THESE DE DOCTORAT

Présentée devant

L'UNIVERSITE DE LILLE

UFR CHIMIE

DOCTEUR DE L'UNIVERSITE DE LILLE

Mention « Molécules et Matière Condensée »

Par

Maxime BEAUVOIS

Ecole Doctorale Science de la Matière, du Rayonnement et de L'Environnement

Unité de Catalyse et de Chimie du Solide, UMR CNRS 8181

Equipe Méthodologie Organométallique en Catalyse Homogène

Synthesis and Characterization of Borohydride/Allyl Rare-Earth Organometallic Complexes Supported by Amino-Pyridine Ligands and their Application towards Ring-Opening Polymerization

Synthèse et caractérisation de complexes allyliques et/ou borohydrure de terres rares supportés par des ligands amido-pyridine et leur application en polymérisation par ouverture de cycle

Soutenue le 05 Mai 2023 à Villeneuve d'Ascq

Thèse Dirigée par

Yohan CHAMPOURET, Chargé de Recherche CNRS, Universités de Lille, directeur de thèse

Marc VISSEAUX, Professeur des Universités, Université de Lille, co-directeur de thèse

Rapporteurs :

Reiner ANWANDER, Professeur des Universités, University of Tübingen, Allemagne

Grégory NOCTON, Chargé de Recherche CNRS, Ecole Polytechnique, Palaiseau

Examinateurs :

Evgueni KIRILLOV, Associate Professor, Université de Rennes, Rennes

Lydie PELINSKI, Professeure des Universités, Université de Lille (Présidente de Jury)

Abstract: During this thesis, the synthesis of borohydride (BH_4) and allyl (C_3H_5) rare earth (RE = Y or Nd) complexes supported by three different amido-pyridine ligands of type (Ar)-N-C(R)(Me)-Py-R' [Ar = 2,6-^{i}Pr-C_6H_3, R = H, R' = H (**Z^1**) or Me (**Z^2**), and R = Me, R' = -C(Me)$_2$=N-Ar (**Z^3**)] have been studied. The borohydride complexes have been obtained using the readily available precursors RE$(BH_4)_3(THF)_3$, the ligand under its protonated form ZH, and one of the two different bases ^{n}BuLi or BEM. On the other hand, the allyl complexes were prepared by reacting the tris-allyl RE and ZH. Coordination of **Z^1** to the neodymium metal center, in both the borohydride and allyl case, resulted in the bis-substituted complexes, while using the bulkier ligand **Z^2** led to the isolation of the mono-substituted complexes. However, depending on the base used, different coordination modes, notably with the possible presence of the magnesium counterpart in the final structure, were observed. While the complexation with the borohydride complexes proceeded as expected, the synthesis of the complex bearing **Z^2** and an allyl moiety led to an, already described in a few cases, C-H activation of the ligand, resulting in dearomatization of the pyridine to a pyridyl moiety and the formation of a dinuclear RE-RE species in which the pyridine is coordinated in η^6 to the RE metal. Obtention of the allylic yttrium complex supported by **Z^1** revealed a unique organometallic chemistry with the formation of an unprecedented allyl bridge between two yttrium moieties. These new families of complexes have been studied for their application in the ring-opening polymerization of cyclic esters (lactide and caprolactone).

Keywords: Rare earth, Yttrium, Neodymium, Borohydride, Magnesium, Allyl, Coordination chemistry, Polymerization, Amido-pyridine, Lactide, Ɛ-Caprolactone

Résumé: Au cours de cette thèse, la synthèse de complexes de terres rares (RE = Y ou Nd) borohydrure (BH_4) et allyle (C_3H_5) supportés par trois différents ligands amido-pyridine de type (Ar)-N-C(R)(Me)-Py-R' [Ar = 2,6-^{i}Pr-C_6H_3, R = H, R' = H (**Z^1**) ou Me (**Z^2**), et R = Me, R' = -C(Me)$_2$=N-Ar (**Z^3**)] a été étudiée. Les complexes de borohydrure ont été obtenus en utilisant les précurseurs faciles à manipuler de type RE$(BH_4)_3(THF)_3$, le ligand sous sa forme protonée ZH, et une base parmi ^{n}BuLi ou BEM, tandis que les complexes allyliques ont été formés en faisant réagir le tris-allyle RE avec ZH. La coordination de **Z^1** au centre métallique du néodyme dans le cas du borohydrure et de l'allyle donne lieu à des complexes bis-substitués, tandis que l'utilisation du ligand **Z^2**, plus volumineux, conduit à l'isolement des complexes mono-substitués. Cependant, différents modes de coordination ont été observés en fonction de la base utilisée, notamment avec la présence éventuelle de la contrepartie en magnésium dans la structure finale. Bien que la complexation avec les complexes borohydrure se soit déroulée comme prévu, la synthèse du complexe portant **Z^2** et un groupement allyle a conduit à une activation C-H habituelle du ligand, déjà décrite dans quelques cas, avec désaromatisation de la pyridine en un groupement pyridyle et formation d'une espèce RE-RE dinucléaire dans laquelle la pyridine est coordonnée en η^6 au métal RE. L'obtention du complexe allylique d'yttrium supporté par **Z^1** a révélé une chimie organométallique unique, avec la formation d'un pont allyle sans précédent entre deux fragments d'yttrium. Ces nouvelles familles de complexes ont été étudiées pour leur application dans la polymérisation par ouverture de cycle d'esters cycliques (lactide et caprolactone).

Keywords: Terres rares, Yttrium, Neodyme, Borohydrure, Magnesium, Allyle, Chimie de coordination, Polymerisation, Amido-pyridine, Lactide, Ɛ-Caprolactone

Acknowledgements

To start I would like to sincerely thanks my director thesis Dr. Yohan Champouret and Prof. Marc Visseaux for the opportunity to do my PhD study under your guidance.

Yohan I am really thankful for the frowns and the constant scolding and asking me to always tidy up after myself it made me grow as a person, even if it's not noticeable. Even helping with the horse shed, somehow help with the thesis. On a more serious note, I am deeply grateful for your guidance, constant support and for sharing all your knowledge with me. I might not have been the model disciple, but thanks for bearing with me.

Marc, (le patron), you have been a great mentor for the last four years. Your expertise on the rare earth metals has been a blessing. It was an honnor and a pleasure to be part of your team. You've known me since I was a DUT student and here, we are now almost ten years later (I bet you regret it but) thanks for making me a part of the team MOCAH. By the I am still waiting for the candies you "borrowed" from me.

I am grateful to Prof. Reiner Anwander and Dr. Gregory Nocton for accepting to read and evaluate this work and to be the rapporteurs of my thesis.

I equally thank Prof. Lydie Pelinsky and Dr. Evgueni Kirillov for being part of my thesis jury and accepting to be examinateurs.

I would like to thank all the members of the CASECO team for the time they shared with me when I went to them for advises or just to talk and blow some steam off. In this team a special thanks is given for the fish lover Nicolas Merles and for the big boss Mathieu Sauthier who gave me advise on chemistry and aquarium.

In the CCM axe a special note for Claudine Butticaz, I have been a pain because of the paperwork for my internship in the US and I am sorry about that.I would also like to thank Celine Delabre for the chatting and elemental analysis and finally than you to my ex-intern Baptiste Lemaire.

More particularly I would like to say thank you to the other student (friends) that share the burden of writing a thesis: Tiphaine Richard, Claudie Simon, Samy Aïssiou and Anthony Saint-Pol. Thanks guys for the moral support and the laughs shared.

Special thanks to the glass blower Maïa Matsakis who repaired all the stuff I broke over the years.

I am also grateful to Dr. Sylvain Duval and Dr. Frédéric Capet who taught me how to use the XRD software but also for their expertise on X-ray crystal structure determination.

Furthermore, I am also grateful to Prof. Evans for welcoming me in his team for two months and to the student present there for all their help during my time over there. In this team I would also like to thank more particularly Cary Stennett for welcoming me and the interesting chemistry conversation.

I would like to acknowledge the University of Lille and the ministry for funding my work and my trip to Irvine.

On a personal note, I am really grateful to my girlfriend Risha Jagdawoo for dealing with me over those years and also helped me a lot when I was down. You are the best!

Table Of Contents

GLOSSARY OF ABBREVIATION

A

α	alpha

B

BEM	n-butylethylmagnesium, (^{n}Bu)(Et)Mg
br	broad

C

[C]	Concentration
Cp	η^5-cyclopentadienyl

D

D	Deuterated
d	doublet
dd	doublet of doublets
ddd	doublet of doublets of doublets
diox	1,4-dioxane, $C_4H_8O_2$
Đ	polydispersity index
δ	chemical shift

E

Et	Ethyl

EtOH	Ethanol
Ɛ-CL	Ɛ-Caprolactone

I

^{i}Pr	isopropyl

L

LA	Lactide
$[LA]_0$	initial concentration of lactide

M

M	metal
m	meta
m	multiplet
Me	methyl
MeOH	Methanol
Mn	number average molecular weight
Mn (theo)	theoretical number average molecular weight
Mw	weight average molecular weight

N

NMR	nuclear magnetic resonance

O

o	ortho
ORTEP	oak ridge thermal ellipsoid program

P

p	para
PCL	poly(Ɛ-caprolactone)
PLA	poly(lactide)
Ph	phenyl, $-C_6H_5$
ppm	part(s) per million

Q

q	quartet

R

R	alkyl or aryl
***rac*-**	racemic mixture
RE	rare earth
REE	rare earth elements
ROP	ring-opening polymerization
RT	room temperature

S

s	singlet
SEC	size exclusion chromatography

T

T	Temperature
t	triplet
TMS	trimethylsilyl, -$SiMe_3$
TOF	turn over frequency
^{t}Bu	tert-butyl

X

XRD	x-ray diffraction

General Introduction

According to the New World Encyclopedia[1], organometallic chemistry is:" the study of chemical compounds containing bonds between carbon and metal atoms. In more general terms, it is the study of compounds containing metal-element bonds that are largely covalent in character." The association between a cationic metal center and a molecule (known as a ligand when coordinated) is called a complex. These complexes can be found in nature such as heme (organometallic iron complex in blood for O_2 transport)[2], vitamin B_{12} (cobalt complexes)[3], among others. These compounds (Fig. 1) can also be synthesized to be used in different applications such as medicine (cancer therapy, medical imaging…)[4], industrial syntheses (fine organic chemistry, obtaining of polymers, electronics application…)[5].

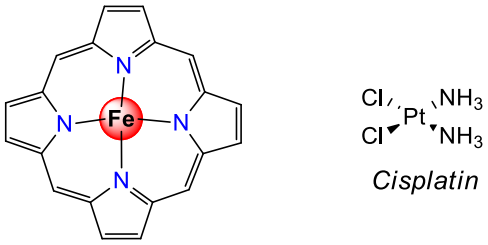

Figure 1: Example of organometallic complexes

My thesis research focuses on synthesizing rare earth complexes. The rare earth elements are constituted of the lanthanides family ([Xe] $4f^x$ $5d^y$ $6s^2$), completed with yttrium ([Kr] $4d^1$ $5s^2$) and scandium ([Ar] $3d^1$ $4s^2$) (Fig. 2).

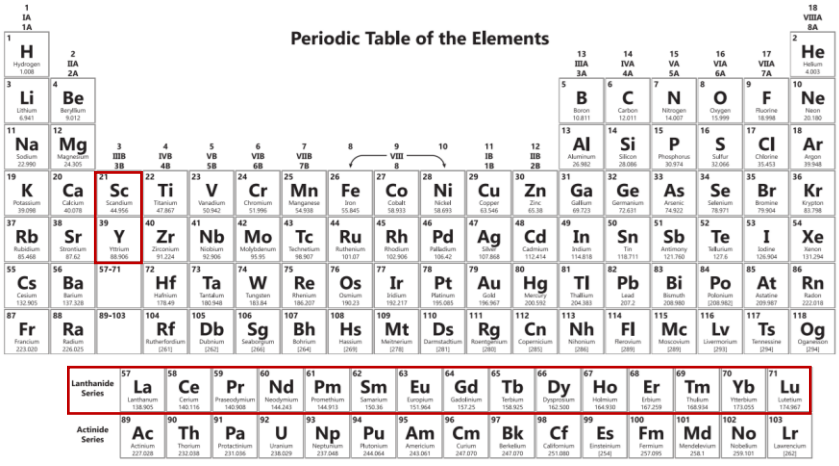

Figure 2: Periodic table with the rare earth elements framed.

The acquisition of rare earth elements has been a geopolitical concern because of China's current virtual monopoly, but the recent discovery of new rare earth mines, particularly the largest

one in Europe found in Sweden in January 2023, may soon alter this scenario. However, the ore extract from the mines is composed of a mix of rare earth elements and, due to their similar chemical properties, the extraction and purification of each element requires the use of a large amount of strong acids and solvents.

Although modern catalysis has been dominated by complexes using transition metals, the use of rare earth (RE) elements was previously underdeveloped for many years, and only recently has their potential been discovered (Chapter 1). In contrast to coordination chemistry involving transition metals (d-blocks metals), the synthesis of complexes using rare earth elements could seem easier due to their two preferred oxidation state (+2 or +3). While the synthesis of transition metals complexes is generally guided by the 18-electron rule, which in turn governs elementary reactions commonly applied to catalysis, such as oxidative reaction, reductive elimination and others, the rare-earth organometallic chemistry is considered more as an ionic chemistry resulting mainly from ligand exchange, with also a reactivity based on insertion/elimination reactions and sigma bond metathesis, and therefore responds to other rules. Even if these parameters might enable an easier chemistry "on paper", this ligand exchange behavior allows to obtain a wide range of complexes with unique coordination mode (anionic product, shared ligand…) and it is only recently that theoretical chemistry has been able to rationalize some of these most particular reactivities.

In this thesis, the formation of complexes using one of the larger rare earth metals (neodymium) and one of the smallest ones (yttrium) will be presented, as typical metals covering general aspects of the REs chemistry. The syntheses that we describe will emphasize some of the drawbacks of this ligand exchange reactivity but also some unexpected products resulting from side-reactions.

Table 1: Main differences between REs and transition metals organometallic chemistry.

	Transition Metals	Rare earth elements
Electronic subshell	(s), (p), (d)	(s), (p), (d), (f)
Typical oxidation number	Wide range (*e.g*. Fe -II to +VI)	+2, +3
Organometallic reactions	Oxidative addition, reductive elimination, β-hydride elimination…	Ligand exchange Insertion/elimination σ-bond metathesis

Some complexes presented in this manuscript will be used as initiator/catalysts for the ring opening polymerization (ROP) of cyclic esters. Polymers can be described as a set of several macro-

chains, which in turn are composed of several small units (monomers) repeated in a definite sequence. One of the most common applications of polymers in today's world is their use as commercial plastics after addition of certain additives. These polymers are mainly obtained from petroleum resource and are, therefore (for the most part), not easily degradable[6]. In recent decades, the synthesis of biodegradable polymers has been widely investigated and is becoming increasingly important due to environmental concerns. In this field, two different polymers have mainly been studied: polycaprolactone and polylactide, which can be easily prepared in a controlled manner by using RE complexes as catalysts.

The present manuscript will be divided into four chapters, as followed:

Chapter 1 provides a small introduction to rare earth elements and their use in everyday life. The history of the rare earth complexes and molecular precursors used during this thesis (allylic and borohydride) will be introduced. A literature review of the borohydride complexes described since the last review in 2011 will be presented.

Chapter 2 describes the results obtained during the synthesis of neodymium and yttrium borohydride complexes supported by amido-pyridine ligands. The first part of this chapter reports the strategies and results in the attempted syntheses of anionic ligands. However, due to the difficulty faced during the syntheses, *in-situ* generation will be preferred by using the protonated form of a ligand combined with a base in the presence of rare earth precursors. Depending on the base and solvent used, the different types of coordination chemistry obtained will be discussed.

Chapter 3 focusses on the complexation of amido-pyridine ligands by using the tris-allyl rare earth as precursors. Usually, the reaction between tris-allyl rare earth complexes and the protonated ligand leads to the formation of propene which facilitates the metal-ligand association. However, this chapter presents uncommon reactions via intra-molecular processes, with a CH activation of the ligand and, consequently, a change in the coordination mode to the RE metal. A possible intermediate of this metalation process is presented, with the formation of an unprecedented allyl bridge between two yttrium centers.

Finally, *Chapter 4* reveals the ability of some of the complexes presented in Chapter 2 and 3 to behave as catalysts for the ring-opening polymerization of cyclic esters (lactide and Ɛ-caprolactone). Some of them were found amongst the most active at room temperature when compared to literature. These polymerization tests were performed in both toluene and THF to evaluate the effect of the solvent. The polymerization of lactide and ε-caprolactone, depending on the complex used as catalyst,

shows some of transesterification side-reaction confirmed by the achievement of small molecular weight of the polymer with narrow polydispersity.

References

[1] www.newworldencyclopedia.org/entry/Organometallic_chemistry

[2] R. Beri, R. Chandra, **Drug Metab. Rev.**, *1993*, 25 (1-2), 49

[3] R. Bonnet, **Chem. Rev.,** *1963*, 63, 6, 573

[4] (a) R. Oun, Y. E. Moussa, N. J. Wheate, **Dalton Trans.**, *2018*, 47 (19), 6645; (b) G. R. Morais, A. Paulo, I. Santos, **Organometallics**, *2012*, 31 (16), 5693

[5] B. M. Gardner, C. C.C. Johansson Seechurn, T. J. Colacot, Organometallic Chemistry in Industry: A Practical Approach, *2020*

[6] A. A. Koutinas, A. Vlysidis, D. Pleissner, N. Kopsahelis, I. Lopez Garcia, I. K. Kookos, S. Papanikolaou, T. Him Kwan, C. Sze Ki Lin, **Chem. Soc. Rev.**, *2014*, 43 (8), 2587

CHAPTER 1 BIBLIOGRAPHY.

1.1 Context

Rare Earth (RE) elements include the whole family of lanthanides ([Xe] $4f^x$ $5d^y$ $6s^2$), which also comprise yttrium ([Kr] $4d^1$ $5s^2$) and scandium ([Ar] $3d^1$ $4s^2$). The International Union of Pure and Applied Chemistry (IUPAC) classifies REs between the light RE elements (from lanthanum to gadolinium) and the heavy RE elements (terbium through lutetium), to which are associated yttrium and scandium. Those elements are part of the same family because of their chemical similarity and the fact that they can be extracted from the same geographic area. However, minerals containing REs can be extracted from almost any region of the world[1] (Fig. 1.1), but they are called "rare" because their concentration is diluted in the earth's crust. Although these elements are used in many fields (catalysis, metallurgy, etc.) (Fig. 1.1), the main problem with these metals is their extraction and refining from the ore, which is, up to now, very polluting for the environment[2].

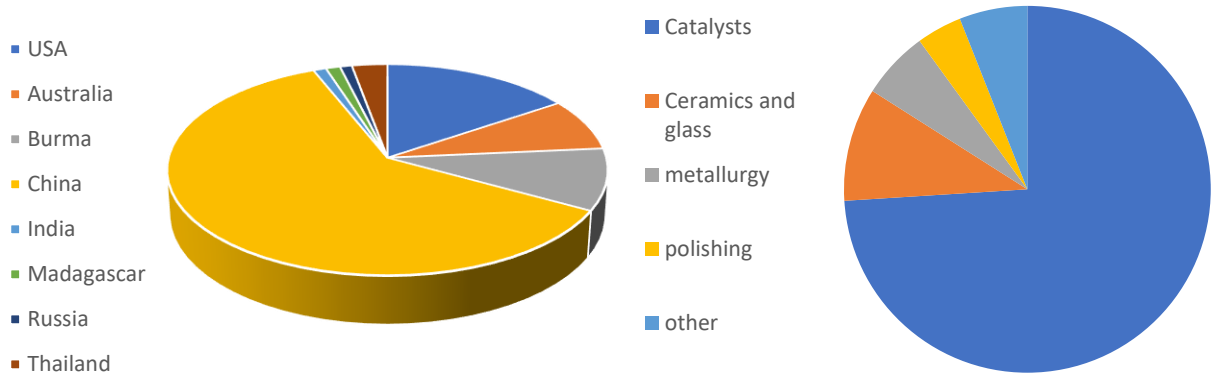

Figure 1.1: Production and utilization of RE elements in 2021[1].

During my thesis, I used RE elements to produce coordination complexes that are expected to serve as catalysts for several applications. The reactivity of complexes in homogeneous catalysis is often driven by the nature of the ligand(s) attached to them. Related ligand(s) cone angle was firstly developed in the 70's using phosphorous based ligand by C. A. Tolman[3]. Computational studies in 2013[4] allowed to extend this theory to nitrogen-based ligand, which was recently applied to REs with a lutetium center[5]. Due to the wide range of RE elements and thus their large size difference, between 1.216 Å and 1.032 Å for CN = 9 (Coordination Number) and even 0.745 Å for Sc (Fig. 1.2)[6], various reactivities and applications can be observed with the same ligand supported by a different metal center.

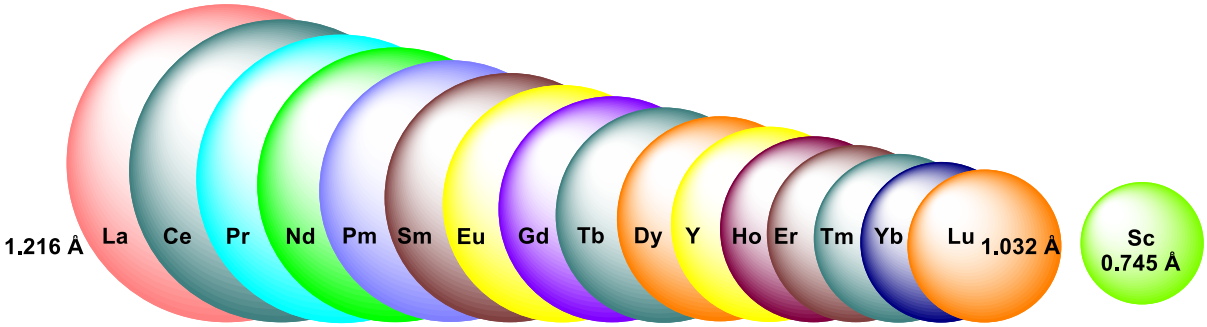

Figure 1.2: Ionic Radii (Å) for Nine Coordinate Trivalent Ions (+ Scandium in Six Coordinate Trivalent Ions; cercle not in scale).

The first organometallic RE complex series was based on the tris(cyclopentadienyl) derivatives $(C_5H_5)_3RE$ (RE = Sc, Y, La, Ce, Pr, Nd, Sm and Gd), which were described in 1954 by G. Wilkinson and J. M. Birmingham[7]. Since then, the REs chemistry has started to develop and many RE catalysts have been designed bearing highly reactive metal-ligand bonds such as: RE-alkyls[8], -amides[9], -alkoxides[10], -triflates[11] among others. These RE complexes can be used in different chemical applications such as electroluminescence[12], catalysis in organic chemistry[13] or polymerization[14], etc.

In this manuscript thesis, I will focus on the synthesis of borohydride (BH_4) and allyl (CH_2CHCH_2) RE-based complexes bearing amido-pyridine derivative ligands, which will be used for the polymerization of cyclic esters. The potential activation of small molecules such as CO_2, CO, H_2, will be also discussed, but only very briefly.

1.2 Generalities on allyl RE complexes

Allyl complexes are a valuable alternative to their alkyl counterparts for reactivity or catalysis purposes, while still exhibiting appropriate levels of activities. This is because the alkyl counterparts are often less stable and usually coordinated by an external base, whereas allyl complexes do not have these limitations. Rare earth allyl complexes have been studied for many reactions such as protonation by acid reagents[15], small molecules activation (H_2, CO_2, NO, NO_2 …)[16], polymerization of various monomers[17] and others. To obtain a wide range of new rare earth allyl complexes, tris-allyl rare earth compounds have been used as valuable precursors for several years. The first synthesis and X-Ray Diffraction (XRD) description of neutral $RE(\eta^3\text{-}C_3H_5)_3$ in 1996 by Taube[18] was made from rare earth tetra-allyl lithium and triethyl borane (Scheme 1.1). The preparation of a tetra-allyl lithium rare earth

complex[19] was performed with a lanthanum center, $[Li(diox)_{1.5}][La(C_3H_5)_4]$, which was synthesized from a mixture of lanthanum tri-chloride with 2 equiv. of tetra-allyl tin and 4 equiv. of ^{n}BuLi. After obtaining this "ate" complex, the series was extended to neodymium by reacting 4 equivalents of $Li(C_3H_5)$ with $NdCl_3$. The lithium reagent was obtained by ligand exchange between tetra-allyl tin and n-butyllithium.

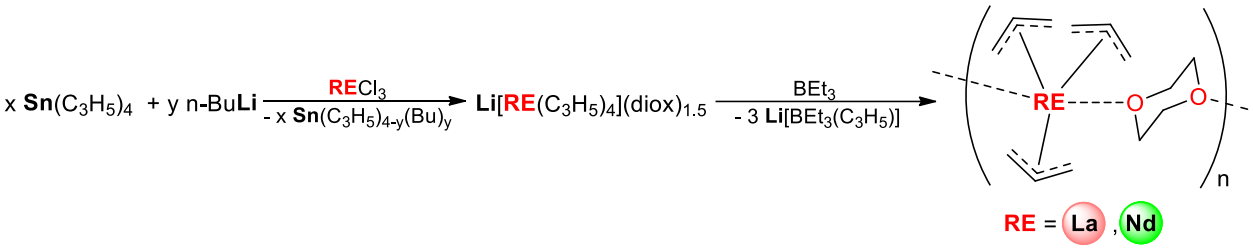

Scheme 1.1: Original synthesis of tris-allyl rare earth complexes.

Since then, various methods have been described in the literature for obtaining these handy precursors of rare earth complexes[20], starting mainly with REI_3 precursor. As an alternative, a direct synthesis using $RECl_3$ has been developed by Bochmann in 2005[21] (Scheme 1.2) to extend the tris-allyl family of RE. During the preparation of $RE(allyl)_3$ complexes, the rare earth precursor $RECl_3$ is subjected to ionic metathesis by a Grignard reagent Mg(allyl)(X) (X = Cl, Br, I). Precipitation of the magnesium salt in dioxane and crystallization allows to obtain clean products. It is worth noting that the use of one type of precursor may not be generalized to the whole family of Res (*cf.* NdI_3, Scheme 1.2).

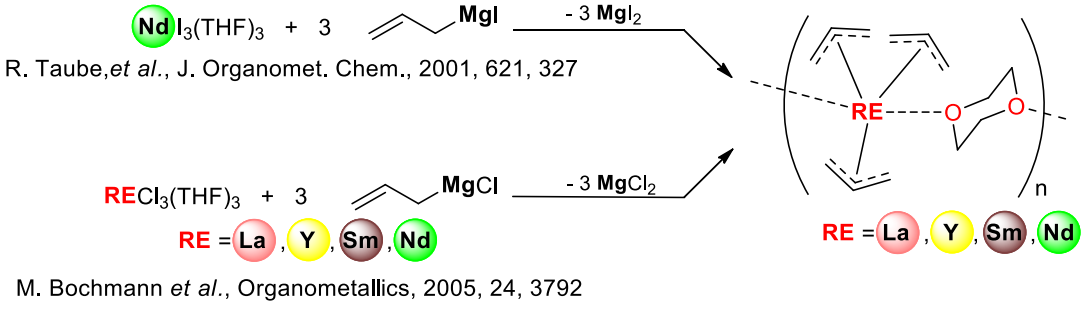

Scheme 1.2: Synthesis of neutral tris-allyl rare earth complexes.

Tris-allyl rare earths are commonly used as convenient precursors for the easy and simple synthesis of $(Z)_xRE(C_3H_5)_{3-x}$ complexes (Scheme 1.3), where Z is referred to as an anionic ligand in this context. Compared to the RE tris-borohydrides, tris-allyl rare earth compounds react straightforwardly with the protonated form of the ligand to obtain the desired product with propene as a sub-product, which can be easily removed under *vacuum*. Numerous studies on rare earth allyl complexes have

been conducted since the last century, and periodic reviews have been published in Comprehensive Organometallic Chemistry[22], including a most recent one which I co-authored.

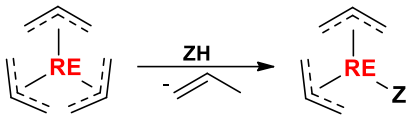

Scheme 1.3: Synthesis of rare earth allyls complexes.

In terms of molecular structure, the allyl group is generally bonded in a tri-hapto η^3-mode to a RE metal center. A fundamental work published in 1999[23] described the fluxional attitude of the allyl moiety from *syn* to *anti,* which is triggered by a switch from η^3 to η^1 followed by a rotation of 180 °, and then the return of the coordination to the η^3 mode (Scheme. 1.4).

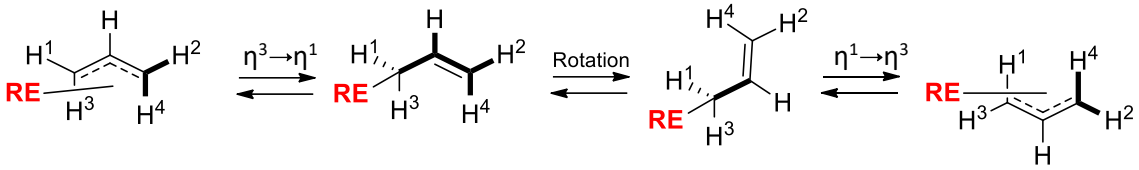

Scheme 1.4: Coordination mode of allyl-RE: switching from η^3 to η^1.

η^1-Coordination arrangement of the allyl moiety is rarely found in the literature for RE coordination chemistry[24], where it is more postulated as an intermediate. The allyl group may be fluxional in solution, which results in a typical 1H/4H or 1H/2H/2H pattern of allyl resonances by ^{1}H NMR spectroscopy. In contrast to borohydride complexes, allyl display preferentially, to our knowledge, two different coordination mode to the metal center as terminal or bridging fashion mode (Fig. 1.3). These bridges will be discussed in more details later in the manuscript.

Being one of the co-authors of a book chapter in Comprehensive Organometallic Chemistry IV in 2022[22d)], included as Appendix 1, $(Z)_xRE(C_3H_5)_{3-x}$ complexes will not be presented further in this bibliographic chapter.

As for RE borohydride complexes, a number of general reviews have been published on that topic over the past decade, with the most recent one being published in 2011[25]. Since then, many new RE borohydride coordination complexes have been synthesized and their catalytic properties have been studied. In this section, we will mostly present the RE complexes bearing at least one BH_4 ligand that have been prepared and described in the literature after 2011.

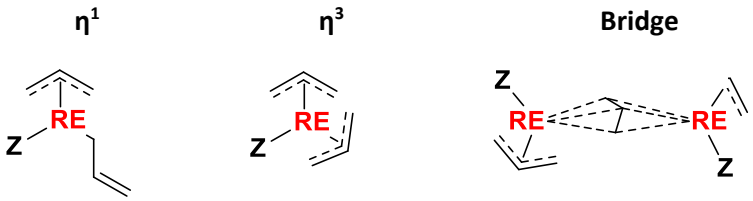

Figure 1.3: Coordination mode of allyl-RE moiety..

1.3 Borohydride RE complexes

1.3.1 Generalities on borohydride RE complexes.

RE tris-borohydrides of the type $RE(BH_4)_3(THF)_x$ were firstly described by reacting RE alkoxides $Ln(OMe)_3$ with diborane in THF[26]. Typical synthesis of these precursors is nowadays pursued by a metathesis reaction in THF between the RE tri-chloride and $NaBH_4$ or $LiBH_4$[27] (Scheme 1.5).

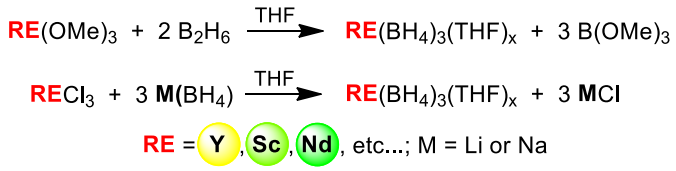

Scheme 1.5: Synthesis of tris-borohydride RE complexes.

Those compounds have been widely used for various applications and, in particular, as valuable precursors for the synthesis of well-defined RE borohydride complexes of the type $RE(BH_4)_{3-y}(Z)_y$ bearing one or more ancillary ligand(s) designated herein as Z^- anionic ligand (note that the THF, generally present as a labile L ligand, has been omitted here for clarity). $RE(BH_4)_{3-y}(Z)_y$ complexes have been extensively applied in molecular chemistry and, more especially, in polymerization catalysis [28]. Although borohydride and chloride ligands are isosteric[29], borohydride is considered to be more electron donating[30] and forms a more covalent bond with a RE metal. Therefore, the use of BH_4 ligand results in complexes that are generally more soluble than their chloride analogs. RE Z-substituted borohydride complexes, $RE(BH_4)_{3-y}(Z)_y$, can be synthesized by different ways. The most commonly used method is to react the RE tris-borohydrides $RE(BH_4)_3(THF)_n$[31] precursor (n = 2 or 3, depending on the RE) with the preformed salt of the anionic ligand (Scheme 1.6), which is referred to the ionic metathesis

route. Another method is to use an *"in-situ"* procedure by means of the *"borohydride/alkyl route" (B/A route)*[32], a strategy developed in our laboratory, where the borohydride starting material $RE(BH_4)_3(THF)$ is mixed with the protonated form of the ligand, ZH, followed by the dropwise addition of an alkyl base such as butylethylmagnesium (BEM), ^{n}BuLi, or others, to yield the desired product after purification steps.

Ionic Metathesis reaction

$$RE(BH_4)_3(THF)_x + y\ MZ \longrightarrow (Z)_yRE(BH_4)_{3-y}(THF)_x + y\ M(BH_4)$$

Borohydride/alkyl route (B/A) route

$$RE(BH_4)_3(THF)_x + y\ ZH \xrightarrow[-\ RH]{M\text{-}R} (Z)_yRE(BH_4)_{3-y}(THF)_x + y\ M(BH_4)$$

RE = Rare Earth; M = Li, K, Na, Mg...; R = alkyl, allyl...; **Z** = Ligand

Scheme 1.6: General methods for the synthesis of borohydride RE complexes.

In the coordination chemistry of borohydride RE complexes, it is important to note that there is no direct bond between the boron atom and the RE center. The bonding mode between the RE element and the borohydride group occurs through hydrogen bridging atoms RE-(μ-H)-B with a three-center two-electron bonds coordination mode. The borohydride can be coordinated as a di-hapto η^2, tri-hapto η^3 or bridging fashion mode. This coordination mode can be identified by the Metal-B distances observed in XRD or by infrared spectroscopy: the di-hapto η^2 is characterized by one strong broad band centered at around 2415 cm^{-1} along with a sharp singlet at ~2125 cm^{-1}, whereas the IR spectrum of tri-hapto η^3 exhibits one sharp band at 2420 cm^{-1} and a strong broad one centered at ~2230 cm^{-1}. This versatile coordination of the borohydride ligand can thus easily complement and adjust the bonding space of the coordination sphere of the metal (Fig 1.4)[33].

Di-hapto **Tri-hapto** **Bridge**

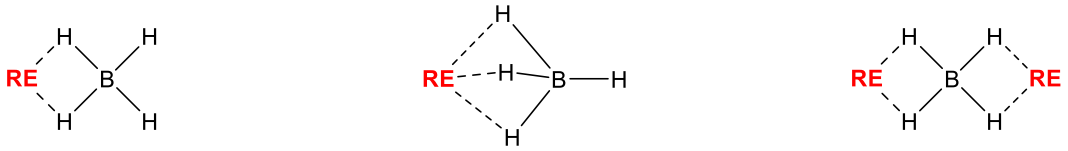

Figure 1.4: Coordination mode of borohydride ligand in RE complexes.

The ^{1}H NMR of the borohydrido ligand is driven by two different parameters. Indeed, depending on the metal center, the signal can give rise to a broad peak for the paramagnetic metal

while it results in a broad multiplet for others such as yttrium [I(^{77}Y) = 5/2]. Displaying a boron coupling of 3/2 [I(^{11}B) = 3/2], the multiplicity of the borohydrido signal (N) can be easily calculated by the formula [I(^{11}B) + I(RE) = N] (for yttrium, N = 4).

Several applications for supported borohydride RE complexes have been studied: polymerization[34], hydrogen storage[35], among others. In recent years, the complexation of various ligands such as cylopentadienyl (Cp), amidino, etc…, which modulate the activity of borohydride complexes, has been studied and an overview of these research works will be compiled in the following section.

1.3.2 Organometallic compounds

1.3.2.1 Mono-substituted complexes

1.3.2.1.1 Cyclopentadienyl derivatives

Cyclopentadienyl-based complexes of RE (**1RE**) have been studied for decades and are still the most used, in the RE complexes field, for a wide range of applications and most notably for polymerization of various monomers. Surprisingly, the neodymium borohydride complex bearing one unsubstituted cyclopentadienyl (Cp) ligand was only very recently isolated by D. M. Roitershtein and colleagues in 2022[36]. The neutral mono(cyclopentadienyl) neodymium complex **1Nd** was obtained from the reaction of $Nd(BH_4)_3(THF)_3$ with an equimolar amount of NaCp in THF (Scheme 1.7). Similar "ate" derivative has already been described by M. Visseaux and coll.[29b] as $[CpNd(BH_4)_3]_2[Mg(THF)_6]$.

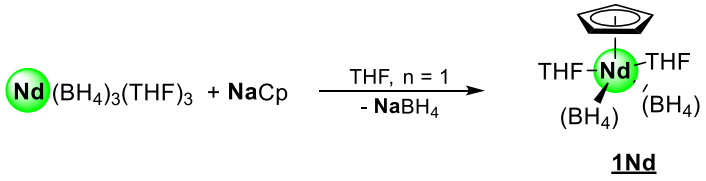

Scheme 1.7: Synthesis of neodymium Cp complex 1Nd.

The crystal structure obtained from XRD studies of **1Nd** depicts a clean mononuclear complex with one cyclopentadienyl ligand coordinated in η^5 fashion and a borohydride group in a η^3 coordination mode. However, to complete the coordination sphere, complex **1Nd** needs two additional THF molecules.

Even if Cp* neodymium (**2Nd**) bis-borohydrides complexes have been known for some years[37], and being already described in 2009 with scandium[38], F. Bonnet *et al*. in 2013[39] isolated crystals suitable for XRD, which revealed the molecular structure of $Cp^*Nd(BH_4)_2(THF)_2$. The authors reported that heating **2Nd** in toluene or benzene allowed to obtain the solvent-free hexamer species $[Cp^*Nd(BH_4)_2]_6$ (**2Nd'**). Solid-state analysis of **2Nd** showed a complex carrying the same coordination environment (*i.e.* two borohydrides in η^3 fashion, two THF molecules and one η^5-Cp) than **1Nd** with the methyl substituents on the Cp ligand. The synthesis of reactive Cp* cationic complexes (**2Nd**$^+$) was achieved from **2Nd** by protonolysis, using a fluorinated Lewis acid at the NMR scale (Scheme 1.8). Due to its high reactivity to polymerize THF, no crystals were obtained for that complex.

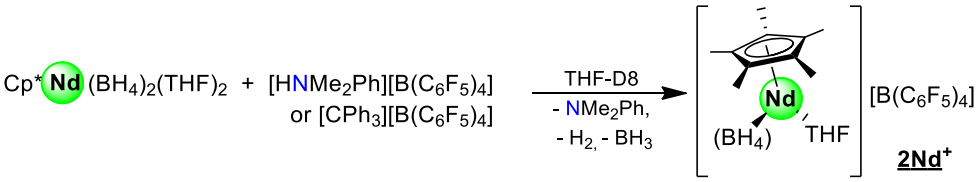

Scheme 1.8: NMR Scale synthesis of $[Cp^*Nd(BH_4)(THF)][B(C_6F_5)]$, 2Nd$^+$.

The synthesis of lanthanum and cerium borohydride complexes using Cp^{tBu3} (Cp^{tBu3} = $\{C_5H_2(^tBu)_3$-1,2,4$\}$) (**3RE**) was reported in 2018 by D.P. Mills and coll.[40]. In the tentative synthesis of the bis-ligand complex, presumably due to steric hindrance, the reaction of two equiv. of KCp^{tBu3} in THF with one equiv. of $La(BH_4)_3(THF)_4$ at room temperature led only to the formation of the mono-substituted complex $Cp^{tBu3}La(BH_4)_2(THF)$ (**3La**), and traces amount of the hexameric form of the mono-substituted $[Cp^{tBu3}La(\mu\text{-}BH_4)_2]_6$ similar to **2Nd'**. The same reaction using $Ce(BH_4)_3(THF)_{3.5}$ resulted in the formation of the dimeric species $[Cp^{tBu3}Ce(BH_4)(\mu\text{-}BH_4)(THF)]_2$ (**3Ce**, Scheme 1.9). The results of this reaction must be caused by the steric hindrance induced by the three tert-butyl groups in the cyclopentadienyl ligand.

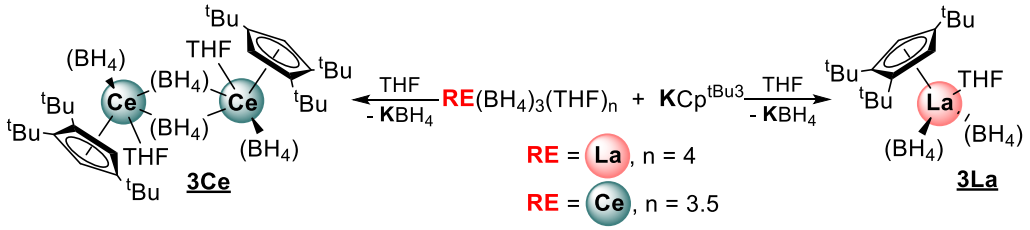

Scheme 1.9: Synthesis of 3La and 3Ce.

XRD suitable crystals of complexes **3Ce**, **3La** and its hexameric form **3La'** were obtained. The molecular structure of the half-sandwich **3La** showed a similar structure to **1Nd** and **2Nd** with a bulkier

cyclopentadienyl ligand. The crystal structure of the hexameric form **3La'** showed a lanthanum cluster with each lanthanum connected to three different BH_4 without the presence of THF molecules. Similar hexameric samarium and neodymium clusters have been previously described with less bulky cyclopentadienyl ligand ($C_5Me_4{}^nPr$)[41]. The solid state XRD structure of **3Ce** exhibited a dimeric complex where each cerium was bounded in a terminal tri-hapto coordination mode to a borohydride group. Each borohydride bridge linked the two cerium centers in a di-hapto coordination mode on one side and in a mono-hapto fashion on the other, which highlights the versatile coordination chemistry of BH_4 ligand.

In 2022, the same team described two new RE bis-borohydrides complexes obtained by reacting KCp''' (Cp''' = {$C_5H_2(SiMe_3)_3$-1,2,4}) (**4RE**) with $RE(BH_4)_3(THF)_3$ (RE = Y, Dy) in THF[42]. While the THF adduct obtained with yttrium is isolated as a [Y(Cp''')$(BH_4)_2$(THF)] structure (**4Y**), the dysprosium adduct is heated 1 hour at 100 °C under *vacuum* to afford a solvent-free adduct in the form of a tetranuclear complex [Dy(Cp''')(BH_4)(μ-BH_4)]$_4$ (**4Dy**, Scheme 1.10). Due to their size, rare earth elements can be prone to produce different clusters after the loss of a solvent molecule [hexameric (**2Nd'**), tetrameric (**4Dy**) and dimeric (**3Ce**)].

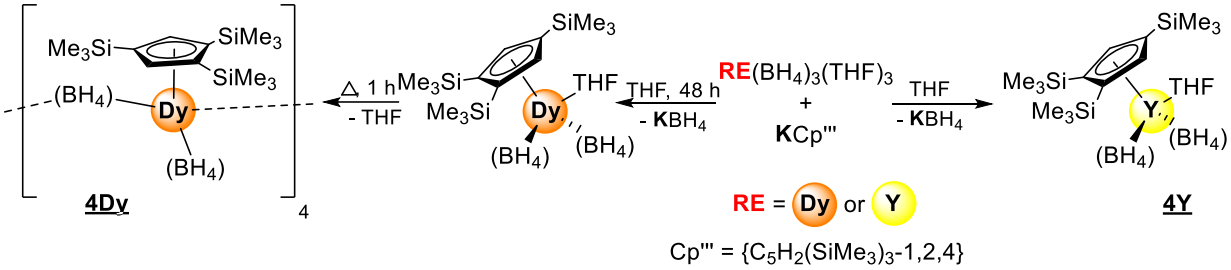

Scheme 1.10: Synthesis of homonuclear 4Y and tetranuclear 4Dy.

Single crystals suitable for XRD were obtained by recrystallization in hexane. The molecular structure of **4Y** exhibited an yttrium complex bonded to two borohydride groups in a η^3 fashion way, a cyclopentadienyl ligand linked in a η^5 manner and a molecule of THF to complete the coordination sphere. Just like with **3Ce**, the **4Dy** tetrameric species exhibited a terminal borohydride group that was bonded through three hydrogens to the metal center, while the borohydride bridges were linked to each dysprosium in a di-hapto fashion.

As discussed in this first part, cyclopentadienyl bis-borohydride complexes are still widely studied for the different coordination mode induced on the borohydride moiety (terminal or bridge). Among those complexes, only **4Dy** and **3Ce** were studied for their application in magnetism. **1Nd** and **2Nd** have been applied as polymerization catalysts or precatalysts as presented in Table 1.1.

In order to increase the reactivity of RE complexes bearing borohydride groups, multidentate ligands have also been assessed as structural elements of new complexes.

1.3.2.1.2 Iminophosphoranyl ligand

A first series of RE borohydride complexes (Y, Lu, La) bearing bis(phosphinimino)methanide (**5RE**) was described in 2010 by J. Jenter *et al*.[43]. These complexes were either (i) synthesized from the tris-borohydride precursors (RE = La or Lu) in the presence of the potassium salt of the ligand in THF at 60 °C (**5La** and **5Lu**) or, (ii) for yttrium, by metathesis between the tri-chloride precursor and the same potassium salt, which led to the chloro dimer yttrium species (omitted for more clarity) that subsequently reacted with $NaBH_4$ to yield the desired borohydride complex (**5Y**, Scheme 1.11). This series of complexes was further extended to neodymium and scandium (**5Sc** and **5Nd**) using the same method (i)[44]. Characterization by X-ray crystallography indicated that all six complexes (**5Sc**, **5La**, **5Y**, **5Lu** and **5Nd**) revealed a similar structure with a phosphinimino ligand and two tri-hapto coordinated borohydride units. However, the presence of a THF molecule was required to complete the coordination space for the two larger elements neodymium and lanthanum.

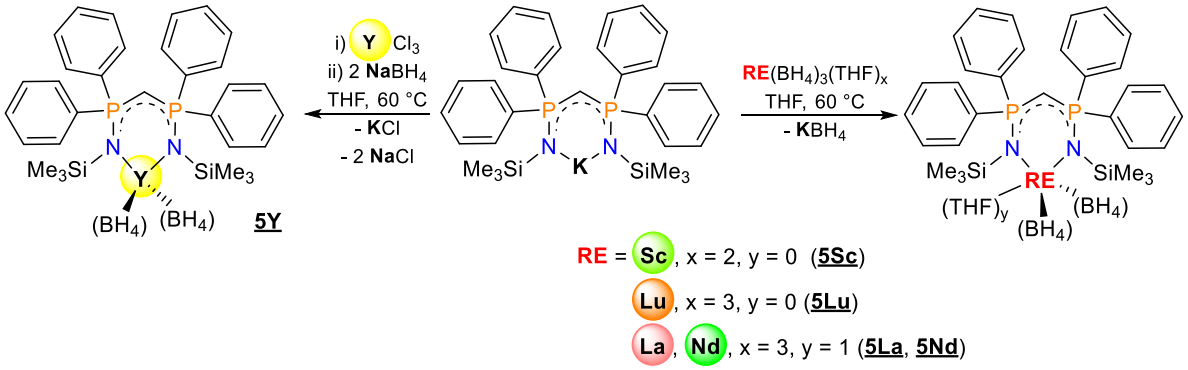

Scheme 1.11: Synthesis of bis(phosphinimino) bis-borohydride complexes.

Following this series, a new family of complexes (**6RE**) was reported in 2015 by the same group with this time a bidentate ligand bearing one thiophosphoranyl arm and an iminophosphoranyl instead of a bis-iminophosphoranyl ligand[45]. This new family was synthesized using the same preparation protocol of ionic metathesis with a dimeric potassium salt (Scheme 1.12).

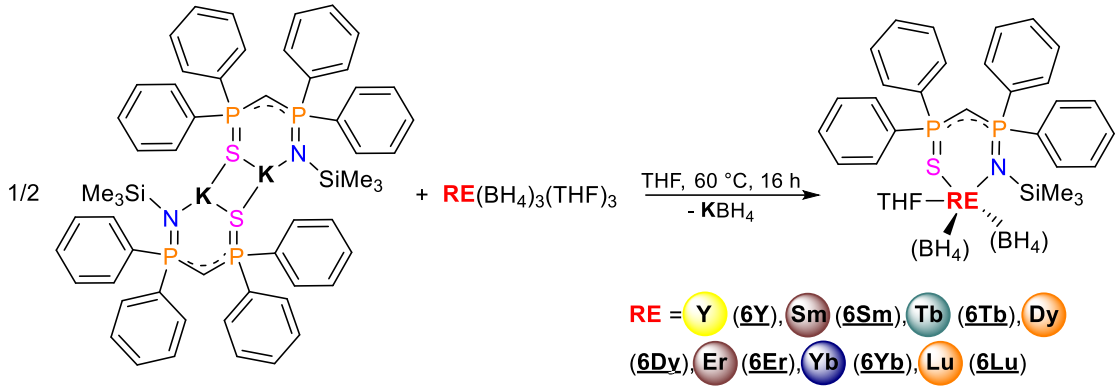

Scheme 1.12: Synthesis of imino-thiophosphoranyl borohydride RE complexes.

Crystal structures of all the complexes have been obtained except for **6Lu**. In each case, the RE center is surrounded by a ligand, which is coordinated by both sulfur and nitrogen, two borohydrides in a η^3 fashion mode and one molecule of THF. The interaction between the methanide carbon atom and the RE atom resulted in the formation of a twisted boat confirmation for the six membered metallacycle.

Although this chemistry is still in its early stage, RE complexes bearing an iminophosphoranyl ligand showed good activity for the ring-opening polymerization of Ɛ-caprolactone, trimethylene carbonate (TMC) and polymerization of methyl methacrylate[46] (MMA) (Table 1.1).

1.3.2.1.3 Nitrogen based ligand.

For decades, complexes resulting from the coordination of nitrogen-based ligands on RE elements permitted numerous applications in different fields like luminescence[47], magnetism[48] and others. For nearly twenty years, Trifonov's group has been investigating the coordination on rare earth borohydride complexes of different types of ligands such as guanidinate[49], bulky diamido ligands[50] and amidinate ligand[51]. New amidinate bis-borohydride complexes were reported in 2015[51] and 2016[52] using amidinate lithium salt combined with $RE(BH_4)_3(THF)_3$ in THF (Scheme 1.13). XRD-suitable single crystals were obtained for **7Y^{iPr}** in a concentrated solution of DME and for **7Y^{Cy}** in a concentrated solution of THF with a layer of hexane. Solid-state analysis revealed for **7Y^{iPr}** and **7Y^{Cy}** the coordination of the ligand by both the nitrogen atoms and the borohydride groups in a tri-hapto fashion. The coordination of an additional solvent molecule (DME or THF) completed the coordination sphere.

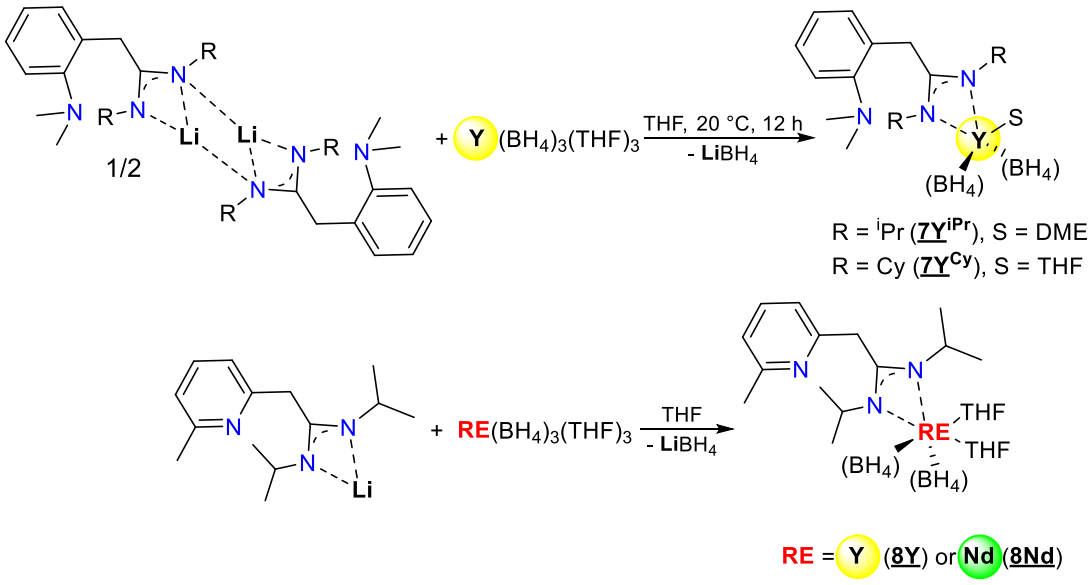

Scheme 1.13: Synthesis of amidinate bisborohydride RE complexes by ionic metathesis with the lithium salt.

Recently, N. Rad'kova *et al.* described the preparation of rare earth borohydride complexes supported by a tetradentate phenoxide ligand (**9RE**)[53]. The *in-situ* deprotonation of the phenolic part was proceeded by the addition of an equimolar amount of ^{n}BuLi at -70°C before the addition of the tris-borohydride precursors. As presented in Scheme 1.14, complex **9Y** is composed of an yttrium metal center coordinated to the ligand through the two nitrogen atoms of the pyridine groups, the tertiary amine and the phenoxide moiety. In addition, the metal center is also coordinated in a tri-hapto fashion to two borohydride parts.

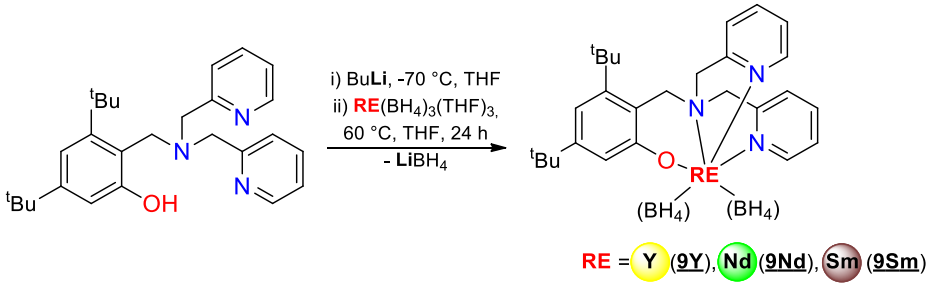

Scheme 1.14: Synthesis of rare earth complexes supported by a tetradentate phenoxide ligand.

In 2013, T. K. Panda and coll. reported the synthesis of an erbium mono-substituted complex bearing an N-aryliminopyrrole ligand[54]. Synthesis of this complex was performed in THF by reacting one equivalent of the potassium salt of the ligand with one equivalent of $Yb(BH_4)_3(THF)_3$ (Scheme 1.15). Obtaining crystals suitable for XRD from a concentrate mixture THF/pentane at -35°C has allowed the

3D arrangement of **10Yb** to be revealed. According to the solid-state analysis, the ytterbium metal center is bound to the ligand *via* the imine group and the pyrrole function, two borohydrides are linked in η^3 mode and two THF molecules are present to complete the coordination sphere.

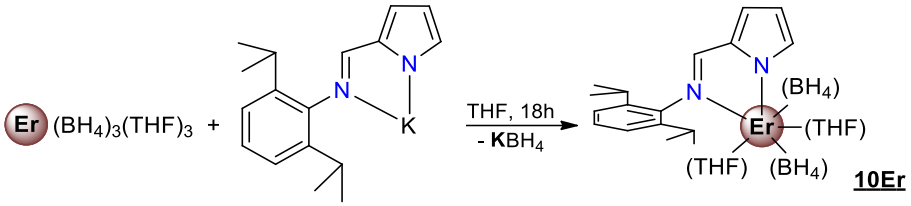

Scheme 1.15: Synthesis of erbium borohydride complexes bearing an N-aryliminopyrrole ligand.

In 2017, the same group was able to isolate new triketiminate bis-borohydride RE (RE = Y or Nd) (**11RE**) complexes using lithium salt metathesis[55] (Scheme 1.16). The molecular structure of **11Nd** was deduced from X-Ray crystallography analysis and revealed that the coordination of the ligand was taking place by the two nitrogen atoms, completed with two THF molecules and both borohydride groups in a η^3 fashion.

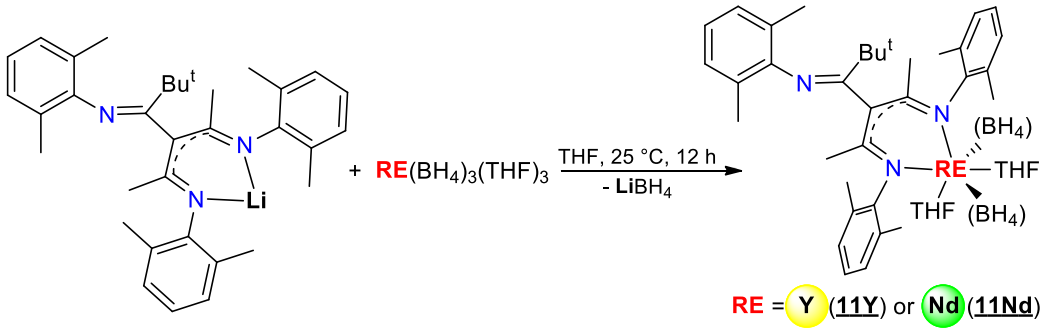

Scheme 1.16: Synthesis of bis-borohydride RE complexes bearing a triketiminate ligand.

Using the amidinate potassium salt, J. Kratsch *et al.* were able to synthesize a new series of borohydride RE complexes (RE = La, Nd, Sm, Yb, Lu, Sc) (**12RE**) *via* an ionic metathesis reaction with tris-borohydride RE precursors in THF[56] (Scheme 1.17). X-ray crystal determination of each compound revealed a RE element supported by one ligand bounded by the two nitrogens, two borohydrides and two THF molecules even though the metals are of different size.

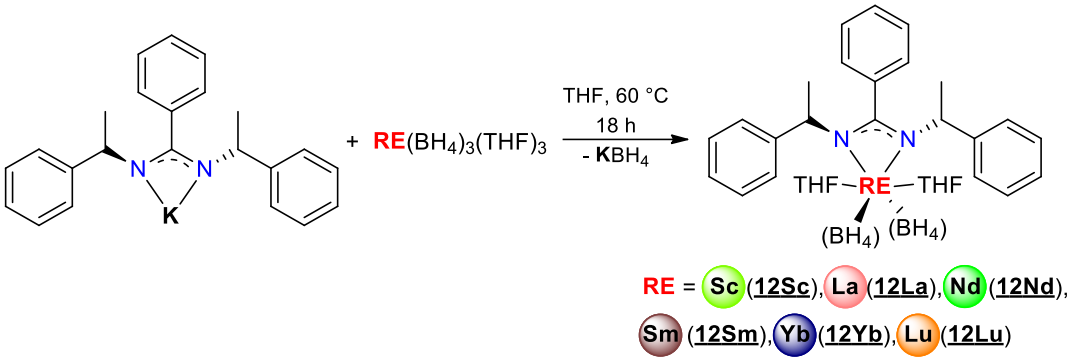

Scheme 1.17: Synthesis of amidinate RE complexes.

As reported in 2014 by M. Schmid *et al.*[57], β-diketiminate RE borohydride complexes (Re = Sc, Dy, Sm, Yb, Lu) were synthesized using the same methodology as above (Scheme 1.18). The typical metathesis reaction between potassium β-diketiminate and RE tris-borohydrides precursors in THF afforded the desired complexes. X ray diffraction analysis of both **13Lu** and **13Sm** complexes showed that the ligand was coordinated by the two nitrogens on the RE element, in addition to two borohydride groups and a THF molecule.

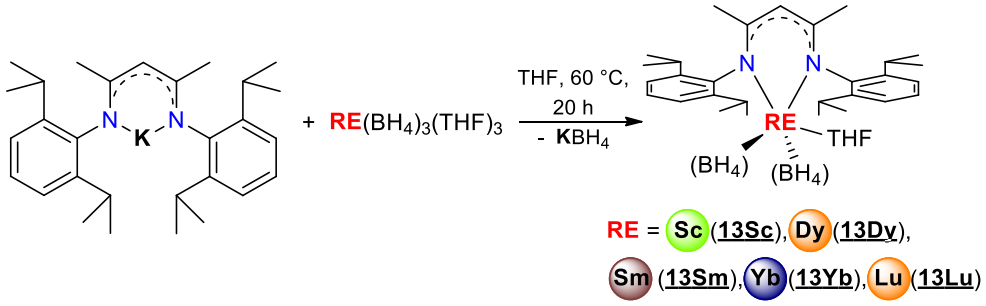

Scheme 1.18: Synthesis of a series of RE borohydride complexes bearing a β-diketiminate ligand.

Complexes comprising of nitrogen-based ligands constitute a wide family for a number of applications in polymerization, with a large choice of ligands (amidinate, guanidinate …) that allow for the formation of different structural assemblies. The above-mentioned complexes have been particularly used for ring-opening polymerization of several polar monomer such as lactide, ε-caprolactone or polymerization of conjugated dienes such as isoprene as depicted in Table 1.1.

Table 1.1: Mono-substituted borohydride RE complexes used in polymerization catalysis.

Borohydride complex	Ɛ-CL	*rac*-La	MMA	TMC	IP	Ref
$CpNd(BH_4)_2(THF)_2$ (**1Nd**)	✓					36
$Cp^*Nd(BH_4)_2(THF)_2$ (**2Nd**)					✓	39
$[CH(PPh_2NsiMe_3)_2]La(BH_4)_2$ (**5La**)	✓		✓	✓		43
$[CH(PPh_2NsiMe_3)_2]Lu(BH_4)_2$ (**5Lu**)	✓		✓	✓		43
$[CH(PPh_2NsiMe_3)_2]Y(BH_4)_2$ (**5Y**)	✓		✓	✓		43
$[CH(PPh_2{=}NsiMe_3)(PPh_2{=}S)]RE(BH_4)_2(THF)$ (**6Y**, **6Tb**, **6Dy**, **6Er** and **6Lu**)	✓					45
$[CH(PPh_2{=}NsiMe_3)(PPh_2{=}S)]RE(BH_4)_2(THF)$ (**6Sm** and **6Yb**)	✓			✓		45
$[o\text{-}Me_2NC_6H_4CH_2C(N^iPr)_2]Y(BH_4)_2(DME)$ (**7Y^{iPr}**)		✓			✓	51
$[o\text{-}Me_2NC_6H_4CH_2C(Ncy)_2]Y(BH_4)_2(THF)$ (**7Y^{Cy}**)		✓			✓	51
$[6\text{-}Me\text{-}C_5H_3N\text{-}2CH_2C(N^iPr)_2]RE(BH_4)_2(THF)_2$ (**8Y** and **8Nd**)					✓	52
$[(C_5H_4NCH_2)_2NCH_2(3,5\text{-}{}^tBu_2C_6H_2O)]RE(BH_4)_2$ (**9RE**) (**9Y**, **9Nd** and **9Sm**)	✓	✓				53
$[(2,6\text{-}Me_2C_6H_3N{=}Cme)_2C(2,6\text{-}Me_2C_6H_3N{=}Cbu^t)]RE(BH_4)_2(THF)_2$ (**11Y** and **11Nd**)	✓	✓			✓	55
$[PhC(NCCH_3Ph)_2]RE(BH_4)_2(THF)_2$ (**12Sc**, **12La**, **12Sm** and **12Lu**)		✓				56
$[(2,6\text{-}C_6H_3{}^iPr_2)NC(Me)CHC(Me)N(2,6\text{-}C_6H_3{}^iPr_2)]RE(BH_4)(THF)$ (**13Sm** and **13Yb**)		✓		✓		57
$[(2,6\text{-}C_6H_3{}^iPr_2)NC(Me)CHC(Me)N(2,6\text{-}C_6H_3{}^iPr_2)]RE(BH_4)(THF)$ (**13Sc**, **13Dy** and **13Lu**)		✓				57

Ɛ-CL = Ɛ-Caprolactone, rac-LA = racemic lactide, MMA = Methyl methacrylate, TMC = Trimethylene carbonate, IP = Isoprene

The preparation of the corresponding bis-substituted complexes of most of these compounds has been attempted. The general method to obtain them by reaction with the tris-borohydride precursors will be presented in the next section.

1.3.2.2 Bis-substituted complexes from tris-borohydride precursors

1.3.2.2.1 Cyclopentadienyl complexes

Compared to the mono-cyclopentadienyl organolanthanide complexes, RE complexes bearing two Cp ligand (or Cp derivatives) have been studied for a longer time and are therefore widely used. The synthesis of the neutral bis-substituted analogous of **1Nd**, **14Nd**, was conducted using the same

protocol and the anionic form **14Nd'** was obtained by adding 18-crown-6 to the reaction mixture[36] (Scheme 1.19). The molecular structure of **14Nd** and **14Nd'** was determined by XRD. While **14Nd** featured a mononuclear neodymium complex supported by two cyclopentadienyl ligands in η^5 coordination mode, one borohydride group and one THF, **14Nd'** resulted in an ionic pair with an anionic neodymium species with two η^5-coordinated Cp ligands. Within these structures, all borohydride units were coordinated to **14Nd** or **14Nd'** in a tri-hapto fashion.

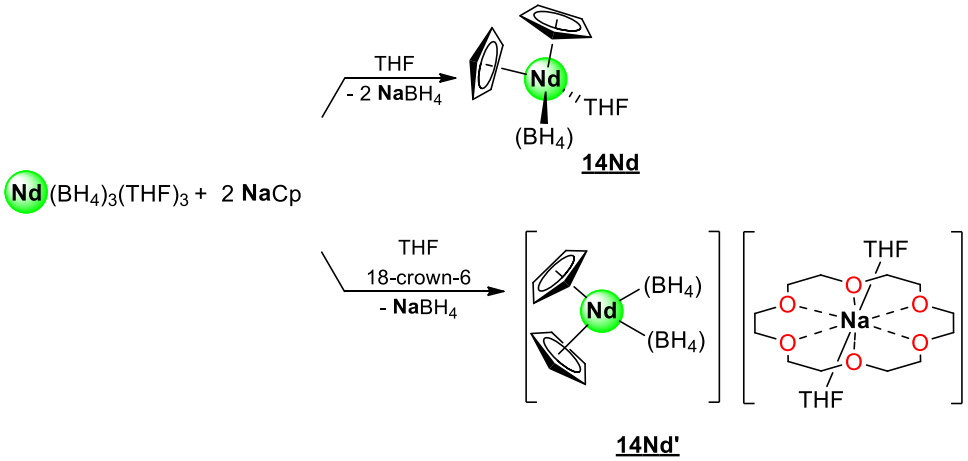

Scheme 1.19: Synthesis of the borohydrido neodymocenes 14Nd and 14Nd'.

It has also been shown that if an excess of $NaBH_4$ is added to the synthesis of **14Nd'** along with 18-crown-6, the isolation of **14Nd'** was accompanied by the formation of two side-products **14Nd''** and **14Nd'''**, as displayed in Scheme 1.20. Single-crystals fitted to X-Ray diffraction studies revealed that the complex **14Nd''** is similar to **14Nd'**, except that Na^+ was coordinated to a single THF molecule and 18-crown-6. On the other hand, the molecular structure of complex **14Nd'''** could be best described as two anionic $[CpNd(BH_4)_2]^-$ species associated with the cationic complexes $[CpNd(18\text{-crown-6})(BH_4)]^+$ and $[Na(18\text{-crown-6})(THF)_2]^+$. Within this structure, it is a rare example of a RE metal center coordinated simultaneously to one Cp ligand and crown ether. According to the author, **14Nd'''** is the unique example of Ln^{3+} where the cyclopentadienyl ligand and crown ether are coordinated simultaneously to a lanthanide. However, the closest similar coordination environment is only known for the divalent Sm^{2+} and Yb^{2+} [58].

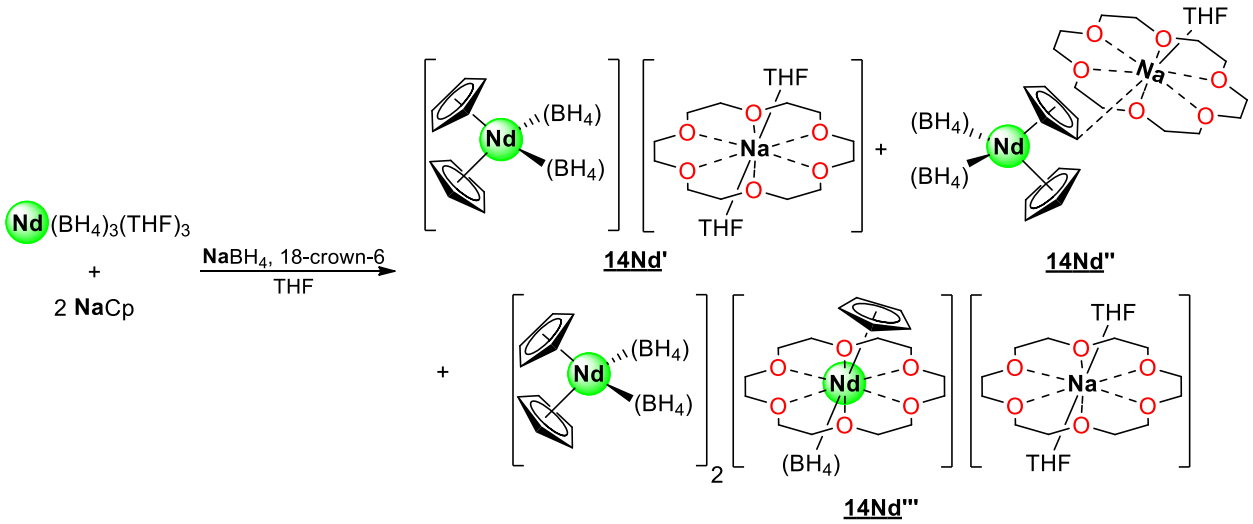

Scheme 1.20: Synthesis of 14Nd' with isolation of side products.

Using the phospholyl potassium salt KHtp (Htp = $PC_4H_2{}^tBu_2$-2,5), a wide range of complexes bearing a phospholyl ligand were isolated[59]. As described by the authors, changing the solvent, and thus using different reaction temperatures, allowed for different forms of the same target product to be obtained (Scheme 1.21). The reaction performed in di-^{n}butyl ether gave the product as a rare earth dimer in the form $[RE(Htp)_2(\mu\text{-}BH_4)]_2$ (**15RE**) but in low yields for **15Nd** and **15Sm**, due to the formation of the by-product $(Htp)_2$. By conducting the same experiment in DME at a lower temperature, the rare earth heterobimetallic RE-K product $[RE(Htp)_2(\mu\text{-}BH_4)_2K(DME)]$ (**16RE**) was obtained and another cerium/potassium heterobimetallic product of the type $[Ce(Htp)(\mu\text{-}Htp)(\mu\text{-}BH_4)_2K(THF)(OEt_2)]$ (**17Ce**), similar to **16RE**, was also obtained in a solvent with a lower boiling point (diethyl ether). In order to prepare the homoleptic complexes, the same procedure using 3 equiv. of the potassium salt of the ligand was attempted, but the desired compound was not obtained. The molecular structure of the different compounds **15RE (RE = La, Ce, Nd, Sn)**, **16RE (RE = La, Ce)** and **17Ce** were achieved but, due to poor quality of the data inherent to the crystal, the metrical parameters of **15Nd** were not given. As seen in scheme 1.21, each metal center is coordinated to the phospholyl ring in η^5 fashion while the BH_4 binding coordination was not specified. In the case of complexes **15RE**, the borohydride bridges stabilized the formation of rare earth dimers. Although the complexes **16RE** exhibited a similar borohydride bridge, the potassium center was coordinated to two DME molecules that allow for the bridging with the potassium center of the other unit. Complex **17Ce** exhibited a different solid-state structure with a potassium center coordinated by a THF molecule, a diethyl ether molecule and a η^5-Htp that forms bridges with the Ce(III) center of the next polymer unit.

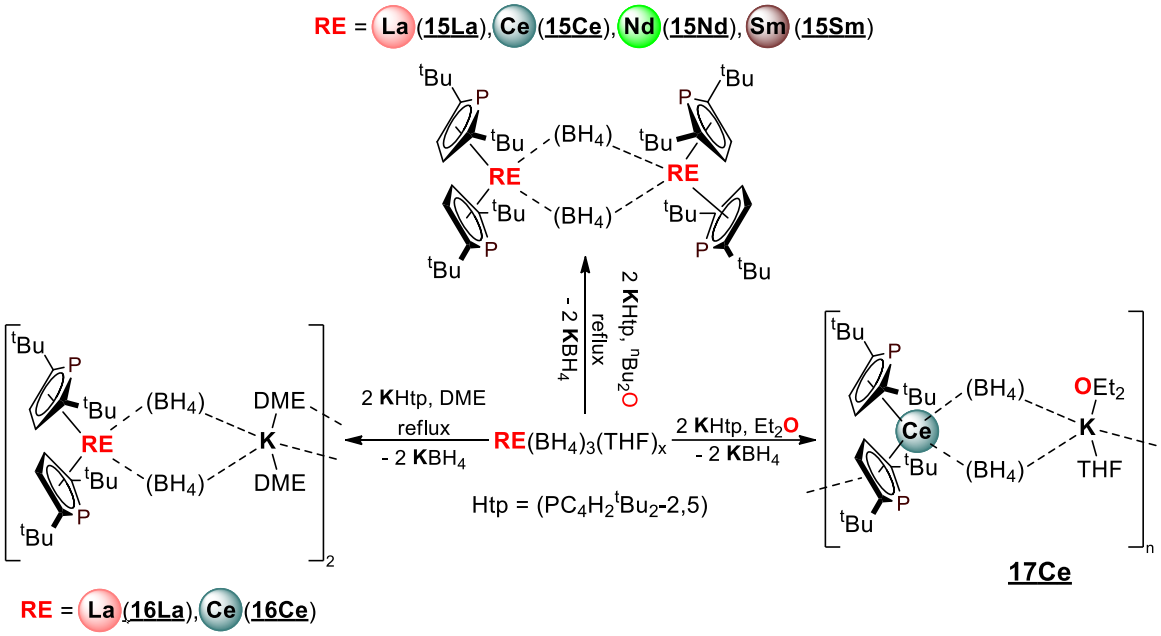

Scheme 1.21: Synthesis of RE borohydride complexes with phospholyl ligands.

Similar syntheses using potassium salt of various cyclopentadienyl derivatives were carried out by D. P. Mills and coll., who fashioned a series of borohydride lanthanum bis-cyclopentadienyl complexes[4040]. Syntheses using KCp''' ({$C_5H_2(SiMe_3)_3$-1,2,4}) and KCp^{tBu3} ({$C_5H_2{}^tBu_3$-1,2,4}) in THF afforded the mononuclear lanthanum complexes (**19La** and **19La**), while the synthesis using KCp^{tBu2} ({$C_5H_3{}^tBu_2$-1,3}) led to a bridged borohydride complex (**20La**, Scheme 1.22). Although the failure to form the cerium bis-substituted complex bearing two Cp^{tBu3} was probably due to steric hindrance, the successful formation of the complex bearing two Cp''' (**18Ce**) was attributed to the ability of the silyl group to bend away from the RE center. A cerium complex supported by two Cp^{tBu2} ligands was previously studied in 1992 that already exhibited this kind of borohydride bridge[60], which could explain that the author presented **20La** as a dimer. The predicted arrangement of both **19La** and **18Ce** were verified by X-Ray analysis and indicated in both cases the coordination of the Cp ring in η^5 mode and a borohydride group in tri-hapto fashion. Complex **18Ce** also showed a THF molecule linked to the metal center.

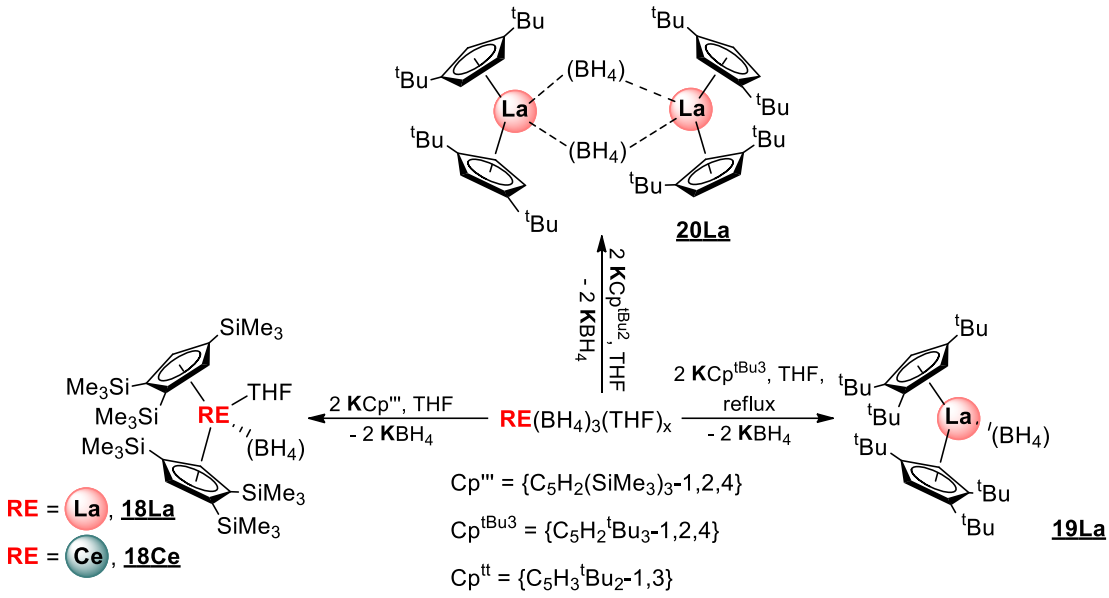

Scheme 1.22: Synthesis of RE complexes with bulky cyclopentadienyl ligands.

The comparison of **19La** and **20La** allowed the authors to assess the hindrance effect brought by the additional ^{t}Bu group, which promoted the formation of a monomeric *vs.* a dimeric form of the complex. Furthermore, the electronic effect could also be noted by the coordination of a THF molecule caused by the coordination of {$C_5H_2(SiMe_3)_3$-1,2,4} instead of {$C_5H_2{}^{t}Bu_3$-1,2,4} (**18La** *vs.* **19La**)

The family of bis-substituted RE complexes bearing two Cp''' ligands was extended to dysprosium and yttrium in 2022 using the same experimental protocol (Scheme 1.23) by the same group[42]. Solid-state analysis of **18Dy** and **18Dy'** revealed similar coordination to **18La** and **18Ce**. The presence of the THF molecule enabled the author to observe the unusual transition from η^3 (**18Dy**) to η^2 coordination (**18Dy'**) of the borohydride group. As expected, the Y analog was found free of THF. The molecular structure of both dysprosium complexes **18Dy** and **18Dy'** was confirmed by XRD analysis.

Just like the mono-substituted Cp RE borohydride complexes, only complexes bearing highly bulkly Cp ligands have been studied for their magnetism properties (**15RE**, **18Ce**, **18Dy**).

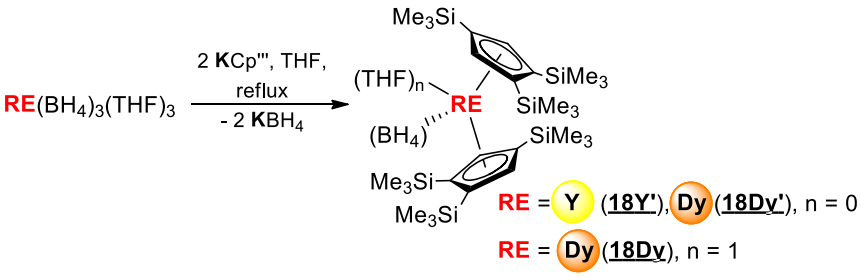

Scheme 1.23: Extension of the bis-Cp''' RE borohydride family.

In summary, the synthesis of bis-substituted mono-borohydride RE complexes might be somewhat more difficult than expected depending on the influence of the substituent on the cyclopentadienyl ligand.

1.3.2.2.2 Nitrogen based ligands.

The synthesis of phenyltrimethylsilylamide borohydride heterobimetallic Nd-Li complexes was reported in 2011[61]. This study showed that depending on the solvent used (THF or hexane), two different products could be isolated (Scheme 1.24). The metathesis reaction using lithium salt Li[N(SiMe$_3$)(C$_6$H$_3$^{i}Pr$_2$-2,6)] and Nd(BH$_4$)$_3$(THF)$_3$ in THF cleanly led to the product **21Nd**, which crystallized as a heterobimetallic species composed of an anionic neodymium bearing two ligands and two borohydrides units coordinated in a typical tri-hapto mode along with the lithium tetra-THF cationic counterpart. The same metathesis reaction in hexane led to a polymeric compound **21Nd'**, whose molecular structure displayed a neodymium moiety coordinated to two ligands through the nitrogen atoms. Both borohydrides were connected to the neodymium by two hydrogens and then linked to the lithium in a mono-hapto fashion.

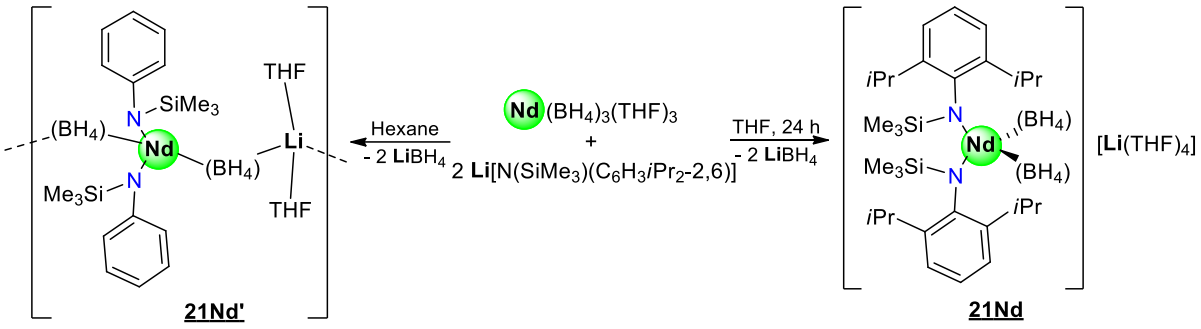

Scheme 1.24: Synthesis of a heterobimetallic compound 21Nd and polymorphic compound 21Nd'.

Further investigations were pursued towards the formation of rare-earth phenyltrimethylsilylamide borohydride complexes. R. Anwander and colleagues were able to prepare Nd and La complexes bearing two phenyltrimethylsilylamide ligands and a BH_4 along with an additional THF solvent molecule by reacting the appropriate $RE(BH_4)_3$ precursor with the potassium salt of the nitrogen ligand. The importance of the solvent used (THF *vs.* hexane) was demonstrated in the synthesis of **22Nd** (Scheme 1.25). Indeed, the apparition of several resonances for the trimethylsilyl groups in THF-D_8 was indicative of the presence of a mixture of products, whereas the synthesis in hexane led to a clean product. The molecular structure of **22Nd** and **22La** was deduced from XRD analysis and exhibited coordination of the ligands through the nitrogen atom, as well as the presence of one molecule of THF. The borohydride group bond length was in a typical range to suggest a tri-hapto coordination mode.

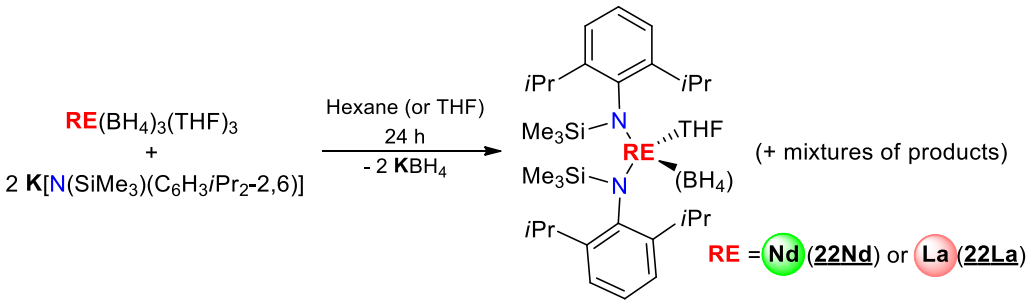

Scheme 1.25: Synthesis of 22Nd and 22La and the importance of the solvent.

In the same publication, the synthesis of the homoleptic lanthanum tris-substituted complex, using either $La(BH_4)_3(THF)_3$ or **22La**, was carried out in the presence of the potassium salt of the ligand in hexane, while the synthesis of the neodymium was not successful. The molecular structure of this lanthanum complex was confirmed by XRD, showing the N-coordination of three ligands to the metal center.

Neodymium borohydride complexes bearing diamino-bisphenoxide ligands[62] have been described by J.-F. Carpentier and A. A. Trifonov and coll. in 2010. The reaction between the two different dilithium salt of diamino-bis(phenoxide) with $Nd(BH_4)_3(THF)_2$ in THF, as seen in Scheme 1.26, led to the formation of the heterobimetallic Nd/Li complex (**23Nd** and **24Nd**). Crystals obtained from a concentrated hexane solution provided the molecular structures where neodymium was coordinated to the ligand through oxygen and nitrogen atoms. The neodymium/Li "core" was constituted in **23Nd** by a μ-BH_4 (in a η^2 mode) bridging a neodymium center to a lithium-THF cation. Meanwhile in **24Nd**, the lithium bis-THF was linked to the neodymium by a borohydride unit in η^2 mode to the lithium and in η^3 to the neodymium.

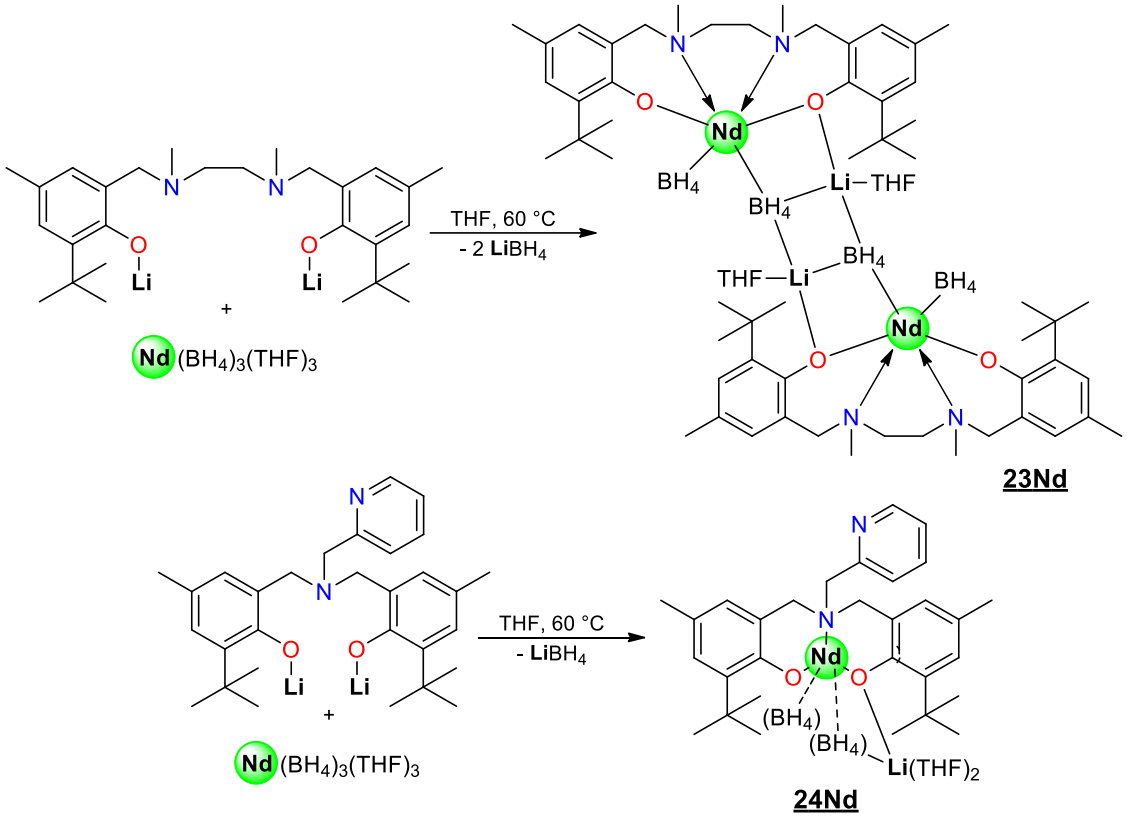

Scheme 1.26: Synthesis of the heterobimetallic 23Nd and 24Nd.

A few years later, following the results obtained in 2005[63] and 2010[64], the family of RE bis(phenolate)amine borohydride complexes was extended in 2015 by F. Bonnet *et al.*[65]**.** Using the same methodology as in 2005, the neodymium complexes were prepared by ionic metathesis from the sodium ligand salt and $Nd(BH_4)_3(THF)_3$ (Scheme 1.27). While **27Nd** crystallized as expected, the crystallization of **25Nd** led to a phenolate-O-bridged dimer by loss of THF molecule (**25Nd'**).

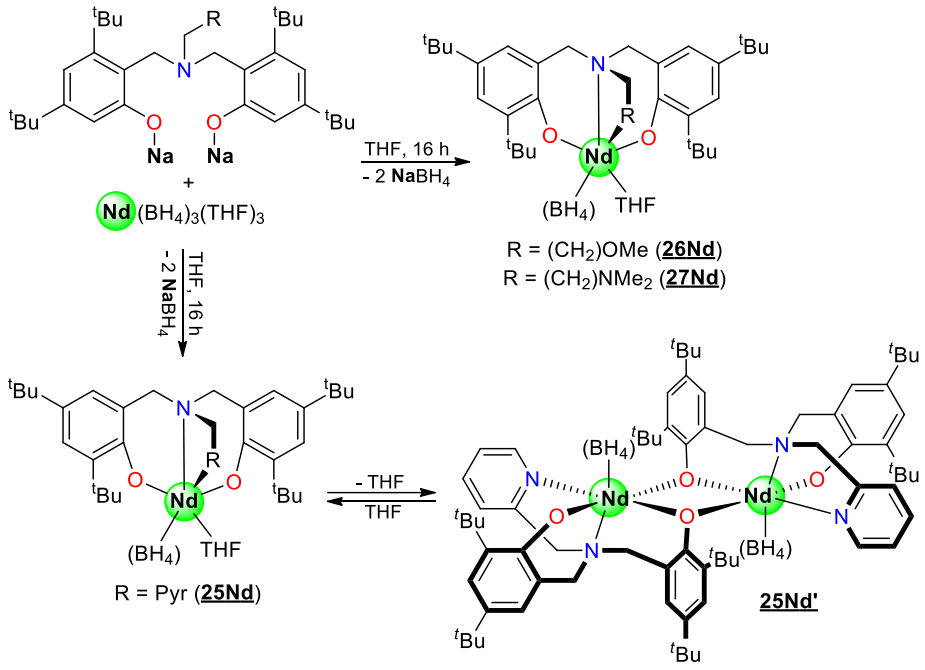

Scheme 1.27: Preparation of borohydrido bis(phenolate)amine neodymium complexes.

Since 2012, the *ansa*-bis(amidinate) ligand has been used for the synthesis of RE complexes[66]. The heterobimetallic Nd-Li and Sm-Li complexes were obtained from the deprotonation of the *ansa*-bis(amidinate) ligand with ^{n}BuLi followed by the addition of the tris-borohydride precursors (**28Sm** and **28Nd** Scheme 1.28). The resulting compounds were crystallized, and the structure of each complex was confirmed by XRD analysis. The solid-state structure revealed both complexes as heterobimetallic "ate" RE-Li compounds, similar to the one obtained previously (**24Nd**), where a borohydride connects the RE element and the lithium atom. According to the authors, the very close distances value Nd-B between terminal and bridge borohydride groups could be explained by the presence of intermolecular Li…B interactions.

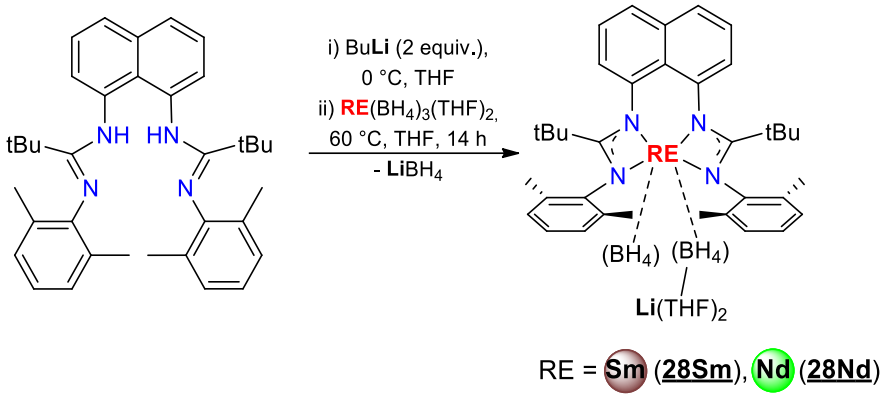

Scheme 1.28: Synthesis of 30Sm and 30Nd.

Trifonov's group also reported the synthesis of a new series of trivalent rare earth complexes supported by a tetradentate bis(amidinato) ligand containing a phenyl linker between the two amidinato parts (Scheme 1.29)[67]. While the synthesis of **29RE** is a "*one-pot*" synthesis by *in-situ* formation of the sodium ligand salt, the lithium salt of the ligand was isolated to lead to **30Y** before reacting with $Y(BH_4)_3(THF)_3$ (synthesis not shown in the scheme for clarity). Although crystals of the THF adduct of **30Y** were obtained, recrystallization from a DME/toluene mixture provides crystals of **30Y** suitable for XRD analysis. The molecular structure of **29Y** and **30Y** was obtained and showed the same coordination environment. In both cases, the yttrium atom is bound to the ligand by the four nitrogen atoms, a molecule of DME and a borohydride group in tri-hapto mode.

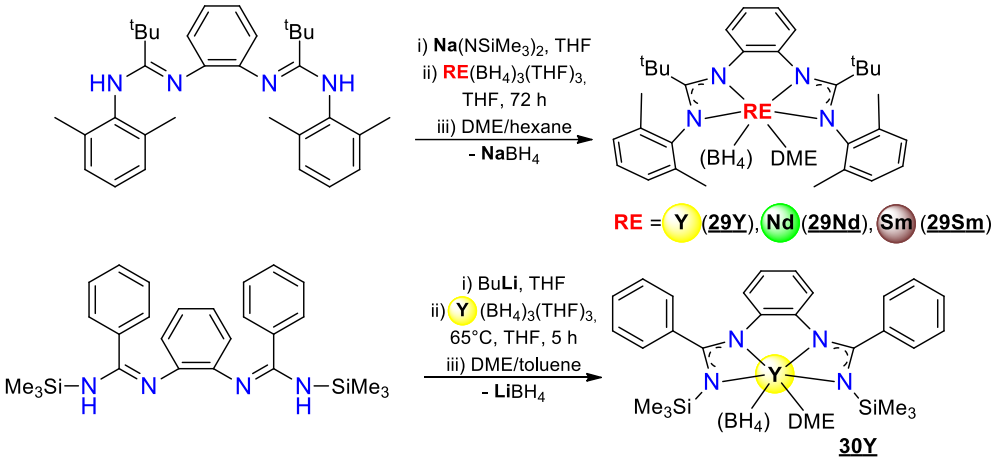

Scheme 1.29: Preparation of the bis(amidinato) complexes 29RE and 30Y.

(Bis)amidinate organo-rare-earth complexes of the type $[(Me_3SiNC(C_6H_5)N)_2(CH_2)_3RE(X)]$ (**31RE**) have been synthesized from years[68], and in 2012, Q. Shen and coll. reported the preparation of a series of borohydride RE analogs (X = BH_4) by two different routes[69]. The first pathway (i) involves

the reaction between the bis lithium salt of the ligand and $RE(BH_4)_3$ in THF, while the second one (ii) proceeds by metathesis of $[(Me_3SiNC(C_6H_5)N)_2(CH_2)_3)RE(Cl)]$ with $NaBH_4$ (Scheme 1.30). Both pathways lead to the same complexes.

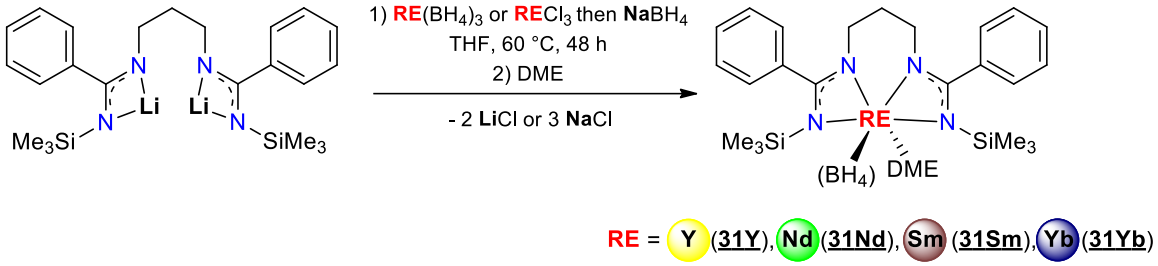

Scheme 1.30: Synthesis of bisamidinate borohydride complexes 31RE.

Crystals suitable for XRD were obtained from a concentrated solution in DME with a layer of toluene. Solid-state analysis was determined and indicated, in each case, a RE center surrounded by a tetradentate ligand coordinated by all four nitrogen atoms. The borohydride unit was connected in a tri-hapto mode and a molecule of DME completed the coordination sphere.

In the same years, this group described the use of the same kind of metathesis strategy, as presented above to obtain RE complexes supported by a bis(guanidinate) ligand (**32RE**)[70] (Scheme 1.31). X-ray diffraction analysis revealed similar structures to those presented above but with the bis(guanidinate) ligand.

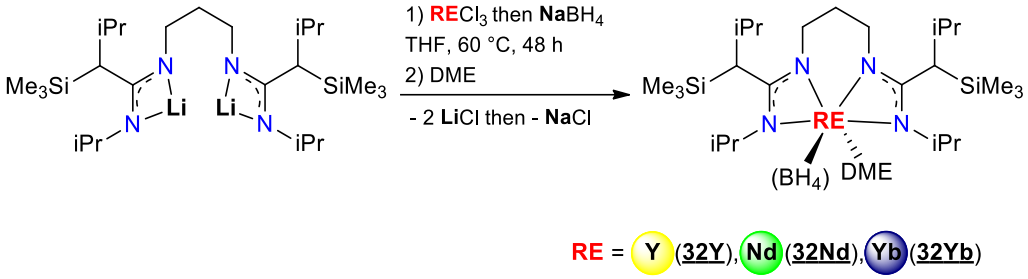

Scheme 1.31: Preparation of bis(guanidinate) RE borohydride complexes.

Quite concomitantly, Q. Shen's team reported bis(β-diketiminate) borohydride rare-earth complexes[71]. Bis(β-diketiminate) chloride rare-earth compounds were firstly synthesized from $RECl_3$ and the sodium salt in THF, and then, these chloro products were treated with $NaBH_4$ in THF to afford the desired products, which were obtained as XRD suitable single crystals (Scheme 1.32). The

molecular structure of all complexes (**33Y**, **34Y**, **33Yb**, **34Yb**) revealed that the metal center was surrounded by two nitrogen ligands and one η^3-coordinated borohydride substituent.

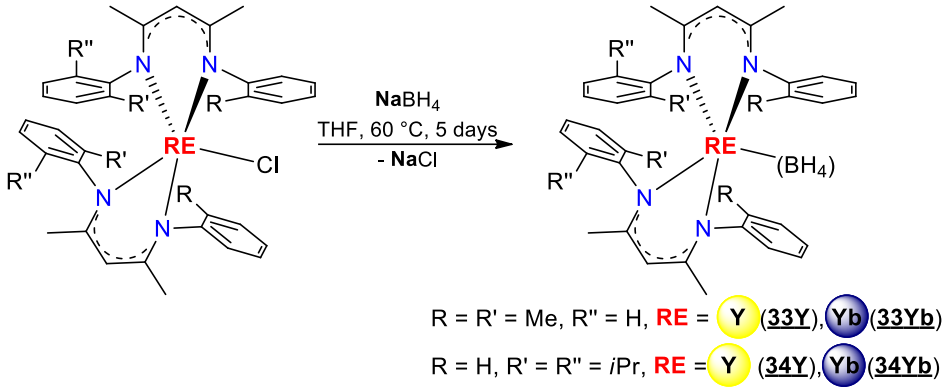

Scheme 1.32: Obtention of yttrium and ytterbium complexes bearing bulky bis(diketiminate) ligands.

Other series of (bis)amidinate supported rare-earth borohydride complexes were reported in 2018 by P. W. Roesky and coworkers[72]. The synthesis of this series of complexes was performed using the lithium salt of the ligand (**35Sc** and **35Lu** Scheme 1.33) instead of the potassium salt as seen previously with **12Sc** and **12Lu**. Single crystals analysis shows the molecular structure of **35Sc** as a complex consisting of a scandium metal center connected to two ligands through the nitrogen atoms and a borohydride in η^3 coordination mode.

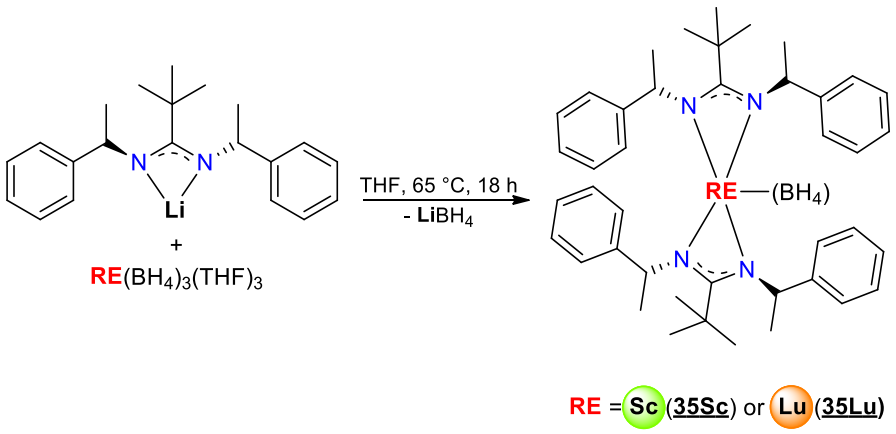

Scheme 1.33: Synthesis of 35Sc and 35Lu.

The synthesis of bis(diazabutadienyl) lutetium borohydride complex, where the ligand is described as a diradical, was carried out in 2021 by W.-X. Zhang and coll.[73]. The reaction proceeded by reduction of ^{Mes}DAD with KC_8, which then reacted with $Lu(BH_4)_3(THF)_3$ in THF to lead to the desired bis-substituted product, as confirmed by XRD (**36Lu**, Scheme 1.34). Solid-state analysis exhibited a

lutetium coordinated to two molecules of ligand bound by the two nitrogen atoms. The borohydride group was connected to the lutetium in a tri-hapto mode.

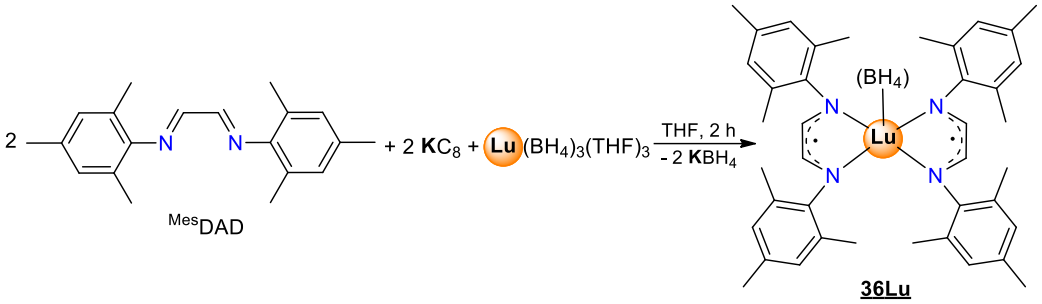

Scheme 1.34: Reduction of ^{Mes}DAD and its complexation on lutetium metal center.

Catalysis reactions involving RE mono-borohydride complexes bearing bis-substituted nitrogen-based ligand towards the polymerization of several monomers: polar (lactide, ε-caprolactone, etc…) and/or unsaturated hydrocarbon (styrene, isoprene, etc…) have been largely studied in the recent years and have shown to display in some cases a high activity.

Also, divalent RE complexes bearing mono-borohydride ligand have been described in the literature and will be subject in the next section.

1.3.2.3 Borohydride complexes of divalent RE metals

Mono-borohydride divalent RE complexes of the type [RE(BH$_4$)(Z)] (Z = Ligand) can be synthesized from the bis-borohydride RE precursors, RE(BH$_4$)$_2$(solvent)$_x$. Nevertheless, such complexes will be limited to RE metals allowing a stable +2 oxidation state.

To this end, the preparation of RE(BH$_4$)$_2$(solvent)$_x$ can be done by multiple pathways: (i) comproportionation between RE^0 metal and [RE(BH$_4$)$_3$(THF)$_3$][74], (ii) salt metathesis from the RE bis-iodide and NaBH$_4$ (or KBH$_4$) or (iii) reduction of [RE(BH$_4$)$_3$(THF)$_3$] with KC$_8$[75] (Scheme 1.35).

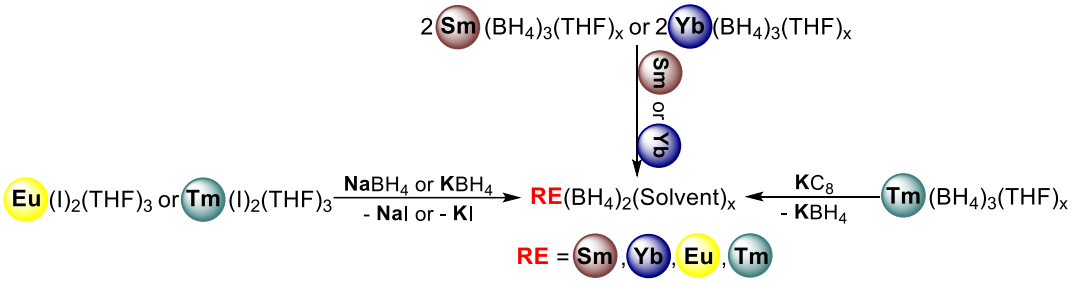

Scheme 1.35: Synthesis of divalent $RE(BH_4)_2$.

Using the divalent precursors of ytterbium and europium along with the potassium salt (DIP$_2$pyr)K [Dip = 2,4-(2,6-^{i}Pr$_2$C$_6$H$_3$N=CH)$_2$–C$_4$H$_3$N], M. Schmid *et al.* reported the synthesis of a series of mono-borohydride rare earth mono-substituted complexes in THF (Scheme 1.36)[76]. The author reported that, while **37Eu** is stable and can be stored for several months under nitrogen at room temperature, **37Yb** decomposes within minutes under the same circumstances. Both molecular structures exhibit a metal center surrounded by three THF molecules and a borohydride group. Surprisingly, while **37Eu** exhibits a europium center connected to the ligand through the three nitrogens atom, **37Yb** features a η^2-coordination mode to the same ligand.

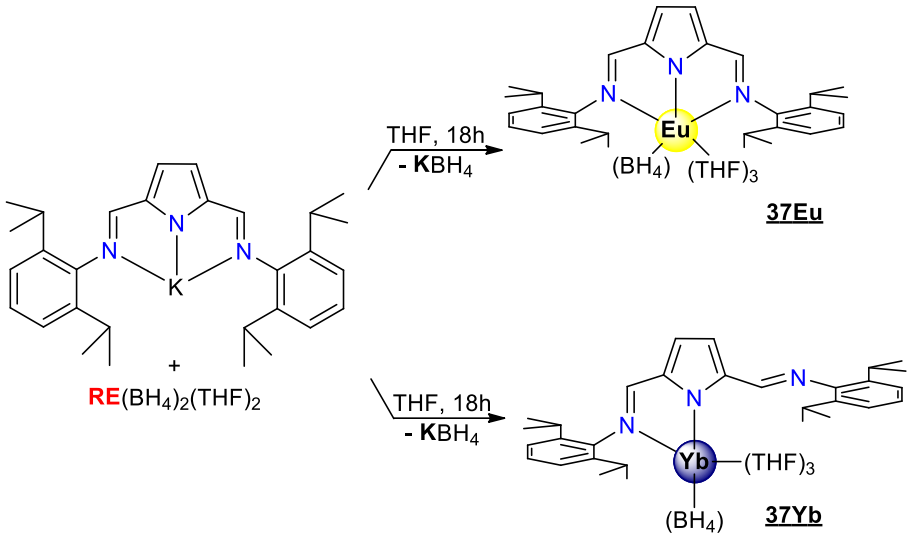

Scheme 1.36: Preparation of ytterbium and europium divalent complexes bearing (DIP$_2$pyr) ligand.

The mono-substituted homologous complexes of **13Sm** and **13Yb** (**38Sm** and **38Yb)** were synthesized from the divalent bis-borohydride complexes $RE(BH_4)_2(THF)_2$ (RE = Sm, Yb, Eu) and the potassium salt of a diketimine ligand, as described by M. Schmid *et al.* (Scheme 1.37)[57]. Crystals of **38Yb** were obtained and the determination of the solid-state structure revealed the same

arrangement as found for the trivalent **13Yb**, but with an additional molecule of THF to fulfill the coordination environment of the Yb metal.

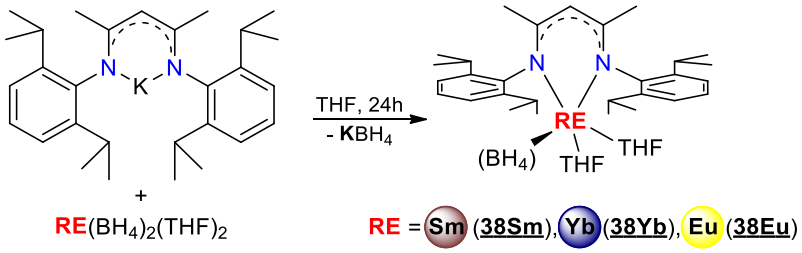

Scheme 1.37: Complexation of divalent RE metal center using β-diketiminate potassium salt.

Using the divalent ytterbium bis-borohydride precursor, synthesis of the mono-substituted imino-thiophosphoranyl homologue of the trivalent **6Yb** was conducted at room temperature, with loss of KBH_4 (Scheme 1.38)[45]. The solid-state structure of **39Yb** was obtained by XRD analysis, and the molecular structure exhibited an ytterbium center with a ligand coordinated by the nitrogen and sulfur atoms. A borohydride unit was bonded to the metal center in a η^3 mode and two molecules of THF were present to complete the coordination sphere.

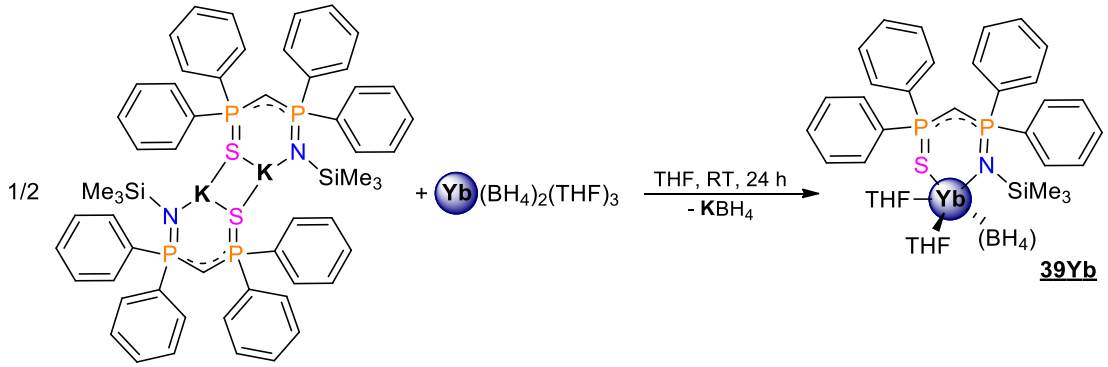

Scheme 1.38: Synthesis of divalent imino-thiophosphoranyl borohydride 39Yb.

F. Nief, F. Bonnet, M. Visseaux and coll. reported in 2011[75b] the synthesis of the heteroleptic tris-(2-^{t}Bu-4-Me)pyrazolylborate divalent thulium borohydrides complexes, which was found to be quite unstable. While metathesis in DME led to the homoleptic complexes, the same reaction carried out in THF resulted in the heteroleptic (**40Tm**, Scheme 1.39) and was confirmed by XRD analysis as a THF solvate thulium borohydride with one equivalent of ligand coordinated by the three nitrogen atoms.

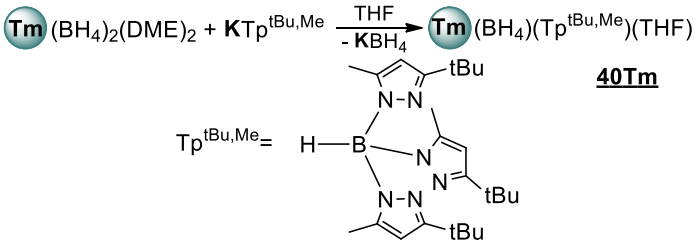

Scheme 1.39: Synthesis by ionic metathesis of 40Tm.

Being quite sensitive, only five RE borohydride divalent compound have been described since 2011.

1.3.2.4 Unusual ionic borohydride RE complexes

In 2014, Q. Shen, M. Xue and coll. reported the synthesis of new RE ionic pairs which were obtained under specific conditions[77]. While the metathesis reaction between $RECl_3$ with $NaBH_4$ is a well-known procedure to yield tris-borohydride complexes, the achievement of ionic pair complexes of formula $[RE(BH_4)_2(THF)_5][RE(BH_4)_4(THF)_2]$ was induced by a change in the reaction temperature. The neutral complexes could be synthesized at 40 °C for 2 days, while the ionic pairs were obtained for the same reaction time but by heating to 75 °C the reaction mixture (Scheme 1.40). The formation of such ionic pair was already described in 1990 with lanthanum[78] and is now also observed for other RE metals (**41Nd**, **41Pr**, **41La**). The molecular structure was elucidated by X-ray crystallography studies for the complexes **41Nd** and **41Pr**. RE-B distances for the cationic part corresponds to a borohydride unit bounded in a tri-hapto mode. For the anionic part, one of the borohydride groups is also in a tri-hapto coordination mode while the other one is in a di-hapto mode.

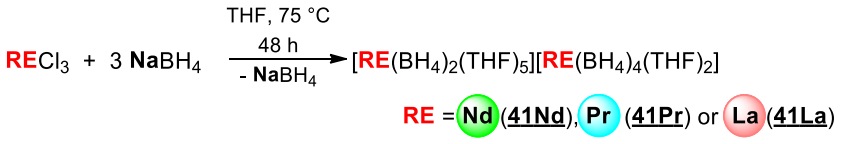

Scheme 1.40: Obtention of ionic borohydride complexes.

In the same publication[54] that presented **10Er**, the authors also reported a smooth reaction that resulted in a tris-substituted anionic samarium mono-borohydride compound, with the potassium hexa-THF as counterpart (Scheme 1.41). Although the reaction is described, the authors did not specify

whether this product was generated regardless of the number of equivalents of potassium salt used. The molecular structure of **42Sm** shows a samarium center coordinated to three ligands and, according to the author, this structure presents the first example of an anionic samarium coordinated in η^1 fashion to a borohydride group.

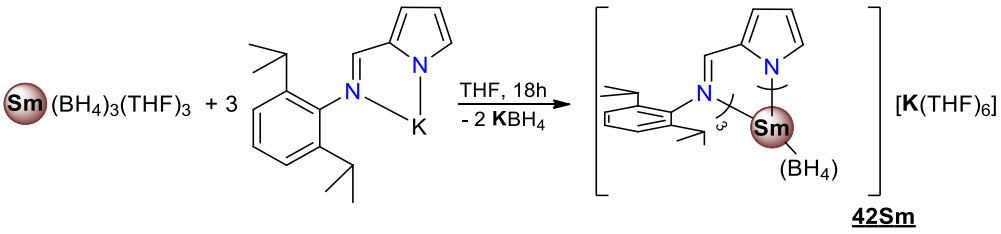

Scheme 1.41: Synthesis of the tris-substituted anionic samarium borohydride complex 42Sm.

D. M. Roitershtein and coworkers reported in 2022 an ionic pair compound that consisted of a cyclopentadienyl terbium complex in which the BH_4 ligands are partially substituted by chloride anions[36]. This product **43Tb** was obtained by reacting $Tb(BH_4)_3(THF)_3$ with NaCp in the presence of 18-crown-6 in THF (Scheme 1.42). The presence of chlorine in the product was explained according to the authors by the presence of $TbCl_3$ within the starting material. Crystals suitable for XRD were obtained and the molecular structure exhibited a cationic part, similar to **14Nd**, with an anionic counterpart having borohydride partially substituted by the chloride anion.

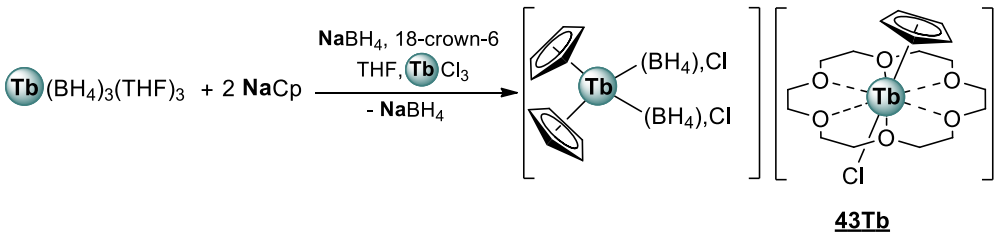

Scheme 1.42: Preparation of partially chloride borohydride Tb complex 43Tb.

1.3.2.5 Mixed RE(BH$_4$)X (X = nucleophilic ligand) complexes

Mixed complexes containing two different nucleophilic and reactive ligands (Nuc), among which amide, triflate, alkyl, etc…, associated to the borohydride ligand in the same molecular species are quite rare, and only a few examples have been described in literature. The nucleophilic ligand is herein described as potentially reactive towards insertion reactions, as BH_4 does in some cases (ROP

processes for example)[25], which excludes halides. To our knowledge, only two examples of such borohydride/Nuc have been published in the literature.

The first example was reported by J. Okuda and L. Maron and coworkers[79] as a cationic borohydride/methyl species. This complex was obtained by reacting one equivalent of the bis-cationic species $[Y(Me)(THF)_6][B(Ph)_4]$ with sodium borohydride in THF to give the desired product (**44Y**, Scheme 1.43). This product was purified by fractional crystallization and led to crystals suitable for XRD analysis, which revealed an yttrium center surrounded by five molecules of THF, one methyl group and a borohydride ligand linked in tri-hapto mode.

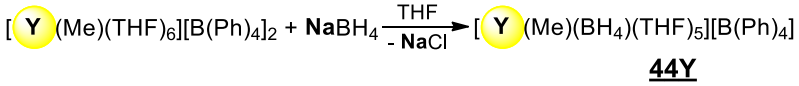

Scheme 1.43: Synthesis of methyl cationic borohydride yttrium complex.

Reported in 2016 by S. Fadlallah *et al.*[80] and later in 2017[81], a series of mixed allyl/BH_4 RE borohydride complexes were obtained by reacting the appropriate $RE(BH_4)_3(THF)_x$ with 0.5 equiv. of $Mg(allyl)_2$ to obtain the targeted complexes (Scheme 1.44). Crystallization of most complexes (**45Sc**, **45Nd** and **45La**) enabled the resolution of the molecular structure by XRD studies and revealed a metal center coordinated with two borohydride groups and one allyl moiety, each in a tri-hapto mode, along with two (**45Sc**) or three (**45Nd**, **45Sm**, **45Y**, **45La**) THF molecules.

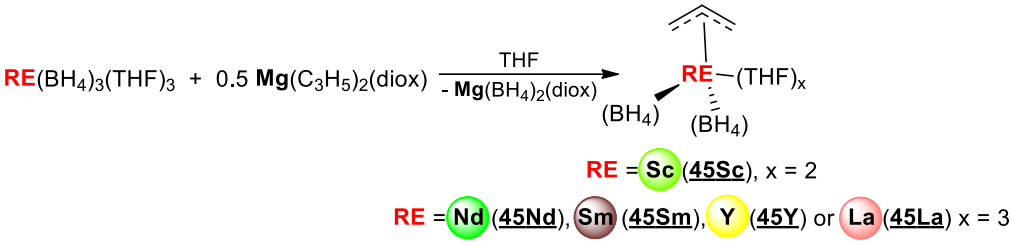

Scheme 1.44: Synthesis of mixed borohydride/allyl complexes.

The synthesis of such mixed complexes is a challenging task, but it holds great potential for high reward. Indeed, the presence of two different reactive ligands on the same metal center could enable several applications, including, for example, polymerization catalysis, by growing two different polymer chains on the same metal (Scheme 1.45).

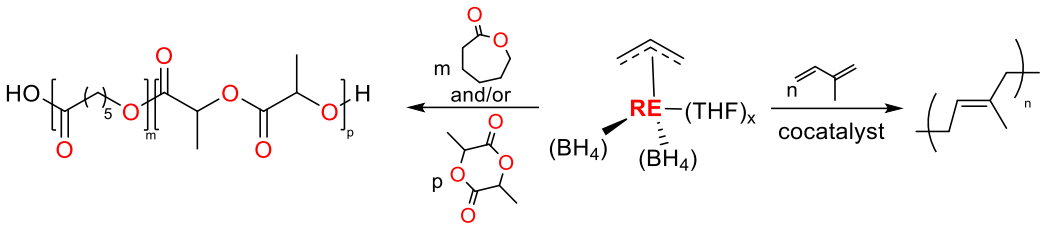

Scheme 1.45: Polymerization using 47RE.

As discussed previuously, many complexes have been synthesized since the last update in the field of RE borohydride complexes. Those complexes show a variety of coordination of BH_4 to the RE metal such as polymorphic form (dimers, hexamers, polymers) with or without the presence of the metallic salt (lithium, potassium…). They have been studied particularly for ROP of cyclic ester (ε-caprolactone, lactide …) and polymerization of 1,3-dienes such as isoprene, as listed below in Table 1.2.

Table 1.2: Bis-substituted, divalent unusual ionic and mixed borohydride RE complexes used in polymerization.

Borohydride complex	Lactones	Lactide	St	IP	MMA	TMC	Ref
$Cp_2Nd(BH_4)(THF)$ (**14Nd**)	✓ (ε-CL)						36
$[Cp_2Nd(BH_4)_2][Na(18\text{-crown-6})(THF)_2]$ (**14Nd'**)	✓ (ε-CL)						36
$[\{CH_2N(Me)CH_2\text{-}3,5\text{-}Me,{}^tBu\text{-}C_6H_2O\}_2 Nd(BH_4)(\mu\text{-}BH_4)Li(THF)]_2$ (**23Nd**)	✓ (*rac*-BBL)	✓(*rac*-LA)					62
$[C_5H_4NCH_2N\text{-}\{CH_2\text{-}3,5\text{-}Me,{}^tBu\text{-}C_6H_2O\}_2 Nd(BH_4)(\mu\text{-}BH_4)Li(THF)_2]$ (**24Nd**)	✓ (*rac*-BBL)	✓(*rac*-LA)					62
$[(2\text{-}C_5H_4N)CH_2N(CH_2\text{-}2\text{-}HO\text{-}3,5\text{-}C_6H_2{}^tBu_2)_2]Nd(BH_4)(THF)$ (**25Nd**)	✓ (ε-CL)		✓	✓			65
$[OMeCH_2\text{-}CH_2N(CH_2\text{-}2\text{-}HO\text{-}3,5\text{-}C_6H_2{}^tBu_2)_2]Nd(BH_4)(THF)$ (**26Nd**)	✓ (ε-CL)		✓	✓			65
$[NMe_2CH_2\text{-}CH_2N(CH_2\text{-}2\text{-}HO\text{-}3,5\text{-}C_6H_2{}^tBu_2)_2]Nd(BH_4)(THF)$ (**27Nd**)	✓ (ε-CL)			✓			65
$[1,8\text{-}C_{10}H_6\{NC({}^tBu)N\text{-}2,6\text{-}Me_2\text{-}C_6H_3\}_2]RE(BH_4)(\mu\text{-}BH_4)Li(THF)_2$ (**28RE**) (**RE** = **28Nd** and **28Sm**)		✓					66
$\{C_6H_4\text{-}1,2\text{-}[NC({}^tBu)N(2,6\text{-}Me_2C_6H_3)_2]\}RE(BH_4)(DME)$ (**29RE**) (**RE** = **29Y**, **29Nd** and **29Sm**)		✓(*rac*-LA)					67
$\{C_6H_4\text{-}1,2\text{-}[NC(C_6H_5)N(SiMe_3)_2]\}Y(BH_4)(DME)$		✓(*rac*-LA)					67

(**30Y**)					
[(Me$_3$SiNC(C$_6$H$_5$)N)$_2$(CH$_2$)$_3$]RE(BH$_4$)(DME) (**31RE**) (**RE** = **31Y**, **31Nd**, **31Sm** and **31Yb**)	✓ (ε-CL)	✓(L-LA, *rac* LA)			69
[{^{i}Pr(Me$_3$Si)NC(N^{i}Pr)N(CH$_2$)}$_2$CH$_2$]RE(BH$_4$)(DME) (**32RE**) (**RE** = **32Y**, **32Nd** and **32Yb**)	✓ (ε-CL)	✓(L-LA, *rac*-LA)			70
[(2,6-^{i}Pr$_2$C$_6$H$_3$)NC(Me)CHC(Me)N-(C$_6$H$_5$)]RE(BH$_4$) (**33Y**)	✓ (ε-CL)	✓(L-LA)			71
[(2,6-^{i}Pr$_2$C$_6$H$_3$)NC(Me)CHC(Me)N-(C$_6$H$_5$)]RE(BH$_4$) (**33Yb**)	✓ (ε-CL)	✓(L-LA)		✓	71
[{N(2-MeC$_6$H$_4$)C(Me)}$_2$CH]RE(BH$_4$) (**34RE**) (**RE** = **34Y** and **34Yb**)	✓ (ε-CL)	✓(L-LA)			71
[{(CH$_3$)(C$_6$H$_5$)CN}$_2$C^{t}Bu]$_2$RE(BH$_4$) (**35RE**) (**RE** = **35Sc** and **35Lu**)		✓ (DL-LA)			72
[2,4-(2,6-^{i}Pr$_2$C$_6$H$_3$N=CH)$_2$–C$_4$H$_3$N]Eu(BH$_4$)(THF)$_3$ (**37Eu**)	✓ (ε-CL)				76
[(2,6-C$_6$H$_3$^{i}Pr$_2$)NC(Me)CHC(Me)N(2,6-C$_6$H$_3$^{i}Pr$_2$)]Eu(BH$_4$)(THF) (**38Eu**)	✓ (ε-CL)				57
[(2,6-C$_6$H$_3$^{i}Pr$_2$)NC(Me)CHC(Me)N(2,6-C$_6$H$_3$^{i}Pr$_2$)]Yb(BH$_4$)(THF) (**38Yb**)	✓ (ε-CL)			✓	57
[CH(PPh$_2$=NSiMe$_3$)(PPh$_2$=S)]Yb(BH$_4$)(THF)$_2$ (**39Yb**)	✓ (ε-CL)			✓	45
[Tp^{tBu,Me}]Tm(BH$_4$)(THF) (**40Tm**)	✓(ε-CL)				75b
[RE(BH$_4$)$_2$(THF)$_5$][RE(BH$_4$)$_4$(THF)$_2$] (**41RE**) (**RE** = **41Nd**, **41Pr** and **41La**)	✓(ε-CL)	✓(L-LA)			77
(C$_3$H$_5$)$_2$RE(BH$_4$)(THF)$_3$ (**45RE**) (**RE** = **45Nd** and **45Sm**)	✓(ε-CL)	✓	✓		80, 81
(C$_3$H$_5$)$_2$RE(BH$_4$)(THF)$_x$ (**47RE**) **(RE = 45Sc**, **45Y** and, **45La)**	✓(ε-CL)	✓			81

*ε-CL = ε-Caprolactone, **rac**-BBL = racemic β-butyrolactone, L-LA = (S,S)-lactide, DL-LA = (R,S)-lactide, **rac**-LA = racemic lactide, MMA = Methyl methacrylate, TMC = Trimethylene carbonate, St = Styrene, IP = Isoprene*

1.4 Conclusion

As seen throughout this introductory chapter, rare earth (RE) elements have diverse applications, and their organometallic compounds can be used to target different catalytic reactions. Notably, a significant difference can be seen between borohydride complexes of light and heavy RE elements, with some exhibiting greater reactivity in polymerization reactions than others. Interestingly, even with the same ligand, the choice of the metal can substantially influence the

reactivity. In general, neodymium is the most commonly used metal center for light RE elements, while yttrium is preferred for heavy REs.

With this in mind, we decided to focus on the synthesis of complexes of neodymium and yttrium during this thesis research work. Our objective is to gain insight into the reactivity light and heavy RE-based catalysis through representative examples.

References

[1] https://pubs.usgs.gov/periodicals/mcs2022/mcs2022.pdf

[2] www.insu.cnrs.fr/fr/cnrsinfo/les-terres-rares-le-paradoxe-environnemental

[3] a) C. A. Tolman, **J. Am. Chem. Soc.**, *1970*, 92 (10), 2953; b) C. A. Tolman, **J. Am. Chem. Soc.**, *1970*, 92 (10), 2956; c) A. Immirzi, A. Musco, **Inorg. Chim. Acta**, *1977*, 25 (2), L41.

[4] J. A. Bilbrey, A. H. Kazez, J. Locklin, W. D. Allen, **J. Comput. Chem.**, 2013, 34 (14), 1189.

[5] (a) V. M. Birkelbach, R. Thim, C. Stuhl, C. Maichle-Mössmer, R. Anwander, **Chem. Eur. J.**, *2019*, 25 (64), 14711; (b) V. M. Birkelbach, C. Stuhl, C. Maichle-Mössmer, R. Anwander, **Organometallics**, *2019*, 38 (22), 4485.

[6] Y. Q. Jia, **J. Solid State Chem.**, *1991*, 95 (1), 184.

[7] G. Wilkinson, J. M. Birmingham, **J. Am. Chem. Soc.**, *1954*, 76, 6210.

[8] P. B. Hitchcock, M. F. Lappert, R. G. Smith, R. A. Bartlett, P. P. Power, **J. Chem. Soc. Chem. Commun**., *1988*, (15) 1007.

[9] D. C. Bradley, J. S. Ghotra, F. Alan Hart**, J. Chem. Soc., Dalton Trans.**, *1973*, (10), 1021.

[10] P. S. Gradeff, K. Yunlu, T. J. Deming, J. M. Olofson, R. J. Doedens, W. J. Evans, **Inorg. Chem.**, *1990*, 29 (3), 420.

[11] (a) S. Kobayashi, I. Hachiya, **J. Org. Chem.**, 1994, 59 (13), 3590; (b) R. W. Marshman, **Aldrichim. Acta**, *1995*, 28 (3), 77.

[12] M. Katkova, A. G. Vitukhnovsky, M. N. Bochkarev, **Russ. Chem. Rev.**, *2005*, 74 (12), 1089

[13] A. Priesto, F. Jaroschik, **Curr. Org. Chem.**, *2022*, 26 (1), 6.

[14] D. M. Lyubov, A. O. Tolpygin, A. A. Trifonov, **Coord. Chem. Rev.**, *2019*, 392, 83; (b) Y. Nakayama, H. Yasuda, **J. Organom. Chem.**, *2004*, 689 (24), 4489.

[15] D. Robert, E. Abinet, T. P. Spaniol, J. Okuda, **Chem. Eur. J.**, *2009*, 15 (44), 11937.

[16] Selected references: (a) W. J. Evans, C. A. Seibel, J. W. Ziller, R. J. Doedens, **Organometallics**, *1998*, 17 (10), 2103; (b) S. Demir, E. Montalvo, J. W. Ziller, G. Meyer, W. J. Evans, **Organometallics**, *2010*, 29 (23), 6608; (c) I. J. Casely, Y. Suh, J. W. Ziller, W. J. Evans, **Organometallics**, *2010*, 29 (21), 5209; (d) E. Abinet, D. Martin, S. Standfuss, H. Kulinna, T. P. Spaniol, J. Okuda, **Chem. Eur. J.**, *2011*, 17 (52), 15014.

[17] Selected references: (a) Z. Jian, D. Cui, Z. Hou, X. Li, **Chem. Commun.**, *2010*, 46 (17), 3022; (b) L. Annunziata, A. Rodrigues, E. Kirillov, Y. Sarazin, J. Okuda, L. Perrin, L. Maron, J. Carpentier, **Macromolecules**, *2011*, 44 (9), 3312; (c) L. N. Jende, C. O. Hollfelder, C. Maichle-Mössmer, R. Anwander, **Organometallics**, *2015*, 34 (1), 32.

[18] R. Taube, H. Windisch, S. Maiwald, H. Hemling, H. Schumann, **J. Organomet. Chem.**, *1996*, 513 (1-2), 49.

[19] R. Taube, H. Windisch, **J. Organomet. Chem.**, *1993*, 445 (1-2), 85.

[20] R. Taube, S. Maiwald, J. Sieler, **J. Organomet. Chem.**, *2001*, 621 (1-2), 327.

[21] L. F. Sánchez-Barba, D. L. Hughes, S. M. Humphrey, M. Bochmann, **Organometallics**, *2005*, 24 (15), 3792.

[22] (a) T. J. Marks, R. D. Ernst, **In Comprehensive Organometallic Chemistry**, G. Wilkinson, F. G. A. Stone, E. W. Abel, Eds., Pergamon: Oxford, UK, *1982*, pp 196–197, 205–206; (b) F. T. Edelmann, In **Comprehensive Organometallic Chemistry II**, E. W. Abel, F. G. A. Stone, G. Wilkinson, Eds., Elsevier: Oxford, UK, *1995*, pp 26–28; (c) F. T. Edelmann, **In Comprehensive Organometallic Chemistry III**, D. M. P. Mingos, R. H. Crabtree, Eds., Elsevier: Oxford, UK, *2007*, pp 17–21; (d) M. Beauvois, Y. Champouret, F.Bonnet, M. Visseaux, **In Comprehensive Organometallic Chemistry IV**, G. Parkin, K. Meyer, D. O'hare, Eds., Elsevier: Oxford, UK, *2022*, 382-448.

[23] M. B. Abrams, J. C. Yoder, C. Loeber, M. W. Day, J. E. Bercaw, **Organometallics**, *1999*, 18 (8), 1389.

[24] S. Standfuss, E. Abinet, T. P. Spaniol, J. Okuda, **Chem. Commun.**, *2011*, 47 (41), 11441.

[25] M. Visseaux, F. Bonnet, **Coord. Chem. Rev**, *2011*, 255 (3-4), 374.

[26] (a) O. Klejnot, **Dissertation, University of Munich**, *1955*; (b) E. Zange, **Chem. Ber.**, *1960*, 93, 652.

[27] (a) J. H. Morris, W. E. Smith, **J. Chem. Soc., Chem. Commun.**, *1970*, (4), 245; (b) U. Mirsaidov, A. Kurbonbekov, T. G. Rotenberg, K. Dzhuraev, **Inorg. Materials (USSR)**, *1978*, 14 (9), 1722; (c) U. Mirsaidov, A. Kurbonbekov, **Dokl. Akad. Nauk. Tadzh. SSR**, *1979*, 22 (5), 313; **Chem. Abstr.**, *1979*, 91, 185190; (d) U. Mirsaidov, A. Rakhimova, T. N. Dymova, **Dokl. Akad. Nauk. SSSR**, *1977*, 236 (1), 120; (e) U. Mirsaidov, **Zh. Neorg. Khim.**, *1977*, 22 (10), 2862; (f) K. N. Semenenko, O. V. Kravchenko, S. E. Kravchenko, V. B. Polyakova, **Inorg. Mater. (USSR)**, *1977*, 13 (12), 2276; (g) O. V. Kravchenko, S. E. Kravchenko, V. B. Polyakova, K. N. Semenenko, **Koord. Khim.**, *1980*, 6 (1), 76; (h) U. Mirsaidov, A. Rakhimova, T. N. Dymova, **Inorg. Mater. (USSR)**, **1979**, 15 (9), 1585; (i) U. Mirsaidov, ; I. B. Shaimuradov, M. Khikmatov, **Russ. J. Inorg. Chem.**, *1986*, 31 (5), 753; (j) U. Mirsaidov, T. G. Rotenberg,

T. N. Dymova, **Dokl. Akad. Nauk Tadzh. SSR**, 1976, 19 (2), 30; (k) E. B. Lobkovskii, S. E. Kravchenko, K. N. Semenenko, **J. Struct. Chem. (USSR)**, *1977*, 18 (2), 312.

[28] T. J. Marks, J.R. Kolb, **Chem. Rev.**, *1977*, 77 (2), 263.

[29] (a) K. W. Bagnall, L. Xing-Fu, **J. Chem. Soc., Dalton Trans.**, *1982*, (7), 1365; (b) X. Feng, A. Guo, Y. Xu, X. Li, P. Sun, **Polyhedron**, *1987*, 6 (5), 1041, (c) C. Baudin, D. Baudry, M. Ephritikhine, M. Lance, A. Navaza, M. Nierlich, J. Vigner, **J. Organomet. Chem.**, *1991*, 41 (5), 59.

[30] (a) S. M. Cendrowski-Guillaume, G. Le Gland, M. Nierlich, M. Ephritikhine, **Organometallics**, *2000*, 19 (26), 5654; (b) D. Barbier-Baudry, O. Blacque, A. Hafid, A. Nyassi, H. Sitzmann, M. Visseaux, **Eur. J. Inorg. Chem.**, *2000*, (11), 2333.

[31] (a) E. Zange, Chem. Ber., 1960, 93, 652; (b) U. Mirsaidov, T. G. Rotenberg, T. N. Dymova, Dokl. Akad. Nauk. Tadzh. SSR, 1976, 19 (2), 30; (c) U. Mirsaidov, A. Kurbonbekov, T. G. Rotenberg, K. Dzhuraev, **Izv. Akad. Nauk. Tadzh. SSR**, *1978*, 14 (9), 1722; (d) U. Mirsaidov, A. Kurbonbekov, **Dokl. Akad. Nauk. Tadzh. SSR**, *1979*, 22 (5), 313.

[32] (a) M. Visseaux, M. Terrier, A. Mottreux, P. Roussel, **C. R. Chimie**, *2007*, 10 (12), 1195; (b) M. Visseaux, P. Zinck, M. Terrier, A. Mortreux, P. Roussel, **J. Alloys Compd.**, *2008*, 451 (1-2), 352.

[33] V. D. Makhaev, **Russ. Chem. Rev.**, *2000*, 69 (9), 727.

[34] Selected reference: (a) I. Palard, M. Schappacher, A. Soum, S. M. Guillaume, **Polym. Int.**, *2006*, 55 (10), 1132;(b) J. Jenter, N. Meyer, P. W. Roesky, S. K.-H. Thiele, G. Eickerling, W. Scherer, **Chem. Eur. J.**, *2010*, 16 (18), 5472;(d) J.-F. Carpentier, **Organometallics**, *2015*, 34 (17), 4175; (e) A. O. Tolpygin, O. A. Linnikova, T. A. Kovylina, A. V. Cherkasov, G. K. Fukin, A. A. Trifonova, **Russ. Chem. Bull., Int. Ed.**, *2020*, 69 (6), 6.

[35] (a) L. Wang, C. Ma, X. Mao, J. Sheng, F. Bai, F. Tang, **Electrochem. Commun.**, *2005*, 7 (12), 1477; (b) T. Arliguie, L. Belkhiri, S.-E. Bouaoud, P. Thuéry, C. Villiers, A. Boucekkine, M. Ephritikhine, **Inorg. Chem.**, *2009*, 48 (1), 221; (c) F. Yuan, Q. Gu, Y. Guo, W. Sun, X. Chena, X. Yu, **J. Mater. Chem.**, *2012*, 22 (3), 1061.

[36] D. A. Bardonov, P. D. Komarov, G. I. Sadrtdinova, V. K. Besprozvannyh, K. A. Lyssenko, A. O. Gudovannyy, I. E. Nifant'ev, M. E. Minyaev, D. M. Roitershtein, **Inorganica Chim. Acta**, *2022*, 529, 120638.

[37] S. M. Cendrowski-Guillaume, G. Le Gland, M. Nierlich, M. Ephritikhine, **Organometallics**, 2000, 19 (26), 5654.

[38] F. Bonnet, C. Da Costa Violante, P. Roussel, A. Mortreux, M. Visseaux, **Chem. Commun.**, *2009*, (23), 3380.

[39] F. Bonnet, C. E. Jones, S. Semlali, M. Bria, P. Roussel, M. Visseaux, P. L. Arnold, **Dalton Trans.**, *2013*, 42 (3), 790.

[40] F. Ortu, D. Packer, J. Liu, M. Burton, A. Formanuik, D. P. Mills, **J. Organomet. Chem.**, *2018*, 857, 45.

[41] F. Bonnet, M. Visseaux, D. Barbier-Baudry, A. Hafid, E. Vigier, M. M. Kubicki, **Inorg. Chem.**, *2004*, 43 (12), 3682.

[42] S. C. Corner, C. A. P. Goodwin, F. Ortu, P. Evans, H. Zhang, G. K. Gransbury, G. F. S. Whitehead, D. P. Mills, **Aust. J. Chem.**, *2022*, 75 (8-9), 684.

[43] (a) J. Jenter, P. W. Roesky, N. Ajellal, S. M. Guillaume, N. Susperregui, L. Maron, **Chem. Eur. J.**, *2010*, 16 (15), 4629; (b) S. M. Guillaume, P. Brignou, N. Susperregui, L. Maron, M. Kuzdrowska, , P. W. Roesky, **Polym. Chem.**, *2011*, 2 (8), 1728; (c) S. M. Guillaume, P. Brignou, N. Susperregui, L. Maron, M. Kuzdrowska, J. Kratsch, P. W. Roesky, **Polym. Chem.**, *2012*, 3 (2), 429.

[44] J. Jenter, G. Eickerling, P. W. Roesky, **J. Organomet. Chem.**, *2010*, 695 (25-26), 2756.

[45] M. Schmid, P. Oña-Burgos, S. M. Guillaume, P. W. Roesky, **Dalton Trans.**, *2015*, 44 (30), 12338.

[46] (a) S. M. Guillaume, P. Brignou, N. Susperregui, L. Maron, M. Kuzdrowskac, P. W. Roesky, **Polym. Chem.**, *2011*, 2 (8), 1728; (b) S. M. Guillaume, P. Brignou, N. Susperregui, L. Maron, M. Kuzdrowska, J. Kratschc, P. W. Roesky, **Polym. Chem.**, *2012*, 3 (2), 429.

[47] Selected references: (a) C. Piguet, A. F. Williams, G. Bernardinelli, J.-C. G. Bünzli, **Inorg. Chem.**, *1993*, 32 (19), 4139; (b) D. A. Bardonov, P. D. Komarov, V. I. Ovchinnikova, L. N. Puntus, M. E. Minyaev, I. E. Nifant'ev, K. A. Lyssenko, V. M. Korshunov, I. V. Taidakov, D. M. Roitershtein, **Organometallics**, *2021*, 40 (9), 1235.

[48] Selected references: (a) N. Ishikawa, M. Sugita, T. Ishikawa, S.-Y. Koshihara, Y. Kaizu, **J. Am. Chem. Soc**, *2003*, 125 (29), 8694; (b) J.Long, F. Habib, P.-H. Lin, I. Korobkov, G. Enright, L Ungur, W. Wernsdorfer, L. F. Chibotaru, M. Murugesu, **J. Am. Chem. Soc.**, *2011*, 133 (14), 5319.

[49] G.G. Skvortsov, M.V. Yakovenko, P.M. Castro, G.K. Fukin, A.V. Cherkasov, J.-F. Carpentier, A.A. Trifonov, **Eur. J. Inorg. Chem.**, *2007*, (20), 3260.

[50] T.V. Mahrova, G.K. Fukin, A.V. Cherkasov, A.A. Trifonov, N. Ajellal, J.-F. Carpentier, **Inorg. Chem.**, *2009*, 48 (9), 4258.

[51] G. G. Skvortsov, A. V. Cherkasov, G. K. Fukin, A. A. Trifonov, **Russ.Chem.Bull., Int.Ed.**, *2015*, 64 (12), 2872.

[52] G. G. Skvortsov, A. O. Tolpygin, D. M. Lyubov, N. M. Khamaletdinova, A. V. Cherkasov, K. A. Lyssenko, A. A. Trifonov, **Russ.Chem.Bull., Int.Ed.**, *2016*, 65 (12), 2832.

[53] N. Rad'kova, V. Rad'kova, A. Cherkasov, T. Kovylina, A. A. Trifonov, **Inorganica Chim. Acta**, *2019*, 489, 132.

[54] K. Naktode, R. K. Kottalanka, T. K. Panda, **Z. Anorg. Allg. Chem.**, 2013, 639 (1), 73.

[55] G. G. Skvortsov, A. V. Cherkasov, A. A. Trifonova, **Russ.Chem.Bull., Int.Ed.**, *2017*, 66 (9), 1665.

[56] J. Kratsch, M. Kuzdrowska, M. Schmid, N. Kazeminejad, C. Kaub, P. Oñ a-Burgos, S. M. Guillaume, P. W. Roesky, **Organometallics**, *2013*, 32 (5), 1230.

[57] M. Schmid, S. M. Guillaume, P. W. Roesky, **Organometallics**, 2014, 33 (19), 5392.

[58] Y. K. Gun'ko, P. B. Hitchcock, M. F. Lappert, **Chem. Commun.**, *1998*, (23), 2663.

[59] J. Liu, L. E. Nodaraki, P. J. Cobb, M. J. Giansiracusa, F. Ortu, F. Tuna, D. P. Mills, **Dalton Trans.**, 2020, 49 (19), 6504.

[60] E.B. Lobkovsky, Y. K. Gun'ko, B.M. Bulychev, V.K. Belsky, G.L. Soloveichik, Y. Antipin, **J. Organomet. Chem.**, *1991*, 406 (3), 343.

[61] C. Schädle, C. Meermann, K. W. Törnroos, R. Anwander, **Eur. J. Inorg. Chem.**, 2010, (18), 2841.

[62] M. A. Sinenkov, G. K. Fukin, A. V. Cherkasov, N. Ajellal, T. Roisnel, F. M. Kerton, J.-F. Carpentier, A. A. Trifonov, **New J. Chem.**, *2011*, 35 (1), 204.

[63] F. Bonnet, A. R. Cowley, P. Mountford, **Inorg. Chem.**, *2005*, 44 (24), 9046.

[64] H. E. Dyer, S. Huijser, N. Susperregui, F. Bonnet, A. D. Schwarz, R. Duchateau, L. Marron, P. Mountford, **Organometallics**, *2010*, 29 (16), 3602.

[65] F. Bonnet, H. E. Dyer, Y. El Kinani, C. Dietz, P. Roussel, M. Bria, M. Visseaux, P. Zinck, P Mountford, **Dalton Trans.**, *2015*, 44 (27), 12312.

[66] M. V. Yakovenko, A. A. Trifonov, E. Kirillov, T. Roisnel, J.-F. Carpentier, **Inorganica Chim. Acta**, *2012*, 383, 137.

[67] A. O. Tolpygin, G. G. Skvortsov, A. V. Cherkasov, G. K. Fukin, T. A. Glukhova, A. A. Trifonov, **Eur. J. Inorg. Chem.**, *2013*, (35),6009.

[68] (a) S. Bambirra, A. Meetsma, B. Hessen and J. H. Teuben, **Organometallics**, *2001*, 20 (4), 782; (b) J. Wang, T. Cai, Y. Yao, Y. Zhang and Q. Shen, **Dalton Trans.**, *2007*, (45), 5275; (c) J. Wang, Y. Yao, Y. Zhang, Q. Shen, **Inorg. Chem.**, *2009*, 48 (2), 744.

[69] W. Li, M. Xue, J. Tu, Y. Zhanga, Q. Shen, **Dalton Trans.**, *2012*, 41 (24), 7258.

[70] X. Zhang, C. Wang, M. Xue, Y. Zhang, Y. Yao, Q. Shen, **J. Organomet. Chem.**, *2012*, 713, 182.

[71] X. Shen, M. Xue, R. Jiao, Y. Ma, Y. Zhang, Q. Shen, **Organometallics**, *2012*, 31 (17), 6222.

[72] T. P. Seifert, T. S. Brunner, T. S. Fischer, C. Barner-Kowollik, P. W. Roesky, **Organometallics**, *2018*, 37 (23), 4481.

[73] H. Yan, J. Wei, W.-X. Zhang, **Organometallics**, *2021*, 40 (19), 3245.

[74] F. Jaroschik, F. Bonnet, X.-F. Le Goff, L. Ricard, F. Nief and M. Visseaux, **Dalton Trans.**, *2010*, 39 (29), 6761.

[75] (a) S. Marks, J. G. Heck, M. H. Habicht, P. Oñ a-Burgos, C. Feldmann, P. W. Roesky, **J. Am. Chem. Soc.**, *2012*, 134 (41), 16983; (b) A. Momin, F. Bonnet, M. Visseaux, L. Maron, J. Takats, M. J. Ferguson, X.-F. Le Goffa, F. Nief, **Chem. Commun.**, *2011*, 47 (44), 12203.

[76] M. Schmid, S. M. Guillaume, P. W. Roesky, **J. Organomet. Chem.**, *2013*, 744, 68.

[77] W. Li, M. Xue, Y. Zhang, Y. Yao, Q. Shen, **Z. Anorg. Allg. Chem.**, *2014*, 640 (7), 1455.

[78] V. K. Bel'skii, A. N. Sobolev, B. M. Bulychev, T. K. Alikhanova, A. Kurbonbekov, U. Mirsaidov, **Koord. Khim.**, *1990*, 16 (12), 1693.

[79] M. U. Kramer, D. Robert, S. Arndt, P. M. Zeimentz, T. P. Spaniol, A. Yahia, L. Maron, O Eisenstein, J. Okuda, **Inorg. Chem.**, *2008*, 47 (20), 9265.

[80] S. Fadlallah, M. Terrier, C. Jones, P. Roussel, F. Bonnet, M. Visseaux, **Organometallics**, *2016*, 35 (4), 456.

[81] S. Fadlallah, J. Jothieswaran, F. Capet, F. Bonnet, M. Visseaux, **Chem. Eur. J.**, *2017*, 23 (62), 15644.

CHAPTER 2 SYNTHESIS AND CHARACTERIZATION OF RARE-EARTH BOROHYDRIDE COMPLEXES SUPPORTED BY AMIDO-PYRIDINE LIGANDS.

As seen in the previous chapter, the coordination chemistry of borohydride group in [RE]-(BH_4) complexes has been widely studied over the past decade and has been recognized as offering high potential for different catalytic reactivities. In order to develop a new family of borohydride complexes, amido-pyridines have been chosen as a valuable ligand platform since they have already proven to be highly versatile in terms of coordination mode with several metal centers, affording complexes with a good ability in polymerization of numerous monomers.

2.1 The amido-pyridine ligand: synthesis and structure

2.1.1 Generalities on amino/amido-pyridine ligands

Amido-pyridine-type ligands are of great interest due to i) the ease of synthesis of the protonated amino counterpart (protio-ligand: ZH), which is achieved by a simple condensation reaction of a suitable amine on the pyridyl-ketone, followed by a reduction reaction of the imine group and ii) the possibility of modification on multiple sites such as R_1 (the group on the pyridine ring), R_2 (the substituent on the carbon at the α-position of the amine nitrogen) and R_3 (the substituent carried by the amine nitrogen), which allows a rich variation of coordination and/or electronic/steric properties (Scheme 2.1). Since M. Westerhausen *et al.* prepared and isolated a series of Zn complexes bearing amido-pyridine ligands[1], a number of modifications to the ligand framework have been investigated, as well as the coordination chemistry with other metal-based systems in order to enhance the reactivity of new complexes in polymerization reactions. For example, amido-pyridine Ni and Pd complexes have been studied for their ability to polymerize ethylene[2], while Zn, Cu and Fe derivatives have been explored for the Ring-Opening Polymerization (ROP) of cyclic esters (*e.g.* lactide[3]), as well as the polymerization of methyl methacrylate (MMA) using amido (or amino)-pyridine Pd, Co, Cu, Zn and Cd complexes[4].

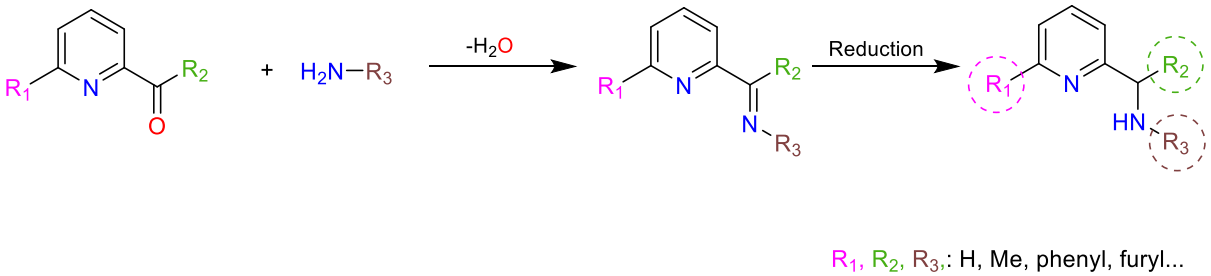

R_1, R_2, R_3,: H, Me, phenyl, furyl...

Scheme 2.1: Synthesis of amino-pyridine protio-ligands ZH.

The chemistry of non-Cp organometallic rare earth complexes has been extensively studied over the past three decades and this family of compounds is becoming increasingly diverse. Notably, post-metallocene rare earth complexes using nitrogen-based ligands[5] such as imidazole, amidinate, amidophosphine, sylilamido, guanidinate[6] and others have been investigated for nearly fifteen years, focusing on diverse applications in homogeneous catalysis such as hydroamination, hydrosilylation reactions and coordinative polymerization of a variety of monomers. As far as amido-pyridine ligands are concerned, organolanthanide complexes of this type were explored as early as 2003[7] and since then, numerous well-defined compounds have been prepared (Fig. 2.1), and some examined for their use in polymerization catalysis of isoprene/ethylene[8].

In this chapter, we will focus on three different amido-pyridine ligands which were selected (Scheme 2.2), two bidentate amido-pyridine and one tridentate amido-pyridine-imine ligand. The impact of the substituent in the α-position of the pyridine ring towards their coordination chemistry with Y and Nd, as well as their application in polymerization catalysis (next chapter 4) will be studied. While **Z^{1}H** and **Z^{3}H** have been known for a few years[9], the ligand **Z^{2}H** was recently developed in our lab starting from the 6-bromo-2-picoline[10]. The first step in synthesizing **Z^{2}H** was starting by the synthesis of 1-(6-methylpyridin-2-yl)ethan-1-one, from the lithiation of commercially available 6-bromo-2-picoline with ^{n}BuLi, followed by addition of *N,N*-dimethylacetamide. For all families of protio-ligand precursors, the condensation reaction of 2,6-diisopropylaniline with the corresponding ketones was undertaken, which allowed us to obtain the three different imines **I^1** – **I^3** in moderate to good yields. The reduction of **I^1** and **I^2** with an excess of $NaBH_4$ gave **Z^{1}H** and **Z^{2}H** in moderate yields. On the other hand, **Z^{3}H** was obtained by the mono-reduction and alkylation of **I^3** using trimethyl aluminum $AlMe_3$, followed by hydrolysis.

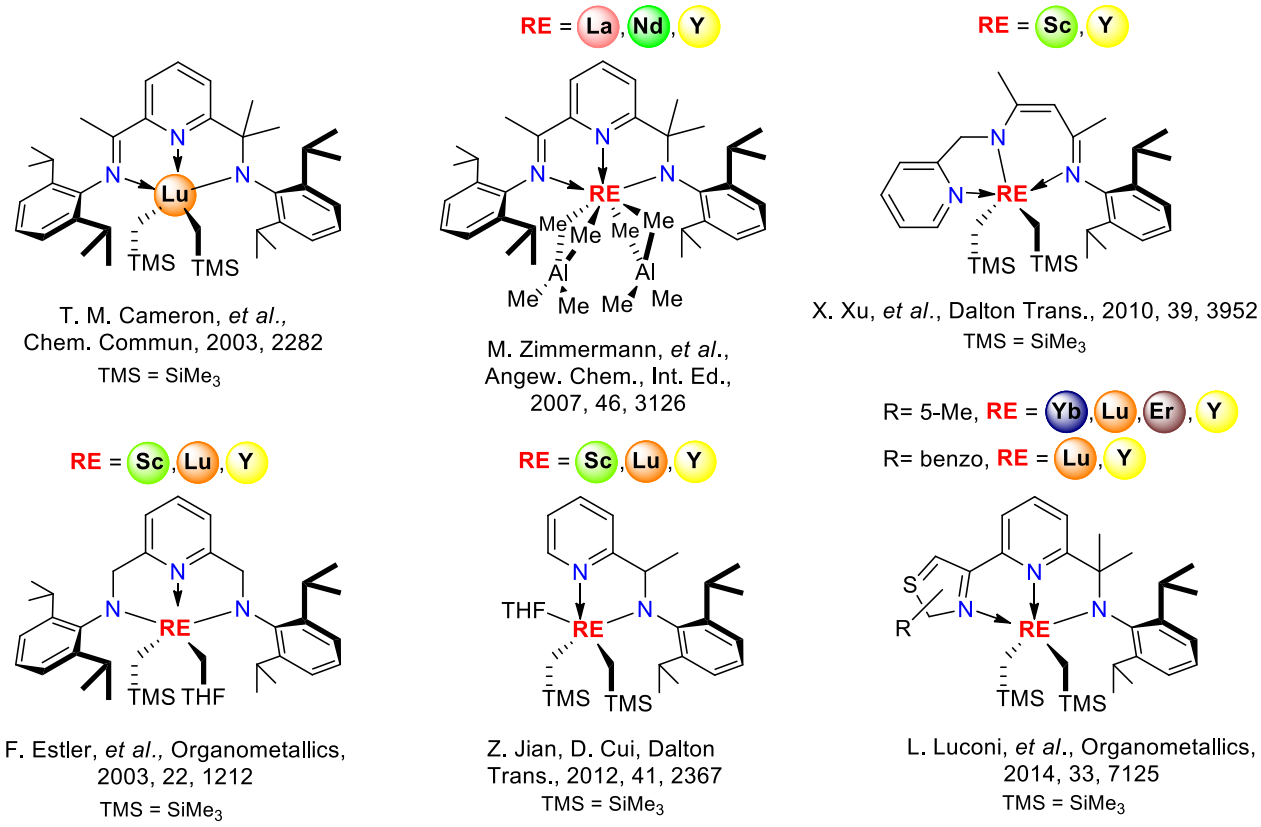

Figure 2.1: Selected examples of organo-rare-earth complexes bearing an amido-pyridine ligand.

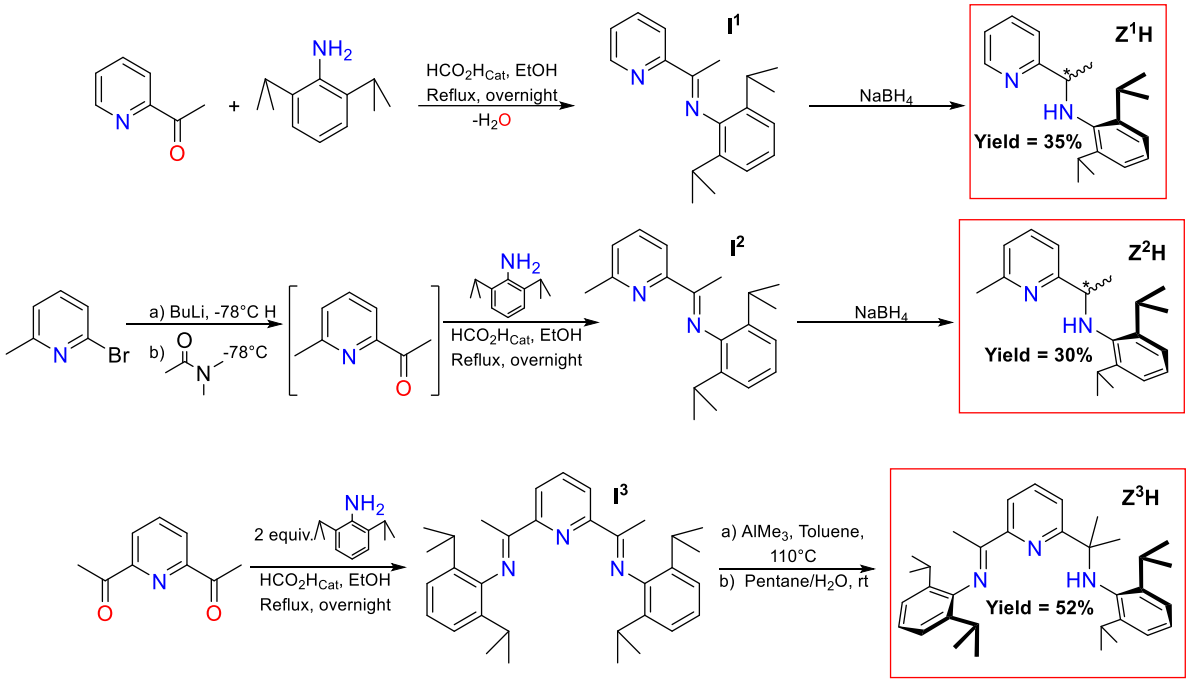

Scheme 2.2: Synthesis strategy of the amido-pyridine ligands used in this work.

All three ligands were characterized by conventional techniques such as NMR, elemental analysis (or HRMS) and the molecular structure of the new **Z^2H** was resolved by X-ray diffraction crystallography.

Single crystals of **Z^2H** suitable for X-ray diffraction analysis were obtained from a slow evaporation of a CH_2Cl_2 solution of the ligand. A view of **Z^2H** is shown in Fig. 2.2; selected bond distances and angles are listed in Table 2.1. The molecular structure of **Z^2H** showed the two enantiomers (R) and (S) in the unit cell with a conformation similar to that of **Z^1H** published previously[9a]. The C-N bond distance [1.478 (3) Å] was comparable to that of **Z^1H** and was in the typical range of a C(sp^3)-N amine bond. Both nitrogen atoms were in a *quasi-cis* position relative to each other, as a weak non-bonding H1-$N2_{pyr}$ interaction was present with a distance of 2.588 Å, as previously noticed for **Z^1H**[9a] (position of the hydrogen calculated by the X-ray software). This weak interaction could be determined by the fact that the sum of the Van der Waals radii between nitrogen (1.55 Å) and hydrogen (1.20 Å) was larger than the distance found in the XRD data (distance $N_{pyridine}$-H = 2.588 Å < $r_N + r_{H=}$ 2.75 Å)[11]. This results in a N2-C15-C13-N1 twist angle of -54.588°, showed a deviation of the amino-methyl moiety from the pyridine plane. The orientation of the two enantiomers in the unit cell resulted from a weak non-bonding C…H interaction between a proton of the methyl in the alpha position of the pyridine nitrogen N2 and the carbon carried by the asymmetric carbon of the enantiomer (r_{found}: 2.78 Å < r_{sum}: 2.90 Å). Finally, it was noticed that the aryl ring and the pyridine plane deviate from the orthogonality with an angle of 68.37°.

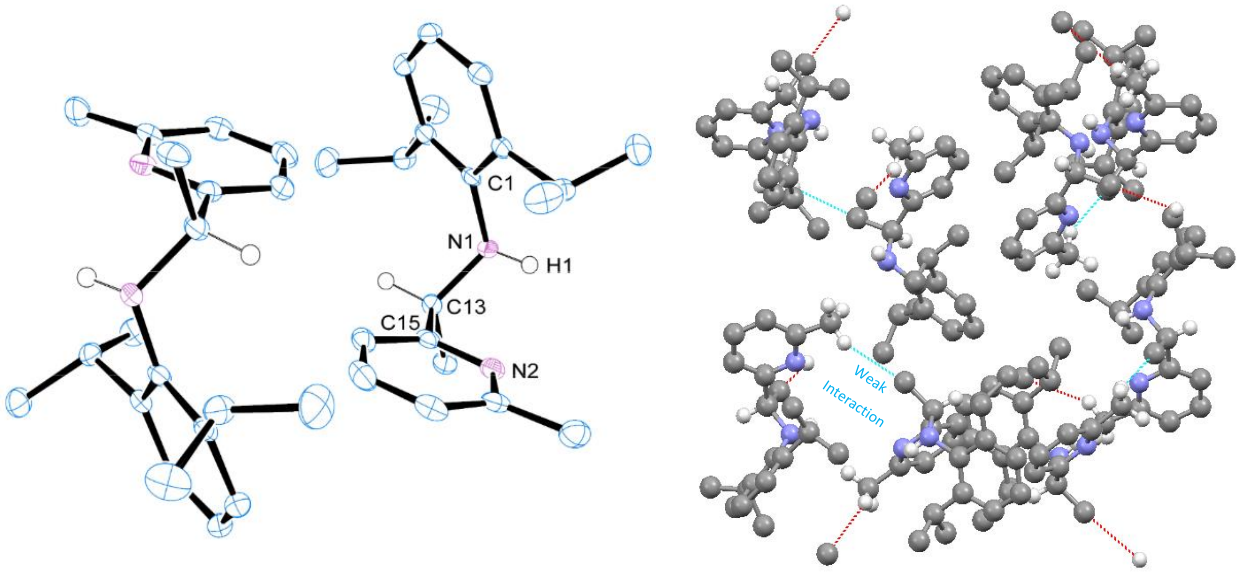

Figure 2.2: Molecular structure of Z^2H, thermal ellipsoids are drawn at the 50% probability level (left). Packing of Z^2H with weak interaction in blue (right).

The ^{1}H NMR spectra of **I^1**, **Z^{1}H**, **I^3** and **Z^{3}H** are depicted in Fig. 2.3. The ^{1}H NMR spectra of **I^2** and **Z^{2}H** being almost identical to that of **I^1** and **Z^{1}H**, they will not be shown here but in Appendix 2 and 3. In any case, ^{1}H NMR spectra of the ligands exhibited a pair of diastereotopic ^{i}Pr methyl resonances between δ = 1.3 and 1.06 ppm (in C_6D_6), instead of one doublet for 12 protons (Fig. 2.3 b-b and d-d). This duplication of the doublet was firstly noticed in the ^{1}H NMR spectrum of iminopyridine precursors **I^1** and **I^3** with a weak split between both signals (Fig. 2.3, a-a and c-c). The presence of one septuplet signal (Fig. 2.3, a-c) integrating for the 2 CH of the isopropyl groups was also noted and reflected an equivalence between both protons, while this was not the case for the protons of the isopropyl CH_3 groups. Such a splitting of the diastereotopic methyl groups in ^{1}H NMR was already described by K. Nienkemper *et al.*[12], who attributes this to a perpendicular arrangement between the C=N imine double bond and the 2,6-diisopropylphenyl plane. This effect could possibly be due to the delocalization of the lone pair on the nitrogen which increases the rotational energy barrier and causes the blocking of the N-C(aryl) bond and thus only one rotamer could be observed in the ^{1}H NMR spectrum.

Unlike the imine precursors **I^1**, rotation of the aryl plan in the amine protio-ligand **Z^{1}H** was present. However, the two isopropyls of the aryl planes were considered as diastereotopic (replacement of one CH_3 with a Br, for example, resulting in the formation of a chiral center). The simultaneous presence of a chiral center and a diastereotopic group resulted in the formation of the two doublets seen in Fig. 2.3 b-b at δ = 1.12 and 1.24 ppm.

Although not discussed in the literature, in the case of **I^1** and **Z^{1}H**, a possible explanation for the CH and CH_3 equivalence (despite the diastereotopic effect) could be the existence of a symmetry plane in the molecule. In the case of the ^{1}H NMR spectrum of **I^3**, the presence of two planes (sheet plane and blue plane in Fig. 2.4) could only lead to two doublets for the 8 methyl groups corresponding to 12H each and thus each doublet would correspond to four CH_3. These two groups of four methyls are depicted in red and green on Fig. 2.4. The reduction of one of the imine groups to form **Z^{3}H** would leave us with only one symmetric plane, the sheet plan. Since the imine part of **Z^{3}H** is quite similar to **I^1**, the two doublets observed could be explained similarly as before. On the other hand, the absence of the chiral center with respect to **Z^{1}H** provided four fully equivalent methyl groups (absence of diastereotopic effect).

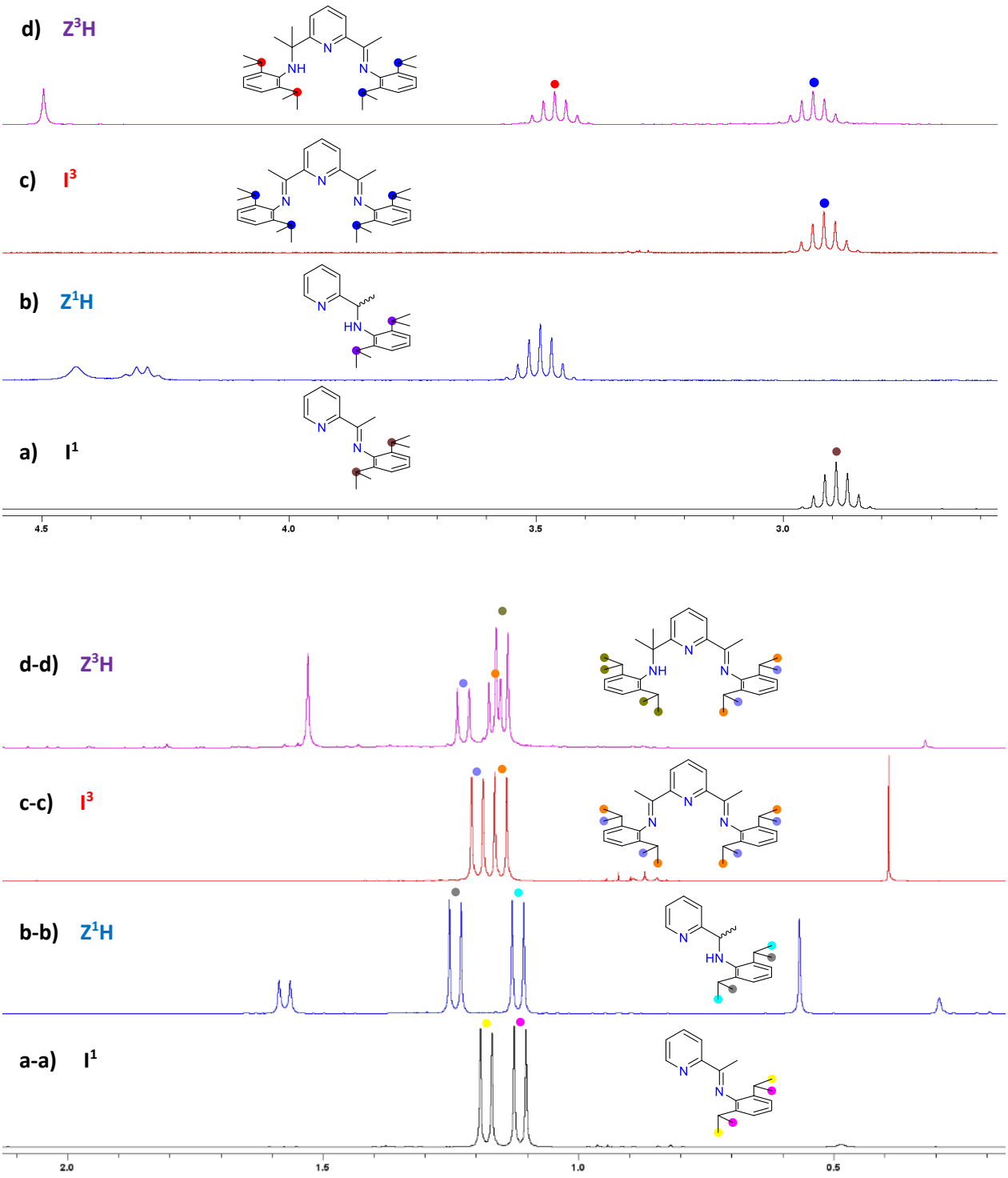

Figure 2.3: Partial ^{1}H NMR spectra of I^1, Z^1H, I^3 and Z^3H showing the proton resonances of isopropyl groups (solvent = C_6D_6).

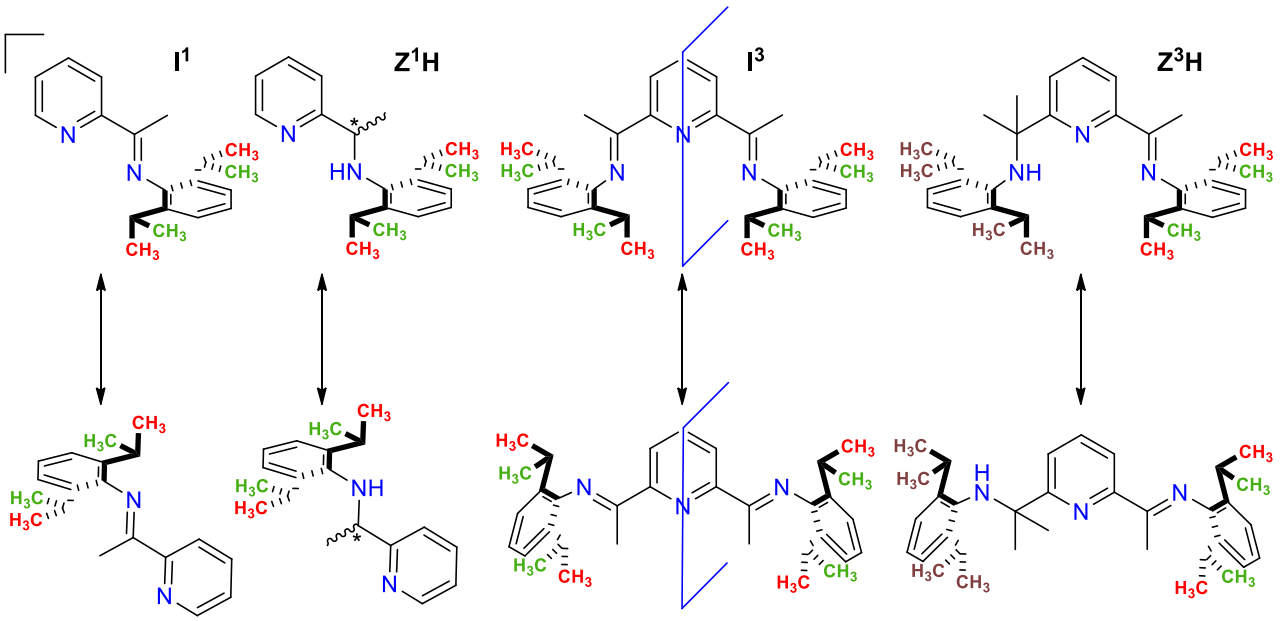

Figure 2.4: Imine/amine corresponding methyl groups for ^{1}H NMR analysis (nitrogens represented in *cis* and *trans*).

2.1.2 Synthesis of anionic amido-pyridine ligands

The preparation of amido-pyridine supported rare earth complexes described in the literature (Fig. 2.1) has been achieved exclusively by "*in-situ*" deprotonation of the protonated ligand with tris-alkyl rare earth precursors. The synthesis of borohydride rare earth complexes in this series, which requires salt metathesis from pre-formed anionic ligands, has not yet been investigated to our knowledge.

Initially, we made several attempts to isolate the anionic salts from their protonated form. According to the literature, different pathways were tested by reacting **Z^{1}H** with various bases. For example, in the case of bis-guanidinate rare-earth borohydride complexes, the deprotonation and isolation of the anionic bis(guanidinate) ligand with a lithium base has been studied by A. A. Trifonov[13]. Another pathway to prepare an anionic ligand is to use a potassium salt as a base. This route is indeed the most commonly used to prepare Cp/Cp* borohydride sandwich complexes[14] (Scheme 2.3).

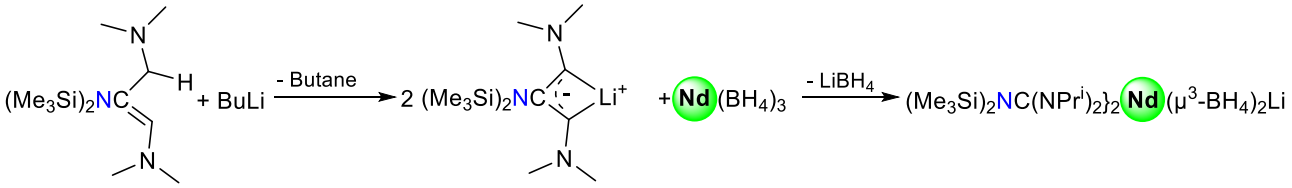

A.A.Trifonov and coll., Russ. Chem. Bull. Int. Ed., 2007, 56, 456

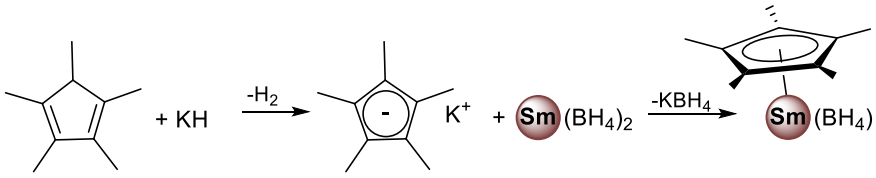

M. Visseaux and coll., Dalton Trans., 2010, 39, 6761.

Scheme 2.3: Synthesis of borohydride rare earth complexes with an anionic ligand. THF are omitted for more clarity.

The synthesis of the anionic **Z^1** ligand was undertaken by using a strong alkyl lithium base, such as MeLi or ^{n}BuLi (pK_a ≈ 48-50). As can be seen in the ^{1}H NMR spectrum, it led to the anionic ligand (Fig. 2.5, +) but unfortunately some impurities (*), which were not attributed to the protio-ligand (Fig. 2.5 a *vs.* b), were also generated in the process. Therefore, this route was dropped.

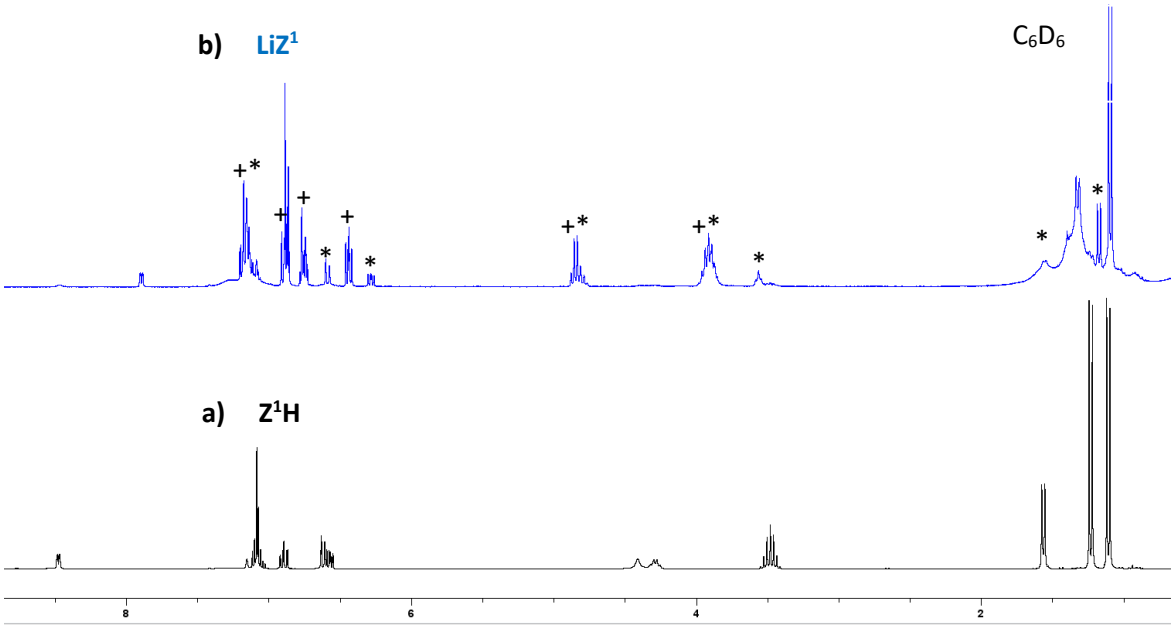

Figure 2.5: ^{1}H NMR spectrum of Z^{1}H and its corresponding lithium salt with impurities (solvent C_6D_6).

The second attempt relied on the use of a less strong base such as KH (pK_a ≈ 35) but the potassium salt of this ligand could not be obtained, and several trials led to different results.

A last attempt to obtain this anionic salt was made using potassium bis(trimethylsilyl) amide [KN(TMS)$_2$] as a smoother base (pK_a ≈ 26), which allowed to isolate a new compound. Surprisingly, after the color change upon addition of KN(SiMe$_3$)$_2$ to a solution containing **Z^{1}H**, the ^{1}H NMR spectrum showed no difference by comparison with that of the protonated ligand alone, but a peak corresponding to KN(TMS)$_2$ appeared (Appendix 4a). Crystals suitable for X-ray determination were obtained at -35 °C from a concentrated solution of this product in pentane and the molecular structure of the isolated compound is shown in Fig. 2.6, with selected bond distances and angles listed in Table 2.1. The molecular structure showed an adduct of the protonated ligand **Z^{1}H** with KN(TMS)$_2$ of the form (**KN(TMS)$_2$.Z^{1}H**).

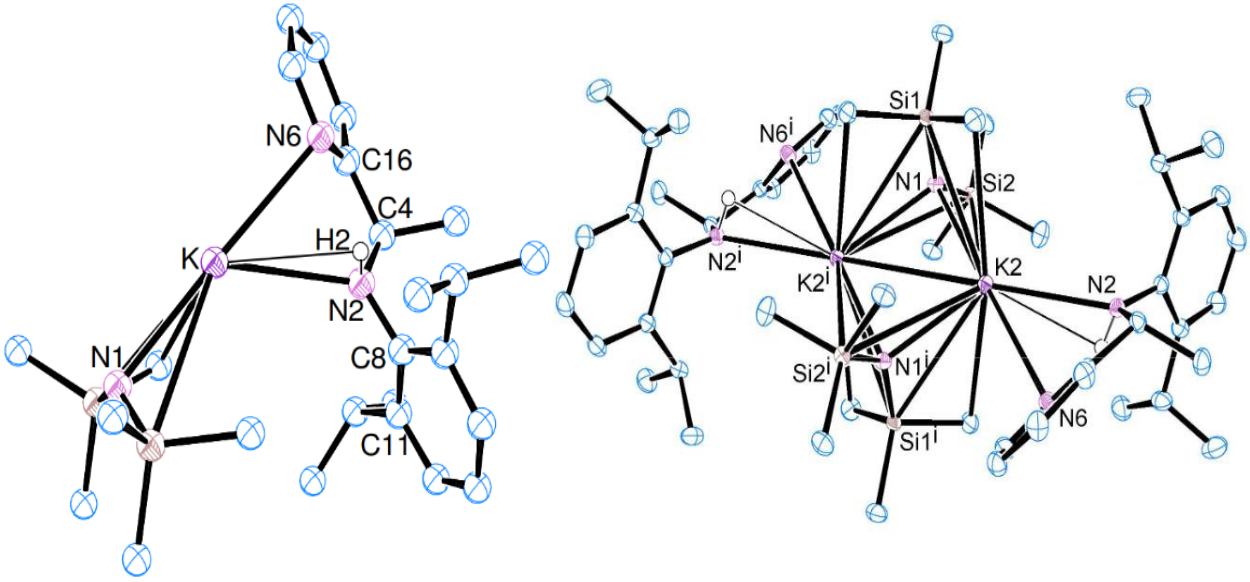

Figure 2.6: Partial molecular structure of KN(TMS)$_2$.Z^{1}H (left) and total view (right) without most of hydrogens for more clarity. Thermal ellipsoids are drawn at the 50% probability level.

Table 2.1: Selected bond and angles for ***Z^{1}H*** *(according to reference 9a),* ***Z^{2}H*** *and the adduct* ***KN(TMS)$_2$.Z^{1}H***

	Z^{1}H	**Z^{2}H**		**KN(TMS)$_2$.Z^{1}H**
N1-H1 (Å)	0.903	0.880	**N2-H2 (Å)**	0.889
N2…H1 (Å)	2.651	2.588	**N6…H2 (Å)**	2.185
C13-N1 (Å)	1.462	1.478	**C4-N2 (Å)**	1.478
N2-C15-C13-N1(°)	-66.38	52.79	**N6-C16-C4-N2 (°)**	-20.455
Pyr *vs.* Aryl plan	60.58	68.37	**Pyr *vs.* Aryl plan**	45.66
			K2-N1 (Å)	2.751
			K2-N1^i (Å)	2.844

The structural differences between the free ligand **Z^{1}H** and its adduct with the potassium amide resulted from a change in the H2-N6 bond distance (H2-N6 $_{\mathbf{KN(TMS)2.Z1H}}$ = 2.185 Å *vs.* H1-N2$_{Z1H}$ = 2.651 Å), which became shorter, while the H2-N2 distance remained close in value (H2-N2$_{\mathbf{KN(TMS)2.Z1H}}$ = 0.889 Å *vs.* H1-N1$_{\mathbf{Z1H}}$ = 0.903 Å). The potassium center was at equal distance from the nitrogen atom of the amino group and the nitrogen of the pyridine ring (K2-N2 = 2.989 Å, K2-N6 = 3.048 Å). The two nitrogen atoms N1 and N1^i were linked to the potassium atom by, a X-type bond (K2-N1 = 2.751 Å), which was similar to the K-N bond distance in KN(TMS)$_2$ (K-N = 2.77 Å)[15]**,** and a L-type bond, which was found to be slightly longer than the K-N distance in KN(TMS)$_2$ (K2-N1^i = 2.844 Å), respectively. A possible explanation for obtaining such acid/base adduct might be deduced from the presence of a weak H2-N6 interaction in the protio-ligand **Z^{1}H** (2.588 Å), which could "trap" the hydrogen in the amino-methyl plane and prevent its deprotonation. Such acid/base adduct might result from the interaction of the nitrogen of the pyridine/amine groups toward the amide moiety of the base that "protects" the hydrogen (K-N = 2.77 Å < K-N1 = 2.844 Å, induced by the repulsion (⇢) between the nitrogen atoms). Thus, the only interaction that could take place would be between the potassium center and the nitrogen of the protonated ligand (K2-N2 = 2.989 Å, K2-N6 = 3.048 Å), which could also cause a repulsion between the potassium center and the δ^+ hydrogen atom and push it into the N6-C16-C4-N2 "cage", making it rather inaccessible for the (trimethylsilyl)amide group (Scheme 2.4).

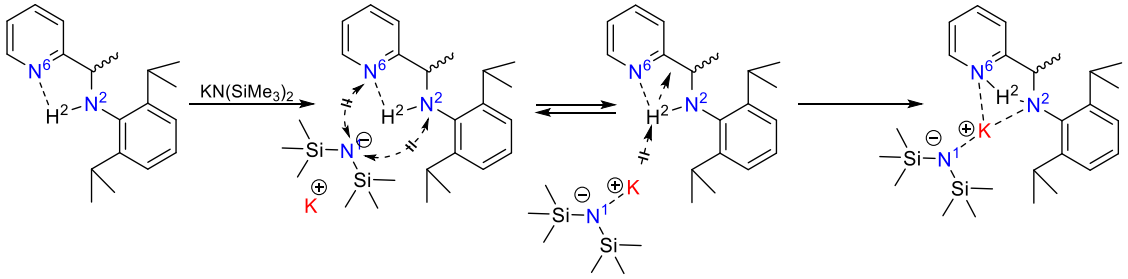

Scheme 2.4: Possible mechanism for the obtention of the potassium adduct KN(TMS)$_2$.Z^{1}H.

The difference in torsion angles between the adduct (N6-C16-C4-N2 = -20.455°) and the free-ligand **Z^{1}H** (N6-C16-C4-N2 = 66.380°) show a structural constraint caused by the coordination of the pyridine/amine nitrogen of the protio-ligand to the potassium center. Compared to **Z^{1}H**, the deviation from orthogonality between the pyridine and the N-aryl plane was more evident in the adduct (**Z^{1}H**: 60.58° *vs.* 45.66°), which might be caused by steric repulsion of the (trimethylsilyl)amide group and the isopropyl of **Z^{1}H**.

After heating the adduct for a week at 50 °C and monitoring the reaction by ^{1}H NMR, no change was observed (Appendix 4b). Due to these inconclusive results, as resumed in Scheme 2.5, isolating the salt from the anionic ligand was discarded and the complexes were synthesized straightforwardly *via* the *"borohydride/alkyl route"* (see below).

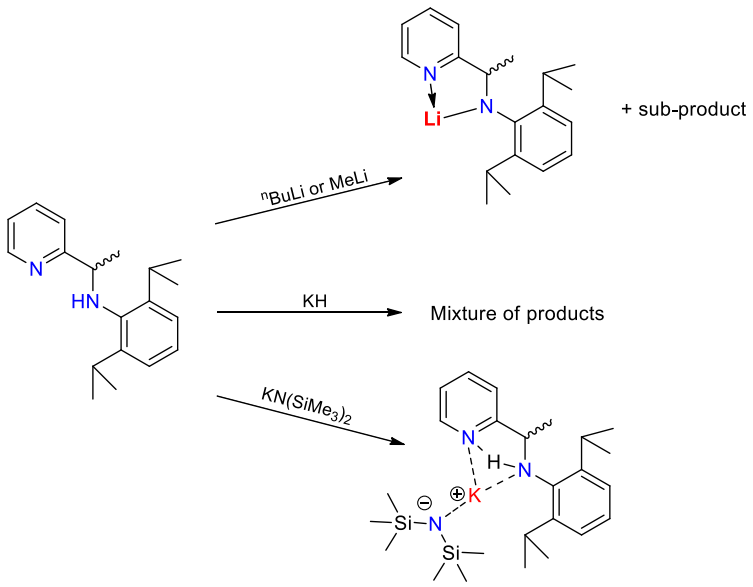

Scheme 2.5: tentative synthesis of the MZ^1 anionic salt (M = Li, K).

2.2 Neodymium amido-pyridine borohydride complexes

2.2.1 Studies with Z^1 ligand

As previously mentioned, neodymium borohydride complexes have been studied for decades and have been proven to behave as active catalysts for many polymerization reactions. For several years now, our laboratory has been using ButylEthylMagnesium (BEM) as a reagent to effectively synthesize rare earth complexes *via* the *"borohydride/alkyl route (B/A route)"*, which involves combining a protio-ligand with BEM. As BEM is a bis-alkyl magnesium base, only half an equivalent is required for the synthesis of mono-substituted complexes (Scheme 2.6). This base, when diluted in an alkane solvent, enables a fast and homogenous synthesis of the complexes with the formation of magnesium borohydride as by-product.

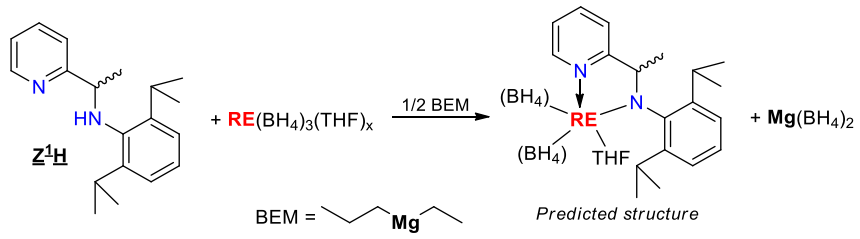

Scheme 2.6: B/A route strategy using BEM for the targeted synthesis of a mono-substituted RE borohydride derivative.

Three different outcomes for the magnesium component are generally observed: i) magnesium by-product can be separated from the final product as Mg(BH$_4$)$_2$(THF)$_x$, ii) the final product can be obtained as an "ate" complex wherein magnesium acts as a counter-cation, iii) formation of a heterobimetallic complex with a magnesium borohydride (μ -BH$_4$) bridge, as seen in Scheme 2.6 and Fig. 2.7, respectively[16].

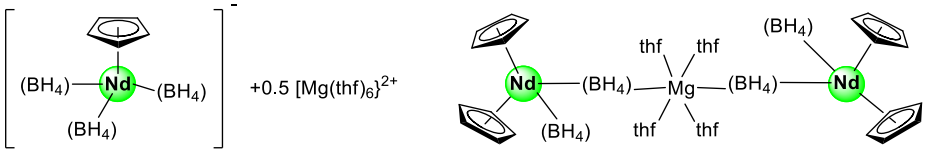

M. Visseaux, *et Al*., C. R. Chim., 2007, 10, 1195

M. Visseaux, *et Al*., Eur. J. Inorg. Chem., 2010, 18,

Figure 2.7: Cyclopentadienyl neodymium borohydride complexes obtained from BEM and Nd(BH$_4$)$_3$(THF)$_3$.

The synthesis of borohydride rare earth complexes bearing an amido-pyridine ligand was first conducted on an NMR scale and was followed by ^{1}H NMR studies (Scheme 2.6). Trivalent neodymium being paramagnetic, ^{1}H NMR studies were recorded between 150 ppm and – 50 ppm (Fig. 2.8) and could only be used as a preliminary step to see the preferential substitution degree (1 or 2 ligands). This substitution degree was determined by the disappearance of the proton resonances of the ligand in the diamagnetic region along with appearance of paramagnetic peaks, indicating coordination of the ligand to the metal center (new paramagnetic peaks = new neodymium complex).

In the ^{1}H NMR spectrum below, the presence of the paramagnetic neodymium tris-borohydride with the **Z^{1}H** ligand (typical resonance at δ = 8.6 ppm, corresponding to the proton in alpha position of the pyridine, Fig. 2.8 a) resulted in a broadening of the ligand peaks, which could be caused by the possible coordination of the nitrogen of the pyridine moiety of the ligand to the metal center. Subsequent reaction with 0.5 equiv. of BEM led to the emergence of a set of resonances in the paramagnetic region of the spectrum (Fig. 2.8 b), which strongly suggested the formation of a [**Z^1**]Nd complex. The resulting complex exhibited a total of fifteen peaks corresponding to the coordinated ligand and the borohydride moiety. Those signals will be further discussed later.

The addition of the second equivalent of **Z^{1}H** ligand in the reaction mixture caused the apparition of broad peak (Fig. 2.8 c-c) (marked ¤), possibly caused by the coordination of protonated form of the ligand. The paramagnetic peaks remained unchanged when an additional half equivalent of BEM was added to the mixture (Fig. 2.8 b *vs*. d), while the broad peak (¤) disappeared (Fig. 2.8 c-c *vs*. d-d).

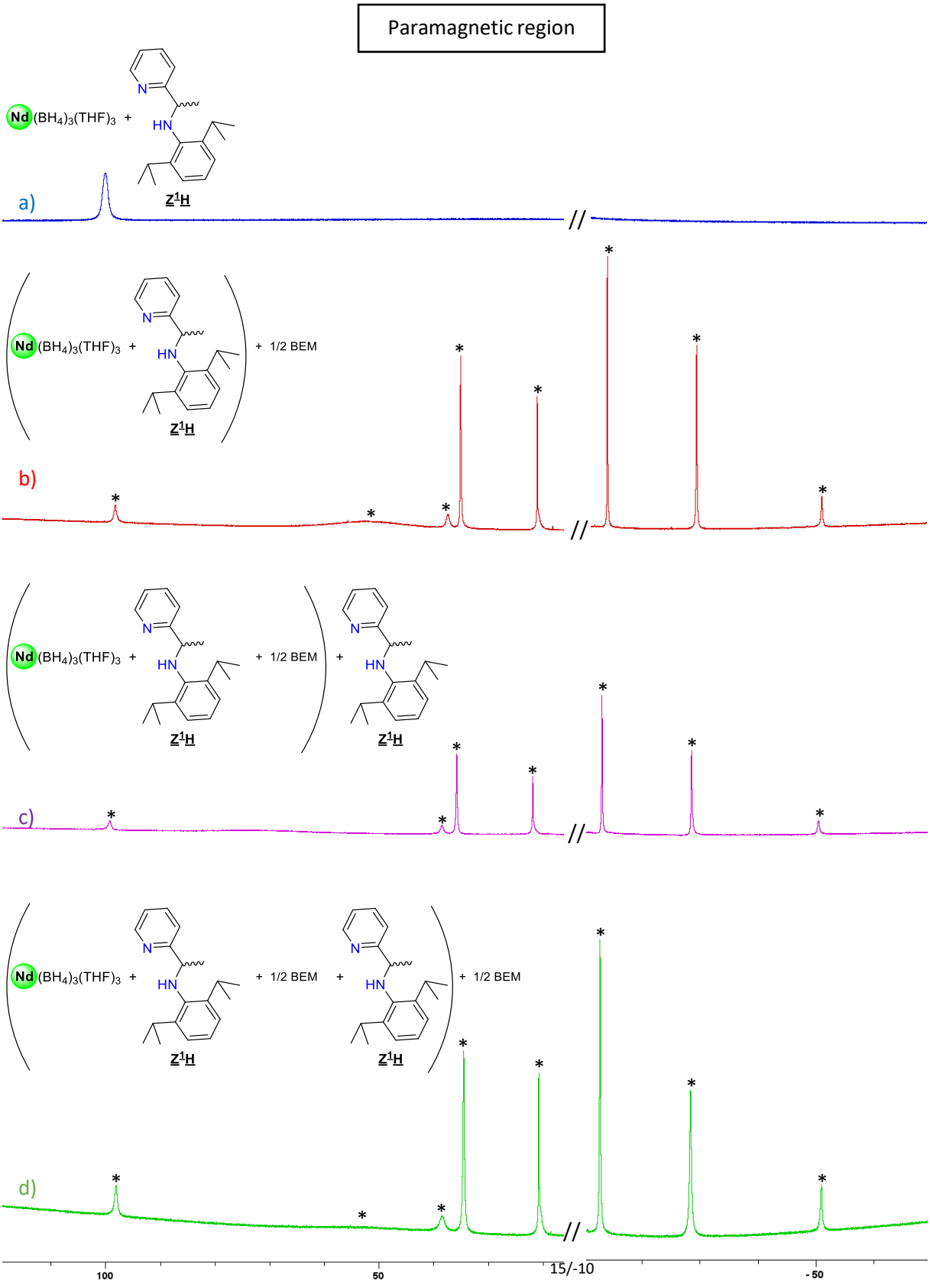
Paramagnetic region
Nd(BH4)3(THF)3 +
Z1H
a)
+ 1/2 BEM
b)
c)
d)
100
50
15/-10
-50

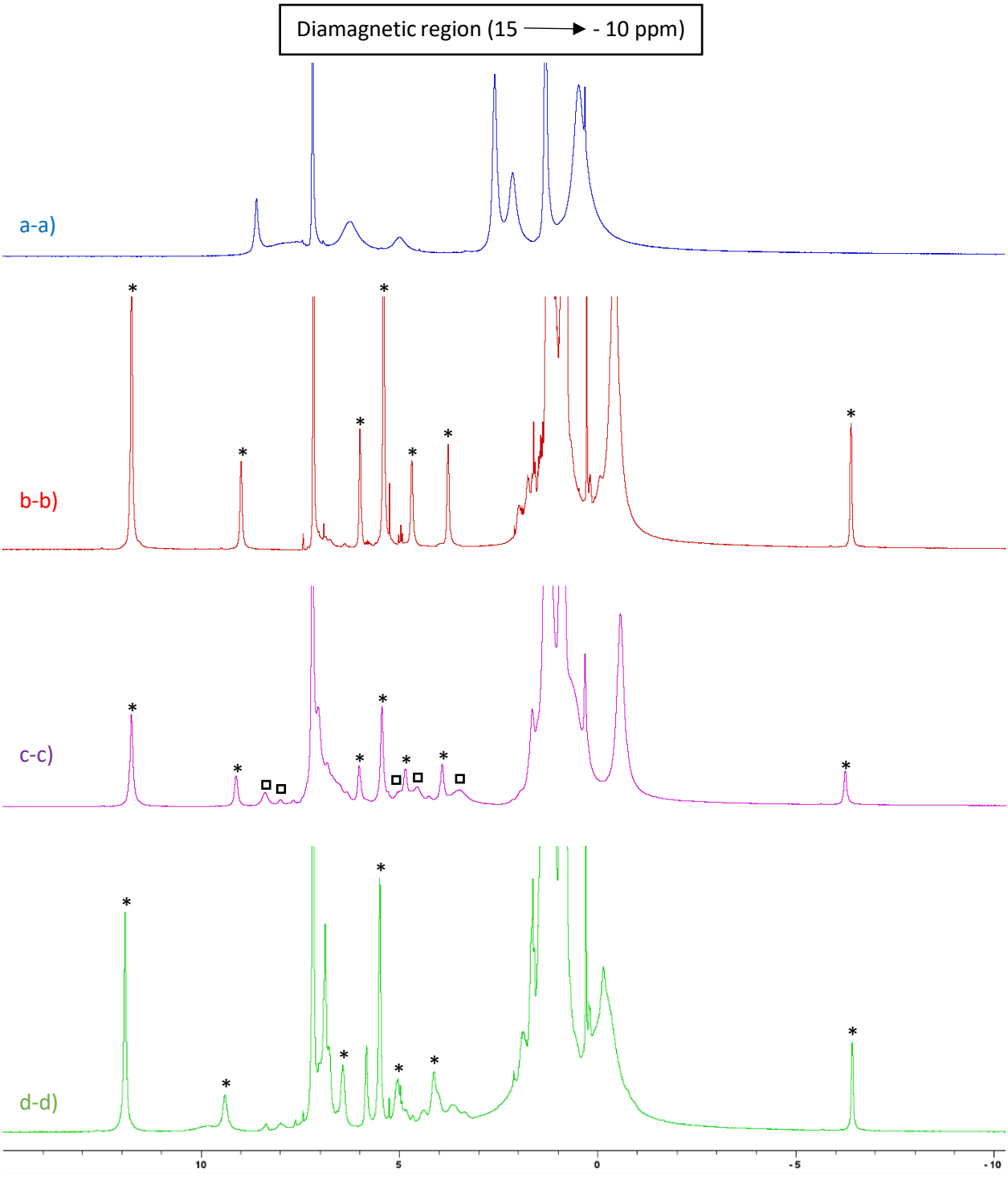

Figure 2.8: Preliminary ^{1}H NMR studies regarding the degree of substitution with Z^{1}H (* new signals for the Nd complex, solvent C_6D_6).

In summary, it appeared that the addition of 2 equiv. of **Z^{1}H** ligand/1 equiv. BEM to Nd(BH$_4$)$_3$ produced the same result as 1 equiv. **Z^{1}H** ligand/0.5 equiv. BEM, while the total amount of ligand was consumed. Thus, we might conclude from this study that a bis-substituted complex (**Z^1**)$_2$Nd(BH$_4$) was obtained at the expense of a mono-substituted derivative (**Z^1**)Nd(BH$_4$)$_2$. Moreover, this reaction

seemed immediate at room temperature at the NMR scale. We believe that the formation of the bis-substituted complex (**Z^1**)$_2$Nd(BH$_4$) from the reaction of 1 equiv. of Nd(BH$_4$)$_3$(THF)$_3$ with 1 equiv. of **Z^{1}H** / 0.5 equiv. of BEM resulted in a 50:50 mixture of bis-substituted complex and residual tris-borohydride of neodymium, as the purple powder of tris-borohydride could be observed in the reaction mixture (Scheme 2.7). Since the molecular structure of the complex, issued from this reaction, is currently only a hypothesis, it will be referred to as complex **1a** at this stage (*vide infra*). However, it might not be excluded that a mono-substituted derivative (in brackets is scheme 2.7) was formed, which rapidly underwent rearrangement into the putative bis-derivative complex (**Z^1**)$_2$Nd(BH$_4$) and Nd(BH$_4$)$_3$.

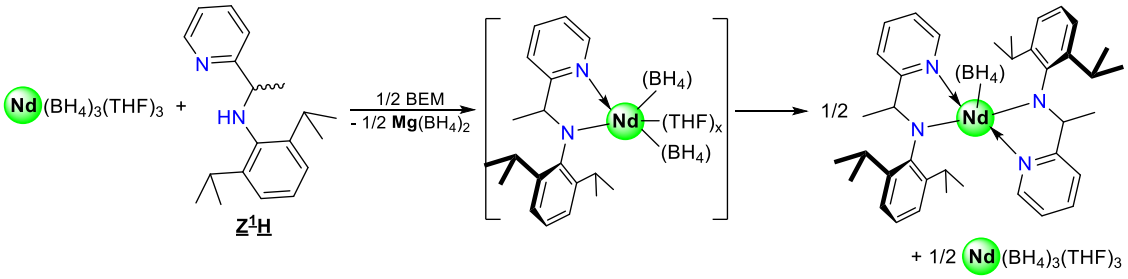

Scheme 2.7: Possible formation of complex (Z^1)$_2$Nd(BH$_4$) using one equivalent of ligand and 0.5 of BEM according to the ^{1}H NMR studies.

While the proton resonances of the Nd complex in the paramagnetic region could be easily identified (Fig. 2.8 d, noted +), a more accurate identification in the diamagnetic region was obtained from the 50:50 Nd(BH$_4$)$_3$: (**Z^1**)$_2$Nd(BH$_4$) mixture (Fig. 2.8 b-b) because no free ligand or impurities were present.

The fifteen observed resonances included a very broad peak (almost in the baseline) around δ = 70 ppm that corresponded to the BH$_4$ group and thus left fourteen signals assignable to the protons of the coordinated ligand. The integration of these signals revealed 8 peaks for 2H [4 x C*H*$_{pyr}$, 1 x CH$_3$(C*H*)-N, 1 x *meta*-C*H*$_{Aryl}$, 2 x C*H*(CH$_3$)$_2$], 1 peak for 4H and 5 peaks for 6H [1 x C*H*$_3$(CH)-N, 4 x CH(C*H*$_3$)$_2$] (Fig. 2.9). In order to clarify these integrations, one possible explanation would be that, compared to the protio-ligand **Z^{1}H** alone, the coordination of the ligand to the neodymium borohydride suppressed the symmetric plane and allowed the discernment of each CH$_3$ unit. As previously suggested for the protio-ligand **Z^{1}H**, the rotational energy barrier of the N-C$_{Aryl}$ bond could be too high, along with the loss of symmetry in the complex, then four signals for the CH$_3$ and two signals for the CH (one isopropyl closer to the borohydride than the other one) were to be expected. Already described in several publications[17,8d], it seems that the coordination of an anionic Z ligand allows this multiplication of peaks. Although most of the peaks could not be assigned to a particular position, one of them could

easily be deduced: indeed, the peak integrating for 4 H at 20.6 ppm could unambiguously be assigned to the *meta*-aryl proton.

After a preliminary examination of the preparation of the presumed complex (**Z^1**)$_2$Nd(BH$_4$) by ^{1}H NMR, the bulk synthesis was then undertaken, with **Z^{1}H**/Nd ratio equal to 2. Addition of BEM led instantly to the change of the blue solution of Nd(BH$_4$)$_3$(THF)$_3$/**Z^{1}H** (2 equiv.) to a green solution. *Vacuum* drying, filtration in toluene and washing with pentane afforded a product that is sufficiently clean for elemental analysis, according to ^{1}H NMR. The ^{1}H NMR spectrum of the clean product was identical to the one depicted in Fig. 2.8 d).

Elemental analysis of the obtained complex was consistent with the formation of the bis-substituted derivative (**Z^1**)$_2$Nd(BH$_4$), but with the presence of an additional molecule of Mg(BH$_4$)$_2$(THF)$_4$,which was under the form of a neutral heterobimetallic Nd/Mg adduct (theo: C = 60.92%, H = 8.91%, N = 5.26%, found: C = 61.25%, H = 8.61%, N = 5.37%). On this basis, the structure of this complex could actually be described in two different forms. The first form would be a 50:50 mixture of the two mononuclear Nd and Mg compounds [(**Z^1**)$_2$Nd(BH$_4$)],[Mg(BH$_4$)$_2$(THF)$_4$], referred to as complex **1a**. The second form would be a Nd-Mg bridged dimer complex [(**Z^1**)$_2$Nd(THF)(μ-BH$_4$)$_2$Mg(BH$_4$)(THF)$_3$], assigned as complex **1b**.

To our surprise, a small amount of crystals suitable for XRD, obtained at cold temperature from a diethylether/pentane mixture, revealed after analysis the isolation of a (possibly a by-product) mono-substituted complex [(**Z^1**)Nd(THF)(BH$_4$)(μ-BH$_4$)]$_2$. As the molecular structure of the complex was different from what was expected (*i.e.* complexes (**Z^1**)$_2$Nd(BH$_4$), **1a** or **1b**), this will be denoted as complex **2** (Fig. 2.10, Table 2.2). The recovery of these crystals showed the possibility of forming the mono-substituted complex by rearrangement at cold temperature, which would probably be much less soluble than its bis-substituted counterpart, with concomitant formation of (**Z^1**)Mg(BH$_4$) as shown in Scheme 2.8, however the reaction pathway has not yet been elucidated. Such behavior in organometallic chemistry of the larger lanthanides has already been reported[18].

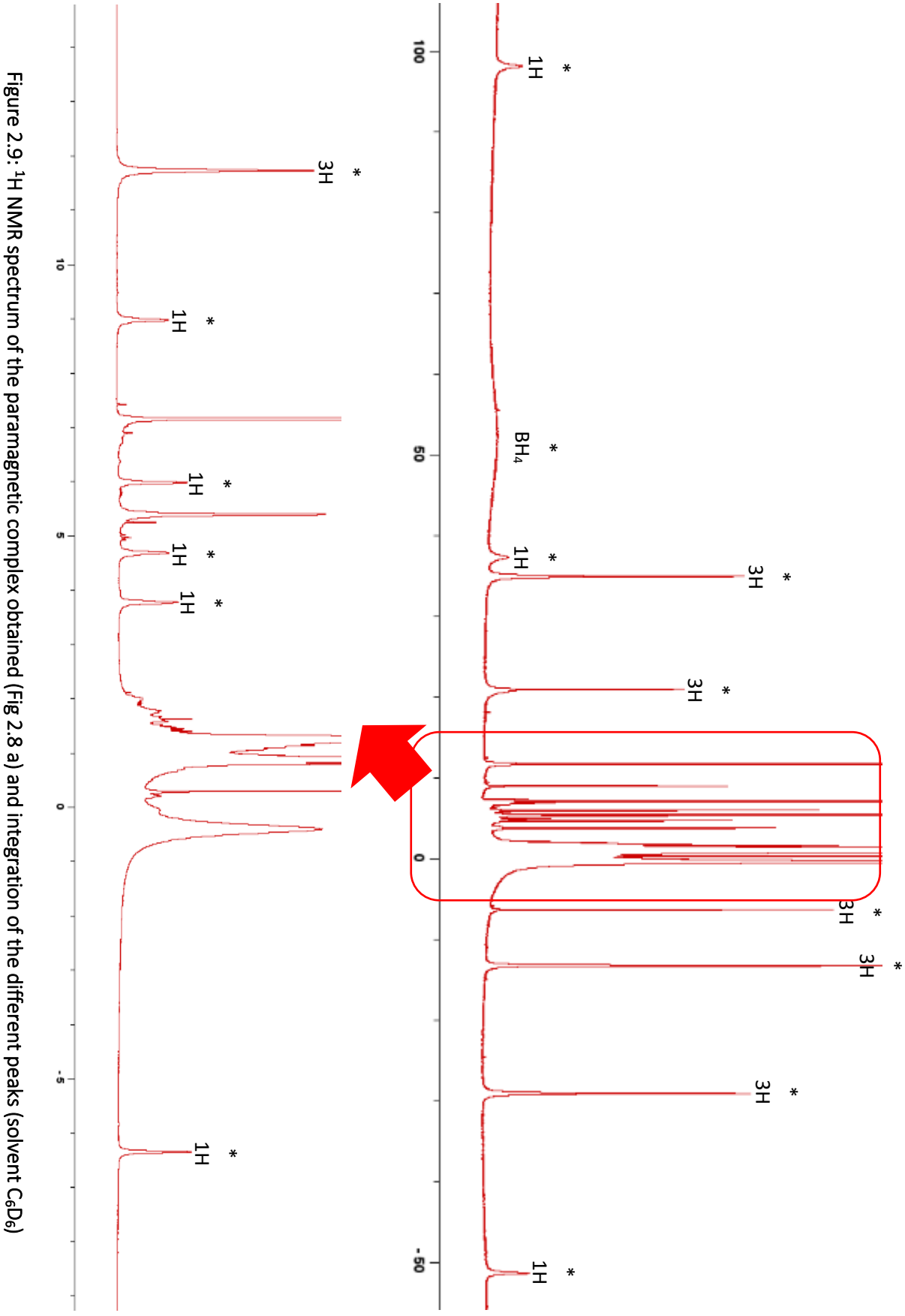

Figure 2.9: ^1H NMR spectrum of the paramagnetic complex obtained (Fig 2.8 a) and integration of the different peaks (solvent C_6D_6)

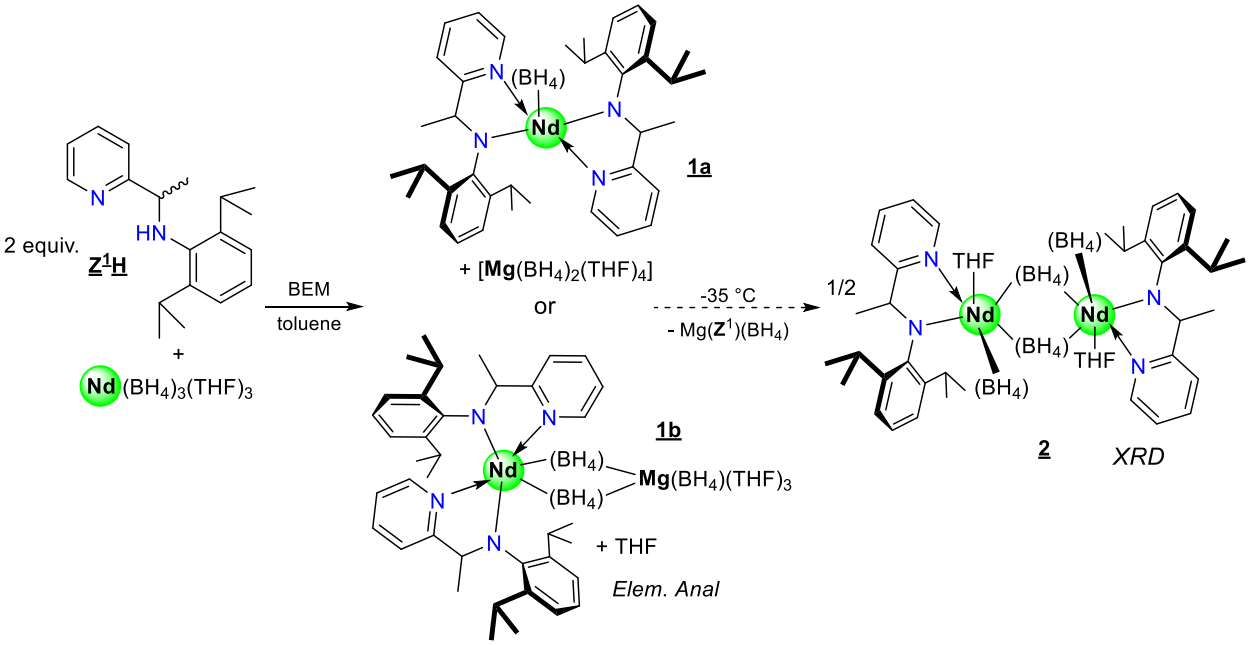

Scheme 2.8: Possible coordination scheme for 1a and 1b with Mg adduct counterpart and rearrangement to obtain complex 2.

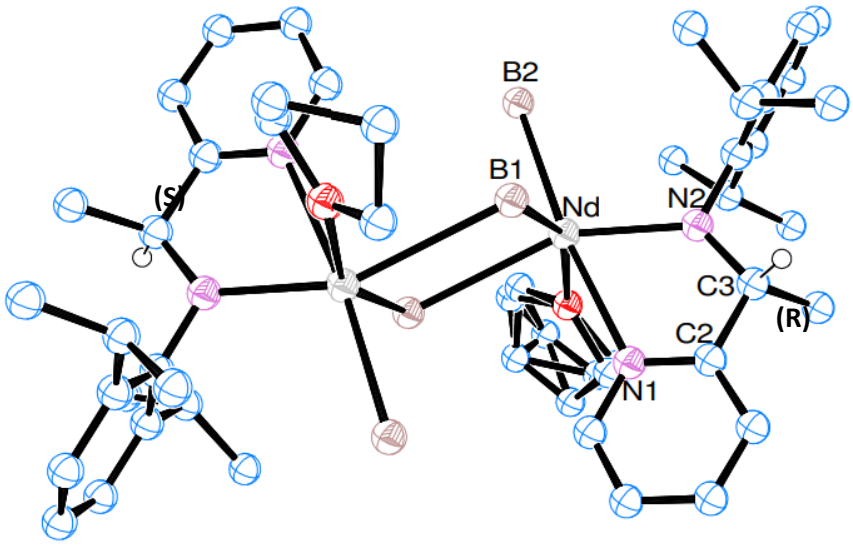

Figure 2.10 Molecular structure of $[(Z^1)Nd(BH_4)(\mu\text{-}BH_4)(THF)]_2$ (2), the hydrogen atoms have been partially omitted for clarity. Thermal ellipsoids are drawn at the 50% probability level.

The molecular structure of **2** exhibited a neutral complex with two neodymium, each bound to a $\mathbf{Z^1}$ ligand (presence of a R and a S ligand in the same compound as seen above) and a borohydride ligand along with two BH_4 groups bridged between the two metals. This complex crystallized in the $P2_1/n$ group. The B2-Nd bond distance of 2.639(8) Å was within the expected range for a

η^3 coordination of the borohydride, while the B1-Nd bond distance of 2.983(8) Å was slightly longer than usual for a bridging fashion mode[19]. To the best of our knowledge, **2** was the first example of a homo-bimetallic neodymium complex that bore both a terminal borohydride group and a borohydride bridge. The twist angle between the pyridine ring and the amidomethyl plane (N1-C2-C3-N2 = 3.331°) exhibited a *quasi*-planarity, while the N-aryl ring deviated from orthogonality to the pyridine ring with an angle of 74.81 °. The distance between both Nd atoms was found at 4.573 Å.

In order to consider the possibility of obtaining a complex without magnesium co-product, the deprotonation of **Z^{1}H** was carried out using 1 equiv. of lithium alkyl base (MeLi or ^{n}BuLi), instead of BEM as reagent, and followed by the addition of ½ equiv. of Nd(BH$_4$)$_3$(THF)$_3$ to give, after extraction and solvent removal, a green product that will be referred to as complex **1'a** (identical to the molecular structure (**Z^1**)$_2$Nd(BH$_4$) depicted in Scheme 2.7) . During the synthesis using this route, a different color change from that observed with BEM was noted: while the synthesis using BEM led straightforwardly to a green solution, the addition of ^{n}BuLi to the blue solution of Nd(BH$_4$)$_3$ precursor and **Z^{1}H** gave a yellow-orange solution that turned green after 5 min. This difference in reactivity/color change of the solution might result from the eventual formation of an [Nd(Alkyl)(BH$_4$)] intermediate species with the BEM pathway, and then this alkyl derivative reacted with the protio-ligand to form the green product **1a** or **1b**. On the contrary, ^{n}BuLi being a strong base, it reacted first with 2 equiv. of **Z^{1}H** (**Z^{1}H**:^{n}BuLi = 2:2) to obtain the orange anionic ligand (2 Li**Z^1**), which subsequently reacted with 1 equiv. of Nd(BH$_4$)$_3$ to presumably form the complex **1'a** bearing two **Z^1**H ligand and one BH$_4$ of the form (**Z^1**)$_2$Nd(BH$_4$), without the presence of main group metals as described in Scheme 2.9.

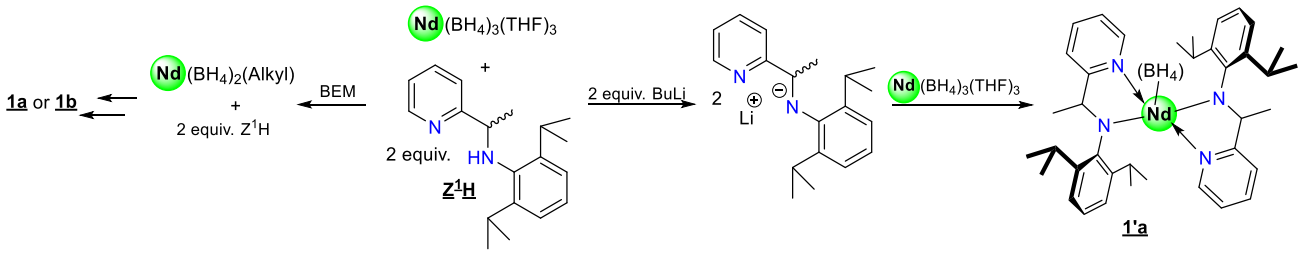

Scheme 2.9: Possible pathway for the synthesis of the bis-substituted complexes.

However, a comparison of the ^{1}H NMR spectra of these two green products (**1a/1b** *vs.* **1'a**) indicated a real difference between the synthesis using BEM and that using a lithium base (Fig. 2.11). One hypothesis may be closely related to the molecular structure of the product. Indeed, this difference might result from the absence of the magnesium counterpart. A possible degradation of the ligand by the lithium pathway was checked by hydrolysis of the NMR tube but clean return to the

spectra of the original **Z^{1}H** protio-ligand excluded this possibility. However, as observed below, two signals between 100 and 130 ppm, normally corresponding to the borohydride unit, are observed, meaning a possible borohydride side-product.

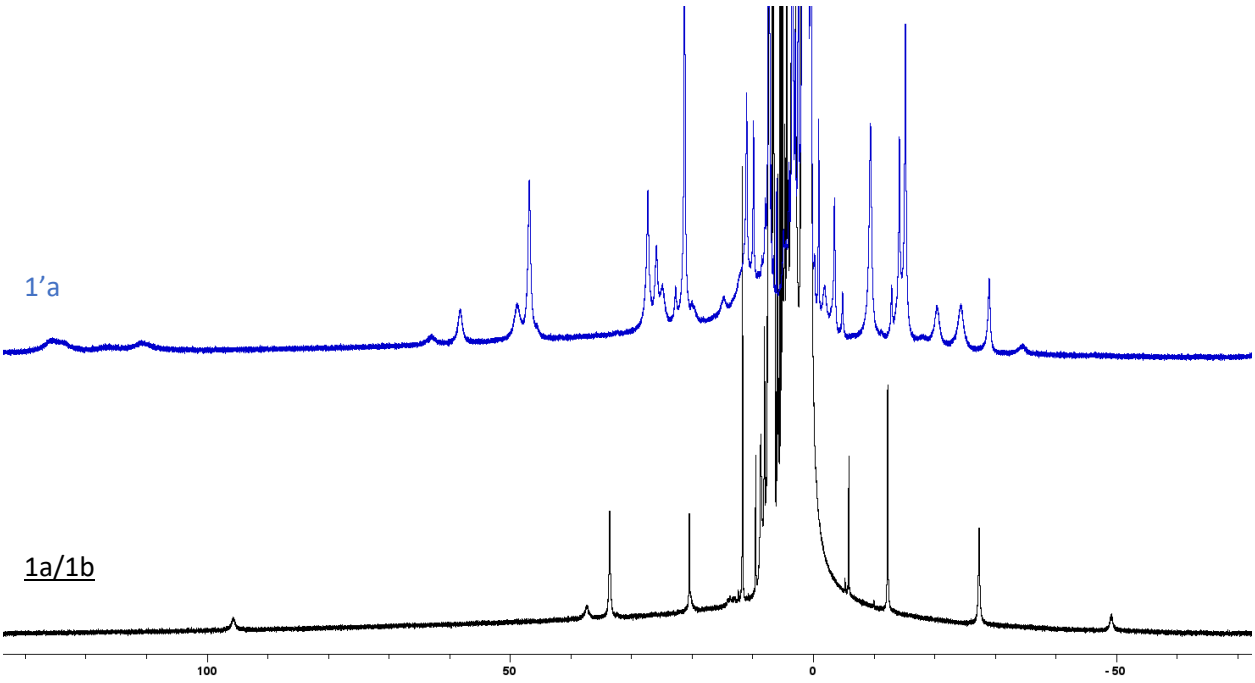

Figure 2.11: ^{1}H NMR of magnesium (1a/1b) *vs.* lithium (1'a) synthesis of a bis-substituted ((Z^1)$_2$Nd(BH$_4$)) derivative (solvent C_6D_6).

Nevertheless, green single crystals suitable for XRD were obtained from the synthesis in bulk, this time using MeLi in toluene. This allowed us to acquire the molecular structure of the isolated compound, shown in Fig. 2.12, which will be denoted as complex **1'b** to differentiate it from complex **1'a** obtained from the reaction using ^{n}BuLi. Selected bond distances and angles are listed in Table 2.2. As anticipated, this structure was obtained without lithium.

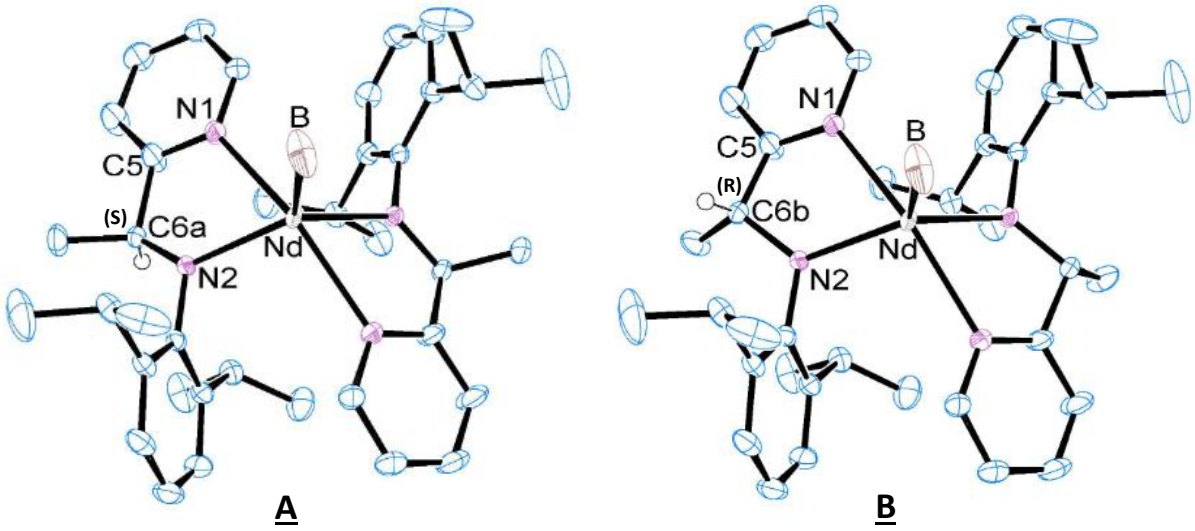

Figure 2.12: Molecular structure of $(Z^1)_2Nd(BH_4)$ – complex 1'b, the hydrogen atoms have been omitted for clarity. Thermal ellipsoids are drawn at the 50% probability level.

The **1'b** complex crystallized in the C2/c space group. The molecular structure revealed a neutral complex bearing two ligands **Z^1** and one BH_4 group. In the crystal packing, the ligand was at 50/50% present in a R or S configuration. In complex **1'b**, the structure showed the two ligands at the same distance from the neodymium center Nd-N1 = Nd-N1' = 2.549(1) and Nd-N2 = Nd-N2' = 2.282(2) Å. Both N-pyridine and N-amido groups of the two ligands were in *trans* of each other. With a Nd-B distance of 2.648 Å, the borohydride was in a classical range for a tri-hapto coordination mode, where this tri-hapto coordinated ligand allowed to complete the coordination sphere without the need of an additional solvent molecule. Since the Nd-B distance was the longest one, it was automatically described as the axial ligand. Surprisingly, the torsion angle of the amido-pyridne chelate was not the same depending on the R or S enantiomers. While the chelate of the S configuration was slightly out of planarity [N1-C5-C6a-N2 = 10.98°], the chelate of the R configuration was highly distorted according to the twist angle N1-C5-C6b-N2 = -31.20°. The N-aryl group slightly deviated from orthogonality with respect to the pyridine ring by a few degrees (angle between the two planes: 85.58 °).

Developed by A. W. Addison *et al.*[20] the calculation of τ in a five substituents system such as this one allowed us to determinate the constraint on the metal and the percentage of distortion from a square pyramidal to a trigonal bipyramidal geometry. The value of τ oscillates between 0 and 1 where 0 correspond to a perfect square pyramidal geometry and 1 to a trigonal bipyramidal geometry. This geometric parameter was determined by the equation: $\tau = (\beta-\alpha)/60$ where β is the largest angle of the base (here N1-Nd-N1' = 152.118 °), α is the angle formed by the two other ligands and the metal (here

N2-Nd-N2': 124.403°). Complex **1'b** had a τ of 0.46 which implied a distortion of the square-based pyramid caused by the borohydride group.

^{1}H NMR of the crystals (**1'b**) presented below (Fig. 2.13) compared to the synthesis performed in ^{n}BuLi (**1'a**) show highly similar but not identical product.

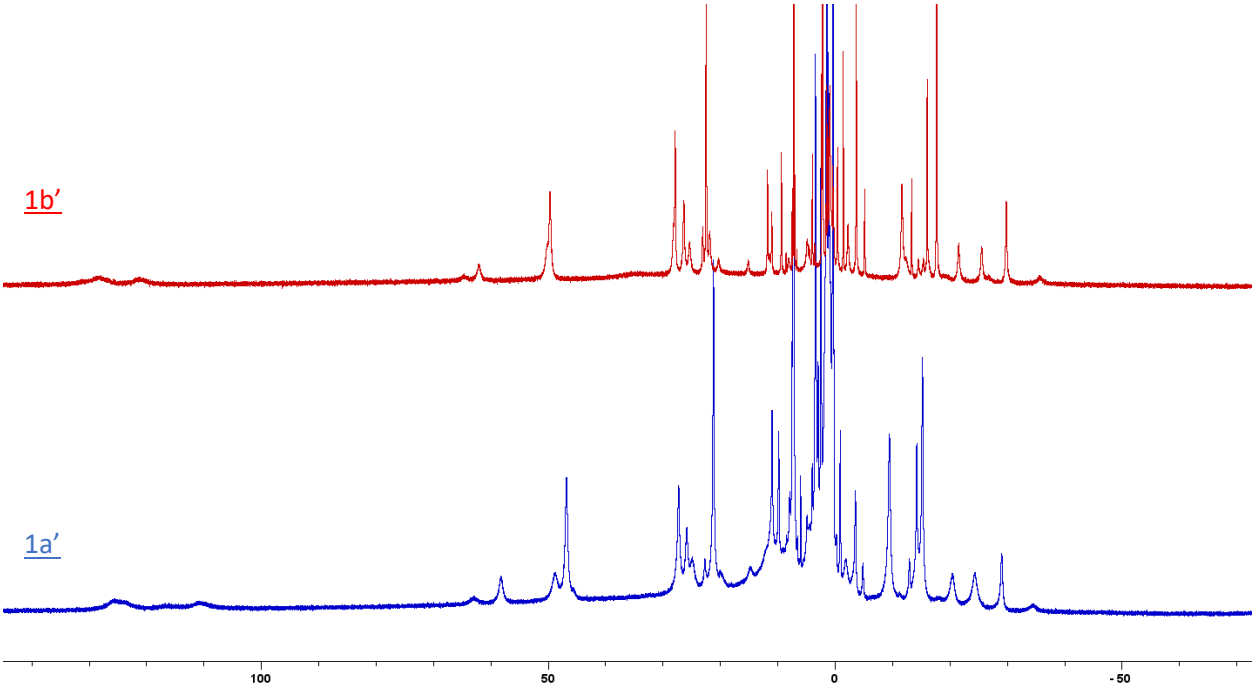

Figure 2.13: ^{1}H NMR of lithium synthesis (1'a) *vs*. the crystallized complex 1'b (solvent C_6D_6).

From this study, we could conclude that while the mono-substituted complex could not be obtained by the "B/A route", the bis-substituted complex was easily achieved with any base (BEM, ^{n}BuLi, MeLi) and whatever the neodymium tris-borohydride/ligand ratio, as illustrated in Scheme 2.10.

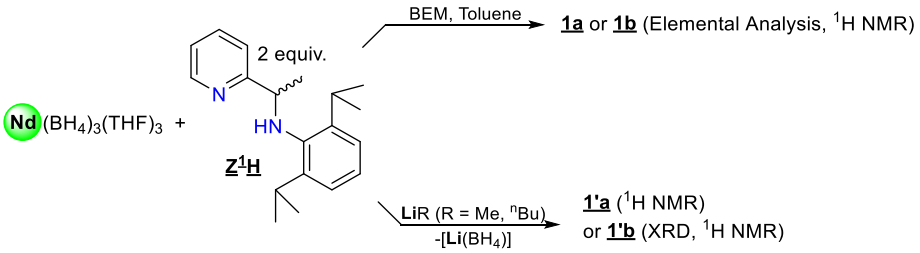

Scheme 2.10: Synthesis of bis-substituted borohydride complexes.

The following studies will focus on the synthesis of complexes with a bulkier ligand, specifically with a methyl group in the alpha position of the pyridine ring (**Z^{2}H**) in order to determine its influence

on structural parameters of the complexes and particularly on the degree of substitution of Nd borohydride.

2.2.2 Studies with Z^2 ligand

As done previously, we performed ^{1}H NMR monitoring using **Z^2H** and BEM, with one and two equivalents of the ligand, to investigate whether the additional methyl group provided sufficient steric hindrance to obtain, or not, a mono-substituted complex (Fig. 2.14). Addition of Nd(BH_4)$_3$(THF)$_3$ onto the protio-ligand **Z^2H,** followed by 0.5 equiv. of BEM, led to the appearance of paramagnetic peaks, which testified the formation of a Nd complex (Fig. 2.14 a). The spectrum represented in Fig. 2.14 a) was quite similar to that of the previously prepared complex (**Z^1**)$_2$Nd(BH_4) (Fig. 2.14 b), which facilitated the identification of the peaks belonging to the [**Z^2**]Nd complex (represented with + in Fig. 2.14). The addition of the second equivalent of protio-ligand/0.5 BEM showed no difference in the spectrum (Fig. 2.14 a *vs.* c): clearly the bis-substituted derivative [**Z^2**]$_2$Nd was not formed. However, upon closer inspection of the diamagnetic region (Fig. 2.14 a-a and c-c), diamagnetic peaks emerged in the spectrum (marked °) that could not be identified with either **Z^2H** (Fig. 2.14 d-d) or BEM + 0.5 **Z^2H** mixture (Fig. 2.14 e-e) and were thus supposed to be free **Z^2** present into the medium. Therefore, based on these preliminary ^{1}H NMR studies, we could assume that the added methyl group provided sufficient steric hindrance to prevent the formation of the bis-substituted compound.

The same approach as in the case of complex (**Z^1**)$_2$Nd(BH_4) could be applied to predict the assignment of the different peaks on the ^{1}H NMR spectra. The integration of the peaks shown in Fig. 2.14 b and b-b) revealed a total of 15 proton resonances. The broad signal observed at 76.5 ppm, which integrated for 8H, could be attributed to the borohydride groups, indicating that there were 14 peaks remaining for the ligand.

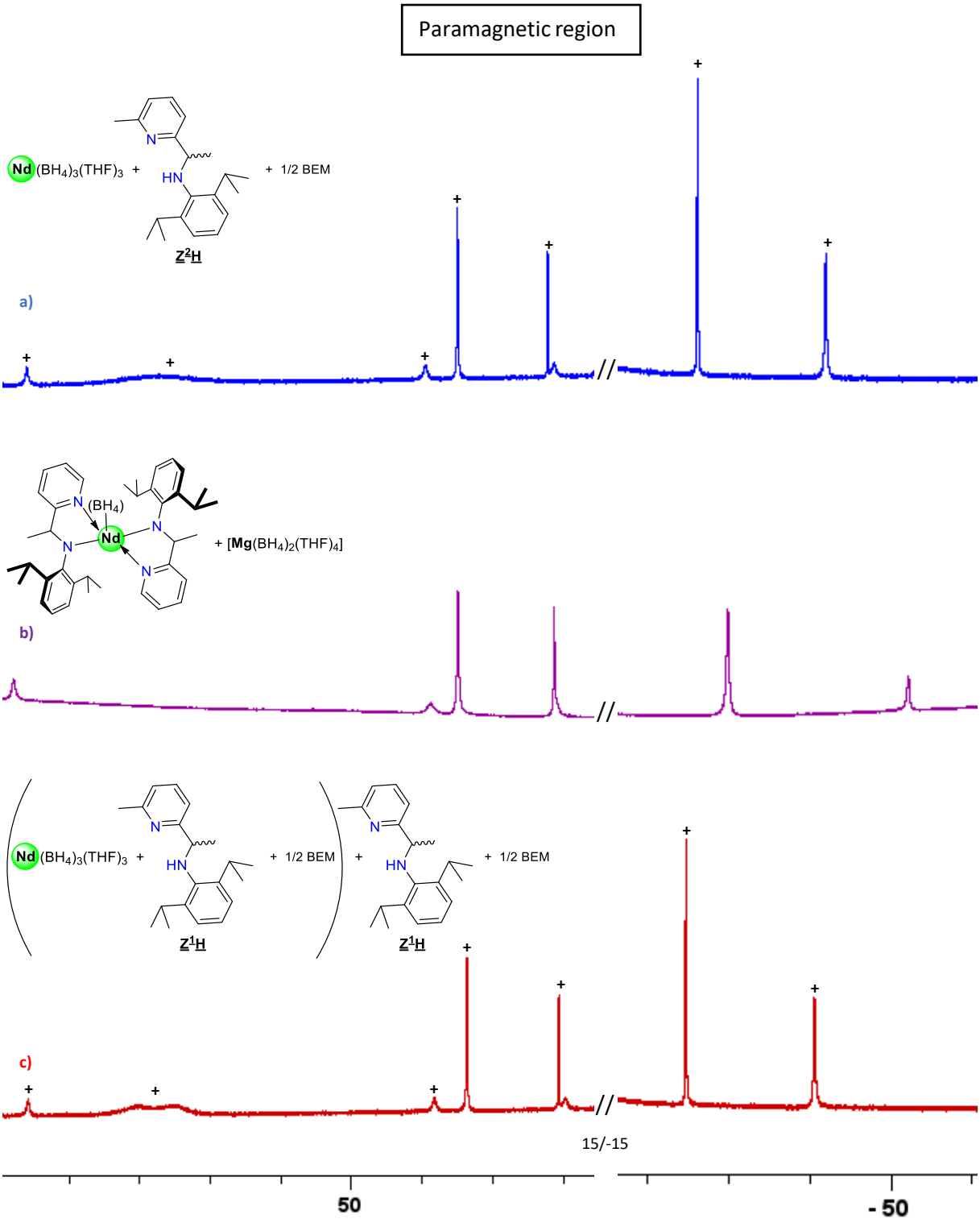
Paramagnetic region
Nd(BH4)3(THF)3 +
+ 1/2 BEM
Z2H
a)
(BH4)
Nd
+ [Mg(BH4)2(THF)4]
b)
Nd(BH4)3(THF)3 +
+ 1/2 BEM
Z1H
+
+ 1/2 BEM
Z1H
c)
15/-15
50
- 50

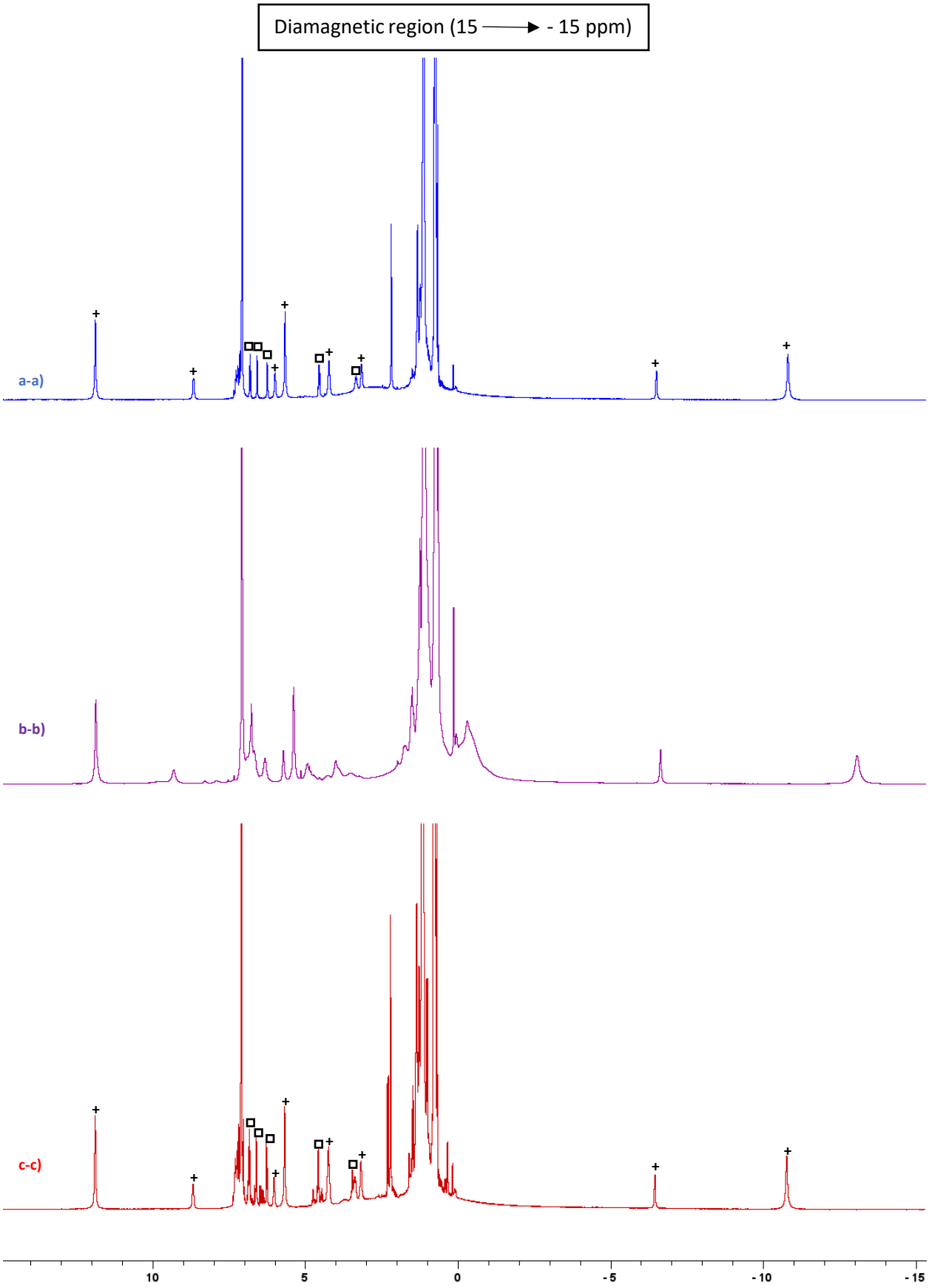
Diamagnetic region (15 ⟶ - 15 ppm)
a-a)
b-b)
c-c)
10
5
0
-5
-10
-15

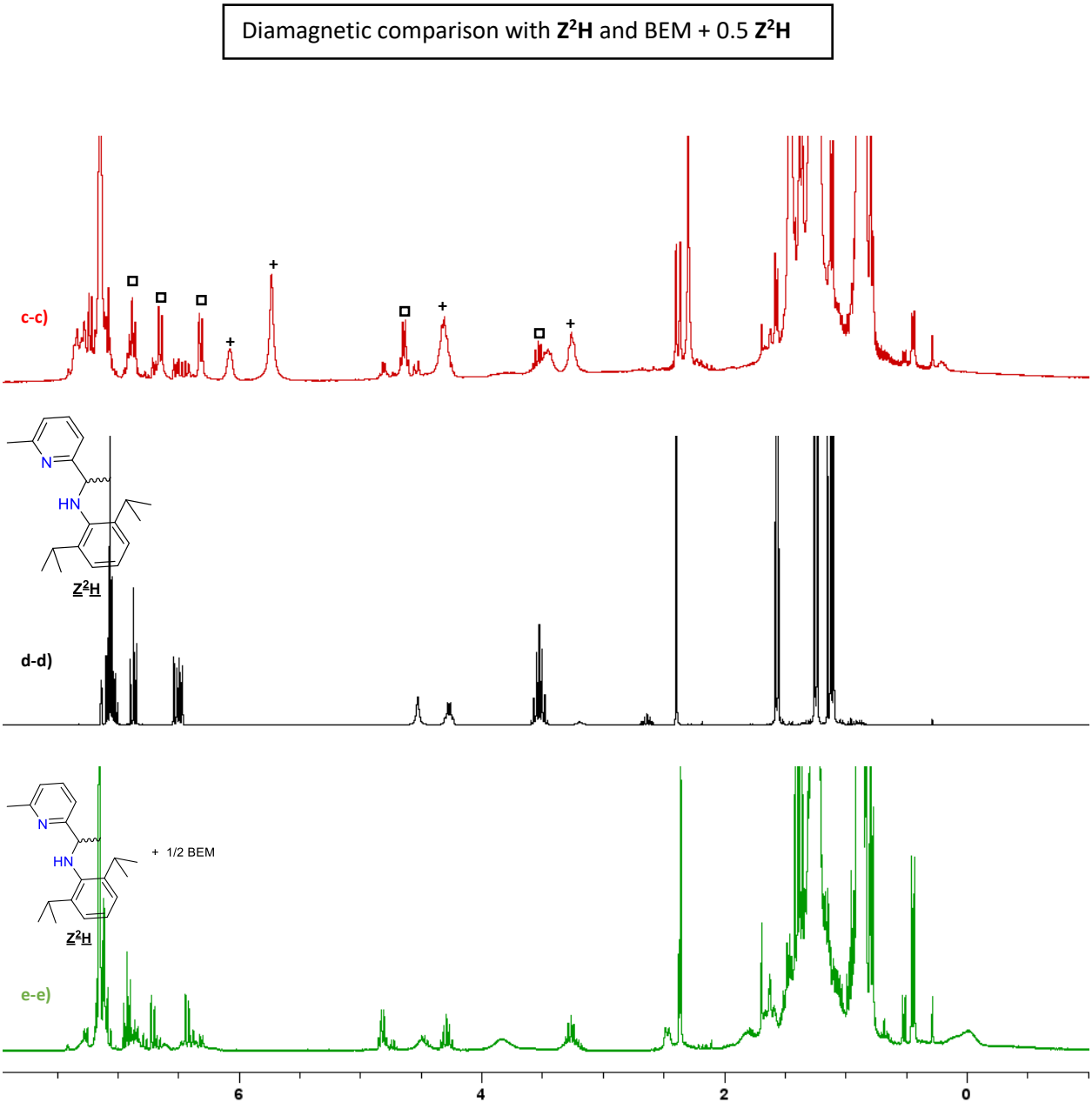

Figure 2.14: Preliminary ^{1}H NMR studies regarding the degree of substitution with Z^{2}H (+ signals of new Nd complex, ¤ additional signals, solvent C_6D_6).

As predicted, among the fourteen peaks related to the coordinated ligand, 7 resonances integrated for one proton at δ (ppm) = 95.86, 38.27, 20.62, 8.73, 6.09, 3.26 and -6.27 [3 x CH_{pyr}, 1 x CH_3(*CH*)-N, 1 x *CH*$_{Aryl}$, 2 x *CH*(CH_3)$_2$], 6 resonances for three at δ (ppm) = 33.68, 11.95, 5.76, -10.55, -24.7 and -40.62 [1 x *CH*$_3$-C_{pyr}, 1 x *CH*$_3$(CH)-N, 4 x CH(*CH*$_3$)$_2$] and 1 resonance at 4.31 ppm integrate for two protons corresponding to the meta-aryl position (Fig. 2.15).

During the bulk synthesis in THF, a similar color change from blue to green, as observed in the case of (**Z^1**)$_2$Nd(BH$_4$) occurred, which could be attributed to the coordination of the ligand to the neodymium center. *Vacuum* drying, filtration in toluene and washing in pentane provided a microcrystalline powder that was sufficiently clean for elemental analysis. The elemental analysis of the product corresponded to a mono-substituted heterobimetallic "ate" complex of formula {(**Z^2**)Nd(BH$_4$)$_3$[Mg(THF)$_6$]$_{0.5}$} (**3**) (Theo: C = 53.84%, H = 9.05%, N = 3.92%, Found: C = 53.70%, H = 8.82%, N = 3.66%), as conventionally obtained by the B/A route[16a-b] (Scheme 2.11).

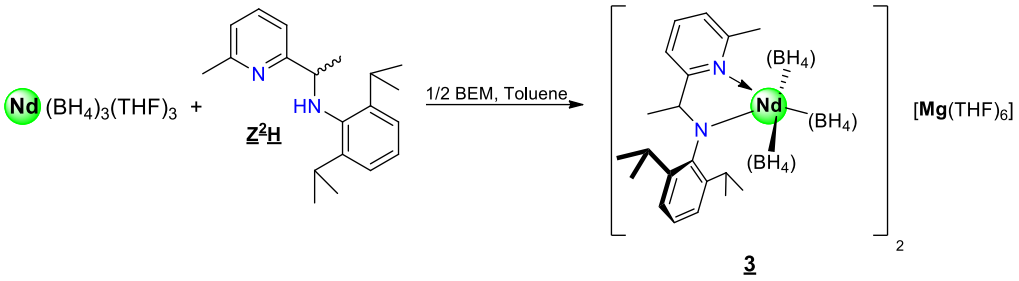

Scheme 2.11: Synthesis of [(Z^2)Nd(BH$_4$)$_3$]$_2$[Mg(THF)$_6$], 3.

Crystals suitable for XRD were obtained from a concentrated solution in THF with a vapor of pentane kept at -40 °C for several days. Quite surprisingly, the molecular structure in Fig. 2.16 displayed a magnesium-free neodymium complex. Selected bond distances and angles are listed in Table 2.2.

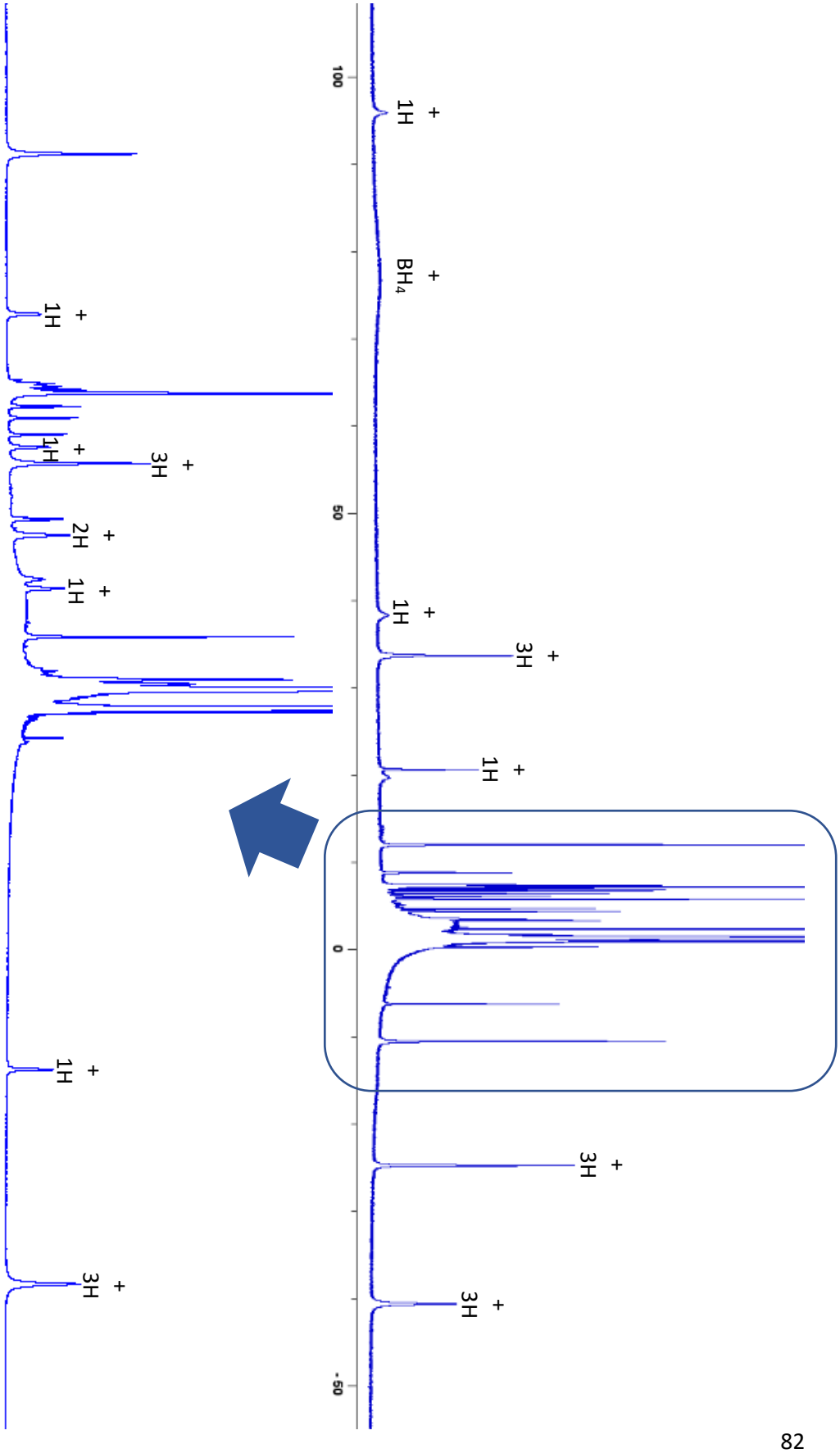

Figure 2.15: ^{1}H NMR spectrum of the paramagnetic complex obtain (Fig 2.14 a) and integration of the different peaks (solvent C_6D_6)

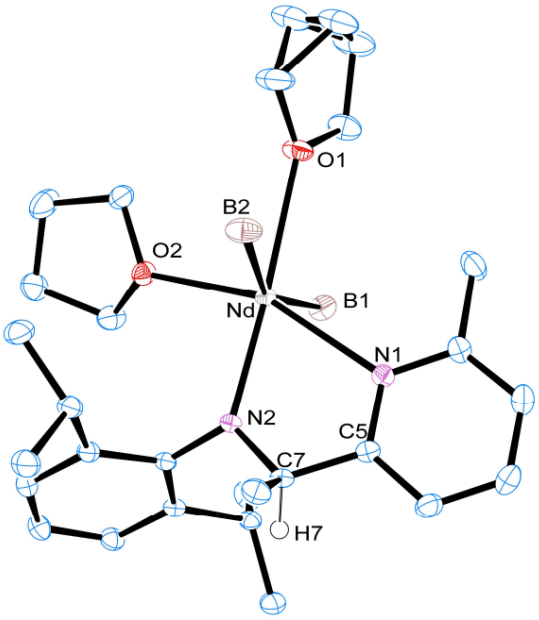

Figure 2.16: Molecular structure of magnesium-free (Z^2)Nd(BH$_4$)$_2$(THF) – complex 4, hydrogen omitted for more clarity. Thermal ellipsoids are drawn at the 50% probability level.

Complex **4** crystallized in the space group P2$_1$/c as a neutral mono-ligand bis-borohydride neodymium complex with two THF molecules coordinated to the neodymium center to complete the coordination sphere. The geometry of this complex was octahedral with the longest bond being Nd-O1 = 2.692 (1) Å. The THF molecule was in the axial position with N2 while N1, O2, B1 and B2 defined the equatorial positions. Packing of complex **4** exhibited both (R) and (S) enantiomers in the same unit cell. The coordinated pyridine and amido nitrogen atoms were at the same distance from the metal center as in the bis-substituted complex **1'b** (**1'b**: N1-Nd = 2.549(1) Å, N2-Nd= 2.282(2) Å *vs.* **4**: N1-Nd = 2.567(1) Å, N2-Nd=2.299(1) Å). Both borohydrides were in a classic range for a tri-hapto coordination mode [Nd-B1= 2.683(2) Nd-B2= 2.682 (2) Å] and were comparable to the Nd-B distance in **1'b**. A slightly higher twist of the amido-pyridine chelate was observed in **4** compared to **1'b** [N1-C5-C7-N2 = 18.90° *vs.* N1-C5-C6a-N2 = 10.98°, respectively]. Moreover, the N-aryl group deviated more from orthogonality with the pyridine plane in **4** (69.19°), compared to **1'b** (85.58°).

With respect to the formation of the mono-substituted **4**, such a compound could result from similar ligand exchange as seen for the formation of **2** at low temperature and subsequent elimination of Mg(BH$_4$)$_2$(THF)$_4$ as presented in Scheme 2.12.

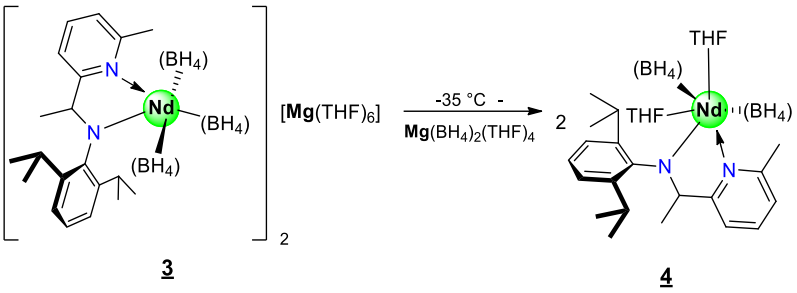

3 **4**

Scheme 2.12: Possible rearrangement leading to 4.

In order to further investigate the electronic/steric effect of an additional imine moiety in the α–position of the pyridine skeleton with this type of ligand on the coordination chemistry with neodymium, syntheses using **Z^{3}H** have been undertaken and are discussed below.

2.2.3 Synthesis of Nd borohydride complexes with Z^3 ligand

Since the additional methyl substituent on the α-position of the pyridine ring was sufficient to limit the coordination of a single **Z^2** ligand to the metal center (**3, 4**), the preparation of the neodymium analog in the presence of the tridentate ligand **Z^{3}H** was performed directly in bulk, according to Scheme 2.13, without prior ^{1}H NMR study. In this context, a solution of BEM was added to a mixture of Nd(BH$_4$)$_3$(THF)$_3$ and one equiv. of **Z^{3}H** in toluene, giving a red solution. After extraction and evaporation of the solvent, the resulting red powder was subjected to NMR analysis. The ^{1}H NMR spectrum revealed a set of paramagnetic peaks typical for a neodymium complex, ranging from -20 to 100 ppm (Figure 2.17). By focusing on the diamagnetic region, we could distinguish the resonances of the protio-ligand **Z^{3}H** (-) (which may have undergone hydrolysis in the solvent), leaving us with a total of 16 peaks corresponding to the complex (+). The broad resonance at 62 ppm integrated for 8H, which is assignable to the two BH$_4$ groups of the complex, and the other 14 signals were easily attributed to the ligand. The integration of the different peaks showed 5 resonances integrating for 1H [3 x C*H*$_{pyr}$, 2 x C*H*$_{Aryl}$], 4 signals integrating for 2H (2 x *meta*-C*H*$_{Aryl}$, 2 x C*H*(CH$_3$)$_2$), 1 signal for 3H which corresponds to the CH$_3$ carried by the imine at 7.33 ppm and 4 signals integrating for 6H [1 x (C*H*$_3$)$_2$C-N, 3 x CH(C*H*$_3$)$_2$] (Fig. 2.17). To match with the supposed structure a missing resonance integrating for 6 protons might be hidden under the solvent pics. Unlike the complexes **1a** and **3** already described, this complex **5** always exhibited a symmetrical plane (plane of the sheet), which allowed an equivalence between the isopropyl groups carried by the same aryl substituent.

Red crystals suitable for XRD and elemental analysis were obtained from standing a toluene solution for couple of days at room temperature. Elemental analysis (Theo: C = 60.87%, H = 8.13%, N = 6.15%, Found: C = 61.49%, H = 9.40%, N = 5.67%) was consistent with the molecular formula (**Z^3**)Nd(BH$_4$)$_2$ (**5**). The solid-state X-ray diffraction analysis, as represented in Fig. 2.18, was consistent with the elemental analysis results.

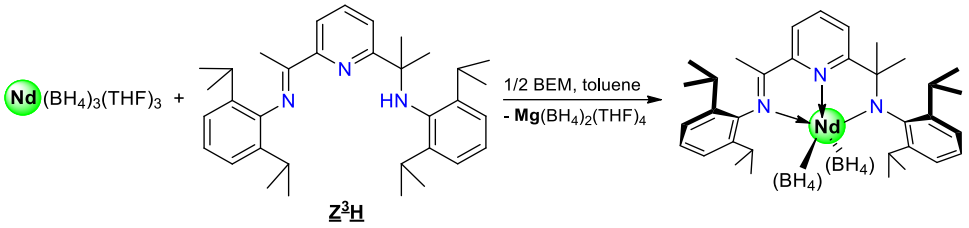

Z^{3}H **5**

Scheme 2.13: Bulk synthesis of amido-imino pyridine neodymium complex 5.

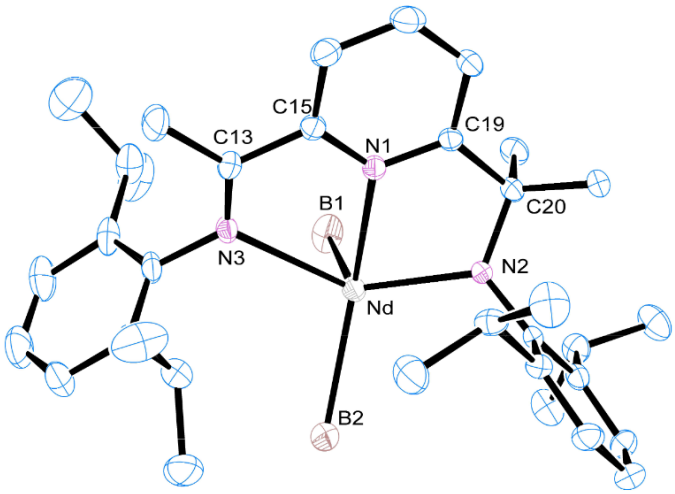

Figure 2.18: Molecular structure of 5, hydrogen omitted for more clarity. Thermal ellipsoids are drawn at the 50% probability level.

The X-ray structure showed a neutral neodymium species supported by one ligand and two borohydride groups, which crystallized in the P2$_1$/c space group. The two distances Nd-B1 = 2.593 Å and Nd-B2 = 2.611 Å were in classic range for the η^3 coordination mode. The imine bond C13-N3 = 1.281 Å and the amido bond C20-N2 = 1.490 Å were also in a typical range by comparison with complexes bearing similar ligands**21**. The bond lengths between the nitrogen of the pyridine and neodymium (N1-Nd = 2.512 Å) along with the nitrogen of the amido group and neodymium (N2-Nd = 2.257 Å) compared well with the ones found in

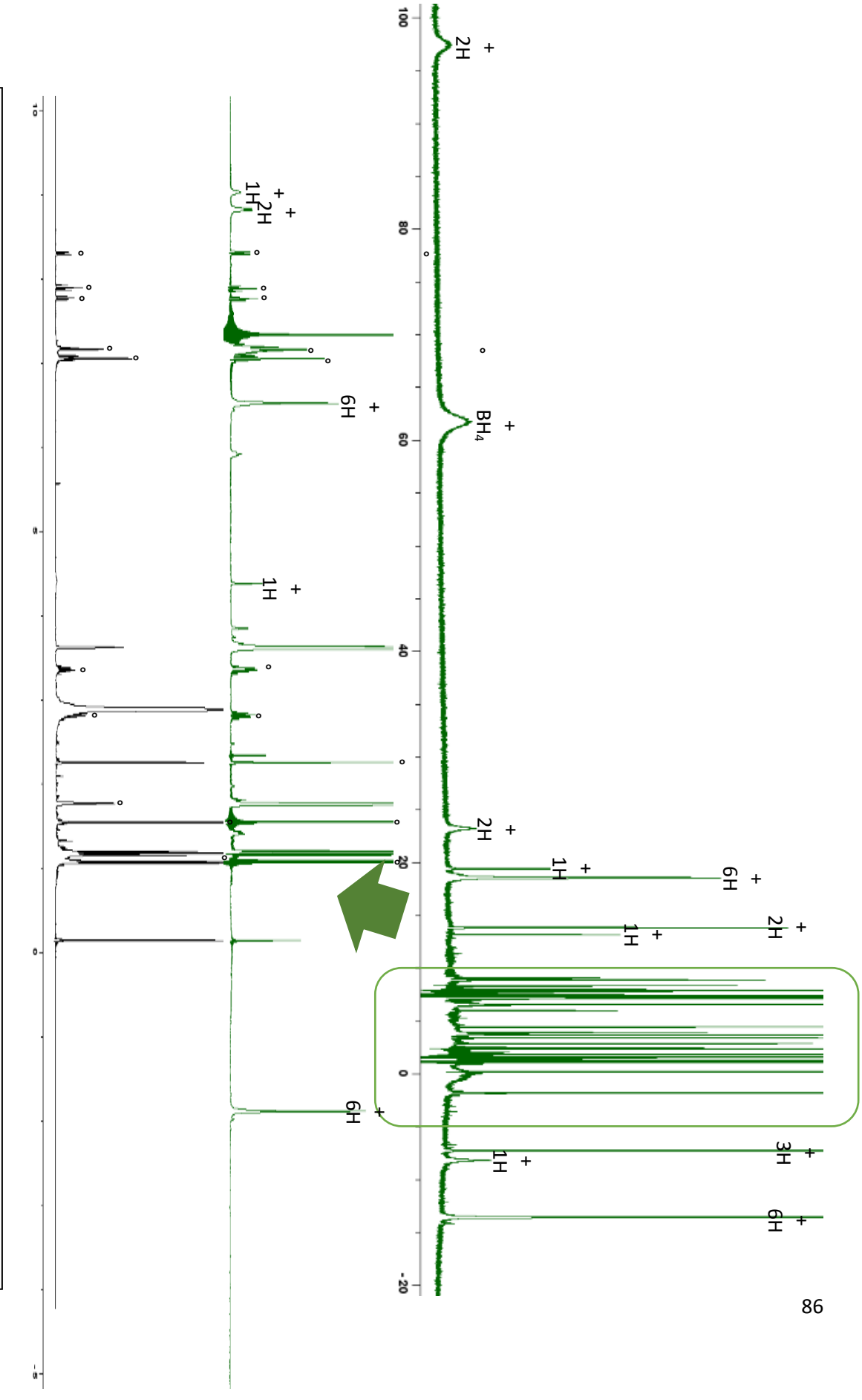

Figure 2.17: ^{1}H NMR spectrum of paramagnetic complex 5 [(Z^3)Nd(BH$_4$)$_2$] and comparison with ligand Z^{3}H (solvent THF-D$_8$)

complexes **1'b** and **4**. The N_{imine}-Nd distance (N3-Nd = 2.612 Å) was in a normal range according to the literature[21]. The torsion angles between the $N_{pyridine}$ and N_{imine} (N3-C13-C15-N1 = -1.26 °) chelating moiety showed that it was more planar than the $N_{pyridine}$ and N_{amido} chelate (N1-C19-C20-N2 = -24.08 °). The difference between N_{imine}-aryl and N_{amido}-aryl groups also influenced the orientation of their respective planes in relation to the pyridine ring. Specifically, the angle formed by the N_{imine}-aryl plane and the pyridine ring is 80.53°, indicating a lesser degree of orthogonality compared to the N_{amido}-aryl plane one, which formed an angle of 88.78° with the pyridine ring. However, after three days in the glovebox at room temperature, instability of the complex was observed by a change of color from red to white, with the product also becoming insoluble in toluene and THF. As described by Zimmermann *et al.* in 2008[22], rare earth complexes bearing amido-imino pyridine ligands can decompose into a white powder. This decomposition is supposed to be due to a poor coordination of the ligand and might be caused by intermolecular Nd-N associations caused by the labile nitrogen part[7b)].

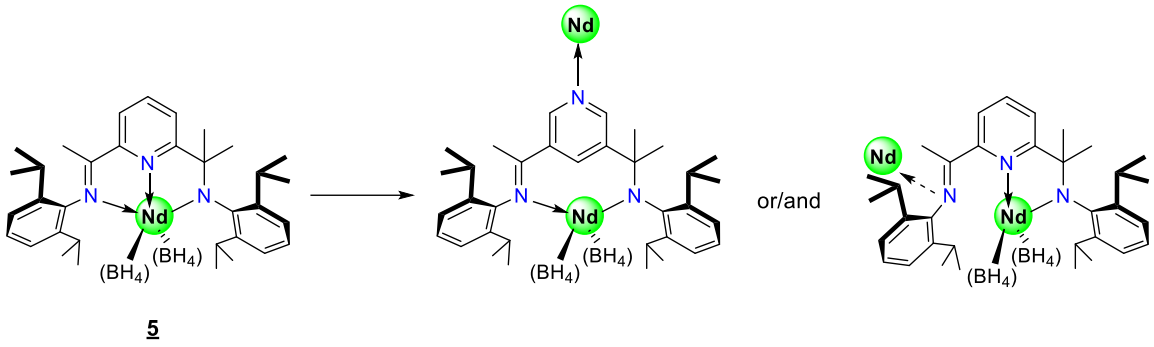

5

Scheme 2.14: Possible intermolecular Nd-N interactions as the result of possible evolution of 5 with time.

*Table 2.2: Selected bond distances and angles for **1'b**, **2**, **4** and **5**.*

	1'b	**2**	**4**	**5**
Nd…..B1 (Å)	2.648	2.983	2.683	2.593
Nd…..B2 (Å)	X	2.639	2.683	2.611
Nd-N_{pyr} (Å)	2.549	2.578	2.567	2.512
Nd-N_{Amine} (Å)	2.282	2.259	2.299	2.257
Twist angles Pyr/Amido	**Z^{1S}** : 12.94 ° **Z^{1R}** : -31.20°	3.31°	18.90 °	-24.08 °
Pyr *vs.* Aryl plan	85.58 °	74.81°	69.19°	88.78 °

This table compares the different neodymium complexes bearing **Z^1**, **Z^2** or **Z^3**. Every borohydride terminal unit were bonded (according to the Nd – B length) in a tri-hapto mode. The neodymium-nitrogen (pyridine or amine) bond length stayed in the same range among these complexes. The mono-substituted bridge [(**Z^1**)Nd(BH_4)(μ-BH_4)(THF)]$_2$ (**2**) showed the most planar chelate and, on the contrary, the most out of planarity was noticed with **1'b** when [**$Z^{1(R)}$**] was coordinated to the metal center. The complex bearing the tridentate ligand **Z^3** (**5**) showed the most orthogonality between the pyridine ring and the aryl plane.

This entire study indicated that the amidopyridine ligand **Z^1** was a particular case: it appeared to be at the steric hindrance limit to allow the formation of a stable bis-substituted derivative, while addition of a small substituent on the pyridine ring led to the formation and isolation of mono-substituted complex.

In summary of these studies, the coordination of amido-pyridine ligands to the neodymium center opened up a wide range of coordination possibilities, which might depend on many factors such as the temperature of synthesis, the nature of the solvent and others. On the other hand, we have shown that the magnesium species issued from BEM could also react and eventually remained associated to the neodymium counterpart under different forms.

In the following section, our investigations will focus on smaller rare earth elements like yttrium.

2.3 Yttrium amido-pyridine borohydride complexes

2.3.1 Study with Z^1 ligand

In addition to neodymium complexes, yttrium borohydride complexes bearing one or two amido-pyridine ligands have also been targeted for their application as potential polymerization catalysts. Since yttrium is smaller than neodymium, a difference in coordination and organometallic reactivity is to be expected. Follow-up ^{1}H NMR studies in C_6D_6 (shown in Fig. 2.19) using 1 and 2 equiv. of Z^1H with 1 equiv. of tris-borohydride of yttrium Y(BH_4)$_3$(THF)$_3$ as precursor, along with the adequate amount of BEM, were performed to determine whether the mono- and/or the bis-substituted derivative could be accessed and formed.

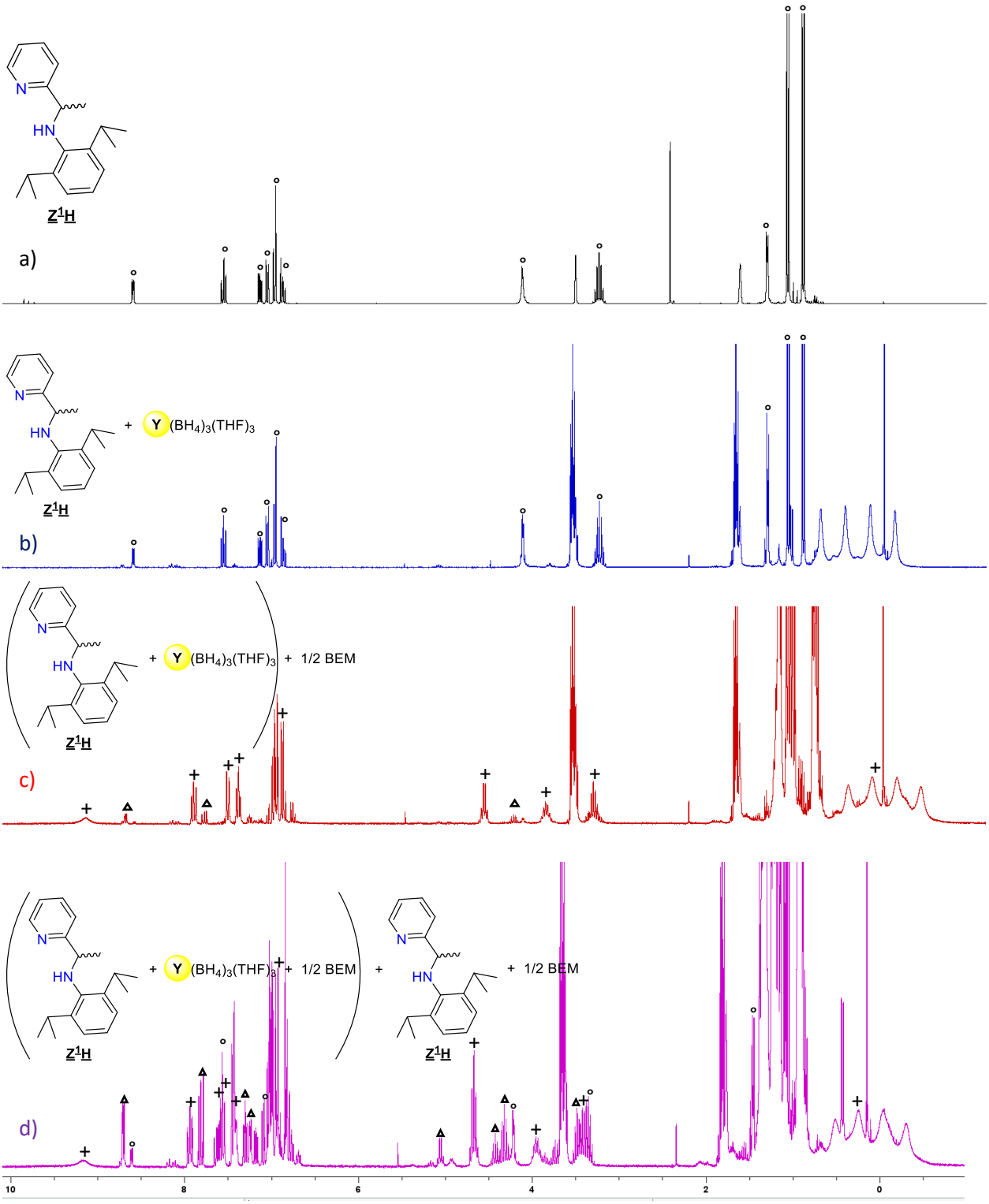

Figure 2.19: ^{1}H NMR monitoring for the reactivity of Y(BH$_4$)$_3$(THF)$_3$/Z^{1}H/BEM (+ = mono-substituted complex, ° = Z^{1}H, ▵ = by-product; solvent THF-D$_8$).

The ^{1}H NMR study, displayed in Fig. 2.19, revealed that no shift of the peak was observed when Y(BH$_4$)$_3$(THF)$_3$ was added to the ligand (Fig. 2.19 a *vs.* b). On the contrary, when half an equivalent of BEM was added in the NMR tube, an instantaneous shift of the signals occurs, indicating the effective coordination of **Z^1** to the metal center, and thus formation of a **Z^1**-substituted complex (+) (Fig. 2.19, c). The ^{1}H NMR spectrum of the formed yttrium borohydride complex exhibited a broad resonance at δ = 9.16 ppm, corresponding to the *ortho*-C*H*$_{pyr}$ proton. Additionally, there are several signals observed between δ = 7.5 and 6.2 ppm, which were consistent with the aryl and pyridine protons. Another typical resonance at δ = 4.66 ppm was observed as a quadruplet and could be attributed to the N-C*H* proton. The duplication of the septuplet shown at δ = 3.95 and 3.42 ppm integrating for 1H each corresponded to the C*H*-isopropyl protons. This duplication was similar to that displayed for **1a/1b** and **3** and could therefore be explained in the same way. Unfortunately, the region between δ = 1.5 and 0.8 ppm corresponding to C*H*$_3$-isopropyl and N-CH(C*H*$_3$) was not clearly visible, while the characteristic broad borohydride quartet at 0.14 ppm was well defined.

Addition of a second equivalent of **Z^{1}H** with another half-equivalent of BEM (Fig. 2.19, d) led to, according to the appearance of a new set of signals (▲), the formation of a second product, albeit in very low yield, which could potentially be a magnesium supported compound as suggested by the absence of a new borohydride signal. Unlike neodymium, the first appearing compound would be the mono-substituted yttrium bis-borohydride complex, which seemed easily reachable, while the bis-substituted derivative would be more difficult to obtain.

The bulk synthesis (Scheme 2.15) of this mono-substituted complex with 0.5 equivalent of BEM and one equiv. **Z^{1}H** was then conducted, leading to the isolation after work-up of a powdery material. This material was identified by elemental analysis (Theo: C = 57.83%, H = 9.57%, N = 4.35%, Found: C = 56.80%, H = 9.31%, N = 4.26%) as a heterobimetallic ionic "ate" yttrium-magnesium complex (**6**) of the form [(**Z^1**)Y(BH$_4$)$_3$]$_2$[Mg(THF)$_6$].

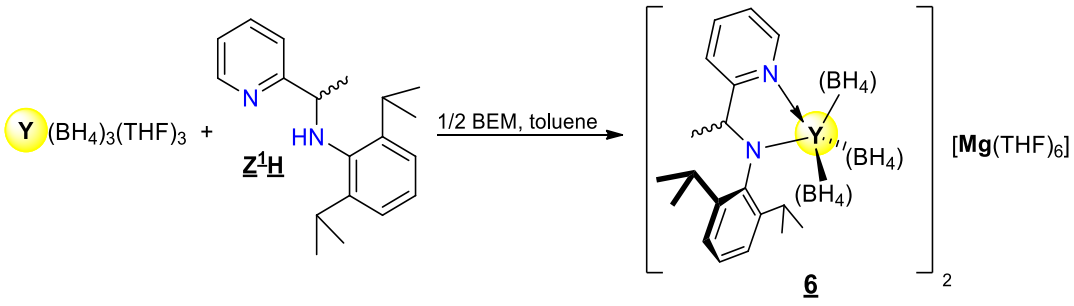

Scheme 2.15: Formation of the ionic pair [(Z^1)Y(BH$_4$)$_3$]$_2$[Mg(THF)$_6$], **6**.

Crystallization from a cold, concentrated THF solution with a pentane layer afforded a quantitative amount of crystals suitable for XRD. The molecular structure (Fig. 2.20) shows the product as drawn above and consistent with the elemental analysis. Selected bond distances and angles are listed in Table 2.3.

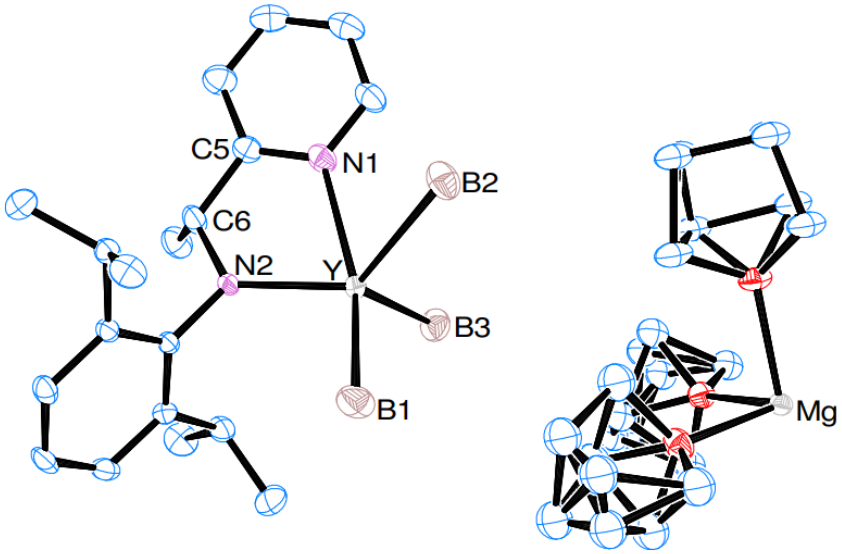

Figure 2.20: Molecular structure of mono-substituted borohydride $[(Z^1)Y(BH_4)_3]^-\{[Mg(THF)_6]^{2+}\}_{0.5}$ - complex 6. Hydrogens omitted for more clarity. Thermal ellipsoids are drawn at the 50% probability level.

Complex **6** crystallized in the P-1 space group and the molecular structure of **6** showed an ionic pair consisting of two anionic yttrium metals bearing one ligand $\mathbf{Z^1}$ as well as three BH_4 and $Mg(THF)_6$ as a counter-cation. While the distance between $N_{pyridine}$ of the chelating ligand $\mathbf{Z^1}$ and the metal center [N1-Y = 2.460(2) Å] was longer than in other neutral or anionic yttrium complexes bearing pyridine[23], the distance between the N_{amido} and yttrium [N2-Y = 2.205 (2) Å] was in a classic range for an "ate" complex[24]. In this complex, two borohydrides were placed in a typical distance range for a tri-hapto coordination mode [Y-B1 = 2.550 (3) Å, Y-B3 = 2.534 (4) Å] and one in a di-hapto mode [Y-B2 = 2.780 (3) Å] with no solvent coordinated to the metal center. The crystal packing showed on the same ionic pair the yttrium bearing the (R) ligand and another bearing the (S) configuration separated by the magnesium cation $[(\mathbf{Z^1})^SY(BH_4)_3][Mg(THF)_6][(\mathbf{Z^1})^RY(BH_4)_3]$. The N-aryl plane deviated from orthogonality with respect to the pyridine ring (68.95°) and was almost identical to that found in complex **4**, while

the amido-pyridine chelate was *quasi*-planar with a torsion angle of N1-C5-C6-N2 = 14.89°. ^{1}H NMR comparison between the crystalized complex and the *in-situ* formed was consistent with the formation of the same complex (Appendix 5).

As same as for the Nd complexes (**Z^1**)$_2$Nd(BH$_4$), which were obtained upon different experimental conditions, a synthesis in the case of Y using MeLi instead of BEM within the same synthetic procedure led to a mixture of products. Crystallization of one of the products from a concentrated yellow solution in toluene surprisingly revealed the formation of a bis-**Z^1** substituted yttrium borohydride (shown in Fig. 2.21) complex **7**. Selected bond distances as well as angles for that compound are listed in Table 2.3.

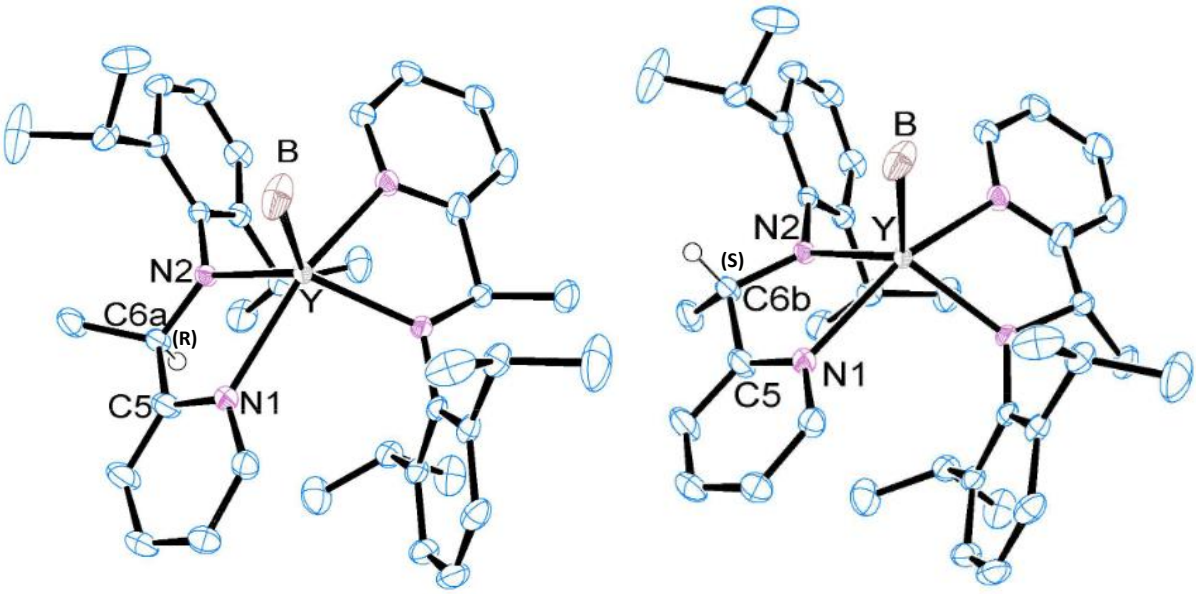

Figure 2.21: Molecular structure of (Z^1)$_2$Y(BH$_4$) – complex 7. Thermal ellipsoids are drawn at the 50% probability level.

Just like its neodymium analog **1'b**, **7** crystallized in the C2/c space group. The molecular structure of complex **7** presented a penta-coordinated yttrium center bound by two **Z^1** ligands (R and S at 50:50% occupancy) and one borohydride group, where its geometry could be best described as a distorted square-based pyramidal with the same geometric parameter τ = 0.47 as complex **1'b**. The N_{amido}-Y (N1-Y = 2.216 Å) bond distance was equivalent for both **Z^1** chelates as well as the $N_{pyridine}$-Y bond length (N2-Y = 2.437 Å), which were similar to those found in complex **6** (N_{amido}-Y = 2.205 and $N_{pyridine}$-Y = 2.461 Å). Both distances showed that the ligands were almost 0.1 Å closer to yttrium as compared to the neodymium complex (**1'b**), which was in accordance with the difference in the

crystalline ionic radius of these elements calculated by Shannon in 1976 for Y^{III} and Nd^{III} (coordination number of 8)[25].

With a Y-B distance of 2.530 Å, the length was in the typical range for a BH_4 coordination in the tri-hapto mode. The N-aryl plane and the pyridine ring were *quasi*-orthogonal to each other with an angle of 85.97°. As already described in **1'b**, the twist angle of the amido-methyl plane differed between the coordination of $\mathbf{Z^{1R}}$ [N2-C6a-C5-N1 = -12.46°] and $\mathbf{Z^{1S}}$ [N2-C6b-C5-N1 = 32.75°] conformers. Surprisingly, the coordination of $Z^{1(R)}$ on the neodymium resulted in the same torsion angle than the coordination of $\mathbf{Z^{1(S)}}$ on the yttrium and *vice versa* [N-C-C-$N_{Nd(\mathbf{Z1R})}$ ≈ N-C-C-$N_{Y(\mathbf{Z1S})}$, N-C-C-$N_{Nd(\mathbf{Z1S})}$ ≈ N-C-C-$N_{Y(\mathbf{Z1R})}$]. The twist angle of the R conformer was practically identical to that found in complex **6** despite the presence of a second ligand $\mathbf{Z^1}$ in **7**. As mentioned earlier, the same difference caused by steric hindrance was also observed in the neodymium complexes between **1'b** and **4**.

To investigate on the formation of this bis-substituted complex, different solvents/bases conditions were used, firstly at the NMR scale. While the synthesis with ^{n}BuLi in C_6D_6 afforded a mixture of products as soon as the first equivalent of the ligand was added (Appendix 6a), the same experiment performed in THF-D_8 upon ^{1}H NMR monitoring showed really interesting results and will be compared with the synthesis using BEM as shown in Fig. 2.22.

As can be seen in Fig. 2.22, the ^{1}H NMR spectra of the reactions mixing yttrium borohydride, $\mathbf{Z^1H}$ (1 or 2 equiv.) and BEM (0.5 or 1 equiv.) (Fig. 2.22, a and b) were quite similar to those using ^{n}BuLi as a base with 1 equiv. of $\mathbf{Z^1H}$ (Fig. 2.22, c), indicating the formation of the mono-substituted complex under these experimental conditions. Thus, it was likely that the same mono-substituted $\mathbf{Z^1}$ yttrium complex was obtained with BEM and with ^{n}Buli. However, complex **6** crystallized under an "ate" form with Mg^{2+} as counterpart, due to the presence of Mg in the reaction medium, which was performed *via* the B/A route.

The ^{1}H NMR spectrum issued from the reaction of 2 equiv. of $\mathbf{Z^1H}$ ligand with 2 equiv. of ^{n}BuLi seemed to lead to a different product (*) than that obtained when a second equivalent of ligand was added with the right equivalent of BEM (▲) (Fig. 2.22, b *vs.* d), suggesting the possible formation of a bis- substituted complex under such circumstances. The formation of this distinct borohydride complex was easily verified by the shift of the borohydride broad quartet resonance at δ = -0.4 ppm in Fig. 2.22, d. Also, the duplication of the isopropyl CH septuplet was observed at δ = 3.12 ppm and 4.3 ppm, as already seen in **6**. The quadruplet for the asymmetric carbon integrating for 2H was shown at δ = 4.76 ppm. Between 6 and 8 ppm, different signals corresponding to CH_{Aryl} and CH_{pyr} were displayed while the signal at δ = 8.46 ppm likely corresponded to the ortho protons of the pyridine.

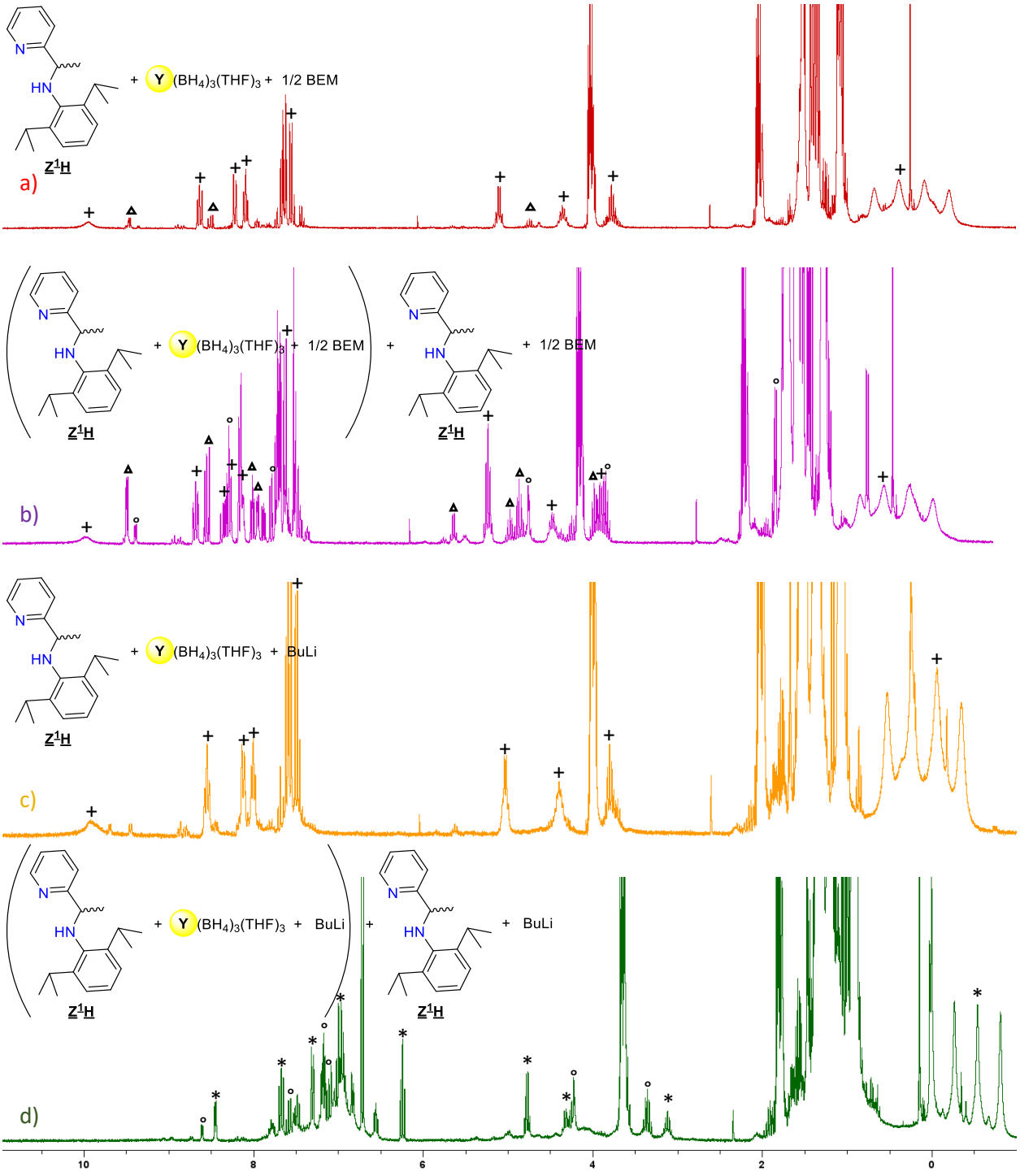

Figure 2.22: ^{1}H NMR BEM *vs.* ^{n}BuLi mono-ligand/ bis-ligand complex (+ = mono-substituted complex, ° = Z^{1}H, * = bis-substituted complex, ▵ = magnesium compound; solvent THF-D$_8$).

As said before, the same experimental procedure was performed in C_6D_6 but the addition of 1 equiv. of ligand with ^{n}BuLi led to an uninterpretable spectrum (Appendix 6a and 6b). The addition of the second equivalent of base/ligand in C_6D_6 led to a cleaner product according to ^{1}H NMR analysis,

but the data was still difficult to interpret compared to the spectra recorded in THF. The only difference between the two experiments lied in the solvent used and thus, the solubility of $Y(BH_4)_3(THF)_3$, which was higher in THF, could be the determining factor for the synthesis of the bis-substituted complex. This change in the coordination mode of the amido-methylpyridine ligand depending on the conditions of synthesis has already been observed by O. Hashmi *et al*. in 2022 for the synthesis of amido-methylpyridine iron complexes[10]: the formation of homoleptic iron complexes bearing two ligands **Z^1** was observed in THF, while the pure mono-substituted complex was obtained from a reaction carried out in pentane.

This study expressed the versatility of the **Z^1** ligand, which was highly dependent on the solvent and base used in relation to the desired product (Scheme 2.16). Based on this study, future syntheses (not described in this thesis) of bis-substituted yttrium complexes will be performed preferentially in THF instead of toluene and with ^{n}BuLi as a base reagent.

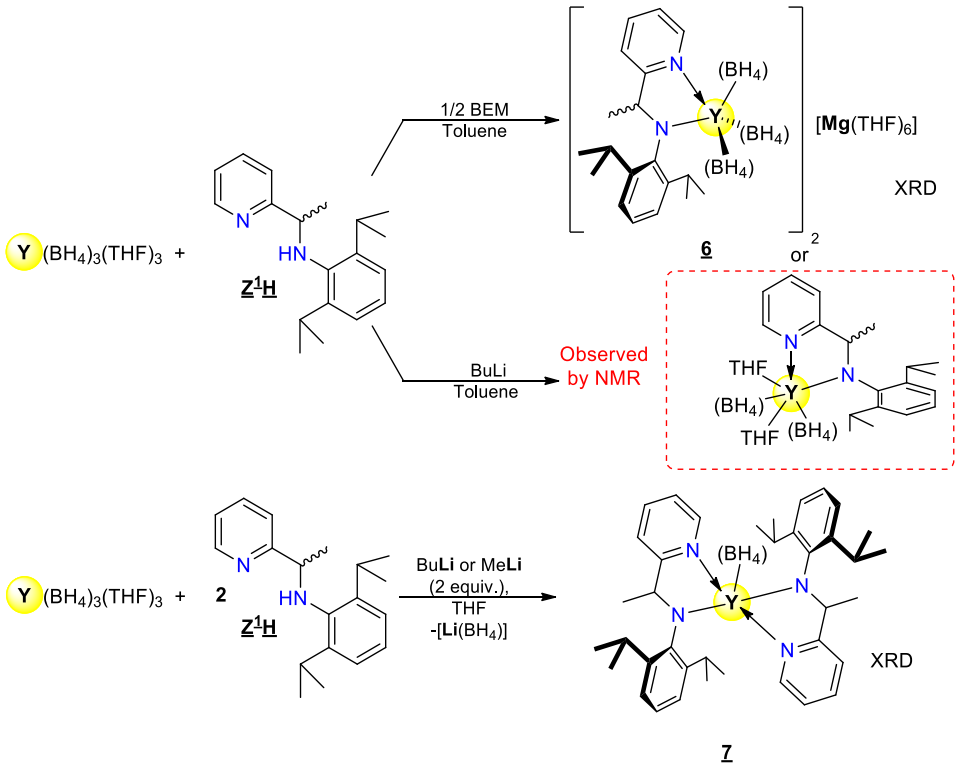

Scheme 2.16: Synthesis of (versatile Z^1 ligand) yttrium borohydride complexes 6 and 7.

2.3.2 Study with Z^2 ligand

As seen previously in the reaction of neodymium borohydride with **Z^2H**, bis-substituted complexes bearing two **Z^2** ligands are difficult to achieve due to the additional methyl group on the pyridine ring that provides more steric hindrance when compared to the ligand **Z^1**. Since the yttrium cation is smaller than the related neodymium, it is evident that the bis-substituted complexes can not be achieved, hence the synthesis of the mono-substituted complex was directly performed on a bulk scale using BEM as a base in toluene (Scheme 2.17). According to the result obtained for the preparation of **6**, we could expect that the general structure of the resulting complex will be that of an anionic yttrium moiety bearing a **Z^2** ligand and three BH_4 associated with the $Mg(THF)_6^{2+}$ cation.

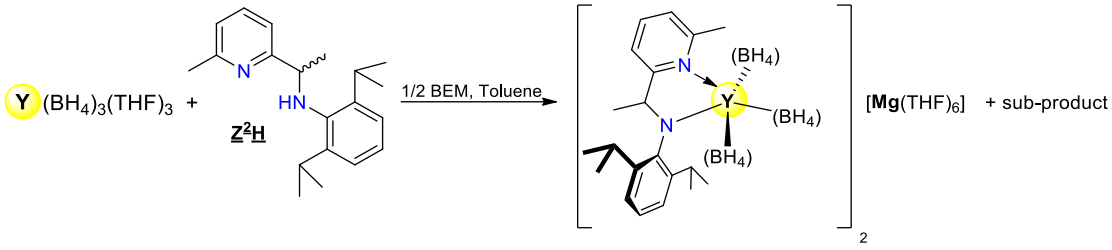

Scheme 2.17: Synthesis of [Z^2]yttrium complex using BEM as a base.

The ^{1}H NMR spectra between δ = 5 and 2 ppm showed (Fig. 2.23) the shift of the resonances from the protio-ligand **Z^2H** to the complex formed (Fig. 2.23 a *vs.* b). The previous ^{1}H NMR spectrum of the mono-substituted **6** revealed the same duplication of the septuplet corresponding to the CH-isopropyl, as observed here, at δ = 3.5 and 4.2 ppm. The presence of a second set of signals corresponding to a by-product (marked as ▲ in the spectrum) was also noted. Notably, a quadruplet at δ = 4.66 ppm could be observed, which corresponded to the proton carried by the carbon of the N-C*H* amido. Relative integration of these signals (quadruplets of the two products at δ = 4.56 and 4.66 ppm) gave an estimate of the by-product of *ca.* 30% of the total mass. The two sets of resonances observed by ^{1}H NMR (Fig. 2.23) might be attributed to the anionic [(**Z^2**)Y$(BH_4)_3]_2$[Mg$(THF)_6$] complex and this by-product.

Several attempts to isolate the mono-substituted ionic complex proved unsuccessful, and purification by crystallization of the desired product was therefore perfomed.

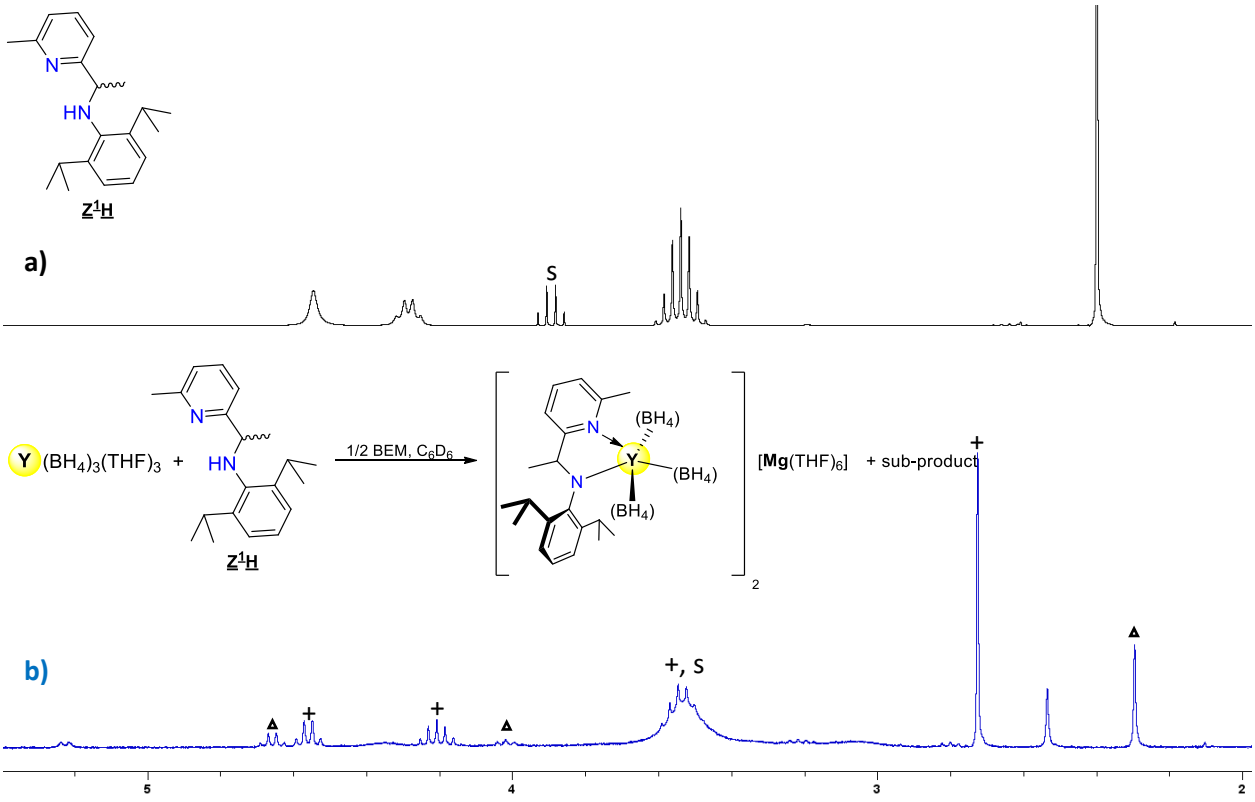

Figure 2.23: ^{1}H NMR of the bulk synthesis of $[(Z^{2})Y(BH_4)_3]_2[Mg(THF)_6]$ in the range 2 – 5 ppm. Yttrium complex (+), by-product (*), solvent (s), recorded in C_6D_6.

Unfortunately, all attempts to crystallize the desired yttrium complex resulted in the isolation of a product that did not contain yttrium [possibly the by-product identified with (▲) in Fig. 2.23 b], which appeared as yellow single-crystals suitable for X-ray diffraction studies. The molecular structure drawn in Fig. 2.24 shows a magnesium center bound by one borohydride and one $\mathbf{Z^2}$ ligand where the coordination was completed by an additionnal THF molecule. Selcted bond distances and angles are listed in table 2.3.

This magnesium complex might result from ligand exchange in solution just after formation of the desired yttrium product in the reaction medium. Already postulated for the formation of 2, the ligand exchange with the RE center might result in obtaining this magnesium compound.

Based on the hypothesis that the by-product observed in Fig. 2.23 corresponded to the magnesium derivative, we could assume that the exchange between the yttrium and the magnesium centers occured more conveniently to lead to $(\mathbf{Z^2})Mg(BH_4)$, whereas in the neodymium series complex 3 crystallized by precipitation from $Mg(BH_4)_2$. This difference in reactivity could be due to the difference of size between Y and Nd. This kind of exchange between magnesium species and allyl rare

earth complexes has already been studied[26] but not with borohydrides. To our knowlegdge only a few examples of mono-borohydride magnesium complex bearing an organic ligand have been synthesized[27].

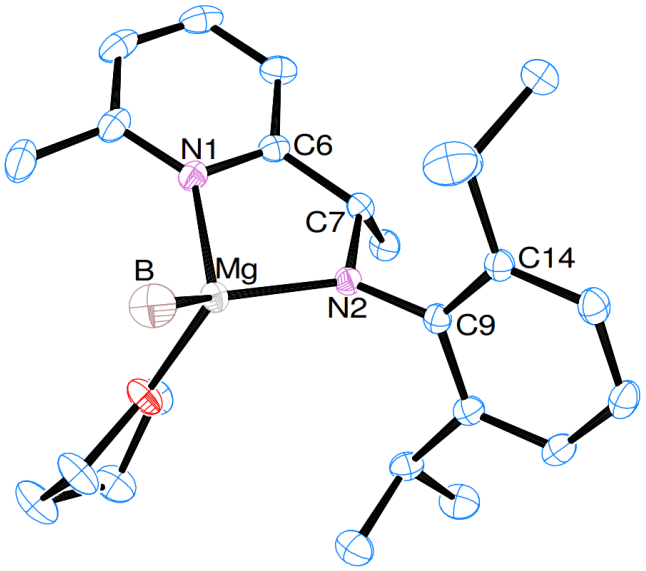

Figure 2.24: Molecular structure of (Z^2)Mg(BH$_4$)—complex 8. Thermal ellipsoids are drawn at the 50% probability level.

This magnesium complex **8** crystallized in the P2$_1$/c space group. The unit cell contained two similar complexes with the two enantiomeric (R) and (S) ligands coordinated to the metal center. The molecular structure displayed shorter N$_{amido}$-Mg [Mg-N2 = 1.963 (1) Å] and N$_{pyridine}$-Mg [Mg-N1 = 2.126 (1) Å] bond lengths[28] than in the yttrium complex **7** (Y-N$_{pyridine}$ = 2.437 Å and Y-N$_{amine}$ = 2.216 Å), in accordance with the ligand being closer to the metal center in **8** than in **7**. The Mg-B bond distance of 2.268 (2) Å was in a typical range for a η^3 coordination mode to magnesium[27]. In this structure, the amido-methylpyridine chelate was slightly distorted as seen with the torsion angle N1-C6-C7-N2 of -10.89 °, which resulted in an angle of 6.54 ° between the pyridine ring and the amido-methyl plane. Meanwhile, the N-aryl plane and the pyridine ring were not orthogonal to each other with an angle of 72.08 ° between the planes.

The possible reaction leading to this magnesium compound presented in Scheme 2.18 proposed a potential rearrangement from the desired yttrium complex under an ionic pair to the magnesium compound, along with the formation of tris-borohydride of yttrium and the neutral yttrium species, which has not yet been isolated. Since both products have similar properties, their separation by solubility differences of one of the products was difficult, and therefore other synthetic routes were

thought of to obtain a pure yttrium complex. The synthesis using BEM in THF was not explored because, as previously mentioned, this solvent helped in the formation of **7** by promoting ligand exchange.

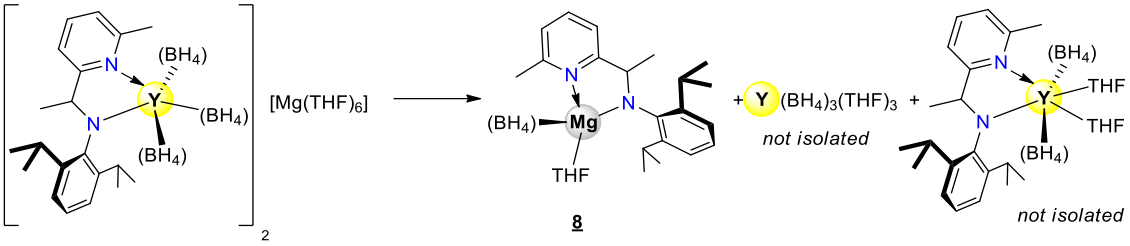

Scheme 2.18: Possible rearrangement pathway leading to 8 and Y by-products.

To avoid the problem of ligand exchange and obtain the targeted yttrium complex, attempts using ^{n}BuLi as a base were made. As can be seen from the ^{1}H NMR spectrum in Fig. 2.25, this strategy proved to be valuable, leading to a cleaner spectrum, with the same peaks shift compared to the ^{1}H NMR of the synthesis with BEM (Fig. 2.25 a *vs.* b). This allowed us to suggest that this product might be the same as the one obtained with BEM. The ^{1}H NMR spectrum shown in Fig. 2.25 b) exhibited three clean signals integrating for 1H at δ = 6.88, 6.55 and 6.33 ppm, while the rest of the pyridine/aryl protons were between δ = 7.2 and 7 ppm. The quadruplet at δ = 4.54 ppm and the singlet at δ = 2.76 ppm were assigned to N-C*H*(CH$_3$) and N-CH(C*H$_3$*). As with complexes **1a/1b**, **3**, **6** and **7**, a splitting of the CH-isopropyl was observed at δ = 4.23 and 3.55 ppm (partly hidden by THF resonance). Unfortunately, the CH$_3$-isopropyl and BH$_4$ peaks could not be observed unambiguously.

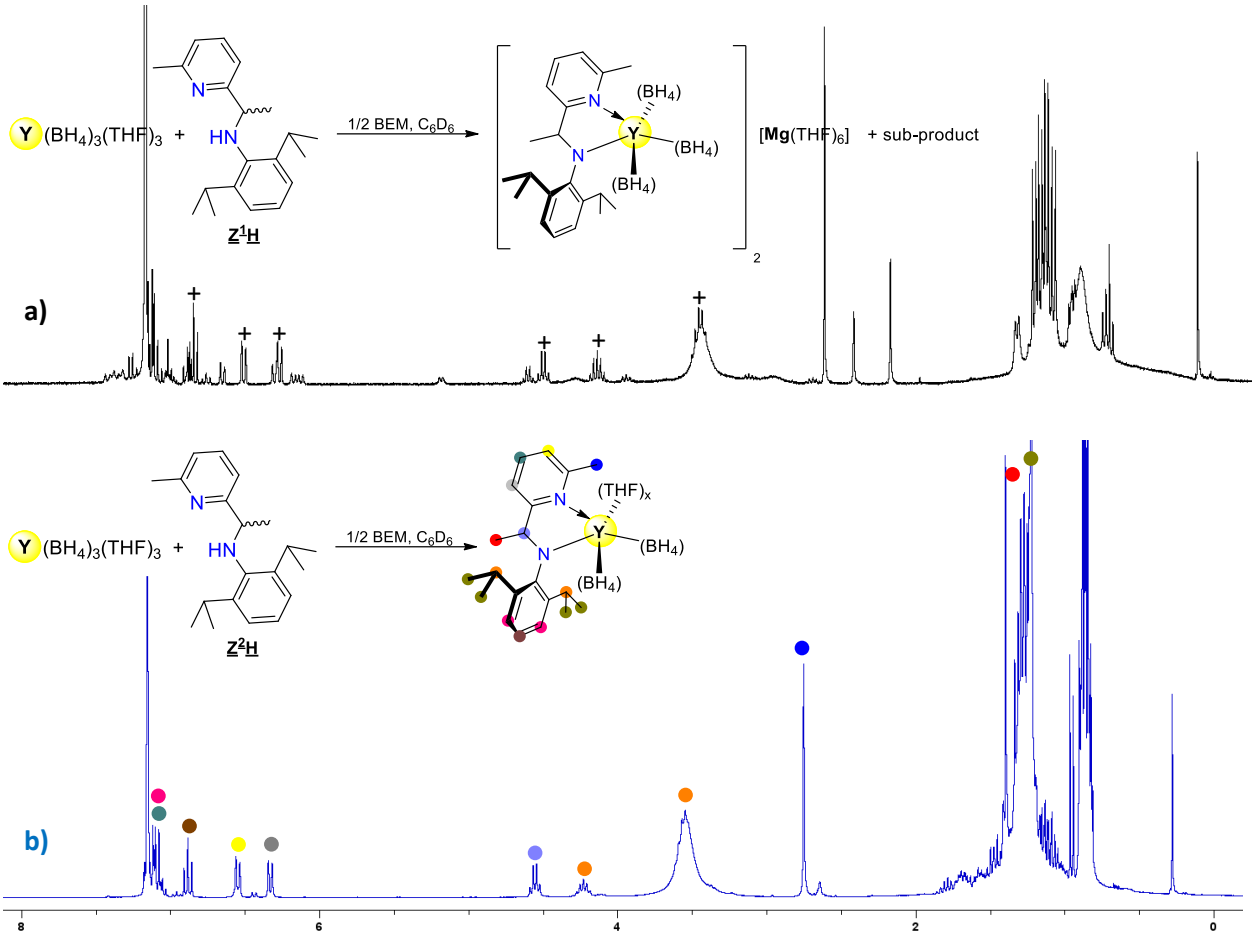

Figure 2.25: Comparison of the synthetic pathway using BEM and ^{n}BuLi for the [Z^2]-yttrium complex (+); solvent C_6D_6.

Based on these ^{1}H NMR studies, the synthesis shown in Scheme 2.19 leading to the neutral complex (**9**) could be deduced, and bulk synthesis will be performed in the future as shown in Scheme 2.19.

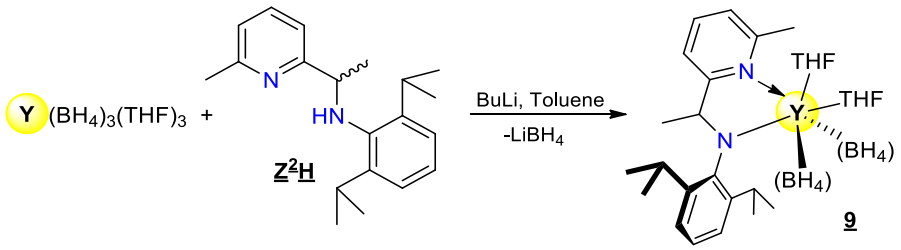

Scheme 2.19: Bulk synthesis of [Z^2]-yttrium complex 9 using ^{n}BuLi.

The study of the coordination chemistry of yttrium borohydride with the **Z^2** ligand demonstrates the importance of the ligand exchange that may occur when magnesium is present in

the reaction mixture. The next study, using the tridentate **Z^3** ligand, will allow us to foresee if the presence of an additional coordination site in the ligand, compared to **Z^1** and **Z^2**, will allow easier coordination with yttrium.

2.3.3 Attempted synthesis of yttrium complexes using amido-imino pyridine ligand Z^3.

Following the results obtained with Z^{2}H, a synthesis using Z^{3}H and BEM as a base was carried out according to Scheme 2.20. The preliminary ^{1}H NMR study using BEM led to an uninterpretable spectrum (Appendix 7).

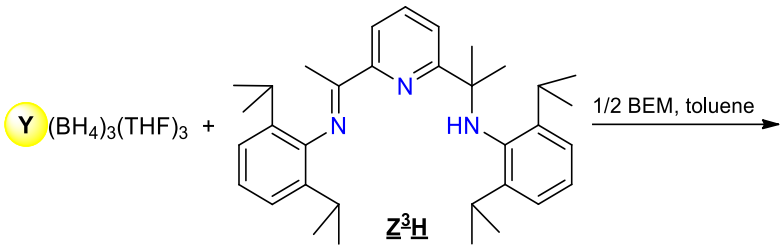

Scheme 2.20: Attempt synthesis of borohydride yttrium complex supported by Z^{3}H.

From the concentrated solution in the NMR tube and after standing for a few days, brown crystals suitable for XRD were obtained, which established the formation of a mono-ligand **Z^3** magnesium borohydride complex (**10**) (Fig. 2.26). Selcted bond distances and angles are listed in table 2.3.

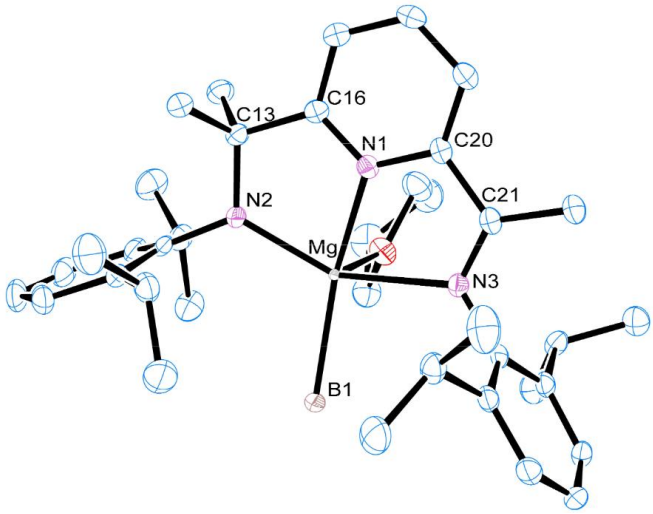

Figure 2.26: Molecular structure of (Z^3)Mg(BH$_4$) – complex 10. Thermal ellipsoids are drawn at the 50% probability level.

Like the precedent magnesium complex **8**, this compound crystallized in the $P2_1/c$ space group. The molecular structure of **10** presented a neutral magnesium center supported by the tridentate $\mathbf{Z^3}$ ligand and a borohydride group, which was completed by an additional THF molecule. The nitrogen-magnesium bond distances [$N1_{amido}$-Mg = 2.059 (2) Å, $N2_{pyridine}$-Mg = 2.150 (2) Å and $N3_{imine}$-Mg = 2.408 (2) Å] were similar to those found for a related Mg complex with an alkyl group instead of BH_4[28], and the carbon-imine bond length [C21-N3 = 1.284 (2) Å] was within the typical range for C(sp^2)-N bond distance. As with 8, the magnesium borohydride bond length of 2.328 (2) Å was consistent with a BH_4-coordination in a tri-hapto mode. Both N-aryl planes and pyridine ring were practically orthogonal with an angle of 82.63 ° for the plane made by the imine moiety and 84.68 ° for the plane of the amines part, while both amido and imino-methyl planes were almost coplanar, as demonstrated by the twist angle (N1-20-C21-N3 = 1.74 °, N1-C16-C13-N2 = -0.37 °). The orthogonality of the N-aryl plane and the planarity of the amido/imino-methyl plane versus the pyridine plane were more marked for this magnesium complex 10 than the previous one 8.

*Table 2.3: Selected bond and angles for **6**, **7**, **8** and **10** (M = Y or Mg)*

	6	7	8	10
M…..B1 (B3) (Å)	2.550 (2.534)	2.530	2.268	2.328
M…..B2 (Å)	2.780	X	X	X
M-N_{pyr} (Å)	2.460	2.437	2.126	2.150
M-N_{Amido} (Å)	2.205	2.216	1.963	2.059
Twist angles Pyr/Amido	14.89	$\mathbf{Z^{1S}}$: 32.75 ° $\mathbf{Z^{1R}}$: -12.46	-10.89	-0.37
Pyr *vs.* Aryl plan	68.95	85.97	72.08	82.63

This table provides an easy comparison of the yttrium $\mathbf{Z^1}$ complexes (mono- vs. bis-substituted). While one Y–B length showed a di-hapto coordination mode of one of the borohydride in **6** [($\mathbf{Z^1}$)Y(BH_4)$_3$]$_2$[Mg(THF)$_6$], all others BH_4 were in a tri-hapto mode. Both complexes showed *quasi*-identical Y-N (pyridine and amido) bond length. The observed twist angle of the amido chelate in complex **6** was quite similar to that obtained when $\mathbf{Z^{1R}}$ was coordinated in the bis-substituted complex (**7**), while that seen with $\mathbf{Z^{1S}}$ was higher. Already discussed previously, the orthogonality of the pyridine ring to the aryl plane was more pronounced in the bis-substituted complex, probably due to steric hindrance induced by the coordination of the second ligand.

The Mg–N (pyridine and amido) and Mg–B present in both magnesium complexes (**8** and **10**) were in the same distances range. Probably caused by the rigidity induced by the imine moiety, the amido-pyridine chelate observed in **10** was more planar than that observed in complex **8** where $\mathbf{Z^2}$ is coordinated.

Unfortunately, the various synthetic tests using ^{n}BuLi, although a color change was observed on some occasions, led to uninterpretable ^{1}H NMR spectra, without the presence of signals characteristic of an yttrium complex (Appendix 7). At the present time, the synthesis of the yttrium borohydride bearing $\mathbf{Z^3}$ ligand is still in progress.

2.4 Conclusion

In summary, the synthesis of borohydride rare earth complexes using amidopyridine ligands is really exciting but a challenge, which depends on many different experimental parameters such as the solvent that may or not allow for better ligand exchange (THF or toluene) and the metal base (lithium or magnesium) used, which can leave metal counterpart in the final structure of the isolated products. These complexes can either crystallize and confirm the substitution degree, as identified by elemental analysis, as neutral bis-substituted complexes (**1'b**, **7**), mono-substituted ion pair complex (**6**) or neutral mono-substituted complex (**5**). However, rearrangement during crystallization may lead to a different degree of substitution than initially identified by elemental analysis. Indeed, crystallization of the ionic pair $[(\mathbf{Z^2})Nd(BH_4)_3]_2[Mg(THF)_6]$ results to the formation of the neutral complex 4 while all attempts to crystallize yttrium complexes lead to the undesirable but interesting magnesium borohydride complexes **8** and **10**. All the complexes synthesized in this chapter are depicted in Fig. 2.27.

Some of these complexes will be studied as initiators for Ring Opening Polymerization of cyclic esters. This is described in Chapter 4 of this manuscript.

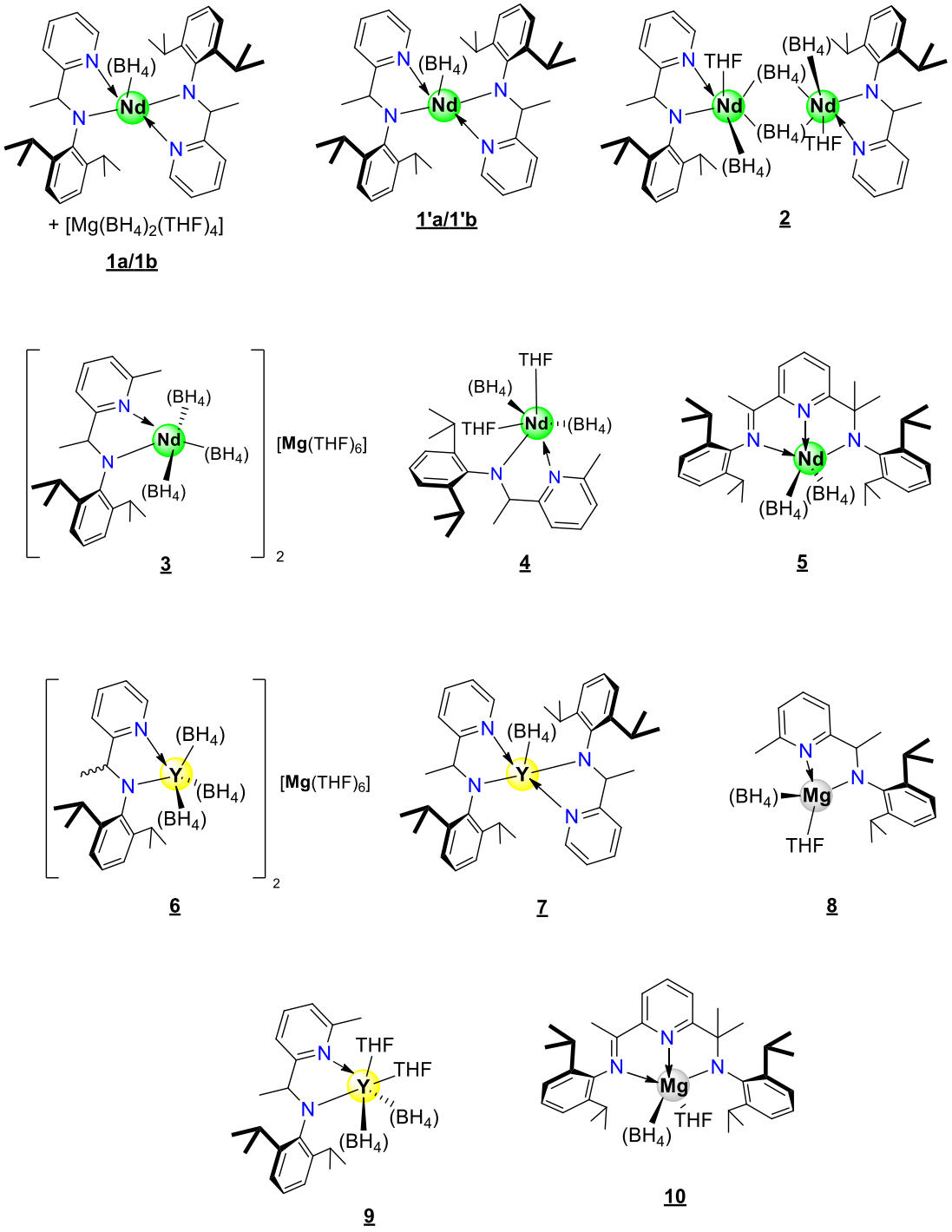

Figure 2.27: The borohydride rare earth amidopyridine complexes synthesized in this work.

References

[1] M. Westerhausen, T. Bollwein, N. Makropoulos, S. Schneiderbauer, M. Suter, H. Nöth, P. Mayer, H. Piotrowski, K. Polborn, A Pfitzner, **Eur. J. Inorg. Chem.**, *2002*, (2), 389.

[2] (a) Y.-C. Lin, K.-H. Yu, S.-L. Huang, Y.-H. Liu, Y. Wang, S.-T. Liu, J.-T. Chen, **Dalton Trans.**, *2009*, (41), 9058; (b) S. Zai, F. Liu, H. Gao, C. Li, G. Zhou, S. Cheng, L. Guo, L. Zhang, F. Zhu, Q. Wu, **Chem. Commun.**, *2010*, 46 (24), 4321; (c) Y.-C. Lin, K.-H. Yu, Y.-F. Lin, G.-H. Lee, Y. Wang, S.-T. Liu, J.-T. Chen, **Dalton Trans.**, *2012*, 41 (22), 6661; (d) K.-H. Yu, S.-L. Huang, Y.-H. Liu, Y. Wang, S.-T. Liu, Y.-C. Cheng, Y.-F. Lin, J.-T. Chen, **Molecules,** *2017*, 22, 1095; (e) D. M. Lovett, L. M. Thierer, E. E. P. Santos, R. L. Hardie, W. G. Dougherty, N. A. Piro, W. S. Kassel, B. M. Cromer, E. B. Coughlin, D. L. Zubris, **J. Organomet. Chem.**, *2018*, 863, 44.

[3] (a) S. Nayab, H. Lee, J. H. Jeong, **Polyhedron**, *2012*, 43 (1), 55; (b) H. Ahn, M. K. Chun, E. Kim, J. H. Jeong, S. Nayab, H. Lee, **Polyhedron**, *2017*, 127, 51; (c) J. Cho, M. K. Chun, S. Nayab, J. H. Jeong, **Polyhedron**, *2019*, 163, 54.

[4] (a) S. Kim, D. Kim, H.-J. Lee, H. Lee, **Polyhedron**, *2014*, 77, 66; (b) S. H. Ahn, J. Shin, S. Nayab, H. Lee, Bull. **Korean Chem. Soc.**, *2016*, 37 (5), 763; (c) H. Cho, M. J. Jung, J. Jeon, H. Lee, S. Nayab, **Inorg. Chim. Acta,** *2019*, 487, 221; (d) S. Park, J. K. Lee, H. Lee, S. Nayab, J. W. Shin, **Appl. Organomet. Chem.**, *2019*, 33 (4), e4797.

[5] A.A. Trifonov, D.M. Lyubov, **Coord. Chem. Rev.**, *2017*, 340, 10.

[6] A.A. Trifonov, **Coord. Chem. Rev.**, *2010*, 254 (11-12), 1327.

[7] (a) T. M. Cameron, J. C. Gordon, R. Michalczyk, B. L. Scott, **Chem. Commun**, *2003*, (18), 2282; (b) F. Estler, G. Eickerling, E. Herdtweck, R. Anwander, **Organometallics**, *2003*, 22 (6), 1212.

[8] Selected reference: (a) M. Zimmermann, K. W. Törnroos, R. Anwande, **Angew. Chem., Int. Ed.**, *2007*, 46 (17), 3126; (b) X. Xu, Y. Chen, G. Zou, J. Sun, **Dalton Trans.**, *2010*, 39 (16), 3952; (c) L. Luconi, D. M. Lyubov, A. Rossin, T. A. Glukhova, A. V. Cherkasov, G. Tuci, G. K. Fukin, A. A. Trifonov, G. Giambastiani, **Organometallics**, *2014*, 33 (24), 7125; (d) Z. Jian, D. Cui, **Dalton Trans.**, *2012*, 41 (8), 2367.

[9] (a) K. Nienkemper, G. Kehr, S. Kehr, R. Fröhlich, G Erker, **J. Organomet. Chem.**, *2008*, 693 (8-9), 1572; (b) B.-Y. Tay, C. Wang, S.-C. Chia, L. P. Stubbs, P.-K. Wong, M. van Meurs, **Organometallics**, *2011*, 30 (21), 6028.

[10] O. H. Hashmi, F. Capet, M. Visseaux, Y. Champouret, **Eur. J. Inorg. Chem.**, *2022, (15)*, 1434.

[11] A. Bondi, **J. Phys. Chem.**, *1964*, 68 (3), 441.

[12] K. Nienkemper, V. V. Kotov, G. Kehr, G. Erker, R. Fröhlich, **Eur. J. Inorg. Chem.**, *2006*, (2), 366.

[13] G.G. Skvortsov, M.V. Yakovenko, G.K. Fukin, E.V. Baranov, Yu. A. Kurskii, A.A.Trifonov, **Russ. Chem. Bull. Int. Ed.**, *2007*, 56 (3), 456.

[14] (a) D. Barbier-Baudry, F. Bouyer, A. S. M. Bruno, M. Visseaux, **Appl. Organometal. Chem.**, *2006*, 20 (1), 24; (b) M. Visseaux, T. Chenal, P. Roussel, A. Mortreux, **J. Organomet. Chem.**, *2006*, 691 (1-2), 86 ; (c) F. Bonnet, M. Visseaux, A. Hafid, D. Baudry-Barbier, M. M. Kubicki, E. Vigier, **Inorg. Chem. Comm.**, *2007*, 10 (6), 690 ; (d) F. Bonnet, C. Da Costa Violante, P. Roussel, A.´ Mortreux, M. Visseaux, **Chem. Commun.**, *2009*, (23), 3380 ; (e) Jaroschik, F. Bonnet, X.F. Le Goff, L. Ricard, F. Nief, M. Visseaux, **Dalton Trans.**, *2010*, 39 (29), 6761.

[15] K. F. Tesh, T. P. Hanusa, J. C. Huffman, **Inorg. Chem.**, *1990*, 29 (8), 1584.

[16] (a) M. Visseaux, M. Terrier, A. Mortreux, P. Roussel, **C. R. Chimie**, 2007, 10 (12), 1195; (b) M. Visseaux, P. Zinck, M. Terrier, A. Mortreux, P. Roussel, **J. All. Comp.**, *2008*, 451 (1-2), 352. (c) M. Visseaux, M. Terrier, A. Mortreux, P. Roussel, **Eur. J. Inorg. Chem.**, *2010*, (18), 2867.

[17] Y. Huo, X. Hu, J. Wang, H. Hu, X. Shi, **New J. Chem.**, *2022*, 46 (17), 8277.

[18] (a) G. V. Khoroshen'kov, A. A. Fagin, M. N. Bochkarev, S. Dechert, H. Schumann, **Russ. Chem. Bull.**, *2003*, 52 (8), 1715; (b) P. L. Arnold, S. T. Liddle, **Organometallics**, *2006*, 25 (6), 1485; (c) C. Pi, Z. Zhu, L. Weng, Z. Chen, X. Zhou, **Chem. Commun.**, *2007*, (21), 2190.

[19] S. M. Cendrowski-Guillaume, M. Nierlich, M. Lance, M. Ephritikhine, **Organometallics**, *1998*, 17 (5), 786.

[20] A. W. Addison, T. N. Rao, J. Reedijk, J. van Rijn, G. C. Verschoor, **J. Chem. Soc., Dalton Trans.**, *1984*, (7), 1349.

[21] S. S. Galley, S. A. Pattenaude, R. F. Higgins, C. J. Tatebe, D. A. Stanley, P. E. Fanwick, M. Zeller, E. J. Schelter, S. C. Bart, **Dalton Trans.**, *2019*, 48 (23), 8021.

[22] M. Zimmermann, K. W. Törnroos, R. M. Waymouth, R. Anwander, **Organometallics**, *2008*, 27 (17), 4310.

[23] B. N. Williams, W. Huang, K. L. Miller, P. L. Diaconescu, **Inorg. Chem.**, *2010*, 49 (24), 11493.

[24] F. Han, J. Zhang, W. Yi, Z. Zhang, J. Yu, L. Weng, X. Zhou, **Inorg. Chem.**, *2010*, 49 (6), 2793.

[25] R. D. Shannon, **Acta Cryst.**, *1976*, A32 (5), 751.

[26] L. F. Sánchez-Barba, D. L. Hughes, S. M. Humphrey, M. Bochmann, **Organometallics**, *2006*, 25 (4), 1012.

[27] (a) J. Prust, K. Most, I. Müller, E. Alexopoulos, A. Stasch, I. Usón, H. W. Roesky, **Z. Anorg. Allg. Chem.**, *2001*, 627 (8), 2032; (b) M. Bremer, G. Linti, H. Nöth, M. Thomann-Albach, G. E. W. J. Wagner, **Z. Anorg. Allg. Chem.**, *2005*, 631 (4), 683; (c) J. Spielmann, M. Bolteb, S. Harder, **Chem. Commun.**, *2009*, (45), 6934; (d) R. A. Collins, J. Unruangsri, P. Mountford, **Dalton Trans.**, *2013*, 42 (3), 759.

[28] P. H. M. Budzelaar, **Eur. J. Inorg. Chem.**, *2012*, (3), 530.

CHAPTER 3 SYNTHESIS AND CHARACTERIZATION OF RARE-EARTH ALLYLIC COMPLEXES BEARING AMIDO-PYRIDINE LIGANDS.

Following the results obtained in the borohydride series, preparation of rare earth allyl complexes supported by the same ligand **Z¹**, **Z²** and **Z³** were pursued. To do so, the first step is the synthesis of the highly sensitive precursors $RE(C_3H_5)_3$. The purity of these precursors being directly related to the experimental procedure, a new synthetic pathway was used. Furthermore, a new possible pathway for the synthesis of the highly desired mixed allyl/borohydride complex $[(BH_4)RE(C_3H_5)_2]$ was imagined.

3.1 New synthesis for tris-allyl rare earth complexes

As mentioned previously, the general synthesis of tris-allyl precursors is performed by reacting the RE tri-chlorides with a diluted solution of magnesium allyl chloride[1]. The synthesis of tris-allyl depends on the experimental conditions, particularly with respect to the reagents/RE molar ratio. An excess or a lack of Mg(allyl)(Cl) can easily lead to the formation of several by-products. To reduce the risk of formation of by-products, an alternative procedure to the one reported was implemented using the highly reactive $Mg(allyl)_2$ in the presence of the same rare earth precursors. This $Mg(allyl)_2$ reagent, which is in the form of a white powder[2], allows for a better control over the amount added to the reaction flask. It can be prepared according to the method described in the literature through the addition of an excess of dioxane to a solution of Mg(allyl)Cl, resulting in the precipitation of white powder of $MgCl_2$. This solution was filtered and evaporated to obtain the desired $Mg(allyl)_2$. The synthesis of the $RE(allyl)_3$ was performed by adding a cold amount of dry and distilled THF to the precursor $RECl_3$, which was then warmed to room temperature. Dioxane was added to the suspension followed by a dropwise addition of the THF solution containing the exact amount of $Mg(allyl)_2$. The white suspension was allowed to stir overnight before being filtered. After evaporation of the solvent, a subsequent extraction in dioxane to remove traces of $MgCl_2$ was done and finally the crystallization in a mixture of toluene/dioxane gave a pure complex in good yield [$Nd(C_3H_5)_3(diox)$: 40%, $Y(C_3H_5)_3(diox)_{0.25}$: 60%) as same as the previous preparation mode (Scheme 3.1).

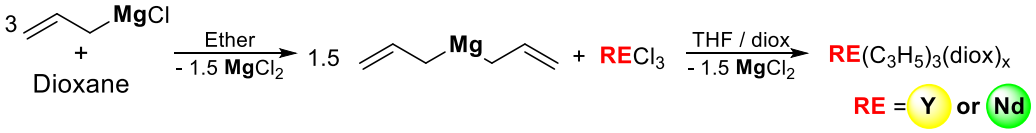

Scheme 3.1: Synthesis of tris-allyl rare earth complexes through magnesium bis(allyl).

The use of magnesium bis-allyl compound for the synthesis of rare earth allyl complexes had already been performed in our laboratory since 2016 for the preparation of mixed mono-allyl bis-borohydride RE complexes of the type $(BH_4)_2RE(C_3H_5)$[3]. These complexes have exhibited very interesting catalytic reactivity towards the ring-opening polymerization (ROP) of cyclic esters or/and the coordinative polymerization of 1,3-diene. In order to modulate the catalytic reactions, the possibility of coordinating a third and different ligand Z was considered**,** in addition to the reactive allyl and borohydride moieties. All reactions with this third potential ligand in the presence of $(BH_4)_2RE(C_3H_5)$, resulted in the activation of the allyl moiety and led to the formation of borohydride complexes due to the allyl part being more reactive than the BH_4[4]. With the aim of obtaining these complexes with three different ligands while preserving both borohydride and allyl units, it was decided to explore the synthesis of the bis-allyl mono-borohydride rare earth complexes $[(BH_4)RE(C_3H_5)_2]$ as a precursor.

3.2 Attempted synthesis of $(BH_4)RE(C_3H_5)_2$

In order to obtain the mixed compound $(BH_4)RE(C_3H_5)_2$, S. Fadlallah (a former PhD student in our research group, 2014-2017) attempted various synthetic methods using tris-borohydride rare earth as the starting material. For example, the use of 2 equivalents of Grignard reagent Mg(allyl)(X) (where X = Cl, Br, etc.) with $RE(BH_4)_3$ led to the formation of the previously described $(BH_4)_2RE(C_3H_5)$. Attempts to form $(BH_4)RE(C_3H_5)_2$ through ligand exchange of $RE(BH_4)_3$ and $RE(C_3H_5)_3$ resulted in a non-reactive mixture as observed in ^{1}H NMR experiments.

After being made aware that the attempt to prepare $(BH_4)RE(C_3H_5)_2$ using tris allyl complexes as precursors was not yet explored, two different pathways were considered for its synthesis (Scheme 3.2). The first proposed route ("Reductive pathway") involves the reaction of tris-allyl rare earth complexes with potassium graphite to obtain the desired reduced divalent compound "$RE(C_3H_5)_2$". This compound will then be combined with a borohydride oxidant such as $Tl(BH_4)$ (which form nanoparticle of Tl^0 afterward) with the aim of affording the mixed borohydride/allyl complexes. The second pathway ("Cationic pathway") will be relying on the synthesis of the known cationic rare earth allyl compound by protonation of the tris-allyl starting materials with an organic acid $([HN(Me)_2(Ph)][B(C_6F_5)_4]$ or $([HN(Et)_3][B(C_6H_5)_4])$[5]. This cationic compound should react with potassium borohydride to give by metathesis $(BH_4)RE(C_3H_5)_2$.

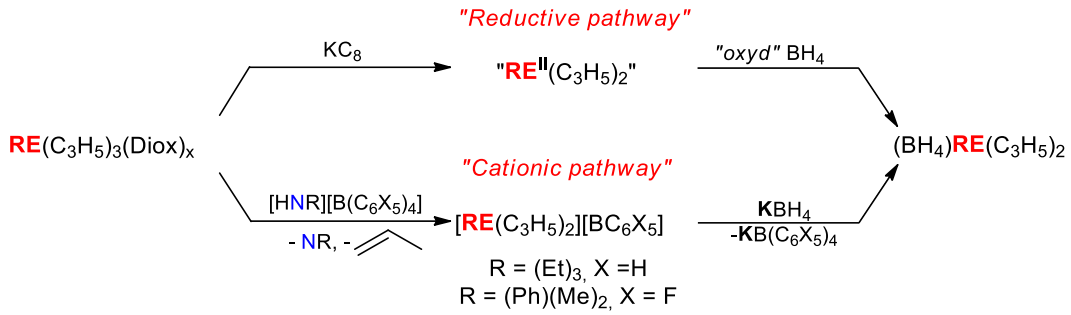

Scheme 3.2: Proposed pathway for the formation of $(BH_4)RE(C_3H_5)_2$.

These different routes will be explored in more details in the following section, starting with the "reductive pathway" and RE = Nd.

3.2.1 Attempted synthesis of $(BH_4)RE(C_3H_5)_2$ using the reductive pathway.

The reduction reaction with rare earth elements being the specialty of Prof. Evans' group[6], the opportunity to spend two months internship at the University of Irvine (USA) was offered to me (August-September 2022), thanks to the financial support of the University of Lille. I would like to thank his team for the opportunity to work with them and for their valuable advices.

The classical synthesis of complexes of a rare earth element at oxidation state +2 requires working at low temperatures (-35 °C) because of their instability[6b]. The formation of divalent rare earth complexes is performed in THF using KC_8 and a cryptand (18-crown-6 or 2-2-2-cryptand) to encapsulate the potassium center. Preliminary cyclic voltammetry studies of a THF solution containing $Nd(C_3H_5)_3(diox)$ showed three different reduction peaks (1, 2, 3 in Fig 3.1) before the reduction of the solvent. Highlighting the area between 0 and 2.5 V revealed the possible presence of a single oxidation peak (4, in Fig 3.1) during the oxidative sweep, meaning that part of the reduction reaction is not reversible (Fig. 3.1 a and b). Usually, the reduction of Nd^{III} complexes to Nd^{II} is easily noticeable by an intense change of color. Indeed, as described in the literature, reduction of Cp_3Nd was observed by a violent color change from green[7] to black[8]. After several attempts at -35 °C in the presence of cryptand, the color change of the solution during the (putative) reduction of neodymium tris-allyl with KC_8 was not noticed. Comparison of the two UV-Vis analyses displayed in Fig. 3.2 of $Nd(C_3H_5)_3$ (blue) and the reduced product (red) showed no difference. Therefore, the formation of divalent species was not established.

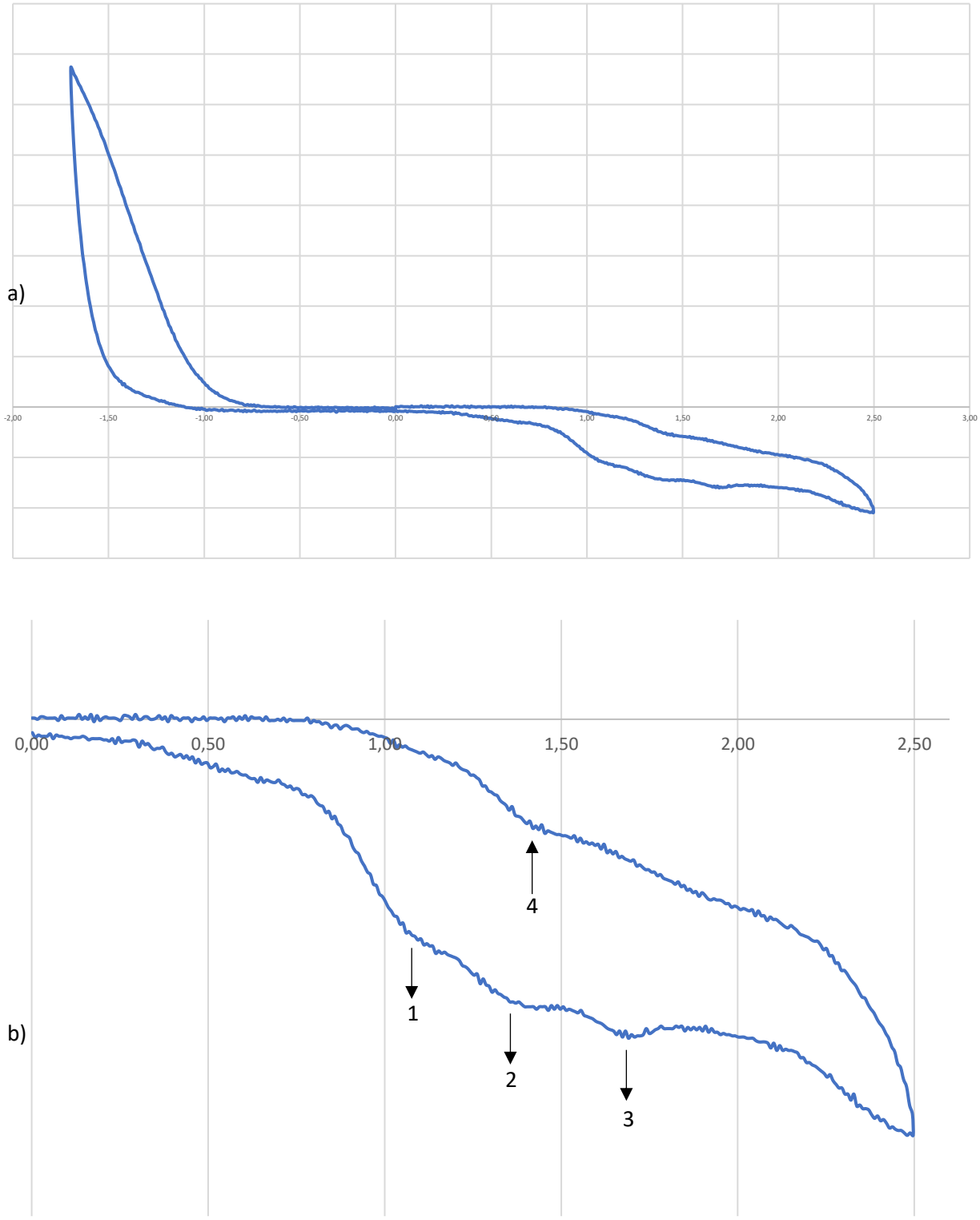

Figure 3.1: Total voltammetry cyclic response for $Nd(C_3H_5)_3(diox)$ (a), zoom between 0 and 2.5 V (b).

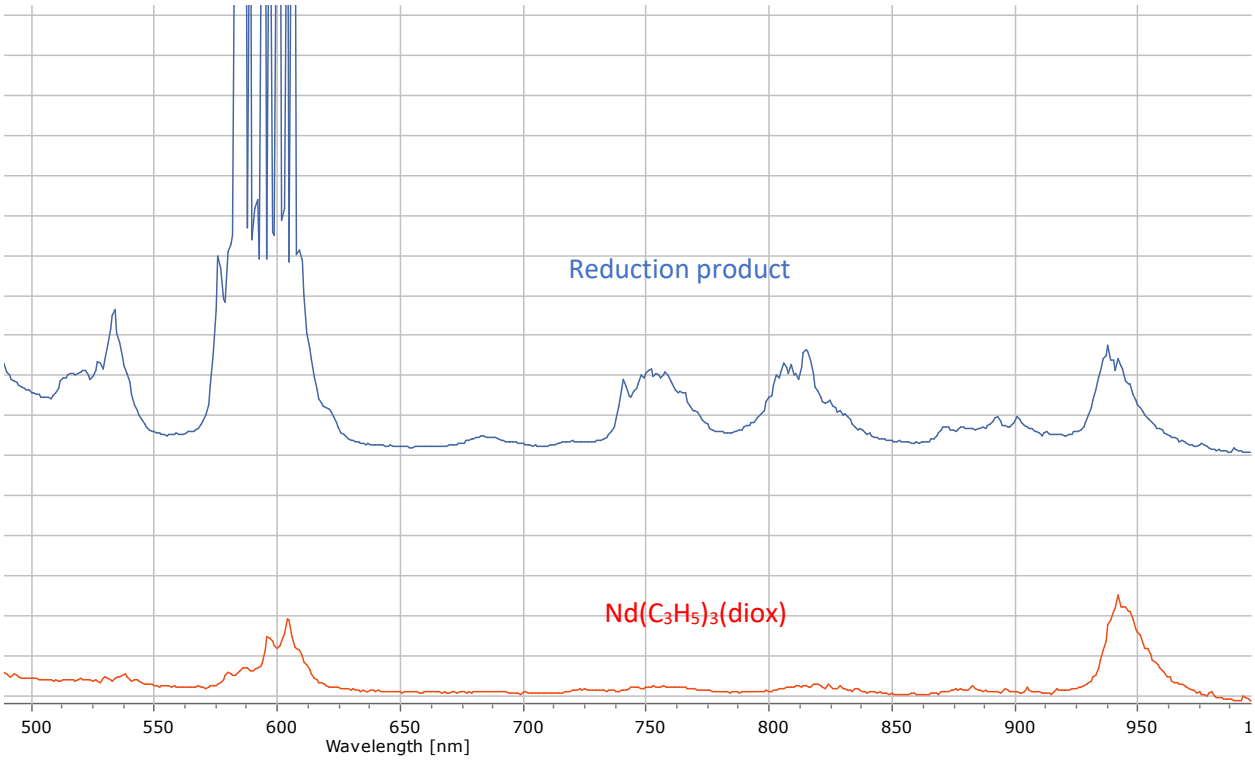

Figure 3.2: UV-VIS analysis of $Nd(C_3H_5)_3(diox)$/reduction product.

On the other hand, it was noticed, a color change of KC_8 from bronze to black (graphene), which clearly indicated that a reaction had occurred. Filtration and addition of a layer of pentane gave the product **11** as green crystals. The ^1H NMR spectra in THF-D8 of the product confirmed the transformation of the tris-allyl compound (Fig. 3.3 a *vs.* b).

The ^1H NMR spectrum displayed in Fig. 3.3 b) shows three different paramagnetic signals at δ = -8.36, -18.75 and -28.33 ppm which correspond, according to their relative integral, to a typical 2H/1H/2H pattern of allyl groups (*). Usually, the cryptand is represented by three peaks, two of which are normally close to each other. Due to the paramagnetic character of neodymium, these latter two peaks merge together to form a broad peak at δ = 3.50 ppm. Integration of this broad resonance at δ = 3.50 ppm for 24 hydrogens and that at δ = 2.52 ppm for 12 hydrogens gives integration of the CH_2CHCH_2 peaks for 8H/4H/8H, which therefore involves four allyls moieties per cryptand molecule.

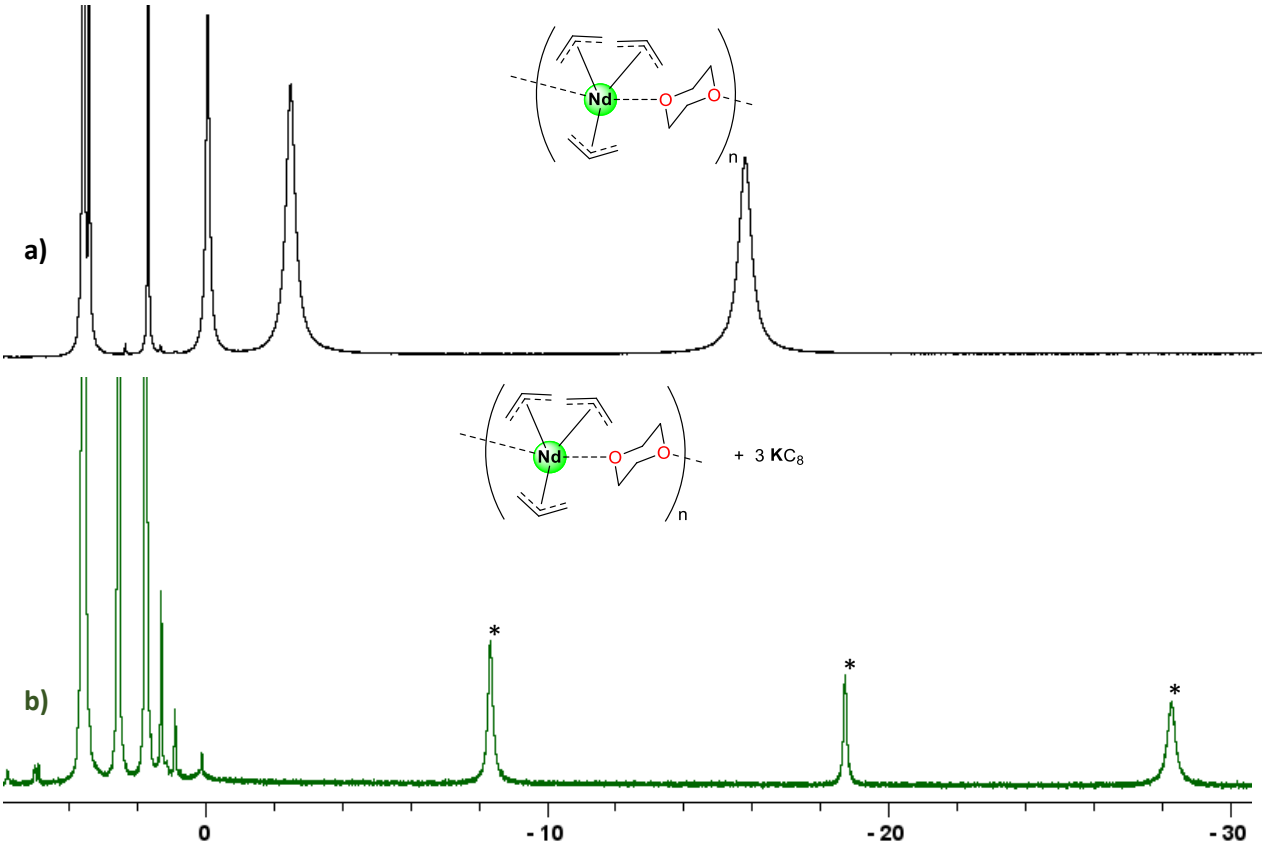

Figure 3.3: ^{1}H NMR spectrum of the reduced product (solvent THF-D8).

As the crystals were XRD-matched, the molecular structure obtained as an anionic tetra-allyl neodymium complex (Fig. 3.4) was in accordance with the ^{1}H NMR spectrum result. Selected bond distances and angles of the molecular structure of **11** are listed in Table 3.1.

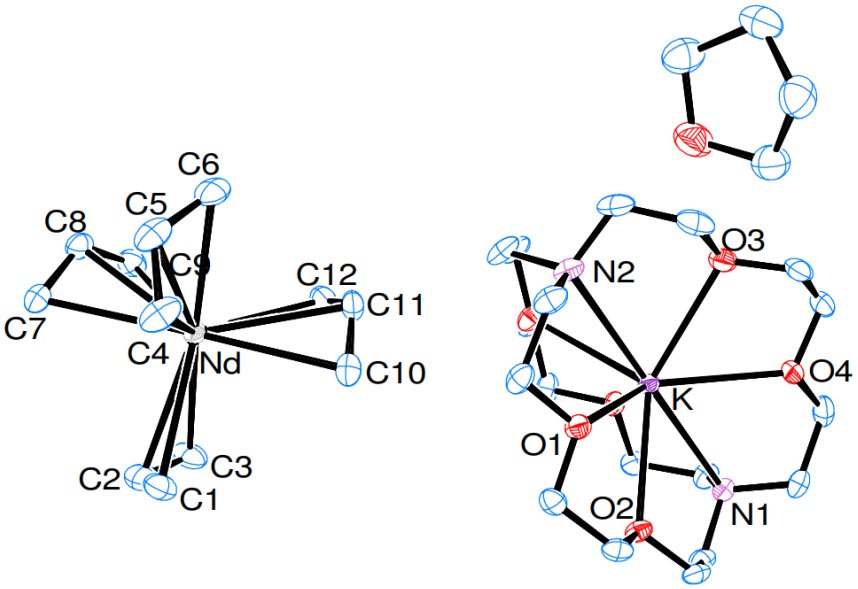

Figure 3.4: Molecular structure of $[Nd(C_3H_5)_4][K(crypt)]$, 11, hydrogens omitted for more clarity. Ellipsoids drawn at 50% probability.

The molecular structure consisted of an ion pair composed of an anionic species of tetra-allyl neodymium and a cationic part of potassium encrypted with crypt-222 and a molecule of THF in the unit cell. This complex crystallized in the $P2_1/n$ group. Similar anionic complexes with different rare earth elements have been obtained with other cationic counterparts (Mg or Li)[9], but not potassium so far. The bond distances between the neodymium atom and the individual carbons of the allyl moieties (C1 to C10) were in a short range between 2.70 and 2.80 Å, which is consistent with the literature for anionic allyl neodymium species. With respect to the allyl ligands, a C-C bond was observed around 1.38 Å along with a slight distortion of the CH_2-CH-CH_2 angles between 126° and 128°, in agreement with a typical delocalized allyl according to literature[9,10] . The distortion of the tetrahedral geometry around the anionic neodymium was observed by the angles C2-Nd-C8: 99.63°, C8-Nd-C5: 78.78°, C5-Nd-C11: 99.81° and C11-Nd-C2: 118.25°, which should have been equal to 109° for a perfect tetrahedral geometry.

The synthesis of a neodymium compound bearing four allylic ligands has been previously described in the literature using a lithium salt as reagent**11**[9], however, the molecular structure has not yet been disclosed. According to the various analyses, a possible reactive route for the synthesis of this tetra-allyl neodymium **11** has been considered. This synthesis involves obtaining the potassium allyl reagent during the course of the reaction. Indeed, according to Fig. 3.1 (a and b) above, three rapid reductions of one equivalent of $Nd(C_3H_5)_3$ could occur with 3 equiv. of KC_8 leading to $K(C_3H_5)$,

which putatively reacts with the tris-allyl neodymium to form the anionic tetra-allyl neodymium species as shown in Scheme 3.3.

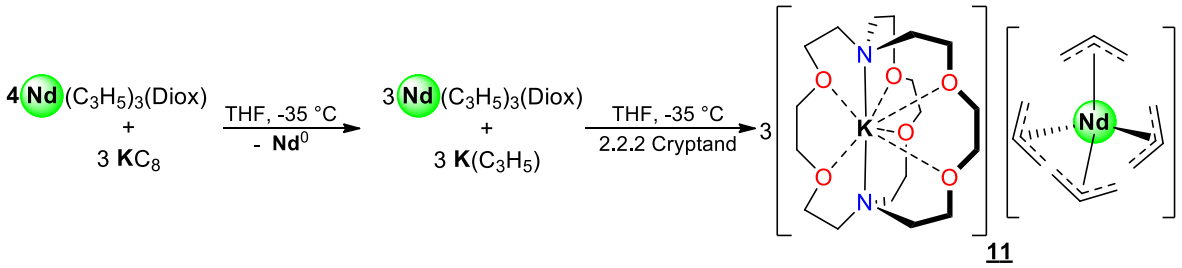

Scheme 3.3: Possible pathway for the synthesis of the tetra-allyl neodymium complex.

As the divalent neodymium allyl species appears to be inaccessible by this reductive approach, obtaining Nd(allyl)$_2$(BH$_4$) seems to be compromised and the "reductive pathway" was not pursued. Instead, the "cationic" pathway was investigated.

3.2.2 Attempted synthesis of (BH$_4$)RE(C$_3$H$_5$)$_2$ using the cationic pathway.

3.2.2.1 Attempts using neodymium.

As said before, the procedure using the cationic pathway consists in preparing the mono-cationic bis-allyl rare earth complex and then reacting it with potassium borohydride to obtain the desired mixed complexes. As reminded in the bibliographic chapter, a similar procedure to obtain mixed complexes has already been studied: in the literature, yttrium bis-cationic methyl compound reacts with sodium borohydride to afford the methyl/borohydride cationic species[12]. Inspired by this methodology, the synthesis of bis-allyl cationic complexes was first performed by protonolysis of the tris-allyl rare earth with a Lewis acid (Scheme 3.4), as described in the literature by the group of Okuda[5]. The plan was to subsequently react the resulting complexes with KBH$_4$.

The two-step synthesis of the mixed borohydride/allyl neodymium [Nd(BH$_4$)(C$_3$H$_5$)$_2$] was first investigated at the NMR scale by monitoring the reaction (Fig. 3.5). For this study, an affordable and easily synthesized Lewis acid [HNEt$_3$][B(Ph)$_4$] was used.

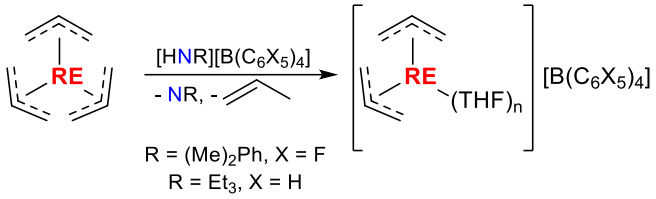

Scheme 3.4: Synthesis of ionic $[RE(C_3H_5)_2][B(C_6F_5)_4]$.

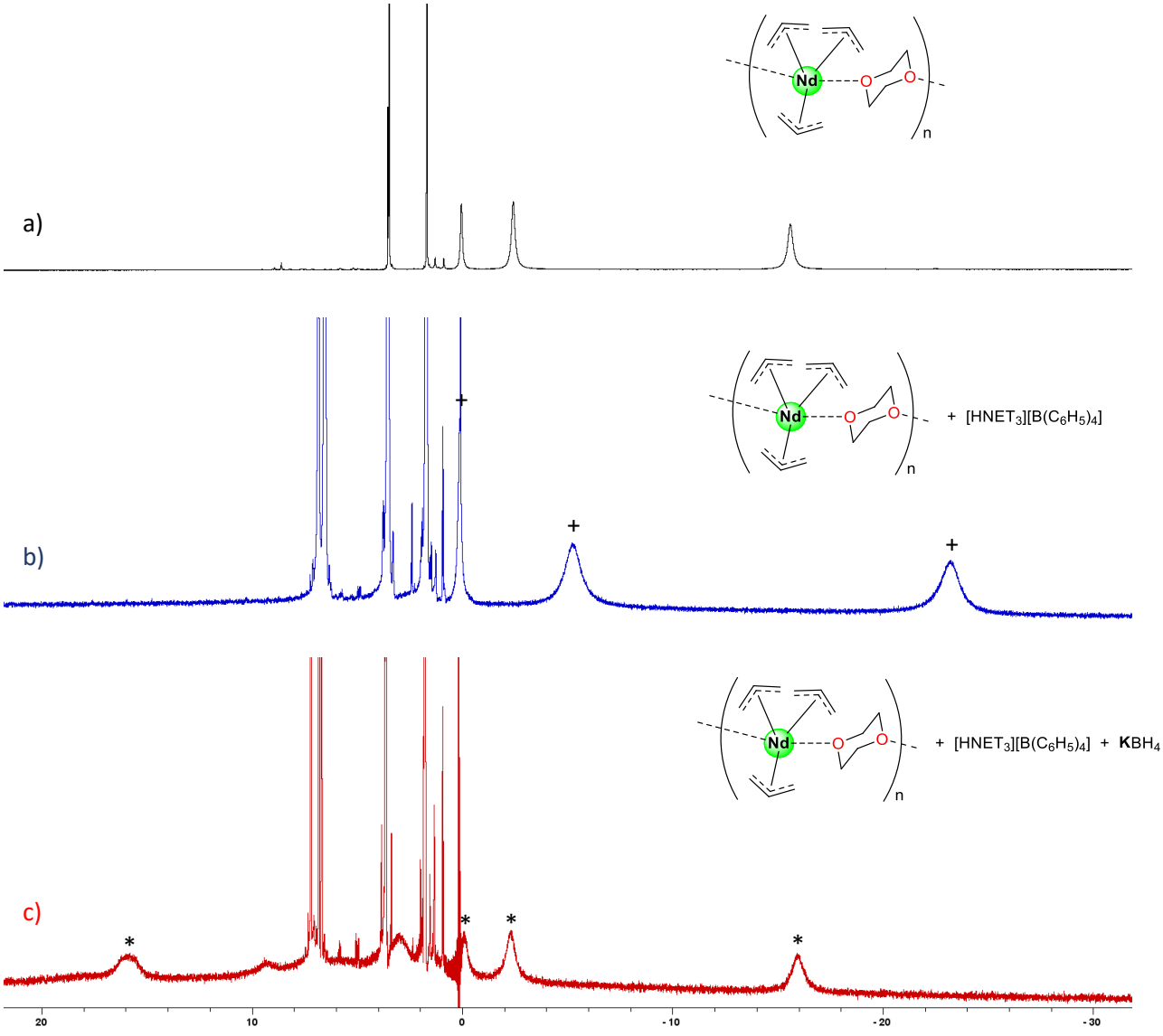

Figure 3.5: ^{1}H NMR study for the expected synthesis of mixed $Nd(C_3H_5)_2(BH_4)$ (solvent THF-D8).

The ^{1}H NMR spectrum of the crystallized $Nd(C_3H_5)_3$(diox) revealed the presence of the three typical signals with a 1H/2H/2H ratio between δ = 20 and -30 ppm (Fig. 3.5 a), similar to that found in the literature [9]. Addition of one equiv. of $[HNEt_3][B(Ph)_4]$ to the NMR tube containing $Nd(C_3H_5)_3$(diox) showed the appearance of three distinct peaks at δ = -23.7, -5.23 and 0.01 ppm, indicating that

$[Nd(C_3H_5)_2][B(Ph)_4]$ (marked as +) was obtained as described in the literature[5]. Attempts to get the mixed complex using KBH_4 led to a new ^1H NMR spectrum, as shown in Fig. 3.5 c). Compared to the spectrum in Fig. 3.5 a) and b), this spectrum indicated a shift of the allyl peaks, which are now oddly at the same position than the one of $Nd(C_3H_5)_3$ (Fig. 3.5 a). In addition, the broad peak observed at *ca.* δ = 16.5 ppm could be attributed to the $Nd(BH_4)$ proton resonance. The integration of this broad peak was set at 4 protons and gave rise to the integration of the other allyl peaks with 2H/4H/4H, which is relevant for a mixed bis(allyl) mono-borohydride $Nd(C_3H_5)_2(BH_4)$ complex (*).

According to the literature, the excess of $[HNEt_3][B(Ph)_4]$ could lead to a di-cationic species and, therefore, the fluorinated $[HNMe_2Ph][B(C_6F_5)_4]$ was preferred for the bulk synthesis. The bulk synthesis of the targeted cationic compound $[Nd(C_3H_5)_2][B(C_6F_5)_4]$ from the tris-allyl precursors and $[HNMe_2Ph][B(C_6F_5)_4]$ was performed at room temperature (Scheme 3.5)[5] and confirmed by ^1H NMR, with the typical allyl signals at δ = -22.1, -4.38, 1.35 ppm (Appendix 8).

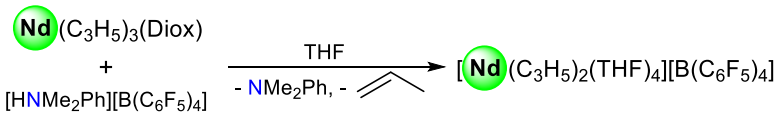

Scheme 3.5: Synthesis of $[Nd(C_3H_5)_2][B(C_6F_5)_4]$.

The addition of potassium borohydride to this cationic neodymium compound led to a new green product, which was soluble in toluene. This product showed characteristic peaks of the allyl and borohydride parts in the ^1H NMR spectrum in THF-D8, identical to those presented in Fig. 3.5 c). Stirring the product in toluene at room temperature allowed the solution to change from green to a biphasic orange solution that evolved into a toluene-insoluble orange product and a colorless solution. However, this green solution appeared to be stable at -35 °C. After decantation and drying, an orange powder soluble in THF was obtained but ^1H NMR analysis, revealed no paramagnetic signals. Thus, no allylic moiety was not any longer coordinated to the metal center. Several attempts to crystallize the green solution at -35 °C led to small green crystals, which corresponded to the unpublished structure of the bis-allyl cation complemented with the perfluorinated borate as seen in Fig. 3.6, where selected bonds and distances are gathered in Table 3.1.

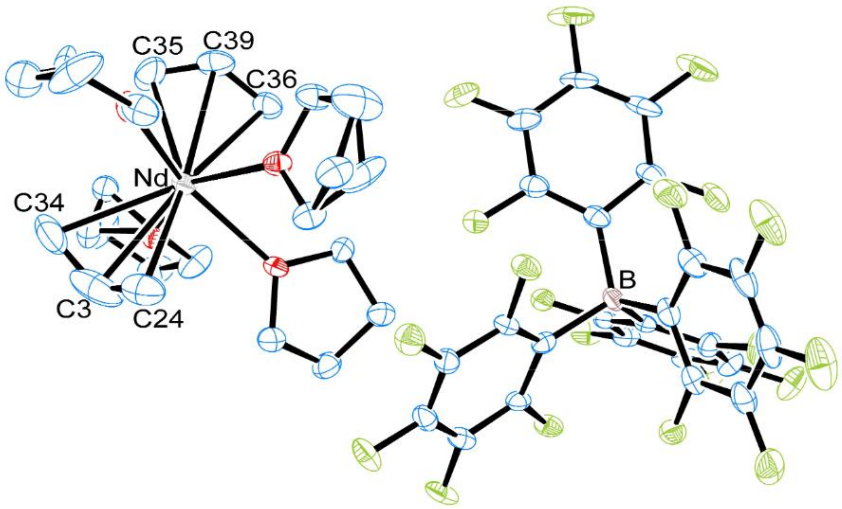

Figure 3.6: Molecular structure of $[Nd(C_3H_5)_2(THF)_4][B(C_6F_5)_4]$.

This molecular structure featured an ionic pair made of a cationic neodymium species composed by two allyl groups and four THF molecules, and the anionic counterpart $[B(C_6F_5)_4]^-$, also known as BARF. The structure crystallized in a C_2/C space group, like the homologous $[Nd(C_3H_5)_2(THF)_4][BPh_4]$ described by D. Robert *et al.*[5]. This complex showed Nd-C bond lengths between 2.65 and 2.75 Å, while the C-C bond mean length of 1.38 Å was coherent with a sp^2-sp^2 carbon bond, in accordance with the delocalization of the negative charge.

*Table 3.1: Selected bond and distances of **11** and $[Nd(C_3H_5)_2(THF)_4][B(C_6F_5)_4]$.*

Mean value	**11**	**$[Nd(C_3H_5)_2(THF)_4][B(C_6F_5)_4]$**
Nd-CH_2[a] (Å)	2.75	2.73
Nd-CH[a] (Å)	2.75	2.72
CH_2- CH[a] (Å)	1.38	1.38
CH_2-CH-CH_2 (°)	127.43	126.22

a) Mean value

At the moment, we could suggest that the instability and decomposition of the green product might be caused either by reaction with $[K][B(C_6F_5)_4]$ or with the residue of $N(Me)_2Ph$. All attempts using the same synthetic procedure have led to the same conclusion. However, the synthesis of the mixed neodymium complexes using different reagents but the same "cationic pathway" is being considered but has not been pursued to date. The synthesis of the mixed yttrium allyl/borohydride complex using the same acidic compounds ($[HN(Et)_3][B(Ph)_4]$ and $[HN(Me)_2Ph][B(C_6F_5)_4]$ followed by addition of the borohydride salt was therefore attempted.

3.2.2.2 Attempts using yttrium.

A cationic yttrium complex $[Y(CH_3)(BH_4)(THF)_5][BPh_4]$ was synthesized using a similar method as described in the previous section[12]. Compared to the paramagnetic nature of neodymium, yttrium is diamagnetic, and this characteristic offers various insights into the coupling observed in ^1H NMR spectra. One of the most important features is the appearance of a highly distinctive broad quadruplet in the ^1H NMR spectra where the borohydride group can be successfully integrated ($[I(^{11}B) = 3/2]$ and $[I(^{77}Y) = 5/2]$). In the same way as for neodymium, ^1H NMR monitoring was performed to follow the possible formation of the mixed complex $Y(allyl)_2(BH_4)(THF)_n$ using $[HNEt_3][BPh_4]$ as Lewis acid and tris-allyl yttrium precursor (Fig. 3.7).

As can be seen in Fig. 3.7, the formation of bis-allyl cationic yttrium from the tris-allyl precursor (Fig. 3.7 a) *vs.* b)) resulted in a set of new peaks (marked as +) accompanied with a shift of the allyl peaks (++), in agreement with what has been found in the literature[5]. The addition of KBH_4 to this poorly soluble product yielded a more soluble material that exhibited the broad and distinct quadruplet of yttrium borohydride around δ = 0 ppm (*) (Fig. 3.7 c). Due to technical problems during the bulk synthesis of yttrium tris-allyl, the synthesis of the mixed "$Y(C_3H_5)_2(BH_4)$" is on hold for the time being, but ^1H NMR studies allow one to see the possibility of a new product emerging.

As discussed in this section, the synthesis of a bis-allyl mono-borohydride mixed rare-earth compound remains highly challenging. Although the "reductive" pathway led to a clean method of producing tetra-allyl of neodymium **11** that could also be applied to the synthesis of other rare earth tetra-allyl complexes, the acidic "cationic" pathway seems promising. Even though the different attempts of bulk synthesis of $Nd(C_3H_5)_2(BH_4)$ resulted in the isolation and crystallization of $[Nd(C_3H_5)_2(THF)_4][BARF]$, the ^1H NMR monitoring using yttrium clearly showed the possible coexistence of both allyl and borohydride moieties on the same RE metal.

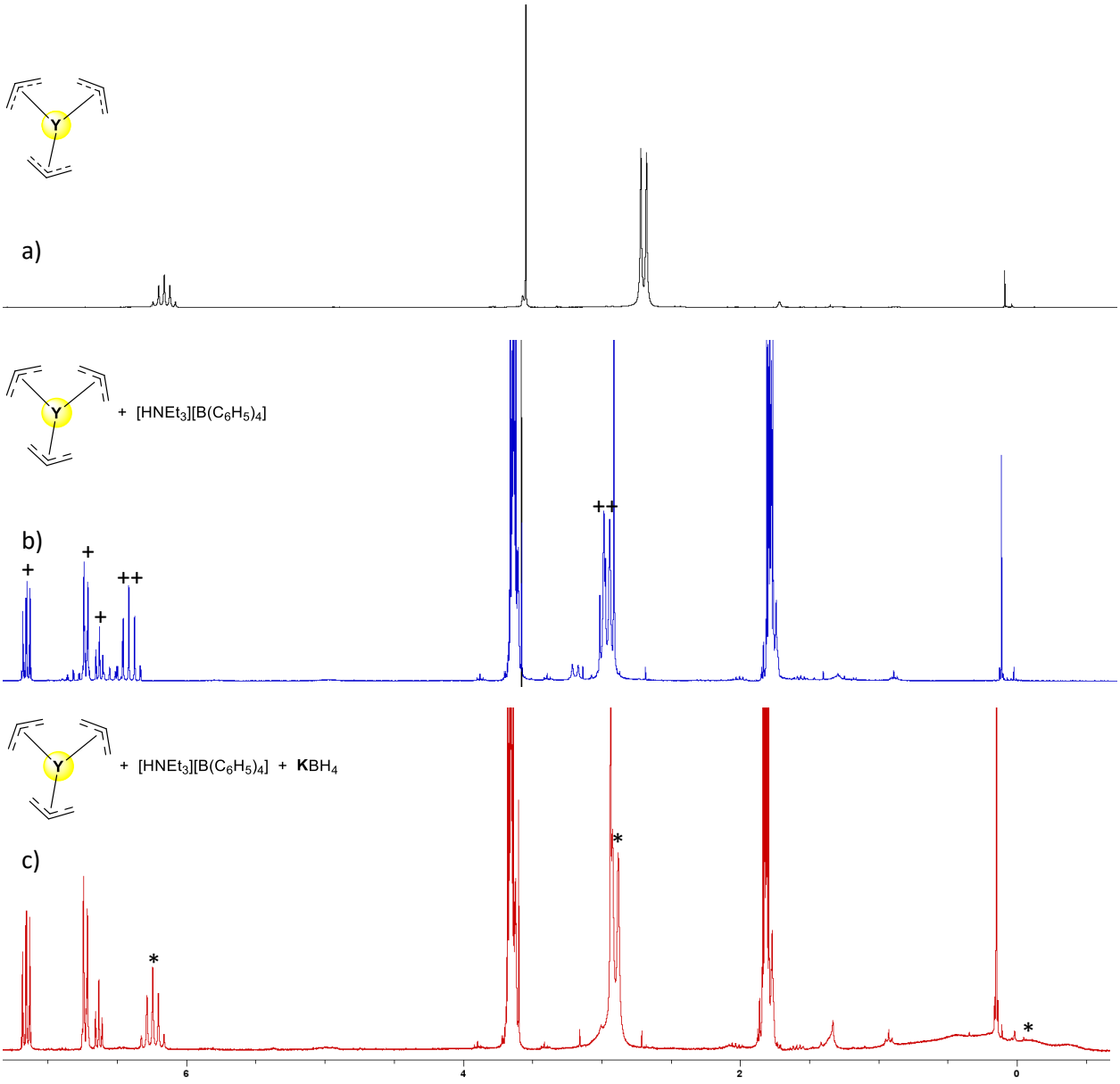

Figure 3.7: ^{1}H NMR study for the formation of the mixed complex $Y(C_3H_5)_2(BH_4)$ (solvent THF-D8).

In parallel of all these tests, the synthesis of new RE allyl complexes supported by the previously described ligands **Z**^{1}, **Z**^{2} and **Z**^{3} was pursued. To compare the results obtained in the borohydride series with the RE tris-borohydrides as precursors, a first set of syntheses using the amino-pyridines as starting materials was carried out with the tris-allyl RE precursors.

3.3 Synthesis of supported rare earth allyl complexes with amido-pyridine ligand.

3.3.1 Syntheses using Z^1H.

3.3.1.1 Studied using the neodymium

As mentioned earlier, "*in-situ*" deprotonation with allyl complexes should give a clean product with propene as by-product and, thus, fewer complications compared to borohydride complexes should be encountered. Following the results presented in the borohydride chapter, a similar approach based on ^{1}H NMR experiments using **Z^1H** and $Nd(C_3H_5)_3$(diox) was performed, aiming at the evaluation of the degree of substitution of the Nd compound formed (Fig. 3.8).

Figures 3.8 a) and a-a) show the neodymium tris-allyl compound, identifiable by its characteristic three broad peaks in a 1H/2H/2H pattern at δ = 0.06, -2.22 and -15.8 ppm (+). The addition of one equivalent of the protio-ligand (Fig. 3.8 b) **Z^1H** resulted in the emergence of numerous paramagnetic signals indicating the coordination of the **Z^1** ligand to the neodymium center. Nevertheless, the peaks of the tris-allyl neodymium complex were still present (Fig. 3.8 b *vs.* a.). Therefore, a second equivalent of **Z^1H** was added to the tube and then the disappearance of the tris-allyl peaks and retention of the same new resonances from b) to c) agreed with the formation of a bis-substituted [(**Z^1**)$_2$Nd(allyl)] complex without formation of the mono-substituted derivative (Scheme 3.6), similar to that found for the Nd borohydride counterpart supported by **Z^1** ligand. Disregarding the signals of the protio-ligand **Z^1H** (marked as °) (c-c *vs.* d-d) and propene, a total of seventeen peaks (*) were obtained. While the broadest resonances are normally related to an allyl moiety, the presence of four peaks appeared inconsistent with a usual 2H/2H/1H or a 4H/1H pattern. Two of these four peaks integrated for 2H, at δ = -8.9 and -19.3 ppm, and the others two for 3H (possibly 2+1) at δ = -11.1 and -15.7 ppm, leaving fourteen peaks corresponding to the proton resonance of the ligand coordinated to the metal center. Integration of the different peaks revealed the presence on the spectrum of eight peaks integrating for 2H [for the two ligands: 4 x C*H*$_{pyr}$, 1 x CH_3(C*H*)-N, 1 x *para*-C*H*$_{Aryl}$, 2 x C*H*(CH_3)$_2$], one peak at δ = -2.32 ppm for 4H (for the two ligands: 2 x *meta*-C*H*$_{Aryl}$) and one peak for 6H [for the two ligands: 1 x C*H*$_3$(CH)-N] along with another four sets of peaks integrating for 6H. These last four peaks [for the two ligands: 4 x CH(C*H*$_3$)$_2$] could indicated, as noticed in the case of the borohydride complexes **1** and **3**, a differentiation between the CH and CH_3 of the two isopropyl groups. As same as in the borohydride series in presence of **Z^1H**, the allyl bis-substituted complex **12** was

formed straightforwardly while the mono-substituted allyl analogue was not attainable at room temperature.

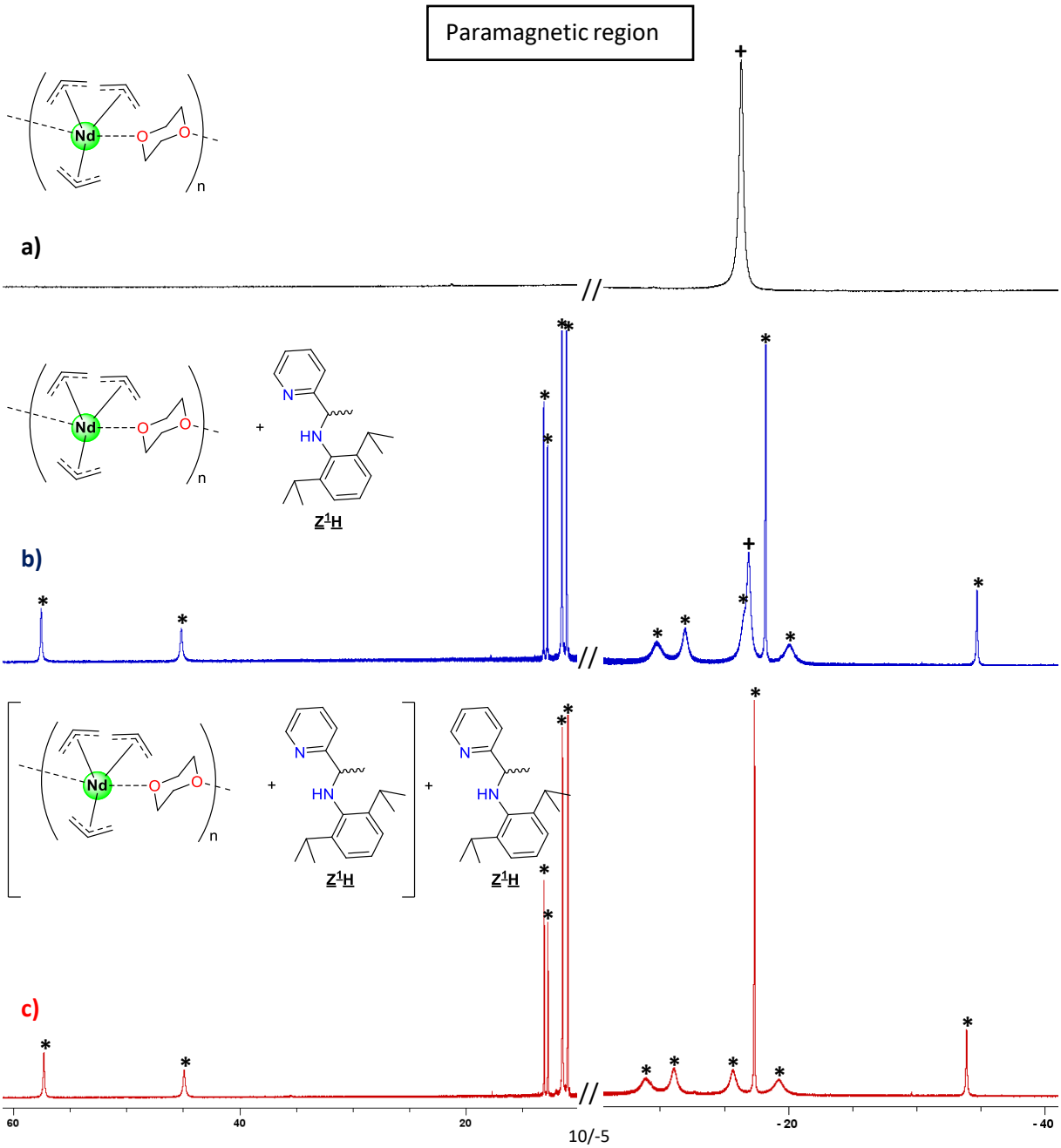

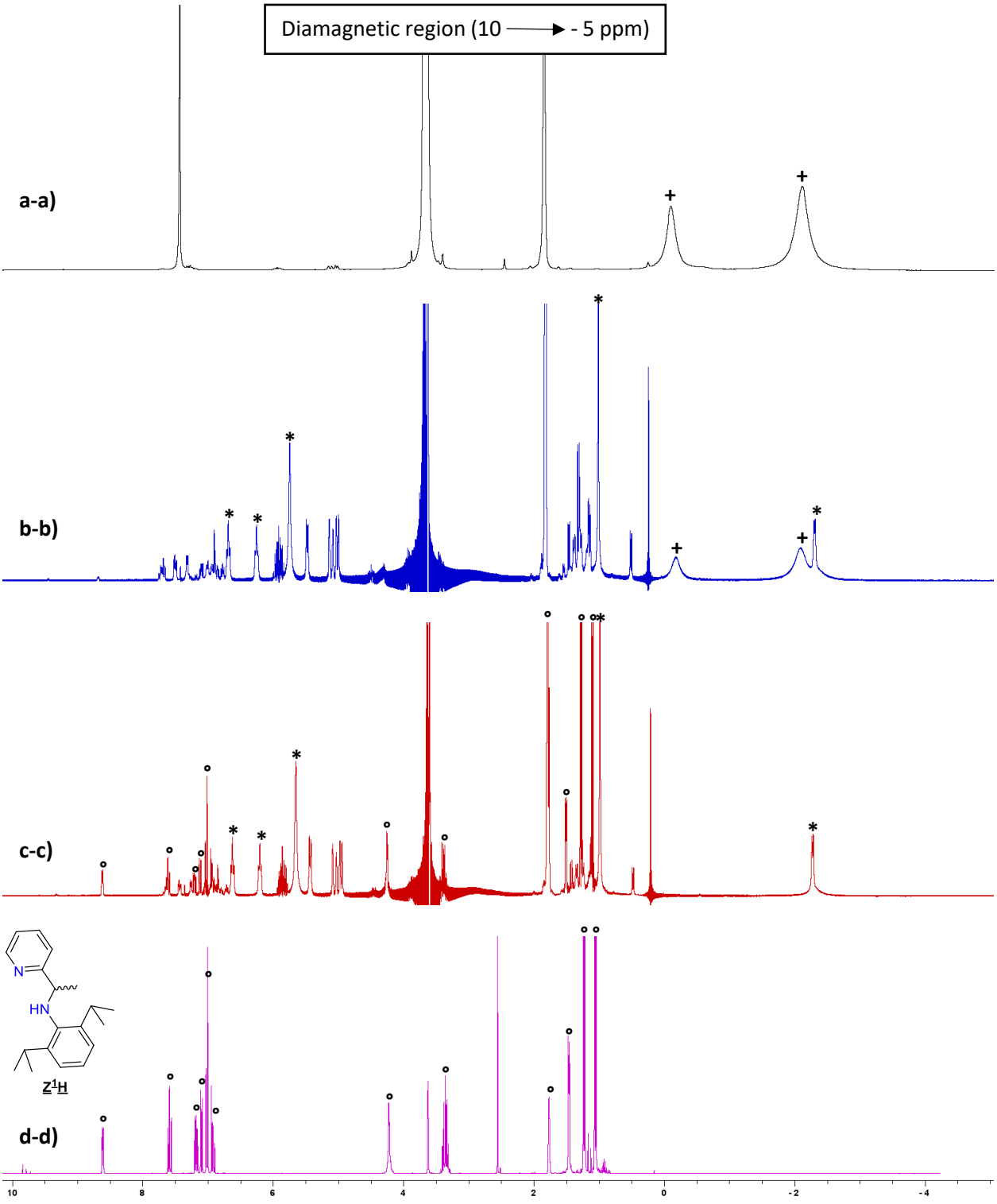

Figure 3.8: ^{1}H NMR monitoring for the formation of $(Z^{1})_{2}$Nd(allyl) complex (solvent THF-D8).

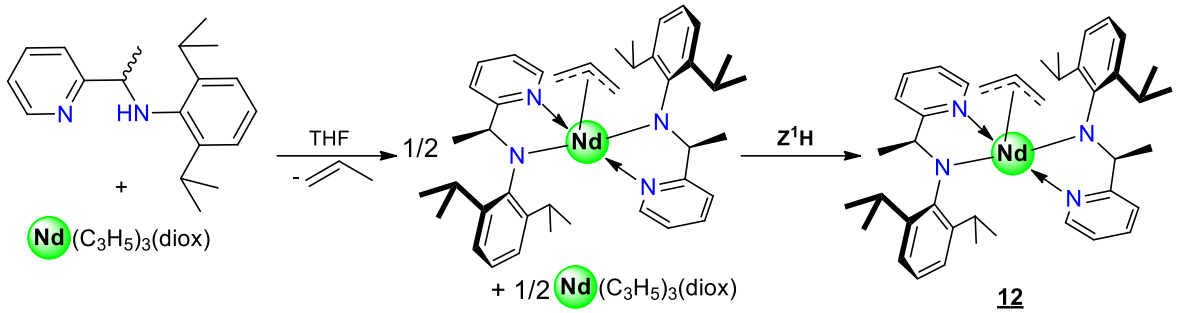

Scheme 3.6: Formation of 12.

The bulk synthesis of the bis-substituted complex **12** was performed at room temperature by addition of two equivalents of the protio-ligand **Z¹H** onto a solution of THF containing the tris-allyl neodymium complex. Evaporation of the solvent from the reaction mixture, followed by dissolution in toluene and filtration, to remove traces of the tris-allyl neodymium complex, afforded the desired product. Single-crystals were obtained from a concentrated solution in pentane at low temperature (-35 °C) and were subjected to elemental analysis, which was consistent with the formation of Nd complex of formula $(\mathbf{Z^1})_2Nd(C_3H_5)$ (theo: C = 65.20%, H = 7.53%, N = 7.07%, found: C = 65.03%, H = 7.65%, N = 7.02%). In addition, these single crystals were submitted to X-ray diffraction analysis and the molecular structure of this compound is presented in Fig. 3.9; selected bond distances and angles are shown in Table 3.3.

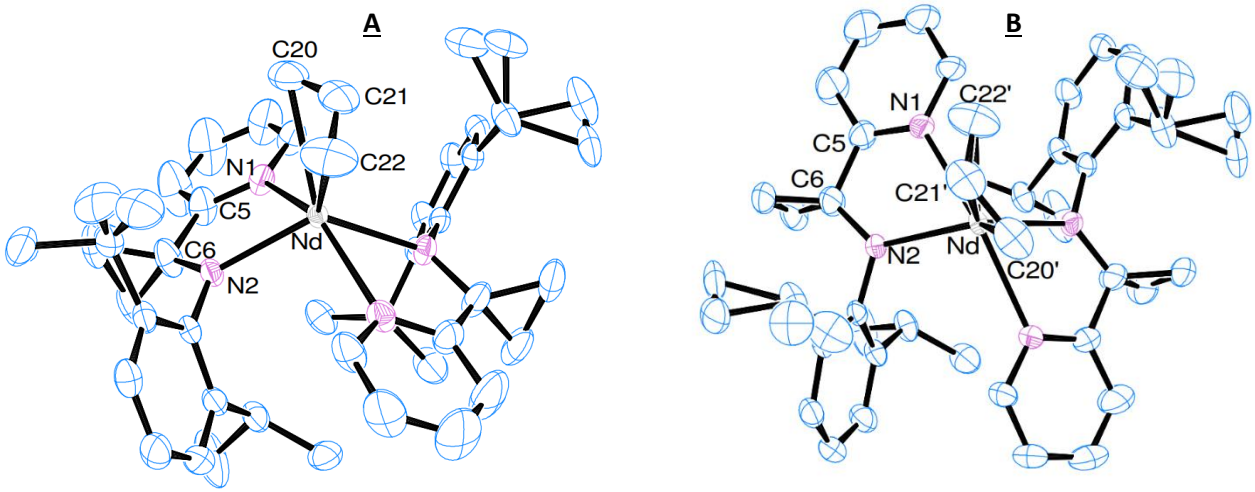

Figure 3.9: Molecular structure of 12 without most of hydrogen for more clarity. Form A and B present in the same packing. Thermal ellipsoids are drawn at the 50% probability level.

X-ray diffraction analysis of the crystals established that the neodymium center was surrounded by two $\mathbf{Z^1}$ ligands and one allyl group. This complex crystallized in the C2/C space group. The unit cell presented each isomer A and B at 50 % of occupancy. The bond distance between the allyl group and the neodymium (Nd-C20 = 2.692 (6), Nd-C21 = 2.731 (5), Nd-C22 = 2.734 (6) Å) were in the typical range for a η^3 coordination; the sp^2 configuration of these carbon was also confirmed by a typical slight distortion in the CH_2-CH-CH_2 angle of 126°, and an average C-C distance of 1.37 Å. Like the borohydride homologous complex **1'**, the Nd–nitrogen ($N1_{pyridine}$ and $N2_{amine}$) distances are in the same range [Nd-$N1_{1'}$: 2.549 (1) *vs.* Nd-$N1_{12}$: 2.550 (2) Å and Nd-$N2_{1'}$: 2.282 (2) *vs.* Nd-$N2_{12}$: 2.311 (2) Å]. The differences between the bis-substituted borohydride and allyl complexes were noticed in the torsion angle between the pyridine ring and the amidomethyl moiety. Contrary to the borohydride complex **1'**, the torsion angle N1-C5-C6-N2 was the same for both enantiomers (R and S) coordinated to the metal center and was shown to be more planar in **12** [**1'**(Mean value): - 10.11° *vs.* **12**: - 2.095°), while the aryl group was *quasi*-orthogonal with the pyridine ring (89.8°). When considering the mean plane formed by the pyridine-amido chelates (defined by the atoms N1, N2, N1', and N2'), it was observed that the Nd atom was slightly displaced from this plane by 0.877 Å. Additionally, the angle between the planes formed by the two pyridine-amido chelates with Nd atom (N1-Nd-N2 and N1'-Nd-N2') was found to be 56.43°.

3.3.1.2 Studied using the yttrium.

As presented in the chapter of this thesis manuscript relative to borohydride complexes, it has been observed that yttrium formed mono-substituted derivatives with $\mathbf{Z^1}$ more readily than the bis-substituted derivatives. Consequently, the bulk synthesis of the mono-substituted yttrium derivative was undertaken at room temperature by the addition of a solution of $\mathbf{Z^1H}$ in THF to a solution of $Y(C_3H_5)_3$(diox) in THF, as same as scheme 3.6. After 30 minutes, the orange solution was evaporated to afford an orange solid. Toluene was added to this orange solid, followed by filtration and evaporation of the solvent to afford an orange oil. A large amount of pentane was added to the orange powder and the resulting solution was filtered and cooled at -35 °C. After a few days, dark orange crystals (yield = 8 %) suitable for XRD analysis were obtained. The molecular structure of complex **13** is depicted in Fig. 3.10, with selected bond distances and angles listed in Tables 3.2 and 3.3.

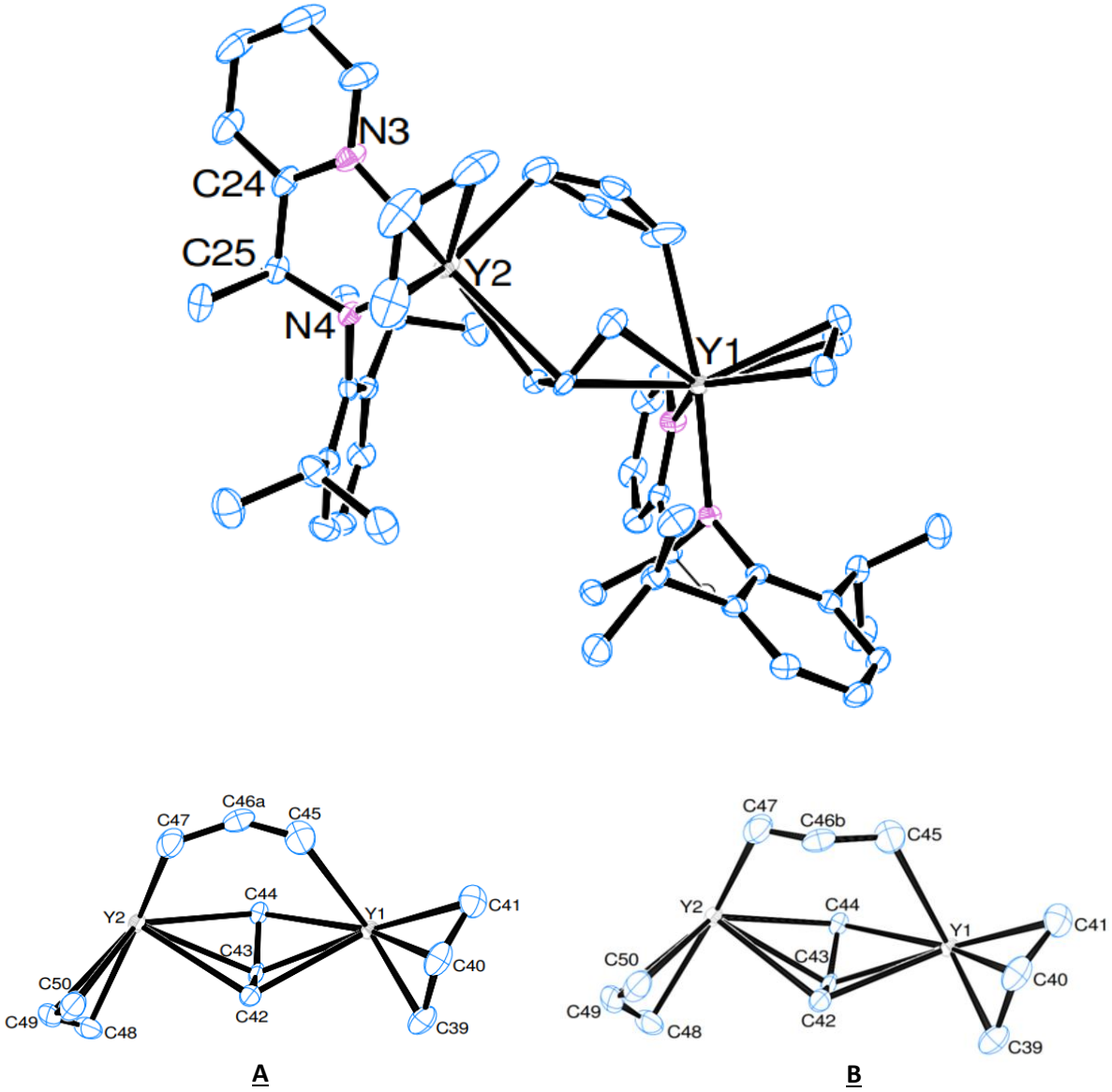

Figure 3.10: Molecular structure of 13. Most of the hydrogen are omitted for clarity. Thermal ellipsoid drawn at 50% of probability.

The compound **13** crystallized in the P-1 space group with a pentane molecule in the unit cell (omitted on the figure above). The molecular structure of the complex was composed of two yttrium centers where each metal was bound to one $\mathbf{Z^1}$ ligand and three different allyl moieties. Of the three different allyls, each yttrium center was coordinated to a typical "terminal" allyl (C41-C40-C39 for Y1 and C50-C49-C48 for Y2). For these terminal allyls, the average Y-C bond lengths (Y-C = 2.62 Å) along with the mean C-C bond distances (C-C = 1.38 Å) and the allyl angle of 126° were within a typical value for a η^3-delocalized allyl moiety[10]. In addition, the two yttrium atoms were connected by a first C44-C43-C42 allyl bridge, with Y1-C44(C43, C42) ≈ Y2-C44(C43) ≈ 2.7-2.6 Å while the Y2-C42 distance was

intriguingly longer at 2.945 Å. A rare example of an η^3-allyl bridge with unsymmetrical bond distances between two RE metal centers was already observed in the formation of the anionic samarium complex $Sm(allyl)_4^-$, which was described in 2005 by the group of M. Bochmann (Fig. 3.11)[9c)]. Among the six Sm-C bond distances shared by the allyl ligand between two Sm atoms, four of them are between 2.7 and 2.8 Å, while the two others are longer at 2.98 Å. This is in contrast to complex **13**, where only one Y-C bond distance was longer than the other five Y-C bonds. Furthermore, another structural feature worth noting in complex **13** is that the two yttrium centers were linked by another unusual allyl bridge, the first of this kind to our knowledge, formed by the allyl C47-C46-C45. This bridge was unsymmetrical, showing a higher Y1-C45 bonding distance than its counterpart Y2-C47 (2.766 *vs.* 2.623 Å, respectively). As already described once with lutetium metal center by W. J. Evans and coll.[13] (Fig. 3.11), we initially assumed that this allyl bridge was η^1-coordinated to the two yttrium centers, but the sum of the yttrium (1.9 Å) and carbon (0.7 Å) radii was slightly shorter than these distances [$r_Y + r_C = 2.6 \leq$ Y-C45(C47)]. Another plausible explanation for these uncommon yttrium-carbon(allyl) distances could involve a "five-center-four electron bonding" (Y-C-C-C-Y), which would extend the concept of five-center-two-electron bonding seen in tri-hapto borohydride seen in the borohydride chapter. To the extent of our knowledge, this bonding pattern has not been observed with an allyl moiety before. In such scenario, the Y2-C47 bond length could be resulting from a mono-hapto coordination while shorter Y1-C45 would be in better agreement with a di-hapto coordination, in this allyl moiety shared between two yttrium. This allyl bridge also featured a short C-C bond length on each side, C45-C46A = 1.255 or C47-C46B = 1.294 Å and a longer one, C47-C46A = 1.382 or C45-C46B = 1.334 Å, respectively (the latter being typical for a double bond). Interestingly, a certain "compensation" in favor of each yttrium center could be observed between the two allyl bridges. Indeed, Y2 was linked by both the shortest distance to one allyl (C47-C46-C45) and the longest to C42 belonging to the other allyl, while the opposite was found to be true for Y1. Furthermore, this unprecedented allyl "core" had C47-Y2-C43 and C45-Y1-C43 angles of 90° and a more open C47-C46-C45 angle than other allyl (C47-C46-C45 = 141.54° *vs*. C42-C43-C44 = 128.26°). Selected bond distances and angles are gathered in Table 3.2.

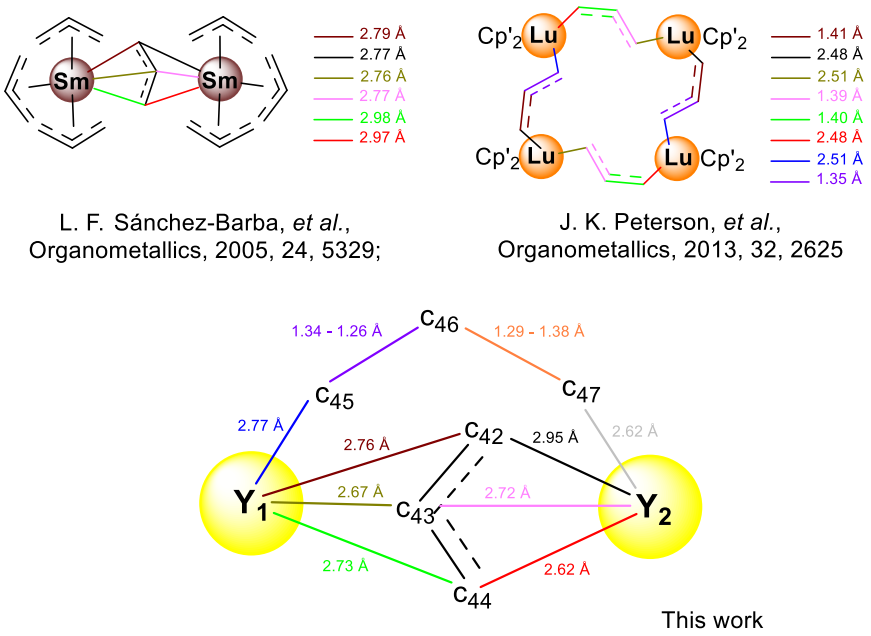

Figure 3.11: Allyl bridges of 13 compared to the ones in literature.

*Table 3.2: Distances and angle of the different allyls in **13***

	13		**13**
Y1-C39 (C41) (Å)	2.536 (2.638)	**Y2-C48 (C50) (Å)**	2.580 (2.680)
Y1-C40 (Å)	2.613 (2)	**Y2-C49 (Å)**	2.639 (2)
C39-C40-C41 (°)	126.72	**C48-C49-C50 (°)**	126.40
C41(C40)-C40(C39) (Å)	1.370 (1.395)	**C48(C49)-C49(C50) (Å)**	1.389 (1.371)
Y1-C42 (Å)	2.756 (2)	**Y2-C42 (Å)**	2.945 (2)
Y1-C43 (Å)	2.670 (2)	**Y2-C43 (Å)**	2.717 (2)
Y1-C44 (Å)	2.730 (2)	**Y2-C44(Å)**	2.673 (2)
Y1-C45 (Å)	2.766 (2)	**Y2-C47 (Å)**	2.623 (2)
Y1-C46A (C46B) (Å)	3.600 (3.596)	**Y2- C46A (C46B) (Å)**	3.506 (3.457)
Y1-C47 (Å)	4.452	**Y2-C45 (Å)**	4.310
C42-C43 (Å)	1.383 (3)	**C45-C46B (Å)**	1.334 (6)
C43-C44 (Å)	1.393 (3)	**C45-C46A (Å)**	1.255 (5)
C42-C43-44 (°)	128.2 (2)	**C46B-C47 (Å)**	1.294 (5)
C45-Y1-C43 (°)	89.70 (7)	**C46A-C47 (Å)**	1.382 (5)
C47-Y2-C43 (°)	92.37 (7)	**C45-C46A(C46B)-C47 (°)**	141.54 (142.72)

Regarding the amido-pyridine ligand coordination mode in **13**, the pyridine and amido nitrogen bond distances were located at a typical distance from the metal center with Y2(Y1)-N4(N2) ≈ 2.22 Å and Y2(Y1)-N3(N1) ≈ 2.45 Å, values almost identical to those observed for complex **7**. The torsion angle between the pyridine plane and the amidomethyl plane (N3-C24-C25-N4 = -9.89°) indicated that the planes deviate slightly from planarity while the aryl plane *vs.* the pyridine plane deviate from orthogonality (73.61°).

*Table 3.3: Selected bond and angles of **12** and **13**.*

	12	**13**
RE-$CH_{2Terminal}$ (Å)	2.713 [a)]	2.609 [a)]
RE-CH (Å)	2.731 [a)]	2.626 [a)]
CH_2-CH-CH_2	125.9 (7)	126.56[a)]
RE-N_{pyr} (Å)	2.549 (2)	2.451 [a)]
RE-N_{Amine} (Å)	2.311 (2)	2.219 [a)]
(N_{pyr}-)C-C(-N_{Amine}) (Å)	1.523	1.510
N_{pyr}-C-C-N_{Amine} (°)	-2.095	-9.890 [a)]
Pyr *vs.* Aryl plane (°)	89.80	74.48[a)]

a) *Mean value*

The ^{1}H NMR spectrum of complex **13** performed in THF-D8 (Fig. 3.12, top) exhibited only one doublet at δ = 2.69 ppm and one quintuplet at δ = 6.23 ppm for the allyl part. In contrast, the ^{1}H NMR spectrum of the same complex in toluene-D8 (Fig. 3.12, bottom) showed a single quintuplet at δ = 6.67 ppm, which overlapped with the signal of one aryl proton, and showed an interesting broad signal between δ = 3.8 and 2.5 ppm, likely corresponding to a *CH_2* of the allyl fragment. Using THF-D8 as the solvent, we could observe only the terminal allyl groups (or possibly a rapid exchange with the η^3—allyl bridge) in the NMR spectrum, with clearly defined resonance peaks for the CH at δ = 6.23 ppm and the two CH_2 at δ = 2.69 ppm integrating respectively for two and eight protons. This observation suggests that the allyl bridges have decomposed, likely leading to a clean mono-substituted **Z^1** yttrium complex with two terminal allyl groups along with the coordination of deuterated THF molecule(s). While the allylic resonances are tricky to understand and to interpret, the peaks corresponding to the **Z^1** ligand coordinated to the metal were easily identifiable (marked as +). Already observed on almost all complexes previously described in this work, the duplication of the CH isopropyl was present on both spectra at δ = 4.51 and 3.72 ppm in Tol-D8 and at δ = 4.05 and 3.25 ppm in THF-D8.

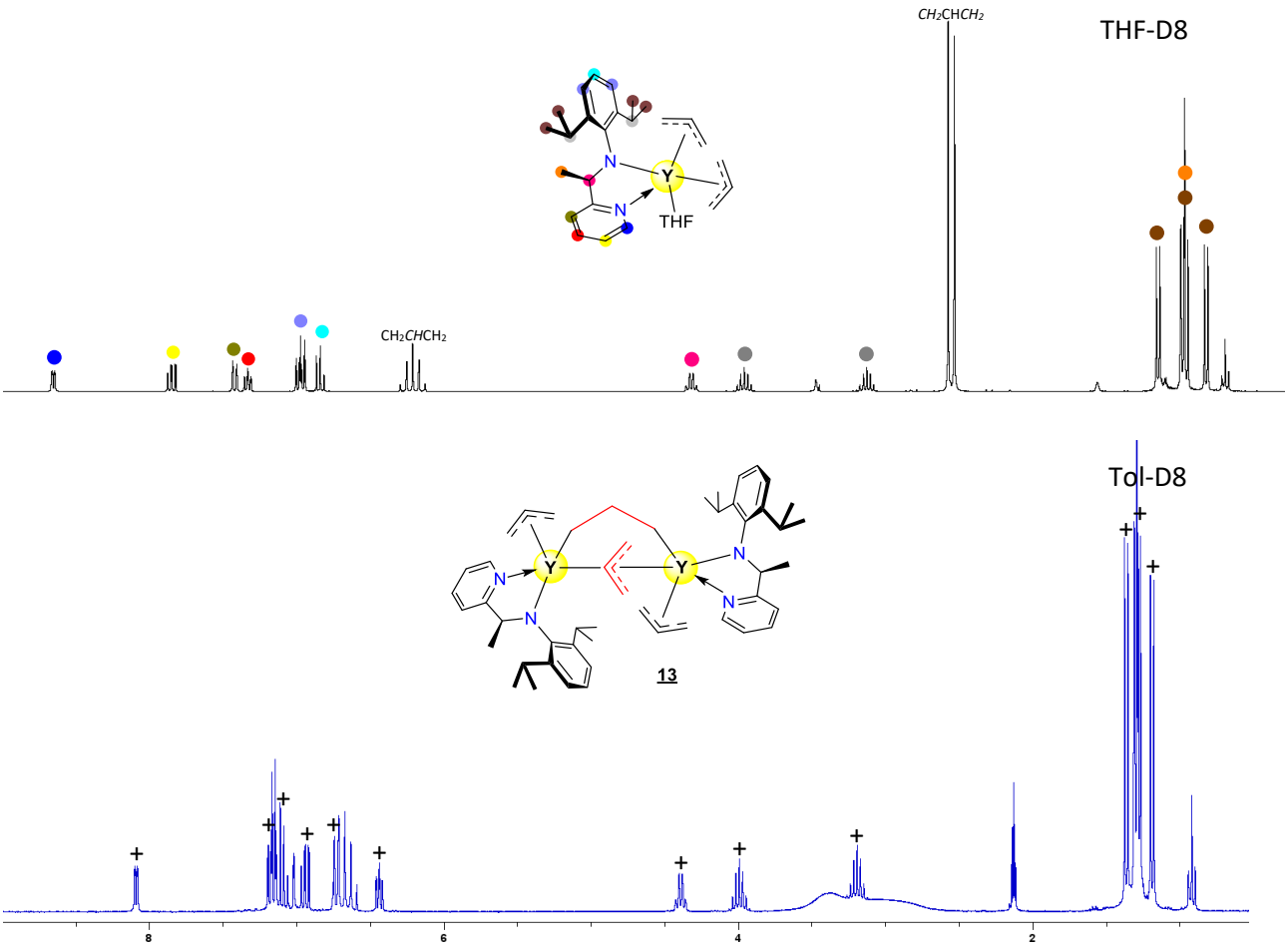

Figure 3.12: ^{1}H NMR of 13 in Tol-D8 (top) and in THF-D8 (bottom).

To come back to the allyl resonances, we would suggest that the CH_2 of the different allyls are capable of exchanging with each other, albeit not fast enough to appear as a well-defined doublet in the spectrum. To investigate the possibility of observing a coalescence phenomenon, ^{1}H NMR studies at different temperatures were performed in toluene-D8, which are presented in Fig. 3.13 a) and b).

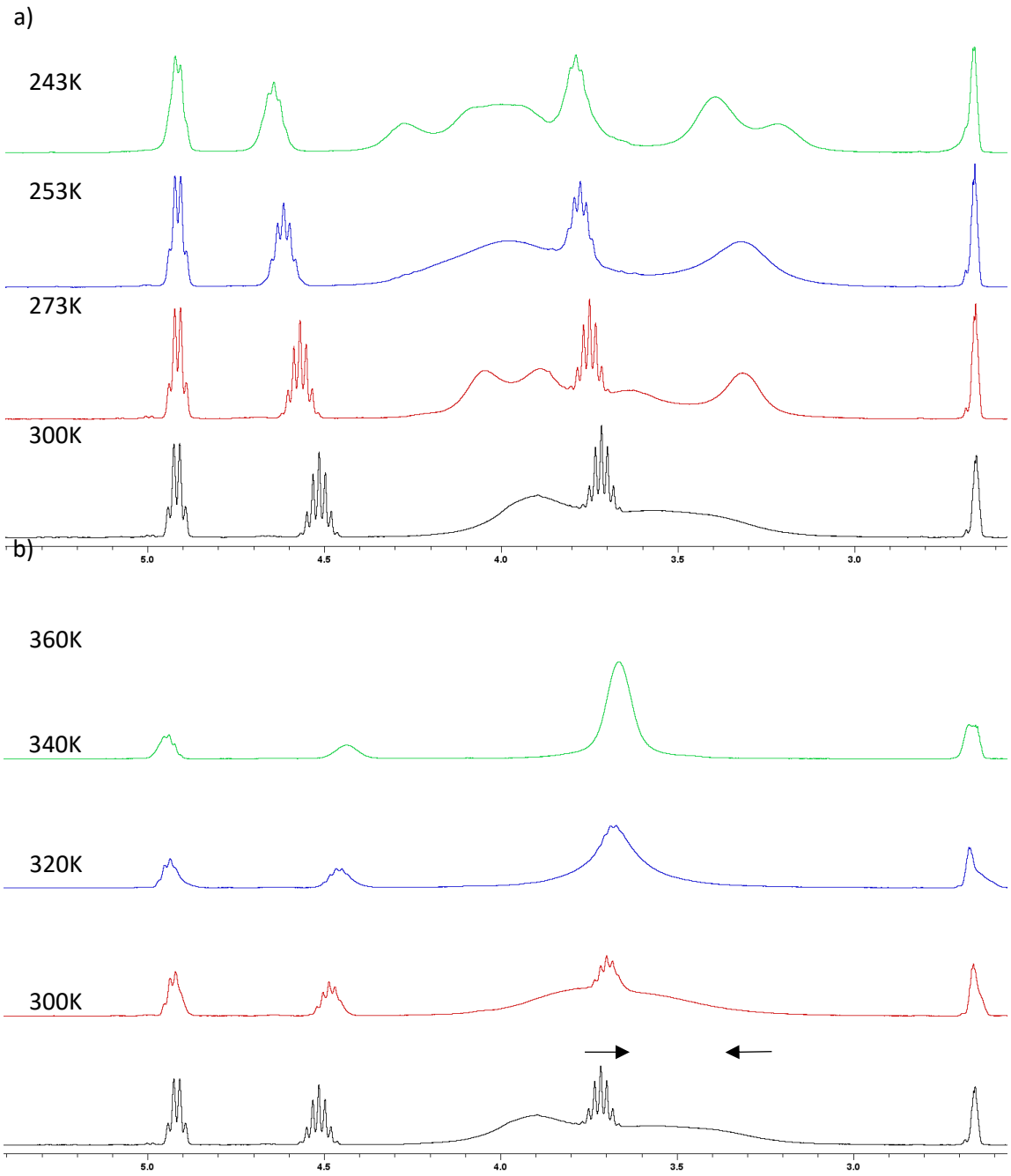

Figure 3.13: ^{1}H NMR of 13 in Toluene-D8 with variation of temperature.

Cooling from 300 K to 273 K (Fig. 3.13 a) allowed to observe a deconvolution of the broad signal around $\delta = 3 - 4$ ppm into three different resonance peaks. Cooling down further to 253 K had no effect on the shape of the peak at δ = 3.3 ppm, while the signals at δ = 3.9 and 4.1 ppm merged into a very broad one at *ca*. δ = 4 ppm. Unfortunately, due to the temperature limit of the instrument fixed at 243 K, the last recorded spectrum was at this temperature, where the resonance at δ = 3.3 ppm began to differentiate as two broad peaks in the same area. The broad signal observed at δ = 4 ppm at

253 K evolved into two signals at δ = 4.3 ppm and a coalescing one at δ = 4.00 ppm. Increasing the temperature from 243 K to 300 K enabled the recovery of the original spectrum.

By heating the same tube from 300 to 360 K with an increase of 20 K [Fig. 3.13 b], the two broad peaks could be seen to merge into one large peak at *ca.* δ = 3.7 ppm, indicating an enhancement of allyl exchange. As with the cold temperature experiments, the original spectrum of **12** was recovered by returning to room temperature.

Following this temperature study, the stability of complex **13** in THF-D8 was also evaluated by ^{1}H NMR study. A first ^{1}H NMR spectrum was recorded after letting complex **13** stand at room temperature in THF for three days (Fig. 3.14, b). This spectrum revealed the appearance of a new product (marked as *) compared to the ^{1}H NMR spectrum of the starting material **13** (Fig. 3.14 a *vs.* b) with the appearance of propene peaks (marked as °). Relative integration of all resonance peaks revealed that the new product was formed at 13% of the total mixture. With the aim of increasing the conversion rate, the NMR tube was heated at 40 °C for several days and the ^{1}H NMR was recorded. After 24 h, the ^{1}H NMR spectrum, displayed in Fig. 3.14 c), showed a conversion of *ca.* 45%. After 3 days, the spectrum (Fig. 3.14, d) revealed a conversion of 80% and, finally, after one week (Fig. 3.14 e) the total consumption of complex **13** was achieved.

Regarding the formation of the new product (marked as *), one can immediately notice on the ^{1}H NMR spectrum (Fig. 3.14 e) the disappearance of most of the aromatic signals (between δ = 7 and 8 ppm) but also the loss of the quadruplet of the proton attached to the asymmetric carbon in **Z^1** (previously at δ = 4.44 ppm). On the other hand, the appearance of two signals between δ = 5 and 6 ppm and a triplet-like resonance at δ = 4.29 ppm could be observed. Interestingly, the evolution of the ^{1}H NMR spectra revealed the disappearance of the duplication of the CH septuplet of the isopropyl at δ = 4.05 ppm and δ = 3.24 ppm. After integration of the ^{1}H NMR spectrum in Fig. 3.14 e), the allyl doublet counted for 4H (δ = 2.46 ppm) and the CH quintuplet for 1H (δ = 6.12 ppm), which testified to the presence of only one allyl group per yttrium center, as could be predicted by the apparition of propene (see above). Among all the other signals, two could be easily identified: the septuplet integrating for 2H at δ = 3.39 ppm is attributed to the CH isopropyl and the meta-aryl CH integrating for 2H at δ = 6.85 ppm. In conclusion, it appeared that the isolated compound **13** could be an intermediate metastable compound that evolves with time, in a polar medium like THF, with release of propene.

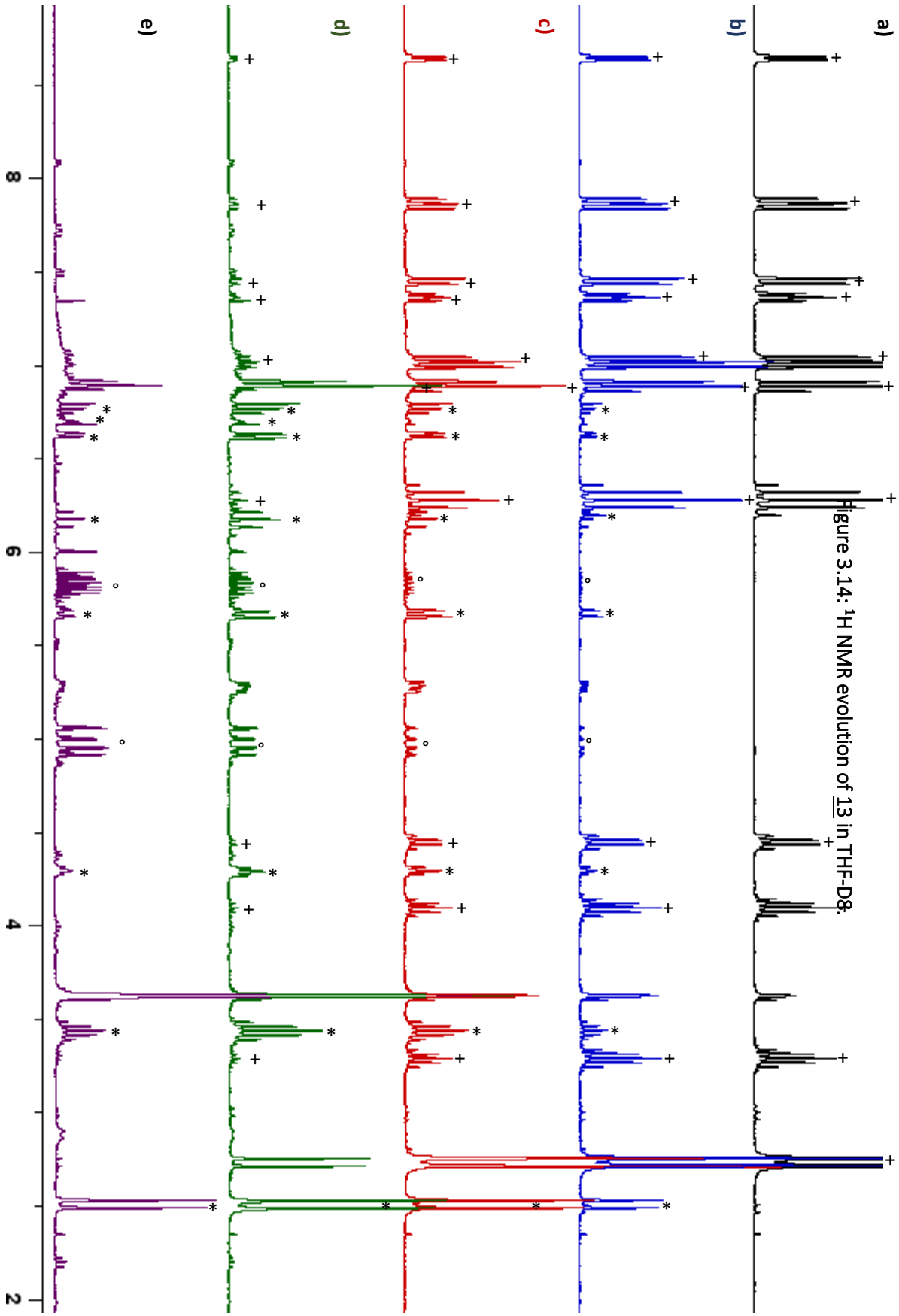

Figure 3.14: ^{1}H NMR evolution of 13 in THF-D8.

This transformation might come from a C-H activation on the asymmetric carbon of the ligand as proposed on Scheme 3.7. Unfortunately, no crystals or elemental analysis of this final product was obtained to confirm this phenomenon.

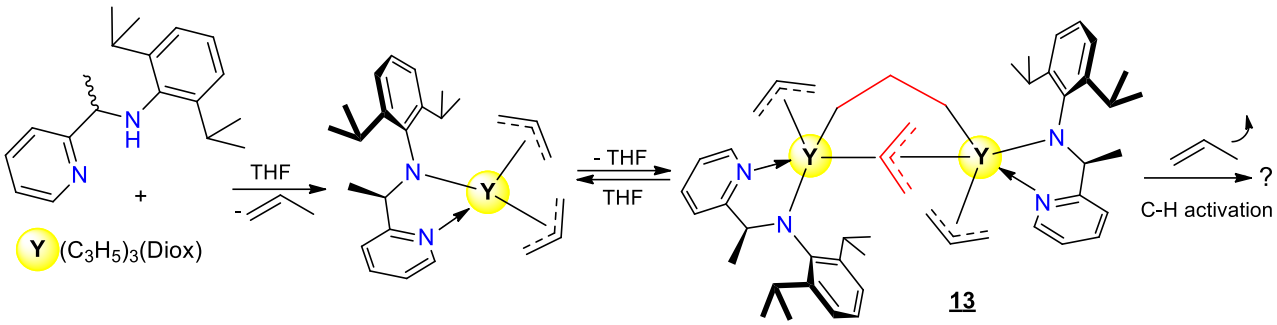

Scheme 3.7: Synthesis of 13 with highlight of allyl bridges and C-H activation.

Expecting to observe this unusual CH activation, similar to that seen with yttrium but using a different rare earth metal, attempts were made to synthesize neodymium mono-substituted complexes with the other ligands **Z^2H** and **Z^3H**.

3.3.2 Syntheses using Z^2H

As seen with the borohydride complexes (Chapter II of this manuscript), the degree of substitution of isolated complexes changed when the ligand **Z^1** was replaced with its methyl substituted **Z^2** counterpart. To confirm the assumption that this (*a priori*) slight modification of the amido-pyridine ligand would lead to a mono-substituted derivative, we attempted to synthesize an allyl complex using **Z^2H** protio-ligand by following the reaction through ^{1}H NMR study, initially in the Nd series.

In Fig. 3.15, the ^{1}H NMR spectra of the starting materials **Z^2H** (in black) and Nd$(C_3H_5)_3$(diox) (in green) (a) were compared to the mixture of these two products displayed in Fig. 3.15 b). It was observed that no reaction occurred 30 minutes after the addition of **Z^2H** to the neodymium tris-allyl solution in THF-D8. The NMR tube was heated at 50 °C for 30 min, which allowed for the deprotonation of **Z^2H** and the formation of a complex that was identified as mono-substituted based on the appearance of several paramagnetic peaks (Fig. 3.15, c and d). Unfortunately, the poor integration of the signal precluded any conclusive interpretation beyond the effectiveness of the coordination of the ligand to Nd metal center. Full spectrum is shown in Appendix 9.

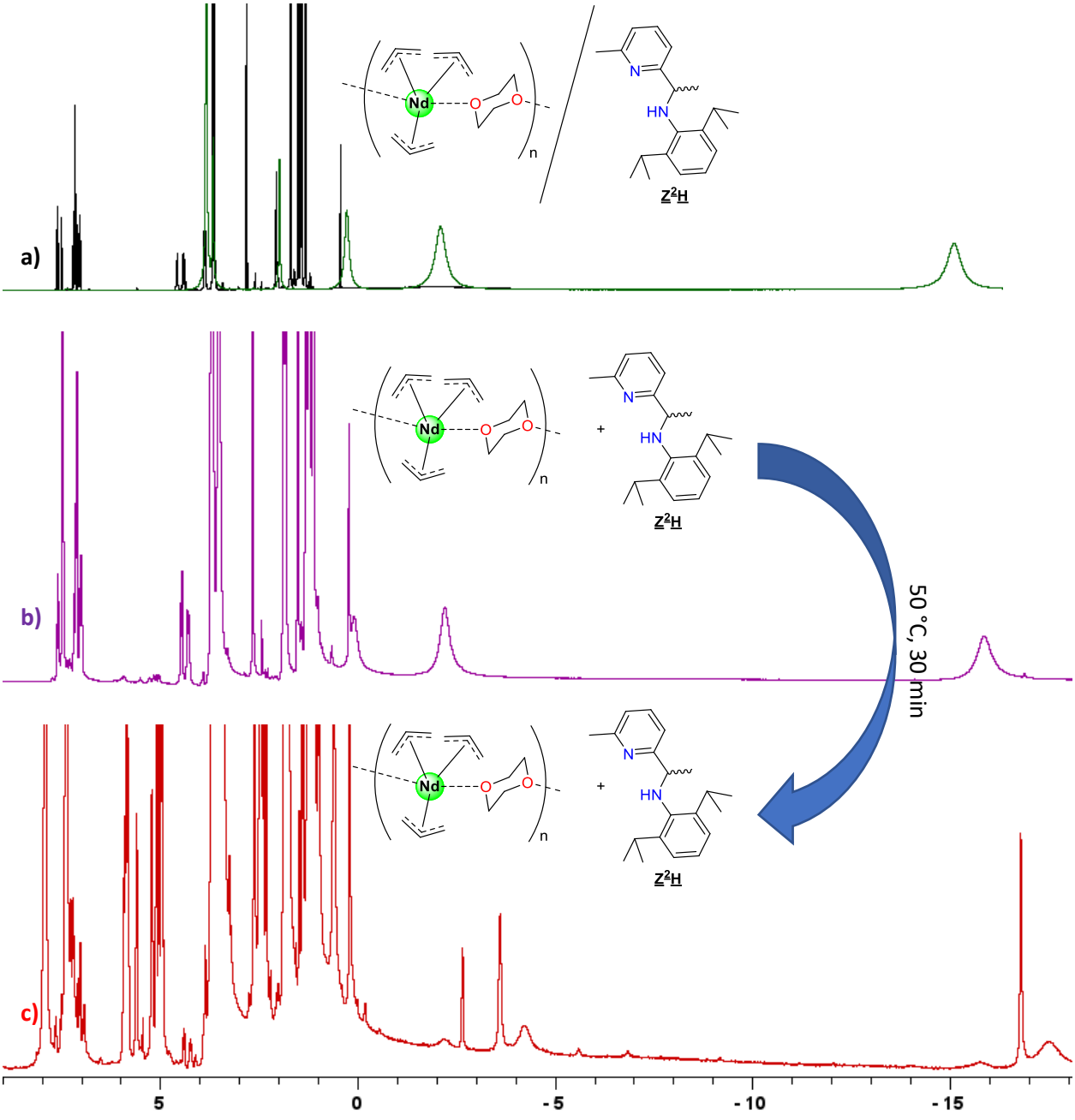

Figure 3.15: ^{1}H NMR monitoring of the reaction of Z^2H with $Nd(C_3H_5)_3(diox)$ (solvent THF-D8)

Bulk synthesis was conducted in THF, where an equimolar mixture of $Nd(C_3H_5)_3(diox)$ and **Z^2H** was heated to 50 °C for one hour. Evaporation of the green solution gave a dark green foam, the product was dissolved in minimal toluene and filtered. The solution was then left to stand at room temperature and dark green crystals suitable for XRD analysis were obtained after a few days. The

molecular structure displayed in Fig. 3.16 shows an interesting sandwich homodinuclear neodymium complex **14**. Selected bond and angles are listed in Table 3.4.

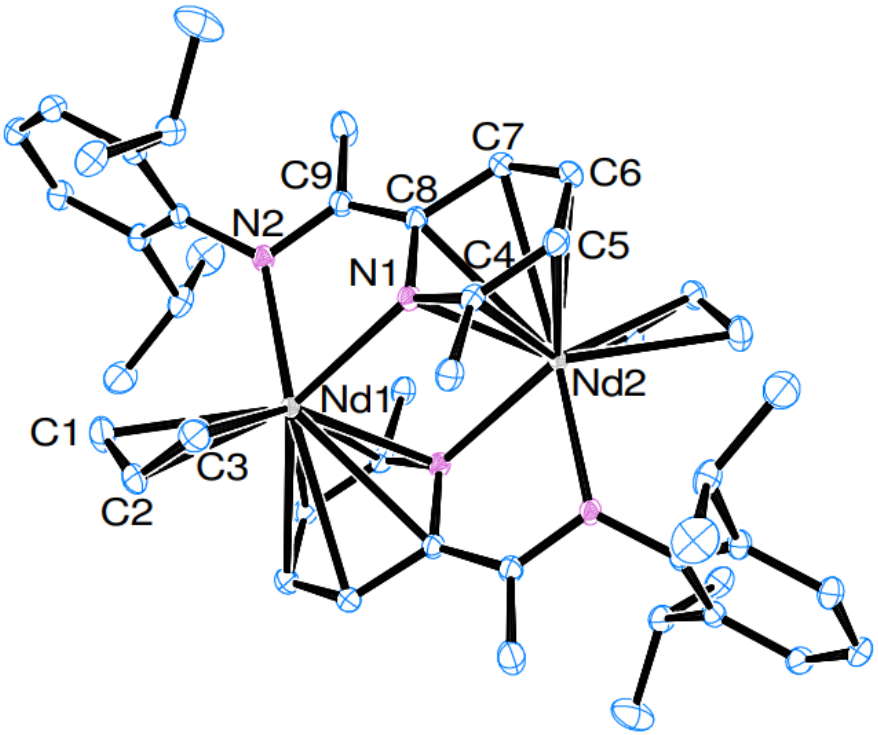

Figure 3.16: Molecular structure of 14 with hydrogens omitted for more clarity. Thermal ellipsoid drawn at 50%.

Complex **14** was crystallized in the Pbca space group and featured two neodymium centers, each of them being coordinated by a ligand $\mathbf{Z^2}$ and an η^3-allyl group. Interestingly, the two Nd centers were bridged by the pyridine nitrogen atom of each $\mathbf{Z^2}$ ligand, providing an unexpected structural feature. The C-C bond between C9 and C8 of 1.383 (2) Å was relevant for a sp^2 hybridized carbon. The length of this bond provided evidence that the proton on the asymmetric carbon C8 was deprotonated by a second allyl moiety (the first being the deprotonation of the amine moiety), as previously considered for the yttrium derivative **13** on the basis of ^{1}H NMR studies. Also, the change in the coordination mode of the pyridine moiety, to a pyridyl moiety, (pyridyl-amido ligand referred to as $\mathbf{Z^{2\prime}}$) was observed in complex **14**. The possibility of a second deprotonation of the amino-pyridine has already been described by M. Westerhausen[14]: the C-H activation of the asymmetric carbon allows the formation of a di-anionic species, which is stabilized by charge delocalization (Scheme 3.8).

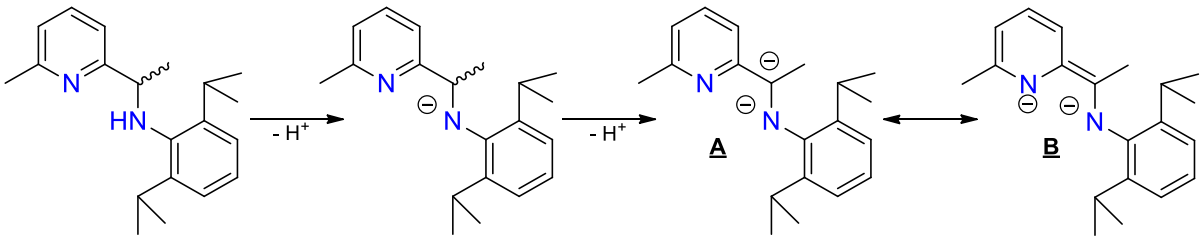

Scheme 3.8: Delocalization of the anionic charge in the Z^2 ligand upon double deprotonation.

While the N2-Nd1 bond length of 2.327 Å in complex **14** was in the same range as that observed in complex **4**, the shrinkage of the $N_{pyridine}$-neodymium bond length from 2.567 Å in complex **4** to 2.455 Å in the present complex was noted. Furthermore, the pyridine ring clearly showed the de-aromatization of pyridine moiety by the presence of two different bond lengths within the ring (C8-C7 ≈ C6-C5 ≈ 1.45 Å and C7-C6 ≈ C5-C4 ≈ 1.37 Å), which accounted for the coordination of the **B** form of the ligand to the Nd center. Analogous magnesium complexes described in the literature[14a)] (Scheme 3.9) exhibit the same pyridyl carbon-carbon and C9-C8 (**14**: 1.383 Å) bond length as found in **14**. Furthermore, a shrinkage of the same kind is observed after the second metalation, allowing the pyridyl unit to be located closer to the magnesium center [Mg(L)(Me), N-Mg: 2.144 Å *vs.* Mg(L'), N-Mg: 2.031 Å]. While the length of the C-N_{Amine} bond is not changed in the magnesium complex [Mg(L)(Me), C-N_{Amine}: 1.480 Å *vs.* Mg(L'), C-N_{Amine}: 1.461 Å], the neodymium complex **14** exhibited a shorter C-N_{Amine} bond compared to that found in complex **4** [1.393 *vs.* 1.465 Å].

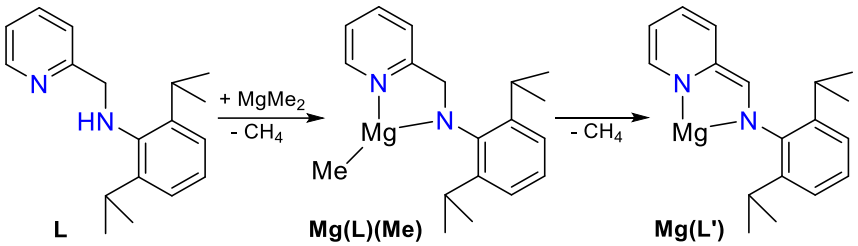

Scheme 3.9: Synthesis of the Mg(L)(Me) and formation of Mg(L') by intramolecular metalation (ref. 14A).

A closer look at the pyridyl bridge gave a Nd2-C4 distance of 2.769 Å in complex **14**, which was shorter than other Nd2-carbon distances (Nd-C5 = 2.857, Nd-C6 = 2.913, Nd-C7 = 2.923, Nd-C8 = 2.879 Å). These distances are close to those observed in toluene adducts of neodymium complexes[15] in which the toluene moiety is η^6-coordinated. In addition, a heterocyclic ligand coordinated to Nd in η^5 mode such as phospholyl[16] has a shorter bond between the metal center and the carbon in the alpha position of the heteroatom. Thus, this unprecedented η^6-coordination of the pyridyl fragment of **$Z^{2\prime}$** ligand to

Nd in complex **14** appeared to be relevant. Particular interest could be showed to another structural point in **14**: the Nd-Nd distance (Nd-Nd = 3.907 Å) was shorter than the sum of the neodymium ionic radius (r_{Nd} = 2.05 Å).

At this stage, a possible interaction between the two Nd centers might be proposed, but further investigations, *i.e*. theoretical calculations, should be performed to get more insights. Although a few complexes have been described in the literature with a short RE-RE distances[17], only two examples have been identified (by DFT and electronic density) to contain an interaction between the two RE centers (bond)[18].

In neodymium chemistry, similar complexes with a tridentate ligand[19] were previously described. They were prepared by three-step reduction of the complex with KC_8 and showed, after the third reduction stage, a homodinuclear structure with an even shorter Nd-Nd distance (3.774 Å) than found in complex **14**.

Considering our previous results with yttrium compound **13,** a possible mechanistical pathway could be suggested as presented in Scheme 3.10. Our proposition is that, similarly to yttrium, a neodymium bis-bridged compound would result from the reaction of Nd(allyl)$_3$(diox) with **Z^{2}H**. However, such compound (that could be isolated successfully as **13** for yttrium) would this time be a transient species that rearranges itself, with loss of propene resulting from C-H activation of the ligand, to lead to the formation of complex **14** (as suggested by the ^{1}H NMR monitoring shown previously in Fig. 3.14). Unfortunately, I was unable to undertake the analog of complex **14** for the yttrium series due to time constraint as these studies were performed towards the end of my PhD contract.

The C1-C2-C3 allyl moiety in **14** was then located at a standard distance from the metal center, with the carbon-neodymium bond distances ranging from 2.62 to 2.72 Å. The angle of the allyl (C1-C2-C3 = 125.62°) was also in a typical range for a full negative charge delocalization. While the torsion angle between the amido-methyl plane and the pyridyl plane showed an almost perfect planarity (N1-C8-C9-N2 = 0.732°), the angle measured between the aryl plane and the pyridyl ring was orthogonal (89.82°).

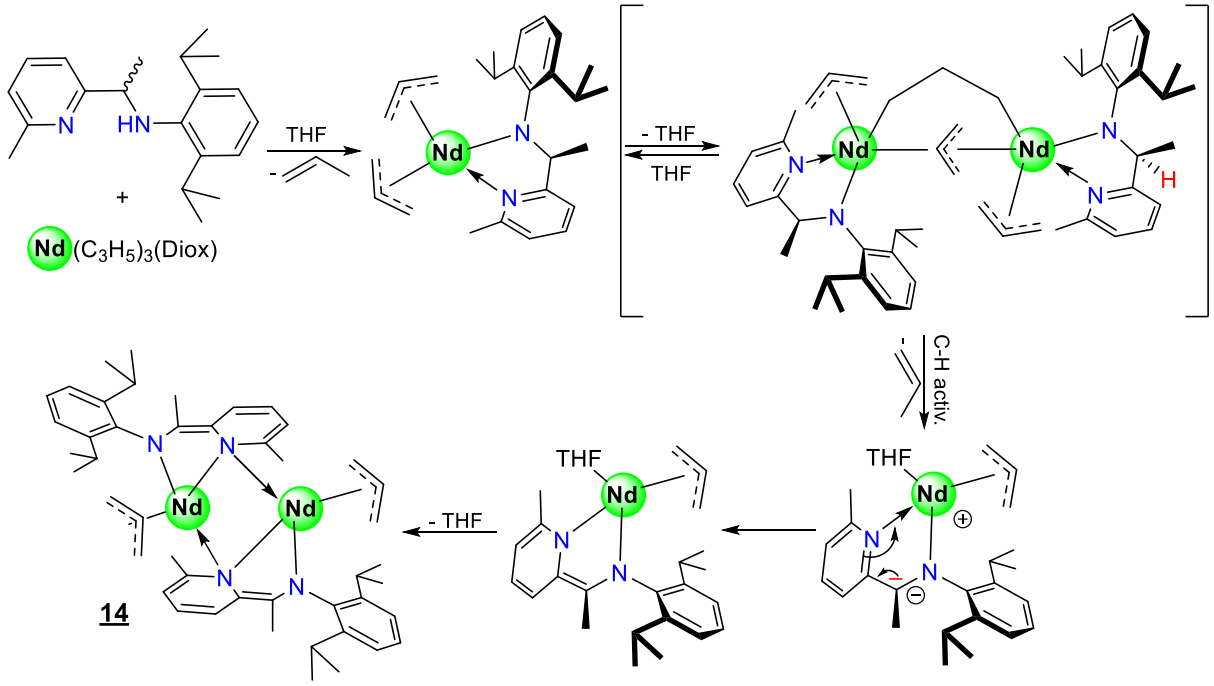

Scheme 3.10: Possible pathway leading to 14.

Following these results, attempts were made to synthesize the neodymium complexes using the **Z^{3}H** ligand, in the hope of observing similar coordination behavior to that of the **Z^{2}H** ligand.

*Table 3.4: Comparison of selected bond length and angles in complexes **14** and **4**.*

	14	**4**
Nd-Nd	3.907	
Nd-$CH_{2Terminal}$ (Å) [a)]	2.663	-
Nd-CH (Å)	2.719 (2)	-
CH_2-CH-CH_2	125.63 (2)	-
Nd02-N1 (Å)	2.610	-
Nd01-N1(Å)	2.455 (2)	2.567 (1)
Nd-N_{Amine} (Å)	2.327 (2)	2.299 (1)
(N_{pyr}-)C-C(-N_{Amine}) (Å)	1.383 (2)	1.511 (2)
C- N_{Amine} (Å)	1.392 (2)	1.465 (2)
N_{pyr}-C-C-N_{Amine} (°)	0.732	18.895
Pyr *vs.* Aryl plan (°)	89.82	69.19

[a)] *Mean value*

3.3.3 Attempt using Z^3H with tris-allyl of neodymium.

It was observed, as exemplified by **Z^2H**, that introducing a methyl substituent onto the pyridine ring made it more difficult for the ligand to coordinate with the Nd metal center. Consequently, heating the mixture of Nd precursor with **Z^2H** was necessary to assist the coordination process, which led to unprecedented coordination chemistry. Thus, with **Z^3H** possessing more steric hindrance than **Z^2H,** ^{1}H NMR studies were performed to foresee the reaction time (Fig. 3.17). As before, the reaction could be easily followed by ^{1}H NMR analysis. Upon adding **Z^3H** in THF-D8 onto the neodymium tris-allyl precursor (marked as +), no reaction was observed after 30 minutes. However, after 3 hours at 50 °C, some paramagnetic resonances began to appear on the spectrum (Fig. 3.17 c) (*). After one day at 50 °C, more paramagnetic signals were present, likely resulting from the coordination of **Z^3**, along with the presence of a portion of the tris-allyl starting material (c *vs.* d). Full conversion was reached in 2 days at 50 °C (Fig. 3.17 e). Unfortunately, due to the highly paramagnetic NMR data, no interpretation was possible (full ^{1}H NMR spectra in appendix 10).

A bulk synthesis was carried out following the ^{1}H NMR result: to the green solution of $Nd(C_3H_5)_3$(diox) in THF was added an equimolar solution of **Z^3H**. The resulting dark red-green solution was left for stirring at 50 °C for 2 days. After that time, the solvent was removed under vacuum before addition of toluene. Filtration and evaporation yielded a dark green powder.

Unfortunately, due to the high solubility of the compound (with an NMR spectrum identical to previous experiment); no crystals were obtained under different solvent conditions, and thus this work is still in progress.

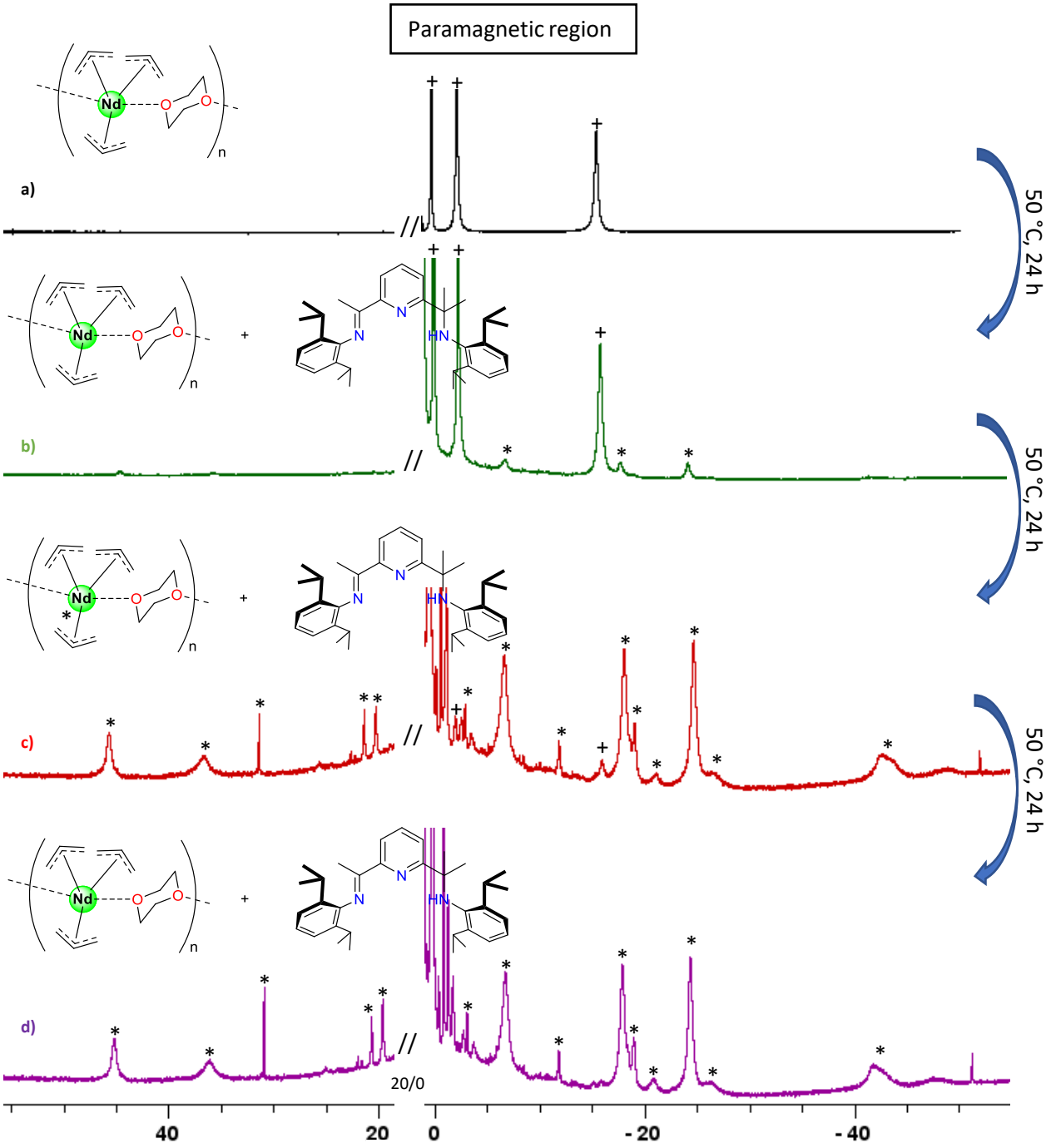

Figure 3.17: ^{1}H NMR monitoring for the complexation of Z^{3}H over neodymium tris-allyl (solvent THF-D8).

3.4 Conclusion

In the attempt to synthesize mixed bis-allyl borohydride complexes, a new clean synthetic

route by reduction of $Nd(C_3H_5)_3(diox)$ leading to the formation of tetra-allyl neodymium (**11**) was found. The most promising preparation pathways to obtain the desired mixed complexes seems to be the cationic routes. The ^1H NMR test with neodymium revealed the possibly of obtaining the product, but the bulk synthesis showed the formation of an unidentified species. The ^1H NMR trials with yttrium appears to be the most promising and bulk synthesis is being considered for the future.

Contrary to our first assumption, the syntheses of amido-pyridine complexes using tris-allyl rare earth precursors were more complicated (but also more exciting!) than anticipated. Although the synthesis of the bis-substituted complex $Nd(\mathbf{Z^1})_2(C_3H_5)$ proceeded as expected, the mono-substituted compound bearing $\mathbf{Z^2}$ underwent a C-H activation by a second deprotonation (**14**).

A very interesting possible intermediate for C-H activation with a unique allyl bridge was isolated (**13**).

References

[1] L. F. Sánchez-Barba, D. L. Hughes, S. M. Humphrey, M. Bochmann, **Organometallics,** *2005*, 24 (15), 3792.

[2] E. A. Hill, W. A. Boyd, H. Desai, A. Darki, L. Bivens, **J. Organomet. Chem.**, *1996*, 514 (1-2),1.

[3] S. Fadlallah, M. Terrier, C. Jones, P. Roussel, F. Bonnet, M. Visseaux, **Organometallics**, *2016*, 35 (4), 456.

[4] S. Fadlallah, J. Jothieswaran, I. D. R., L. Maron, F. Bonnet, M. Visseaux, **Catalysts**, *2020*, 10 (8), 820.

[5] D. Robert, E. Abinet, T. P. Spaniol, J. Okuda, **Chem. Eur. J.**, *2009*, 15 (44), 11937.

[6] (a) M. R MacDonald, J. W. Ziller, W. J. Evans, **J. Am. Chem. Soc.**, *2011*, 133 (40), 15914; (b) M. R. MacDonald, J. E. Bates, M. E. Fieser, J. W. Ziller, F. Furche, W. J. Evans, **J. Am. Chem. Soc.**, *2012*, 134 (20), 8420; (c) M. R. MacDonald, J. E. Bates, J. W. Ziller, F. Furche, W. J. Evans, **J. Am. Chem. Soc.**, *2013*, 135 (26), 9857; (d) P. B. Hitchcock, M. F. Lappert, L. Maron, A. V. Protchenko, **Angew. Chem., Int. Ed.**, *2008*, 47 (8), 1488; (e) J. F. Corbey, D. H. Woen, C. T. Palumbo, M. E. Fieser, J. W. Ziller, F. Furche, W. J. Evans, **Organometallics**, *2015*, 34 (15), 3909.

[7] C. J. Windorff, M. T. Dumas, J. W. Ziller, A. J. Gaunt, S. A. Kozimor, W. J. Evans, **Inorg. Chem.**, *2017*, 56 (19), 11981.

[8] T. F. Jenkins, D. H. Woen, L. N. Mohanam, J. W. Ziller, F. Furche, W. J. Evans, **Organometallics**, *2018*, 37 (21), 3863.

[9] (a) A. Mazzei, **Makromol. Chem. Suppl.**, *1981*, 4, 61; (b) R. Taube, S. Maiwald, J. Sieler, **J. Organomet. Chem.**, *1996*, 513 (1-2), 37; (c) L. F. Sánchez-Barba, D. L. Hughes, S. M. Humphrey, M. Bochmann, **Organometallics**, *2005*, 24 (22), 5329; (d) S. Standfuss, E. Abinet, T. P. Spaniol, J. Okuda, **Chem. Commun.**, *2011*, 47 (41), 11441.

[10] Selected reference: (a) L. F. Sánchez-Barba, D. L. Hughes, S. M. Humphrey, M. Bochmann, **Organometallics**, *2005*, 24 (15), 3792; (b) S. Maiwald, R. Taube, H. Hemling, H. Schumann, **J. Organomet. Chem.**, 1998, 552 (1-2), 195.

[11] M. Brunelli, S. Poggio, U. Pedretti, G. Lugli, **Inorg. Chim. Acta**, *1987*, 131 (2), 281.

[12] M. U. Kramer, D. Robert, S. Arndt, P. M. Zeimentz, T. P. Spaniol, A. Yahia, L. Maron, O Eisenstein, J. Okuda, **Inorg. Chem.**, *2008*, 47 (20), 9265.

[13] J. K. Peterson, M. R. MacDonald, J. W. Ziller, W. J. Evans, **Organometallics**, *2013*, 32 (9), 2625.

[14] (a) M. Westerhausen, T. Bollwein, N. Makropoulos, S. Schneiderbauer, M. Suter, H. Nöth, P. Mayer, H. Piotrowski, K. Polborn, A. Pfitzner, **Eur. J. Inorg. Chem.**, *2002*, (2), 389; (b) M. Westerhausen, A. N. Kneifel, N. Makropoulos, **Inorg. Chem. Comm.**, *2004*, 7 (8), 990; (c) D. Olbert, H. Görls, D. Conrad, M. Westerhausen, **Eur. J. Inorg. Chem.**, *2010*, (12), 1791.

[15] (a) Q. Liu, Y.-H. Lin, Q. Shen, **Acta Cryst.**, *1997*, C53 (11), 1579; (b) Y.-M. Yao, Y. Zhang, Q. Shen, Q.-C. Liu, Q.-J. Meng, Y.-H. Lin, **Chin. J. Chem.**, 2001, 19 (6), 588.

[16] S. M. Cendrowski-Guillaume,G. Le Gland, M. Nierlich, M. Ephritikhine, **Eur. J. Inorg. Chem.**, *2003*, (7), 1388.

[17] R. E. White, T. P. Hanusa, B. E. Kucera, **J. Am. Chem. Soc.**, *2006*, 128 (30), 9622.

[18] (a) F.-S. Guo, B. M. Day, Y.-C. Chen, M.-L. Tong, A. Mansikkamäki, R. A. Layfield, **Science**, *2018*, 362 (6421), 1400; (b) C. A. Gould, K. R. McClain, D. Reta, J. G. C. Kragskow, D. A. Marchiori, E. Lachman, E.-S. Choi, J. G. Analytis, R. D. Britt, N. F. Chilton, B. G. Harvey, J. R. Long, **Science**, *2022*, 375 (6577), 198.

[19] (a) H. Sugiyama, I. Korobkov, S. Gambarotta, **Inorg. Chem.**, *2004*, 43 (18), 5771; (b) S. S. Galley, S. A. Pattenaude, R. F. Higgins, C. J. Tatebe, D. A. Stanley, P. E. Fanwick, M. Zeller, E. J. Schelter, S. C. Bart, **Dalton Trans.**, *2019*, 48 (23), 8021.

CHAPTER 4 APPLICATION OF THE SYNTHESIZED RARE-EARTH AMIDO-PYRIDINE COMPLEXES IN RING-OPENING POLYMERIZATION

Preliminary studies of ring opening polymerization using some of the complexes described through this thesis will be presented in this chapter. Effects of the solvent as well as side-reactions noted by a difference between the experimental molecular weight and that expected will be discussed.

4.1 General presentation of the polymerization

4.1.1 Commonly used polymers

A polymer is an assembly of macromolecules composed of a large number of repeating monomers or units. Although polymers can be found in the natural environment (called biopolymers), most polymers used in everyday life are synthetic (plastics) and are mostly issued from the petrochemical industry[1] (Fig. 4.1).

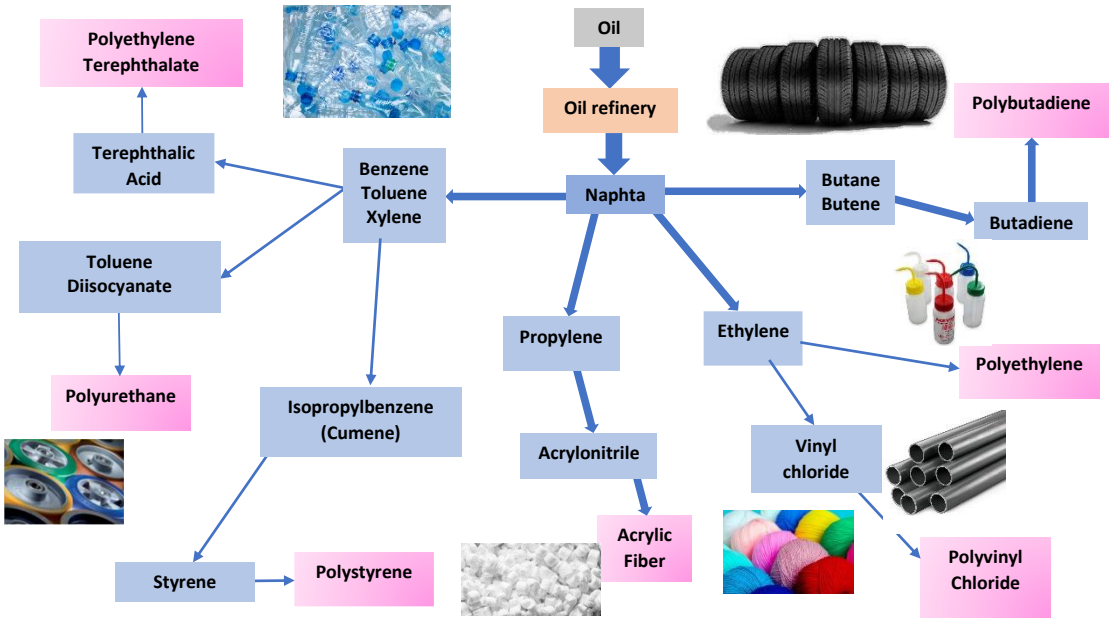

Figure 4.1: Examples of petrochemical based polymers.

In recent decades, the environmental impact caused by petrochemical polymers has significantly increased, with waste problems a growing threat to the oceanic ecosystem. Therefore, multiple solutions have been considered such as: recycling existing polymers[2], production of biodegradable polymers[3]…. However, a world without plastic is not imaginable and thus, polymers from bio-sourced monomers (such as lactide or myrcene…) seem to be one of the most promising alternatives. Several

polymers are also naturally available, for example from trees (starch, cellulose, 1.4-*cis* polyisoprene from *Hevea*, 1.4-*trans* polyisoprene from *Gutta-Percha*…) but unfortunately, they do not meet all the desired mechanistical properties for the numerous applications of plastics in our "modern" way of life. To date, chemists and polymer scientists are not able to perfectly replicate nature. For example, the latex obtained from the *Hevea* tree is made of 1.4-*cis* polyisoprene with a stereoregularity of up to 99.9%, which is currently not possible to synthesize chemically.

Different synthetic methods have been used over the years to prepare polymers, for instance radical polymerization[4], ionic polymerization[5] and coordinative polymerization as studied here.

As discussed in the bibliographic chapter, most of the rare earth borohydride complexes have been investigated for lactone and lactide polymerization to afford biodegradable and biocompatible polymers by ring opening polymerization (ROP) of these cyclic ester monomers[6]**.** Lactide can be find, thanks to the two asymmetric carbons, under different form: meso- (R and S on the same molecule), enantiopure or in racemic mixture.

4.1.2 Ring opening polymerization.

The mechanism of the ROP of cyclic esters [lactide (LA), Ɛ-caprolactone (ε-CL), among others] using metal-based complexes has been elucidated through experimental and theoretical studies, and it has been established that a coordination-insertion pathway is taking place[7]. In this mechanism, the first step is the coordination of the oxygen atom of the carbonyl group of the monomer to the metal center. Then, the initiating group (or the growing polymer chain) (Z) attacks the carbon of the carbonyl group. Subsequently, the migration of the Z group triggers the opening of the ring, which is then followed by the de-coordination of the oxygen atom from the metal center. The polymerization continues (propagation) with the coordination of a new monomer unit followed by the attack and migration of the polyester chain, and so on (Scheme 4.1).

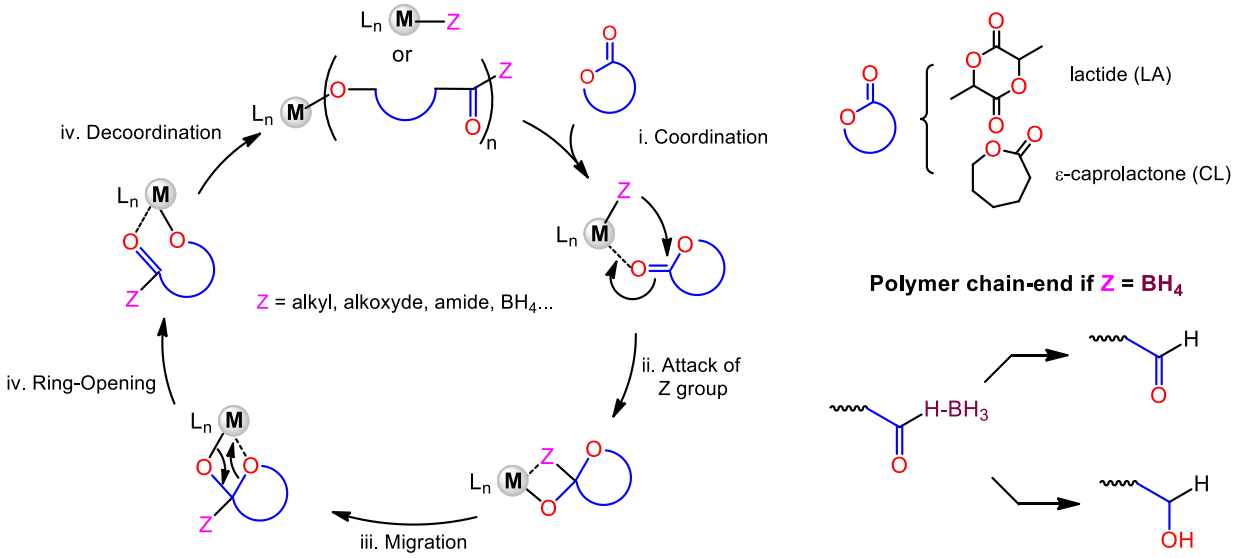

Scheme 4.1: Mechanism for the ROP of lactide with metal-based catalyst.

The use of a complex where Z = BH_4 can lead to different chain end-functions. The terminal carbonyl bearing the borohydride function may undergo a reduction and, taking into account the other hydroxy end-group after hydrolysis of the metal-oxygen bond, a polymer bearing two hydroxide groups at both chain-ends is obtained. On the other hand, the absence of this reduction leads to polymers bearing both a hydroxy and a formyl functions[8].

4.1.3 Noticeable allyl and borohydride rare earth complexes used in ROP.

The first mention of a rare earth complex involving a borohydrido function for ROP was reported nearly twenty years ago by S. Guillaume *et al.*[9]. Since then, many complexes have been studied for this kind of polymerization. As presented in Fig. 4.2, the different borohydride complexes of RE used for ROP of cyclic esters exhibit different activities [ranked by TOF (h^{-1})][10]. Among them, our laboratory described the synthesis of a mixed complex of RE containing both borohydride/allyl reactive groups. Through DFT studies[11] and polymers chain-ends analysis, it was confirmed that the ring-opening polymerization using this mixed complex is initiated by the borohydride moiety.

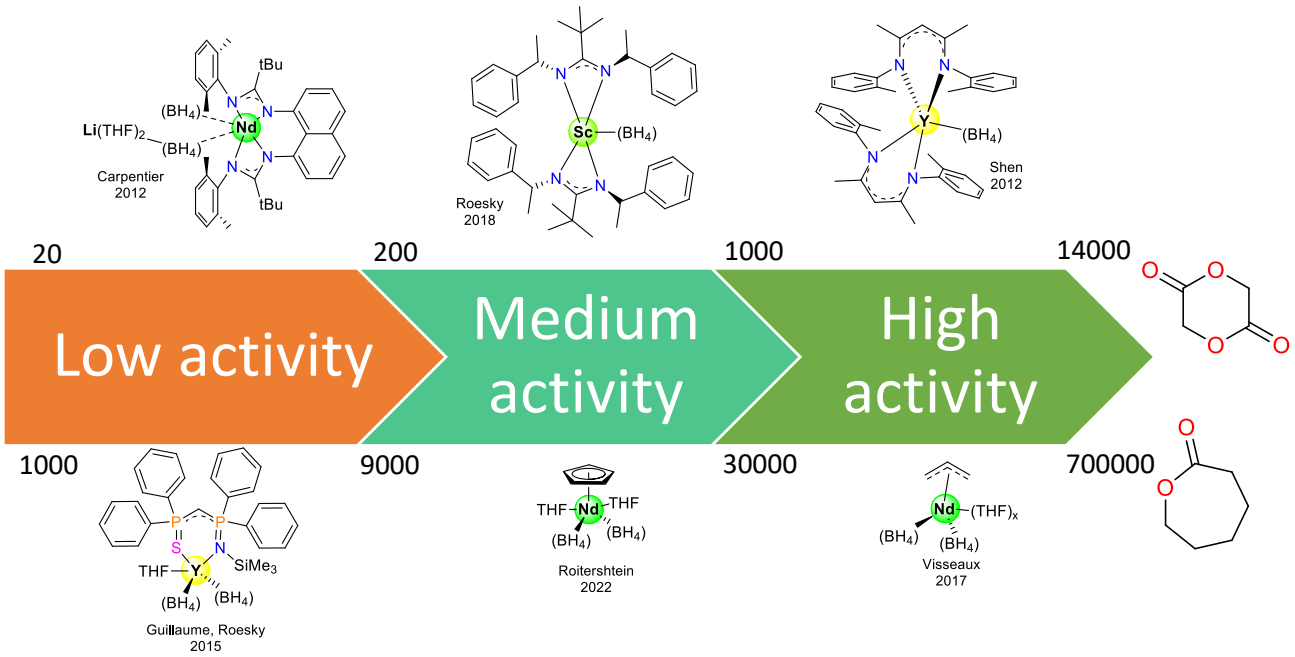

Figure 4.2: Unofficial chart of the TOF activity of selected catalysts toward ROP of lactide (top) and ε-caprolactone (bottom)[10].

In contrast to the borohydride complexes, to our knowledge, only a few allylic (CH_2CHCH_2) RE complexes have been used for ring-opening polymerization of cyclic esters and are shown in Fig. 4.3 (with Ar = 2,6-$C_6H_5{}^iPr_3$)[12]. The turnover frequencies of these products are given in Table 4.1.

Since rare earth metals have a strong oxophilicity, according to various examples in the literature, polymerization in THF leads to competition between monomers and solvent coordination to the metal center, resulting in a longer time to complete the polymerization. To increase the rate of polymerization and prevent this issue, the reaction can be performed in a non-coordinating and nonpolar solvent, such as toluene, even though the monomer solubility in this solvent may be lower.

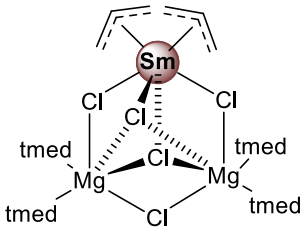

M. Yuan, *et al.*, J. Appl. Polym Sci.,1999, 73, 2857

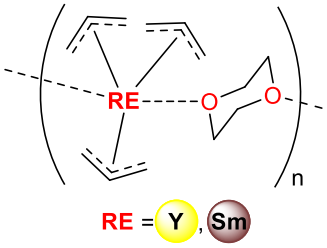

L. F. Sánchez-Barba, *et al.*, Organometallics, 2005, 24, 3792

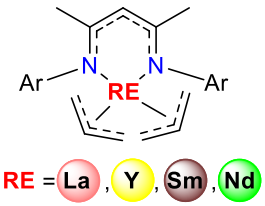

L. F. Sánchez-Barba, *et al.*, Organometallics, 2005, 24, 3792

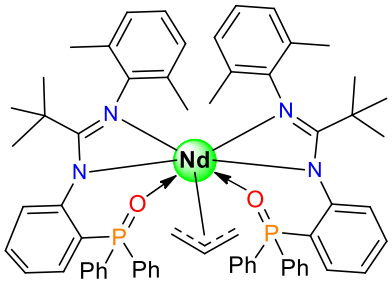

A. O. Tolpygin,*et al.* Russ. Chem. Bull., Int. Ed., 2020, 69, 6, 1114

Figure 4.3: Allylic complexes using for ROP of cyclic esters.

Table 4.1: Activity of the rare earth complexes bearing allyl (C_3H_5) ligand.

Complexes	TOF_{CL} (h^{-1})	TOF_{LA} (h^{-1})
$(\eta^3C_3H_5)Sm(\mu_2\text{-}Cl)_2(\mu_3\text{-}Cl)_3Mg(tmed)(\mu_2\text{-}Cl)Mg(tmed)$[a]	-	17[c]
$RE(\eta^3C_3H_5)_3$[a]	5 600 - 29 000[c]	10 – 60[d]
$RE(\eta^3C_3H_5)_2[HC(MeCN\text{-}2.6\text{-}^iPr_2C_6H_3)_2]$[a]	6 000 - 12 000[c]	10 - 30[d]
$Nd(C_3H_5)[2\text{-}(Ph_2P(O)]C_6H_4NC(But)N(2.6\text{-}Me_2C_6H_3]_2$[b]	15 000[c]	6000[c]

a) Reaction carrier out in THF, b) Reaction carried out in toluene, c) Reaction performed in at 20°C or 25°C, d) Reaction performed 40°C.

The polymerization rate scales depicted previously (Fig. 4.2) are used for comparison with the complexes presented in this thesis manuscript. Only four different complexes (**1a/1b**, **5**, **6** and **12**) were tested in ROP polymerization catalysis (Fig. 4.4). The number-average molar mass values and dispersity ($Đ = \bar{M}_w/\bar{M}_n$) were determined by size exclusion chromatography (SEC) in THF using polystyrene for calibration. Using the correction coefficient Y, the number average molecular weight can be easily calculated ($\bar{M}_n = \bar{M}_{n\,GPC(raw)} \times Y$)**13** , where Y = 0.58 for lactide and 0.56 for ε-caprolactone.

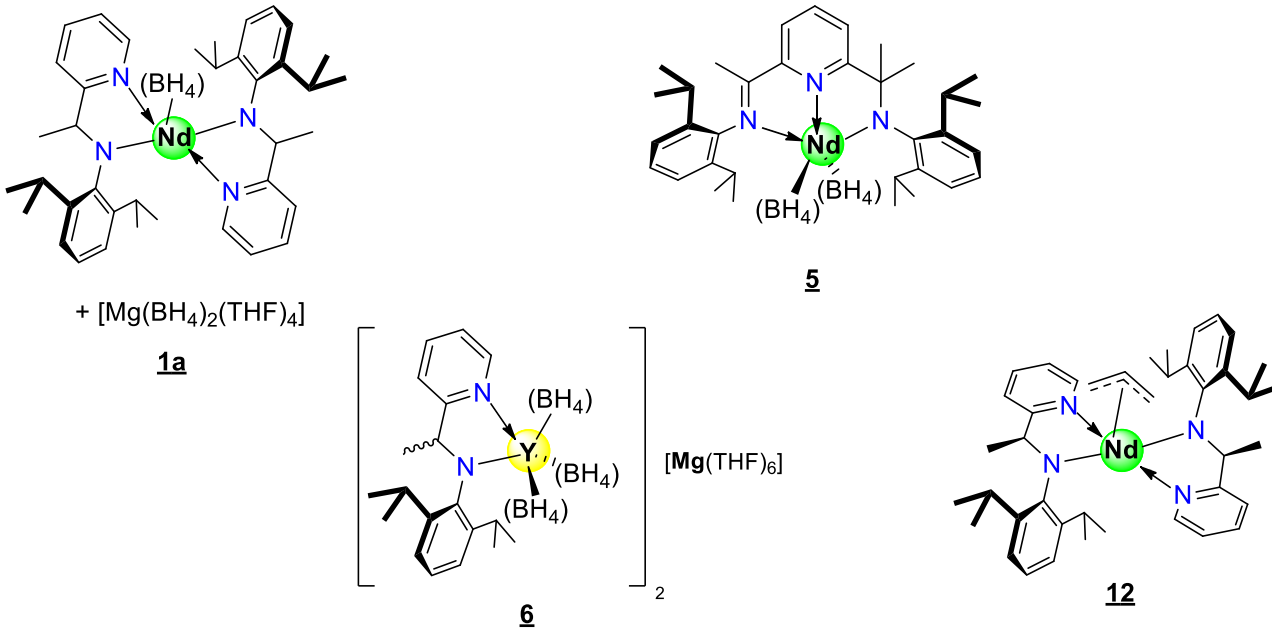

Figure 4.4: Complexes used for ring-opening polymerization preliminary studies. 1b omitted for more clarity.

4.2 ROP using the complexes described in the thesis.

4.2.1 Polymerization using neodymium complexes.

Prior to starting the polymerization, the monomers were purified. Ɛ-CL was first dried over CaH_2 before being distilled to obtain a H_2O and oxygen-free monomer. The purification of lactide was somewhat more difficult. The crude lactide was solubilized in hot toluene and then crystallized at 0 °C before filtering the toluene to remove the possible traces of lactic acid. This operation was repeated twice and final sublimation of the lactide, in the presence of desiccant guard tube filled withP_2O_5, gave the dry lactide.

With the idea of assessment of a mono-substituted complex for such ROP experiments and before the synthesis and isolation of the bis-substituted complex of the form $(\mathbf{Z^1})_2Nd(BH_4)$, the first study using neodymium borohydride aminopyridine complex was done in a "*one pot*" process. To do so, one equivalent of $\mathbf{Z^1H}$ and one equiv. of neodymium tris-borohydride in the presence of a half equivalent of BEM were mixed in a reactor. Subsequently, the monomer was added to evaluate its activity as polymerization catalyst. Although the results seemed really interesting, with activity at room

temperature and total conversion of 100 equiv. of *L*-lactide within 1 h 30 min, each reagent has been tested individually to compare their activity in lactide polymerization (Table 4.2).

Table 4.2: Polymerization of lactide using the synthesis reagents and the "one pot" complex.

Entry [a]	*L*-LA (eq)	Conversion	$\bar{M}_{n\,th}$ (g/mol)[d]	$\bar{M}_{n\,exp}$ (g/mol)[e]	*Đ*
*$Nd(BH_4)_3(THF)_3$ + **Z^1H** + 0.5 BEM*[c]	100	98%	14 120	7 900	2.2
Z^1H[b]	100	0%	-	-	-
$Nd(BH_4)_3(THF)_3$[b]	100	0%	-	-	-
BEM[b]	200	91%	13 150	26 500	1.7
***Z^1H** + 0.5 BEM*[b]	100	98%	14 200	28 900	1.7

[a] Reaction conducted at room temperature, during 1 h 30 min, [b] concentration of lactide: 0.33 M in toluene, [c] concentration of lactide: 0.67 M in toluene, [d] $\bar{M}_{n\,th}$(LA)= $\bar{M}_n[LA]_0/[Cat]$×conversion×(molecular weight of LA), [e] the results were obtained from GPC analysis. $\bar{M}_n$(LA)= $\bar{M}_{n\,GPC(raw)}$×0.58.

The assessment of each reagent showed that magnesium compounds (BEM and BEM + **Z^1H**) were active towards the ring-opening polymerization of *L*-LA at room temperature. The results obtained from the two last entries showed an experimental molecular weight that was twice the theoretical molecular weight. This probably suggests that only 50% of the alkyl species initiated the polymerization. Since ring-opening polymerization can be triggered by an excess of BEM, polymerization using the isolated complex **1a/1b** was preferred to avoid confusion regarding the reactive species (Table 4.3). In a reactor, the correct amount of monomer was dissolved (partial dissolution) in a solvent, and then a solution of the complex was added to the medium. After some time, the polymerization medium resulted in the formation of a gel and after a given time, stirring was completely blocked, and therefore, the reaction was stopped. The polymer material was obtained by precipitation in a large amount of ethanol.

*Table 4.3: ROP using complex **1a/1b** in toluene.*

Entry[c]	Monomer	m/M	*t* (min)	Conversion	$\bar{M}_{n\,th}$ (g/mol)[f]	$\bar{M}_{n\,exp}$ (g/mol)[g]	*Đ*
1[a]	*L*-LA	200/1	5	98%[d]	28 300	26 800	1.8
2[a]	*L*-LA	400/1	10	52%[d]	30 000	32 200	1.8
3[b]	Ɛ-CL	200/1	<1	98%[e]	22 400	14 900	2.2
4[b]	Ɛ-CL	1000/1	<5	98%[e]	111 900	38 400	1.7

M = Catalyst, m = monomer.
*[a] Polymerization carried out with 0.02 mmol of **1a/1b**; [b] polymerization carried out with 0.01 mmol of **1a/1b**; [c] reaction performed with a monomer concentration of 0.67M in toluene; [d] conversion was determined by integration of the methine resonances by ^1H NMR; [e] conversion was determined according to the yield, by*

gravimetry; [f] $\bar{M}_{n}{}^{th}$ = $[LA]_0$ / [Cat] × conversion × (molecular weight of LA) + $[CL]_0$ / 2 / [Cat] × conversion × (molecular weight of CL); [g] the results were obtained from GPC analysis: $\bar{M}_{n}{}^{exp}$(LA) = $\bar{M}_{n}{}^{GPC(raw)}$ × 0.58, $\bar{M}_{n}{}^{exp}$(CL) = $\bar{M}_{n}{}^{GPC(raw)}$ × 0.56.

Polymerization of *L*-Lactide (entries 1 and 2) at room temperature with **1a/1b** showed a low to medium activity with reference to our previous scale (1250 < TOF_{LA} < 2350 h^{-1}). The experimental and theoretical number-average molar mass were in close agreement for one polymer chain growing per metal center.

However, the polymerization of Ɛ-caprolactone (entries 3 and 4) showed a high activity (TOF_{CL} = 11 800 h^{-1}) with an experimental molecular weight much lower than expected, as already described and discussed several times in the literature. Indeed, while ROP for a low ratio of [m]/[M] (m = monomers, M = metal) promoted by rare earth borohydride complexes yields polymers of a predicted chain lenght, polymerization catalysis performed with a high [m]/[M] ratio (>250) often produces smaller $\bar{M}_{n}$ than anticipated. The observed deviation is frequently justified by intramolecular (back-biting) and/or intermolecular transesterifications[6, 7a),14] leading to cyclic and linear polymers (Scheme 4.2, example with lactide).

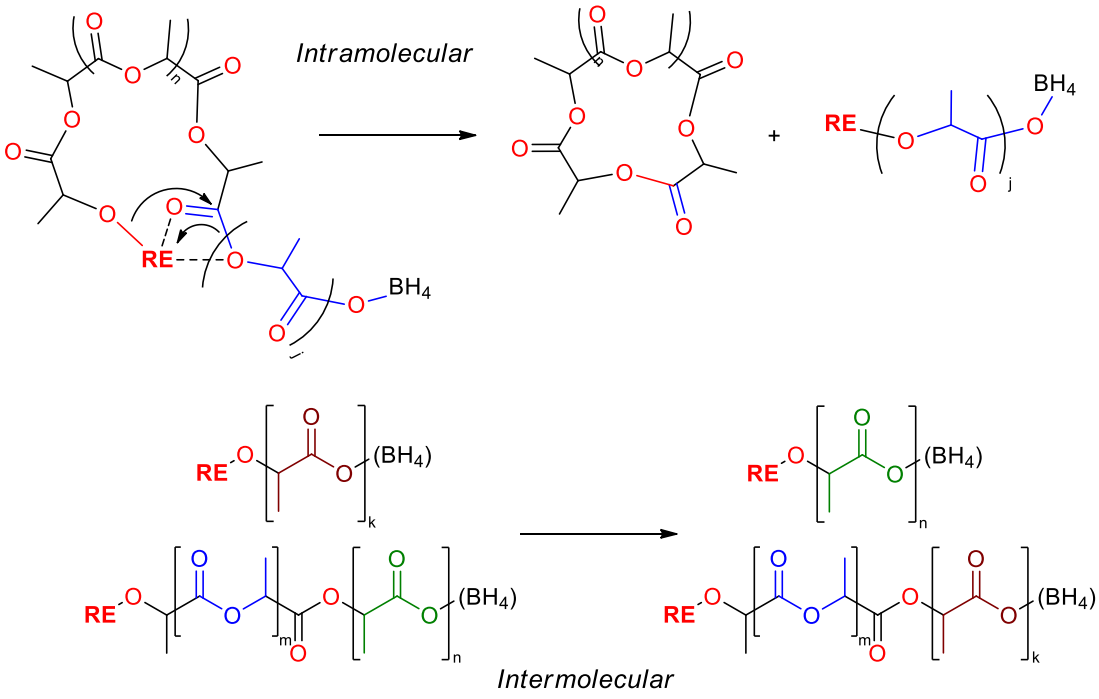

Scheme 4.2: Intra- and intermolecular transesterification.

Following this study, the polymerization of 1000 equiv. of Ɛ-caprolactone with **5** [(Z^3)Nd(BH_4)$_2$] was attempted. Due to poor solubility of the complex in toluene, and as evidenced by the GPC-SEC

chromatogram depicted in Fig. 4.5, the non-homogenous reaction mixture led to a polymer containing several populations. Indeed, while a part of the complex initiates the polymerization process as soon as the monomer is added, the other part that was not solubilized starts the polymerization with a delay.

To avoid this large dispersity, the polymerization reactions were performed in THF. Even if, as discussed previously, polymerization in THF might increase the reaction time, it is also noticed that the better solubility of lactide in this solvent likely contributed to the formation of polymers with narrower dispersity. Thus, the polymerizations of lactide were pursued in THF, but this time at 50 °C (no polymerization performed at room temperature) to increase the polymerization rate. In addition, in the hope of observing a possible selectivity, the switch from *L*-Lactide to *rac*-Lactide was performed. Polymerization using the complex **1a/1b** was also carried out to compare the activity of the two complexes **1a/1b** and **5** (Table 4.4). Although the methodology did not change, the polymerization of lactide in THF did not lead to gel formation compared to the polymerization presented previously in toluene.

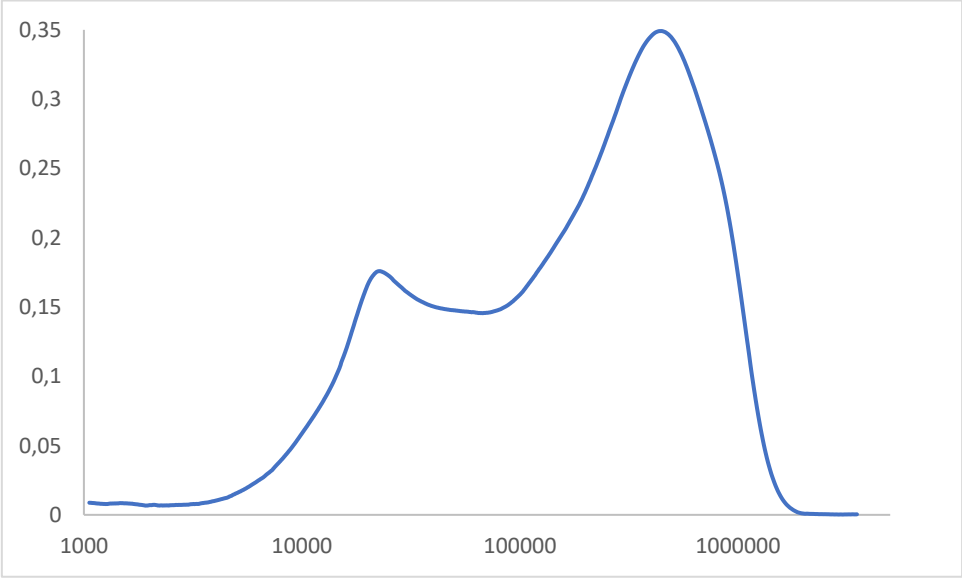

Figure 4.5: GPC trace of the polymerization of 1000 equiv. of Ɛ-CL with 5.

*Table 4.4: Polymerization of rac-LA using **1a/1b** and **5** in THF.*

Entry[a)]	Catalyst	*rac*-LA/BH_4	*t* (min)	Conversion[b)]	$\bar{M}_{n\,th}$ (g/mol)[c)]	$\bar{M}_{n\,exp}$ (g/mol)[d)]	*Đ*
1	**1a/1b**	250	40	99%	35 600	12 600	1.4
2	**1a/1b**	1000	960	97%	139 700	28 200	1.4
3	**5**	250	35	99%	18 000	8 600	1.4
4	**5**	1000	180	93%	67 000	26 800	1.4

Reaction time was not necessarily optimized.
[a)] Polymerization carried out with 0.005 mmol of catalyst with a monomer concentration of 1 M at 50 °C in THF; [b)] conversion was determined by integration of the methine resonances by ^{1}H NMR, [c)] $\bar{M}_{n\,th}$ = $[LA]_0/[Cat]$ × conversion × (molecular weight of LA) + $[CL]_0$ / 2 / [Cat] × conversion × (molecular weight of CL); [d)] the results were obtained from GPC analysis. $\bar{M}_{n\,exp}(LA) = \bar{M}_{n\,GPC}(raw) \times 0.58$.

Unfortunately, due to time constraints, it was not possible to optimize the reaction time. As already discussed above, the polymerization reaction performed in THF with **1a/1b** showed a longer reaction time than in toluene for a full conversion, due to the coordination of THF molecules. Nevertheless, this allowed a better solubility of the lactide and led to polymers with a narrower dispersity (THF, *Đ* = 1.4 *vs.* toluene, *Đ* = 1.7-2.2). Compared to the polymerization of lactide in toluene, transfer reactions appeared to occur according to a smaller $\bar{M}_n$(exp) than expected. However, the narrow dispersity allowed one to imagine a certain regularity in the occurrence of this side reaction.

Polymerization using **5** compared to **1a/1b** appeared to be faster and, surprisingly, the experimental $\bar{M}_n$s were of the same magnitude order than the ones obtained with **1a/1b**.

Following the results obtained with *rac*-LA, ROP experiments of Ɛ -CL were carried out (table 4.5) with **1a/1b** and **5** as catalysts in THF. Due to the rapid formation of a gel (at 250 equiv. of Ɛ-CL), these reactions were conducted at room temperature.

*Table 4.5: Polymerization of Ɛ-CL using **1a/1b** and **5** in THF.*

Entry[a)]	Catalyst	Ɛ -CL/BH_4	*t* (min)	Yield[b)]	$\bar{M}_{n\,th}$ (g/mol)[d)]	$\bar{M}_{n\,exp}$ (g/mol)[e)]	*Đ*
1	**1a/1b**	250	1	73%	20 800	8 200	1.3
2	**1a/1b**	1000	30	75%	85 500	18 700	1.3
3	**5**	250	1	81%	11 400	11 500	1.3
4	**5**	1000	180	-	-	-	-

Reaction time was not necessarily optimized.
[a)] Polymerization carried out with 0.005 mmol of catalyst with a monomer concentration of 1M at room temperature in THF, [b)] Yield: weight of polymer/weight of monomer used, [c)] Conversion was determined according to the yield, [d)] $\bar{M}_{n\,th}$ = $[LA]_0/[Cat]$ × conversion × (molecular weight of LA) + $[CL]_0$ / 2 / [Cat] ×

conversion × (molecular weight of CL), [e] The results were obtained from GPC analysis. $\bar{M}_{n}^{exp}(CL) = \bar{M}_{n}^{GPC}(raw) \times 0.56$.

Similarly, to the polymerization conducted with lactide, the polymerization conducted in THF took longer time than those performed in toluene (Table 4.3). The GPC results for the polymerization of Ɛ-CL using **1a/1b** reveals experimental $\bar{M}_n$s lower than the theoretical values expected (entries 1 and 2).

However, polymerization using complex **5** showed an almost perfect match between the theoretical and experimental $\bar{M}_n$, but the increase in monomer loading failed to produce a polymer after precipitation in ethanol (entry 4). This experiment will be repeated in the near future in order to confirm the results.

The following studies using complex **12** [$(\mathbf{Z^1})_2Nd(C_3H_5)$] were pursued using the same protocol. However, due to the high activity of this complex noted by the rapid formation of a highly viscous medium, the polymerization reactions were conducted at room temperature in THF.

Table 4.6: Ring-opening polymerization using $(\mathbf{Z^1})_2Nd(C_3H_5)$, **12** *(solvent = THF)*

Entry[a]	Monomers	m/M	*t* (min)	Conversion	$\bar{M}_{n}^{th}$ (g/mol)[d]	$\bar{M}_{n}^{exp}$ (g/mol)[e]	*Đ*
1	*rac*-LA	250	<2	99% [b]	35 600	77 000	1.6
2	*rac*-LA	1000	10	98% [b]	141 100	86 800	1.9
3	Ɛ-CL	250	10	73% [c]	18 000	54 000[f]	3.1
4	Ɛ-CL	1000	10	-	-	-	-

Reaction time was not necessarily optimized. M = Catalyst, m = monomers.
[a] Polymerization carried out with 0.005 mmol of **12** *with a monomer concentration of 1M in THF, [b] Conversion was determined by integration of the methine resonances in the* ^1H *NMR, [c] Conversion was determined according to the yield, [d]* $\bar{M}_{n}^{th} = [LA]_0/[Cat] \times conversion \times (molecular\ weight\ of\ LA) + [CL]_0 / 2 / [Cat] \times conversion \times (molecular\ weight\ of\ CL)$, *[e] The results were obtained from GPC analysis.* $\bar{M}_{n}^{exp}(LA) = \bar{M}_{n}^{GPC}(raw) \times 0.58$ $\bar{M}_{n}^{exp}(CL) = \bar{M}_{n}^{GPC}(raw) \times 0.56$, *[f] GPC in progress.*

Entries 1 and 2 show that the catalyst had a very high activity for lactide polymerization (TOF_{LA} > 6000 h^{-1}), which should be higher if the reaction time was optimized. In comparison, such an activity was only produced by the fastest complexes $\{Nd(C_3H_5)[2\text{-}(Ph_2P(O)]C_6H_4NC(But)N(2.6\text{-}Me_2C_6H_3]_2\}$[12c] in toluene. Thus, this "speed record" could be overpassed by switching from the solvent THF to toluene (which could not be tested for the time being). However, as proven before, this change was consistently accompanied by an increase in polydispersity. Furthermore, in entry 1, since the experimental $\bar{M}_n$ was higher than the theoretical value, it may reflect a slow initiation compared to the propagation step (the polymerization might have been initiated by only 50% of the catalyst).

Increasing the monomer/catalyst ratio to 1000 equiv. revealed the presence of side-reactions ($\bar{M}_{n\,exp}$ **<** $\bar{M}_{n\,th}$) as observed previously with **1a/1b**.

The activity of complex **12** for the polymerization of 250 equiv. of Ɛ-CL (entry 3) was found lower than that of **1a/1b** under the same conditions (experiment conducted at room temperature and solvent = THF) (**12**: TOF_{CL} = 1 095 h^{-1}, **1**: TOF_{CL} = 10 950 h^{-1}). Even though the GPC-SEC chromatogram exhibited a bimodal trace, due to some technical issues at that time, the experimental value of $\bar{M}_n$ could already be considered higher than expected. However, as seen with entry 4 of Table 4.5, increasing the loading to 1000 equiv. of Ɛ-CL prevents the system from functioning properly. Just like the reaction between **5** and a 1000 equivalent of Ɛ-CL, this reaction too will have to be repeated in the future.

Attempting statistical copolymerization using 250 equiv. of *rac*-LA and 250 equiv. of Ɛ-CL at 50 °C in THF overnight resulted in polymerization of LA only. The competition between lactide and Ɛ-caprolactone, which had been proven several times before**15**, was in favor of the lactide due to the presence of more coordination sites (oxygen), and other factors.

In order to observe, or not, the difference between the catalysis activity of neodymium and yttrium, polymerization, experiments using complex **6** {[(**Z**^{1})Y$(BH_4)_3$][$Mg(THF)_6]_{0.5}$} as a catalyst were attempted.

4.2.2 Polymerization attempts using the yttrium complex 6.

Due to time constraints, only one trial in toluene of each polymerization (lactide and caprolactone) was done using 6. The same methodology was used in which the solution of catalyst was added to the monomer. While the polymerization of Ɛ-CL was done at room temperature, polymerization of *L*-lactide was performed at 50 °C.

*Table 4.7: Ring-opening polymerization using **6** in toluene.*

Entry[a)]	Monomers	m/M	*t* (min)	Conversion	$\bar{M}_{n\,th}$ (g/mol)[d)]	$\bar{M}_{n\,exp}$ (g/mol)[e)]	*Đ*
1	*L*-LA	500	30	58%[b)]	20 900	21 500	1.4
2	Ɛ-CL	1000	10	56%[c)]	32 100	33 100	1.4

M = Catalyst, m = monomers.
*[a)] Polymerization carried out with 0.005 mmol of **5** with a monomer concentration of 1M, [b)] Conversion was determined by integration of the methine resonances in the ^{1}H NMR, [c)] Conversion was determined according to the yield, [d)] $\bar{M}_{n\,th}$ = [LA]$_0$/[Cat] × conversion × (molecular weight of LA) + [CL]$_0$ / 2 / [Cat] × conversion × (molecular weight of CL), [e)] The results were obtained from GPC analysis. $\bar{M}_{n\,exp}$(LA) = $\bar{M}_{n\,GPC}$(raw) × 0.58 $\bar{M}_{n\,exp}$(CL) = $\bar{M}_{n\,GPC}$(raw) × 0.56.*

Polymerization using **5** in toluene exhibited, according to the previous scale (Fig. 4.2), a medium activity towards lactide (TOF_{LA} = 580 h^{-1}) but a low activity for Ɛ-CL (TOF_{CL} = 3 400 h^{-1}). As previously seen with complex **1**, polymerization in toluene yielded the desired $\bar{M}_n$ but with a narrower dispersity.

4.3 Conclusion

In conclusion, based on these preliminary experiments, ring-opening polymerization using borohydride or allyl complexes of rare earths bearing an amido-pyridine ligand seems to be quite promising.

Even if these results were issued from preliminary studies, and were mostly not optimized, a first scale of reactivity can be implied. In terms of catalysis activity, the best reactivity in THF was obtained with the allyl complex **12** (TOF_{LA} value between 6 000 and 7 500h^{-1}) followed by the two borohydride complexes **5** and **1a/1b** with a TOF value near 400 h^{-1}. Oddly, this scale is reverse for the polymerization of Ɛ-CL (TOF_{CL}**12** (3 000h^{-1}) < TOF_{CL} **5** ≈ TOF_{CL} **1a/1b** (11 000 and 12 000 h^{-1}). In the same solvent (toluene), the yttrium complex **6** showed a small activity than the neodymium complex [TOF_{LA} **1a/1b** > TOF_{LA} **6** (1 200 > 600 h^{-1}), TOF_{LA} **1a/1b** > TOF_{LA} **6** (12 000 > 3 000 h^{-1})].

Regarding the control over macromolecular data, while ring-opening polymerization with RE borohydride complexes in toluene allowed the fast formation of polymers, with somewhat broad dispersity, switching to THF solvent for **1a/1b** led to longer reaction time, possibly due to the coordination competition between THF and monomer molecules. Furthermore, the used of THF as solvent permitted the acquisition of polyesters (PLA, PCL) with a smaller $\bar{M}_n$ than anticipated. In turn,

the same syntheses with **6** afforded polymers with the expected $\bar{M}_n$. Although the polymers obtained with **1a/1b** do not meet the expected number-average molar mass values, some control is observed (providing by the narrow dispersity) over the side-reaction. Further examination of these polymers by MALDI-TOF technique should reveal whether transesterification is intra- or intermolecular (formation of cyclic or linear polymers). The ROP experiments performed in THF with **12** exhibit high activity for the polymerization of lactide, but because of this fast polymerization, the reaction is not perfectly controlled.

In the future, it is planned to assess the polymerization of isoprene with the amido-pyridine RE complexes prepared in this thesis work, using different co-catalysts, for which positive results might be expected based on the literature.

References

[1] A. A. Koutinas, A. Vlysidis, D. Pleissner, N. Kopsahelis, I. Lopez Garcia, I. K. Kookos, S. Papanikolaou, T. Him Kwan, C. Sze Ki Lin, **Chem. Soc. Rev.**, *2014*, 43 (8), 2587. Picture from: https://www.lapeyregroup.com /produit/pissette-de-securite-antigoutte-a-col-large/, https://autocomponentsindia.com/tyre-industry foresees-lot-of-challenges-in-spite-of-raw-material-costs-remain-favourable/, https://www.Thehydrobro s.com/en-fr/products/floraflex-34-pvc-pipe-fittings, https://www.fibre2fashion.com/news/textile-news /nitma-hails-reduction-of-add-on-imported-acrylic-fibre-269623-newsdetails.htm, https://www.futura-sciences.com/sciences/definitions/chimie-polystyrene-10176/, https://www.barroneq.com/5-reasons-to-get-polyurethane-wheels-on-your-casters/, https://www.modeintextile.fr/cycle-logic-bouteilles-plastiqu es -pet-chimie-textile/.

[2] Selected references: (a) I. A. Ignatyev, W. Thielemans, B. Vander Beke, **ChemSusChem.**, *2014*, 7 (6), 1579; (b) N. Yang, **Science**, *2022*, 378 (6616), 132; (c) K. P. Sullivan, A. Z. Werner, K. J. Ramirez, L. D. Ellis, J. R. Bussard, B. A. Black, D. G. Brandner, F. Bratti, B. L. Buss, X. Dong, S. J. Haugen, M. A. Ingraham, M. O. Konev, W. E. Michener, J. Miscall, I. Pardo, S. P. Woodworth, A. M. Guss, Y. Román-Leshkov, S. S. Stahl, G. T. Beckham, **Science**, *2022*, 378 (6616), 207.

[3] C. M. Plummer, L. Li, Y. Chen, **Macromolecules,** *2023*, 56 (3), 731.

[4] S. Dworakowska, F. Lorandi, A. Gorczyński, K. Matyjaszewsk, **Adv. Sci.**, *2022*, 9 (19), 2106076.

[5] A. Hirao, Y. Matsuo, R. Goseki, **J. Polym. Res .**, *2019*, 26 (12), 263.

[6] M. Visseaux, F. Bonnet, **Coord. Chem. Rev.**, *2011*, 255 (3-4), 374.

[7] (a) O. Dechy-Cabaret, B. Martin-Vaca, D. Bourissou, **Chem. Rev.**, *2004*, 104 (12), 6147; E. Stirling, Y. Champouret, M. Visseaux, **Polym. Chem.**, *2018*, 9 (19), 251.

[8] I. Palard, M. Schappacher, B. Belloncle, A. Soum, S. M. Guillaume, **Chem. Eur. J.**, *2007*, 13 (5), 1511.

[9] S. Guillaume, M. Schappacher, A. Soum, **Macromolecules**, *2003*, 36 (1), 54 ; I. Palard, A. Soum, S.M. Guillaume, **Macromolecules**, *2005*, 38 (16), 6888.

[10] Selected references: (a) X. Shen, M. Xue, R. Jiao, Y. Ma, Y. Zhang, Q. Shen, **Organometallics**, *2012*, 31 (17), 6222; (b) M. V. Yakovenko, A. A. Trifonov, E. Kirillov, T. Roisnel, J.-F. Carpentier, **Inorganica Chim. Acta**, *2012*, 383, 137; (c) S. Fadlallah, M. Terrier, C. Jones, P. Roussel, F. Bonnet, M. Visseaux, **Organometallics**, *2016*, 35 (4), 456; (d) S. Fadlallah, J. Jothieswaran, F. Capet, F. Bonnet, M. Visseaux,

Chem. Eur. J., *2017*, 23 (62), 15644; (e) M. Schmid, P. Oña-Burgos, S. M. Guillaume, P. W. Roesky, **Dalton Trans.**, *2015*, 44 (30), 12338; (f) T. P. Seifert, T. S. Brunner, T. S. Fischer, C. Barner-Kowollik, P. W. Roesky, **Organometallics**, *2018*, 37 (23), 4481; (g) D. A. Bardonov, P. D. Komarov, G. I. Sadrtdinova, V. K. Besprozvannyh, K. A. Lyssenko, A. O. Gudovannyy, I. E. Nifant'ev, M. E. Minyaev, D. M. Roitershtein, **Inorganica Chim. Acta**, *2022*, 529, 120638.

[11] S. Fadlallah, J. Jothieswaran, I. Del Rosal, L. Maron, F. Bonnet, M. Visseaux, **Catalysts**, *2020*, 10 (8), 820.

[12] (a) M. Yuan, C. Xiong, X. Li, X. Deng, **J. Appl. Polym. Sci.**, 1999, 73 (14), 2857; (b) L. F. Sánchez-Barba, D. L. Hughes, S. M. Humphrey, M. Bochmann, **Organometallics**, *2005*, 24 (15), 3792; (c) A. O. Tolpygin, O. A. Linnikova, T. A. Kovylina, A. V. Cherkasov, G. K. Fukin, A. A. Trifonov, **Russ. Chem. Bull., Int. Ed.**, *2020*, 69 (6), 1114.

[13] M. Save, M. Schappacher, A. Soum, **Macromol. Chem. Phys.**, 2002, 203 (5-6), 889.

[14] (a) J. Kratsch, M. Kuzdrowska, M. Schmid, N. Kazeminejad, C. Kaub, P. Oñ a-Burgos, S. M. Guillaume, P. W. Roesky, **Organometallics**, *2013*, 32 (5), 1230; (b) M. V. Yakovenko, A. A. Trifonov, E. Kirillov, T. Roisnel, J.-F. Carpentier, **Inorganica Chim. Acta**, *2012*, 383, 137.

[15] R. D. Rittinghaus, S. Herres-Pawlis, **Chem. Eur. J.**, *2023*, 29 (1), e2022022.

General conclusion and perspectives

Throughout this thesis, a new series of borohydride and allyl rare earth complexes bearing $\mathbf{Z^n}$ amido-pyridine ligands [$\mathbf{Z^n}$ = $\mathbf{Z^1}$, $\mathbf{Z^2}$ and $\mathbf{Z^3}$ (Chart 1)] were synthesized. Those new complexes were characterized by ^{1}H NMR spectroscopy, elemental analysis for several of them, and the coordination of the ligand to the metal center was confirmed in most cases by XRD analysis. Some of these complexes were assessed as initiators for the ring-opening polymerization of cyclic esters (lactide and Ɛ-caprolactone), which showed medium to high catalytic activity.

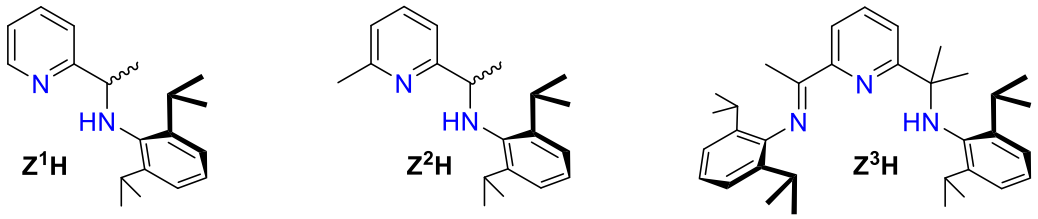

Chart 1: Amido-pyridine protio-ligand used during this work.

In order to synthesize borohydrides rare earth complexes, the anionic approach using the upstream preparation of anionic salt of $\mathbf{Z^1H}$ ligand was attempted with different bases [KH, ^{n}BuLi and $KN(TMS)_2$]. Unfortunately, this route turned out to be trickier than expected, and only the stable acid-base adduct $KN(TMS)_2.\mathbf{Z^1H}$ could be isolated and crystallized. The syntheses of rare earth borohydride complexes bearing those ligands were therefore obtained by the *in situ "borohydride/alkyl route"*.

In neodymium chemistry, the use of $\mathbf{Z^1H}$ led preferentially to the formation of the bis-substituted complex $[(\mathbf{Z^1})_2Nd(BH_4)],[Mg(BH_4)_2(THF)_4]/[(\mathbf{Z^1})_2Nd(THF)(\mu\text{-}BH_4)_2Mg(BH_4)(THF)_3]$ and $(\mathbf{Z^1})_2Nd(BH_4)$ (**1a/1b** and **1'a/1'b**, respectively). The formation of the mono-substituted complex $[(\mathbf{Z^1})Nd(BH_4)(\mu\text{-}BH_4)(THF)]_2$ (**2**) from **1a/1b** indicated that a ligand exchange process between the neodymium and the magnesium, present in the final structure [loss of $Mg(\mathbf{Z^1})(BH_4)$], could have occurred. Interestingly, increasing the steric hindrance by the simple presence of a methyl group in the α-position of the pyridine ring ($\mathbf{Z^2H}$) greatly influenced the preferential coordination mode: a mono-substituted complex was isolated. While the elemental analysis of the crude powder was consistent with an "*ate*" complex of formula $\{(\mathbf{Z^2})Nd(BH_4)_3[Mg(THF)_6]_{0.5}\}$ (**3**), crystallization afforded a neutral neodymium complex $(\mathbf{Z^2})Nd(BH_4)_2(THF)$ (**4**), after loss of $Mg(BH_4)_2$. The synthesis of a neodymium complex bearing the tridentate $\mathbf{Z^3}$ ligand was easily conducted, which was characterized by X-ray analysis and elemental analysis to confirm the formation of a neutral complex $(\mathbf{Z^3})Nd(BH_4)$ (**5**).

In yttrium chemistry, it was demonstrated that the solvent and the base used for the reaction have both an impact regarding the coordination of the ligand **Z^1**. The use of BEM limited the synthesis to a mono-substituted complex [(**Z^1**)Y(BH_4)$_3$]$_2$[Mg(THF)$_6$] (**6**) in which the two anionic yttrium moieties were associated with a magnesium cationic counterpart. However, using a lithium base (MeLi or ^{n}BuLi) in THF allowed a more efficient ligand exchange that resulted in the coordination of a second equivalent of the ligand to the metal center, leading to the complex (**Z^1**)$_2$Y(BH_4) (**7**). The different crystallization attempts of the presumed complexes (**Z^2**)Y(BH_4)$_2$ and (**Z^3**)Y(BH_4)$_2$, obtained *via* the used of BEM, ended to the formation of (**Z^2**)Mg(BH_4) and (**Z^3**)Mg(BH_4) (**8** and **10**), validating the hypothesis of a ligand exchange between the metal centers.

Our investigations to extend the family of mixed allyl/borohydride complexes have led to a new method for the clean synthesis of tetra-allyl anionic neodymium complex [Nd(C_3H_5)$_4$][K(crypt)] (**11**), through the reduction of tris-allyl of neodymium with KC_8. Furthermore, the effort to combine one borohydride and two allyl ligand on neodymium to create a mixed precursor produced a highly unstable complex and unfortunately, only the bis-cationic compound [Nd(C_3H_5)$_2$(THF)$_4$][B(C_6F_5)$_4$], was obtained through XRD examination.

Synthesis of the allyl analogs of the **Z^n**-substituted borohydride complexes were performed in the hope of observing a similar coordination of the ligands. The synthesis using two equivalents of **Z^{1}H** with tris-allyl Nd precursors resulted, as expected, to the formation of the bis-substituted neodymium (**Z^1**)$_2$Nd(C_3H_5) complex **12**, which was confirmed by elemental analysis along with its molecular structure that was resolved by X-Ray diffraction studies. Following this result, the synthesis of the mono-substituted **Z^1**-yttrium allyl complex, analogous to the borohydride **6**, was undertaken. Crystals suitable for X-ray diffraction revealed a unique molecular structure of the form [(**Z^1**)Y(C_3H_5)(μ-C_3H_5)$_2$(**Z^1**)Y(C_3H_5)] (**13**) within which three different allyl moieties were depicted (one terminal allyl and two unsymmetrical bridge allyl). Monitoring the evolution of this product allowed us to propose a possible intramolecular C-H activation. This kind of intramolecular reactivity was further evidenced by obtaining the molecular structure of the **Z^2**-neodymium allyl complex [(μ-**Z$^{2\prime}$**)Nd(C_3H_5)]$_2$ **14**, which exhibited two neodymium metal centers connected by a pyridyl fragment, coming from C-H activation of **Z^2** ligand, carried by each neodymium atom.

Preliminary results of ring-opening polymerization of lactide and ε-caprolactone exhibited a rather good activity for the borohydride complexes **1a/1b**, **5**, **6** as initiators, and a very high activity for the allyl complex **12**. However, GPC-SEC results indicated that the polymer chains displayed lower $\bar{M}_n$

than expected, due to possible transesterification processes. The transesterifications reactions did not seem to be random since narrow dispersities were observed.

On the basis of the results obtained in this thesis work, future research objectives will possibly include the following:

i. Clean bulk synthesis of the borohydride yttrium complex bearing the ligand **Z^2** using ^{n}BuLi, according to the ^{1}H NMR monitoring of the "*in-situ*" reaction performed in this thesis.

ii. The reduction of rare-earth tris-allyl complexes with KC_8 to obtain a rapid and clean synthetic method to tetra-allyl species.

iii. The synthesis and isolation of the mixed RE(allyl)$_2$(BH_4) complexes using the "*acidic pathway*". In the hypothesis where these mixed complexes could not be isolated, "*in-situ*" reactions with a protio-ligand **Z^nH** could be undertaken to tentatively isolate the expected products (allyl)RE(**Z^n**)(BH_4).

iv. Theoretical calculations must be performed on yttrium allyl-bridged complex **13** to confirm its role as a possible intermediate in the C-H activation of the asymmetric carbon of the ligand noted with neodymium. Complex **13** is of high interest: it must be re-synthesized and its reactivity, especially the potentially highly reactive Y-CCC-Y allyl bridge, must be thoroughly investigated towards a third ligand, small molecules or monomers, amongst others.

v. Theoretical calculations and magnetism studies should be done on the neodymium complex **14** to evaluate the degree of interaction (and eventually of bonding) between the two Nd centers.

vi. Further and more completed ring opening polymerization studies of lactide and ε-caprolactone should be conducted, also including the other complexes described in this manuscript. Moreover, polymerization of isoprene using cocatalysts such as: BEM, Al^{i}Bu$_3$, MAO, etc. would probably give rise to interesting results in terms of activity and selectivity.

vii. Finally, the rare earth allyl complexes described throughout this thesis should be studied for their reactivity towards small molecules such as CO_2, CO, H_2...

These are only lines of thought and we are convinced that continuing this work could lead to promising results and interesting advances in the organometallic chemistry of rare earths.

EXPERIMENTAL PART

General methods and materials: All the syntheses of rare earth products have been performed in air-free condition under argon. All the prepared complexes have been stored in a dry solvent-free glovebox (Jacomex O_2 < 1ppm, H_2O < 1ppm) under argon. Toluene, THF and pentane were purified through an alumina column (Mbraun, Mérignac, France), stored, deoxygenated by freeze-pump-thaw method, and then stored over benzophenone sodium. Solvents were either transferred to the reaction flask by trap-to-trap condensation at cold temperature or stored on 4 Å molecular sieves in the glovebox before use.

All the organic compounds (6-bromo-2-picoline, 2-acetylpyridine, 2,6-diisopropylaniline, 2,6-diacetylpyridine, N,N-dimethylacetamide), borohydride salts (potassium or sodium borohydride), acidic salts and bases [N,N-dimethylanilinium tetrakis(pentafluorophenyl)borate, n-butyllithium, methyllithium, butyl(ethyl)magnesium], monomers (lactide, *L*- and *rac*-, and ε-caprolactone), rare earth precursors (neodymium and yttrium tri-chloride) were acquired from Sigma-Aldrich, TCI or Fisher scientific.

The organic compounds were used as received while the borohydride and acidic salts, bases and rare earth precursors were stored before use in the glovebox.

Lactide (*L*- and *rac*-) used for polymerization was purified by recrystallization twice from a hot solution in toluene and filtered after each crystallization to remove traces of residual lactic acid. The lactide was then sublimed under *vacuum* over P_2O_5 and then stored in the glovebox.

Ɛ-caprolactone was dried under argon over CaH_2 before trap-to-trap distillation and then stored at -20 °C in the glovebox.

^{1}H NMR spectra were recorded on a Brucker Advance 300 instrument at 300 K. All ^{1}H chemical shifts (reported in ppm) were determined by using the residual signal of the deuterated solvent according to the literature[1]. Elemental analyses were performed by Céline Delabre on an Elementar Vario Cube apparatus at UCCS, University Lille Nord de France. For the polymers, the conversion was determined by mean of ^{1}H NMR spectroscopy by using Topspin software. Size exclusion chromatography (SEC) analyses of the samples were performed in THF (+ 0.1 % toluene) as an eluant at 35 °C (1 mL/min) with an Agilent 1260 pump, a Wyatt Optilab refractometer, and Waters Styragel columns (HR1, HR3 and HR4) calibrated with polystyrene standards. The GPC profile was further retraced in MS Excel with calibration equation and the data were verified.

General polymerization reaction: a reactor was loaded with the desired equivalent of monomer (200, 250, 400, 500 or 1000 equiv.) and stirred in the solvent (THF or toluene) for 2 minutes.

The catalyst was then added in the reactor and the reaction mixture was stirred either in an oil bath at 50 °C or at room temperature. Once the reaction was completed (after a given time or in case of any gel formation), the solution was quenched with a few drops of toluene containing a small amount of acidified water. An aliquot was collected to get the ^{1}H NMR conversion and the polymer was isolated by precipitation in a large volume of ethanol (250 mL).

$AgNO_3$ test: a few milligrams of the product are placed in a small flask and melted in the presence of potassium hydroxide to form a white foam. Water is then added, followed by a solution of concentrated HNO_3 to neutralize the pH giving a colorless solution. A few drops of a 1 M $AgNO_3$ solution are added, and the presence of chlorine can be verified by the appearance of AgCl as a white precipitate. This test allows to detect residual chloride traces in the compounds.

Synthesis of Ligands.

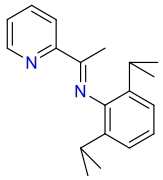

Preparation of 2,6-diisopropylphenyl-1-(pyridin-2-yl)ethan-1-imine (I^1) (according to reference [2]): to a yellowish solution of 2-acetylpyridine (5 mL, 44.6 mmol) in 20 mL of methanol, 2,6-diisopropylaniline (8.4 mL, 44.6 mmol) and a few drops of formic acid are added at room temperature. The mixture is refluxed at 80 °C overnight. After cooling to room temperature, the solution is evaporated under *vacuum* and the product is dissolved in 50 mL of pentane before being dried over Na_2SO_4. After evaporation of the pentane under *vacuum*, the product was dissolved in a minimal amount of methanol and allowed to stand at -40 °C overnight to give the compound as yellow crystals. This last step was repeated several times to recover additional crops of the final product **I^1**. Yield: 7.0 g (24.1 mmol, 54%). ^{1}H NMR (300 MHz, C_6D_6): δ (ppm) = 1.11 (d, 6H, $^3J_{HH}$ = 6.9 Hz, CH(C*H*$_3$)$_2$, 1.18 (d, 6H, $^3J_{HH}$ = 6.9 Hz, CH(C*H*$_3$)$_2$), 2.31 (s, 3H, N=C(C*H*$_3$)), 2.87 (sept, 2H, $^3J_{HH}$ = 6.9 Hz, C*H*(CH$_3$)$_2$), 6.69 (m, 1H, *para*-CH$_{Aryl}$), 7.15 (m, 5H, CH$_{Aryl}$ + C*H*$_{pyr}$), 8.48 (m, 1H, *ortho*-C*H*$_{pyr}$).

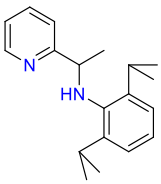

Preparation of 2,6-diisopropyl-1-(pyridin-2-yl)ethyl)aniline (Z^1H) (according to reference [2]): to a yellow solution of **I^1** (7 g, 24.1 mmol) in a methanol/dichloromethane mixture (1:2, respectively, total = 30 mL), a large excess of $NaBH_4$ (100 equiv.) is added. The evolution of the reaction is monitored by TLC (silica, ethyl acetate/petroleum ether 10:1). After disappearance of the starting material, the reaction mixture is quenched with water and extracted with dichloromethane (2 x 30 mL) and washed with deionized H_2O to obtain, after column

chromatography (silica, ethyl acetate/petroleum ether 30:1), the product **Z^{1}H** as a white powder. Yield: 4.6 g (16.2 mmol, 65%). ^{1}H NMR (300 MHz, C_6D_6): δ (ppm) = 1.12 (d, 6H, $^3J_{HH}$ = 6.83 Hz, CH(C*H*$_3$)$_2$), 1.24 (d, 6H, $^3J_{HH}$ = 6.83 Hz, , CH(C*H*$_3$)$_2$), 1.57 (d, 3H, $^3J_{HH}$ = 6.6 Hz, NH-CH(C*H*$_3$)), 3.49 (sept., 2H, $^3J_{HH}$= 7 Hz, C*H*(CH$_3$)$_2$), 4.29 (q, 1H, $^3J_{HH}$ = 6.17 Hz, NH-C*H*) 4.30 (s, 1H, N*H*), 6.56 (ddd, 1H, $^3J_{HH}$ = 7.53 Hz, $^4J_{HH}$ = 4.75 Hz, $^5J_{HH}$ = 1.25 Hz, *meta*-C*H*$_{pyr}$), 6.62 (dt, 1H, $^3J_{HH}$ = 7.67 Hz, $^5J_{HH}$ = 1.1 Hz, *meta*-C*H*$_{pyr}$), 6.89 (td, 1H, $^3J_{HH}$ = 7.75 Hz, $^5J_{HH}$ = 1.88 Hz, *para*-CH$_{Aryl}$), 7.07 (m, 3H, *para*-C*H*$_{pyr}$ + *meta*-CH$_{Aryl}$), 8.48 (m, 1H, *ortho*-C*H*$_{pyr}$).

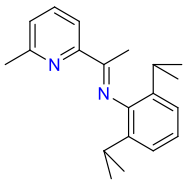

Preparation of 2,6-diisopropylphenyl-1-(6-methylpyridin-2-yl)ethan-1-imine (I^2) (according to reference [3]): in a three-neck round bottom flask under argon atmosphere, a colorless solution of 6-bromo-2-picoline (4 mL, 34 mmol) in THF (80 mL) is treated with a 2.5 M solution of ^{n}BuLi (14 mL, 35.7 mmol, 1.05 equiv.), which is added dropwise at -78 °C. This solution is left stirred for 15 min at – 78 °C and *N,N*-dimethylacetamide (6.3 mL, 68 mmol, 2 equiv.) is added. After 15 min stirring, the mixture is allowed to warm to RT over one hour. The solvent is evaporated, and the crude product is extracted with dichloromethane (2 x 30mL), washed with deionized water and dried over Na_2SO_4 to give the ketone, which is directly placed in a round bottom flask with 20 mL of methanol. 2,6-diisopropylaniline (6.03 g, 34 mmol) is added with a few drops of formic acid and the reaction mixture is heated to reflux overnight. After evaporation of the solvent, the product is extracted with pentane (50 mL), washed with water and dried over Na_2SO_4. The pentane is removed under *vacuum* and the residual product is placed in minimum of ethanol, which is left at – 40 °C to yield yellow crystals of **I^2.** Yield: 4.9 g (2.88 mmol, 49%). ^{1}H NMR (300 MHz, CD_2Cl_2): δ (ppm) = 1.34 ppm (m, 12H, CH(C*H*$_3$)$_2$), 2.17 (s, 3H, C*H*$_{3pyr}$), 2.60 (s, 3H, N=C(C*H*$_3$)), 2.74 (sept., 2H, $^3J_{HH}$ = 7.2 Hz, C*H*(CH$_3$)$_2$), 7.04-7.17 (m, 3H, *meta*-C*H*$_{Aryl}$ + *para*-C*H*$_{pyr}$), 7.26 (d, 1H, $^3J_{HH}$ = 8 Hz, *meta*-C*H*$_{pyr}$), 7.70 (t, 1H, $^3J_{HH}$ = 7.67 Hz, *para*-CH$_{Aryl}$), 8.13 (d, 1H, $^3J_{HH}$ = 7.95 Hz, *meta*-C*H*$_{pyr}$).

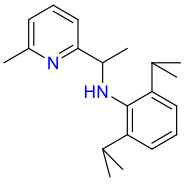

Preparation of 2,6-diisopropylphenyl-1-(6-methylpyridin-2-yl)ethyl)aniline (Z^{2}H) (according to reference [3]): to a yellow solution of **I^2** (0.85 g, 2.9 mmol) in a methanol/dichloromethane (1:2, respectively, total = 30mL) mixture, a large excess of $NaBH_4$ (100 equiv.) is added. The evolution of the reaction is monitored by TLC (silica, ethyl acetate/petroleum ether, 10:1). After the consumption of the starting materials, the reaction is quenched with water and extracted with dichloromethane (2 x 30mL), then washed with deionized water to obtain, after column chromatography (silica, ethyl acetate/petroleum ether, 30:1), the

product **Z²H** as a white oil. Yield: 0.9 g (1.74 mmol, 90%). ^{1}H NMR (300 MHz, CD_2Cl_2): δ (ppm) = 1.04 (d, 6H, $^3J_{HH}$ = 6.7 Hz, CH(C*H*$_3$)$_2$), 1.21 (d, 6H, $^3J_{HH}$ = 6.7 Hz, CH(C*H*$_3$)$_2$), 1.42 (d, 3H, $^3J_{HH}$ = 6.6 Hz, NH-CH(C*H*$_3$)), 2.56 (s, 3H, C*H*$_{3pyr}$), 2.32 (sept., 2H, $^3J_{HH}$ = 7 Hz, *CH*(CH$_3$)$_2$), 4.15 (q, 1H, $^3J_{HH}$ = 6.8 Hz, NH-*CH*) 4.31 (s, 1H, N*H*), 6.81 (dd, 1H, $^3J_{HH}$ = 7.68 Hz, *para*-CH$_{Aryl}$), 6.96 (m, 4H, CH$_{Aryl}$ + C*H*$_{pyr}$), 7.43 (m, 1 H, *meta*-C*H*$_{pyr}$).

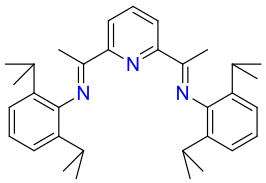

Preparation of 1,1'-(pyridine-2,6-diyl)bis(2,6-diisopropylphenyl)ethan-1-imine) (I³) (according to reference [4]): to a yellowish solution of 2,6 diacetylpyridine (1.0 g, 6.13 mmol) in 20 mL of ethanol, 2,6-diisopropylaniline (2.18 g, 12.26 mmol) and a few drops of formic acid are added at room temperature. The mixture is refluxed at 80 °C overnight and the product starts to precipitate. Filtration of the hot solution and washing with cold ethanol (2 x 15 mL) allows to recover the product as a yellow solid. Yield: 1.85 g (3.84 mmol, 63%).^{1}H NMR (300 MHz, C_6D_6): δ (ppm) = 1.15 (d, 12H, $^3J_{HH}$ = 6.8 Hz, CH(C*H*$_3$)$_2$), 1.19 (d, 12H, $^3J_{HH}$ = 6.8 Hz, CH(C*H*$_3$)$_2$), 2.27 (s, 6H, N=C(C*H*$_3$)), 2.91 (sept., 4H, $^3J_{HH}$ = 6.9 Hz, C*H*(CH$_3$)$_2$), 7.08-7.32 (m, 7H, CH$_{Aryl}$ + *para*-C*H*$_{pyr}$), 8.49 (d, $^3J_{HH}$ = 7.8 Hz, 2H, *meta*-C*H*$_{pyr}$).

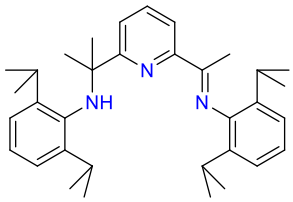

Preparation of (1-(6-(2-((2,6-diisopropylphenyl)amino)propan-2-yl)pyridin-2-yl)ethylidene)-2,6-diisopropylaniline (Z³H) (according to reference [5]): in a Schlenk tube under argon atmosphere, a yellow solution of **I³** (0.8 g, 1.6 mmol) in toluene is treated with a 1 M heptane solution of Al(Me)$_3$ (1.8 mL, 1.1 equiv.). After addition the brown solution is left to stir at 110 °C overnight. After cooling back to room temperature, the solution is quenched with 30 mL of pentane containing 0.02 mL of H_2O for 3 h to result to an orange solution with a white precipitate. The solvents are evaporated, and the crude product is extracted with CH_2Cl_2 (30 mL), washed with deionized water and dried over $NaSO_4$. The orange product is obtained after evaporation of the CH_2Cl_2. Yield: 0.68 g (1.3 mmol, 83%). ^{1}H NMR (300 MHz, CD_2Cl_2): δ (ppm) = 1.06 (d, 12H, $^3J_{HH}$ = 6.8 Hz, CH(C*H*$_3$)$_2$), 1.15 (d, 6H, $^3J_{HH}$ = 6.8 Hz, CH(C*H*$_3$)$_2$), 1.16 (d, 6H, $^3J_{HH}$ = 6.8 Hz, CH(C*H*$_3$)$_2$), 1.51 (s, 6H, NH-CH(C*H*$_3$)$_2$), 2.23 (s, 3H, N=C(C*H*$_3$)), 2.77 (sept., 2H, $^3J_{HH}$ = 6.9 Hz, C*H*(CH$_3$)$_2$), 3.28 (sept., 2H, $^3J_{HH}$ = 7 Hz, C*H*(CH$_3$)$_2$), 4.39 (s, 1H, N*H*), 7.06-7.2 (m, 6H, C*H*$_{Aryl}$), 7.6 (m, 1H, *meta*-C*H*$_{pyr}$), 7.82 (d, $^3J_{HH}$ = 7.9 Hz, 1H, *meta*-C*H*$_{pyr}$), 8.25 (m, 1H, *para*-C*H*$_{pyr}$).

Synthesis of Reagents

Preparation of potassium graphite (KC_8) (according to reference [6]): in the glovebox, 8 equiv. of graphite (2.45 g, 204.64 mmol) are added to a vial containing 1 g of melt potassium (25.58 mmol). The solid mixture is grinded until obtention of a copper-colored powder.

Preparation of triethylammonium tetraphenylborate $[HNEt_3][B(Ph)_4]$ (according to reference [7]): NEt_3 (1.22 mL, 8.77 mmol) is added dropwise to a 20% wt HCl aqueous solution. This colorless solution is then added dropwise to a solution of $NaBPh_4$ (3 g, 8.77 mmol) in acetone (15 mL). The product precipitates instantaneously as a colorless powder. Then, the solution is filtered, washed twice with cold water and dried under *vacuum* to afford the product as a white powder. Yield: 2.96 g (7.19 mmol, 82%). ^{1}H NMR (300 MHz, THF-D8): δ (ppm) = 0.98 (t, 9H, $^3J_{HH}$ = 7.26 Hz, C*H*$_3$), 2.68 (q, 6H, $^3J_{HH}$ = 7.28 Hz, C*H*$_2$), 6.73 (m, 4H, *para*-C*H*$_{Aryl}$), 6.88 (m, 8H, *meta*-C*H*$_{Aryl}$), 7.29 (m, 8H, *ortho*-C*H*$_{Aryl}$).

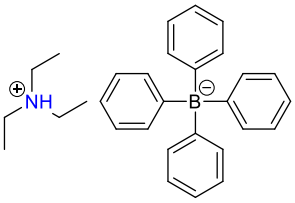

Preparation of $Mg(\eta^3\text{-}C_3H_5)_2$ (according to reference [8]): In a dried Schlenk tube, 30 mL (51 mmol) of a 1.7 M THF solution of $Mg(C_3H_5)(Cl)$ are treated at room temperature with 1.2 equiv. of dioxane (5.23 mL, 61 mmol) to give a grey solution with a grey precipitate. This mixture is stirred for 1 h before adding Et_2O (60 mL) followed by further stirring for 20 min. Filtration of the solution affords a light grey solution that is dried under *vacuum*. The whitish solid obtained is triturated in toluene (25 mL) and dried under *vacuum* to obtain the product as a white powder. Yield: 2.2 g (20.6 mmol, 39%). ^{1}H NMR (300 MHz, THF-D8): δ (ppm) = 2.34 (d, 8H, $^3J_{HH}$ = 11.22 Hz, C*H*$_2$CHC*H*$_2$), 6.23 (q, 2H, $^3J_{HH}$ = 11.19 Hz, CH_2C*H*CH_2).

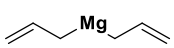

Preparation of $KN(TMS)_2.Z^1H$: In a dried Schlenk tube, to a solution of **Z^1H** (0.208 g, 0.74 mmol) in THF is added $KN(TMS)_2$ (0.147 g, 0.74 mmol). The yellow starting solution is left under stirring overnight to turn dark brown. Evaporation, filtration in toluene and *vacuum* drying yields a dark brown powder. The powder is dissolved in the minimum amount of pentane and then left at -35 °C for crystallization. 0.193 g (0.4 mmol, 54%) of dark crystals suitable for XRD were obtained. ^{1}H NMR (300 MHz, THF-D8): δ (ppm) = -0.20 (br, 16H, C*H*$_{3TMS}$), 1.01 (d, 6H, $^3J_{HH}$ = 6.83 Hz, CH(C*H*$_3$)$_2$), 1.18 (d, 6H, $^3J_{HH}$ = 6.83 Hz, , CH(*CH*$_3$)$_2$), 1.42 (d, 3H, $^3J_{HH}$ = 6.6 Hz, NH-CH(C*H*$_3$)), 3.31 (sept.,

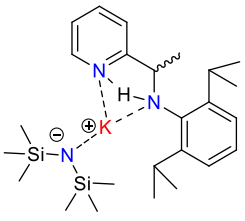

2H, $^3J_{HH}$= 7 Hz, C*H*$(CH_3)_2$), 4.14 (q, 1H, NH-C*H* + s, 1H, N*H*), 6.87 (m, 1H, *meta*-CH_{pyr}), 6.96 (d, 2H, *meta*-CH_{Aryl}), 7.05 (m, 1H, CH_{pyr}), 7.13 (m, 1H, CH_{pyr}), 7.54 (m, 1H, para-CH_{Aryl}), 8.56 (m, 1H, *ortho*-CH_{pyr}).

Synthesis of Rare Earth precursors:

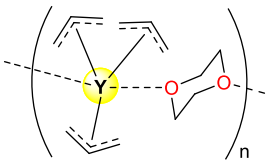

Preparation of Y(η^3-C_3H_5)$_3$(diox)$_{0.25}$ (modified version of [9]): YCl_3 (4 g, 20.47 mmol) was suspended in THF (50 mL) and stirred overnight at 50 °C. The white suspension was then treated with a THF solution (10 mL) of 1.5 equiv. of $Mg(C_3H_5)_2$ (3.27g, 30.7 mmol) at room temperature and dioxane (20 mL) is added to the reaction medium. The yellow starting solution turns into orange with formation of a white precipitate overnight. Filtration of the reaction mixture and evaporation of the solvents results to an orange oil, which is extracted twice with dioxane (2 x 15 mL). After drying under *vacuum*, the orange solid is washed with pentane (3 x 15 mL) to afford the desired product as an orange powder. Yield: 2.88 g (12.3 mmol, 60%). Possible recrystallisation in a dioxane/toluene (1:6 respectively, total = 70 mL) mixture is possible to obtain a purer product. ^{1}H NMR (300 MHz, THF-D8): δ (ppm) = 2.73 (d, 12H, $^3J_{HH}$= 12.14 Hz, CH_2CHCH_2), 3.56 (s, 2H, 0.25 $C_4H_8O_2$) 6.19 (quint, 3H, $^3J_{HH}$ = 12.08 Hz, CH_2CHCH_2).

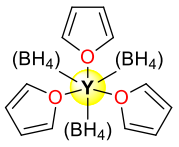

Preparation of Y(BH_4)$_3$(THF)$_3$ (modified version of [10]): to a white suspension of $YCl_3(THF)_3$ (5 g, 12.1 mmol) in THF (50 mL) are added 3.5 equiv. of $NaBH_4$ (1.61 g, 42.5 mmol). The mixture is refluxed at 80 °C for 3 days. The reaction mixture is filtered and evaporation of the solvent provides a white solid. This solid is extracted several times in THF (30 mL) until the $AgNO_3$ test is negative. The product is obtained as a white powder (1.95 g, 5.6 mmol, 46%). ^{1}H NMR (300 MHz, C_6D_6): δ (ppm) = 0.83-1.67 (q, 12H, BH_4), 1.20 (br. s, 12H, THF), 3.73 (br. s, 12H, THF).

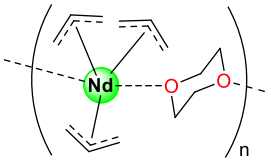

Preparation of Nd(η^3-C_3H_5)$_3$(diox) (according to reference [9]): $NdCl_3$ (2g, 8 mmol) is treated with a solution of $Mg(C_3H_5)_2$ (1.27 g, 12 mmol, 1.5 equiv.) in THF (10mL). Dioxane (20 mL) is added to the solution and the green solution with white suspension is left under stirring overnight. Filtration and evaporation yield a green oil. This oil is extracted twice with dioxane (2 x 15 mL) and the resulting green oil is diluted in a dioxane/toluene

(1:2, respectively, total = 30 mL) mixture at -40 °C. The product is obtained as a microcrystalline solid (1.1 g, 3.1 mmol, 39%). ^{1}H NMR (300 MHz, THF-D8): δ (ppm) = -15.81 (br. s, 6H, anti-C*H*$_2$CHC*H*$_2$), δ = -2.16 ppm (br. s, 6H, syn-C*H*$_2$CHC*H*$_2$), δ = 0.09 ppm (br. s, 3H, CH$_2$C*H*CH$_2$), δ = 3.67 ppm (br. s, 8H, C$_4$*H*$_8$O$_2$).

Preparation of Nd(BH$_4$)$_3$(THF)$_3$ (modified version of [10]): to a blue suspension of NdCl$_3$(THF)$_3$ (5 g, 10.7 mmol) in THF (50 mL) are added 3.5 equiv. of NaBH$_4$ (1.42 g, 37.4 mmol). The mixture is refluxed at 80 °C for 24 h. The purple solution is filtered and evaporated to produce a purple solid. This solid is extracted multiple times with THF (30 mL) until the AgNO$_3$ test is negative. The product is obtained as a purple powder (3 g, 7.4 mmol, 69%). ^{1}H NMR (300 MHz, C$_6$D$_6$): δ (ppm) = 1.93 (br. s, 12H, THF), 3.16 (br. s, 12H, THF), 99.48 (br. s, 12H, B*H*$_4$).

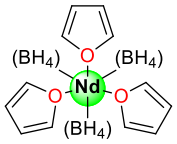

<u>Synthesis of Rare Earth ionic/mixed complexes:</u>

Preparation of [Nd(η^3-C$_3$H$_5$)$_4$][K(crypt)$^+$] (<u>11</u>): a mixture of Nd(η^3-C$_3$H$_5$)$_3$(diox) (0.3 g, 0.84 mmol) and 2,2,2 cryptand (0.318 g, 0.84 mmol) in THF (5 mL) at -35 °C is treated with 1.5 equiv. of KC$_8$ (0.171 g, 1.27 mmol). The reaction is left to stir for less than 5 min before filtering. The product is obtained by crystallization from a concentrated solution in THF with a layer of pentane at -35 °C. Yield: 0.305 g (0.42 mmol, 50%). ^{1}H NMR (300 MHz, THF-D8): δ (ppm) = -28.3 (br. s, 8H, anti-C*H*$_2$CHC*H*$_2$), -18.72 (br. s, 4H, CH$_2$C*H*CH$_2$), -8.35 (br. s, 8H, syn-C*H*$_2$CHC*H*$_2$), 2.51 (br. s, 12H, N-C*H*$_2$), 3.51 (br. s, 12H, N-CH$_2$(C*H*$_2$)), 3.57 (br. s, 12H, O(C*H*$_2$)$_2$O).

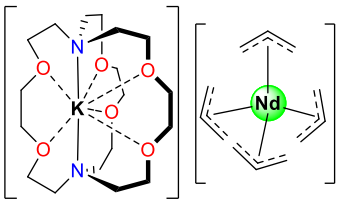

Attempted preparation of Nd(η^3-C$_3$H$_5$)$_2$BH$_4$: i) [Nd(η^3-C$_3$H$_5$)$_2$][B(C$_6$F$_5$)$_4$] was prepared according to the literature[9b]: to a solution of Nd(η^3-C$_3$H$_5$)$_3$(diox) (0.3 g, 0.84 mmol) in THF (10 mL), was added dropwise under stirring a solution of [HNMe$_2$Ph][B(C$_6$F$_5$)] (0.67 g, 0.84 mmol) in THF. After 5 min, the solution was filtered, dried under *vacuum* and washed twice with pentane (2 x 15 mL). A crop of the green powder was analyzed in NMR and the ^{1}H NMR in THF-D8 confirmed the obtention of the bis-allyl cationic complex with the presence of N(Me)$_2$Ph. ii) the complex was dissolved again in THF (10 mL) and was left under stirring for one hour after the addition of 1.1 equiv. of KBH$_4$ (0.05g, 0.9 mmol).

Evaporation of the solvent under *vacuum* resulted in a green powder. Addition of toluene (10 mL) and filtration to remove the excess of KBH_4 allowed the obtention of a light green colored solution. The beginning of the color change was observed after one hour to give an orange product while the solution seemed stable at -35 °C for a few days. ^{1}H NMR of the orange powder revealed after isolation and drying the absence of paramagnetic peaks while the product obtained after drying the green solution revealed by ^{1}H NMR the presence of some paramagnetic peaks at δ (ppm) = -15.61 (br. s, 6H, anti-C*H*$_2$CHC*H*$_2$), δ = -2.35 ppm (br. s, 6H, syn-C*H*$_2$CHC*H*$_2$), δ = 0.00 ppm (br. s, 3H, CH_2CHCH_2), 16.5 (br s, BH_4). The attempts of crystallization from the concentrated solution in toluene resulted to the obtention of crystals, which revealed the molecular structure of the cationic species [Nd(η^3-$C_3H_5)_2(THF)_4$][$B(C_6F_5)_4$].

<u>Synthesis of Rare Earth amido-pyridine supported complexes:</u>

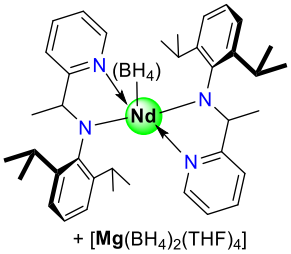

Preparation of [(Z^1)$_2$Nd(BH_4)][Mg(BH_4)$_2$(THF)$_4$] (1a/1b): from a solution of Nd(BH_4)$_3$(THF)$_3$ (0.28 g, 0.69 mmol) and two equiv. of **Z^1H** (0.4 g, 1.14 mmol) in toluene (10 mL) is added one equiv. of a 1.28 M BEM solution in hexane (0.44 mL, 0.69 mmol). The solution turned from light blue to green and was left to stir for 30 min at room temperature. After evaporation of the solvent, the green foam was extracted with 20 mL of toluene and evaporated to dryness to give the product as a green powder that was washed with pentane (2 x 10 mL) (0.46 g, 0.43 mmol, 63%). ^{1}H NMR (300 MHz, C_6D_6): δ (ppm) = -51.01 (s, 1H), -28.41 (s, 3H), -12.79 (s, 3H), -6.46 (s, 1H), 3.77 (s, 1H) 5.04 (s, 1H), 5.48 (s, 2H), 5.98 (s, 1H), 9.39 (s, 1H), 11.92 (s, 3H), 20.65 (s, 3H), 34.47 (s, 3H), 38.01 (br s, 1H), 50.72 (br, 4H, BH_4), 98.05 (br s, 1H). Anal. calcd. for **[(Z^1)$_2$Nd(BH_4)][Mg(BH_4)$_2$(THF)$_4$]**: C, 60.92; H, 8.91; N, 5.26. Found: C, 61.25; H, 8.61; N, 5.37.

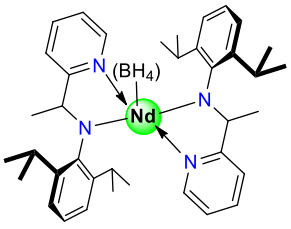

Preparation of (Z^1)$_2$Nd(BH_4) <u>1'b</u>: as in the synthesis of [(Z^1)$_2$Nd(BH_4)][Mg(BH_4)$_2$], a solution of Nd(BH_4)$_3$(THF)$_3$ (0.22 g, 0.54 mmol) and 1.95 equiv. **Z^1H** (0.3 g, 1.06 mmol) in toluene (10 mL) was treated with a 1.6 solution of MeLi in THF (0.66 mL, 1.06 mmol, 1.95 equiv.). The solution turned from light blue to green with apparition of a white precipitate and was left for stirring for 30 min at room temperature. After evaporation of the THF, the green foam was extracted with 10 mL of toluene and left at room temperature with a vapor of pentane for

crystallization. After 24 h green crystals suitable for XRD were obtained (0.15 g, 0.2 mmol, 19%). The ^{1}H NMR spectrum was not interpretable and can been seen in the annex XX. Unfortunately, no elemental analysis was done.

Preparation of (Z^2)Nd(THF)$_2$(BH$_4$)$_2$ (3): to a blue solution of Nd(BH$_4$)$_3$(THF)$_3$ (0.3 g, 0.74 mmol) and 1 equiv. of **Z^2H** (0.22 g, 0.74 mmol) in toluene (10 mL) is added 0.5 equiv. of a 1.28 M BEM solution in hexane (0.29 mL, 0.37 mmol). The solution changed from light blue to green (with presence of a precipitate) and was left to stir for 1 h at room temperature. After evaporation of the solvent, the green foam was extracted with 20 mL of toluene and dried under *vacuum* to give the product as a green powder, which was washed with pentane (2 x 10 mL) (0.35 g, 0.57 mmol, 77%). Crystals suitable for XRD were obtained from a concentrated solution in THF at -40 °C with a layer of pentane and revealed the molecular structure of **4**. ^{1}H NMR (300 MHz, C_6D_6): δ (ppm) = -40.62 (s, 3H), -24.7 (s, 3H), -10.55 (s, 3H), -6.27 (s, 1H), 3.26 (s, 3H), 4.31 (s, 2H), 5.76 (s, 3H), 6.09 (s, 1H), 8.73 (s, 1H), 11.95 (s, 3H), 20.62 (s, 1H), 33.68 (s, 3H), 38.27 (s, 1h), 68 - 86 (br, BH$_4$), 95.86 (s, 1H). Anal. calcd. for **[(Z^2)Nd(BH$_4$)$_3$]$_2$[Mg(THF)$_6$]**: C, 53.84; H, 9.05; N, 3.92. Found: C, 53.70; H, 8.82; N, 3.66.

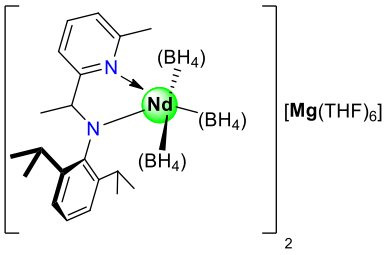

Preparation of (Z^3)Nd(BH$_4$)$_2$ (5): a solution of Nd(BH$_4$)$_3$(THF)$_3$ (0.167 g, 0.4 mmol) and 1 equiv. **Z^3H** (0.2 g, 0.4 mmol) in toluene (10 mL) is treated with a 1.28 M solution of BEM in hexane (0.16 mL, 0.2 mmol, 0.5 equiv.). The solution turned from orange to purple with a white solid and was left to stir for 1 h at room temperature. After evaporation of the THF, the purple-red oil is extracted with 20 mL of toluene (red solution) and concentrated to half of the solution, then left at room temperature for crystallization. 0.077 g of red crystals (0.11 mmol, 29%) were obtained and the resulting solution was dried under *vacuum* to yield a red powder (0.072 g, 0.10 mmol, 27%). (300 MHz, THF-D8): δ (ppm) = -13.58 (s, 6H), -8.21 (s, 1H), -7.31(s, 3H), -1.85 (s, 6H), 2.27 (s, 1H), 6.54 (s, 6H), 8.83 (br, 2H), 9.05 (br s, 1H) 13.15 (s, 1H), 13.77 (s, 2H), 18.51 (s, 6H), 19.37 (s, 1H), 23.22 (s, 2H), 61.68 (br, BH$_4$), 97.48 (br, 2H). Anal. Calc. for (Z^3)Nd(BH$_4$)$_2$: C = 60.87%, H = 8.13%, N = 6.15%; found: C = 61.49%, H = 9.40%, N = 5.67%).

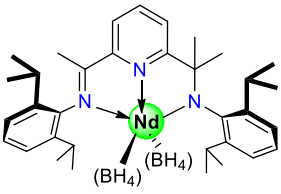

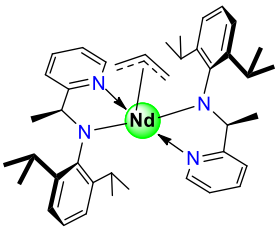

Preparation of $(Z^1)_2Nd(\eta^3\text{-}C_3H_5)$ (12): a solution of $Nd(\eta^3\text{-}C_3H_5)_3(diox)$ (0.15 g, 0.42 mmol) in THF (10 mL) is treated with a solution of 1.95 equiv. **Z^1H** (0.232 g, 0.82 mmol) in THF (5 mL). The green solution is stirred for 1 h before evaporation. The obtained green product was extracted with toluene (15 mL) and dried under *vacuum* to afford a green powder. (0.215 g, 0.29 mmol, 68%). ^{1}H NMR (300 MHz, THF-D8): δ (ppm) = -33.81 (s), -19.23 (br s), -17.35 (s), -15.76(br s), -11.13 (br s), -8.95 (br s), -2.32 (s), 0.96 (s,), 5.65 (br), 6.19(br), 6.62 (br), 11.0 (s), 11.52 (s), 12.80 (s), 13.1 (s), 44.94 (s), 57.33 (s). Crystals suitable for XRD were obtained from a concentrated solution in pentane at -40 °C (molecular structure of **12**). Anal. calcd. for **$(Z^1)_2Nd(\eta^3\text{-}C_3H_5)(diox)_{0.5}$**: C, 65.2; H, 7.53; N, 7.07. Found: C, 65.03; H, 7.65; N, 7.02.

Attempted preparation of $(Z^2)Nd(\eta^3\text{-}C_3H_5)_2$: a solution of $Nd(\eta^3\text{-}C_3H_5)_3(diox)$ (0.2 g, 0.56 mmol) in THF (10 mL) was treated with a solution of 0.95 equiv. of **Z^2H** (0.158 g, 0.53 mmol). The green solution was stirred for 1 h at 50 °C. The resulting brown solution was dried, and the resulting dark brown oil was then dissolved in toluene (20 mL), followed by filtration and evaporation which provided the product as a dark brown oil. Pentane (10 mL) was added and after drying a dark green powder was obtained. (0.16 g). Small amount (0.034g, 0.07mmol, 13%) of crystals suitable for XRD were obtained from a concentrated solution in toluene allowing to determine the molecular structure **14** **$\{[(\mu\text{-}Z^{2'})Nd(\eta^3\text{-}C_3H_5)]_2\}$**. ^{1}H NMR of powder (300 MHz, C_6D_6): δ (ppm) = -34.57 (s), -23.57 (s), -20.98 (s), -7.26(s), -5.41 (s), -3.01 (s), -0.49 (s), 2.9 (s), 3.20 (s), 6.10 (s), 8.80 (s), 9.80 (s), 10.83 (s), 11.20 (s), 16.73 (s), 36.00 (s), 48.10 (s).

Attempted preparation of $(Z^3)Nd(\eta^3\text{-}C_3H_5)_2$: a solution of $Nd(\eta^3\text{-}C_3H_5)_3(diox)$ (0.2 g, 0.56 mmol) in THF (10 mL) is treated with a solution of 0.95 equiv. of **Z^3H** (0.26 g, 0.53 mmol). The brown solution is stirred 3 days at 50 °C before evaporation. The dark brown oil is extracted twice with pentane (2 x 15 mL). After filtration and evaporation, a brown powder is obtained (0.12 g). Due to poor NMR data quality only a few peaks could be attributed to the complex. ^{1}H NMR (300 MHz, THF-D8) of the brown powder: δ (ppm) = -41.9 (br), -24.3 (s), -17.91 (br), -6.76 (br), 19.54 (br), 20.66 (br), 36.25 (br), 45.20 (br).

Preparation of $[(Z^1)Y(BH_4)_3]^-_2[Mg(THF)_6]^{2+}$ (6): a colorless solution of $Y(BH_4)_3(THF)_3$ (0.4 g, 1.14 mmol) and **Z^1H** (0.32 g, 1.14 mmol) in toluene is treated with an 1.28 M solution of BEM (0.440 mL, 0.57 mmol, 0.49 equiv.) to give a yellow solution with the presence of a white precipitate. This solution is left under stirring for 30 min. Evaporation of the solvents yields a yellow foam. Toluene (15 mL) is then added to the foam, followed by filtration and evaporation to obtain a new yellow foam. This foam is triturated in pentane and washed twice with it to afford a light-yellow product (0.52 g, 0.81 mmol, 71%). Crystals suitable for XRD were obtained from a concentrated solution in THF/pentane at -40 °C. ^{1}H NMR (300 MHz, C_6D_6): δ (ppm) = 1.21 (d, 6H, $^3J_{HH}$ = 6.61 Hz, CH(CH_3)$_2$), 1.26 (dd, 6H, $^3J_{HH}$ = 6.31 Hz, , CH(CH_3)$_2$), 1.31 (d, 3H, $^3J_{HH}$ = 6.91 Hz, N-CH(CH_3)), 3.51 (sept., 2H, $^3J_{HH}$= 6.68 Hz, C*H*(CH_3)$_2$), 4.17 (sept., 2H, $^3J_{HH}$= 6.68 Hz, C*H*(CH_3)$_2$), 4.63 (q, 1H, $^3J_{HH}$ = 6.27 Hz, N-C*H*), 6.36 (br. t, 1H, $^3J_{HH}$ = 6.83 Hz, *meta*-CH_{pyr}), 6.59 (br. d, 1H, $^3J_{HH}$ = 8.03 Hz, *meta*-CH_{pyr}), 6.82 (td, 1H, $^3J_{HH}$ = 7.53 Hz, $^5J_{HH}$ = 1.1 Hz, *para*-CH_{pyr}), 8.66 (m, 1H, *ortho*-CH_{pyr}). The peaks integrating for the borohydride function are certainly hidden by the CH_3 peaks and the aryl peak missing under the peak of solvent. Anal. calcd. for **$[Y(BH_4)_3(Z^1)]^-_2[Mg(THF)_6]^2$**: C, 57.83; H, 9.57; N, 4.35. Found: C, 56.80; H, 9.31; N, 4.26.

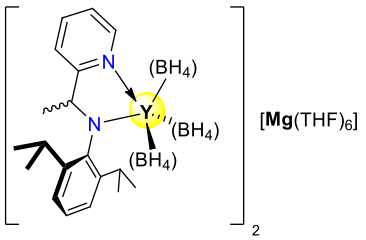

Attempted preparation of $(Z^1)Y(BH_4)_2$ (7): a colorless solution composed of 0.4 g of $Y(BH_4)_3(THF)_3$ (1.14 mmol) and 0.32 g of **Z^1H** (1.14 mmol) in toluene is treated with a 1.6 M solution of MeLi in THF (0.7 mL, 1.12 mmol, 0.98 equiv.) and left to stir during 10 minutes. Evaporation of the solvent, filtration in toluene (20 mL) and drying under *vacuum* affords the product as a yellow foam which is washed twice with pentane (2 x 10mL) to yield a yellow powder. ^{1}H NMR shows the presence of numerous signals sign of a mixture of product Appendix 5. Crystallization from a concentrated solution in toluene with a pentane vapor allowed the obtention of crystals suitable for XRD. The molecular structure revealed the formation of **$(Z^1)_2Y(BH_4)$**.

Attempted preparation of $[(Z^2)Y(BH_4)_3]^-_2[Mg(THF)_6]^{2+}$: a colorless solution of $Y(BH_4)_3(THF)_3$ (0.235 g, 0.67 mmol) and **Z^2H** (0.2 g, 0.67 mmol) in toluene is treated with half an equiv. of BEM (BEM solution in hexane at 1.28 M) (0.26 mL, 0.34 mmol) to obtain a yellow solution and a white precipitate. This solution is left to stir for 30 min. Evaporation of the solvent allows to obtain a yellow foam to which toluene (15 mL) is added. Subsequent filtration and evaporation yielded a yellow powder (0.32 g, 0.36 mmol, ^{1}H NMR yield according to 30 % of by-product: 37%). Several crystallization attempts resulted

only in crystals of **8** [**(Z^2)Mg(BH_4)**]. ^{1}H NMR of the powder (300 MHz, C_6D_6) showed in the same spectrum typical peaks related to the yttrium complex at δ (ppm) = 4.21 (sept., 2H, $^3J_{HH}$= 6.73 Hz, C*H*(CH_3)$_2$) and 4.55 (q, 1H, $^3J_{HH}$ = 6.69 Hz, N-C*H*) but also that of the magnesium complex **8**, δ (ppm) = 4.02 (sept., 2H, $^3J_{HH}$= 6.73 Hz, C*H*(CH_3)$_2$) and 4.65 (q, 1H, $^3J_{HH}$ = 6.69 Hz, N-C*H*).

Attempted preparation of [(Z^3)Y(BH_4)$_3$]$^-_2$[Mg(THF)$_6$]$^{2+}$: a colorless solution of **5** (0.147 g, 0.42 mmol) and **Z^3H** (0.21 g, 0.42 mmol) in toluene is treated with half an equiv. of BEM (BEM solution in hexane at 1.28 M) (0.16 mL, 0.21 mmol). Upon addition of BEM, the solution turns from orange to purple with the presence of a white precipitate. This solution is left under stirring for 30 minutes. Evaporation of the solvents afforded a purple foam to which toluene (15 mL) was added. Subsequent filtration and evaporation resulted in a purple powder (0.135 g). Several attempts of crystallization resulted only by the obtention of crystals of **10** [**(Z^3)Mg(BH_4)**]. ^{1}H NMR of the powder could not be interpreted as seen in Annex 7.

Preparation of (Z^1)Y(C_3H_5)$_2$ (13): to an orange solution of Y(C_3H_5)(diox)$_{0.25}$ (0.303 g, 1.29 mmol) in THF (20 mL) is added 0.347 g of **Z^1H** (1.22 mmol, 0.95 equiv.)**.** The orange solution is left under stirring for 30 min. Evaporation and addition of toluene (15 mL) lead to an orange solution with an orange precipitate. Filtration and *vacuum* drying allowed the obtention of an orange dark oil. 30 mL of pentane was added to the oil and after filtration the orange solution was stored at -35 °C. Dark orange crystals suitable for XRD were obtained and the molecular structure was revealed as **13 [(Z^1)Y(C_3H_5)(μ-C_3H_5)$_2$(Z^1)Y(C_3H_5)]**. ^{1}H NMR of the crystals (300 MHz, THF-D8): δ (ppm) = 1.07 (d, 6H, $^3J_{HH}$ = 6.72 Hz, CH(*CH*$_3$)$_2$), 1.16 (d, 3H, $^3J_{HH}$ = 6.87 Hz, N-CH(*CH*$_3$)), 1.24 (dd, 6H, $^3J_{HH}$ = 6.72 Hz, , CH(*CH*$_3$)$_2$), 2.68 (d, 8H, $^3J_{HH}$ = 12.24 Hz, *CH*$_2$CH*CH*$_2$), 3.24 (sept., 2H, $^3J_{HH}$= 6.76 Hz, *CH*(CH_3)$_2$), 4.04 (sept., 2H, $^3J_{HH}$= 6.76 Hz, *CH*(CH_3)$_2$), 4.39 (q, 1H, $^3J_{HH}$ = 6.67 Hz, N-*CH*), 6.22 (quint.d, $^3J_{HH}$ = 12.24 Hz, J_{HY} = 1.09 Hz, 2H, CH_2*CH*CH_2),6.83 (br t, 1H, $^3J_{HH}$ = 7.52 Hz, para-CH_{Aryl}), 6.96 (m, 2H, *meta*-CH_{Aryl}), 7.31 (br t, 1H, $^3J_{HH}$ = 6.36 Hz, *para*-C*H*$_{pyr}$), 7.40 (br. d, 1H, $^3J_{HH}$ = 8.12 Hz, *meta*-C*H*$_{pyr}$), 7.81 (m, 1H, H^{Py}), 8.58 (m, 1H, *ortho*-C*H*$_{pyr}$). ^{1}H NMR of the crystals (300 MHz, Tol-D8): δ (ppm) = 2.48 – 3.74 (br., 8H, *CH*$_2$CH*CH*$_2$), 3.14 (sept., 2H, $^3J_{HH}$= 6.76 Hz, *CH*(CH_3)$_2$), 3.93 (sept., 2H, $^3J_{HH}$= 6.67 Hz, *CH*(CH_3)$_2$), 4.34 (q, 1H, $^3J_{HH}$ = 6.67 Hz, N-*CH*), 6.39 (br. t, 1H, H^{Ar}), 6.61 (quint, $^3J_{HH}$ = 12.24 Hz, 2H, CH_2*CH*CH_2),6.68 (br d, 2H, , *meta*-CH_{Aryl}), 6.89 (br. t, 1H, *para*-CH_{Aryl}), 7.04 (br d, 1H, *meta*-C*H*$_{pyr}$), 7.12 (br. d, 1H, *meta*-C*H*$_{pyr}$), 7.86 (m, 1H, *para*-C*H*$_{pyr}$), 8.04 (m, 1H, *ortho*-C*H*$_{pyr}$). The peaks corresponding to N-CH(*CH*$_3$)) and the isopropyl methylene being too close to each other, a clear distinction could not be done in Tol-D8.

References

[1] G. R. Fulmer, A. J. M. Miller, N. H. Sherden, H. E. Gottlieb, A. Nudelman, B. M. Stoltz, J. E. Bercaw, K. I. Goldberg, **Organometallics**, *2010*, 29 (9), 2176.

[2] K. Nienkemper, G. Kehr, S. Kehr, R. Fröhlich, G Erker, **J. Organomet. Chem.**, *2008*, 693 (8-9), 1572.

[3] O. H. Hashmi, F. Capet, M. Visseaux, Y. Champouret, **Eur. J. Inorg. Chem.**, *2022, (15)*, 1434.

[4] G. J. P. Britovsek, M. Bruce, V. C. Gibson, B. Kimberley, P. J. Maddox, S. Mastroianni, S. J. McTavish, C. Redshaw, G. A. Solan, S. Strömberg, A. J. P. White, D. J. Williams, **J. Am. Chem. Soc.**, *1999*, 121 (38), 8728.

[5] B.-Y. Tay, C. Wang, S.-C. Chia, L. P. Stubbs, P.-K. Wong, M. van Meurs, **Organometallics**, *2011*, 30 (21), 6028.

[6] D. E. Bergbreiter and J. M. Killough, **J. Am. Chem. Soc.,** *1978*, 100 (7), 2126.

[7] D. M. Amorose, R. A. Lee, J. L. Petersen, **Organometallics**, *1991,* 10 (7), 2191.

[8] (a) W. Schlenk, J. W. Schlenk, **Ber.**, *1929*, 62B, 920; (b) C. R. Noller, W. R White, **Am. Chem. Soc.**, *1937*, 59, 1354; (c) R. Kullman, **Compt. Rend.**, 1950, 231, 866.

[9] (a) L. F. Sanchez-Barba, D. L. Hughes, S. M. Humphrey, M. Bochmann, **Organometallics,** *2005*, 24 (15), 3792; (b) D. Robert, E. Abinet, T. P. Spaniol, J. Okuda, **Chem. Eur. J.,** *2009*,15 (44), 11937.

[10] U. Mirsaidov, A. Kurbonbekov, **Dokl. Akad. Nauk. Tadzh. SSR**, *1979*, 22 (5), 313; **Chem. Abstr.**, *1979*, 91, 185190.

APPENDICES

Appendices for the thesis of Maxime Beauvois

Appendix 1: Comprehensive organometalic chemistry

Alkenes and Allyl Complexes of the Group 3 Metals and Lanthanides

Maxime Beauvois[a], Yohan Champouret[a], Fanny Bonnet[b], and Marc Visseaux[a], [a]Univ. Lille, CNRS, Univ. Artois, Centrale Lille, UMR 8181 - UCCS - Unité Catalyse et Chimie du Solide, Lille, France; [b]Univ. Lille, CNRS, INRAE, Centrale Lille, UMR 8207 - UMET - Unité Matériaux et Transformations, Lille, France

Abbreviations

Bd	1,3-Butadiene
CCG	Catalyzed chain growth
CGC	Constrained geometry catalyst
Cp	Cyclopentadienyl
Cp*	Pentamethylcyclopentadienyl
diox	Dioxane
DFT	Density functional theory
Dipp	$2,6\text{-}^{i}Pr_2C_6H_3$
DME	Dimethoxyethane
Fc	Ferrocene
Flu	Fluorenyl
Ip	Isoprene
Ind	Indenyl
MAO	Methyl aluminoxane
NMR	Nuclear magnetic resonance
PB	Polybutadiene
PI	Polyisoprene
PS	Polystyrene
ROP	Ring opening polymerization
THF	Tetrahydrofuran

TMEDA	*N*,*N*,*N*′,*N*′-Tetramethylethylenediamine
TOF	Turn-over frequency
TON	Turn-over-number
St	Styrene
XRD	X-Ray diffraction

1 Introduction

This chapter reviews the chemistry of lanthanide and group 3 metals (which corresponds to rare earth metals and herein designed as Ln or *lanthanides*) alkene and allyl organometallic complexes over the period 2006–20. It follows previous developments on the chemistry of these complexes in preceding editions of COMC in 1982, 1995 and 2007.[1]

Alkene and alkyne complexes are compounds in which the hydrocarbon molecule behaves as L-type ligand toward the metal center. In this chapter, we will also present literature works regarding alkenyl and alkynyl (X-type ligand).

As far as allyl organolanthanides are concerned, we wish to bring to the reader's attention that this field has been addressed by Carpentier and collaborators in their well-documented review published in 2010 in *C.R. Chimie*.[2] However, with the aim to be as exhaustive as possible, we included herein all information that seemed essential to us and was already cited earlier. All complexes comprising the "simple" [Ln](C_3H_5) and "substituted" [Ln]($C_3H_nR_{5-n}$) (R = alkyl, n = 1–4) allyl motive will be the subject of this chapter. The complexes bearing an heteroallyl (i.e., allyl comprising a heteroatom in the carbon framework) group will be also addressed.

Allyl complexes are a valuable alternative to their alkyl counterparts, which are often less stable and coordinated by an external base, for reactivity or catalysis purposes, while having appropriate activities. Regarding synthetic approaches, a convenient method to prepare [Ln]-allyl compounds is to use ionic metathesis, by reacting a lanthanide precursor ([Ln]-X, X = halide, borohydride, etc.) with an anionic allyl reagent, typically a Grignard (allyl)MgX (X = Cl, Br) or $(allyl)_nM$ (n = 1, 2; M = alkaline, alkaline-earth metal) reagent. Alternatively, the homoleptic tris(allyl)Ln(solvent)$_x$[3–6] may be used as starting material, which is reacted with a given proligand (i.e., the conjugate acid of an anionic ligand). In some rare cases, the strategy of the insertion reaction of an allene into a lanthanide hydride bond has been reported too to create the lanthanide-allyl motive[7] (or the insertion of a ketenimine to produce an (azallyl)-Ln moiety).

In terms of molecular structure, the allyl group is generally bonded in a trihapto η^3-mode to a lanthanide metal. However, the ligand can occasionally be found under an η^1-coordination arrangement. The allyl group may be fluxional in solution, which results in a typical 1H/4H or 1H/2H/2H pattern of allyl resonances by ^{1}H NMR spectroscopy.

Concerning chemical reactivity, the lanthanide allyl moiety has been the subject of numerous reactions, including insertions of small molecules, hydrogenolysis, protonation by acid reagents, hydrosilylation, substitution, photolytic activation, and reduction. All these kinds of reactivity will be addressed in this chapter. In addition, polymerization catalysis represents a whole and very specific part of the applications of lanthanide allyl complexes. In particular, it is well-established that Ln-allyl species are involved in polymerization processes of conjugated dienes when lanthanide catalysts are implemented.[8–13] Advances in this field have been reviewed recently[14] and they will be included here when relevant for the period covered in this chapter.

Finally, complexes in which an unusual coordination mode of allyl-type is found are also reviewed. In turn, fluorenyl rare earth complexes where the ligand is in some cases coordinated in an η^3-trihapto mode to the metal are not included herein. Such complexes, which have been reviewed in 2005,[15] are covered in another chapter of the present edition of COMC.

For ease of reading and for all practical purposes, a table containing the main structural information on the complexes described is provided at the end of each section.

2 Alkene, alkyne, alkenyl, alkynyl complexes of the lanthanides

2.1 Alkene and alkyne complexes

Isolated lanthanide-alkene species are extremely rare in the literature, even though there are some evidence of their existence via NMR studies. As a matter of facts, they are most of the time found as intermediates in various catalytic reactions such as olefin[16,17] and 1,3-diene[18,19] polymerization, hydrogenation,[20] hydroamination,[21,22] hydrophosphination[23] and hydrosilylation.[24] Nearly all structurally characterized lanthanide-alkene complexes involve an alkene that is tethered to another coordinating group due to the weakness and lability of the lanthanide-alkene bond. Ethylene coordination to [$(C_5Me_5)_2$Eu] was highlighted via NMR paramagnetic shifts[25] and dynamic NMR behavior of the yttrium alkyl-tethered alkene complex $(C_5Me_5)_2Y(\eta^1{:}\eta^5\text{-}CH_2CH_2CR_2CR'{=}CH_2)$ [$\mathbf{1_Y}$] (R = H, Me and R′ = H, Me) was extensively studied.[26–34]

In 1987, Andersen and Burns reported the first lanthanide-alkene structure of a divalent ytterbium-platinum (μ-bridged) alkene complex, $(C_5Me_5)_2Yb(\mu\text{-}\eta^2{:}\eta^2\text{-}C_2H_4)Pt(PPh_3)_2$ [$\mathbf{2_{Yb}}$].[35] In 1999, the synthesis and X-ray structure of the interesting alkene ytterbium complex $[Yb\{\eta^1{:}\eta^2\text{-}C(SiMe_3)_2SiMe_2CH{=}CH_2\}\{OEt_2\}]_2(\mu\text{-}I)_2$ [$\mathbf{3_{Yb}}$] (Fig. 1, left) was reported by the group of Smith and co-workers.[36] Some years later, Evans[37] and Schumann[38,39] and coworkers detailed the structures of several alkene-tethered cyclopentadienyl complexes of divalent lanthanides ($\mathbf{4_{Yb}}$, $\mathbf{5_{Sm}}$, $\mathbf{5_{Eu}}$, $\mathbf{5_{Yb}}$, Fig. 1, middle and right) and the closely related alkaline earths that display alkene coordination.

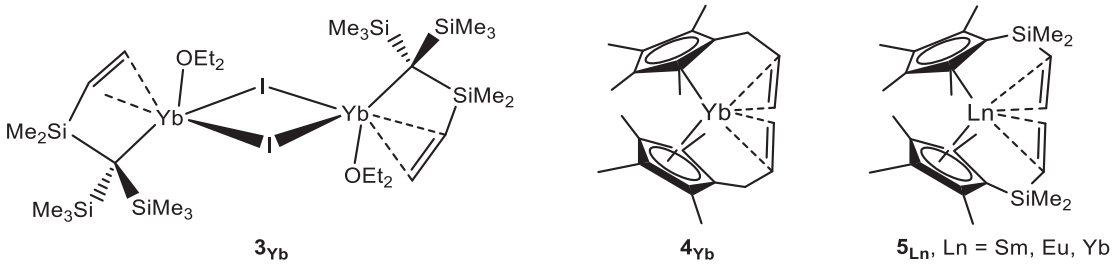

Fig. 1 Molecular structures of some alkene complexes of the lanthanides.

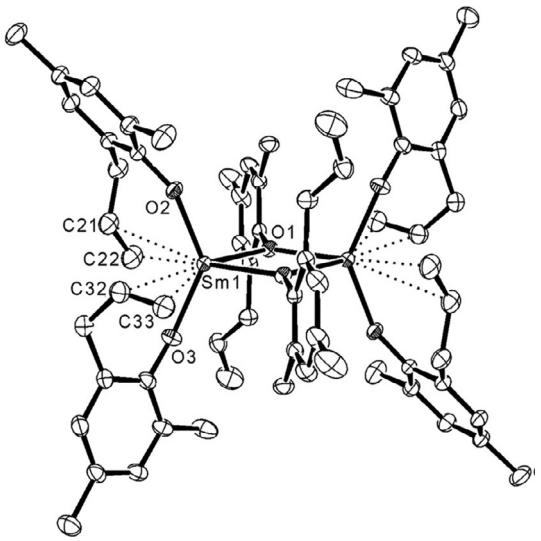

Fig. 2 Molecular structure of $\mathbf{7_{Sm}}$ (thermal ellipsoids are drawn at the 30% probability level). Reprinted from Berg, D. J.; Tosha, B.; Xuening, F. *J. Organomet. Chem.* **2010**, *695*, 2703–2712, with the authorization of Elsevier.

Regarding more recent work, Berg et al. reported in 2010 the synthesis, solid state structure and the solution behavior of dimeric lanthanide aryloxides bearing one or two allyl groups in the *o*-aryl positions: $\{Ln[DALP]_2\}_2[\mu\text{-DALP}]_2$ $[\mathbf{6_{Ln}}]$ (with H-DALP = 2,6-diallyl-4-methylphenol and Ln = La, Ce, Nd, Er, Yb, Y) and $\{Ln[MALP]_2\}_2[\mu\text{-MALP}]_2$ $[\mathbf{7_{Ln}}]$ (with H-MALP = 2-allyl-4, 6-dimethylphenol and Ln = La, Sm, Y) complexes.[40] The coordination of the alkenes from the allyl groups to the Ln^{3+} center was observed crystallographically across the lanthanide series (Fig. 2). Variable temperature NMR studies revealed that the dimeric structures remain intact in non-coordinating solvents with rapid bridge-terminal aryloxide exchange taking place above about 275–295 K for all DALP complexes, except erbium. These complexes were the first neutral trivalent lanthanide-alkene complexes that have been structurally characterized.

More recently, the group of Trifonov described the synthesis of divalent $(Cp^{Bn5})_2Ln$ $[\mathbf{8_{Ln}}]$ ($Cp^{Bn5} = C_5(CH_2Ph)_5$, Ln = Yb, Sm and Eu) by combining the potassium salt KCp^{Bn5} with 0.5 equiv. of $LnI_2(THF)_n$ (Scheme 1).[41]

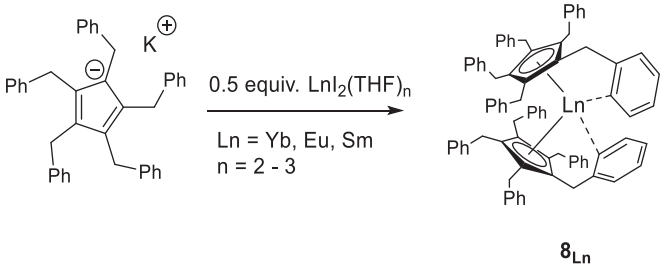

Scheme 1 Synthesis of $\mathbf{8_{Ln}}$ complexes.

The X-ray diffraction studies revealed that the three complexes are isostructural with the Ln(II) metal being coordinated by two η^5-Cp^{Bn5} rings with an additional interaction of one C-sp^2 carbon in ortho position of the two pendant phenyl moiety (Fig. 3).

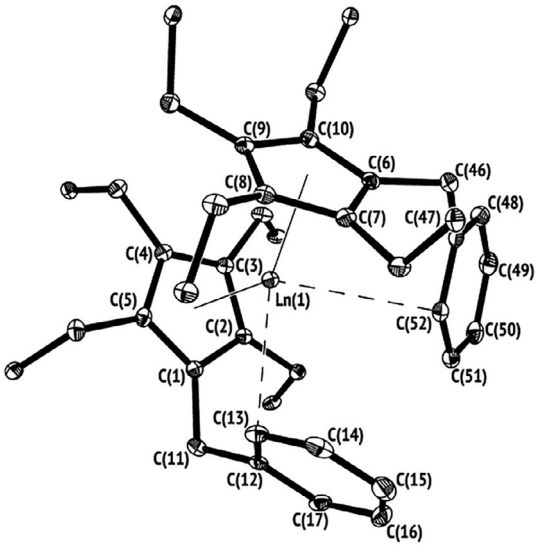

Fig. 3 Molecular structure of $\mathbf{8_{Ln}}$ complexes (Ln = Yb, Sm and Eu) (thermal ellipsoids are drawn at the 30% probability level). Carbon atoms of Ph groups and hydrogen atoms are omitted for clarity. Reprinted from Selikhov, A. N.; Mahrova, T. V.; Cherkasov, A. V.; Fukin, G. K.; Larionova, J.; Long, J.; Trifonov, A. A. *Organometallics* **2015**, *34*, 1991–1999, with the authorization of the American Chemical Society.

Reaction of $\mathbf{8_{Sm}}$ with 1 equiv. of phenazine afforded the $[(Cp^{Bn5})_2Sm]_2[\mu\text{-}\eta^3\text{:}\eta^3\text{-}(C_{12}H_8N_2)]$ $[\mathbf{8'_{Sm}}]$ adduct that was isolated as single crystals (Scheme 2).

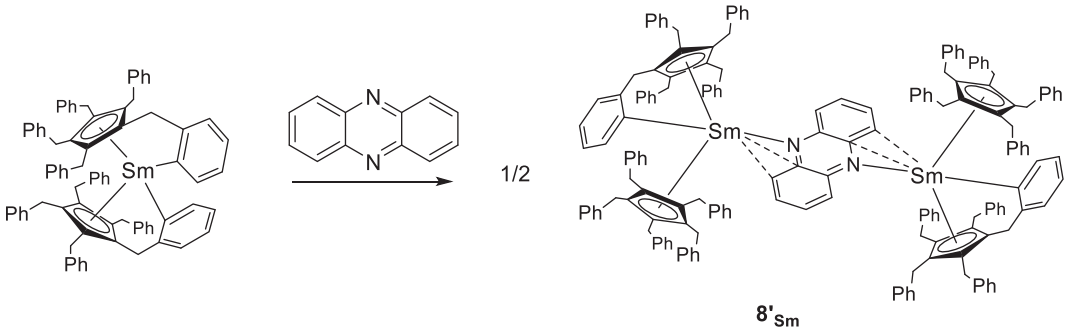

Scheme 2 Synthesis of $\mathbf{8'_{Sm}}$ adduct.

X-ray diffraction analysis of $\mathbf{8'_{Sm}}$ showed that the μ-bridged phenazine ligand is coordinated to both samarium centers through one nitrogen atom and two neighboring carbon atoms of the phenazine (Fig. 4). Furthermore, it was found that the Sm-C(Cp) bond distances fall in the range typical for Sm(III) compounds, indicating that oxidation of Sm(II) occurs during the reaction.

The preparation of lanthanide complexes supported with a functionalized indolyl ligand was carried out by the group of Wang using $[Ln(CH_2SiMe_3)_3(THF)_2]$ (Ln = Yb, Er and Y) precursors in presence of 1 equiv. of 3-(CyN=CH)C_8H_5NH proligand in toluene, which yields the dinuclear lanthanide alkyl complexes $[\mathbf{9_{Ln}}]$ (Scheme 3).[42]

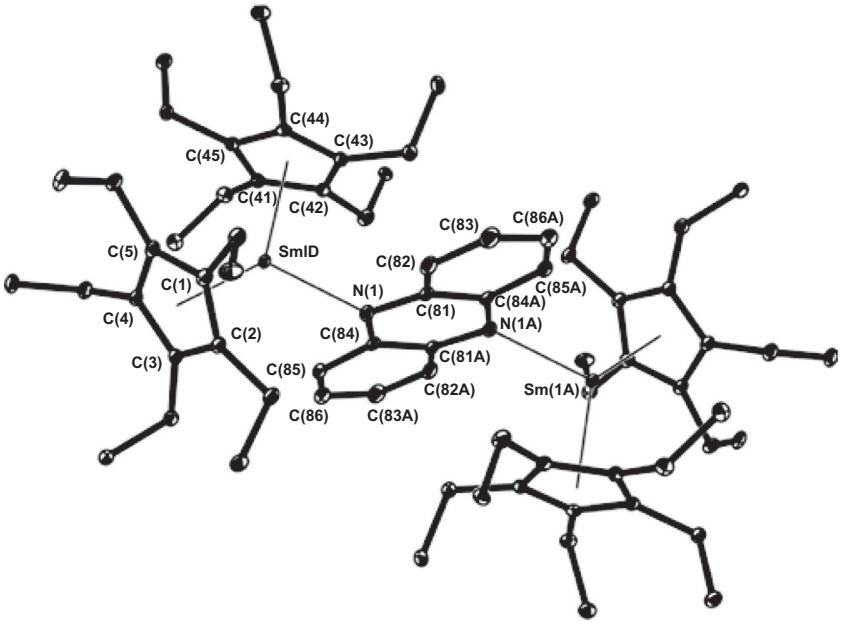

Fig. 4 Molecular structure of $\mathbf{8'_{Sm}}$ (thermal ellipsoids with a 30% probability level). Carbon atoms of Ph groups and hydrogen atoms are omitted for clarity. Reprinted from Selikhov, A. N.; Mahrova, T. V.; Cherkasov, A. V.; Fukin, G. K.; Larionova, J.; Long, J.; Trifonov, A. A. *Organometallics* **2015**, *34*, 1991 – 1999, with the authorization of the American Chemical Society.

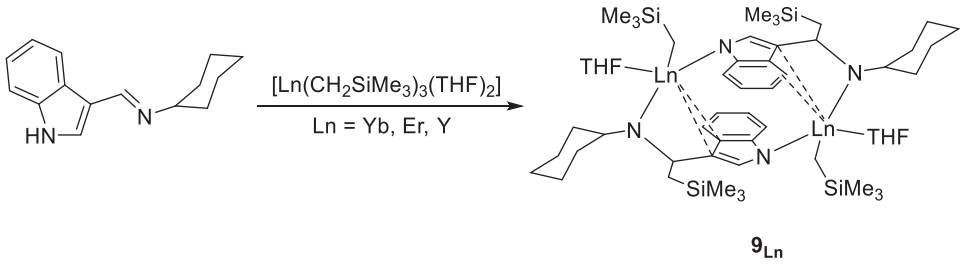

$\mathbf{9_{Ln}}$

Scheme 3 Synthesis of complexes $\mathbf{9_{Ln}}$.

The molecular structure of the three complexes was determined by X-ray diffraction studies and revealed, in particular, that the two metal centers are bridged by the indolyl ligand through the two carbons of the five membered ring in η^2-fashion and through the nitrogen atom in an η^1-mode (Fig. 5). Interestingly, the η^2-coordination mode of the two carbons of the five-membered ring was not observed when the reaction was conducted in THF, due to the presence of an additional THF ligand in the coordination sphere of the metal center.

In the same study, upon treatment of 3-(^{t}BuNH-CH$_2$)C$_8$H$_5$NH proligand with Ln(CH$_2$SiMe$_3$)$_3$(THF)$_2$ (Ln = Y, Er and Dy) in THF, trinuclear complexes $\mathbf{10_{Ln}}$ were formed (Scheme 4, up). On the other hand, a dinuclear species $\mathbf{11_{Yb}}$ could be isolated just 1 year earlier from the reaction of the same 3-(^{t}BuNH-CH$_2$)C$_8$H$_5$NH proligand with Yb(CH$_2$SiMe$_3$)$_3$(THF)$_2$, which includes a metal with a smaller ionic radius (Scheme 4, down).[43]

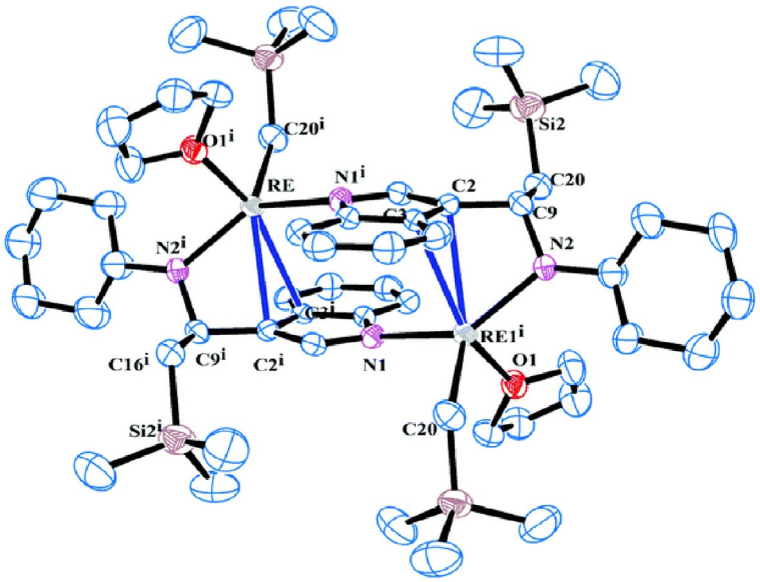

Fig. 5 Representative molecular structure of complexes $\mathbf{9_{Ln}}$ showing the bridging mode as {[η^2:η^1-μ-η^1-3-[(CyNCH(CH_2SiMe_3))Ind]RE(THF)(CH_2SiMe_3)}$_2$ (Cy = cyclohexyl, Ind = indolyl, RE = Ln = Yb, Er, Y) lanthanide complexes (thermal ellipsoids are drawn at the 30% probability level). Hydrogen atoms are omitted for clarity. Reprinted from Zhang, G.; Deng, B.; Wang, S.; Wei, Y.; Zhou, S.; Zhu, X.; Huang, Z.; Mu, X. *Dalton Trans.* **2016**, *45*, 15445–15456, with the authorization of the Royal Society of Chemistry.

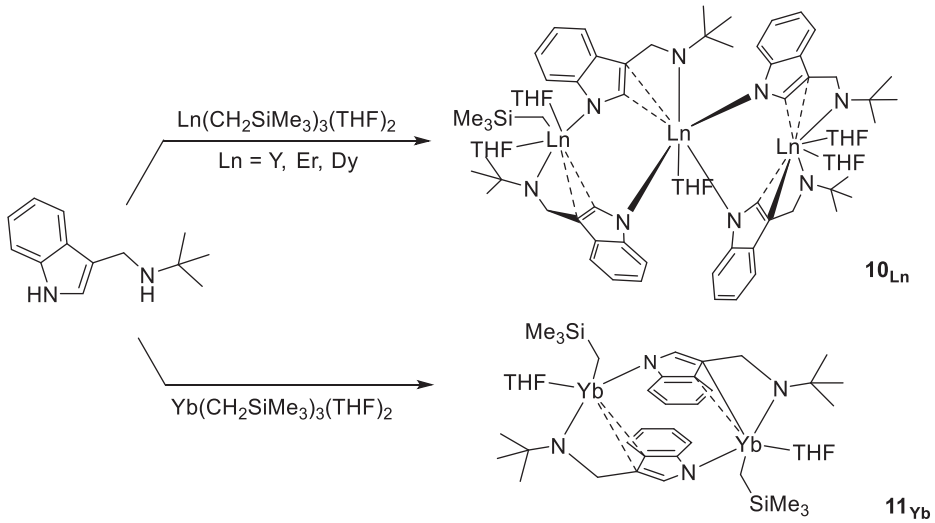

Scheme 4 Synthesis of indenyl alkyl complexes $\mathbf{10_{Ln}}$ and $\mathbf{11_{Yb}}$ showing a different result depending on the nature of the lanthanide precursor.

In the case of the trinuclear complexes $\mathbf{10_{Ln}}$, the X-ray diffraction analysis indicates a distorted octahedral geometry around the metal center that comprises an η^2-coordination mode of the carbon atoms and η^1-fashion of the nitrogen atom from the indolyl moiety, one nitrogen atom from the amido group and two additional THF molecules (Fig. 6, left). Similar η^2-coordination binding mode of the carbon atom of the indolyl ring was observed for the dinuclear $\mathbf{11_{Yb}}$, which was obtained under two forms, with indolyl groups in *trans* (major) or *cis* (minor) position from each other (Fig. 6, right).

In parallel, dinuclear species $\mathbf{12_{Ln}}$ were prepared from the one-pot treatment of 3-(^{t}BuNH-CH_2)C_8H_5NH proligand and [Ln(CH_2SiMe_3)$_3$(THF)$_2$] in the presence of [(2,6-^{i}Pr$_2$C$_6$H$_3$)N=CHNH-($C_6H_3^iPr_2$-2,6)] amidine (Ln = Er, Y, Scheme 5).

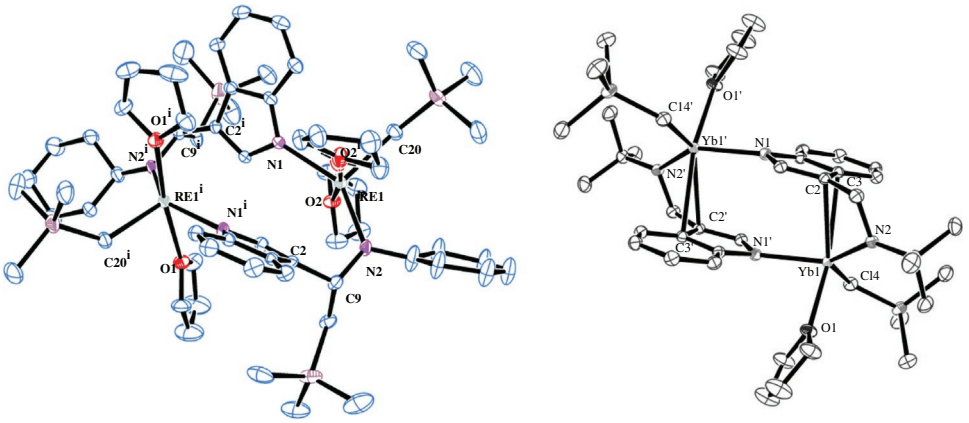

Fig. 6 Molecular structure of $[\eta^2{:}\eta^1\text{-}\mu\text{-}\eta^1\text{-}3\text{-}(^t\text{BuNCH}_2)\text{Ind}]_4\text{Ln}_3(\text{THF})_5(\text{CH}_2\text{SiMe}_3)$ $\mathbf{10_{Ln}}$ (RE = Ln = Y, Er, Dy, left) and of complex *trans*-$[\{\mu\text{-}\eta^2{:}\eta^1{:}\eta^1\text{-}3\text{-}(^t\text{BuNCH}_2)\text{Ind}\}\text{Yb}(\text{THF})(\text{CH}_2\text{SiMe}_3)]_2$ $\mathbf{11_{Yb}}$ (right). Thermal ellipsoids are set at the 30% probability level. Reprinted from (left) Zhang, G.; Deng, B.; Wang, S.; Wei, Y.; Zhou, S.; Zhu, X.; Huang, Z.; Mu, X. *Dalton Trans.* **2016**, *45*, 15445–15456, with the authorization of the Royal Society of Chemistry; (right) Zhang, G.; Wei, Y.; Guo, L.; Zhu, X.; Wang, S.; Zhou, S.; Mu, X. *Chem. Eur. J.* **2015**, *21*, 2519–2526, with the authorization of the Wiley-VCH Verlag GmbH.

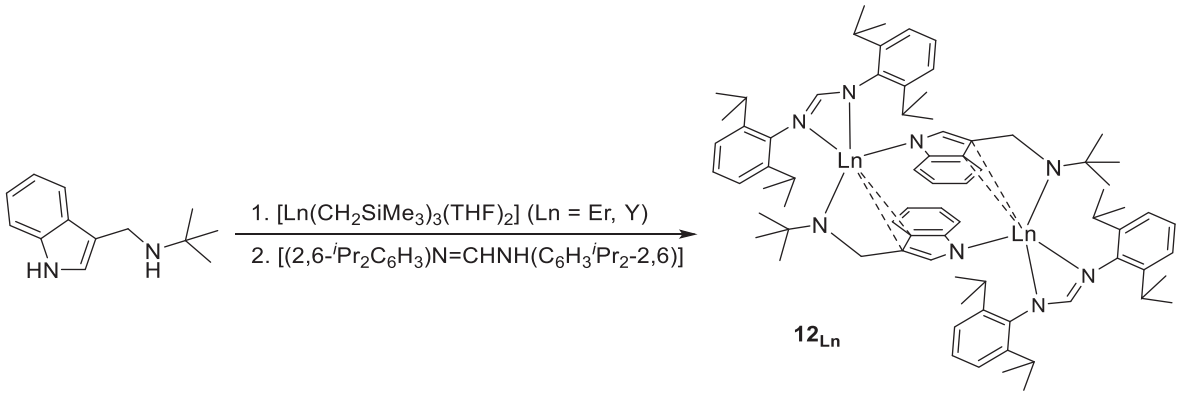

Scheme 5 Synthesis of dinuclear complexes $\mathbf{12_{Ln}}$.

The X-ray molecular structure revealed that in $\mathbf{12_{Ln}}$ the metal center is also coordinated to the carbon of the indolyl ring in η^2-mode and the nitrogen atom in η^1-fashion (Fig. 7).

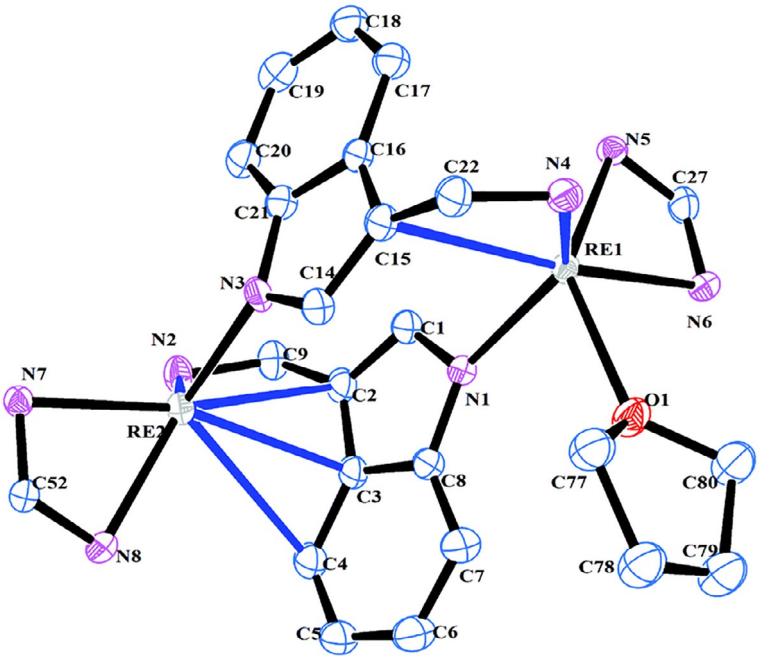

Fig. 7 Molecular structure of $[\eta^1\text{-}\mu\text{-}\eta^1{:}\eta^1\text{-}3\text{-}(^t\text{BuNCH}_2)\text{Ind}][\eta^1\text{-}\mu\text{-}\eta^1{:}\eta^3\text{-}3\text{-}(^t\text{BuNCH}_2)\text{Ind}]\text{RE}_2(\text{THF})[(\eta^3\text{-}2,6\text{-}^i\text{Pr}_2\text{C}_6\text{H}_3)\text{NCHN}(\text{C}_6\text{H}_3^i\text{Pr}_2\text{-}2,6)]_2$ [$\mathbf{12_{Ln}}$] (RE = Ln = Er, Y, ellipsoid are drawn at the 30% probability level). Reprinted from Zhang, G.; Deng, B.; Wang, S.; Wei, Y.; Zhou, S.; Zhu, X.; Huang, Z.; Mu, X. *Dalton Trans.* **2016**, *45*, 15445–15456, with the authorization of the Royal Society of Chemistry.

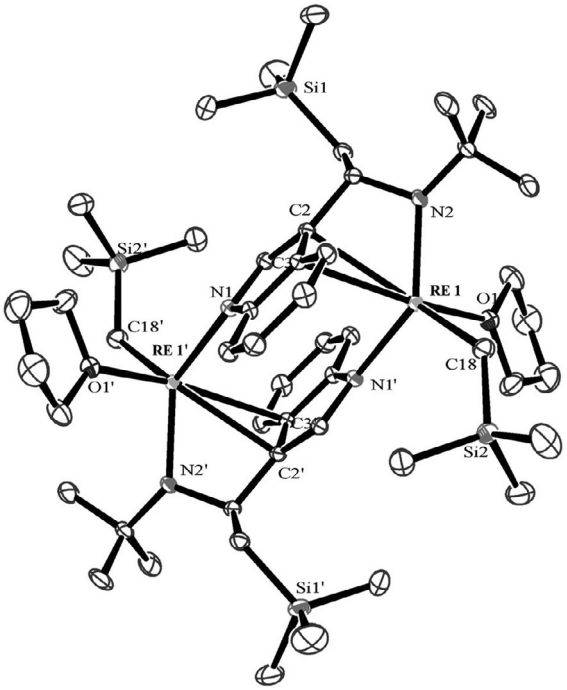

Fig. 8 Representative molecular structure of [*trans*-[{μ-η^2:η^1:η^1-3-{^{t}BuNCH(CH_2SiMe_3)}Ind}Ln(THF)(CH_2SiMe_3)]$_2$] [$\mathbf{13_{Ln}}$] (RE = Ln = Y, Dy, Yb, ellipsoid are drawn at the 30% probability level). Reprinted from Zhang, G.; Wei, Y.; Guo, L.; Zhu, X.; Wang, S.; Zhou, S.; Mu, X. *Chem. Eur. J.* **2015**, *21*, 2519–2526, with the authorization of the Royal Society of Chemistry.

Following the same strategy as for the synthesis of complexes $\mathbf{9_{Ln}}$ (Scheme 3), but using 3-(^{t}BuN=CH)C_8H_5NH as proligand, afforded the dinuclear lanthanide complexes [*trans*-[{μ-η^2:η^1:η^1-3-{^{t}BuNCH(CH_2SiMe_3)}Ind}Ln(THF)(CH_2SiMe_3)]$_2$] [$\mathbf{13_{Ln}}$] (Ln = Y, Dy, Yb), where *trans* represents the orientation of six membered rings of the indolyl ligands in opposite directions. According to X-ray analysis, dinuclear rare-earth metal alkyl complexes with central symmetry were isolated as dianionic species bridges with two metal alkyl units in μ-η^2:η^1:η^1 bonding mode (Fig. 8).[43]

In a more recently published work by Trifonov and coworkers, divalent benzhydryl Ln(II) derivatives of the formula [(p-^{t}Bu-C_6H_4)$_2$CH]$_2$Ln(L)$_n$ ($\mathbf{14_{Sm}}$, Ln = Sm, L = DME, n = 2; $\mathbf{14'_{Ln}}$, Ln = Sm, Yb, L = TMEDA, n = 1) were synthesized.[44] The complexes display structural peculiarities: X-ray diffraction studies showed that the benzhydryl ligands are bound to the metal center in an η^2-coordination mode in $\mathbf{14_{Sm}}$, where short contacts between Sm(II) ion and the *ipso*-carbon atom of one of the phenyl rings were detected, whereas $\mathbf{14'_{Yb}}$ displays η^3-coordination of the benzhydryl moieties to the metal center (Fig. 9). In $\mathbf{14'_{Sm}}$, one benzhydryl is η^3-coordinated while the second one is η^4-coordinated to the Sm(II) ion. Theoretical calculations were carried out in order to get more details on the nature of M–L bonding, which corroborates the presence of short interactions between the metal center and the *ortho*- and *ipso*-carbons of the benzhydryl ligands, highlighting the variety of hapticities observed.

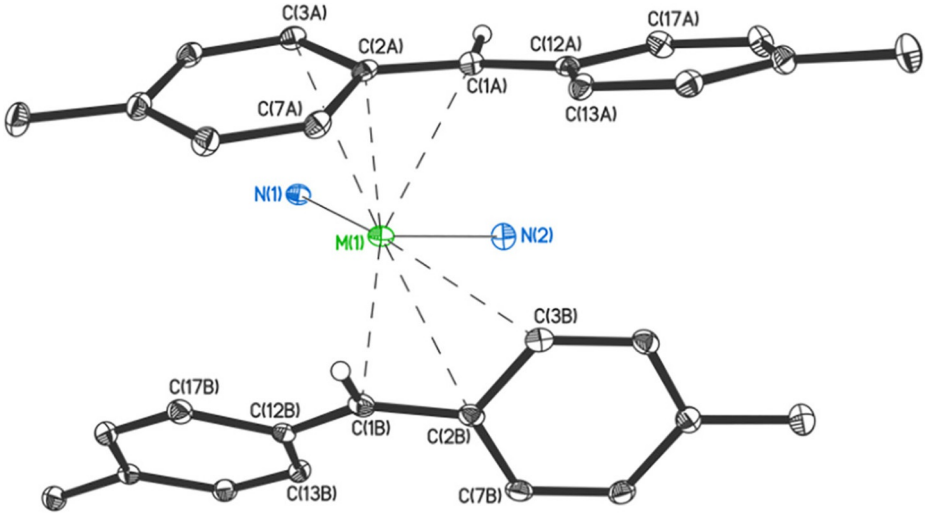

Fig. 9 Molecular structure of a representative complex [(p-^{t}Bu-C_6H_4)$_2$CH]$_2$Ln(L)$_n$ ($\mathbf{14'_{Ln}}$, M = Ln = Sm, Yb). Ellipsoids are set at the 30% probability, hydrogen atoms, methyl groups of ^{t}Bu-substituents, and carbon atoms of TMEDA molecules are omitted for clarity. Reprinted from Selikhov, A. N.; Plankin, G. S.; Cherkasov, A. V.; Shavyrin, A. S.; Louyriac, E.; Maron, L.; Trifonov, A. A. *Inorg. Chem.* **2019**, *58*, 5325–5334, with the authorization of the American Chemical Society.

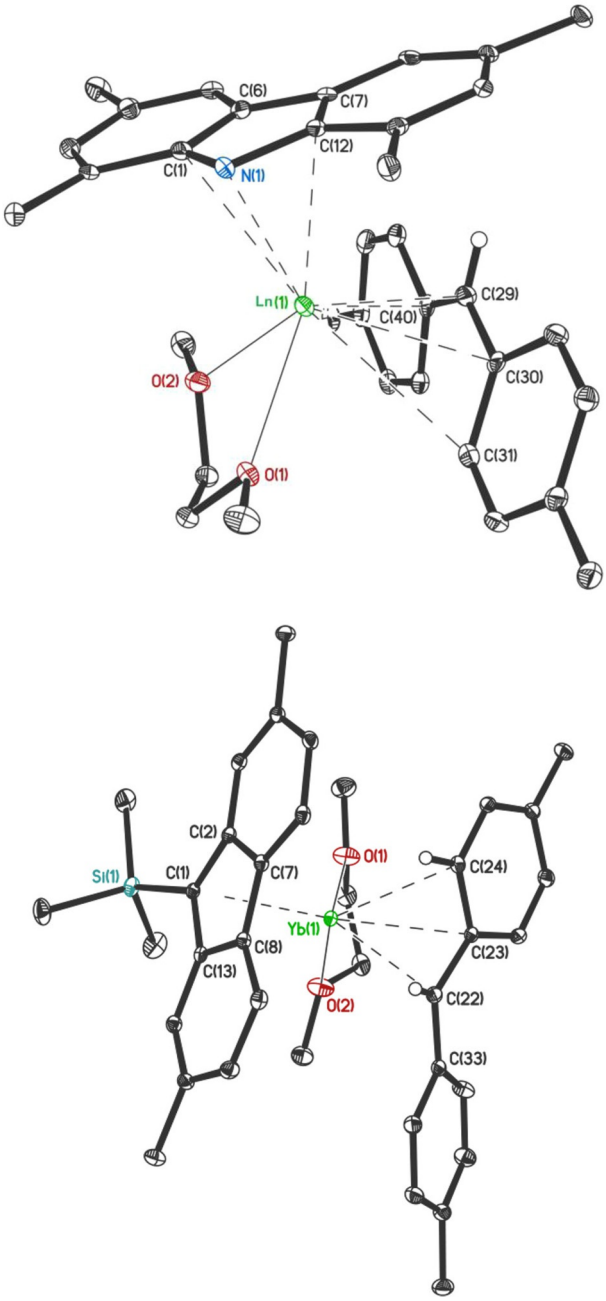

Fig. 10 Molecular structure of the half-sandwich complexes $\mathbf{15_{Sm}}$ (left) and $\mathbf{15_{Yb}}$ (right). Methyl fragments of ^{t}Bu groups and all hydrogen atoms except the methine hydrogen are omitted for clarity. Ellipsoids are given at 30% of the probability level. Reprinted from Selikhov, A. N.; Shavyrin, A. S.; Cherkasov, A. V.; Fukin, G. K.; Trifonov, A. A. *Organometallics* **2019**, *38*, 4615–4624, with the authorization of the American Chemical Society.

Substitution of one benzhydryl ligand by *tert*-butylcarbazol-9-yl (^{t}Bu$_4$Carb) or 2,7-di-*tert*-butyl-fluoren-9-trimethylsilyl (^{t}Bu$_2$FluTMS) was also performed later by the same group.[45] The molecular structure of the DME adducts of samarium and ytterbium [^{t}Bu$_4$Carb]Ln[(p-^{t}Bu-C$_6$H$_4$)$_2$CH](DME) [$\mathbf{15_{Sm}}$, $\mathbf{15_{Yb}}$] revealed an η^3-coordination mode of the benzhydryl ligand to the metal (Fig. 10, left and right, respectively) while the ytterbium complex [^{t}Bu$_2$FluTMS]Yb[(p-^{t}Bu-C$_6$H$_4$)$_2$CH](TMEDA) bearing TMEDA ligand [$\mathbf{16_{Yb}}$] shows an η^1-coordination mode.

Following the synthesis of [(p-^{t}Bu-C$_6$H$_4$)$_2$CH]$_2$Ln(L)$_n$, Trifonov and coworkers prepared a series of Ln(III) (Ln = La, Nd and Y) complexes supported by three benzhydryl ligands, $\mathbf{17_{Ln}}$, from salt metathesis of [(p-^{t}Bu-C$_6$H$_4$)$_2$CH]Na in presence of 1/3 equiv. of LnX$_3$(THF)$_{3.5}$ (X = Cl, I) (Scheme 6).[46]

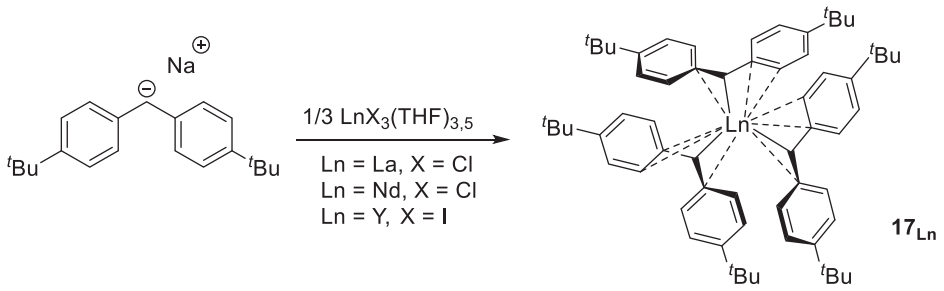

Scheme 6 Synthesis of complexes $\mathbf{17_{Ln}}$.

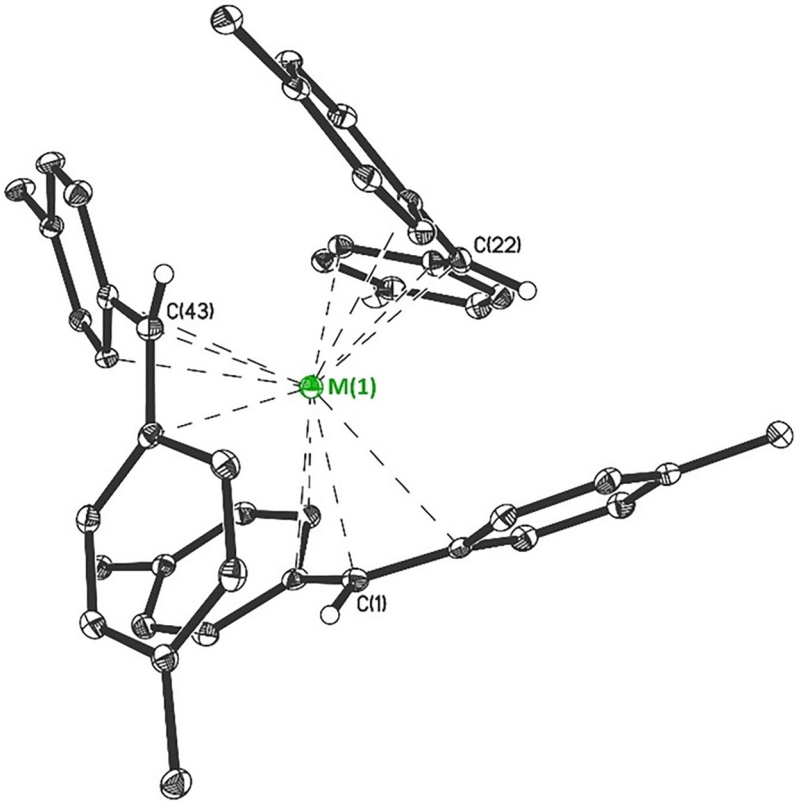

Fig. 11 Molecular structure of complexes $\mathbf{17_{Ln}}$ (M = Ln = La, Nd, Y). Thermal ellipsoids are given at the 30% probability level. Methyl groups of *tert*-butyl substituents and hydrogen atoms except bonded with methanide carbons were omitted for clarity. Reprinted from Selikhov, A. N.; Boronin, E. N.; Cherkasov, A. V.; Fukin, G. K.; Shavyrin, A. S.; Trifonov, A. A. *Adv. Synth. Catal.* **2020**, *362*, 5432–5443, with the permission of Wiley-VCH GmbH.

Single crystals of $\mathbf{17_{Ln}}$ suitable for X-ray diffraction studies revealed that, for each lanthanide element, the benzhydryl ligand is rather coordinated in an η^4-mode to the metal center with one covalent bond between Ln and the methanide carbon as well as short contacts with two *ipso* and one *ortho*-phenyl carbons of the benzhydryl part (Fig. 11).

Upon reaction of the potassium salt $\{[2,2\text{-}(4\text{-}MeC_6H_3NMe_2)_2CH]K(THF)\}_2$ with $LnI_2(THF)_2$(Ln = Yb and Sm), the replacement of the ^{t}Bu substituent on the *para* position of the benzhydryl ligand by NMe_2 group led to the formation of the homoleptic $[2,2\text{-}(4\text{-}MeC_6H_3NMe_2)_2CH]_2Ln$ $[\mathbf{18_{Ln}}]$ (Scheme 7).[47]

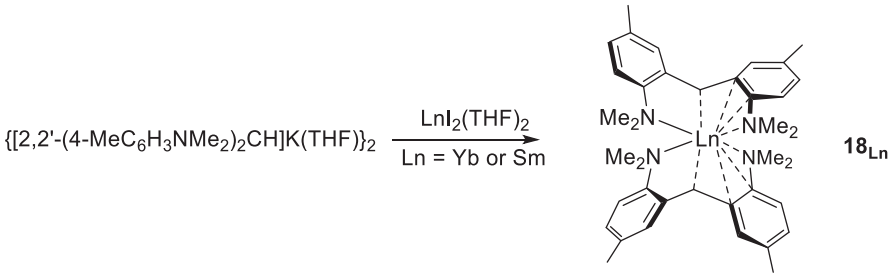

Scheme 7 Synthesis of complexes $\mathbf{18_{Ln}}$.

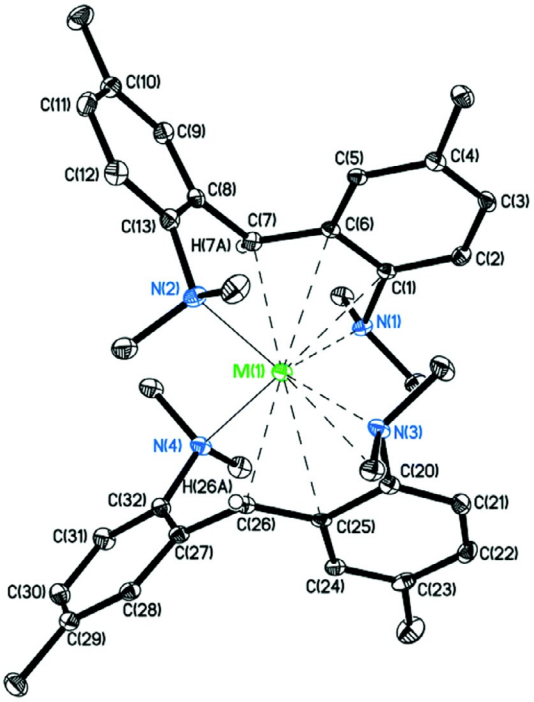

Fig. 12 Molecular structure of $\mathbf{18_{Ln}}$ (M = Yb and Sm) with a 30% thermal ellipsoid probability level. All hydrogen atoms except that of M–CH are omitted for clarity. Reprinted from Khristolyubov, D. O.; Lyubov, D. M.; Shavyrin, A. S.; Cherkasov, A. V.; Fukin, G. K.; Trifonov, A. A. *Inorg. Chem. Front.* **2020**, *7*, 2459–2477, with the permission of the Royal Society of Chemistry.

The X-ray diffraction studies revealed that, in both cases, the divalent lanthanide centers in $\mathbf{18_{Ln}}$ are coordinated by two [2,2-(4-$MeC_6H_3NMe_2)_2CH]^-$ ligands through the carbon of the methanido group as well as two additional nitrogen atoms of the NMe_2 substituents (Fig. 12), although, the coordination mode of both [2,2-(4-$MeC_6H_3NMe_2)_2CH]^-$ ligands was shown to be different. Upon closer examination of the distances and angles between the metals and the ligands, it was observed that one ligand coordinates in κ^1-N mode while the other revealed a short contact between *ipso*- and *ortho*-carbons of one phenyl substituent, resulting in an η^4-CCCN coordination mode with the metal.

Long et al. described the preparation of two half-sandwich complexes of the type (Cp*)Dy(2,6-^{i}Pr$_2$C$_6$H$_3$N–CMe=CMe–NC$_6$H$_3^i$Pr$_2$–2,6)(THF) [$\mathbf{19_{Dy}}$] and [Li(THF)$_3$][Dy(2,6-^{i}Pr$_2$C$_6$H$_3$N–CMe=CMe–NC$_6$H$_3$ ^{i}Pr$_2$–2,6)(Cp*)Cl] (Cp* = C$_5$Me$_5$) [$\mathbf{19'_{Dy}}$] by treatment of $DyCl_3$ with [K(THF)$_x$(2,6-^{i}Pr$_2$C$_6$H$_3$N–CMe=CMe–NC$_6$H$_3^i$Pr$_2$–2,6)K(THF)$_x$] in the presence of either KCp* or LiCp*, respectively (Scheme 8).[48]

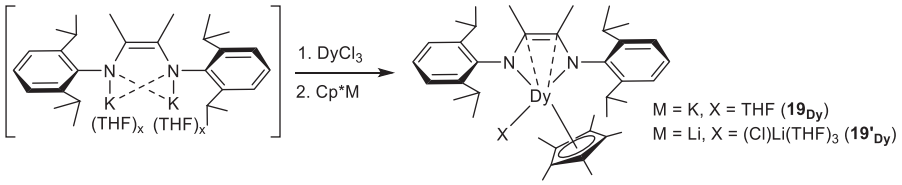

Scheme 8 Synthesis of $\mathbf{19_{Dy}}$ and $\mathbf{19'_{Dy}}$ starting from potassium or lithium reagent, respectively.

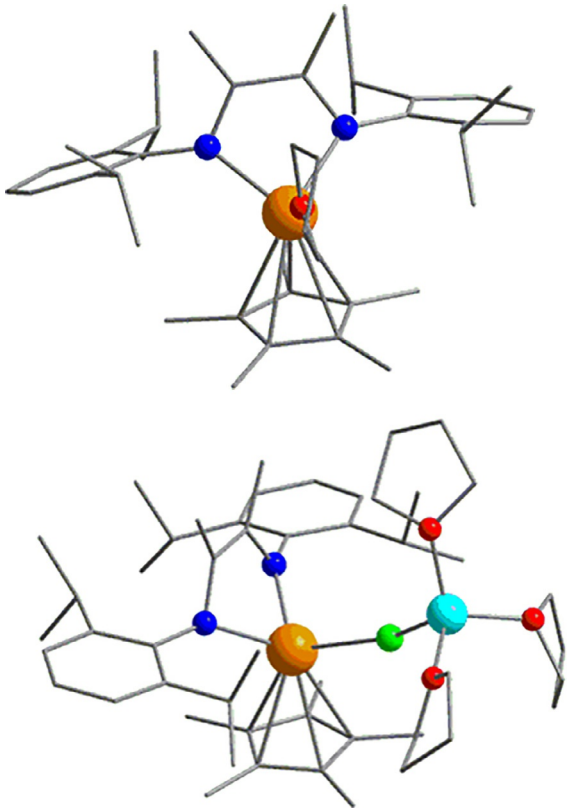

Fig. 13 Structure of $\mathbf{19_{Dy}}$ (left) and $\mathbf{19'_{Dy}}$ (right). Color code: orange, Dy; red, O; gray, C; green, Cl; light blue, Li. Hydrogen atoms have been omitted for clarity. Reprinted from Long, J.; Tolpygin, A. O.; Cherkasov, A. V.; Lyssenko, K. A.; Guari, Y.; Larionova, J.; Trifonov, A. A. *Organometallics* **2019**, *38* (4), 748–752, with the permission of the American Chemical Society.

In both cases, the X-ray diffraction measurement revealed that the metal centers of both $\mathbf{19_{Dy}}$ and $\mathbf{19'_{Dy}}$ are coordinated to one dianionic NC═CN ligand, one Cp* ligand and one THF or (Cl)Li(THF)$_3$ moiety, respectively (Fig. 13). The weak interaction of the Dy(III) cation with the carbon atoms of the NC═CN part is consistent with an η^2-coordination mode of the carbon double bond to the metal center (Table 1).

2.2 Alkenyl and alkynyl complexes

The reactivity of lanthanide complexes with unsaturated hydrocarbon substrates has been the subject of numerous investigations in the 1980s, but it was only in 1990 that the group of Evans succeeded in identifying the first examples of an η^2-alkene lanthanide complexes $[(Cp^*)_2Sm]_2(\mu\text{-}\eta^2\text{:}\eta^4\text{-}CH_2CHPh)$ $[\mathbf{20_{Sm}}]$ and $[(Cp^*)_2Sm]_2(\mu\text{-}\eta^2\text{:}\eta^4\text{-}PhCHCHPh)$ $[\mathbf{20'_{Sm}}]$ by reduction of styrene and stilbene precursors, respectively, in the presence of divalent $(Cp^*)_2Sm$.[9] A decade later, the same group extended the reactivity of the decamethylsamarium with isoprene and myrcene to produce the bimetallic $[(Cp^*)_2Sm]_2[\mu\text{-}\eta^2\text{:}\eta^4\text{-}CH_2CHC(Me)CH_2]$ $[\mathbf{21_{Sm}}]$ and $[(Cp^*)_2Sm]_2[\mu\text{-}\eta^2\text{:}\eta^4\text{-}CH_2CHC(CH_2)CH_2CH_2CHCMe_2]$ $[\mathbf{21'_{Sm}}]$ complexes, respectively.[49] In addition, the coordination chemistry of yttrium was also explored by reacting YCl_3 with tetraphenylethylenyl M[PhCCPh$_2$] (M = Na or K) to form complexes of the type $[M(THF)_x][Y(Ph_2CCPh_2)_2]$ $[\mathbf{22_Y}]$.[50]

The extension of the chemistry of alkenyl lanthanides was at the same period pursued by Floriani and coworkers by reacting the *meso*-octaethylporphyrinogen (oepg) lanthanide complexes, {(oepg)Ln}Na(THF)$_2$ (Ln = Pr, Nd) with $NaC_{10}H_8$ in an ethylene atmosphere in the presence of 18-crown-6 in THF that yields dimeric species of formula $[\{(oepg)Ln\}Na(THF)_2(\mu\text{-}\eta^2\text{:}\eta^2\text{-}C_2H_4)]_2$ $[\mathbf{23_{Ln}}]$ where the metals are bridged by the $[C_2H_4]^-$ moiety.[51] According to the X-ray crystal structure of

Table 1 Structural and analytical data of alkene and alkyl complexes (in brackets for relevant complexes only, otherwise for all complexes).

Compound number	*Molecular formula*	*X-ray data typical Ln-C (alkene or alkyl) distances (Å)*	*NMR data*	*References*
$\mathbf{1_Y}$	$[(Cp^*)_2Y(\eta^1{:}\eta^5\text{-}CH_2CH_2CR_2CR'{=}CH_2)]$	–	^1H, ^1H NOESY, ^{13}C, VT ^1H and ^{13}C NMR, ^1H-^{13}C HMQC	26–34
$\mathbf{2_{Yb}}$	$[(Cp^*)_2Yb(\mu\text{-}\eta^2{:}\eta^2\text{-}C_2H_4)Pt(PPh_3)_2]$	Yb-C = 2.770(3), 2.793(3)	^1H, ^{31}P	35
$\mathbf{3_{Yb}}$	$[[Yb\{\eta^1{:}\eta^2\text{-}C(SiMe_3)_2SiMe_2CH{=}CH_2\}(OEt_2)]_2(\mu\text{-}I)_2]$	Yb-C = 2.50(2)	^1H attempts (broad signals/ rearrangements)	36
$\mathbf{4_{Yb}}$	$[Yb(C_5Me_4CH_2CH_2CH{=}CH_2)_2]$	Yb-C = 2.941(7), 3.132(7) 2.881(7), 3.032(7)	^1H, ^{13}C	38,39
$\mathbf{5_{Sm}}$, $\mathbf{5_{Eu}}$, $\mathbf{5_{Yb}}$	$[Ln\{(C_5Me_4)SiMe_2(CH_2{-}CH{=}CH_2)]_2\}]$ (Ln = Sm, Eu, Yb)	Sm-C = 3.249(4), 3.004(3) Eu-C = 3.293(4), 3.008(3) Yb-C = 3.182(3), 2.905(3)	^1H, ^{13}C ($\mathbf{5_{Yb}}$)	37
$\mathbf{6_{La}}$, $\mathbf{6_{Ce}}$, $\mathbf{6_{Nd}}$, $\mathbf{6_{Er}}$, $\mathbf{6_{Yb}}$, $\mathbf{6_Y}$	$[\{Ln[DALP]_2\}_2[\mu\text{-}DALP]_2]$ (Ln = La, Ce, Nd, Er, Yb, Y)	Nd-C = 3.122(6), 3.024(5), 3.185(6), 3.256(5) Er-C = 3.122(6), 2.928(5), 3.186(6), 3.126(5) Y-C = 3.128(5), 2.970(5), 3.187(5), 3.153(5)	^1H, ^{13}C for ($\mathbf{6_{Nd}}$, $\mathbf{6_Y}$)	40
$\mathbf{7_{La}}$, $\mathbf{7_{Sm}}$, $\mathbf{7_Y}$	$[\{Ln[MALP]_2\}_2[\mu\text{-}MALP]_2]$ (Ln = La, Sm, Y)	Sm-C = 3.120(4), 3.099(3), 3.149(4), 3.252(3) Y-C = 3.090(3), 3.140(4), 3.123(3), 3.288(4)	^1H	40
$\mathbf{8_{Yb}}$, $\mathbf{8_{Sm}}$, $\mathbf{8_{Eu}}$	$[(Cp^{Bn5})_2Ln]$ ($Cp^{Bn5} = C_5(CH_2Ph)_5$, Ln = Yb, Sm, Eu)	Yb-C = 2.952(2), 3.197(2) Sm-C = 2.996(2), 3.161(2) Eu-C = 2.991(2), 3.163(2)	^1H, ^{13}C ($\mathbf{8_{Yb}}$, $\mathbf{8_{Eu}}$)	41
$\mathbf{8'_{Sm}}$	$[(Cp^{Bn5})_2Sm]_2[\mu\text{-}\eta^3{:}\eta^3\text{-}(C_{12}H_8N_2)]]$	Sm-C = 2.869(2), 2.901(2)	^1H, ^{13}C	41
$\mathbf{9_{Yb}}$, $\mathbf{9_{Er}}$, $\mathbf{9_Y}$	$[\{[\eta^2{:}\eta^1{-}\mu{-}\eta^1\text{-}3\text{-}(CyNCH(CH_2SiMe_3))Ind]Ln(THF)(CH_2SiMe_3)\}_2]$ (Cy = cyclohexyl, Ind = indolyl, Ln = Yb, Er, Y)	Yb-C = 2.675(6), 2.811(7) Er-C = 2.717(6), 2.825(5) Y-C = 2.709(5), 2.816(5)	^1H ($\mathbf{9_Y}$), ^{13}C ($\mathbf{9_Y}$)	42
$\mathbf{10_Y}$, $\mathbf{10_{Er}}$, $\mathbf{10_{Dy}}$	$[\eta^2{:}\eta^1{-}\mu{-}\eta^1\text{-}3\text{-}(^t\text{BuNCH}_2)Ind]_4Ln_3(THF)_5(CH_2SiMe_3)$ Ln = Y, Er, Dy	Y-C = 2.963(3), 3.044(3) Er-C = 2.969(6), 3.026(5) Dy-C = 2.989(5), 3.027(6)	^1H ($\mathbf{10_Y}$), ^{13}C ($\mathbf{10_Y}$)	42
$\mathbf{11_{Yb}}$	*trans*-$[\{\mu\text{-}\eta^2{:}\eta^1{:}\eta^1\text{-}3\text{-}(^t\text{BuNCH}_2)Ind\}Yb(THF)(CH_2SiMe_3)]_2$	Yb-C = 2.681(4), 2.787(5)	–	43
$\mathbf{12_{Er}}$, $\mathbf{12_Y}$	$[[\eta^1\text{-}\mu\text{-}\eta^1{:}\eta^1\text{-}3\text{-}(^t\text{BuNCH}_2)Ind][\eta^1\text{-}\mu{-}\eta^1{:}\eta^3\text{-}3\text{-}(^t\text{BuNCH}_2)Ind]Ln_2(THF)[(\eta^3\text{-}2,6\text{-}^i\text{Pr}_2C_6H_3)NCHN(C_6H_3^iPr_2\text{-}2,6)]_2]$ (Ln = Er, Y)	Er1-C = 2.794(7), Er2-C = 2.733(8), 2.712(7), 3.031(6) Y1-C = 2.825(6), Y2-C = 2.759(7), 2.738(7), 3.022(7)	^1H($\mathbf{12_Y}$), ^{13}C ($\mathbf{12_Y}$)	42
$\mathbf{13_Y}$, $\mathbf{13_{Dy}}$, $\mathbf{13_{Yb}}$	$[$*trans*$\text{-}[\{\mu\text{-}\eta^2{:}\eta^1{:}\eta^1\text{-}3\text{-}\{^t\text{BuNCH}(CH_2SiMe_3)\}Ind\}Ln(THF)(CH_2SiMe_3)]_2]$ (Ln = Y, Dy, Yb)	Y-C = 2.725(4), 2.810(4) Dy-C = 2.745(3), 2.775(3) Yb-C = 2.636, 2.838(3)	^1H($\mathbf{13_Y}$), ^{13}C ($\mathbf{13_Y}$)	43
$\mathbf{14_{Sm}}$, $\mathbf{14'_{Yb}}$, $\mathbf{14'_{Sm}}$	$[[(p\text{-}^t\text{Bu-}C_6H_4)_2CH]_2Ln(L)_n]$ ($\mathbf{14_{Sm}}$, Ln = Sm, L = DME, $n = 2$; $\mathbf{14'_{Ln}}$, Ln = Sm, Yb, L = TMEDA, $n = 1$)	$\mathbf{14_{Sm}}$: Sm-C = 2.863(2), 2.662(2), 2.701(2), 2.944(2), 2.963(2), 3.060(2) $\mathbf{14'_{Yb}}$: Yb-C = 2.668(2), 2.555(2), 2.617(2), 2.853(2), 2.889(2), 2.895(2) No R-xay for $\mathbf{14'_{Sm}}$	^1H, ^{13}C ($\mathbf{14_{Sm}}$, $\mathbf{14_{Yb}}$)	44
$\mathbf{15_{Sm}}$, $\mathbf{15_{Yb}}$	$[[^t\text{Bu}_4\text{Carb}]Ln[(p\text{-}^t\text{Bu-}C_6H_4)_2CH](DME)]$ (Ln = Sm, Yb)	Sm-C = 2.670(4), 2.904(3), 3.220(4), 3.125(4) Yb-C = 2.540(4), 2.806(4), 3.084(4), 3.350(4)	^1H ($\mathbf{15_{Sm}}$), ^{13}C ($\mathbf{15_{Sm}}$)	45
$\mathbf{16_{Yb}}$	$[(^t\text{Bu}_2\text{FluTMS})Yb[(p\text{-}^t\text{Bu-}C_6H_4)_2CH](DME)]$	Yb-C = 2.589(2), 2.721(2), 2.737(2)	^1H, ^{13}C	45
$\mathbf{17_Y}$, $\mathbf{17_{La}}$, $\mathbf{17_{Nd}}$	$[Ln[(p\text{-}^t\text{Bu-}C_6H_4)_2CH]_3]$ (Ln = Y, La, Nd)	Y-C_{ipso} = 2.720(2) to 2.844(2) Y-C_{ortho} = 2.812(2), 2.814(2), 2.814(2) La-C_{ipso} = 2.841(2) to 2.915(2) La-C_{ortho} = 2.948(2), 2.958(2), 2.971(2) Nd-C_{ipso} = 2.795(3) to 2.867(3) Nd-C_{ortho} = 2.905(3), 2.918(3), 2.920(3)	^1H ($\mathbf{17_Y}$, $\mathbf{17_{La}}$), ^{13}C ($\mathbf{17_Y}$, $\mathbf{17_{La}}$)	46
$\mathbf{18_{Yb}}$, $\mathbf{18_{Sm}}$	$[Ln[2,2\text{-}(4\text{-}MeC_6H_3NMe_2)_2CH]_2]$ (Ln = Yb, Sm)	Yb-C = 2.576(4), 2.585(4), 2.730(4), 2.742(4), 2.852(3), 2.864(4) Sm-C = 2.710(2), 2.728(2), 2.779(2), 2.804(2), 2.854(2), 2.883(2)	^1H, ^{13}C	47
$\mathbf{19_{Dy}}$	$(Cp^*)Dy(2,6\text{-}^i\text{Pr}_2C_6H_3N{-}CMe{=}CMe{-}NC_6H_3^iPr_2{-}2,6)(THF)$	Dy-C = 2.837(2), 2.845(2)	–	48
$\mathbf{19'_{Dy}}$	$[Li(THF)_3][Dy(2,6\text{-}^i\text{Pr}_2C_6H_3N{-}CMe{=}CMe{-}NC_6H_3^iPr_2{-}2,6)(Cp^*)Cl]$	Dy-C = 2.764(2), 2.769(2)	–	48

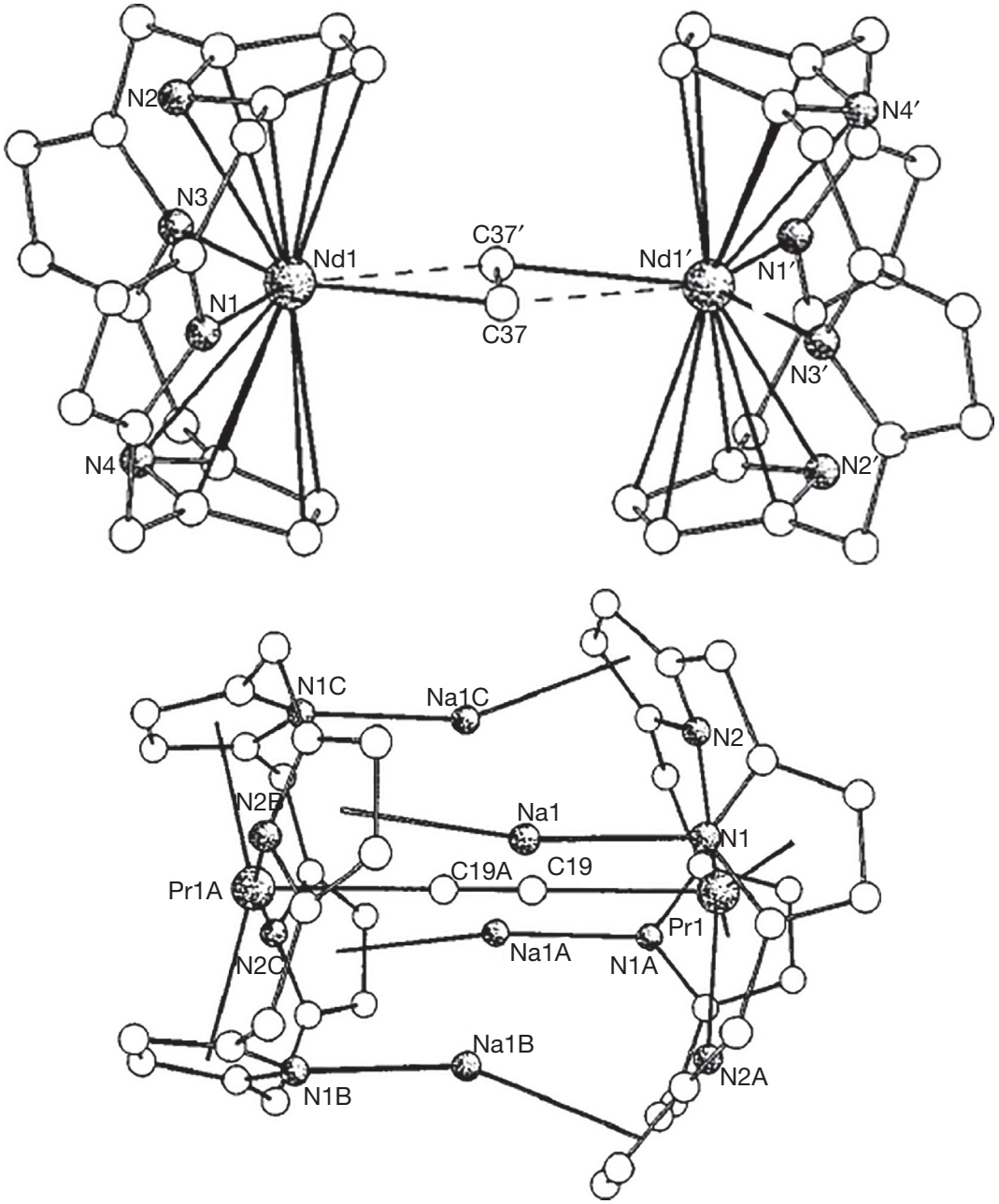

Fig. 14 Molecular structure of $\mathbf{23_{Nd}}$ (left, $Na(THF)_2$ and counter-cationic part and *meso*-ethyl groups omitted for clarity) and $\mathbf{24_{Pr}}$ (right, *meso*-ethyl groups omitted for clarity). Reprinted from Campazzi, E.; Solari, E.; Scopelliti, R.; Floriani, C. *Chem. Commun.* **1999**, 1617, with the permission of the Royal Society of Chemistry.

the Nd derivative $\mathbf{23_{Nd}}$, the $[C_2H_4]^-$ unit is side-on bonded to the two metal atoms (Fig. 14, left). In the presence of acetylene and sodium metal, the resulting acetylido complexes were formed where the two metal centers in $[\{(oepg)Ln\}(Na)_2(\mu\text{-}\eta^2\text{:}\eta^2\text{-}C_2)]_2$ $[\mathbf{24_{Ln}}]$ are bridged by the C_2^{2-} $\mu\text{-}\eta^2\text{:}\eta^2$-bonded anion as shown in the X-ray structure of $\mathbf{24_{Pr}}$ (Fig. 14, right).

$[(Cp''_2Sc)_2\text{-}(\mu\text{-}\eta^2\text{:}\eta^2\text{-}C_2H_4)]$ $[\mathbf{25_{Sc}}]$ was isolated in low yield (<5%) from the tentative reduction of $(Cp'')_2ScI$ with lipophilic reducing agent $[K(18\text{-crown-6})]_2[C_6H_2(SiMe_3)_4\text{-}1,2,4,5]$ ($Cp'' = [\eta^5\text{-}C_5H_3(SiMe_3)_2\text{-}1,3]$). This compound was suspected to arise from transient Sc(II)-induced cleavage of the crown ether.[52] The X-ray structure (Fig. 15) features a centrosymmetric ethylene-bridged binuclear scandium compound where the Sc-C(ethylene) distances of 2.314(3) Å are comparable to previously observed.[53]

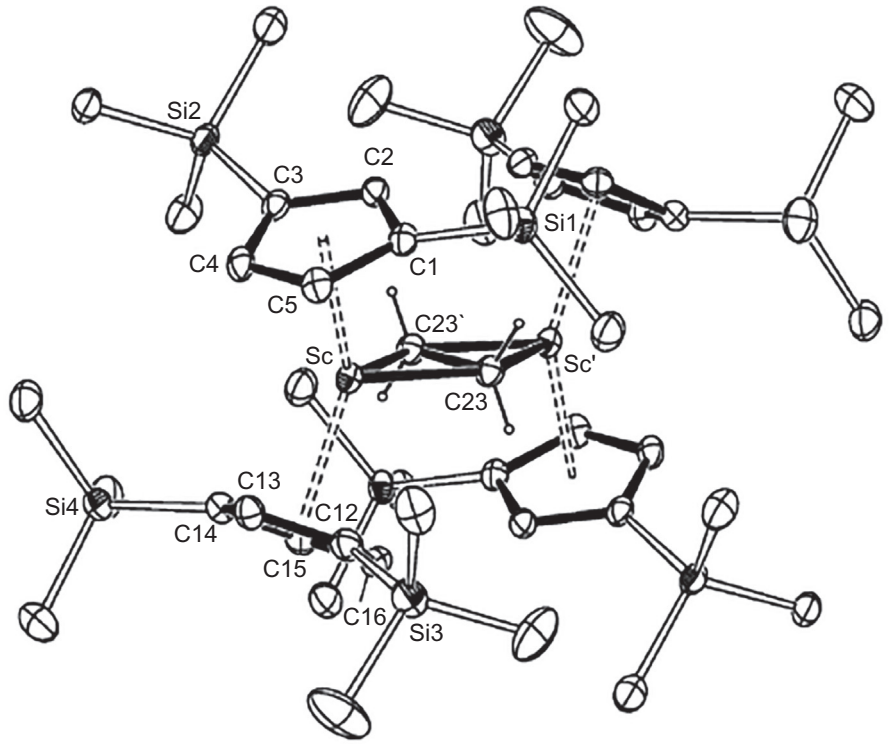

Fig. 15 Molecular structure of $\mathbf{25_{Sc}}$. Thermal ellipsoids are drawn at the 30% probability level. Hydrogen atoms except $H_2C=$ are omitted for clarity. Reprinted from Coles, M. P.; Hitchcock, P. B.; Lappert, M. F.; Protchenko, A. V. *Organometallics* **2012**, *31*, 2682–2690, with the authorization of the American Chemical Society.

In 2014, Diaconescu and coworkers reported that the reduction of (*E*)-stilbene using (NNTBS)LnI(THF)$_2$ (NNTBS = 1,1-Fc(NSi^{t}BuMe$_2$)$_2$, Ln = Y and La, Fc = ferrocene) in presence of potassium graphite KC_8 resulted in the formation of [(NNTBS)Ln(THF)]$_2$[μ–η^3:η^3-(E)-PhCHCHPh] ($\mathbf{26_{Ln}}$) as illustrated in Scheme 9.[54]

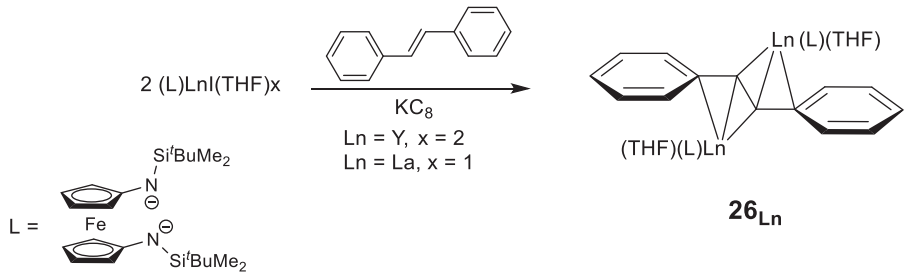

Scheme 9 Synthesis of complexes $\mathbf{26_{Ln}}$.

The molecular structure of $\mathbf{26_Y}$ was determined by X-ray diffraction analysis and revealed that the bridging stilbene coordinates to the metal center in an η^3-fashion through the central C–C bond and one *ipso*-carbon (Fig. 16).

The three-decker Yb(II) complex [Cp^{Bn5}Yb(DME)]$_2$[μ-$C_{10}H_8$] ($\mathbf{27_{Yb}}$) (Cp^{Bn5} = pentabenzylcyclopentadienyl, $C_{10}H_8$ = naphtalene) was synthesized by reacting [Cp^{Bn5}Yb(DME)(μ-I)]$_2$ with 2 molar equiv. of [$C_{10}H_8$]K or [YbI(DME)$_2$]$_2$[μ-$C_{10}H_8$] in the presence of Cp^{Bn5}K in a 1:2 molar ratio in DME (Scheme 10).[55] This complex contained a dianionic μ-η^4:η^4 naphthalene bridge between the two metal centers. Upon oxidation with 1,4-diphenyl-buta-1,3-diene, the three-decker [Cp^{Bn5}Yb(DME)]$_2$(μ-η^4:η^4-PhCHCHCHCHPh) Yb(II) complex $\mathbf{27'_{Yb}}$, where the dianionic diphenylbutadiene replaced the naphthalene moiety, was isolated. Both complexes were structurally characterized and the peculiar nature of the bonding in their bridging unit was additionally investigated by DFT studies.

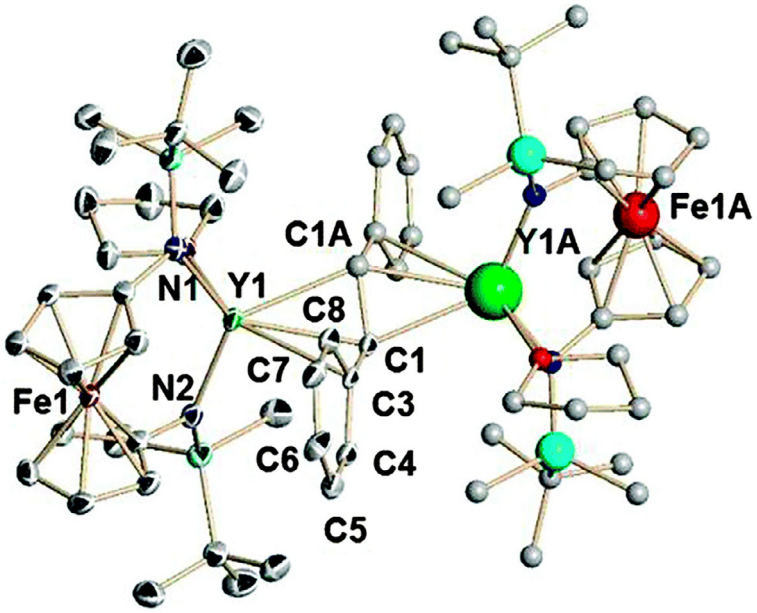

Fig. 16 Molecular structure of **26$_Y$**. Thermal ellipsoids are drawn at the 50% probability level. Hydrogen atoms and disordered counterparts are omitted for clarity. Reprinted from Huang, W.; Abukhalil, P. M.; Khan, S. I.; Diaconescu, P. L. *Chem. Commun.* **2014**, *50*, 5221–5223, with the authorization of the Royal Society of Chemistry.

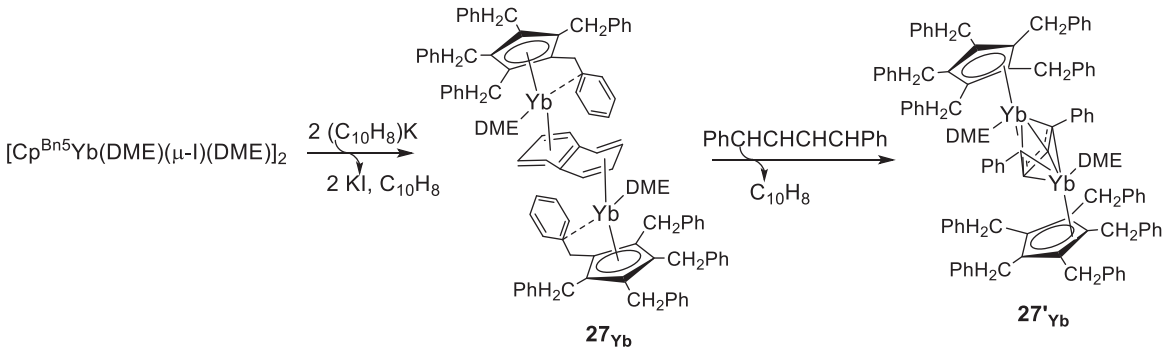

Scheme 10 Successive steps of the synthesis of **27$_{Yb}$** and **27′$_{Yb}$**.[55]

The sp^2 C–H activation of the ligand 1-R-3-(2,6-^{i}Pr$_2$C$_6$H$_3$N=CH)C$_8$H$_5$N (R = Bn or Me) in the presence of 0.5 equiv. of Ln(CH$_2$SiMe$_3$)$_3$(THF)$_2$ (Ln = Y, Er, Dy) resulted in the formation of the σ-bonded indolyl-supported rare earth complexes of the type [1-R-3-(2,6-^{i}Pr$_2$C$_6$H$_3$N=C)C$_8$H$_5$N]$_2$Ln(CH$_2$SiMe$_3$) [**28$_{Ln}$**, R = Bn; **28′$_{Ln}$**, R = Me], while a single ligand coordinates to the smaller ytterbium precursor to yield the [1-Bn-3-(2,6-^{i}Pr$_2$C$_6$H$_3$N=C)C$_8$H$_5$N]Yb(CH$_2$SiMe$_3$)$_2$(THF)$_2$ complex [**29$_{Yb}$**] (Scheme 11; Table 2).[56]

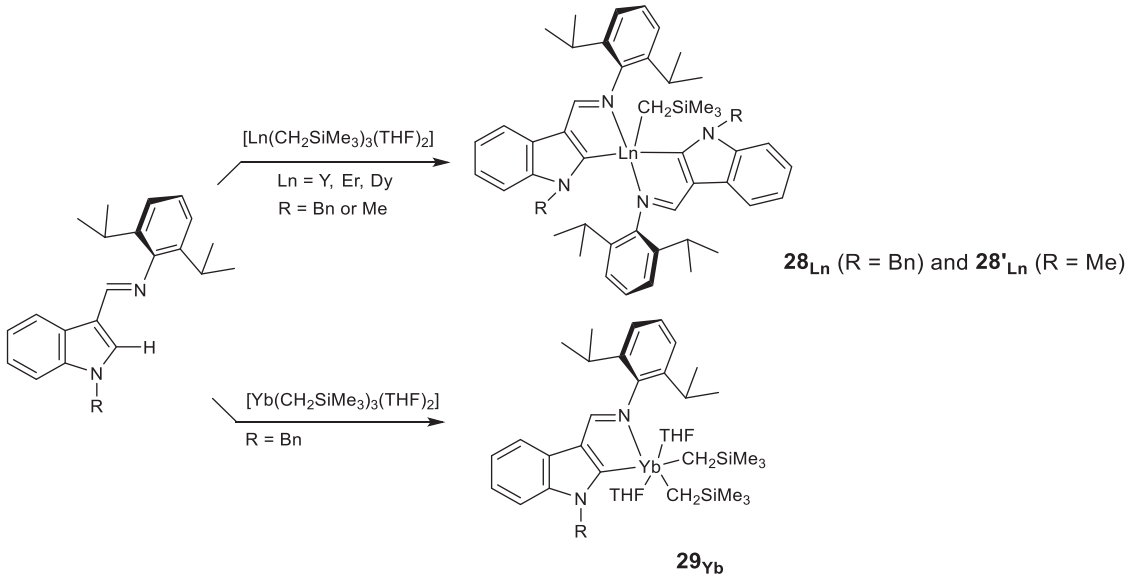

Scheme 11 Synthesis of bis-indolyl $\mathbf{28}_{Ln}$ and $\mathbf{28'}_{Ln}$ and mono-indolyl $\mathbf{29}_{Yb}$.

Table 2 Structural and analytical data of alkenyl and alkynyl complexes (in brackets only the relevant complexes only, otherwise for all complexes).

Compound number	*Molecular formula*	*X-ray data Typical Ln-C (alkenyl or alkynyl) distances (Å)*	*NMR data*	*References*
$\mathbf{20}_{Sm}$, $\mathbf{20'}_{Sm}$	$[(Cp^*)_2Sm]_2(\mu\text{-}\eta^2\text{:}\eta^4\text{-}CH_2CHPh)$; $[(Cp^*)_2Sm]_2(\mu\text{-}\eta^2\text{:}\eta^4\text{-}PhCHCHPh)$	Not available	–	9
$\mathbf{21}_{Sm}$, $\mathbf{21'}_{Sm}$	$[(Cp^*)_2Sm]_2[\mu\text{-}\eta^2\text{:}\eta^4\text{-}CH_2CHC(Me)CH_2]$; $[(Cp^*)_2Sm]_2[\mu\text{-}\eta^2\text{:}\eta^4\text{-}CH_2CHC(CH_2)CH_2CH_2CHCMe_2]$	Sm-C = 2.544(9), 2.674(9) Sm-C = 2.5294(4), 2.672(4)	^1H, ^{13}C	49
$\mathbf{22}_{Y}$	$[M(THF)_x][Y(Ph_2CCPh_2)_2]$ (M = Na, K)	Y-C = 2.518(6)	–	50
$\mathbf{23}_{Nd}$, $\mathbf{23}_{Pr}$	$[\{(oepg)Ln\}Na(THF)_2(\mu\text{-}\eta^2\text{:}\eta^2\text{-}C_2H_4)]_2$ (Ln = Nd, Pr)	Nd-C = 2.497(7), 2.790(7)	–	51
$\mathbf{24}_{Nd}$, $\mathbf{24}_{Pr}$	$[\{(oepg)Ln\}(Na)_2(\mu\text{-}\eta^2\text{:}\eta^2\text{-}C_2)]_2$ (Ln = Nd, Pr)	Pr-C = 2.670(4)	–	51
$\mathbf{25}_{Sc}$	$[(Cp''_2Sc)_2\text{-}(\mu\text{-}\eta^2\text{:}\eta^2\text{-}C_2H_4)]$	Sc-C = 2.314(3)	–	52
$\mathbf{26}_{La}$, $\mathbf{26}_{Y}$	$[(NNTBS)Ln(THF)]_2[\mu\text{-}\eta^3\text{:}\eta^3\text{-(E)-PhCHCHPh}]$ (Ln = La, Y)	Y-C = 2.603(4), 2.581(5) and 2.741(7)	^1H, ^{13}C	54
$\mathbf{27}_{Yb}$, $\mathbf{27'}_{Yb}$	$[(Cp^{Bn5})Yb(DME)]_2[\mu\text{-}C_{10}H_8]$; $[(Cp^{Bn5})Yb(DME)]_2(\mu\text{-}\eta^4\text{:}\eta^4\text{-PhCHCHCHCHPh})$ (Cp^{Bn5} = pentabenzylcyclopentadienyl, $C_{10}H_8$ = naphtalene)	Yb-C = 2.687(2), 2.681(2), 2.695(2), 2.720(2) Yb-C = 2.726(6), 2.745(6), 2.789(6), 2.821(4)	^1H, ^{13}C	55
$\mathbf{28}_{Y}$, $\mathbf{28}_{Er}$, $\mathbf{28}_{Dy}$, $\mathbf{28'}_{Y}$, $\mathbf{28'}_{Er}$, $\mathbf{28'}_{Dy}$, $\mathbf{28'}_{Yb}$	[1-*R*-3-(2,6-^{i}Pr$_2$C$_6$H$_3$N=C)C$_8$H$_5$N]$_2$Ln(CH$_2$SiMe$_3$) (R = Bn, Ln = Y, Er, Dy; R = Me, Ln = Y, Er, Dy, Yb)	Y-C = 2.483(2), Er-C = 2.468(3), Dy-C = 2.489(3) Y-C = 2.473(4), Er-C = 2.466(4), Dy-C = 2.472(4), Yb-C = 2.422(3)	^1H ($\mathbf{28}_{Y}$, $\mathbf{28'}_{Y}$), ^{13}C ($\mathbf{28}_{Y}$, $\mathbf{28'}_{Y}$)	56
$\mathbf{29}_{Yb}$	[1-Bn-3-(2,6-^{i}Pr$_2$C$_6$H$_3$N=C)C$_8$H$_5$N]Yb(CH$_2$SiMe$_3$)$_2$(THF)$_2$	Yb-C = 2.522(4)	–	56
$\mathbf{30}_{Er}$	$[MeC(NDipp)CHC(Me)NCH_2CH_2NC_4H_2\text{-}2,5\text{-}Me_2]Er(CH_2SiMe_3)(\mu\text{-}C{\equiv}CPh)]_2$	Er-C = 2.521(5)	–	57
$\mathbf{31}_{Y}$, $\mathbf{31'}_{Yb}$	$\{(R\text{-}C{\equiv}C)Ln[2\text{-}(^tBuN{=}CH)C_8H_5N]_2\}_2$ ($\mathbf{31}_{Y}$, Ln = Y, R = Ph; $\mathbf{31'}_{Yb}$, Ln = Yb, R = SiMe$_3$)	Y-C = 2.502(8), 2.524(8) Yb-C = 2.483(4), 2.488(4)	^1H ($\mathbf{31}_{Y}$), ^{13}C ($\mathbf{31}_{Y}$)	58
$\mathbf{32}_{Gd}$	(Tp^{Me2})Gd(THF)(Cp)(C=PhC) (Tp^{Me2} = tri(3,5-dimethylpyrazolyl)borate)	Gd-C = 2.519(8)	–	59

The X-ray diffraction analysis of the yttrium complexes $\mathbf{28_Y}$ and $\mathbf{28'_Y}$ indicated a rather similar five-coordinate distorted trigonal bipyramidal geometry around the metal center with Csp^2-Y bond distances in the same range (2.48–2.47 Å) (Fig. 17, left, $\mathbf{28'_Y}$). On the other hand, the ytterbium complex $\mathbf{29_{Yb}}$ showed a six-coordinate octahedral geometry around the metal center (Fig. 17, right).

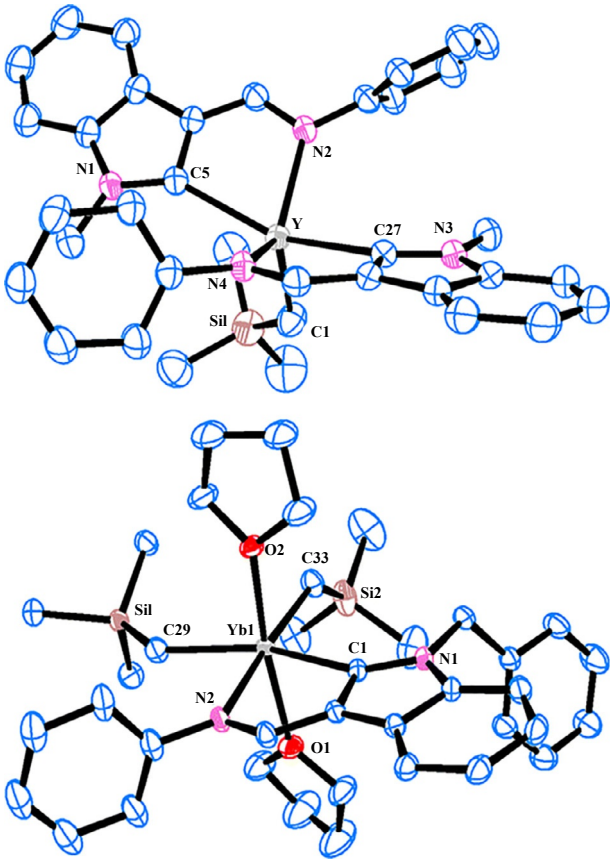

Fig. 17 Molecular structure of $\mathbf{28'_Y}$ (left) and of $\mathbf{29_{Yb}}$ (right) with thermal ellipsoids drawn at the 30% probability level. All hydrogen atoms and isopropyl groups are omitted for clarity. Reprinted from Guo, L.; Zhu, X.; Zhang, G.; Wei, Y.; Ning, L.; Zhou, S.; Feng, Z.; Wanf, S.; Mu, X.; Chen, J.; Jiang, Y. *Inorg. Chem.* **2015**, *54*, 5725–5731, with the permission of the American Chemical Society.

Zhu et al. reported recently that the dinuclear pyrrolyl-functionalized β-diketiminato erbium alkynyl complex [MeC(NDipp)CHC(Me)NCH$_2$CH$_2$NC$_4$H$_2$-2,5-Me$_2$]Er(CH$_2$SiMe$_3$)(μ-C≡CPh)]$_2$ ($\mathbf{30_{Er}}$, Dipp = 2,6-^{i}Pr$_2$C$_6$H$_3$) is obtained by the reaction of the lanthanide dialkyl precursor with phenylacetylene (Scheme 12).[57] According to the authors, activation of the terminal *sp*C–H bond in the alkyne takes place to afford dinuclear alkynyl $\mathbf{30_{Er}}$.

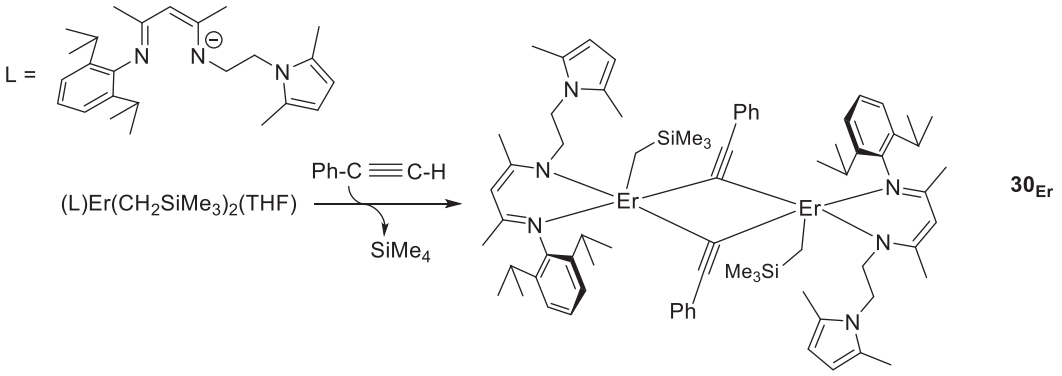

Scheme 12 Synthesis of alkynyl complex $\mathbf{30_{Er}}$.

From XRD, it was established that the alkynyl complex $\mathbf{30_{Er}}$ exhibits a centrosymmetric structure with phenylacetylene as a bridge bonded to the erbium ions, and the core of the molecule is a four-membered ring (Fig. 18).

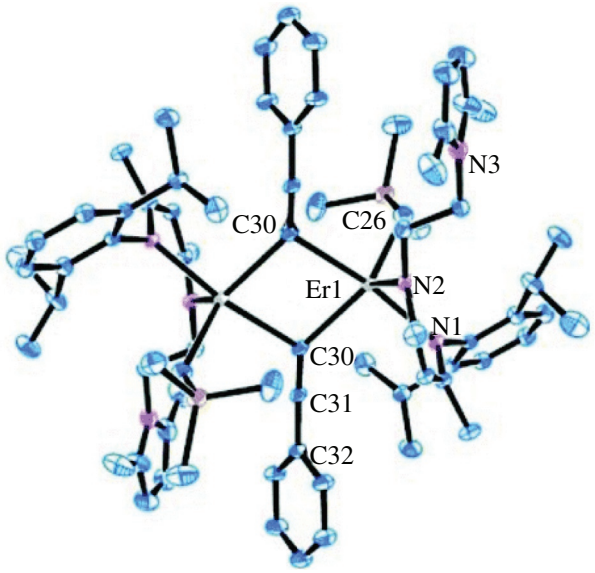

Fig. 18 Molecular structure of $\mathbf{30_{Er}}$ (hydrogen atoms and isopropyl groups are omitted for clarity). Reprinted from Zhu, X.; Li, Y.; Guo, D.; Wang, S.; Wei, Y.; Zhou, S. *Dalton Trans.* **2018**, *47*, 3947–3957, with the authorization of the Royal Society of Chemistry.

The group of Wang described the synthesis of $\{(R{-}C{\equiv}C)Ln[2\text{-}(^tBuN{=}CH)C_8H_5N]_2\}_2$ complexes ($\mathbf{31_Y}$, Ln = Y, R = Ph; $\mathbf{31'_{Yb}}$, Ln = Yb, R = $SiMe_3$) starting from $[2\text{-}(^tBuN{=}CH)C_8H_5N]Ln[N(SiMe_3)_2]_2$ combined with R—C≡CH (Scheme 13) that were prepared with the aim to study the mechanism of the catalytic addition of terminal alkynes on carbodiimide substrates.[58]

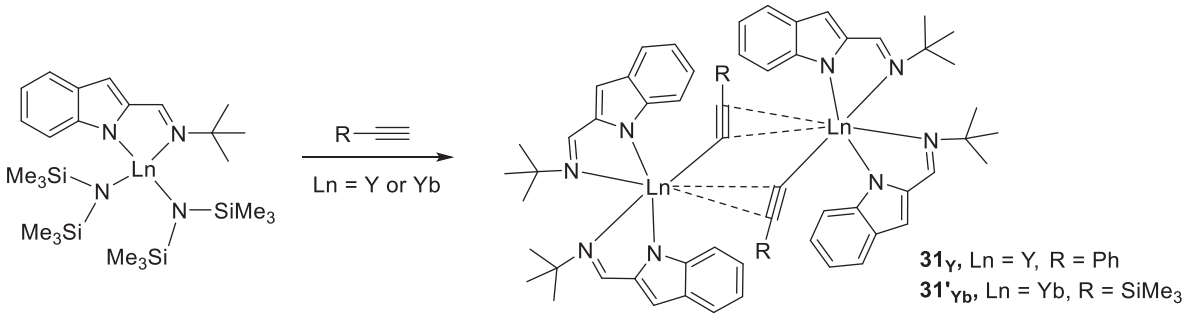

Scheme 13 Synthesis of alkynyl complexes $\mathbf{31_Y}$ and $\mathbf{31'_{Yb}}$.

The X-ray diffraction analysis on single-crystals of $\mathbf{31_Y}$ and $\mathbf{31'_{Yb}}$ revealed the formation of dimeric structures, with the alkynyl ligand being coordinated to the metal center in $\mu\text{-}\eta^1{:}\eta^2$ haptic mode (Fig. 19).

The addition of 1 equiv. of phenylacetylene to the monoalkyl $(Tp^{Me2})Gd(THF)(Cp)(CH_2Ph)$ (Tp^{Me2} = tri(3,5-dimethylpyrazolyl)borate) in toluene afforded the corresponding phenylacetylide gadolinium complex $[\mathbf{32_{Gd}}]$ (Scheme 14, Fig. 20).[59]

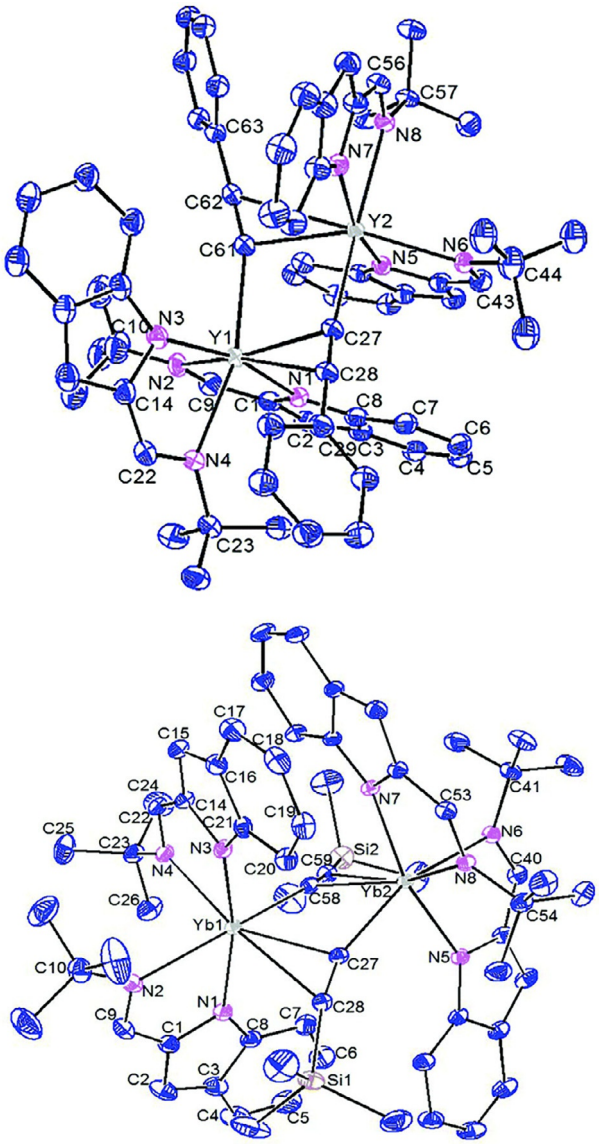

Fig. 19 Molecular structures of $\mathbf{31_Y}$ (left) and $\mathbf{31'_{Yb}}$ (right) with thermal ellipsoids set at the 15% probability level. All hydrogen atoms are omitted for clarity. Reprinted from Feng, Z.; Huang, Z.; Wang, S.; Wei, Y.; Zhou, S.; Zhu, X. *Dalton Trans.* **2019**, *48* (29), 11094–11102, with the permission of the Royal Society of Chemistry.

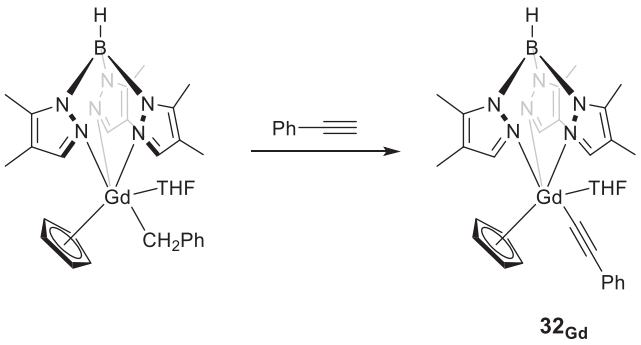

$\mathbf{32_{Gd}}$

Scheme 14 Synthesis of alkynyl complex $\mathbf{32_{Gd}}$.

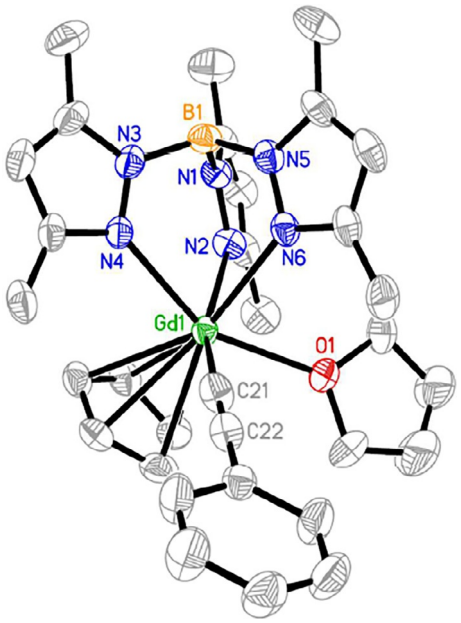

Fig. 20 Molecular structure of $\mathbf{32_{Gd}}$ with 30% probability thermal ellipsoids. All hydrogen atoms are omitted for clarity. Reprinted from Zhang, F.; Zhang, J.; Zhang, Y.; Hong, J.; Zhou, X. *Organometallics* **2014**, *33* (21), 6186–6192, with the permission of the American Chemical Society.

3 Allyl complexes of the lanthanides

3.1 Homoleptic allyl complexes

3.1.1 Bis-allyl complexes

The substituted-allyl complexes of ytterbium under the form of THF adducts ($[1\text{-}(SiMe_3)C_3H_4]_2Yb(THF)_2$ $[\mathbf{33_{Yb}}]$ and $[1\text{-}(SiPh_3)\text{-}3\text{-}(SiMe_3)C_3H_3]_2Yb(THF)$ $[\mathbf{34_{Yb}}]$ and terpyridine adducts $[1,3\text{-}(SiMe_3)_2C_3H_3]_2Yb(tpy)$ $[\mathbf{35_{Yb}}]$, $[1,3\text{-}(SiMe_3)_2C_3H_3]_2Yb(tpyCN)$, $[\mathbf{35'_{Yb}}]$ $[1,3\text{-}(SiMe_3)_2C_3H_3]_2Yb(tpy(CN)_2$ $[\mathbf{35''_{Yb}}]$, $[1\text{-}(SiMe_3)C_3H_4]_2Yb(tpyCN)$ $[\mathbf{33'_{Yb}}]$ and $[1\text{-}(SiPh_3)\text{-}3\text{-}(SiMe_3)C_3H_3]_2Yb(tpyCN)$ $[\mathbf{34'_{Yb}}]$ were synthesized (Scheme 15) and studied regarding the effect of allyl ligands on the internal charge-transfer process. The two allyl ligands are η^3-coordinated in the THF complexes according to their crystal structures and ^{1}H NMR data.[60]

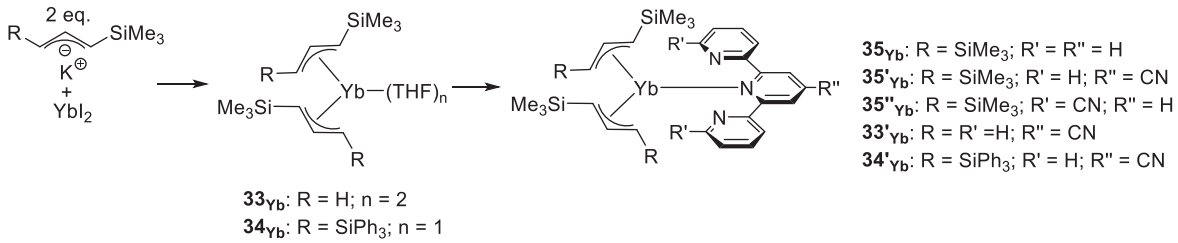

Scheme 15 Synthesis of bis(allyl) ytterbium complexes and their terpyridine adducts.

The X-ray structure of $\mathbf{35_{Yb}}$ displays η^3-coordinated allyl ligands and shorter Yb-C distances (2.52(2) to 2.62(2) Å) than previously noticed in divalent $[1,3\text{-}(SiMe_3)_2C_3H_3]_2Yb(THF)_2$, which was explained by the +III oxidation state of Yb in the tpy adduct (Fig. 21).[61]

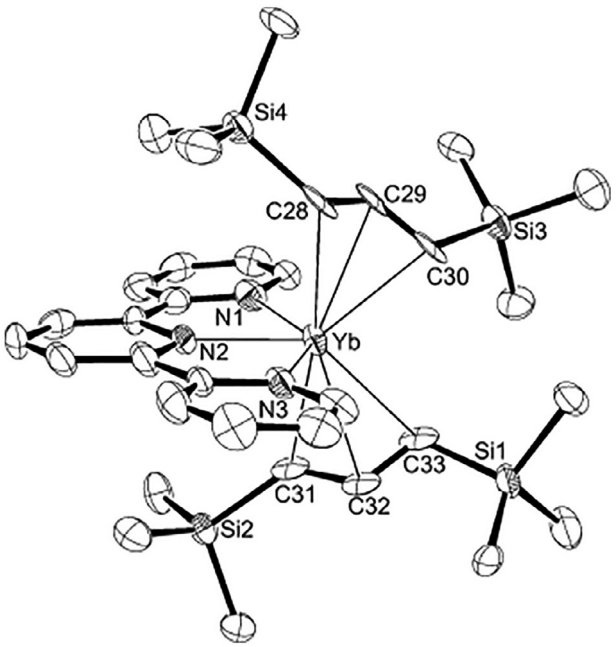

Fig. 21 Thermal ellipsoid representation of **35$_{Yb}$** (50% probability ellipsoids). H atoms have been omitted for clarity. Reprinted from White, R. E.; Carlson, C. N.; Veauthier, J. M.; Simpson, C. K.; Thompson, J. D.; Scott, B.L.; Hanusa, T. P.; John, K. D. *Inorg. Chem.* **2006**, *45*, 7004–7009, with the permission of the American Chemical Society.

3.1.2 Tris-allyl complexes

The tris-allyl complexes of the group 3 metals and the lanthanides are known since the seminal work of Taube's research group,[3,4] later completed by Bochmann.[5]

In another study published in 2005, Bochmann and coworkers, trying to generalize the synthetic route to the tris-allyl derivatives of lanthanides, isolated the mixed lanthanide/magnesium derivatives **36$_{Ln}$** where Ln = La, Y, whereas anionic allyl species were obtained with neodymium and samarium (see further).[62] These compounds **36$_{Ln}$**, which were afforded in moderate yields, resulted from the reaction of $LnI_3(THF)_n$ with (allyl)magnesium iodide according to Scheme 16. From ^{1}H NMR analysis, it was deduced that the allyl moiety is η^3-coordinated to the lanthanide atom and η^1-bonded to Mg.

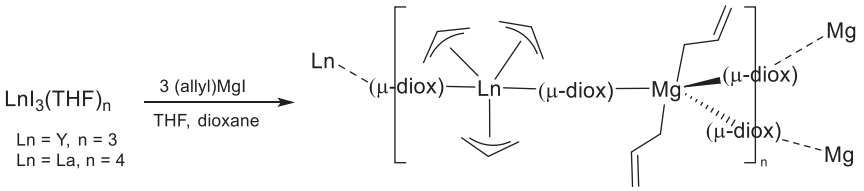

36$_{Ln}$

Scheme 16 Synthesis of $[Ln(\eta^3\text{-}C_3H_5)_3(\mu\text{-dioxane})Mg(\eta^1\text{-}C_3H_5)_2(\mu\text{-dioxane})_{1.5}]_\infty$ (**36$_{Ln}$**, Ln = La, Y).

From X-ray studies, the mode of coordination of the allyl groups was confirmed and it was also established that these complexes are coordination polymers, featuring sheets of parallel zigzag $-[Mg\text{-}(\mu\text{-dioxane})\text{-}Mg\text{-}(\mu\text{-dioxane})]_{n-}$ chains, linked by $-[(\mu\text{-dioxane})\text{-}Ln(\eta^3\text{-}C_3H_5)_3\text{-}(\mu\text{-dioxane})\text{-}Ln(\eta^3\text{-}C_3H_5)_3]_{n-}$ units as shown in Fig. 22 (for Ln = Y).

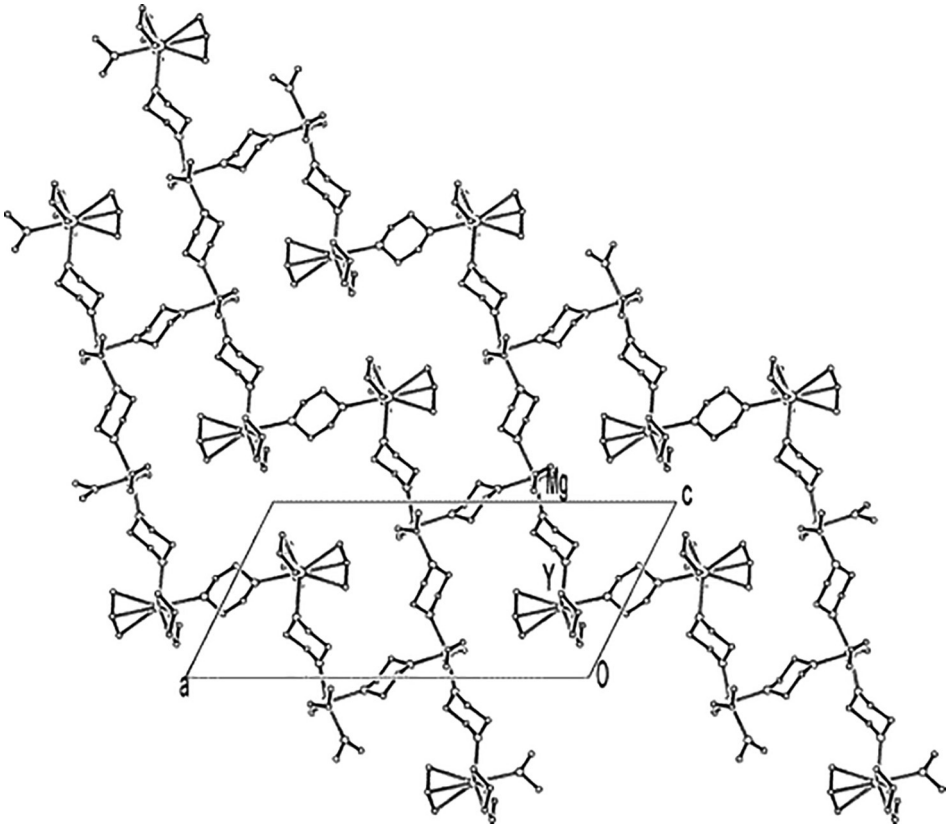

Fig. 22 Projection of the planar polymeric chains down the *b*-axis in $\mathbf{36_Y}$. Reprinted from Sanchez-Barba, L. F., Hughes, D. L., Humphrey, S. M., Bochmann, M. *Organometallics* **2005**, *24*, 5329–5334, with the authorization of the American Chemical Society.

A few years later, Okuda brought an important contribution with the isolation of the tris-allyl complex [{Ce(η^3-C_3H_5)$_3$(diox)}$_2$(μ-diox)] [$\mathbf{37_{Ce}}$] that was obtained by recrystallization in neat dioxane of [Ce(η^3-C_3H_5)$_3$(diox)] (diox = 1, 4-dioxane) synthesized according to the published procedure (reaction of $LnCl_3$ with 3 equiv. of (allyl)MgCl, *vide infra*). From XRD analysis (Fig. 23, left), the geometry around the cerium center in $\mathbf{37_{Ce}}$ was found to be best described as distorted trigonal bipyramidal. In turn, recrystallization of [Ln(η^3-C_3H_5)$_3$(diox)] (Ln = Ce, Pr) in THF/pentane afforded the bis-THF adducts [Ln(η^3-C_3H_5)$_3$(THF)$_2$] [$\mathbf{37'_{Ln}}$] as crystals suitable for X-ray diffraction studies. In the molecular structure of $\mathbf{37'_{Ce}}$, two allyl groups and a THF molecule are found in the equatorial plane, with the third allyl group and an additional THF molecule occupying the apical positions (Fig. 23, right).[6]

Quite surprisingly, it is only in 2011 that the tris(allyl)scandium compounds [Sc(C_3H_5)$_3$(THF)$_n$] (n = 0, 2) were obtained, by the simple reaction of anhydrous $ScCl_3$ with three equivalents of allylpotassium or 1.5 equivalents of bis(allyl)calcium in THF at 0 °C (Scheme 17).[63]

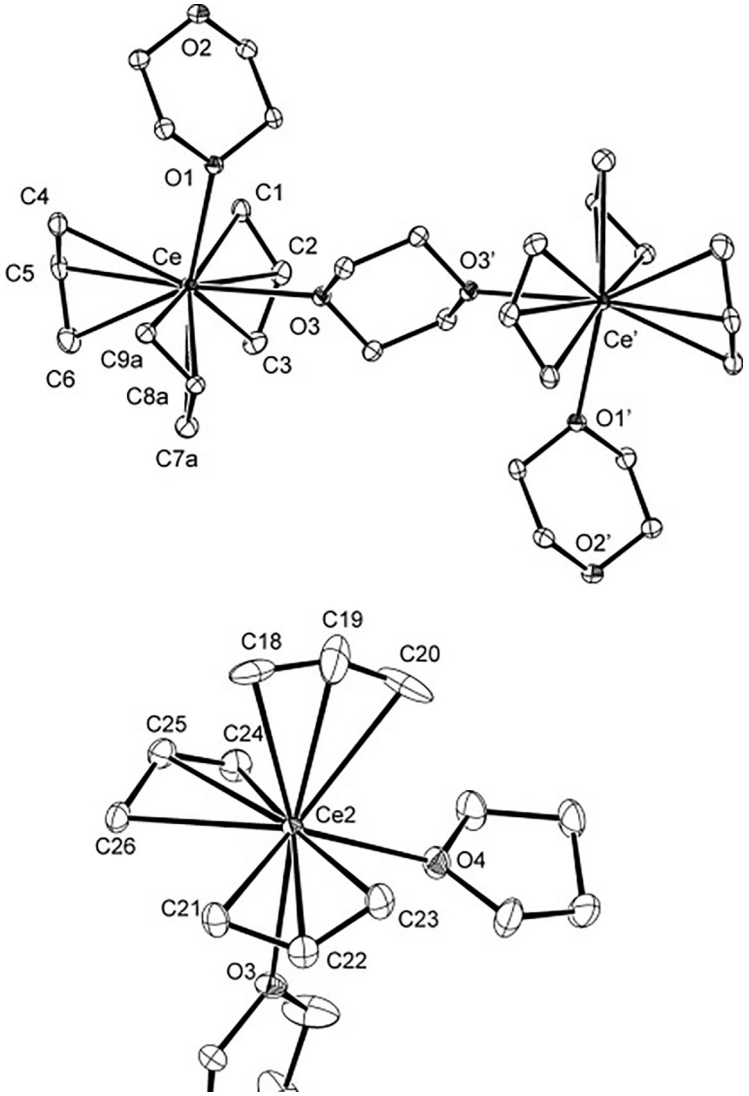

Fig. 23 Molecular structures of $\mathbf{37}_{Ce}$ (left) and $\mathbf{37'}_{Ce}$ (right). Thermal ellipsoids are drawn at the 30% probability level, hydrogen atoms are omitted for clarity. Reprinted from Robert, D.; Abinet, E.; Spaniol, T. P.; Okuda, J. *Chem. Eur. J.* **2009**, *15*, 11937–11947, with the authorization of Wiley-VCH Verlag GmbH.

$$ScCl_3(THF)_n \xrightarrow[\text{or } 3/2\ Ca(C_3H_5)_2]{3\ K(C_3H_5)} \underset{\mathbf{37'_{Sc}}}{Sc(\eta^3\text{-}C_3H_5)_2(\eta^1\text{-}C_3H_5)(THF)_2} \xrightarrow{\text{vacuum}} \underset{\mathbf{37''_{Sc}}}{Sc(C_3H_5)_3}$$

Scheme 17 Synthesis of $\mathbf{37'}_{Sc}$ followed by subsequent vacuum treatment affording $\mathbf{37''}_{Sc}$.

Drying *in vacuo* of the bis-THF adduct $\mathbf{37'}_{Sc}$ afforded the homoleptic uncoordinated $Sc(C_3H_5)_3$ ($\mathbf{37''}_{Sc}$). X-ray diffraction studies on crystals isolated from THF solution revealed that, in the bis-THF adduct $\mathbf{37'}_{Sc}$, two allyl ligands are coordinated in an η^3-fashion while one allyl ligand is in the η^1-mode, consistent with the formula $Sc(\eta^1\text{-}C_3H_5)_3(\eta^3\text{-}C_3H_5)_2(THF)_2$ (Fig. 24). This structural arrangement is in good agreement with the *ab initio* calculations carried out by the group of Schaefer, in which the theoretical study performed on divalent and trivalent homoleptic allyl complexes $Sc(C_3H_5)_2$ and $Sc(C_3H_5)_3$ suggested that in both complexes, the allyl groups are bonded as fluxional trihapto to the Sc metal.[64]

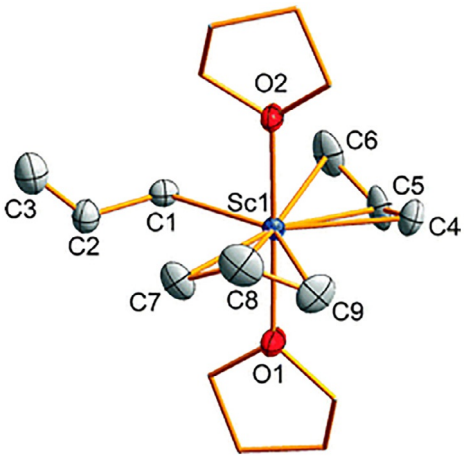

Fig. 24 Molecular structure of $\mathbf{37'_{Sc}}$ (ellipsoids are set at the 50% probability level, hydrogen atoms are omitted for clarity). Reprinted from Standfuss, S.; Abinet, E.; Spaniol, T. P.; Okuda J. *Chem. Commun.* **2011**, *47*, 11441–11443, with the permission of the Royal Society of Chemistry.

In 2006, Hanusa and coworkers attempted the synthesis of a non-solvated tris-allyl derivative of lanthanide bearing the bis-trimethylsilylallyl ligand. They carried out the reaction with an holmium precursor, a metal of small ionic radius among the lanthanides family (thus belonging to the *late* sub-group of lanthanides),[65] since THF-adducts Ln[1,3-$(SiMe_3)_2C_3H_3]_3$(THF) were formed with lanthanides of larger ionic radius (belonging to the *early* sub-group of lanthanides).[61] Instead of the presumably formed tris-allyl derivative, the isolated holmium compound was a dimeric complex of formula {[1,3-$(SiMe_3)_2C_3H_3$]Ho[CH$(SiMe_3)$CHCH$SiMe_2$-μ-CH_2]}$_2$ [$\mathbf{38_{Ho}}$] in which hydrogen abstraction from a trimethylsilyl group has occurred on two allyl ligands, resulting in the formation of dimethylsilylene units that bridge the holmium atoms (Fig. 25, left).[66]

Furthermore, when the reaction time was prolonged, a second and different product was isolated and structurally characterized, {(THF)Ho[CH$(SiMe_3)$CHCH$SiMe_2$-μ-CH_2]}$_2$[μ-η^1,η^3-C$(SiMe_3)$CHCH$SiMe_3$] [$\mathbf{39_{Ho}}$], in which, in addition to two dimethylsilylene bridges, the metal centers are joined with a μ-η^1,η^3-allylidene ligand (Fig. 25, right). Evidence for delocalized bonding in the allylidene fragment was provided from both crystallographic and computational studies. A tentative explanation of the successive formation of the two compounds, due to the presence of residual water in the starting holmium triflate material, is given in Scheme 18.

A generalization about the strategy of synthesis of allyl complexes of the lanthanides with [1,3-bis(trimethylsilyl)allyl] ligand was then proposed by Hanusa and coworkers in 2007.[67] The authors succeeded in the preparation in good yields (>75%) of tris-allyl lanthanide Ln[1,3-$(SiMe_3)_2C_3H_3]_3$ complexes $\mathbf{40_{Ln}}$, by starting from rigorously anhydrous triflates Ln$(OTf)_3$ (Ln = Dy, Ho, Er, Tm, Lu) with 3 equiv. of K[1,3-$(SiMe_3)_2C_3H_3$] in THF (Scheme 19).

All complexes in this small ionic radius lanthanide series were found to be non-solvated. The thulium compound Tm[1,3-$(SiMe_3)_2C_3H_3]_3$ ($\mathbf{40_{Tm}}$) could be crystallographically characterized (Fig. 26), showing the three allyl ligands η^3-bounded to the metal and the Tm–C bond distances range from 2.326(2) to 2.606(2) Å, with an average of 2.53(1) Å (Table 3).

Starting from the trichlorides with Ln = Ho or Er, the (bistrimethylsilyl)allyl complexes were isolated as well, whether with two or three equivalents of allyl ligand as starting material, as same as previously observed with yttrium.[68] The same tris(allyl) product $\mathbf{40_{Ho}}$ was isolated in the case of starting with HoI_3 as precursor. However, this was an unexpected result, as anionic "ate" complexes of formula [Ln[1,3-$(SiMe_3)_2C_3H_3]_3$I]$^-$ were previously shown to be formed in the dysprosium and erbium series when the triiodides were used as precursors.[69] To isolate the tetra-allyl lanthanate holmium complex $\mathbf{41_{Ho}}$, the authors found that it was necessary to carry out the reaction from the lithium allyl reagent (Scheme 20). Unfortunately, they could not obtain X-ray quality crystals of that complex.

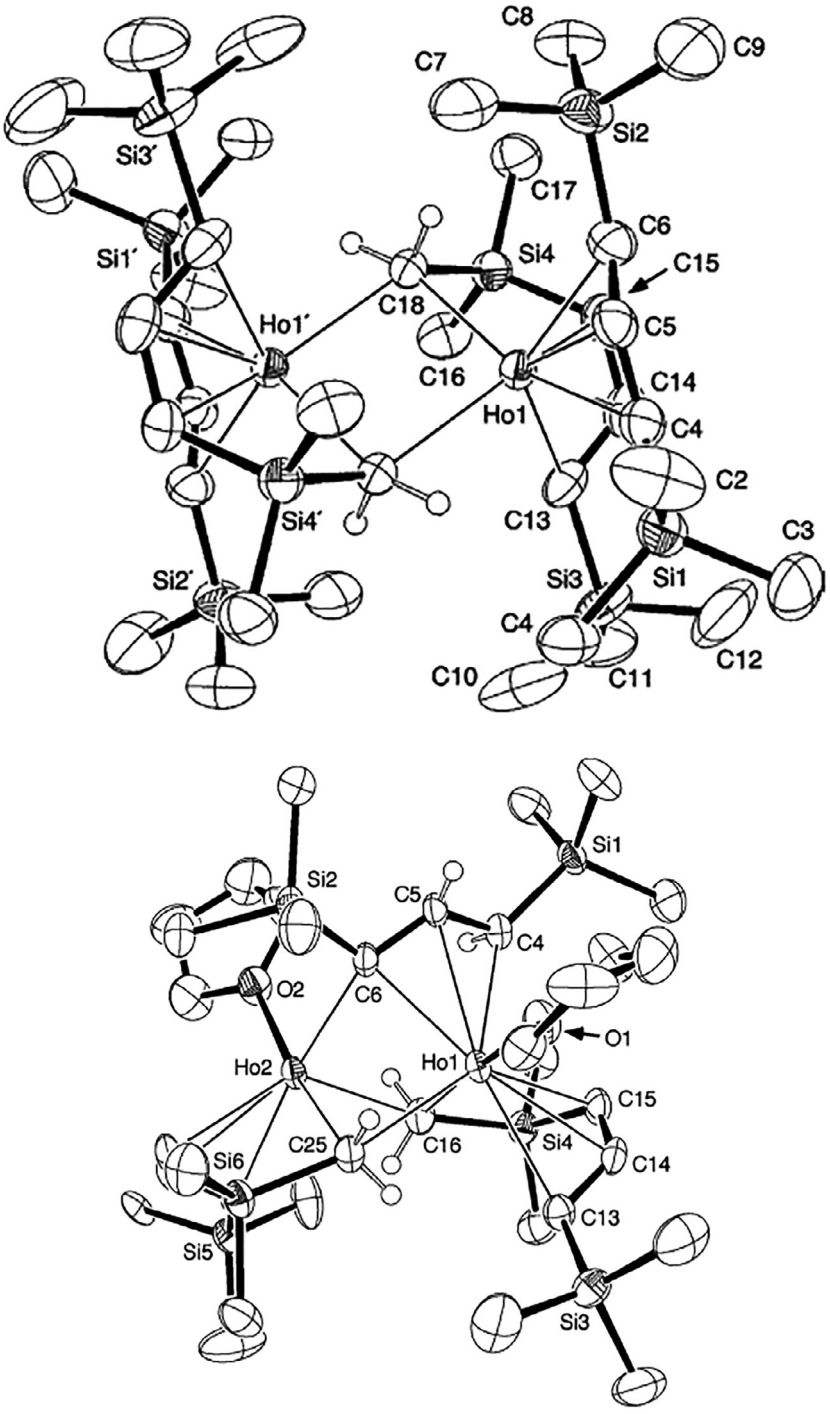

Fig. 25 Molecular structure of $\mathbf{38_{Ho}}$ (left) and $\mathbf{39_{Ho}}$ (right) (ellipsoids are set at the 50% probability level, hydrogen atoms of the dimethylsilylene and allylidene bridges are omitted for clarity). Reprinted from White, R. E.; Hanusa, T. P.; Kucera, B. E. *J. Am. Chem. Soc.* **2006**, *128*, 9622–9623, with the permission of the American Chemical Society.

It was not until 2014 that the tris-allyl scandium complex Sc[1,3-$(SiMe_3)_2C_3H_3]_3$ [$\mathbf{42_{Sc}}$] comprising the same bulky tris [1,3-bis(trimethylsilyl)allyl] groups was prepared, by mechanochemical synthesis *via* ionic metathesis between $ScCl_3$ and the potassium salt of the allyl anion. The X-ray crystal structure of this hexane-soluble compound revealed monomeric compound having three π-bound η^3-allyl ligands (Fig. 27), which was confirmed by ^{1}H NMR analysis in solution.[70]

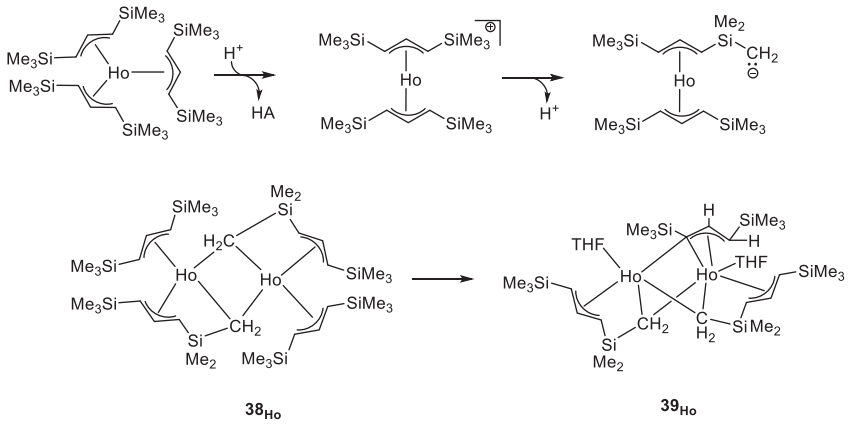

Scheme 18 Proposed explanation for the formation of bis(trimethylsilyl)allyl holmium complexes $\mathbf{38_{Ho}}$ and $\mathbf{39_{Ho}}$.[66]

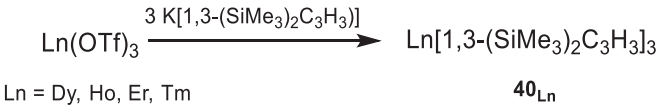

Scheme 19 Straightforward synthesis of tri-[(bistrimethylsilyl)allyl] complexes $\mathbf{40_{Ln}}$ using the potassium allyl reagent as starting material.

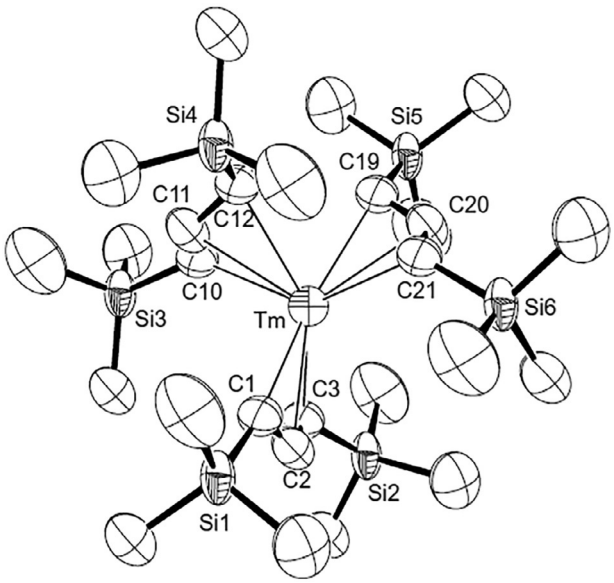

Fig. 26 Molecular structure of $\mathbf{40_{Tm}}$ (ellipsoids are set at the 50% probability level, hydrogen atoms are omitted for clarity). Reprinted from White, R. E.; Hanusa, T. P.; Kucera, B. E. *J. Organomet. Chem.* **2007**, *692*, 3479–3485, with the permission of Elsevier.

Table 3 Structural and analytical data of homoleptic allyl complexes (in brackets only the relevant complexes only, otherwise for all complexes).

Compound number	*Molecular formula*	*X-ray data* *Ln-C(allyl) distances (Å)*	*NMR data*	*References*
33_{Yb}, $33'_{Yb}$	$[1\text{-}(SiMe_3)C_3H_4]_2Yb(L)_2$	**$35'_{Yb}$**: Yb-C = 2.52(2) to 2.62(2)	^{1}H	60,61
34_{Yb}, $34'_{Yb}$	(L = THF, tPyCN)			
35_{Yb},$35'_{Yb}$, $35''_{Yb}$	$[1\text{-}(SiPh_3)\text{-}3\text{-}(SiMe_3)C_3H_3]_2Yb(L)$ (L = THF, tPyCN) $[1,3\text{-}(SiMe_3)_2C_3H_3]_2Yb(L)$ (L = THF, tPyCN, $tPy(CN)_2$)			
36_Y, 36_{La}	$[Ln(\eta^3\text{-}C_3H_5)_3(\mu\text{-dioxane})Mg(\eta^1\text{-}C_3H_5)_2(\mu\text{-dioxane})_{1.5}]_\infty$	Y-C = 2.600(8), 2.589(8), 2.525(11); 2.770(9), 2.704(9), 2.686(8); 2.622(5), 2.645(5), 2.709(5); Mg-C = 2.188(8); 2.189(8) La-C = 2.794(6), 2.827(6), 2.756(6); 2.815(7), 2.8068, 2.739(6); 2.731(6), 2.783(6), 2.763(6); Mg-C = 2.197(6), 2.195(6)	^{1}H, ^{13}C	62
37_{Ce}	$[\{Ce(\eta^3\text{-}C_3H_5)_3(diox)\}_2(\mu\text{-diox})]$	Ce-C = 2.765(3), 2.780(3), 2.719(3)	–	6
$37'_{Ce}$, $37'_{Pr}$	$[Ln(\eta^3\text{-}C_3H_5)_3(THF)_2]$ (Ln = Ce, Pr)	–	^{1}H, ^{13}C	6
$37'_{Sc}$	$[Sc(\eta^1\text{-}C_3H_5)(\eta^3\text{-}C_3H_5)_2(THF)_2]$	η^1-C_3H_5: Sc-C = 2.373(4) η^3-C_3H_5: Sc-C = 2.434(4), 2.479(4), 2.557(4), 2.493(4), 2.485(4), 2.447(4)	^{1}H, ^{13}C	63
$37''_{Sc}$	$[Sc(\eta^3\text{-}C_3H_5)_3]$	–	–	63,64
38_{Ho}	$\{[1,3\text{-}(SiMe_3)_2C_3H_3]Ho[CH(SiMe_3)CHCHSiMe_2\text{-}\mu\text{-}CH_2]\}_2$	Ho-C = 2.603(4), 2.617(4), 2.510(4)	–	66
39_{Ho}	$\{(THF)Ho[CH(SiMe_3)CHCHSiMe_2\text{-}\mu\text{-}CH_2]\}_2[\mu\text{-}\eta^1,\eta^3\text{-}C(SiMe_3)CHCHSiMe_3]$	Ho-C = 2.564(5), 2.645(5), 2.500(5)	–	66
40_{Dy}, 40_{Ho}, 40_{Er}, 40_{Tm},40_{Lu}	$Ln[1,3\text{-}(SiMe_3)_2C_3H_3]_3$ (Ln = Dy, Ho, Er, Tm, Lu)	Tm-C = 2.326(2) to 2.606(2)	–	67
41_{Ho}	$[Ho[1,3\text{-}(SiMe_3)_2C_3H_3]_3I]^-[Li(THF)_4]^+$	–	–	67
42_{Sc}	$Sc[1,3\text{-}(SiMe_3)_2C_3H_3]_3$	Sc-C = 2.38(3) average distance	^{1}H	70
43_Y, 43_{La}, 43_{Nd}	$[Ln(\eta^3\text{-}C_3H_5)_2(THF)_3]^+[B(C_6F_5)_4]^-$ (Ln = Y, La, Nd)	–	^{1}H, ^{13}C, ^{11}B, ^{19}F	6
$43'_Y$, $43'_{La}$, $43'_{Ce}$, $43'_{Pr}$, $43'_{Nd}$	$[Ln(\eta^3\text{-}C_3H_5)_2(THF)_3]^+[BPh_4]^-$ (Ln = Y, La, Ce, Pr, Nd)	Y-C = 2.617(3), 2.597(3), 2.515(3), 2.584(3), 2.608(3), 2.593(3) La-C = 2.783(4), 2.757(4), 2.711(4), 2.753(4), 2.798(4), 2.772(4) Nd-C = 2.704(17), 2.747(16), 2.725(16), 2.689(18), 2.691(18), 2.729(17)	^{1}H ^{13}C (**$43'_{La}$**, **$43'_{Ce}$**, **$43'_{Pr}$**, **$43'_{Nd}$**) ^{11}B (**$43'_{La}$**, **$43'_{Ce}$**, **$43'_{Pr}$**, **$43'_{Nd}$**)	6
$43''_Y$, $43'''_Y$, $43'''_{La}$	$[Ln(\eta^3\text{-}C_3H_5)_2(THF)_3]^+[ER_3(\eta^1\text{-allyl})]^-$ (E = Al, Ln = Y; E = B, Ln = Y, La)	–	^{1}H, ^{13}C, ^{27}Al (**$43''_Y$**) ^{11}B (**$43'''_Y$**, **$43'''_{La}$**)	6
44_{La}	$[La\{OCPh_2(CH_2CH{=}CH_2)\}_2(THF)_3]^+[BPh_4]^-$	–	^{1}H, ^{13}C, ^{11}B	6
$43'_{Sc}$, $43''_{Sc}$, 43_{Sc}	$[Sc(\eta^3\text{-}C_3H_5)_2(THF)_3][B(C_6X_3Z_2)_4]$ (X = Z = H; X = H, Z = Cl; X = Z = F)	**$43'_{Sc}$**: Sc-C = 2.5071(16), 2.4662(16), 2.4117(16), 2.3854(16), 2.474(2), 2.486(6), 2.5870(17)	^{1}H (**$43'_{Sc}$**)	63
45_{La}, 45_{Nd}	$[Ln(\eta^3\text{-}C_3H_5)(THF)_6]^{2+}[BPh_4]^-_2$ (Ln = La, Nd)	**45_{La}**: distorted structure	^{1}H, ^{13}C, ^{11}B	6
46_{Sc}	$K[Sc(C_3H_5)_4]$	–	^{1}H	63
$46'_{Sc}$	$[Ca(THF)_6][Sc(C_3H_5)_4]_2$	–	^{1}H, ^{13}C	63
$46''_{Sc}$	$[Mg(THF)_6][Sc(\eta^1\text{-}C_3H_5)_2(\eta^3\text{-}C_3H_5)_2]_2$	η^3-C_3H_5: Sc-C = 2.450(5), 2.436(6), 2.450(6); Sc-C = 2.488(5), 2.453(5), 2.424(5) η^1-C_3H_5: Sc-C = 2.271(5), 2.277(5)	^{1}H, ^{13}C	63
$46''_{Nd}$, $46''_{Sm}$	$\{[Mg(THF)_6][Ln(\eta^3\text{-}C_3H_5)_4]_2(THF)_2\}$	Sm-C = 2.761(5), 2.708(4), 2.648(4); 2.673(4), 2.712(5), 2.751(5); 2.739(5), 2.738(4), 2.734(4); 2.709(4), 2.736(4), 2.743(4)		62
47_{Sm}	$\{[Mg(THF)_6][Sm_2(\eta^3\text{-}C_3H_5)_6(\mu\text{-}\eta^3{:}\eta^3\text{-}C_3H_5)]_2(toluene)\}$	Bridging allyl: Sm(1)-C = 2.793(6), 2.762(6), 2.977(6); Sm(2)-C = 2.774(6), 2.765(6), 2.972(6) η^3-allyl: Sm(1)-C = 2.675(5), 2.700(5), 2.680(5); 2.725(5), 2.710(5), 2.651(5); 2.713(5), 2.701(5), 2.623(5); Sm(2)-C = 2.699(5), 2.712(5); 2.712(5); 2.655(5), 2.717(5), 2.712(6); 2.632(5), 2.691(5), 2.673(5)	–	62

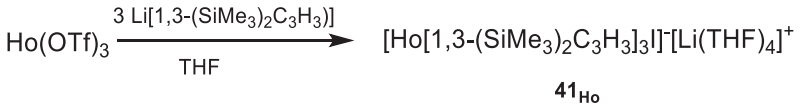

Scheme 20 Synthesis of tetra-[(bistrimethylsilyl)allyl] "ate" complex $\mathbf{41_{Ho}}$ starting from the lithium allyl reagent.

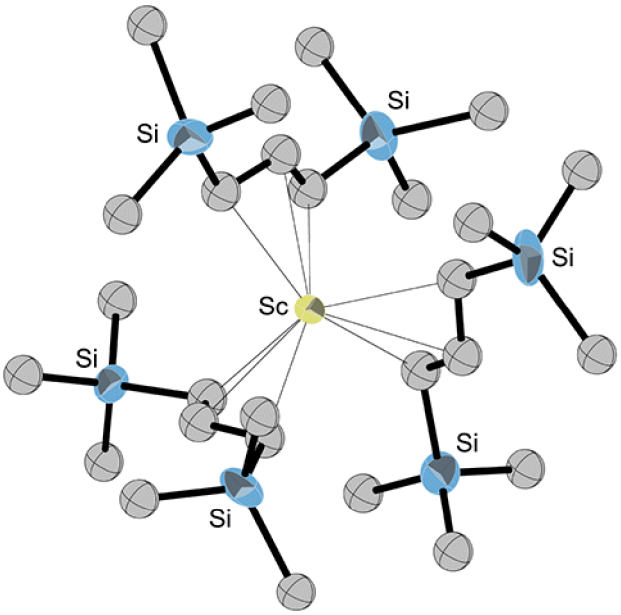

Fig. 27 Molecular structure of $\mathbf{42_{Sc}}$ with the thermal ellipsoids drawn at the 50% probability level, hydrogen atoms are excluded for clarity. Reprinted from Rightmire, N. R.; Hanusa, T. P.; Rheingold, A. L. *Organometallics* **2014**, *33*, 5952–5955, with the authorization of the American Society of Chemistry.

3.1.3 Bis-allyl cationic complexes

The lanthanum and the neodymium $[Ln(allyl)_2][B(C_6F_5)_4]$ ionic pairs were briefly described and assessed as single-component catalysts for butadiene polymerization in 1999.[71] It is however a decade later that Okuda and co-workers reported the full synthesis of a series of mono-cationic bis-allyl complexes $[Ln(\eta^3\text{-}C_3H_5)_2(THF)_3]^+[B(C_6F_5)_4]^-$ ($\mathbf{43_{Ln}}$, Ln = Y, La, Nd), by reacting the tris-allyl complexes $Ln(\eta^3\text{-}C_3H_5)_3(diox)$, described by Taube, with one equivalent of $[HNMe_2Ph][B(C_6F_5)_4]$ in THF (Scheme 21).[6] The mono-cationic bis-allyl analogs, bearing a non-perfluorinated counteranion $[Ln(\eta^3\text{-}C_3H_5)_2(THF)_3]^+[BPh_4]^-$ ($\mathbf{43'_{Ln}}$, Ln = Y, La, Nd) were prepared similarly using $[HNEt_3][BPh_4]$.

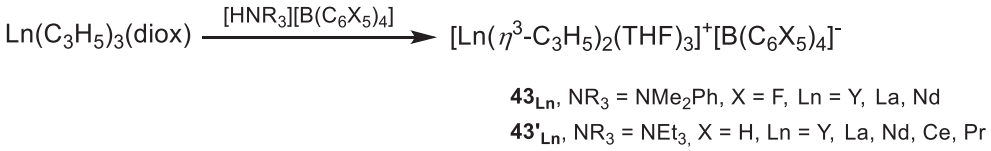

Scheme 21 Synthesis of ionic pairs $\mathbf{43_{Ln}}$ and $\mathbf{43'_{Ln}}$ by protonation of the tris-allyl precursors with ammonium borates.

An X-ray crystal study of the mono-cationic yttrium complex $\mathbf{43'_Y}$ showed that all three allyl ligands are η^3-coordinated with similar bond lengths between each allyl ligand and yttrium metal (Fig. 28). The neodymium and lanthanum analogs (the cerium and praseodymium complexes were not analyzed) were found to contain a fourth THF molecule. Shorter metal-allyl bonds were noticed in these complexes by comparison with the neutral tris-allyl parent complexes, revealing a higher Lewis acidity of the rare earth metal from neutral to cationic species.

The ^{1}H NMR analysis of both yttrium complexes $\mathbf{43_Y}$ and $\mathbf{43'_Y}$ displayed two signals (1H/4H relative ratio) for the allyl group, corresponding to fast *syn*/*anti* exchange on the NMR timescale. In contrast, three distinct signals were seen for the lanthanum and neodymium ones, typical of slow *syn*/*anti* exchange.

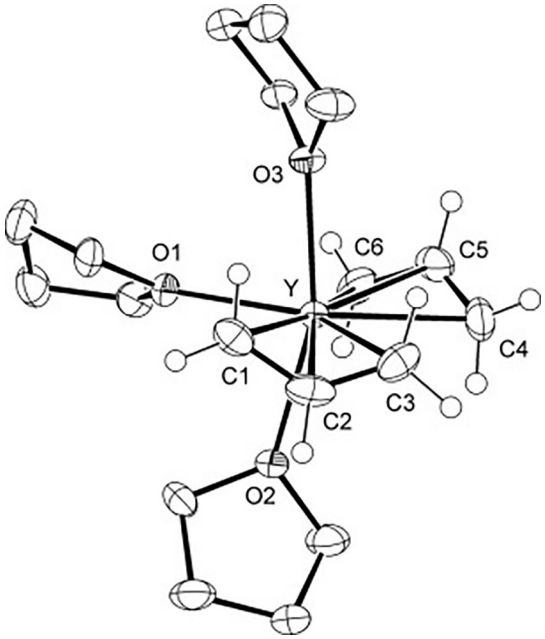

Fig. 28 Molecular structure of **43′$_Y$** with displacement ellipsoids set at the 50% probability level (the counter-anion and hydrogen atoms are omitted for the sake of clarity). Reprinted from Robert, D.; Abinet, E.; Spaniol, T. P.; Okuda, J. *Chem. Eur. J.* **2009**, *15*, 11937–11947, with permission of WILEY-VCH Verlag GmbH.

Upon reaction of the tris-allyl precursors with a Lewis acid ER_3 ($Al(CH_2SiMe_3)_3$ or BPh_3), allyl abstraction took place, affording the ion pair $[Ln(\eta^3\text{-}C_3H_5)_2(THF)_3]^+[ER_3(\eta^1\text{-allyl})]^-$ (**43″$_Y$**, E = Al, Ln = Y; **43‴$_{Ln}$**, E = B, Ln = Y, La), where the abstracted allyl group is found η^1-coordinated to the E element (Scheme 22).

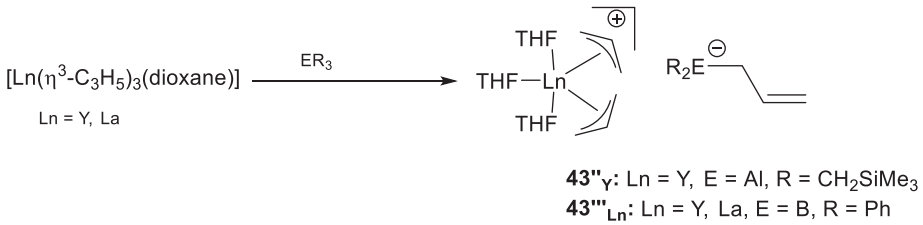

Scheme 22 Synthesis of ionic pairs **43″$_Y$** and **43‴$_{Ln}$** by allyl abstraction with a Lewis acid.

Interestingly, it was found that benzophenone inserts into the La-C(allyl) bond of **43′$_{La}$** to form the bis(alkoxy) complex $[La\{OCPh_2(CH_2CH{=}CH_2)\}_2(THF)_3]^+[BPh_4]^-$ (**44$_{La}$**). It is noteworthy that, however, the yttrium derivative **43′$_Y$** failed to react under the same conditions.

The bis-allyl cation $[Sc(\eta^3\text{-}C_3H_5)_2(THF)_3]^+$ was isolated 2 years after the other lanthanide counterparts, upon protonation of the tris-allyl scandium **37′$_{Sc}$** with a Brønsted acid similarly as shown in Scheme 21. Depending on the acid reagent, three ionic pairs of formula $[Sc(\eta^3\text{-}C_3H_5)_2(THF)_3]^+[B(C_6X_3Z_2)_4]^-$ (**43′$_{Sc}$**: X = Z = H; **43″$_{Sc}$**: X = H, Z = Cl; **43$_{Sc}$**: X = Z = F) could be isolated. The X-ray structure of **43′$_{Sc}$** showed that the allyl ligands are η^3-coordinated. The ^{1}H NMR analysis indicated dynamic behavior of the allyl ligand.[63] This cationic complex was also isolated by the reaction of two equiv. of Brønsted acid with tetraanionic $K[Sc(C_3H_5)_4]$ (*vide supra*).

The bis-allyl mono-cationic complexes **43$_{Ln}$** were found to be active toward the polymerization of 1,3-butadiene when combined with $Al(^iBu)_3$ as co-catalyst.[6,63] Among the resulting catalytic combinations, the yttrium catalyst was found to be the most active (TOF 10,000 h^{-1}) leading to the formation of polybutadiene (PB) with the highest 1,4-*cis* stereoregularity of 90% in rare contradiction of the well-known "neodymium effect," where neodymium exhibits the best performances along the rare earths family for this kind of polymerization catalysis.[12] The addition of one extra equivalent of $[NPhMe_2H][B(C_6F_5)_4]$ to the mono-cationic **43$_Y$**/$Al(^iBu)_3$ catalyst system in the butadiene polymerization mixture led to an increase in both the activity (up to TOF—12,000 h^{-1}) and the selectivity (92.5% of 1,4-*cis* PB). The *in situ* formation of mono-allyl di-cationic species was likely to be responsible for the better reactivity according to the authors.[6] In the case of scandium, the complex displayed low activity (TOF 95 h^{-1}) in styrene polymerization to afford atactic PS, with little improvement when $[HNMe_2Ph][B(C_6F_5)_4]$ was added in the reaction mixture.[63]

3.1.4 Mono-allyl dicationic complexes

The first examples of mono-allyl di-cationic complexes of the early lanthanides La and Nd $[Ln(\eta^3\text{-}C_3H_5)(THF)_6]^{2+}[BPh_4]_2^-$ [**45$_{Ln}$**] could be prepared by protonation of their tris-allyl precursors with two equivalents of $[HNEt_3][BPh_4]$. The same products were isolated from the single protonation of the mono(allyl) cationic complexes **43′$_{Ln}$** with one equivalent of acid (Scheme 23).[6]

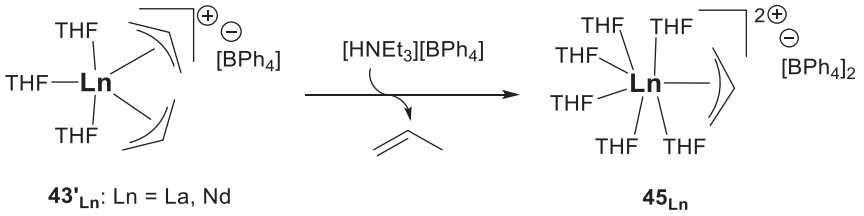

Scheme 23 Protonation of the mono-cationic precursors **43′$_{Ln}$** with ammonium borates leading to di-cationic **45$_{Ln}$** complexes.

X-ray quality crystals were obtained for the lanthanum complex [**45$_{La}$**], where a distorted pentagonal-bipyramidal coordination geometry was observed, with the remaining allyl group occupying the axial position.

Slow reaction with pyridine indicated a rather inertness of the remaining allyl group in these di-cationic **45$_{Ln}$** ion pairs (Ln = La, Nd), in contrast to what was expected from the reactivity observed in butadiene polymerization where the *in situ* formation of similar species was postulated (*vide infra*).

3.1.5 Tetra-allyl anionic complexes

When $[Sc(C_3H_5)_3(THF)_2]$ [**37′$_{Sc}$**] was treated with one equivalent of allylpotassium, the "ate" complex $K[Sc(C_3H_5)_4]$ [**46$_{Sc}$**] was obtained, which could also be synthesized directly by treating $ScCl_3$ with four equivalents of allylpotassium (Scheme 24). The ^{1}H NMR spectrum of this complex shows a doublet and a quintet for the allyl groups, indicating fluxional behavior of the allyl moiety in solution.[63]

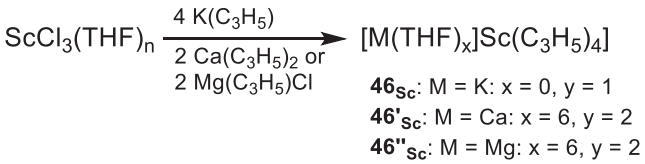

Scheme 24 Synthesis of tetra-allyl ionic scandium complexes.

When $ScCl_3$ was treated with two equivalents of bis(allyl)calcium, $[Ca(THF)_6][Sc(C_3H_5)_4]_2$ [**46′$_{Sc}$**] was obtained, while the reaction of $ScCl_3$ with two equivalents of (allyl)MgCl afforded X-ray quality crystals of the adduct $[Mg(THF)_6][Sc(C_3H_5)_4]_2$ [**46″$_{Sc}$**]. In this latter complex, two allyl ligands are found η^1- and the two others are η^3-coordinated to the scandium center (Fig. 29).

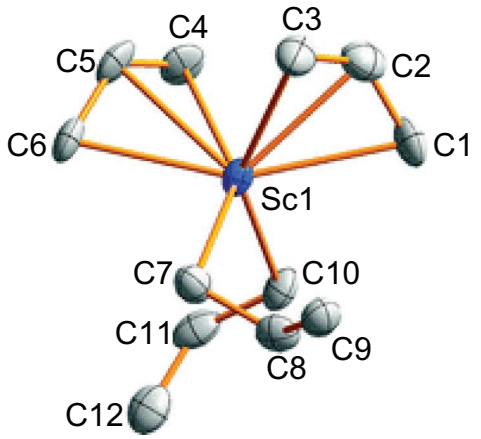

Fig. 29 Molecular structure of **46″$_{Sc}$**. The cationic counter-cation and hydrogen atoms are omitted for clarity. Thermal ellipsoids drawn at the 50% probability level. Reprinted from Standfuss, S.; Abinet, E.; Spaniol, T. P.; Okuda J. *Chem. Commun.* **2011**, *47*, 11441–11443, with the authorization of the Royal Society of Chemistry.

Tetra-allyl ionic compounds of the larger lanthanides were prepared some years before these scandium derivatives.[62] The heterobimetallic trinuclear $\{[Mg(THF)_6][Nd(\eta^3\text{-}C_3H_5)_4]_2(THF)_2\}$ [**46″$_{Nd}$**] was isolated from the room temperature reaction between $NdI_3(THF)_{3.5}$ and 3 equiv. of (allyl)MgI in a THF/dioxane mixture. On the other hand, under the same experimental conditions, the tetra-allyl samarium complex was first isolated as $\{[Mg(THF)_6][Sm_2(\eta^3\text{-}C_3H_5)_6(\mu\text{-}\eta^3\text{:}\eta^3\text{-}C_3H_5)]_2(toluene)\}$ [**47$_{Sm}$**],

which yielded {[Mg(THF)$_6$][Sm(η^3-C$_3$H$_5$)$_4$]$_2$(THF)$_2$} [**46″$_{Sm}$**] after reaction in hot THF with the diketimine ArN=C(Me)CH=C(Me)NHAr (Ar = 2,6-C$_6$H$_3^i$Pr$_2$), along with the previously reported allyl(diketiminate)Sm(η^3-C$_3$H$_5$)$_2${HC-(MeCNAr)$_2$}[5] and the known Sm(η^3-C$_3$H$_5$)$_3$.

X-ray crystal analysis of **47$_{Sm}$** showed a binuclear anion [Sm$_2$(η^3-C$_3$H$_5$)$_7$]$^-$ that involves two samarium centers in distorted tetrahedral arrangements, with three terminal and one bridging η^3-allyl ligand (Fig. 30). The X-Ray structure of **46″$_{Nd}$** was also elucidated, featuring the tetra-allyl anion [Nd(η^3-C$_3$H$_5$)$_4$]$^-$ of the type already discussed in details by Taube in [Li(dioxane)$_{1.5}$][Ln(η^3-C$_3$H$_5$)$_4$] (Ln = La, Nd).[3]

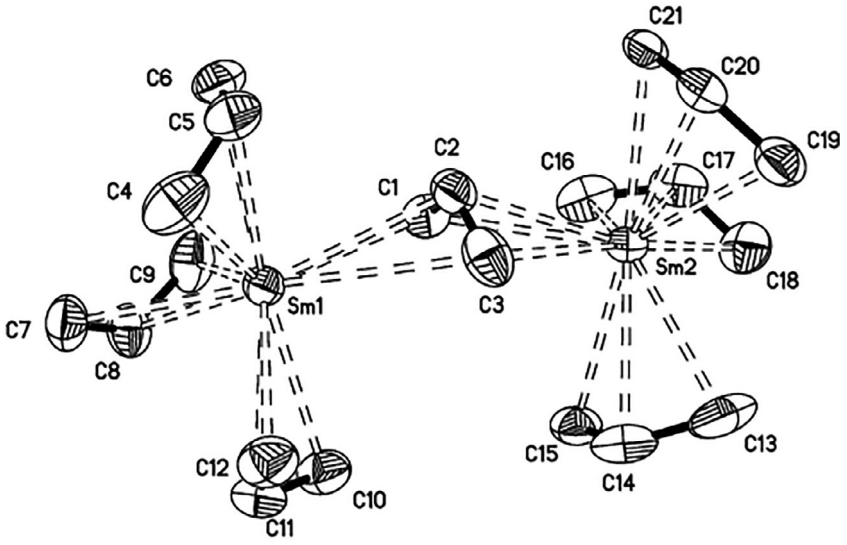

Fig. 30 X-ray molecular structure of **47$_{Sm}$**. The cationic Mg counter-cation and hydrogen atoms are omitted for clarity. Thermal ellipsoids drawn at the 50% probability level. Reprinted from Sanchez-Barba, L. F., Hughes, D. L., Humphrey, S. M., Bochmann, M. *Organometallics* **2005**, *24*, 5329–5334, with the authorization of the American Chemical Society.

3.2 Mono-substituted bis-allyl complexes: (Allyl)$_2$LnX compounds

3.2.1 (Allyl)$_2$LnX compounds with halide ligand

In 2006, Carpentier and coworkers extended the family of heterobimetallic bis-allyl derivatives of formula Ln(allyl)$_2$Cl(MgCl$_2$)$_2$(THF)$_4$ to Ln = Y and La [**48$_{Ln}$**], after the pioneering synthesis of their neodymium congener by Porri and coworkers.[72] All complexes were synthesized from LnCl$_3$(THF)$_n$ and (allyl)MgCl in THF (Scheme 25). Two sets of broadened resonances for two inequivalent allyl groups were observed by ^{1}H NMR spectroscopy.[73]

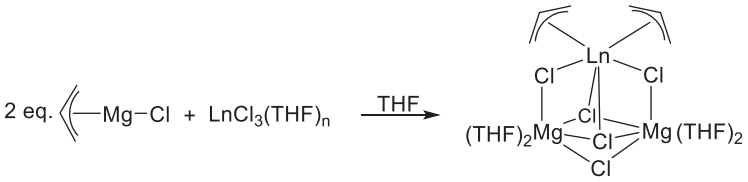

48$_{Ln}$ (Ln = Y, La)

Scheme 25 Synthesis of mixed chloro-bis(allyl) complexes **48$_{Ln}$**.

All three complexes (Nd, Y, La) were assessed as precatalysts toward isoprene polymerization, they were found to be active only when activated with an alkylaluminum or MAO, along with good control over macromolecular data. The Nd(allyl)$_2$Cl(MgCl$_2$)$_2$(THF)$_4$/MAO combination gave high 1,4-*cis* selectivity (>96%) along with high activity (TOF up to 50,000 h^{-1}). Reversal in stereoregularity was observed with **48$_Y$** when this bis-allyl derivative was associated with AlEt$_3$ or Al*i*Bu$_3$, affording PI with up to 91% 1,4-*trans* content (TOF *ca.* 100 h^{-1}), while MAO as co-catalyst lead to 75% 1,4-*cis* PI.

3.2.2 (Allyl)$_2$LnX compounds with amide and related N-donor ligands

The preparation and characterization of a series of neutral solvent-free bis(allyl) rare-earth metal complexes [Ln(Me$_3$TACD)(η^3-C$_3$H$_5$)$_2$] (**49$_{Ln}$**, Ln = Y, La, Ce, Pr, Nd, Sm) supported by the 1,4,7-trimethyl-1,4,7,10-tetraazacyclododecane anion (Me$_3$TACD$^-$) have been reported by Okuda and coworkers.[74] These complexes were synthesized by the clean reaction of the proligand (Me$_3$TACD)H with the tris(allyl) [Ln(η^3-C$_3$H$_5$)$_3$(diox)] precursors (Scheme 26).

X-ray diffraction studies on single crystals of the complexes **49$_{Ln}$** (Ln = Y, La, Pr, and Sm) show similar arrangement around the metal center, which can be described as a square antiprism formed by the nitrogen atoms of the ligand and the terminal carbon

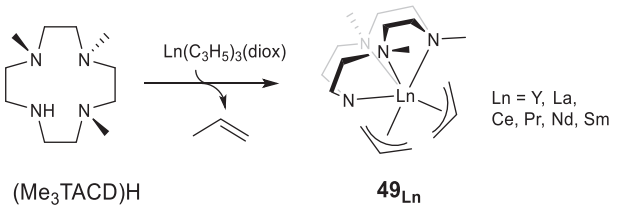

Scheme 26 Synthesis of mixed amido-bis(allyl) complexes **49$_{Ln}$** by reaction of the tris(allyl) derivatives with (Me_3TACD)H.

atoms of both allyl ligands. ^{1}H NMR investigations in solution of **49$_{La}$**, conducted in the temperature range −80 °C to +80 °C, established that the allyl ligands retain the η^3-binding mode on the NMR timescale.

Upon treatment with Brønsted acids, the series of monocationic mono-allyl complexes [Ln(Me_3TACD)(η^3-C_3H_5)(THF)$_2$][B(C_6X_5)$_4$] (**50$_{La}$**, X = F; **50′$_{Ln}$**, Ln = La, Ce, Nd, X = H) were isolated and characterized (Scheme 27).

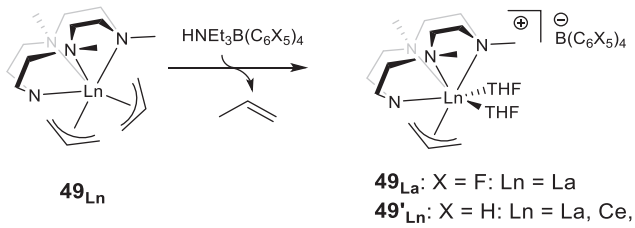

Scheme 27 Synthesis of mixed amido-mono(allyl) ionic complexes **50$_{Ln}$** and **50′$_{Ln}$** by reaction of the bis(allyl) precursors **49$_{Ln}$** with Bronsted acids.

The cerium compound **50′$_{Ce}$** was found to crystallize as a separated ion pair without close interactions between the cation and anion. The comparison of the structural parameters (distances and angles) in neutral [Ce(Me_3TACD)(η^3-C_3H_5)$_2$] [**50$_{Ce}$**] and cationic [Ce(Me_3TACD)(η^3-C_3H_5)(THF)$_2$][B(C_6X_5)$_4$] [**50′$_{Ce}$**] compounds in the solid state did not reveal significant difference, in relation with the higher Lewis acidity of the metal center in the cationic cerium analog, as same as already observed when comparing the pure allyl Ce(η^3-C_3H_5)$_3$(THF)$_3$ and [Ce(η^3-C_3H_5)$_2$(THF)$_4$][BPh_4] derivatives.[6]

Hydrogenolysis of **49$_{Ln}$** with H_2 afforded the hydride complexes [Ln(Me_3TACD)H_2]$_n$ (Ln = Y, La, Sm, n = 3–4), which crystallize under a tetrameric form for the lanthanum complex (Scheme 28). Allyl complexes of the lighter lanthanides can therefore be considered as a valuable alternative to the commonly used alkyl precursors for the synthesis of hydrido compounds.

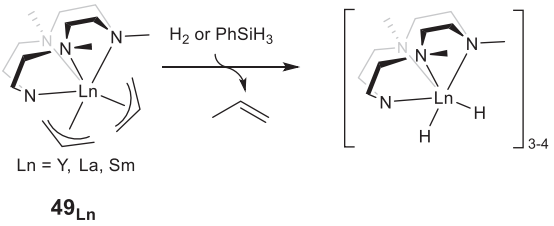

Scheme 28 Hydrogenolysis of mixed amido-(allyl) **49$_{Ln}$** affording the Me_3TACD-supported dihydride complexes.

Further reactivity studies of mixed amido-bis(allyl) complexes **49$_{Ln}$** toward furan derivatives were reported in the same article, i.e. hydrosilylation of furfural and hydrodeoxygenation of furan and 2-methylfuran. The active species was proposed to be the dihydride complex formed by hydrogenation of the neutral bis(allyl) moiety.[6]

3.2.3 (Allyl)$_2$LnX compounds with cyclopentadienyl/indenyl ligands

The half-sandwich bis-allyl scandium complexes ($C_5Me_4SiMe_3$)Sc(η^3-C_3H_5)$_2$ [**51$_{Sc}$**], (C_5Me_5)Sc(η^3-C_3H_5)$_2$ [**52$_{Sc}$**] and (C_5Me_5)Sc(η^3-2-MeC_3H_4)$_2$ [**53$_{Sc}$**] were synthesized in 2008 by Hou and coworkers from the straightforward reaction of $ScCl_3$ with the cyclopentadienyl lithium derivatives and allyl magnesium chlorides, as described in Scheme 29 for complex **51$_{Sc}$**.[75]

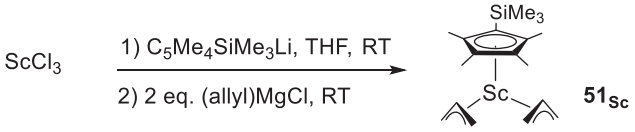

Scheme 29 Synthesis of half-sandwich bis(allyl) scandium complex **51$_{Sc}$**.

All three scandium complexes were isolated as base-free and were structurally characterized. They displayed similar characteristics in the solid state, but whereas one allyl ligand is found prone and the other supine in the two C_5Me_5 complexes $\mathbf{52}_{Sc}$ and $\mathbf{53}_{Sc}$, the two allyl groups are all prone in $\mathbf{51}_{Sc}$ (Fig. 31). All three complexes were found to be fluxional in solution from ^{1}H NMR studies in deuterated toluene, the two allyl units being non-equivalent at very low temperature (−80 °C).

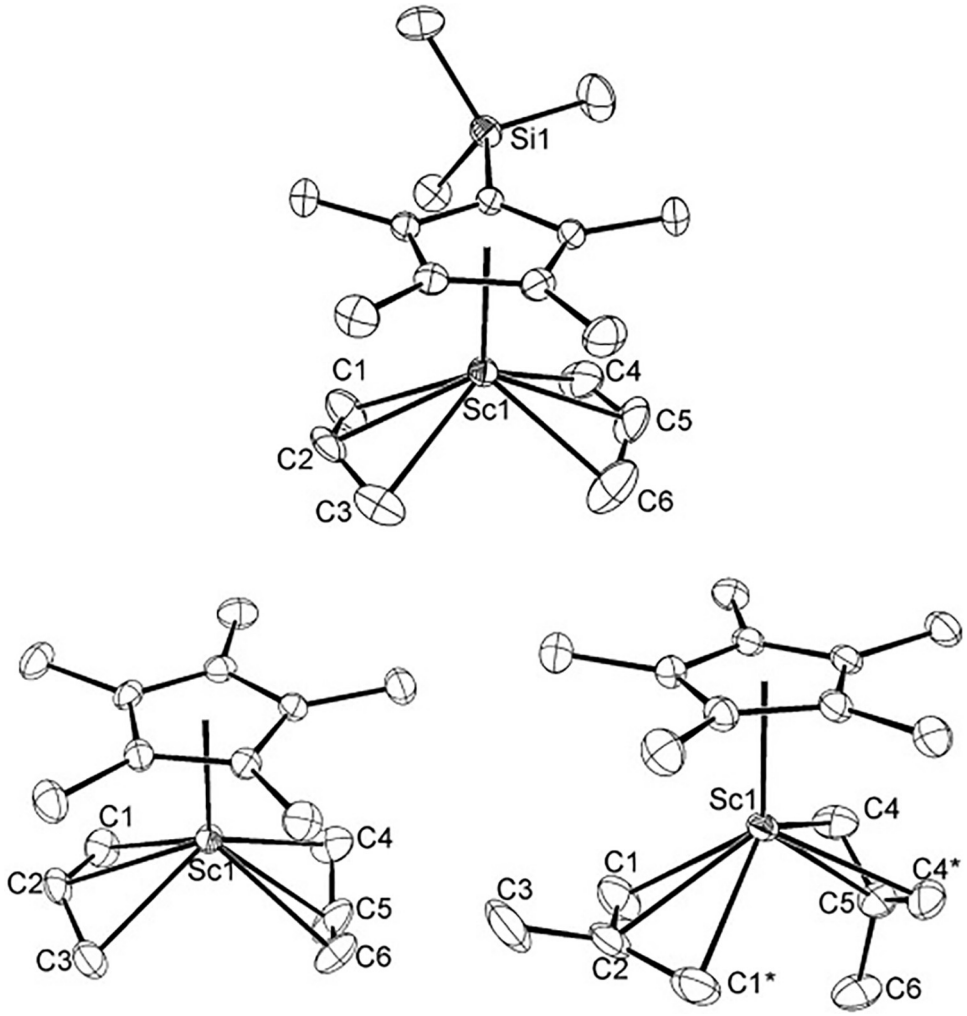

Fig. 31 ORTEP drawings of $\mathbf{51}_{Sc}$ (left) and of $\mathbf{52}_{Sc}$ (right). Displacement ellipsoids are set at the 30% probability level and the hydrogen atoms are excluded for clarity. Reprinted from Yu, N; Nishiura, M.; Li, X.; Xi, Z.; Hou, Z. *Chem. Asian J.* **2008**, *3*, 1406–1414, with the permission of WILEY-VCH Verlag GmbH.

When combined with $[HNMe_2][B(C_6F_5)_4]$, the bis(allyl) derivative $\mathbf{51}_{Sc}$ was found to be active toward the polymerization of isoprene and its copolymerization with norbornene.[75]

One year later, the reaction of the neutral tris-allyl complexes $Ln(\eta^3\text{-}C_3H_5)_3(diox)$ (Ln = Y, La) with the proligand $HC_5Me_4SiMe_3$ was used by Okuda to cleanly prepare the half-sandwich bis(allyl) complexes $(C_5Me_4SiMe_3)Ln(\eta^3\text{-}C_3H_5)_2(THF)$ [$\mathbf{51'}_{Ln}$] with propene release (Scheme 30), where the allyl group was noted as fluxional by ^{1}H NMR analysis.[6]

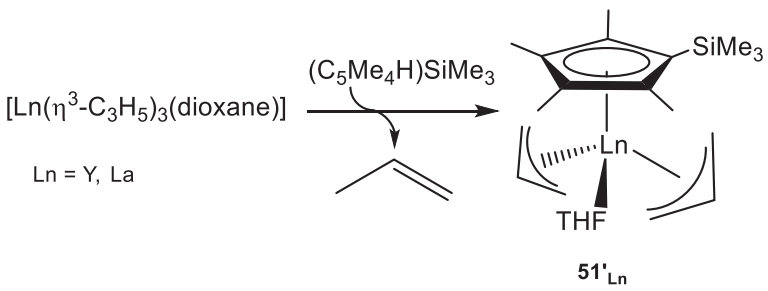

Scheme 30 Synthesis of half-sandwich bis(allyl) complexes $\mathbf{51'}_{Ln}$.

The syntheses of a series of rare earth bis(allyl) complexes with constrained geometry ($C_5Me_4C_6H_4$-*o*-NMe_2)Ln(η^3-C_3H_5)$_2$ (**54$_{Ln}$**, Ln = Y, Nd, Gd, Dy, Lu), ($C_5Me_4C_6H_4$-*o*-PPh_2)Ln(η^3-C_3H_5)$_2$ (**55$_{Ln}$**, Ln = Y, Gd), ($C_9H_6C_6H_4$-*o*-NMe_2)Ln(η^3-C_3H_5)$_2$ (**56$_{Ln}$**, Ln = Y, Dy), ($C_9H_6C_6H_4$-*o*-PPh_2)Ln(η^3-C_3H_5)$_2$ (**57$_{Ln}$**, Ln = Y, Gd) (Fig. 32) were mentioned in a patent in 2010.[76] Upon combination with an alkylaluminum reagent and an organic boron activator, all these complexes showed high catalytic performances in 1,4-*cis* selective polymerization of conjugated dienes (isoprene and butadiene) along with full conversion. The polymerization reaction displayed the characteristics of a living polymerization.

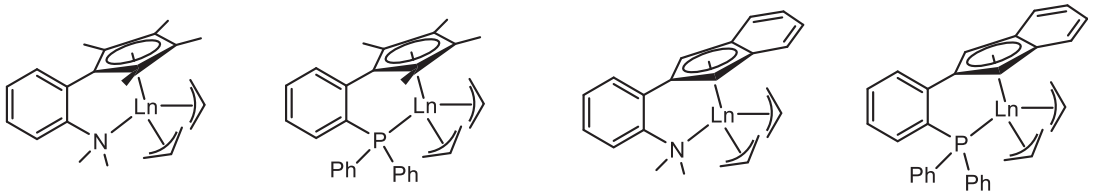

54$_{Ln}$ Ln = Y, Nd, Gd, Dy, Lu

55$_{Ln}$ Ln = Y, Gd

56$_{Ln}$ Ln = Y, Dy

57$_{Ln}$ Ln = Y, Gd

Fig. 32 Constrained geometry bis(allyl) complexes **54$_{Ln}$**, **55$_{Ln}$**, **56$_{Ln}$**, **57$_{Ln}$**.

The preparation of the lanthanide aminophenyl-Cp bis(allyl) complexes **54$_{Ln}$** (Ln = Y, Nd, Gd, Dy) was described in further details in a communication reported in 2010[77] and 2 years later in a full paper for the lutetium derivative,[78] by the sequential metathesis reactions of $LnCl_3$ with (C_5Me_4-C_6H_4-*o*-NMe_2)Li and (C_3H_5)MgCl (Scheme 31).

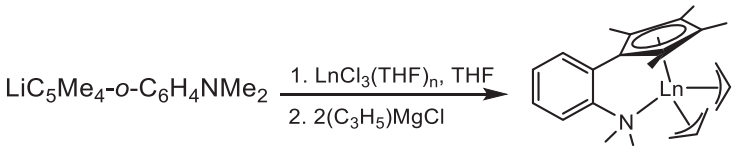

54$_{Ln}$
Ln = Y, Nd, Gd, Dy, Lu

Scheme 31 Synthesis of the aminophenyl-Cp bis(allyl) complexes **54$_{Ln}$**.

Thanks to ^{1}H NMR studies, the allyl group in the yttrium complex [**54$_Y$**] was found fluxional with the typical 1H/4H resonances. The yttrium, gadolinium, and dysprosium complexes (**54$_Y$**, **54$_{Gd}$**, **54$_{Dy}$**, respectively) were characterized by X-ray crystallography as solvent-free—even though the reaction was performed in THF solvent—isostructural complexes and it was shown that both allyl moieties coordinate in the η^3-mode. The molecular structure of the lutetium complex **54$_{Lu}$** was also later deduced from X-ray studies, in which both of the allyl groups, in the solid state as well as in solution, coordinated to the metal center in classical trihapto η^3-mode (Fig. 33). The coordination of the amino moiety corroborated the absence of additional solvent in the molecule.

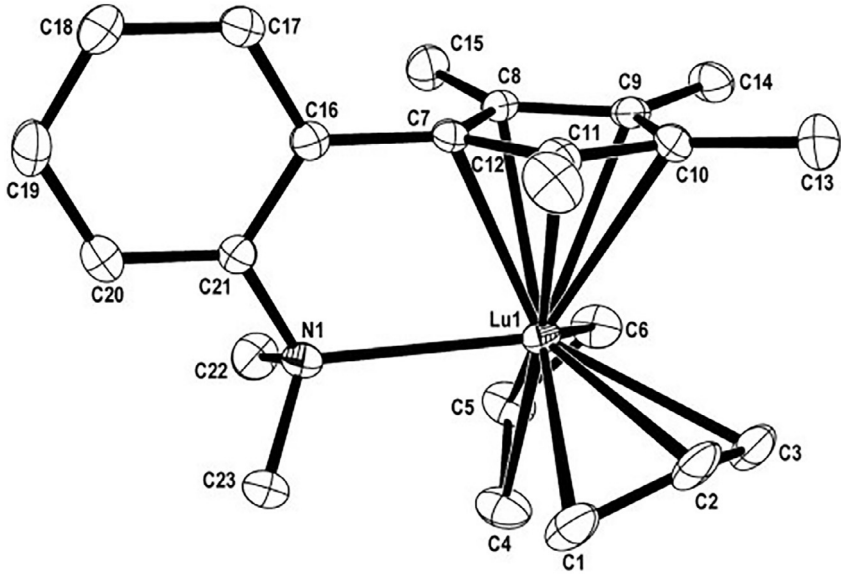

Fig. 33 ORTEP plot of **54$_{Lu}$**. Displacement ellipsoids are set at the 40% probability level and the hydrogen atoms are excluded for clarity. Reprinted from Jian, Z.; Cui, D.; Hou, Z. *Chem. Eur. J.* **2012**, *18*, 2674–2684, with the permission of WILEY-VCH Verlag GmbH.

The yttrium- and scandium–bis (allyl) complexes, $(C_5Me_4\text{-}C_5H_4N)Ln(\eta^3\text{-}C_3H_5)_2$ ($\mathbf{58_{Ln}}$, Ln = Y, Sc), which contained pyridyl-Cp, another electron-withdrawing ligand, were obtained following a similar two-step procedure as described in the same publication (Scheme 32, left).[78] A more-crowded environment in $\mathbf{54_{Lu}}$—due to this aminophenyl-Cp—than in the pyridyl-Cp lutetium bis(allyl) complex $(C_5Me_4\text{-}C_5H_4N)Lu(\eta^3\text{-}C_3H_5)_2$ ($\mathbf{58_{Lu}}$), which was published separately,[79] was advanced to explain the lower reactivity of the former complex (see further).

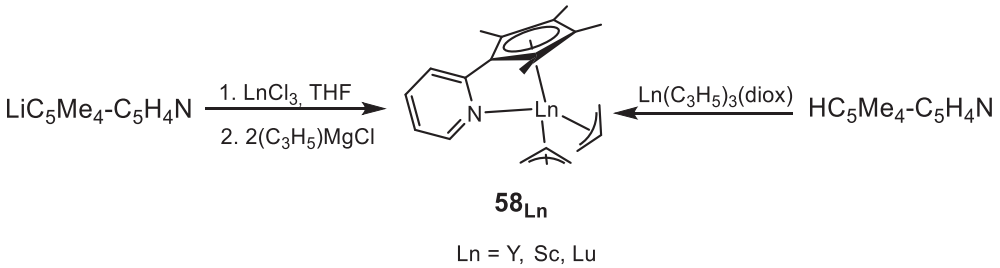

Scheme 32 Two synthetic approaches for the preparation of complexes $\mathbf{58_{Ln}}$.

Alternatively, these compounds $\mathbf{58_{Ln}}$ were prepared, including their lutetium congener, by protonolysis reaction of $Ln(allyl)_3(diox)$ with the proligand $HC_5Me_4\text{-}C_5H_4N$ (Scheme 32, right).[78,79] The ^{1}H NMR analysis of the yttrium complex $\mathbf{58_Y}$ suggested slow *syn/anti* exchange of the allylic protons, in contrast to what was observed in previously mentioned $\mathbf{54_Y}$[78] and $(C_5Me_4SiMe_3)Y(\eta^3\text{-}C_3H_5)_2(THF)$.[6] On the other hand, in the case of the scandium analog $\mathbf{58_{Sc}}$, only two allyl signals (1H/4H) were observed, as for its lutetium analog. All three complexes $\mathbf{58_{Ln}}$ (Ln = Y, Sc, Lu) displayed the same solvent-free monomeric arrangement in which the ligand generates a CGC configuration with the two allyl units bounded in η^3-fashion to the metal and one allyl group prone while the other supine (Fig. 34, only shown here for $\mathbf{58_{Lu}}$).[79]

Upon activation with $[Ph_3C][B(C_6F_5)_4]$, the electron withdrawing pyridine-Cp-based lutetium complex $\mathbf{58_{Lu}}$ afforded highly active catalyst toward butadiene polymerization (TOF 60,000 h^{-1}), which was also *cis*-1,4-selective, up to 97%. Moreover, the three $\mathbf{58_{Ln}}$ complexes in the same pyridine-Cp-based series (Y, Lu, Sc), in particular the scandium complex, exhibited outstanding activity (TOF 60,000 h^{-1}) for styrene polymerization, when combined with trityl borate as activator, to give perfectly syndiotactic polystyrene (*s*PS). As such, the scandium and the lutetium complexes in this series are among the rare examples of precatalysts having a dual ability in both syndiotactic styrene polymerization and *cis*-selective 1,3-diene polymerization.[80] In contrast, the

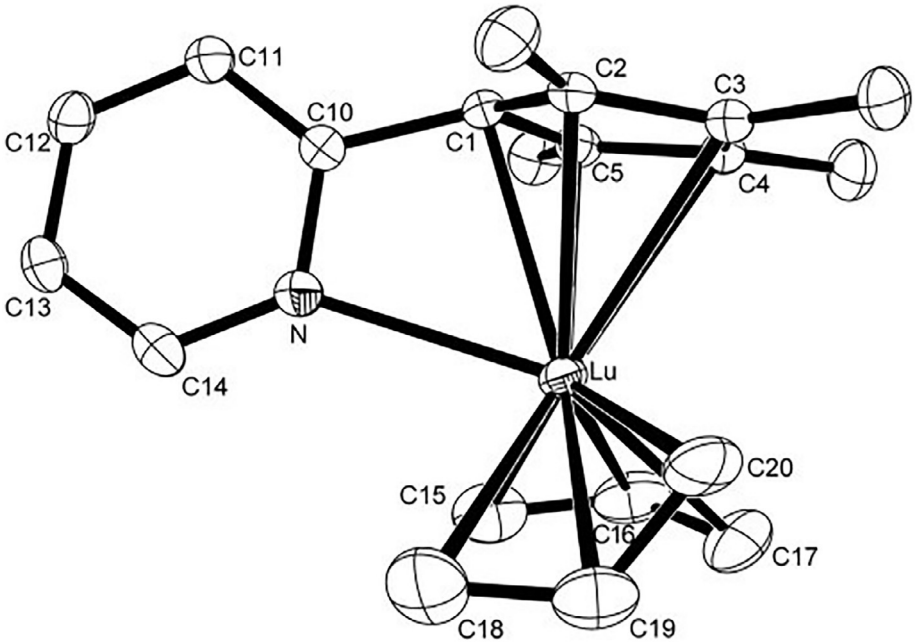

Fig. 34 ORTEP plot of constrained geometry Cp-Pyridyl bis(allyl) $\mathbf{58_{Lu}}$. Displacement ellipsoids are set at the 40% probability level and the hydrogen atoms are excluded for clarity. Reprinted from Jian, Z.; Tang, S; Cui, D. *Chem. Eur. J.* **2010**, *16*, 14007–14015, with the permission of WILEY-VCH Verlag GmbH.

amino-phenyl Cp yttrium and lutetium complexes (C_5Me_4-C_6H_4-*o*-NMe_2)Ln(η^3-C_3H_5)$_2$ **54$_{Ln}$** failed to polymerize styrene under the same conditions of activation. This result was explained in terms of bite angle, which hinders the coordination and insertion of the styrene monomer, while being more favorable for Cp-pyridine complexes.

In combination with tritylborate [Ph_3C][$B(C_6F_5)_4$], **58$_{Lu}$** afforded as well a highly active catalyst (TOF up to 5100 h^{-1}) for the statistical and the sequenced copolymerization of butadiene and styrene. Copolymers having highly *cis*-1,4-PB and syndiotactic PS segments, along with high molecular weight and narrow dispersity were obtained. Kinetic studies demonstrated that in the presence of a mixture of the two monomers butadiene was consumed first, followed by the growing of the syndiotactic PS sequence, finally affording diblock styrene-butadiene copolymers in all cases. The same kind of copolymer was isolated from sequenced butadiene/styrene copolymerization.[79]

The pyridine-cyclopentadienyl bis(allyl) complex ($C_5Me_4C_5H_4N$)Lu(η^3-C_3H_5)$_2$ (**58$_{Lu}$**) was also used as precatalyst for the copolymerization of isoprene with styrene, in combination with [Ph_3C][$B(C_6F_5)_4$].[81] The resulting Ip/St copolymers displayed multiblock microstructure with high *cis*-1,4-polyisoprene (PI) units (80%) and crystalline *s*PS sequences. The terpolymerization of styrene with isoprene and butadiene with the same catalytic combination gave unprecedented terpolymers that were composed of perfect *s*PS blocks, high *cis*-1,4-PI units and almost pure *cis*-1,4-PB sequences arranged in multiblock mode, with excellent control over the regio- and stereoregularity as well as the composition (Scheme 33).

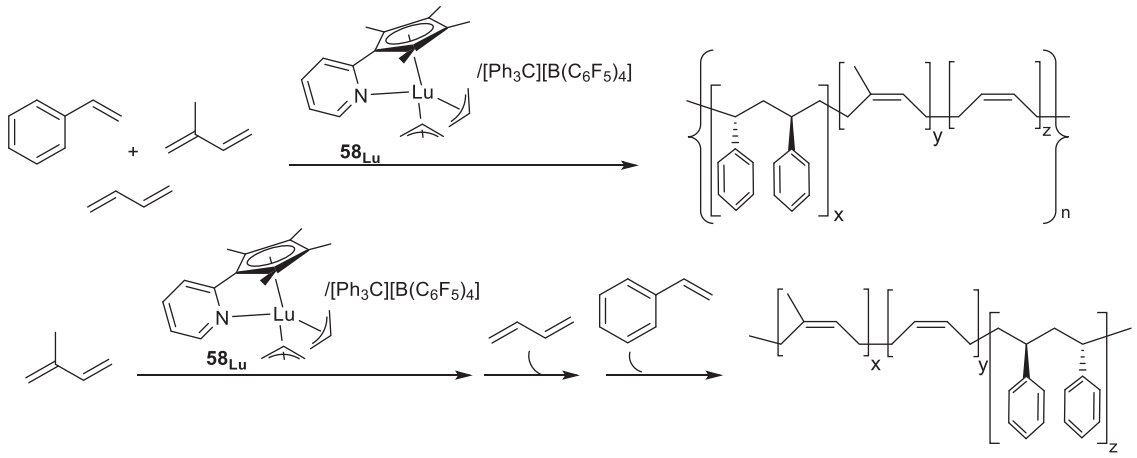

Scheme 33 Terpolymerization experiments performed with **58$_{Lu}$**-based catalyst.

The activity of the bis(allyl) complexes **54$_{Ln}$** (Ln = Y, Nd, Gd, Dy) was assessed toward the polymerization of isoprene in the presence of AlR_3 (mainly Al(^{i}Bu)$_3$) and [$PhMe_2NH$][$B(C_6F_5)_4$] in toluene at 20 °C. The neodymium complex had the highest activity (TOF 3000 h^{-1}). The gadolinium complex afforded the highest *cis*-1,4 regular PI at 99.2% (at 0 °C) along with the living character of the polymerization. It was observed that when the Al/Gd ratio was increased, a typical catalyzed chain growth (CCG) process was operating, with systematic decrease of the molecular weight of the PI while the molecular weight distribution remained unchanged. Again, upon activation with [Ph_3C][$B(C_6F_5)_4$]/Al(^{i}Bu)$_3$, (C_5Me_4–C_6H_4-*o*-NMe_2)Gd(η^3-C_3H_5)$_2$ (**54$_{Gd}$**) afforded, *via* sequential monomer addition of isoprene and butadiene, unprecedented *cis*-PI-*b*-*cis*-PB and *cis*-PI-*b*-*cis*-PB-*b*-*cis*-PI block copolymers. This was possible thanks to the living polymerization process occurring through reversible Gd/Al chain transfer.[77]

More recently, Anwander and coworkers synthesized the allyl half-sandwich complexes of the heavier lanthanides, Cp^{NMe2}Ln(η^3-C_3H_5)$_2$ (**59$_{Ln}$**, Ln = Y, Ho, Lu; Cp^{NMe2} = $C_5Me_4CH_2CH_2NMe_2$) having a more flexible N-functionalized cyclopentadienyl ligand than in the aminophenylCp complexes **54$_{Ln}$**.[82] The reaction was conducted in two steps by first reacting $LnCl_3(THF)_x$ with Cp^{NMe2}Li at room temperature, and then adding two equivalents of the Grignard reagent C_3H_5MgCl (Scheme 34).

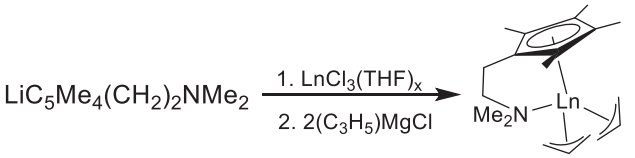

Ln = Y, Ho, Lu

59$_{Ln}$

Scheme 34 Synthesis of constrained-geometry allyl complexes **59$_{Ln}$**.

X-ray analysis showed that the three complexes were under a bis-allyl half-sandwich monomeric form and were all isostructural, in an overall arrangement similar to that found for complexes $\mathbf{54_{Ln}}$. One of the allyl groups showed similar bond lengths between terminal and central carbon atoms, while the second allyl group showed a significantly longer bond length between the rare earth metal and the terminal carbon. The ^{1}H NMR spectra of diamagnetic yttrium [$\mathbf{59_Y}$] and lutetium [$\mathbf{59_{Lu}}$] complexes showed the typical quintet (1H)/doublet (4H) set of signals characteristic of dynamic exchange of the allylic protons, along with splitting of the quintet in the case of the yttrium derivative, due to the coupling with ^{89}Y.

An [Allyl]/[Cl] exchange was observed when yttrium and holmium complexes reacted with $AlEt_2Cl$, leading to multi(μ-chlorido) hexametallic [Ln_6Cl_{12}] clusters, consistent with the absence of any reactivity toward isoprene polymerization when adding $AlEt_2Cl$. When activated with either [Ph_3C][$B(C_6F_5)_4$] or [$PhNMe_2H$][$B(C_6F_5)_4$] borates, only the lutetium half-sandwich displayed a noticeable activity (TOF 500 h^{-1}) toward the polymerization of isoprene, affording non stereo-regular PI. However, in the presence of 10 additional equiv. Al^iBu_3, all three $\mathbf{59_{Ln}}$-based catalysts displayed improved activity (TOF 1000–2000 h^{-1}). A decrease in the polymer molecular weights with narrow dispersities was also noticed, which indicated chain transfer to aluminum.

The pyrrolidine-functionalized half-sandwich complexes ($C_5Me_4SiMe_2NC_4H_8$)Ln(η^3-C_3H_5)$_2$ ($\mathbf{60_{Ln}}$, Ln = Sc, Y, Lu) were synthesized by Luo and coworkers by reacting $LnCl_3$ with one equivalent of $C_5Me_4SiMe_2$-NC_4H_8Li followed by the addition of two equivalents of (C_3H_5)MgCl in THF at room temperature (Scheme 35).[83]

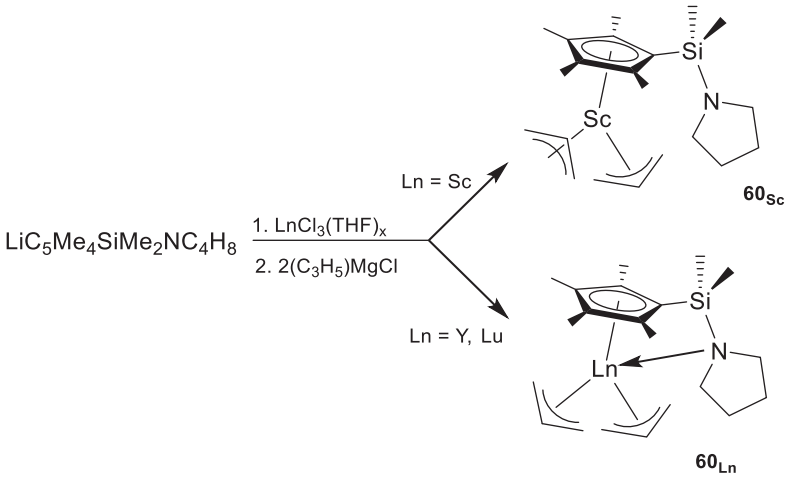

Scheme 35 Synthesis of half-sandwich allyl complexes $\mathbf{60_{Ln}}$.

The ^{1}H NMR spectra of the three $\mathbf{60_{Ln}}$ complexes indicated the fluxional allyl ligand in solution, with the typical doublet signal for the terminal allylic protons and one multiplet for the central allylic protons. X-ray analysis showed that the pendant pyrrolidine moiety coordinates to the metal center in the yttrium and lutetium complexes (Fig. 35, left), where this coordination is absent for the scandium complex due to smaller size of the scandium cation (Fig. 35, right).[65] In the three complexes, the two allyl moieties were coordinated to the central metal in an η^3-mode, but with one allyl group prone and the other supine in the case of the scandium complex.

The half-sandwich scandium complex $\mathbf{60_{Sc}}$ was found to be highly active toward styrene polymerization when activated with one equivalent of [Ph_3C][$B(C_6F_5)_4$], producing pure *s*PS at room temperature (TOF 250 h^{-1}). When Al(^{i}Bu)$_3$ was added in excess, the activity increased drastically (TOF 1500 h^{-1}). On the other hand, yttrium and lutetium complexes proved to be much less active.

3.3 Bis-substituted mono-allyl complexes: (Allyl)LnX_2 compounds

3.3.1 (Allyl)LnX_2 compounds with borohydride ligands

Recently, Fadlallah et al. synthesized the first lanthanide complexes bearing both allyl and borohydride ligands, Ln(BH_4)$_2$(η^3-C_3H_5)(THF)$_3$ ($\mathbf{61_{Ln}}$, Ln = Nd, Sm) from the reaction of the precursor Ln(BH_4)$_3$(THF)$_3$ with half an equivalent of Mg(C_3H_5)$_2$(L)$_n$ (L = THF, dioxane) at room temperature in THF solution.[84] This family of complexes, which are the counterparts of the $LnCl_2$(allyl)(THF)$_2$ in chloride series,[85] was a little later extended to yttrium, lanthanum and scandium, the latter being isolated as a bis-THF adduct (Scheme 36; Table 4).[86]

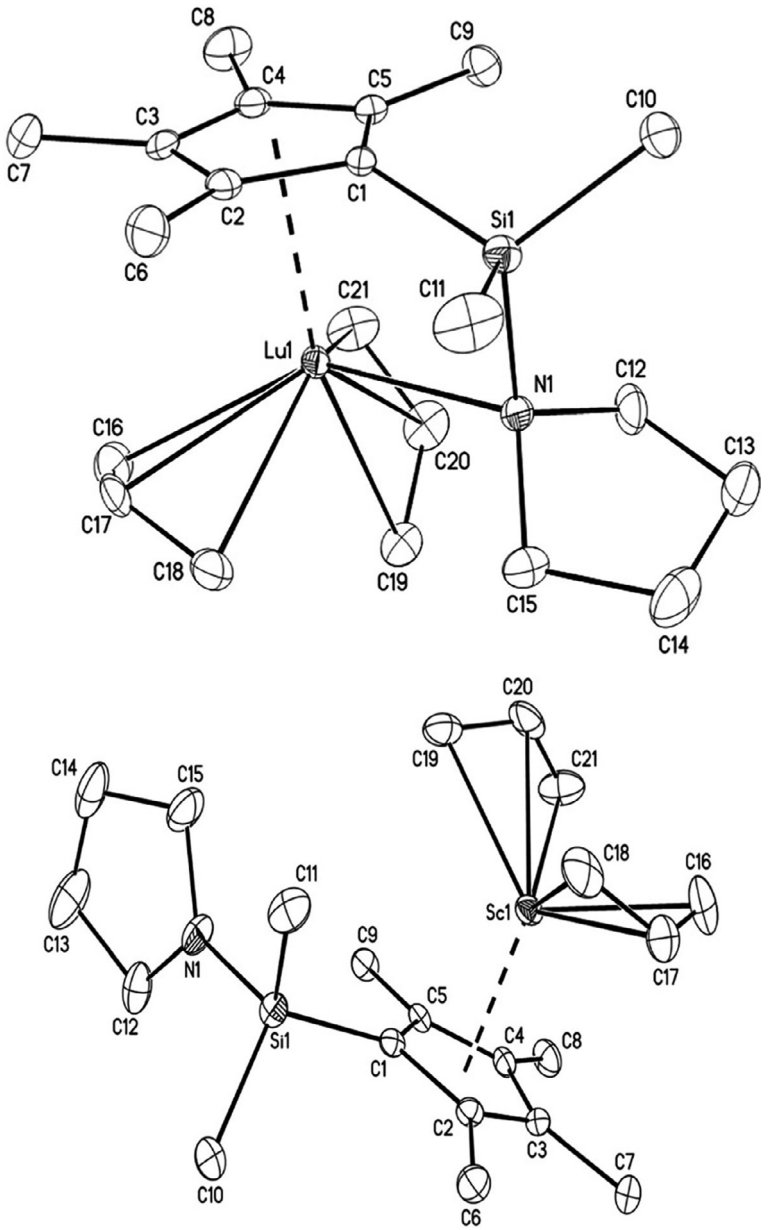

Fig. 35 ORTEP plot of $(C_5Me_4SiMe_2NC_4H_8)Ln(\eta^3\text{-}C_3H_5)_2$ (**60**$_{Ln}$, Ln = Lu, left and Sc, right). Thermal ellipsoids are drawn at the 10% probability level and the hydrogen atoms are excluded for clarity. Reprinted from Luo, Y.; Chi, S.; Chen, J. *New J. Chem.* **2013**, 37, 2675–2682, with the permission of the Royal Society of Chemistry.

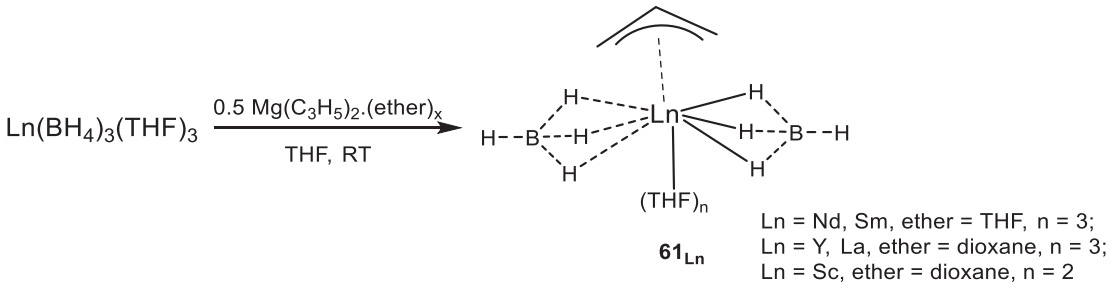

Scheme 36 Synthesis of mixed allyl-borohydride **61**$_{Ln}$ complexes.

Table 4 Structural and analytical data of monosubstituted bis(allyl) complexes (in brackets only the relevant complexes only, otherwise for all complexes).

Compound number	*Molecular formula*	*X-ray data* *Ln-C(allyl) distances (Å)*	*NMR data*	*References*
48$_{Y}$, 48$_{La}$	$Ln(allyl)_2Cl(MgCl_2)_2(THF)_4$ (Ln = Y, La)	–	^{1}H	73
49$_{Y}$, 49$_{La}$, 49$_{Ce}$, 49$_{Pr}$, 49$_{Nd}$, 49$_{Sm}$	$[Ln(Me_3TACD)(\eta^3\text{-}C_3H_5)_2]$ (Ln = Y, La, Ce, Pr, Nd, Sm)	Y-C = 2.641(3), 2.684(4)[a], 2.610(8)[a], 2.754(4); 2.740(3), 2.698(3), 2.697(3) La-C = 2.808(4), 2.859(4), 2.837(4); 2.791(4), 2.918(4), 2.887(4) Pr-C = 2.782(5), 2.751(7), 2.744(5); 2.824(14)[a], 2.83(2)[a] Sm-C = 2.743(3), 2.700(5), 1.337(4); 2.716(3), 2.779(9)[a], 2.758(15)[a]	^{1}H, ^{13}C	74
50$_{La}$, 50′$_{La}$, 50'$_{Ce}$, 50'$_{Nd}$	$[Ln(Me_3TACD)(\eta^3\text{-}C_3H_5)(THF)_2][B(C_6X_5)_4]$ (X = F, Ln = La; X = H, Ln = La, Ce, Nd)	Ce-C = 2.822(3), 2.816(3), 2.792(3)	^{1}H, ^{13}C	74
51$_{Sc}$	$(C_5Me_4SiMe_3)Sc(\eta^3\text{-}C_3H_5)_2$	**51$_{Sc}$:** Sc-C = 2.419(4) to 2.466(5)	^{1}H, ^{13}C	75
52$_{Sc}$	$(C_5Me_5)Sc(\eta^3\text{-}C_3H_5)_2$	**52$_{Sc}$:** Sc-C = 2.415(3) to 2.460(3)		
53$_{Sc}$	$(C_5Me_5)Sc(\eta^3\text{-}2\text{-}MeC_3H_4)_2$	**53$_{Sc}$:** Sc-C = 2.397(2) to 2.512(3)		
51′$_{Y}$, 51′$_{La}$	$Ln(C_5Me_4SiMe_3)(\eta^3\text{-}C_3H_5)_2(THF)$ (Ln = Y, La)	–	^{1}H, ^{13}C	6
54$_{Y}$, 54$_{Nd}$, 54$_{Gd}$, 54$_{Dy}$, 54$_{Lu}$	$(C_5Me_4\text{-}C_6H_4\text{-}o\text{-}NMe_2)Ln(\eta^3\text{-}C_3H_5)_2$ (Ln = Y, Nd, Gd, Dy, Lu)	Gd-C = 2.648(4), 2.674(4) Dy-C = 2.612(3), 2.637(3) Lu-C = 2.579(3), 2.582(3) (average distances)	^{1}H, ^{13}C (**54$_{Y}$**, **54$_{Lu}$**)	76–78
55$_{Y}$, 55$_{Gd}$	$(C_5Me_4C_6H_4\text{-}o\text{-}PPh_2)Ln(\eta^3\text{-}C_3H_5)_2$ (Ln = Y, Gd)	–	–	76
56$_{Y}$, 56$_{Dy}$	$(C_9H_6C_6H_4\text{-}o\text{-}NMe_2)Ln(\eta^3\text{-}C_3H_5)_2$ (Ln = Y, Dy)	–	–	76
57$_{Y}$, 57$_{Gd}$	$(C_9H_6C_6H_4\text{-}o\text{-}PPh_2)Ln(\eta^3\text{-}C_3H_5)_2$ (Ln = Y, Gd)	–	–	76
58$_{Sc}$, 58$_{Y}$, 58$_{Lu}$	$(C_5Me_4\text{-}C_5H_4N)Ln(\eta^3\text{-}C_3H_5)_2$ (Ln = Sc, Y, Lu)	Sc-C = 2.483(4), 2.476(4) Y-C = 2.600(3), 2.617(3) Lu-C = 2.567(4), 2.603(3) (average distances)	^{1}H, ^{13}C	78,79
59$_{Y}$, 59$_{Ho}$, 58$_{Lu}$	$Cp^{NMe2}Ln(\eta^3\text{-}C_3H_5)_2$ (Cp^{NMe2} = $C_5Me_4CH_2CH_2NMe_2$; Ln = Y, Ho, Lu)	Y-C = 2.590(5) to 2.663(7) Ho-C = 2.587(7) to 2.660(13) Lu-C = 2.534(4) to 2.633(9)	^{1}H (**59$_{Y}$**, **59$_{Lu}$**)	82
60$_{Sc}$, 60$_{Y}$, 60$_{Lu}$	$(C_5Me_4SiMe_2NC_4H_8)Ln(\eta^3\text{-}C_3H_5)_2$ (Ln = Sc, Y, Lu)	Sc-C = 2.418(8), 2.431(7), 2.395(7); 2.438(7), 2.414(7), 2.428(8) Y-C = 2.625(3), 2.617(3), 2.600(3); 2.656(3), 2.637(3), 2.554(3) Lu-C = 2.596(4), 2.564(4), 2.539(5); 2.633(4), 2.592(4), 2.506(4)	^{1}H, ^{13}C	83

[a]Distorted.

From ^{1}H NMR analysis, the allyl moiety appeared as a 1H/2H/2H set of resonances for the complexes made with the larger lanthanides (La, Nd and Sm), revealing no dynamic behavior at the ^{1}H NMR timescale. In contrast, the allyl group was found to be fluxional (1H/4H pattern by ^{1}H NMR spectroscopy) in the case of the smaller yttrium and scandium. All complexes **61$_{Ln}$** displayed a monomeric structure according to X-ray studies. Complex **61$_{Sc}$** is the only one to crystallize as a bis-THF adduct. Among the five complexes, **61$_{Y}$** stands out, with one borohydride trihapto and the other dihapto, while for the other four complexes the ligands are coordinated in tridentate mode to the metal. In all five complexes, the allyl moiety binds the metal in an η^3-mode (Fig. 36).

The neodymium derivative **61$_{Nd}$** was the only one in the series to be active toward the polymerization of isoprene (TOF 177–1000 h^{-1}), either on its own, due to the presence of the Nd-allyl bond, or combined with various alkylating reagents among which Mg(^{n}Bu)(Et), Al(^{i}Bu)$_3$ or MAO (methylaluminoxane). In every case, the selectivity of the reaction was 1,4-*trans*, up to 95.5%. In turn, all five complexes **61$_{Ln}$** were found very active toward the ring-opening polymerization (ROP) of ε-caprolactone (TOF up to 700,000 h^{-1} with neodymium), *L*-lactide (TOF up to 1300 h^{-1} with neodymium), and statistical copolymerization of both monomers. It is noteworthy that the initiation of the polymerization was demonstrated to take place *via* the borohydride rather than the

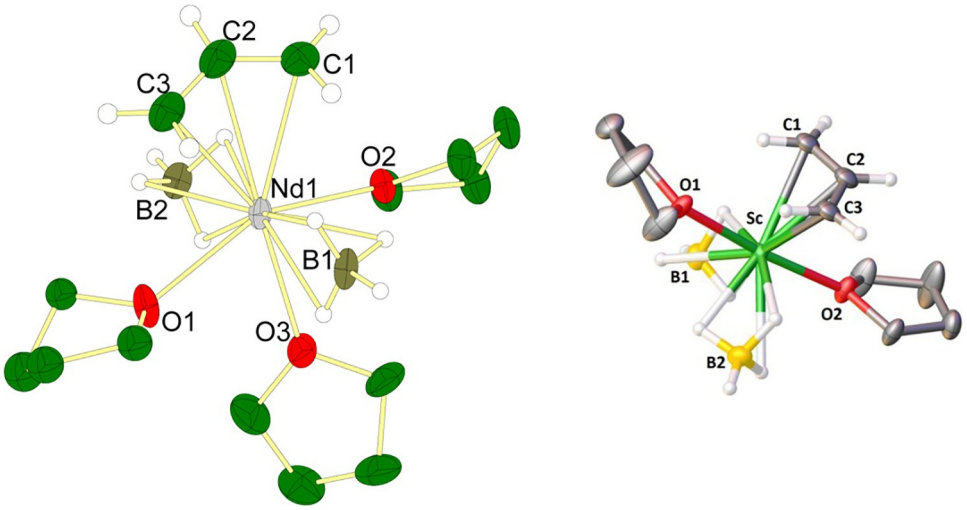

Fig. 36 ORTEP plot of $\mathbf{61_{Nd}}$ (left) and $\mathbf{61_{Sc}}$ (right). Hydrogen atoms are partially omitted for clarity. Reprinted from Fadlallah, S.; Terrier, M.; Jones, C.; Roussel, P.; Bonnet, F.; Visseaux, M. *Organometallics* **2016**, *35*, 456–461; Fadlallah, S.; Jothieswaran, J.; Capet, F.; Bonnet, F.; Visseaux, M. *Chem. Eur. J.* **2017**, *23*, 15644–15654, with the permission of WILEY-VCH Verlag Gm and the American Chemical Society, respectively.

allyl moiety by means of ^{1}H NMR spectroscopy end-group analysis. This experimental result was just recently corroborated by DFT studies, where the peculiar reactivity of the borohydride *vs* the allyl group was explained by the lower stability of the product resulting from monomer insertion into Ln-allyl rather than Ln-(BH_4) in $\mathbf{61_{Ln}}$ complexes.[87] In contrast, the metal-allyl bond was found to be more reactive than the metal-borohydride one toward the insertion of benzophenone, as expected from the literature,[6] and toward the protonation reaction with $[HNMe_2Ph][B(C_6F_5)_4]$ and HC_5Me_4R (R = Me, Et, Scheme 37).

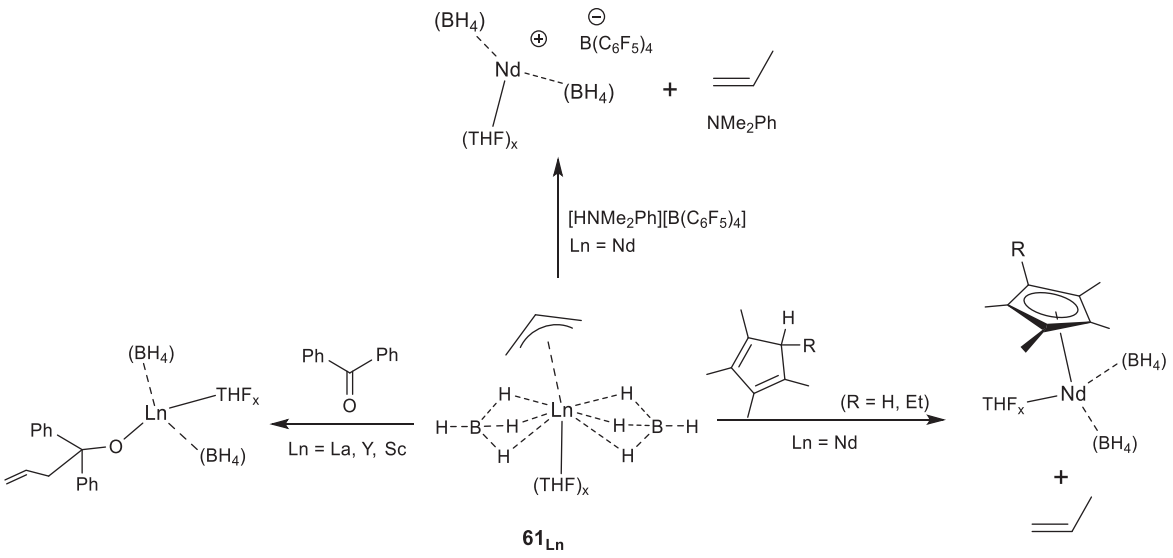

Scheme 37 Reactivity of complexes $\mathbf{61_{Ln}}$ toward various reagents.[87]

3.3.2 (Allyl)LnX$_2$ compounds with amide and related N-donor ligands

In 2013, Okuda and coworkers used a dianionic (L_4X_2)-type surrogate for the bis(cyclopentadienyl) scaffold to synthesize the mono(allyl) complexes $[(1,7\text{-}Me_2TACD)Ln(\eta^3\text{-}C_3H_5)]_2$ ($\mathbf{62_{Ln}}$, Ln = Y, La) by the acid-base 1:1 reaction of the protio form of the macrocyclic ligand $(1,7\text{-}Me_2TACD)H_2$ ($1,7\text{-}Me_2TACD$ = 1,7-dimethyl-1,4,7,10-tetraazacyclododecane, $1,7\text{-}Me_2[12]aneN_4$) with $[Ln(\eta^3\text{-}C_3H_5)_3(diox)]$ in THF (Scheme 38, left).[88]

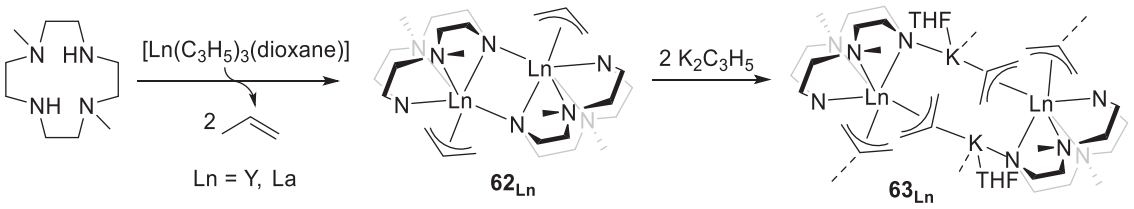

Scheme 38 Synthetic scheme for the preparation of allyl complexes of the series $\mathbf{62_{Ln}}$ and $\mathbf{63_{Ln}}$.

From XRD studies, it was established that the lanthanum congener $\mathbf{62_{La}}$ is a centrosymmetric dimer with lanthanum atoms bridged by one of the two amido nitrogen atoms (Fig. 37). The average La–C(allyl) bond length was found similar to the value found in the mono substituted bis-allyl $(Me_3TACD)La(\eta^3\text{-}C_3H_5)_2$ [$\mathbf{49_{La}}$][71] and in $La(\eta^3\text{-}C_3H_5)_3(TMEDA)$.[89]

By subsequent reaction of complexes $\mathbf{62_{Ln}}$ with K(allyl), the corresponding heterometallic allyl "ate" complexes $[(1,7\text{-}Me_2TACD)Ln(\eta^3\text{-}C_3H_5)_2K(THF)]_n$ ($\mathbf{63_{Ln}}$, Ln = Y, La) were isolated (Scheme 38, right), which were found to be both polymeric in the solid state *via* allyl bridges according to X-ray analysis. One allyl ligand is nearly symmetrically η^3-bonded to the potassium ion, while the other is η^3-bonded in an unsymmetrical fashion (Fig. 38).

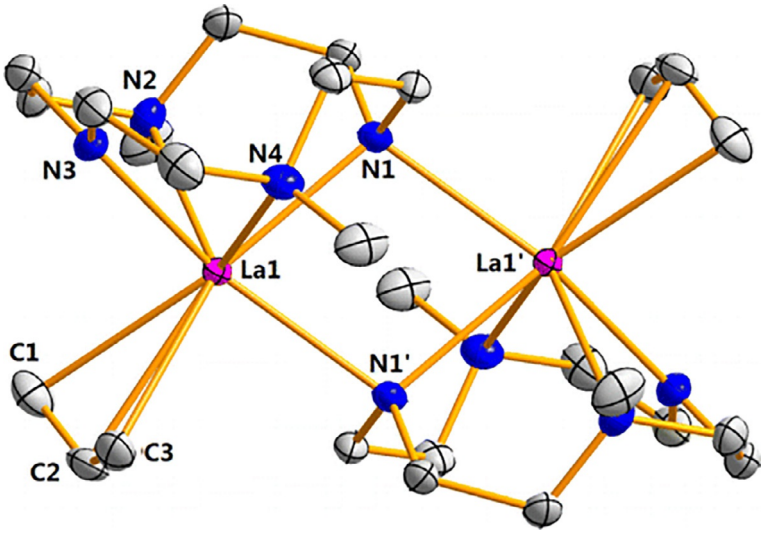

Fig. 37 ORTEP plot of dimeric $\mathbf{62_{La}}$. Displacement parameters are set at 50% probability level and the hydrogen atoms are omitted for clarity. Reprinted from Cui, P.; Spaniol, T. P.; Okuda, J. *Organometallics* **2013**, *32*, 1176–1182, with the authorization of the American Chemical Society.

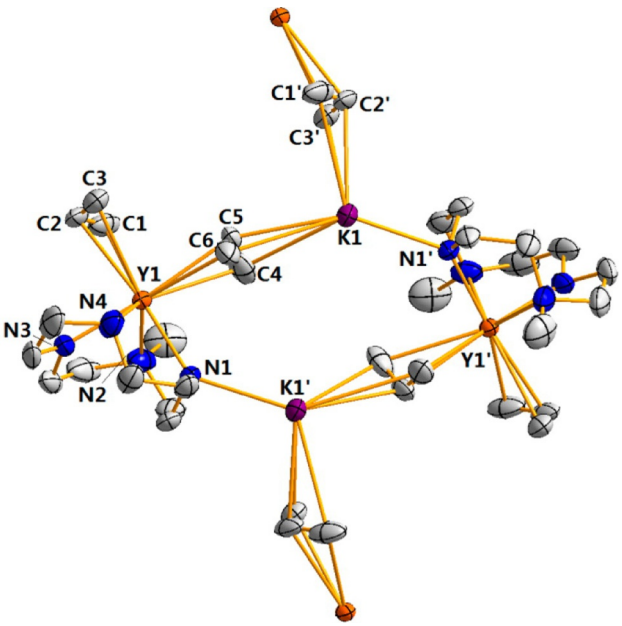

Fig. 38 Molecular structure of $\mathbf{63_Y}$. Displacement parameters are set at the 50% probability level and the hydrogen atoms are omitted for clarity. Reprinted from Cui, P.; Spaniol, T. P.; Okuda, J. *Organometallics* **2013**, *32*, 1176–1182, with the authorization of the American Chemical Society.

In terms of reactivity, hydrogenolysis of the yttrium/potassium compound $\mathbf{63_Y}$ afforded the heterobimetallic hydrido complex $[(1,7\text{-}Me_2TACD)_2Y_2H_3K(THF)_2]_2$. In turn, upon the same treatment, $\mathbf{63_{La}}$ led to the formation of the heptanuclear La_3K_4 heptahydrido complex $[(1,7\text{-}Me_2TACD)_3La_3H_7K_4(THF)_7]$.

The same research group prepared 1 year later, similarly as for its yttrium and lanthanum counterparts, the scandium mono(allyl) complex $(1,7\text{-}Me_2TACD)Sc(\eta^3\text{-}C_3H_5)$ $[\mathbf{62_{Sc}}]$ from the diamino diamine $(1,7\text{-}Me_2TACD)H_2$ and $(C_3H_5)_3Sc(THF)_2$ $[\mathbf{37'_{Sc}}]$ in THF (Scheme 39).[90]

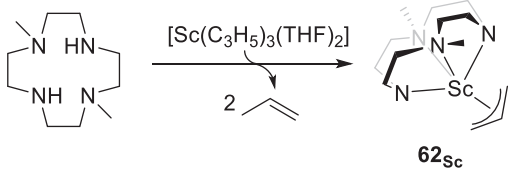

$\mathbf{62_{Sc}}$

Scheme 39 Synthesis of diamino-diamido(allyl) $\mathbf{62_{Sc}}$.

Unlike its dinuclear yttrium and lanthanum homologs, $\mathbf{62_{Sc}}$ was readily soluble in hydrocarbon solvents. Its monomeric nature as well as the η^3-coordination mode of the allyl group was confirmed by variable temperature NMR spectroscopy studies, where the allyl group was shown to be fluxional in solution.

Hydrogenolysis of $\mathbf{62_{Sc}}$ with H_2 in THF gave the bimetallic hydride ionic complex $[(1,7\text{-}Me_2TACD)_3Sc_3H_2]$ $[(1,7\text{-}Me_2TACD)_3Sc_3H_4]$. Interestingly, monitoring this reaction in THF-d_8 indicated the formation of mixed allyl–hydrido intermediates, leading to the production of the hydride as the main compound after 2 days.

Mixed allyl-hydrido complexes could be obtained in the Me_3TACD series previously discussed: $[Ln(Me_3TACD)(\eta^3\text{-}C_3H_5)(\mu\text{-}H)]_2$ dimeric complexes ($\mathbf{64_{Ln}}$, Ln = Nd, Sm) were isolated from the reaction of the neutral bis(allyl) compounds $\mathbf{49_{Ln}}$ with phenylsilane but only in the case of neodymium and samarium (Scheme 40). It is interesting to note that the same reaction afforded the bis(hydride) $[Ln(Me_3TACD)(\mu\text{-}H)_2]_4$ when Ln = Ce, Pr.[91]

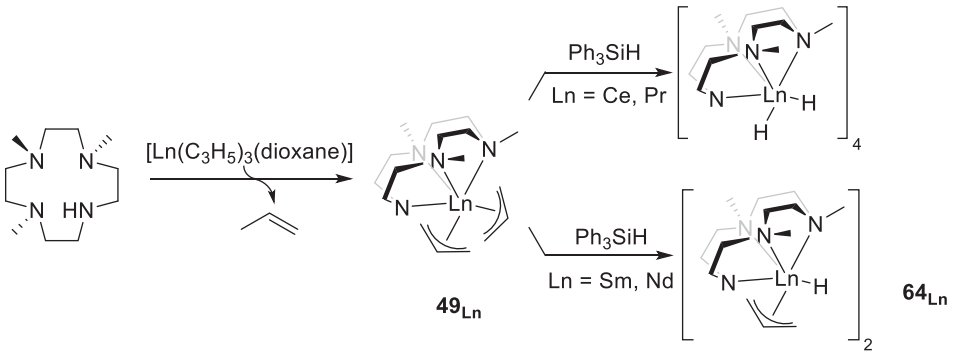

$\mathbf{49_{Ln}}$ $\mathbf{64_{Ln}}$

Scheme 40 Reaction of complexes $\mathbf{49_{Ln}}$ with triphenylsilane yielding mixed (allyl)(hydride) $\mathbf{64_{Ln}}$.

These exceptional mixed allyl-hydride complexes $\mathbf{64_{Ln}}$ were structurally characterized by X-ray analysis, showing that the allyl moiety coordinates in a η^3-bonding mode to the metal center (Fig. 39). So far, these complexes are the only rare-earth metal hydride compounds that possess an allyl moiety.

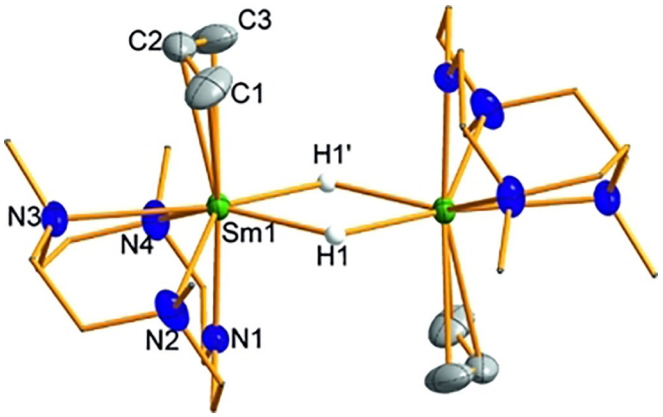

Fig. 39 ORTEP plot of $\mathbf{64_{Sm}}$. Thermal ellipsoids of the Sm, N and C atoms are set at the 50% probability level. Hydrogen atoms of the Me_3TACD and allyl ligands are omitted for clarity. Reprinted from Martin, D.; Kleemann, J.; Abinet, E.; Spaniol, T. P.; Maron, L.; Okuda J. *Eur. J. Inorg. Chem.* **2013**, 3987–3992, with the authorization of WILEY-VCH Verlag GmbH.

In the same article, it was found that the mixed allyl-hydride complexes $\mathbf{64_{Ln}}$ are able to promote the copolymerization of cyclohexene oxide with CO_2. As usually observed for such polymerization,[92] TON of order of magnitude of *ca.* 100 and broad dispersities of copolymers are noticed, which possess an alternating, atactic microstructure.

In 2020, the tridentate amidine 2-[$Ph_2P(O)$]$C_6H_4NHC(^tBu)$=N(2,6-$Me_2C_6H_3$) containing the side-chain donor group Ph_2P=O was introduced by Trifonov and coworkers in the chemistry of lanthanide allyls. The reaction of the tris-allyl precursor $Nd(C_3H_5)_3(diox)_2$ with this tridentate ligand in a 1:2 molar ratio gave the bis(amidinate)mono(allyl) neodymium complex {2-[$Ph_2P(O)$]$C_6H_4NC(^tBu)$N(2,6-$Me_2C_6H_3$)}$_2$Nd(C_3H_5) ($\mathbf{65_{Nd}}$). This complex was alternatively prepared by the reaction between the monochloride complex {2-[$Ph_2P(O)$]$C_6H_4NC(^tBu)$N(2,6-$Me_2C_6H_3$)}$_2$NdCl and allylmagnesium bromide (C_3H_5)MgBr (Scheme 41).[93]

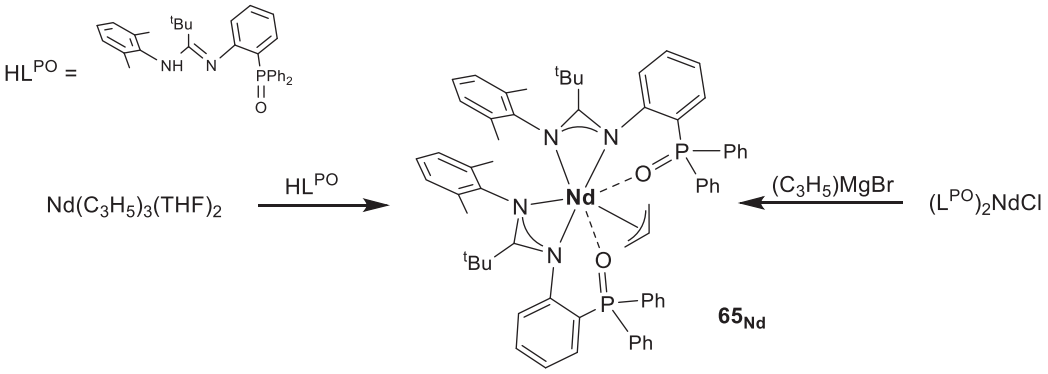

Scheme 41

X-ray studies revealed that complex $\mathbf{65_{Nd}}$ crystallizes as a solvate with 3.5 molecules of dioxane per Nd in the asymmetric unit (Fig. 40). The η^3-coordination mode of the allyl ligand was deduced by the CH_2–CH bond lengths in the complex that have similar values. It was also established that the Nd–C(allyl) bond lengths are slightly longer than the corresponding ones in the heteroleptic cyclopentadienyl neodymium allyl chloride complex [$CpNMe_2Nd(\eta^3$-$C_3H_5)(\mu$-Cl)]$_2$, where $CpNMe_2$ is 1-[2-(*N*,*N*-dimethylamino) ethyl]-2,3,4,5-tetramethylcyclopentadienyl (see further),[82] but are to some extent smaller than the Nd–C(allyl) distances in the allyl-hydride complex $\mathbf{64_{Nd}}$,[91] providing an overview of the steric/electronic properties of this amidino phosphine-oxide ligand.

Allyl complexes of the lanthanides are known to initiate the ring opening polymerization (ROP) of cyclic esters, although such studies are rather scarce in the literature.[5,88,94–97] The monoallyl complex $\mathbf{65_{Nd}}$ was as well found efficient toward *rac*-lactide and

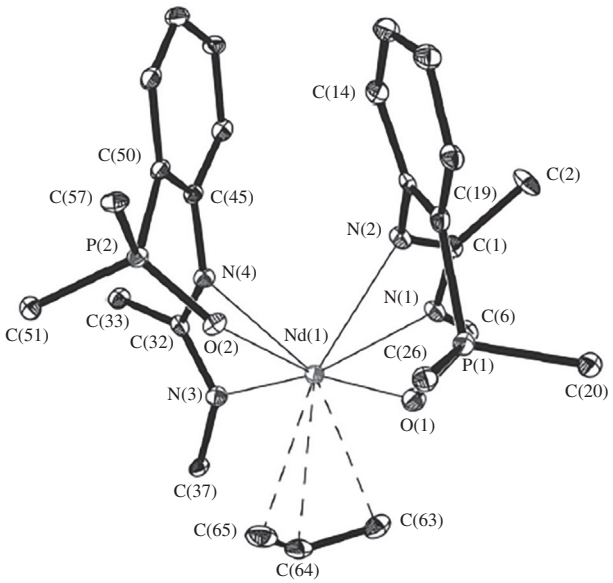

Fig. 40 ORTEP plot of {2-[$Ph_2P(O)$]$C_6H_4NC(^tBu)$N(2,6-$Me_2C_6H_3$)}$_2$Nd(C_3H_5) [$\mathbf{65_{Nd}}$]. The displacement ellipsoids are drawn at the 30% probability level. Hydrogen atoms, methyl groups of the ^{t}Bu substituent, 2,6-$Me_2C_6H_3$ moieties and aryl substituents of Ph_2P=O are omitted for clarity. Reprinted from Tlpygin, A. O.; Linnikova, O. A.; Kovylina, T. A.; Cherkasov, A. V.; Fukin, G. K.; Trifonov, A. A. *Russ. Chem. Bull. Int. Ed.* **2020**, *69* (6), 1114–1121, with the permission of Springer.

ε-caprolactone, exhibiting higher activity compared to the neodymium diketiminate bis(allyl) complex $Ln(\eta^3\text{-}C_3H_5)_2\{\kappa^2\text{-}HC(MeCNAr)_2\}$ (Ar = 2,6-^{i}Pr$_2$C$_6$H$_3$) previously described by Bochmann and coworkers,[5] but the process was rather uncontrolled with both monomers.

3.3.3 (Allyl)LnX$_2$ compounds with alkoxide ligands

A series of non-metallocene allyl complexes of early lanthanide containing a 1,ω-dithiaalkenediyl-bridged bis(phenolate) ligand $[Ln(L)(\eta^3\text{-}C_3H_5)(THF)_{1-2}]$ (**66$_{Ln}$**, L = tbbp, Y, La; **67$_{Ln}$**, L = etbbp, La, Ce, Nd, Sm) (Fig. 41) were synthesized by Okuda and coworkers by reacting the tris(allyl) complex $Ln(\eta^3\text{-}C_3H_5)_3(diox)$ with the corresponding bis(phenol) through propene elimination.[98] The (OSO)-type bisphenolate tbbp ligand was best suited for yttrium and lanthanum, whereas the larger lanthanides lanthanum, cerium, neodymium and samarium accommodated the tetradentate (OSSO)-type bis(phenolate) etbbp ligand.

Variable-temperature ^{1}H NMR spectroscopy of the lanthanum complex [**67$_{La}$**] showed the typical fluxional behavior for the allyl protons at room temperature, while the *syn* and *anti* H resonances could be observed at lower temperature (−30 °C). The tbbp-yttrium [**66$_Y$**] (Fig. 42) and etbbp-lanthanum [**67$_{La}$**] and cerium [**67$_{Ce}$**] complexes were obtained as suitable single-crystals for further X-ray structure determination.

The (OSSO)-type complexes **67$_{Ln}$** were found very efficient and versatile catalysts toward the hydrosilylation of various olefins. According to the authors, lanthanum and cerium compounds were among the most active and regioselective homogeneous rare-earth metal catalysts for the hydrosilylation of styrene.[98]

3.3.4 Cationic (allyl)LnX compounds with cyclopentadienyl or related ligands

The reaction of complex $(C_5Me_4SiMe_3)Sc(\eta^3\text{-}C_3H_5)_2$ (**51$_{Sc}$**, *vide infra*, Section 3.2.3), with $[HNMe_2Ph][B(C_6F_5)_4]$ cleanly afforded the *N*,*N*-dimethylaniline-coordinated cationic mono-(η^3-allyl) complex $[(C_5Me_4SiMe_3)Sc(\eta^3\text{-}C_3H_5)(\eta^6\text{-}PhNMe_2)][B(C_6F_5)_4]$ [**68$_{Sc}$**]. Upon treatment with the trityl reagent $[Ph_3C][B(C_6F_5)_4]$, complex **51$_{Sc}$** yielded the separated ion pair

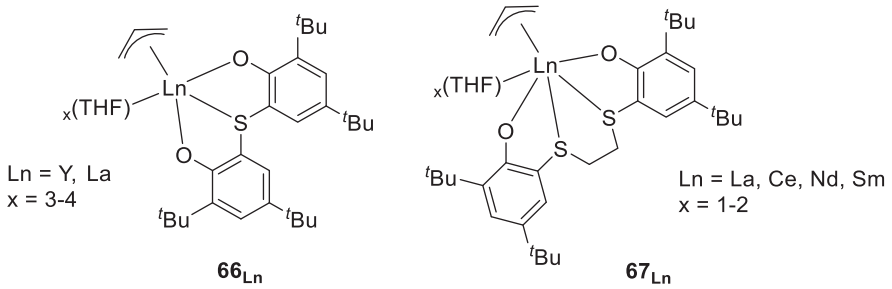

Fig. 41 1,ω-Dithiaalkenediyl-bridged bis(phenolate) $[Ln(L)(\eta^3\text{-}C_3H_5)(THF)_{1-2}]$ complexes (**66$_{Ln}$**, L = tbbp, Y, La; **67$_{Ln}$**, L = etbbp, La, Ce, Nd, Sm).

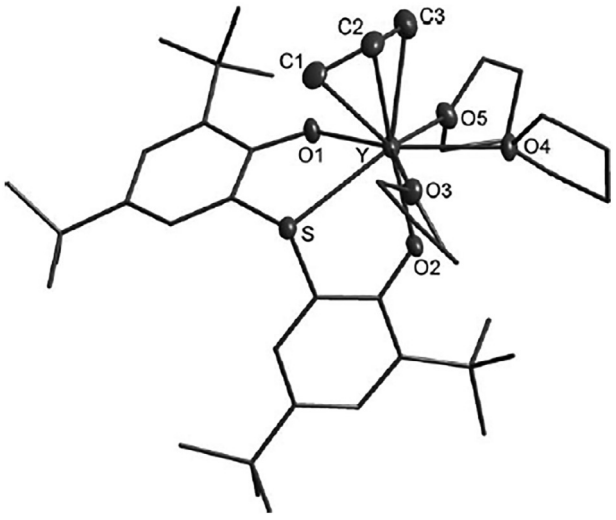

Fig. 42 ORTEP diagram of $[\{Y(tbbp)(\eta^3\text{-}C_3H_5)(THF)_3\}\cdot THF]$ [**66$_Y$**]. Thermal ellipsoids are drawn at the 30% probability level. Hydrogen atoms as well as the non-coordinated THF solvent molecules are omitted for clarity. Reprinted from Abinet, E.; Spaniol, T. P.; Okuda, J. *Chem. Asian J.* **2011**, *6*, 389–391, with the permission of WILEY-VCH Verlag GmbH.

$[(C_5Me_4SiMe_3)Sc(\eta^3\text{-}C_3H_5)(\eta^6\text{-}PhMe)][B(C_6F_5)_4]$ [**68′$_{Sc}$**], whereas the same starting complex afforded the contact ion pair $(C_5Me_4SiMe_3)Sc(\eta^3\text{-}C_3H_5)(\mu,\eta^6\text{-}Ph)BPh_3]$ [**68″$_{Sc}$**] when reacted with $[HNMe_2Ph][BPh_4]$ (Scheme 42).[75]

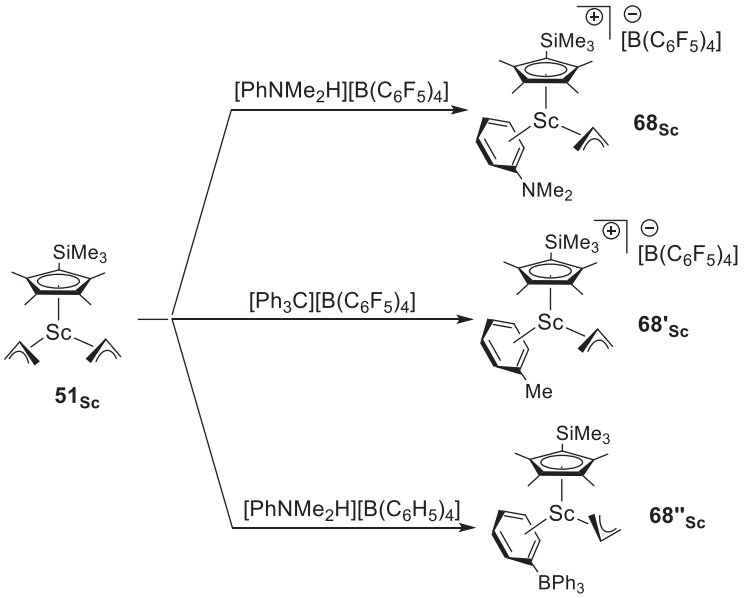

Scheme 42 Synthesis of allyl cationic scandium complexes.

These cationic allyl complexes were found to be fluxional in solution from ^{1}H NMR analysis. They were all three isolated as X-ray suitable crystals and hence structurally characterized. Among them, **68$_{Sc}$** was the first example of a crystallographically characterized *N,N*-dimethylaniline-coordinated cationic metal complex, especially in allyl series. The isolation of the Lewis base free contact-ion-pair complex **68″$_{Sc}$** was an illustration that BPh_4 is more strongly coordinating than $B(C_6F_5)_4$, where one of the four Ph groups in BPh_4 showed bonding interactions with the Sc atom in an η^6 manner (Fig. 43). From recrystallization of the latter complexes in THF, THF-separated ion pairs $[(C_5Me_4SiMe_3)Sc(\eta^3\text{-}C_3H_5)(THF)_2][B(C_6F_5)_4]$ and $[(C_5Me_4SiMe_3)Sc(\eta^3\text{-}C_3H_5)(THF)_2][BPh_4]$ were isolated.

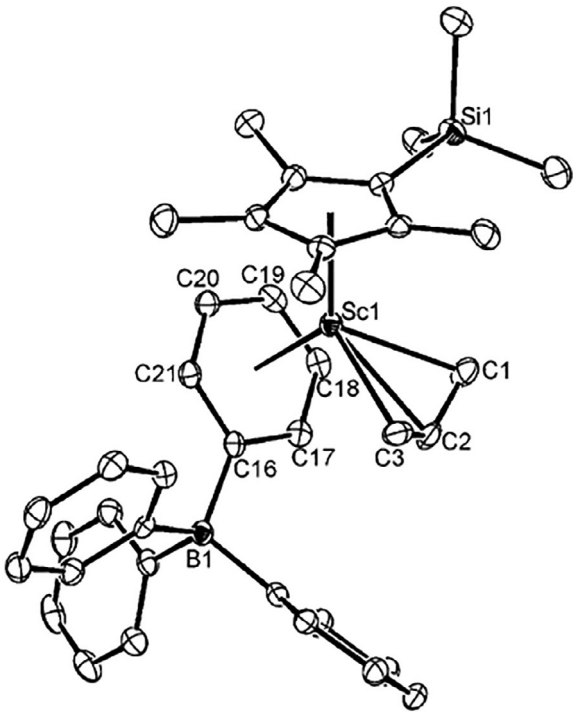

Fig. 43 ORTEP diagram of $[(C_5Me_4SiMe_3)Sc(\eta^3\text{-}C_3H_5)][BPh_4]$ [**68″$_{Sc}$**]. Thermal ellipsoids are drawn at the 30% probability level. Hydrogen atoms are omitted for clarity. Reprinted from Yu, N; Nishiura, M.; Li, X.; Xi, Z.; Hou, Z. *Chem. Asian J.* **2008**, *3*, 1406–1414, with the permission of WILEY-VCH Verlag GmbH.

The THF-free ionic complexes $\mathbf{68}_{\mathbf{Sc}}$ and $\mathbf{68'}_{\mathbf{Sc}}$ were found to be highly active, without addition of any borate activator, toward the polymerization of isoprene and its copolymerization with norbornene.[75]

In a no less remarkable paper, Okuda and coworkers reported, shortly after these above mentioned studies of the Hou's group on scandium, that acid treatment of the half-sandwich bis-allyl complexes $Ln(C_5Me_4SiMe_3)(\eta^3\text{-}C_3H_5)_2(THF)$ ($\mathbf{51'}_{\mathbf{Ln}}$) with $[NEt_3H][BPh_4]$ or $[HNMe_2Ph][B(C_6F_5)_4]$ afforded the mono-allyl mono-cations $[(C_5Me_4SiMe_3)Ln(\eta^3\text{-}C_3H_5)(THF)_2]^+[B(C_6X_5)_4]^-$ (Ln = Y, La; $\mathbf{68}_{\mathbf{Ln}}$: X = F, $\mathbf{68'}_{\mathbf{Ln}}$: X = H) (Scheme 43).[6]

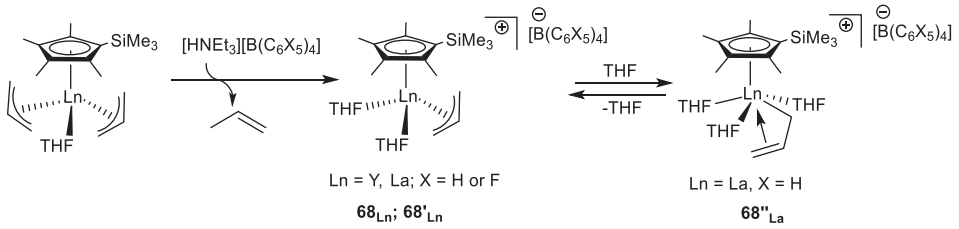

Scheme 43 Synthesis of half-sandwich allyl cationic complexes $\mathbf{68}_{\mathbf{Ln}}$ and formation of related THF adducts in THF solution.

In the molecular structure of the lanthanum derivative $\mathbf{68''}_{\mathbf{La}}$, which was determined from X-ray quality crystals obtained in THF, one shorter C–C bond within the allyl ligand was found opposite to the Cp ligand, indicating an increased double-bond character (Fig. 44). ^{1}H NMR spectroscopy revealed little rigidity for the allyl group of the lanthanum complexes $\mathbf{68}_{\mathbf{La}}$ and $\mathbf{68'}_{\mathbf{La}}$, whereas the yttrium derivatives $\mathbf{68}_{\mathbf{Y}}$ and $\mathbf{68'}_{\mathbf{Y}}$ displayed higher fluxionality with fast *syn*/*anti* exchange.

1,3-Butadiene polymerization was assessed with the monocationic half-sandwich allyl complexes $\mathbf{68}_{\mathbf{La}}$ and $\mathbf{68}_{\mathbf{Y}}$ in the presence of Al^iBu_3. The yttrium-based catalyst $\mathbf{68}_{\mathbf{Y}}$ showed much higher activity (TOF 12,000 h^{-1}), in comparison to the lanthanum one (TOF 1600 h^{-1}) at room temperature in toluene with fair selectivity (86% 1,4-*cis*).

In a recently published joint experimental/theoretical study,[99] cationic Sc-allyl active species are described as intermediates that are formed during the uncommon ethylene/*cis*-1,4 butadiene copolymerization by means of catalysts issued from specially designed half-sandwich thiophene-fused cyclopentadienyl scandium complexes (see Fig. 45, **A** and **A'**).[100] From DFT calculations, it is proposed that it is the open coordination sphere of the scandium active species that facilitates butadiene η^4-*cis* coordination/insertion to give 1,4-*cis* regularity *via* the *anti* Sc-π-allyl intermediate.

At the same time, the Marks' group has prepared mononuclear and binuclear half-scandocenes (see Fig. 45, **B**) to study the impact of both pre-catalyst and co-catalyst nuclearity on the selectivity of isoprene (co-)polymerization. They concluded that the isomerization of allyl active species during the polymerization process was related to this nuclearity, which explained the different selectivities obtained.[101]

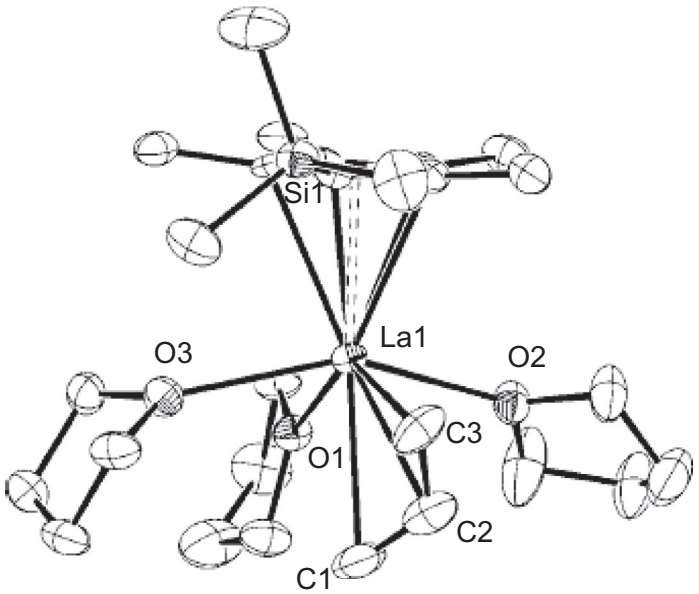

Fig. 44 ORTEP view of the cationic part of one of the two independent sets of ion pairs in $\mathbf{68''}_{\mathbf{La}}$. Thermal ellipsoids are set at the 50% probability level. Hydrogen atoms are omitted for clarity. Reprinted from Robert, D.; Abinet, E.; Spaniol, T. P.; Okuda, J. *Chem. Eur. J.* **2009**, *15*, 11937–11947, with the permission of WILEY-VCH Verlag GmbH.

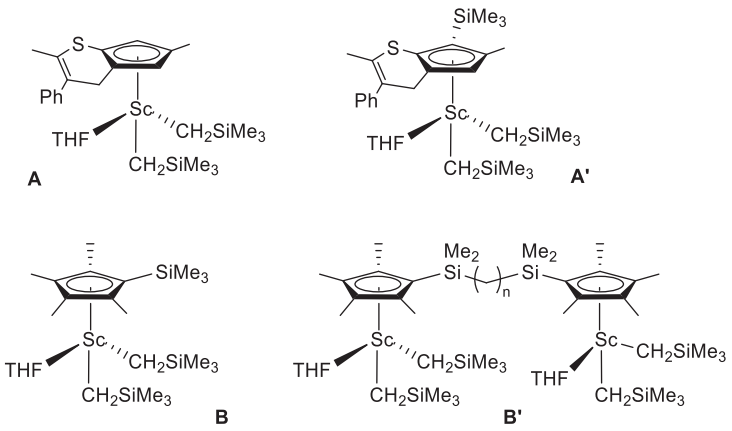

Fig. 45 Structures of thiophene-fused Cp and mononuclear/binuclear scandium complexes.

3.3.5 (Allyl)LnX_2 compounds with cyclopentadienyl ligands

The mono(allyl)metallocene of scandium $(C_5Me_4H)_2Sc(\eta^3\text{-}C_3H_5)$ [$\mathbf{69_{Sc}}$] was synthesized similarly as described by Tsutsui in the pioneer studies related to mono(allyl) lanthanidocenes in the C_5H_5 series,[102] by the simple ionic metathesis between $(C_5Me_4H)_2ScCl(THF)$ and allylmagnesium chloride (Scheme 44).[103]

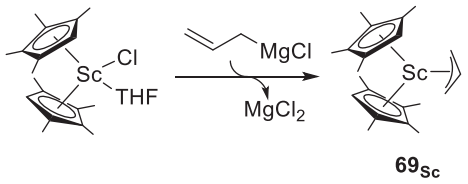

Scheme 44 Synthesis of monoallyl complex $\mathbf{69_{Sc}}$.

Previously in the chemistry of scandium, the *ansa*-cyclopentadienyl mono-allyl derivative $\{Me_2Si[C_5H_2\text{-}2,4\text{-}(CHMe_2)_2]_2\}Sc(\eta^3\text{-}C_3H_5)$ had been prepared in a similar way.[104] This ionic metathesis strategy differs from the one developed ten years ago where $(C_5Me_5)_2Sc(C_3H_5)_3$ and $[Me_2Si(C_5H_3\text{-}3\text{-}CMe_3)_2]Sc(\eta^3\text{-}C_3H_5)$ resulted from the insertion reaction of an allene with the corresponding metallocene hydrides.[7]

The complex $\mathbf{69_{Sc}}$ displayed fluxional behavior in solution and was characterized by X-ray diffraction as a non-solvated monomer (Fig. 46). This allyl scandocene was further used as precursor of the ion pair $[(C_5Me_4H)_2Sc]\text{-}[(\mu\text{-}Ph)BPh_3]$ upon

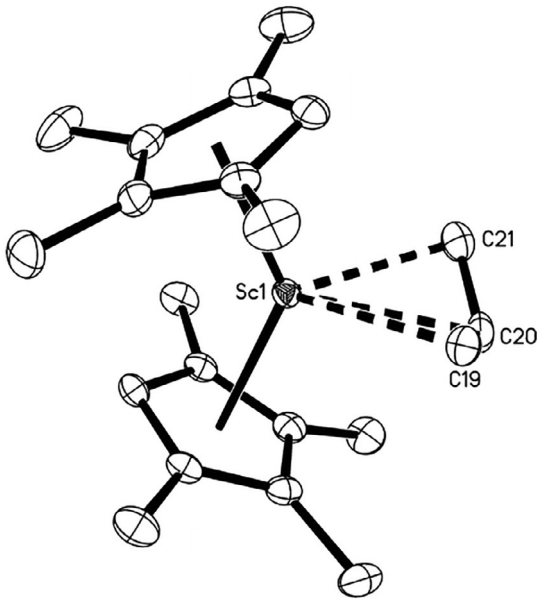

Fig. 46 ORTEP plot of $\mathbf{69_{Sc}}$ with thermal ellipsoids set at the 50% probability level. Hydrogen atoms are omitted for clarity. Reprinted from Demir, S.; Lorenz, S. E.; Fang, M.; Furche, F.; Meyer, G.; Ziller, J. W.; Evans, W. J. *J. Am. Chem. Soc.* **2010**, *132*, 11151–11158, with the authorization of the American Chemical Society.

protonation with $HNEt_3BPh_4$. The latter complex was subjected to KC_8 reduction in the presence of N_2, yielding the dinitrogen complex $[(C_5Me_4H)_2Sc]_2(\mu\text{-}\eta^2\text{:}\eta^2\text{-}N_2)$. This strategy, which involves the initial synthesis of an allyl derivative, is of high interest for the activation of small molecules with low reactivity such as molecular nitrogen.

The mono(allyl) metallocene $(C_5Me_4H)_2Y(\eta^3\text{-}C_3H_5)$ [**69$_Y$**] was obtained as same as its scandium analog by treatment of the chlorometallocene precursor with one equiv. of allylmagnesium, followed by prolonged heating under vacuum (Scheme 45).[105]

Monoallyl yttrium complex **69$_Y$** was extensively characterized, including by single crystal X-ray diffraction. In this complex, the longest Y-(C_3H_5) interaction is the central carbon of the allyl moiety, as is typical of other $(C_5Me_4R)_2Ln(\eta^3\text{-}C_3H_5)$ (R = H or Me) complexes ((**Lu, Cp***),[106] (**Nd, Sm, Tm, Cp***),[107] (**Sm, Cp***),[9] (**Lu, Y, Cp***)[108]).

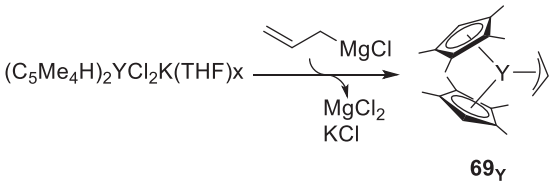

Scheme 45 Synthesis of monoallyl complex **69$_Y$**.

The reaction of **69$_Y$** with 1 equiv. $HNEt_3BPh_4$ yielded the non-solvated cation $[(C_5Me_4H)_2Y][(\mu\text{-}Ph)_2BPh_2]$ (Scheme 46).

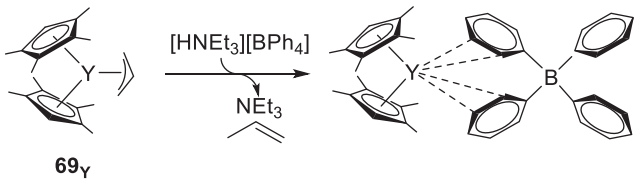

Scheme 46 Protonation of allyl yttrocene **69$_Y$** to yield the corresponding cationic yttrium species.

Upon hydrogenation with 1 atm of H_2, **69$_Y$** yielded the yttrium hydride complex, $[(C_5Me_4H)_2Y(\mu\text{-}H)]_x$ in 98% yield (Scheme 47). The allyl hydrogenation method clearly appears, again, as a valuable route for the preparation of hydride complexes.[105]

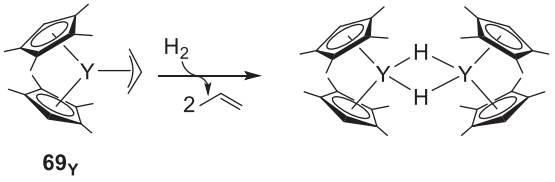

Scheme 47 Hydrogenolysis of allyl yttrocene **69$_Y$** to yield the corresponding yttrium hydride.

A well-known synthetic strategy in organolanthanide chemistry was developed by Evans, which was devoted to the synthesis of sterically hindered tris-cyclopentadienyl derivatives of the smallest lanthanides (from Tb to Lu and also including Y and Sc). This methodology uses the peculiar chemical reactivity of allyl complexes of lanthanides, as an alternative route to the classical ionic metathesis. It involves the intermediate preparation of an allyl complex $[(C_5H_4SiMe_3)_2Lu(\mu\text{-}C_3H_5)]_4$ [**70$_{Lu}$**] *via* the metathetic reaction of $[(C_5H_4SiMe_3)_2Lu(\mu\text{-}Cl)]_2$ with $(C_3H_5)MgCl$ according to Scheme 48.[109]

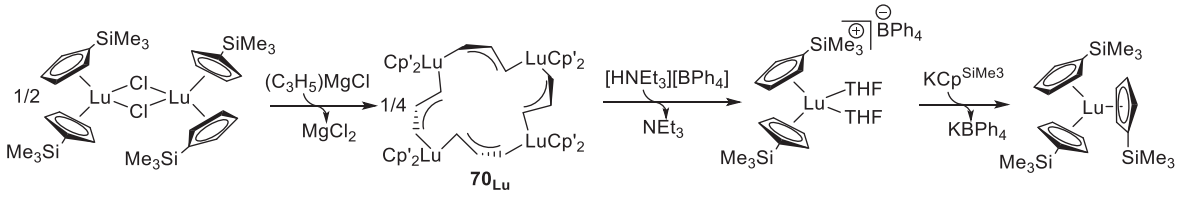

Scheme 48 Synthetic strategy for the preparation of sterically hindered triscyclopentadienyl complexes of the late lanthanides involving the intermediate allyl complex **70$_{Lu}$** (Cp′ = $C_5H_4SiMe_3$).

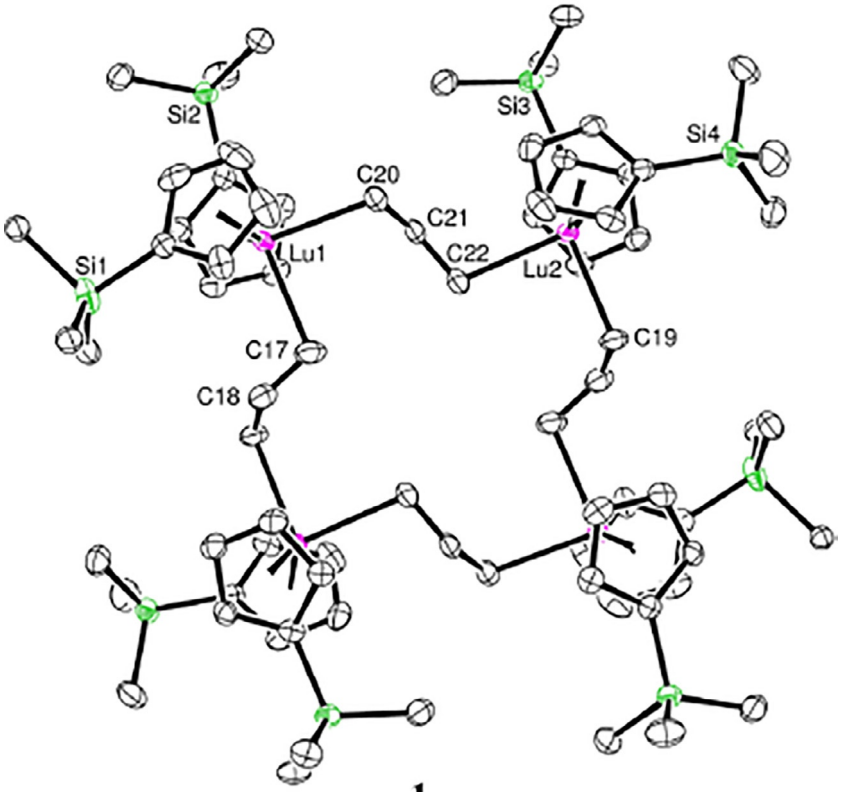

Fig. 47 ORTEP plot of $\mathbf{70_{Lu}}$ with thermal ellipsoids set at the 50% probability level and hydrogen atoms are omitted for clarity. Reprinted from Peterson, J. K.; MacDonald, M. R.; Ziller, J. W.; Evans, W. J. *Organometallics* **2013**, *32*, 2625–2631, with the permission of the American Chemical Society.

The resulting allyl complex $\mathbf{70_{Lu}}$ crystallizes as a non-solvated tetramer as determined by X-ray diffraction studies (Fig. 47).

In a second step, this monoallyl derivative subsequently reacts with $[HNEt_3][BPh_4]$ to generate the ionic pair $[(C_5H_4SiMe_3)_2Lu(THF)_2]^+[BPh_4]^-$, which affords upon addition of $KC_5H_4SiMe_3$ the triscyclopentadienyl $(C_5H_4SiMe_3)_3Lu$ in good yield.

More recently, the methylallyl yttrium derivative $(Cp^*)_2Y(\eta^3\text{-}CH_2CMeCH_2)$ ($(Cp^* = C_5Me_5$, $\mathbf{71_Y}$) was classically synthesized from (methylallyl)magnesium chloride and $(Cp^*)_2YCl_2K(THF)$. This compound was prepared as a model to help at identifying by-products of photochemical activation. Its X-ray crystal structure was determined (Fig. 48).[110]

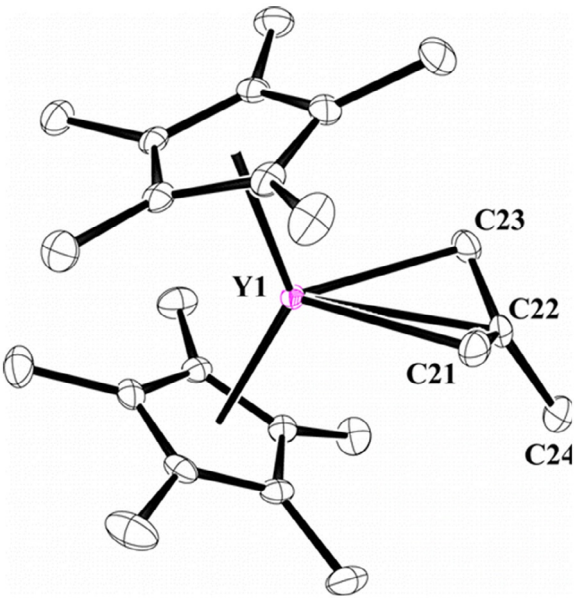

Fig. 48 ORTEP plot of $\mathbf{71_Y}$. Ellipsoids are drawn at the 50% probability level. The second molecule and the hydrogen atoms are omitted for clarity. Reprinted from Fieser, M. E.; Johnson, C. W.; Bates, J. E.; Ziller, J. W.; Furche, F.; Evans, W. J. *Organometallics* **2015**, *34*, 4387–4393, with the authorization of the American Chemical Society.

Photochemical activation of rare-earth-metal bis-(pentamethylcyclopentadienyl) allyl complexes $(Cp^*)_2Ln(\eta^3\text{-}C_3H_4R)$ (Ln = Y, Lu; **71$_{Ln}$**: R = Me; **72$_{Ln}$**: R = H) was used by Evans and co-workers to reduce dinitrogen, affording $[(Cp^*)_2Ln]_2(\mu\text{-}\eta^2\text{:}\eta^2\text{-}N_2)$ complexes. In the presence of isoprene, similar photolytic activation of complexes **72$_{Ln}$** (Ln = Y, Lu) provided polyisoprene, which was the result of radical rather than coordinative polymerization, according to the authors, while sulfur was reduced under the same conditions to generate $[(Cp^*)_2Ln]_2(\mu\text{-S})$ complexes (Scheme 49).[110]

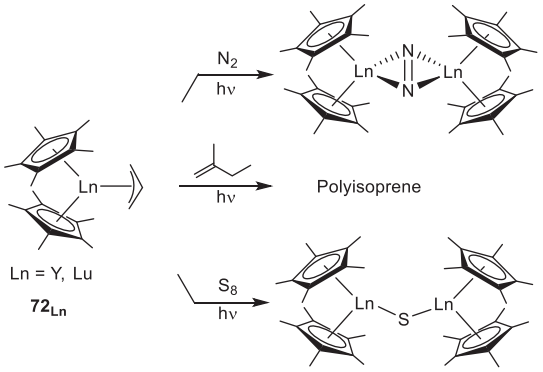

Scheme 49 Photochemical activation of **72$_{Ln}$** (Ln = Y, Lu) in the presence of various substrates.

The mono(allyl) complexes in the bis(pentamethylcyclopentadienyl) series, $Cp^*_2Ln(C_3H_5)$ [**72$_{Ln}$**], were the subject of several reactivity studies during the last two decades, and they have in part been mentioned in the previous edition of COMC.[1] Among these studies, the most important contribution came from the group of Evans, who investigated, apart from above-mentioned activation reactions, the chemical potential of the Ln-(allyl) bond toward several insertion reactions and hydrogenolysis.

This group examined in 2008 the reaction of complexes **72$_{Ln}$** (Ln = Y, La, Sm) with (trimethylsilyl)diazomethane. Elements of different ionic radius (small yttrium, large lanthanum and intermediate samarium) were chosen in order to get an overview of the reactivity of these complexes. It was observed that in all three cases clean insertion takes place, instead of the more classical metalation encountered with $(Cp^*)_2Sm$ or $[(Cp^*)_2SmH]_2$,[111] affording the lanthanide hydrazonato complexes of formula $(Cp^*)_2Ln[\eta^2(N,N')\text{-RNN=CHSiMe}_3]$ (R = CH_2=$CHCH_2$, Scheme 50).[112] The complexes were crystallographically characterized where the double bond of the allyl substituent is oriented toward the metal center in the lanthanum complex, with no detection of a metal-carbon interaction, whereas in samarium and yttrium ones this bond points away from the metals.

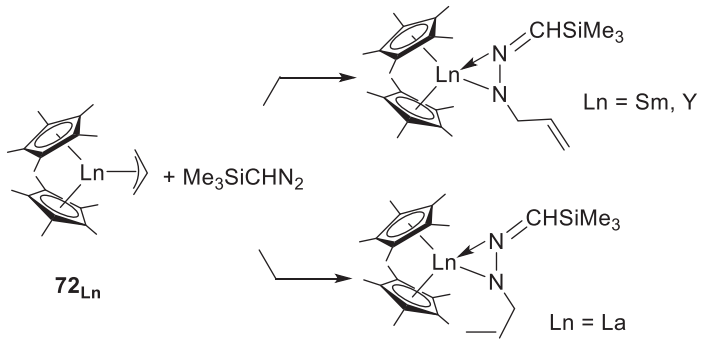

Scheme 50 Reaction of complexes **72$_{Ln}$** (Ln = Y, La, Sm) with (trimethylsilyl)diazomethane.

Very soon after, the lanthanide metallocene allyl complexes $(Cp^*)_2Ln(C_3H_5)(THF)$ (**72'$_{Ln}$**, Ln = Ce, Sm, Y) were readily transformed into $(Cp^*)_2Ln(hpp)$ (hpp = 1,3,4,6,7,8-hexahydro-2*H*-pyrimido[1,2-α]pyrimidinate) by deprotonation in the presence of Hhpp,[113] which is another illustration of the acid-base reactivity of the Ln(allyl) moiety (Scheme 51). It must be emphasized however that both $(Cp^*)_2Sm$ and $[(Cp^*)_2SmH]_2$ led to the same $(Cp^*)_2Ln(hpp)$ when submitted to the reaction with Hhpp, which shows the duality of reactivity of the metal-allyl fragment depending on the reagent considered (see the reactivity observed toward (trimethylsilyl)diazomethane, as discussed immediately above).

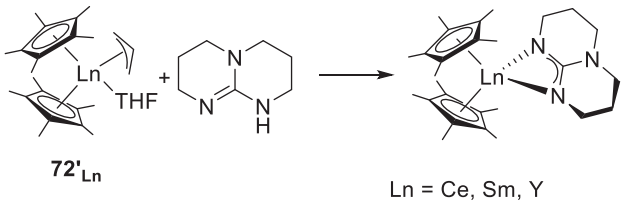

Scheme 51 Acid-base reaction of complexes **72'$_{Ln}$** (Ln = Ce, Sm, Y) with Hhpp (hpp = 1,3,4,6,7,8-hexahydro-2*H*-pyrimido[1,2-α]pyrimidinate).

In 2010, nitric oxide NO was found to cleanly react with $(Cp^*)_2Ln(C_3H_5)(THF)$ (**72'$_{Ln}$**, Ln = Y, La, Sm) to form $\{(Cp^*)_2Ln[\mu\text{-}ONN(CH_2CH{=}CH_2)O]\}_2$ complexes, which were structurally characterized. The formation of $ONN(CH_2CH{=}CH_2)O^-$ anion was proposed to arise from insertion of NO into the Ln-C(allyl) bond followed by coupling of the (allyl-NO) radical anion with a second molecule of NO (Scheme 52).[114]

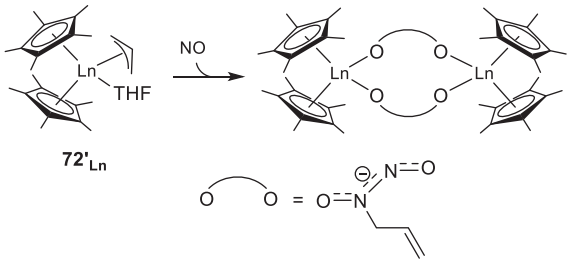

Scheme 52 Insertion of NO into Ln-allyl fragment in **72'$_{Ln}$** allyl complexes (Ln = Y, La, Sm).

The same group also showed at the same time that N_2O undergoes facile insertion into metal-carbon bonds of several allyl metallocene complexes to form $(C_3H_5N_2O)$ ligands: the products $[(Cp^*)_2Ln(\mu\text{-}\eta^1{:}\eta^2\text{-}O\text{–}N{=}N{—}C_3H_5)]_2$ (Ln = Y, Sm, La) were obtained in reactions of N_2O with the bis(Cp^*) allyl complexes (as THF adducts **72'$_{Ln}$**, Ln = Y, Sm, La), instead of the expected metallocene oxides. Similar reactivity was observed in the tetramethylcyclopentadienyl series, with the formation of $[(C_5Me_4H)_2Ln(\mu\text{-}\eta^1{:}\eta^2\text{-}O{—}N{=}N{—}C_3H_5)]_2$ (M = Sc, Y) from the mono(allyl) lanthanidocenes **71$_{Ln}$** (Ln = Sc, Y).[115]

Later, the Evans' group studied insertion reactions with chalcogenides reagents. They reported that **71$_{Sc}$** reacts with PhEEPh (E = S, Se, Te) to form the products $[(C_5Me_4H)_2Sc(SPh)]_2$, $(C_5Me_4H)_2Sc(SePh)$ and $(C_5Me_4H)_2Sc(TePh)$, respectively, along with $(C_3H_5)EPh$ release (Scheme 53, up).[116] In presence of 2,2′-dipyridyl disulfide, pySSpy, the monometallic sulfur derivative $(C_5Me_4H)_2Sc(Spy\text{-}\kappa^2\text{-}S,N)$ is obtained (Scheme 53, down).

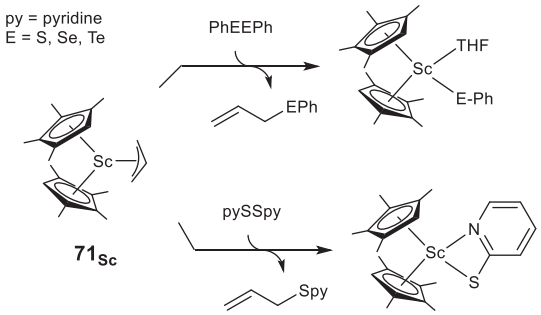

Scheme 53 Reactions of allyl scandocene **71$_{Sc}$** with chalcogenides.

A σ-bond metathesis mechanism was proposed to account for such experimental results, as an example of Sc-C (*via* η^1-allyl) bond reactivity (Scheme 54).

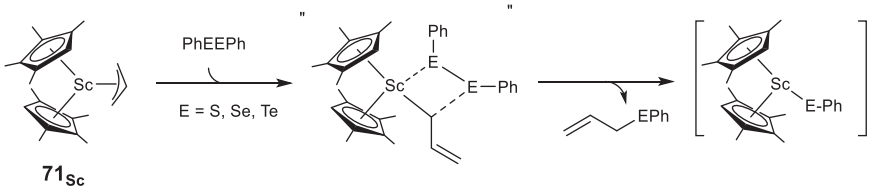

Scheme 54 Mechanistic pathway of the insertion of chalogenides in Sc-allyl moiety.[116]

Beside these reactions, which are related to the insertion in a Ln-allyl bond of a metallocene derivative, a particular reactivity is to be reported. It concerns the reaction of **72$_Y$** with the borane 9-borabicyclo[3.3.1]nonane (9-BBN) that afforded a compound containing two yttrium metallocene borane complexes $(Cp^*)_2Y[\eta^3\text{-}C_3H_4(BC_8H_{14})]$ **[73$_Y$]** and $(Cp^*)_2Y(\mu\text{-}H)_2(BC_8H_{14})$, in a single crystal, as revealed by X-ray crystallographic analysis (Fig. 49).[117]

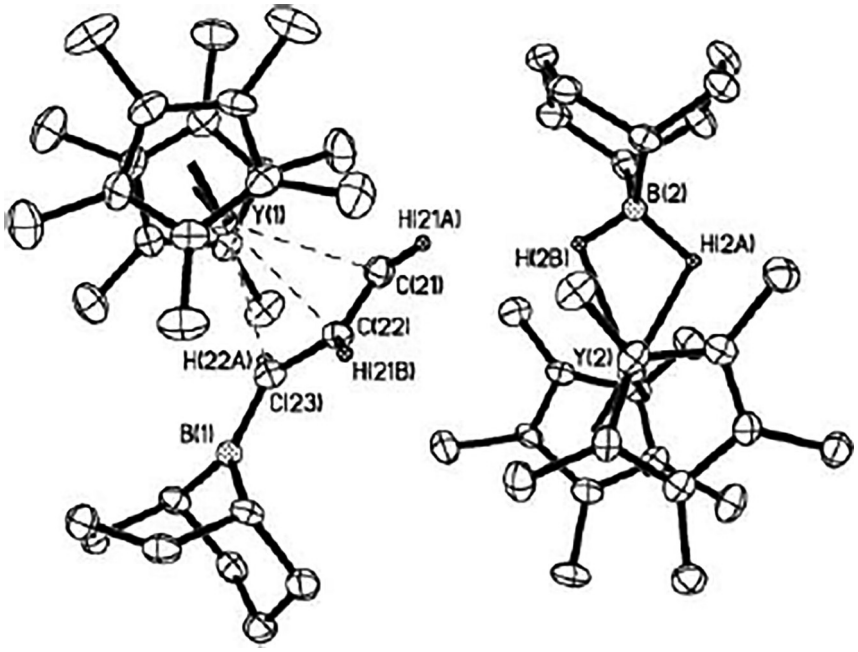

Fig. 49 ORTEP plot of $(Cp^*)_2Y[\eta^3\text{-}C_3H_4(BC_8H_{14})]$ [**73$_Y$**] and $(Cp^*)_2Y(\mu\text{-}H)_2(BC_8H_{14})$, in a single crystal, thermal ellipsoids are drawn at the 50% probability level. The second molecule and the hydrogen atoms are omitted for clarity. Reprinted from Evans, W. J.; Lorenz, S. E., Ziller, J. W. *Chem. Commun.* **2007**, 4662–4664, with the authorization of the Royal Chemical Society.

The two compounds are proposed to be formed after a several steps process, **73$_Y$** being the result of the uncommon addition of 9-BBN in the olefin—arising from the yttrium allyl starting compound **62$_Y$**—with the allyl group in an η^1-coordination mode, based on *in situ* ^{1}H and ^{11}B NMR spectroscopy studies (Scheme 55).

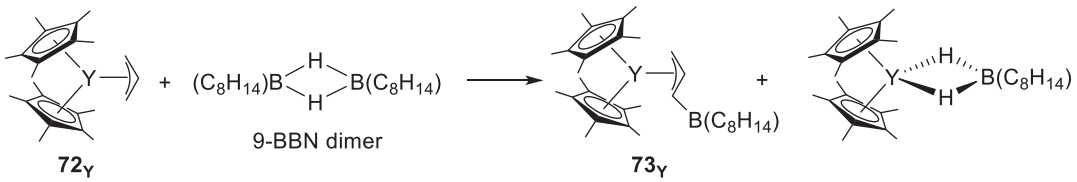

Scheme 55 Reactions of allyl yttrocene **72$_Y$** with 9-BBN.

Later, in 2014, it was found that hydrogenolysis of a 1:1 mixture of $(Cp^*)_2Lu\text{-}(\eta^3\text{-}C_3H_5)$ [**72$_{Lu}$**] and $(Cp^*)_2Y(\eta^3\text{-}C_3H_5)$ [**72$_Y$**] forms a mixture of hydride complexes, from which the heterobimetallic "tuckover" compound $(Cp^*)_2Lu(H)_2YCp^*_2$ could be isolated, in addition to the already known $[(Cp^*)_2LuH]_2$ and $[(Cp^*)_2YH]_2$ (Scheme 56). Also, 1:1 mixtures of bis(Cp^*) allyl complexes with lanthanum and lutetium or yttrium yielded exclusively the heterobimetallic products under the same conditions.[118]

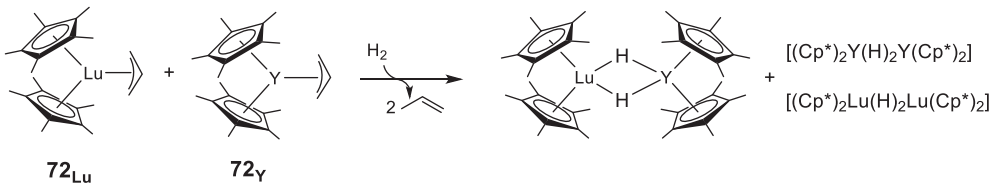

Scheme 56 Heterobimetallic hydride preparation from hydrogenolysis of mixtures of allyl lanthanidocenes.

The previously mentioned review from Carpentier[2] cites quite extensively the two families of *ansa*-cyclopentadienyl-fluorenyl[119,120] (Cp-Flu) and *ansa*-indenyl-allyl complexes of the lanthanides published in the mid-2000s (Fig. 50).[121] In terms of reactivity, these complexes were initially found as efficient and stereoselective (*syndio*- for the former ones and *iso*- for the latter ones) single-component catalysts for styrene polymerization. We can however specify that in the Cp-Flu series (complexes (a) in Fig. 50), the combination of the chloro neodymium precursor with Mg(allyl)$_2$, which leads to the *in situ* formation of the corresponding allyl-Nd derivative, is much less active than the single-component catalyst, although almost as *syndio*-selective.[122] Among these catalysts, some were the subject of more in-depth studies of their reactivity in polymerization that were not reported in the above cited review.

The mechanism of initiation of the syndiospecific styrene polymerization catalyzed by single-component *ansa*-(Cp-Flu) neodymium allyl was investigated by experimental/computational joint studies.[123] It was found by ^{13}C NMR studies of oligomers prepared by chain-growth polymerization using $\{C_5H_4CMe_2(9\text{-}C_{13}H_8)\}Nd[\eta^3\text{-}1,3\text{-}(SiMe_3)_2C_3H_3]$/excess Mg($n$Bu)$_2$ that 2,1-insertion is preferential to 1,2-insertion pathway. Moreover, according to the authors, the DFT studies revealed that with both *ansa*-dimethylmethylene **74$_{Ln}$** and *ansa*-dimethylsilylene **74‴$_{Ln}$** the insertion of styrene monomer takes place in the η^3-coordinated allyl moiety without the need to switch to η^1 hapticity (calculations performed on the europium complex), in contrast to the mechanism proposed in the case of organoaluminum-mediated chain transfer polymerization of 1,3-dienes with Nd-based catalysts.[124] In the same paper from Carpentier and coworkers, when comparing the two CMe_2- and $SiMe_2$-bridged complexes, it was concluded that the activity in styrene polymerization could be predicted to be higher in the former series.[123] Finally, the nature of the initiating ligand was deduced to be of prime importance in these single-component *ansa*-(Cp-Flu) neodymium complexes, with a very clear preference for Nd-allyl *vs* Nd-alkyl according to DFT.

Seeking to determine the origin of syndiospecificity in styrene polymerization observed with the bulky *ansa*-lanthanidocene allyl in the Cp-Flu series, authors from the same research group performed other DFT investigations, which were published posteriorly in 2010. It was proposed that the origin of the *syndio* control was due to a chain-end control mechanism (CEM), resulting from the conjunction of the minimization of two repulsion effects: the classical phenyl (incoming monomer)-phenyl (last unit inserted) one during the growing of the polymer chain, and also of the repulsion between the fluorenyl ligand and the incoming styrene unit.[125] This family of *ansa*-(Cp-Flu) allyl complexes were finally shown to display high versatility, with the possibility of producing syndiotactic styrene-rich co-polymer materials including isoprene and/or ethylene.[126]

Later, in 2011, Carpentier and coworkers found that the combination of the bulky allyl *ansa*-lanthanidocene **74′$_{Nd}$** (Fig. 50) with di(n-butyl)magnesium in excess behaved efficiently as binary catalytic system for the stereo-controlled coordinative polymerization of styrene under reversible chain transfer regime (CCTP, coordinative chain transfer polymerization), yielding syndiotactic PS with high activity (TOF 2500 h^{-1}).[127] A CCTP behavior was observed as well for *rac*-$\{Me_2C(Ind)_2\}Y[\eta^3\text{-}1,3\text{-}(SiMe_3)_2C_3H_3]$ (**75′$_Y$**, Ind = indenyl) under reversible transfer coordinative polymerization conditions, while this complex was previously shown to be active as single-component catalyst, but the dispersity was improved in the presence of an excess of Mg(^{n}Bu)$_2$. By adjusting the amount of Mg(^{n}Bu)$_2$, up to 200 polymer chains can be generated per lanthanide center.[128] In terms of selectivity, isotactic PS was produced with this yttrium catalyst combination with high activities (TOF up to 2100 h^{-1}).[127] Thorough mechanistic investigations, also confirmed by the support of theoretical studies, demonstrated that the initiation of the polymerization resulted from the insertion of styrene into the Ln-allyl (single component) or Ln-alkyl (chain transfer) moiety, and that an enantiomorphic site control mechanism (ECM) was operative to account for the *iso*-selectivity observed.[129]

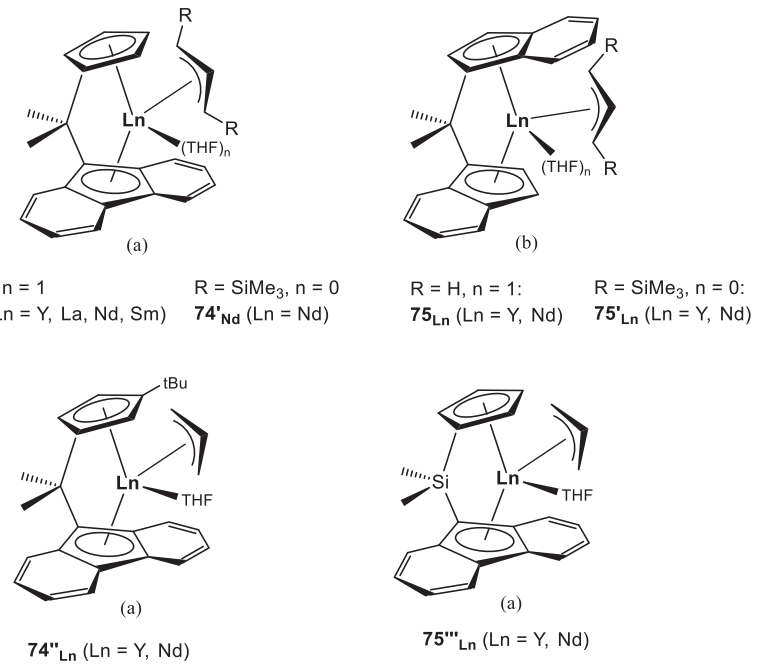

Fig. 50 Examples of *ansa*-(Cp-Flu)(allyl) ((a) form) and *ansa*-(indenyl)(allyl) ((b) form) complexes of the lanthanides.

The *ansa*-indenyl allyl complex of yttrium *rac*-{$Me_2C(Ind)_2$}Y[η^3-1,3-$(SiMe_3)_2C_3H_3$] [**75′$_Y$**] (Fig. 50) was also reported in 2007 as active as single-component catalyst toward isoprene homopolymerization, affording 1,4-*trans* rich PI with moderate activity (TOF 70 h^{-1}). The same authors subsequently showed that when di(ethyl)zinc was added in excess, reversible Y/Zn chain transfer was observed, with a comparable activity (TOF 76 h^{-1}), while maintaining the 1,4-*trans* selectivity (ca. 90%). In turn, in combination with $Mg(^nBu)_2$ a good level of transfer was noticed, but at the expense of the 1,4-*trans* selectivity (up to 47% 3,4 units).[128]

To complete the polymerization studies with this complex, the copolymerization of isoprene and styrene mediated by *rac*-{$Me_2C(Ind)_2$}Y[η^3-1,3-$(SiMe_3)_2C_3H_3$] [**75$_Y$**] in the absence of co-reagent afforded statistical copolymers with blocky distribution of the two monomers. Well-defined and crystalline 1,4-*trans*-PI-*b*-iPS diblock copolymers were also prepared by sequential addition of the two monomers.[128]

3.3.6 (Allyl)LnXX′ compounds

When the same synthetic procedure as for the synthesis of $Cp^{NMe2}Ln(\eta^3\text{-}C_3H_5)_2$ (Ln = Y, Ho, Lu) complexes was done in the case of the larger size neodymium element (Scheme 34, *vide infra*), it gave a mono(allyl) chloro derivative [$Cp^{NMe2}Nd(\eta^3\text{-}C_3H_5)(\mu\text{-Cl})]_2$ [**76$_{Nd}$**], instead of the expected bis allyl half-sandwich (Scheme 57). This neodymium complex was found to be dimeric through (μ-Cl) bridges with one substantially longer Nd–Cl bond than the other one, anticipating a possible reactivity.[82]

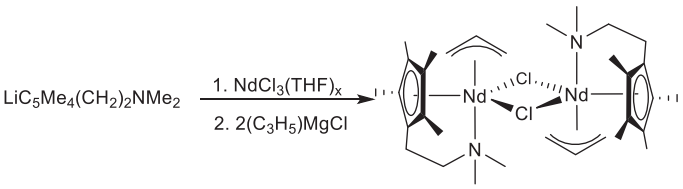

76$_{Nd}$

Scheme 57 Synthesis of mono(allyl)(chloro) complex **76$_{Nd}$**.

This chloro-allyl half-sandwich neodymium complex was found to be fairly active (TOF 1000–2000 h^{-1}) toward the polymerization of isoprene when combined with a borate activator and excess (10 equiv.) of AlR_3 cocatalyst. Interestingly, the selectivity switched from 85% 1,4-*trans* PI ($AlMe_3$) to 85% 3,4-PI ($Al(^iBu)_3$) depending on the aluminum reagent used. In common with the other complexes bearing this Cp^{NMe2} ligand (*vide infra*), the use of Al^iBu_3 *vs.* $AlMe_3$ with **76$_{Nd}$** provided reversible transfer between the lanthanide metal and the aluminum during the polymer chain growing process. Finally, the neodymium complex **76$_{Nd}$** was found to be inactive on its own without activator/co-catalyst, as already observed for the bis(allyl)Cp^{NMe2} complexes (Table 5).

Table 5 Structural and analytical data of bis-substituted mono(allyl) complexes (in brackets only the relevant complexes only, otherwise for all complexes).

Compound number	*Molecular formula*	*X-ray data* *Ln-C(allyl) distances (Å)*	*NMR data*	*References*
61$_{Sc}$, **61$_Y$**, **61$_{La}$**, **61$_{Sm}$**, **61$_{Nd}$**	$Ln(BH_4)_2(\eta^3\text{-}C_3H_5)(THF)_n$ (Ln = Sc, n = 2; Ln = Y, La, Sm, Nd, n = 3)	Y-C = 2.629, 2.636, 2.619 Sc-C = 2.508, 2.467, 2.419 La-C = 2.717, 2.810, 2.813 Sm-C = 2.663(3), 2.696(3), 2.685(3) Nd–C = 2.719(7), 2.740(6), 2.699(6)	^1H ^{11}B (**61$_Y$**, **61$_{La}$**)	84,86
62$_Y$, **62$_{La}$**	[(1,7-Me_2TACD)Ln($\eta^3\text{-}C_3H_5$)]$_2$ (Ln = Y, La)	La-C = 2.834(5), 2.843(5), 2.828(5)	^1H, ^{13}C (**62$_{La}$**)	88
62$_{Sc}$	(1,7-Me_2TACD)Sc($\eta^3\text{-}C_3H_5$)	–	^1H, ^{13}C	90
63$_Y$, **63$_{La}$**	[(1,7-Me_2TACD)Ln($\eta^3\text{-}C_3H_5$)$_2$K(THF)]$_n$ (Ln = Y, La)	–	^1H, ^{13}C	88
64$_{Nd}$, **64$_{Sm}$**	[Ln(Me_3TACD)($\eta^3\text{-}C_3H_5$)(μ-H)]$_2$ (Ln = Nd, Sm)	Sm-C = 2.749(4), 2.762(4), 2.825(3) Nd-C = 2.759(3), 2.799(3), 2.853(2)	^1H, ^{13}C (**64$_{Sm}$**)	91
65$_{Nd}$	{2-[Ph_2P(O)]C_6H_4NC(^{t}Bu)N(2,6-$Me_2C_6H_3$)}$_2$Nd(C_3H_5)	Nd-C = 2.67(2) to 2.78(2)	–	93
66$_Y$, **66$_{La}$**	[Ln(tbbp)($\eta^3\text{-}C_3H_5$)(THF)$_{1\text{-}2}$] (Ln = Y, La)	Y-C = 2.611(4), 2.646(4), 2.670(4)	^1H, ^{13}C	98
67$_{La}$, **67$_{Ce}$**, **67$_{Nd}$**, **67$_{Sm}$**	[Ln(etbbp)($\eta^3\text{-}C_3H_5$)(THF)$_{1\text{-}2}$] (Ln = La, Ce, Nd, Sm)	La = 2.744(2), 2.8009(17), 2.8087(18) Ce-C = 2.729(4), 2.765(3), 2.770(3)	^1H, ^{13}C	98

(*Continued*)

Table 5 (Continued)

Compound number	*Molecular formula*	*X-ray data Ln-C(allyl) distances (Å)*	*NMR data*	*References*
68_{Sc} **$68'_{Sc}$** **$68''_{Sc}$**	$[(C_5Me_4SiMe_3)Sc(\eta^3\text{-}C_3H_5)(\eta^6\text{-}PhNMe_2)][B(C_6F_5)_4]$ $[(C_5Me_4SiMe_3)Sc(\eta^3\text{-}C_3H_5)(\eta^6\text{-}PhMe)][B(C_6F_5)_4]$ $(C_5Me_4SiMe_3)Sc(\eta^3\text{-}C_3H_5)(\mu,\eta^6\text{-}Ph)BPh_3]$	Sc-C = 2.575(6), 2.584(9), 2.523(5) Sc-C = 2.454(3), 2.498(5), 2.417(3) Sc-C = 2.409(2), 2.452(2), 2.515(2)	^1H, ^{13}C (**$68'_{Sc}$**, **$68''_{Sc}$**), ^{19}F(**$68'_{Sc}$**), ^{11}B (**$68'_{Sc}$**)	75
68_Y, **$68'_Y$**, **68_{La}**, **$68'_{La}$**	$[(C_5Me_4SiMe_3)Ln(\eta^3\text{-}C_3H_5)(THF)_2]^+[B(C_6X_5)_4]^-$ (Ln = Y, La; X = H, F)	**$68''_{La}$**: La-C = 2.844(5), 2.803 (5), 2.684(5)	^1H, ^{13}C, ^{11}B, ^{19}F (**68_Y**, **68_{La}**)	6
69_{Sc}, **69_Y**	$(C_5Me_4H)_2Ln(\eta^3\text{-}C_3H_5)$ (Ln = Sc, Y)	Sc-C = 2.4702(11), 2.4774 (11), 2.4618(11) Y-C = 2.590(3), 2.594(3), 2.603(3); 2.585(3), 2.592(3), 2.603(3)	^1H, ^{13}C, ^{45}Sc (**69_{Sc}**)	103,105
70_{Lu}	$[(C_5H_4SiMe_3)_2Lu(\mu\text{-}\eta^1\text{:}\eta^1\text{-}C_3H_5)]_4$	Lu-C = 2.508(3), 2.482(3), 2.485(3)	^1H	109
71_Y	$(C_5Me_5)_2Y(\eta^3\text{-}CH_2CMeCH_2)$	Y-C = 2.562(2), 2.7021(2), 2.570(2)	^1H, ^{13}C	110
73_Y	$(Cp^*)_2Y[\eta^3\text{-}C_3H_4(BC_8H_{14})]$	Y-C = 2.681(5), 2.661(5), 2.632(5)	^1H, ^{11}B	117
74_Y, **74_{La}**, **74_{Nd}**, **74_{Sm}**; **$74'_{Nd}$**; **$74''_Y$**, **$74''_{Nd}$** ; **$74'''_Y$**, **$74'''_{Nd}$**	$\{C_5H_3R\text{-}EMe_2(9\text{-}C_{13}H_8)\}Ln[\eta^3\text{-}1,3\text{-}(R')_2C_3H_3(THF)_n]$: E = C, Si; R = H, ^{t}Bu; R′ = H, $SiMe_3$; n = 0, 1	**71_{Nd}**: Nd-C = 2.656(12) , 2.700(11), 2.725(9) **$71''_{Nd}$**: Nd-C = 2.639(5), 2.756 (5), 2.818(5) **$71'''_Y$**: Y-C = 2.583(2), 2.571 (10); 2.649(2)	^1H (**71_Y**, **71_{La}**, **$71''_Y$**, **$71'''_Y$**), ^{13}C (**71_Y**, **$71''_Y$**, **$71'''_Y$**)	120
75_Y, **75_{Nd}**; **$75'_Y$**, **$75'_{Nd}$**	*rac*-$\{Me_2C(Ind)_2\}Ln[\eta^3\text{-}1,3\text{-}R_2C_3H_3(THF)_n]$: R = H, $SiMe_3$; n = 0, 1	**$72'_Y$**: Y-C in CCDC-648472	^1H (**$72'_Y$**), ^{13}C (**$72'_Y$**)	121
76_{Nd}	$[Cp^{NMe2}Nd(\eta^3\text{-}C_3H_5)(\mu\text{-}Cl)]_2$	Nd-C = 2.666(5), 2.702(4), 2.685(5)	–	82

3.4 Aza-allyl lanthanide complexes

Zhang et al. reported in 2010 a new method to prepare lanthanide hetero-allyl complexes by insertion of a ketenimines into the Ln-C σ-Bond of a lanthanide precursor[130]: the reaction of $[Cp_2Ln(\mu\text{-}Me)]_2$ and Cp_2LnPh with $PhRC{=}C{=}N^tBu$ gives 1-aza-allyl organometallic complexes $Cp_2Ln[^tBuNC(R')CRPh]$ (Ln = Y, Er, Yb; **77_{Ln}**: R = Ph, R′ = Me; **78_{Ln}**: R = Ph, R′ = Ph; **79_{Ln}**: R = H, R′ = Me; **80_{Ln}**: R = H, R′ = Ph) (Scheme 58).

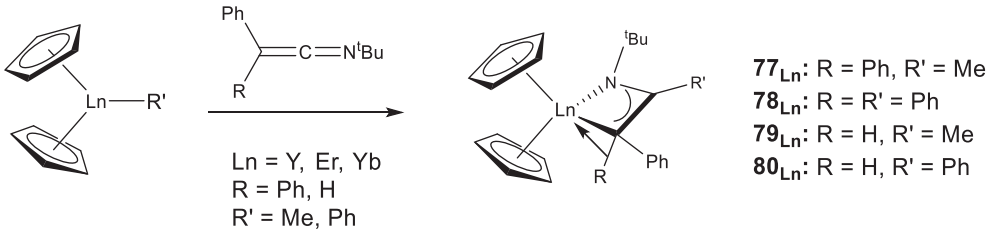

Scheme 58 Synthesis of aza(allyl) complexes **77_{Ln}**, **78_{Ln}**, **79_{Ln}**, **80_{Ln}**.

The erbium congener **77_{Er}** was isolated as X-ray quality crystals (Fig. 51). The structural data revealed that the resulting aza(allyl) ligand in that complex has a strong η^3-interaction with the Er^{3+} ion. Thus, the coordination sphere of the metal atom is partly saturated by one agostic interaction to one hydrogen atom from the ligand. A similar structure was observed for ytterbium (**77_{Yb}**) and yttrium (**77_Y**) congeners.

Recently, it was observed that the treatment of rare-earth metal dialkyl complexes supported by a pyrrolyl-functionalized β-diketiminato ligand with the formula $[MeC(NDipp)CHC(Me)NCH_2CH_2NC_4H_2\text{-}2,5\text{-}Me_2]Ln(CH_2SiMe_3)_2(THF)$ (Ln = Y, Er; Dipp = 2,6-^{i}Pr$_2$C$_6$H$_3$) with 2,4,6-trimethylpyridine leads to the mononuclear azaallyl [MeC(NDipp)CHC(Me)

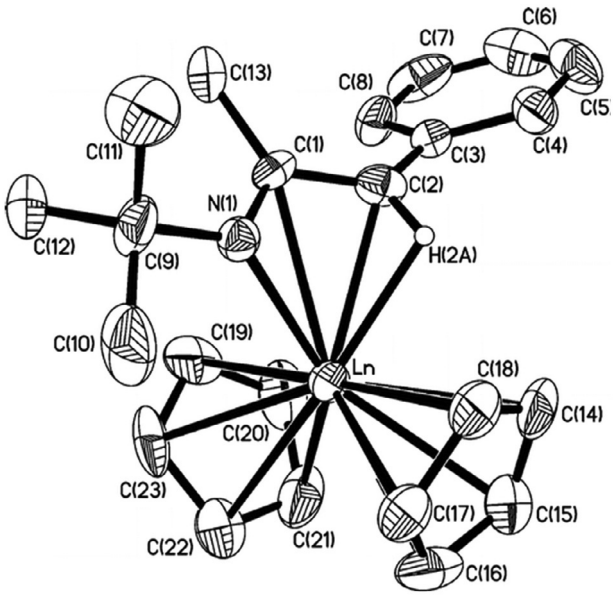

Fig. 51 ORTEP plot of $Cp_2Er[^tBuNC(Me)CHPh]$ (**77**$_{Er}$) with the probability ellipsoids drawn at the 30% level. Hydrogen atoms are omitted for clarity. Reprinted from Zhang, Z.; Bu, X.; Zhang, J.; Liu, R.; Zhou, X.; Weng L. *Organometallics* **2010**, *29*, 2111–2117, with the permission of the American Chemical Society.

$NCH_2CH_2NC_4H_2$-2,5-Me_2]Ln(η^3-CH_2-2-NC_5H_2-4,6-Me_2)$_2$ (**81**$_{Ln}$, Ln = Y, Er) *via* sp^3 C–H activation (Scheme 59, shown for the erbium congener). The complexes were isolated as suitable X-ray crystals, where the η^3-aza-allyl arrangement was evidenced by Ln–C and Ln–N bond lengths of *ca.* 2.4–2.8 Å, i.e. in the typical range for this coordination mode[57] (Table 6).

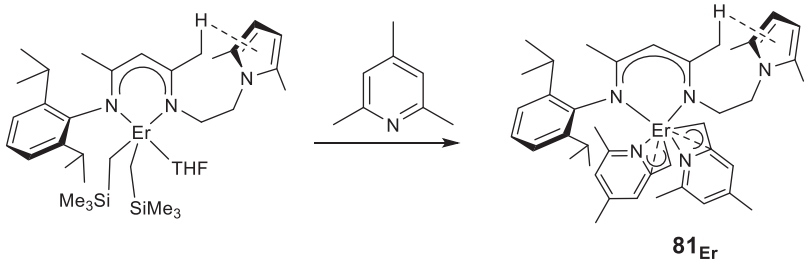

81$_{Er}$

Scheme 59 Synthesis of **81**$_{Er}$ via C–H activation of 2,4,6-trimethylpyridine by the (pyrrolyl-functionalized β-diketiminato)dialkyl erbium precursor.

Table 6 Structural and analytical data of aza-allyl complexes (in brackets only the relevant complexes only, otherwise for all complexes).

Compound number	*Molecular formula*	*X-ray data Ln-C(allyl) distances (Å)*	*NMR data*	*References*
77$_Y$, **77**$_{Er}$, **77**$_{Yb}$; **78**$_Y$, **78**$_{Er}$, **78**$_{Yb}$; **79**$_Y$, **79**$_{Er}$, **79**$_{Yb}$; **80**$_Y$, **80**$_{Er}$, **80**$_{Yb}$	$Cp_2Ln[^tBuNC(R')CRPh]$ (R = Ph, R′ = Me; R = Ph, R′ = Ph; R = H, R′ = Me; R = H, R′ = Ph)	**77**$_{Ln}$: Y-C = 2.917(6), 2.902(5), 2.754(5) Er-C = 2.892(5), 2.903 (5), 2.725(5) Yb-C = 2.892(7), 2.940 (7), 2.740(6) **78**$_{Ln}$: Y-C = 2.874(10), 2.907(8), 2.795(8) Yb-C = 2.856(7), 2.899 (7), 2.743(7) Yb-C = 2.880(7), 2.943 (7), 2.761(7)	^{1}H (**77**$_Y$, **78**$_Y$, **79**$_Y$, **80**$_Y$), ^{13}C (**77**$_Y$, **78**$_Y$, **79**$_Y$, **80**$_Y$)	130
81$_Y$, **81**$_{Er}$	[MeC(NDipp)CHC(Me) $NCH_2CH_2NC_4H_2$-2,5-Me_2] Ln(η^3-CH_2-2-NC_5H_2-4,6-Me_2)$_2$ (Ln = Y, Er; Dipp = 2,6-$^iPr_2C_6H_3$)	Y-C = 2.465(5), 2.727 (5) Er-C = 2.450(5), 2.709 (5)	^{1}H, ^{13}C (**81**$_Y$)	57

3.5 Lanthanide complexes with unusual allyl coordination mode

The equimolar reaction between $Y(CH_2SiMe_3)_3(THF)_2$ precursor and $HL^2(^iPr)$ pro-ligand [$HL^2(^iPr)$ = $Cp^{Me}PN$-type ligand $C_5Me_4H—PPh_2=N—2,6\text{-}^iPr_2\text{-}C_6H_3$] in the presence of LiCl afforded two distinct bis(alkyl) complexes based on ^1H NMR spectroscopic analysis (Scheme 60).[131]

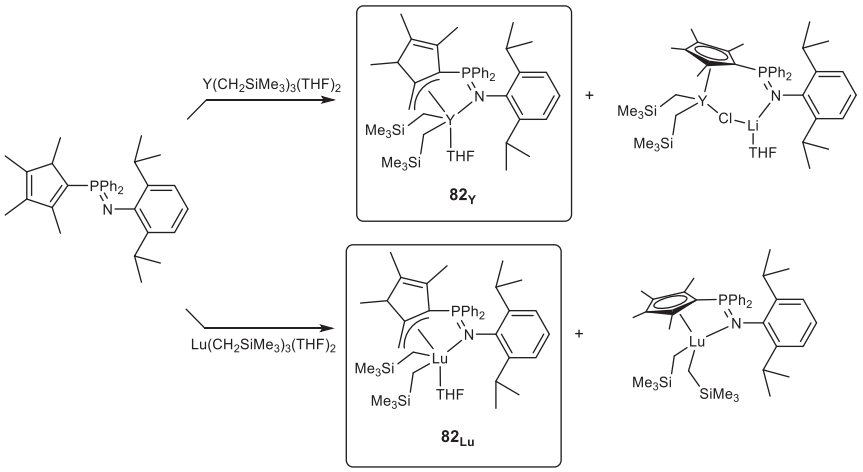

Scheme 60 Synthesis of complexes $\mathbf{82_{Ln}}$.

Recrystallization of the crude material from these reaction mixtures furnished the complexes $[C_5HMe_3(\eta^3\text{-}CH_2)—PPh_2=N—2,6\text{-}^iPr_2\text{-}C_6H_3]Y(CH_2SiMe_3)_2(THF)$ [$\mathbf{82_Y}$] and $(C_5Me_4—PPh_2=N—2,6\text{-}^iPr_2\text{-}C_6H_3)Y(CH_2SiMe_3)_2(LiCl)(THF)$ in a ≈9/1 ratio, respectively. The X-ray diffraction studies of the former complex revealed an uncommon η^3-allyl/κ-N coordination mode of the ligand with Y^{3+} (Fig. 52). The Y-C(allyl) distances [2.749(3), 2.669(3), and 2.724(3) Å] are similar, suggesting a symmetrical allylic moiety bounded to yttrium atom. Such a coordination mode has been already observed in $(\eta^5\text{-}C_5Me_4–C_5H_4N)[C_5HMe_3(\eta^3\text{-}CH_2)–C_5H_4N\text{-}\kappa]Y(CH_2SiMe_3)$[132] and $(C_5Me_5)Y(\eta^5\text{-}C_5Me_4CH_2–C_5Me_4CH_2\text{-}\eta^3)$,[133] although the allyl was found to be dissymmetric in both cases. When the central metal was changed to lutetium, a mixture of two bis(alkyl) complexes was further isolated, one of which, $[C_5HMe_3(\eta^3\text{-}CH_2)—PPh_2=N—C_6H_3^iPr_2]Lu(CH_2SiMe_3)_2(THF))$ [$\mathbf{82_{Lu}}$], exhibited a η^3-allyl/κ-N coordination mode similar to that found for the yttrium derivative from ^1H NMR studies.

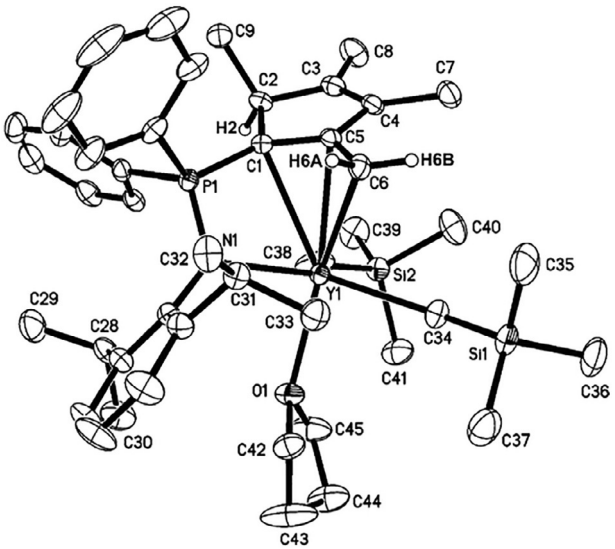

Fig. 52 Molecular structure of $\mathbf{82_Y}$. Thermal ellipsoids are set at the 40% probability level. Reprinted from Jian, Z.; Petrov, A. R.; Hangaly, N. K.; Li, S.; Rong, W.; Mou, Z.; Rufanov, K. A.; Harms, K.; Sundermeyer, J.; Cui, D. *Organometallics* **2012**, *31*, 4267–4282, with the permission of the American Chemical Society.

In the reaction of $[(C_5Me_5)_2YH]_2$ with cyclooctatetraene C_8H_8, $(C_5Me_5)Y[(\eta^5\text{-}C_5Me_4CH_2\text{-}C_5Me_4CH_2\text{-}\eta^3)]$ [**83$_Y$**] formed unexpectedly among other by-products solely in benzene (Scheme 61).[133]

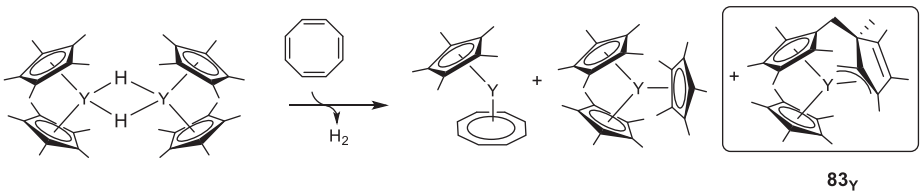

Scheme 61 Formation of complex **83$_Y$** from ligands redistribution after reaction with cyclooctatetraene.

The X-ray diffraction analysis of **83$_Y$** (Fig. 53) indicated that the Y^{3+} metal center is coordinated to one $(C_5Me_5)^-$ ligand in η^5-coordination mode and two $(C_5Me_5)^-$ rings that are linked by a CH_2 group to form a new type of *ansa-allyl*-cyclopentadienyl dianion ligand of the type $(C_5Me_4CH_2\text{-}C_5Me_4CH_2)^{2-}$. The coordination of the dianion to Y^{3+} reveals an unusual pentahapto-trihapto chelation $(\eta^5\text{-}C_5Me_4CH_2\text{-}C_5Me_4CH_2\text{-}\eta^3)^{2-}$ where the Y-C(η^3-allyl) bonds are not symmetrical [Y-C(allyl) in the range of 2.450–2.990 Å].

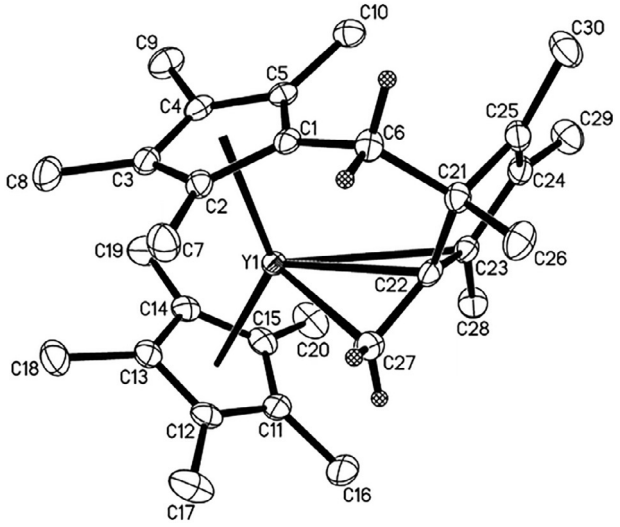

Fig. 53 ORTEP plot drawn at the 50% probability level of **83$_Y$**. Hydrogen atoms are omitted for clarity. Reprinted from Evans, W. J.; Schmiege, B. M.; Lorenz, S. E.; Miller, K. A.; Champagne, T. M.; Ziller, J. W.; DiPasquale, A. G.; Rheingold, A. L. *J. Am. Chem. Soc.* **2008**, *130*, 8555–8563, with the authorization of the American Chemical Society.

An allylic Ln,C,P π-type interaction was proposed in phosphoniomethylidene complexes of scandium and lutetium, [{MeC(NDipp)CHC(NDipp)Me}Ln(CHPPh$_3$)X] (**84$_{Sc}$**: R = Me; **84$_{Lu}$**: R = CH_2SiMe_3; **84′$_{Sc}$**: X = I; **84″$_{Sc}$**: X = OTf), on the basis of X-ray diffraction studies corroborated with DFT calculations (Scheme 62, Fig. 54a,b,c).[134]

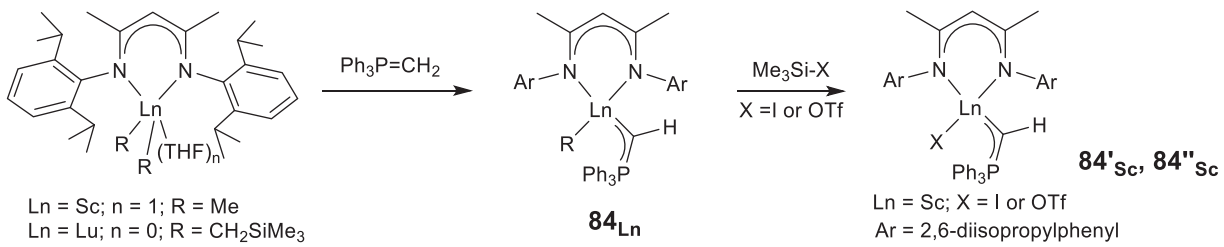

Scheme 62 Synthesis of complexes **84$_{Ln}$**, **84′$_{Sc}$**, **84″$_{Sc}$**.

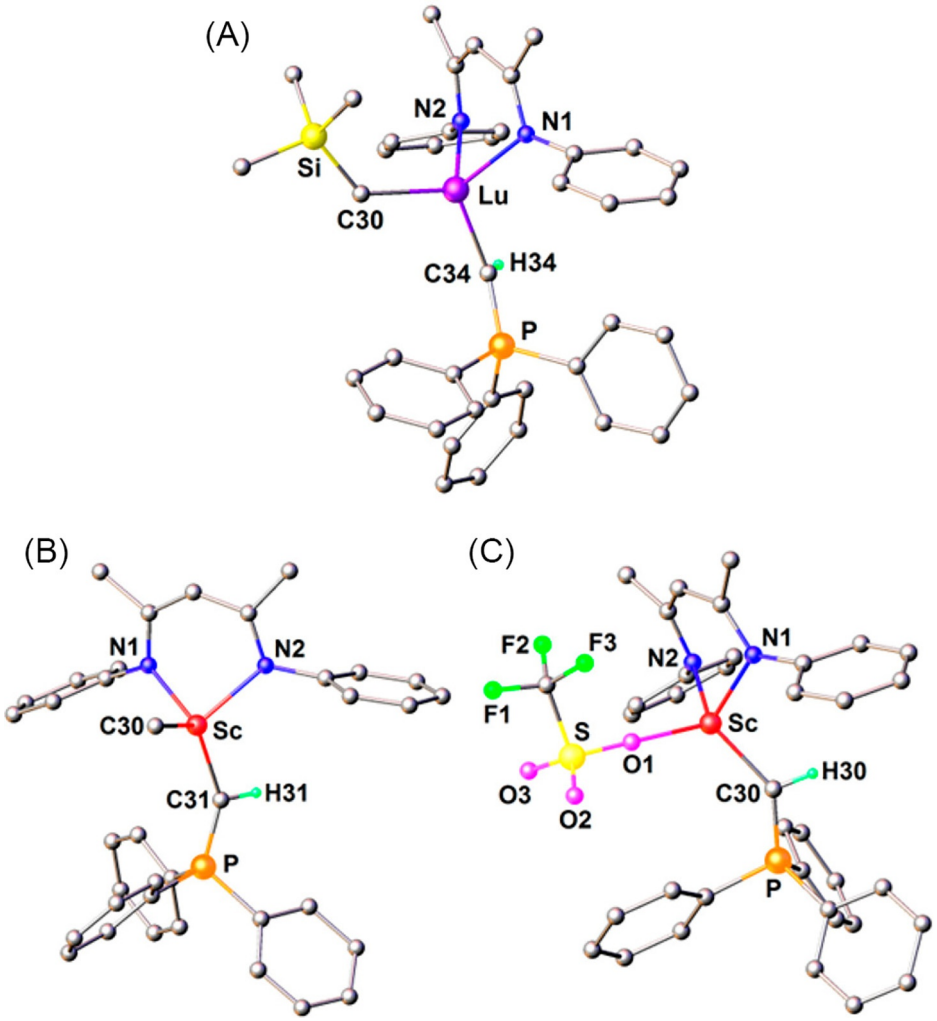

Fig. 54 Molecular structure of $\mathbf{84_{Lu}}$ (a), $\mathbf{84_{Sc}}$ (b) and $\mathbf{84''_{Sc}}$ (c), represented with ball and stick. Isopropyl groups and hydrogen atoms are omitted for clarity. Reprinted from Mao, W.; Xiang, L.; Maron, L.; Leng, X.; Chen, Y. *J. Am. Chem. Soc.* **2017**, *139*, 17759–17762, with the permission of the American Chemical Society.

An η^3-benzyl-type coordination mode is observed in the dihydrido-1,2-diphenylethane-1,2-diyl complex $[(NCN)LuH(THF)]_2$-(PhCHCHPh) ($\mathbf{85_{Lu}}$), which results from the reaction of the dihydride $[(NCN)LuH_2]_2(THF)_3$ with diphenylacetylene in THF after 24 h (NCN = $PhC(NC_6H_3^iPr_2\text{-}2,6)_2$) (Scheme 63).[135] This interaction is replaced by a π-interaction of the phenyl group in benzene.

The "PhCHCHPh" moiety in complex $\mathbf{85_{Lu}}$ is linked to one lutetium metal atom in an η^2-fashion with the ethane-1,2-diyl carbon atoms and to the other lutetium metal atom in an η^3-coordination mode with one benzyl carbon, one *ipso*-phenyl carbon and one *ortho*-phenyl carbon atoms (Fig. 55).

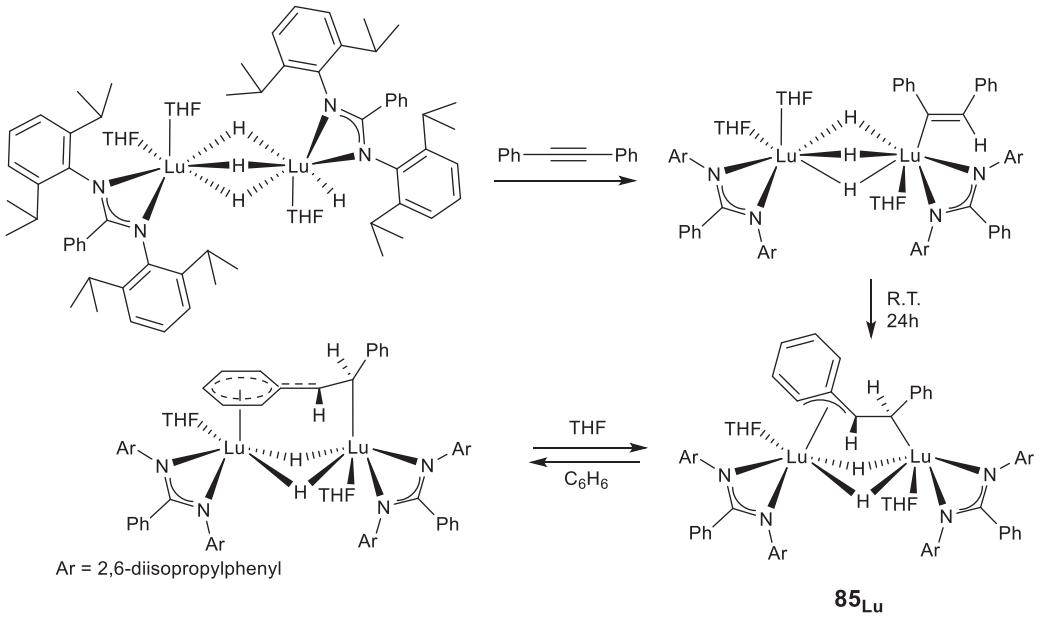

Scheme 63 Formation of complex $\mathbf{85_{Lu}}$.

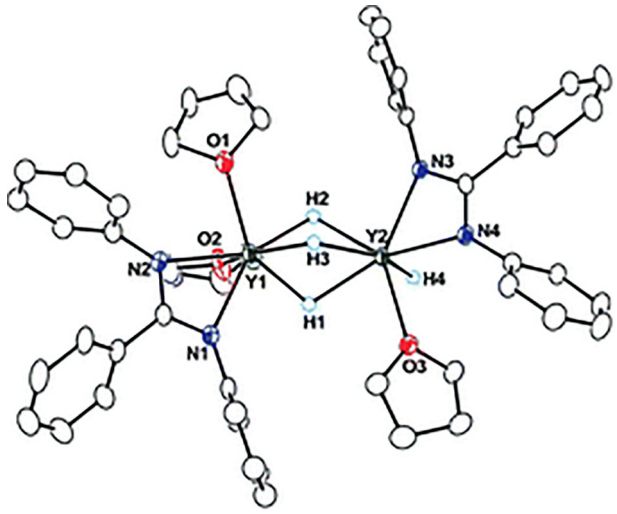

Fig. 55 ORTEP plot of the dihydrido-1,2-diphenylethane-1,2-diyl complex [(NCN)LuH(THF)]$_2$-(PhCHCHPh) ($\mathbf{85_{Lu}}$) with thermal ellipsoids drawn at the 30% probability level. The isopropyl group and hydrogen atoms (except the bridging hydride) are omitted for clarity. Reprinted from Cheng J.; Wang H.; Nishiura M.; Hou Z. *Chem. Sci.* **2012**, *3*, 2230–2233, with the authorization of the Royal Chemical Society.

Addition of 2 equiv. of the pyridyl-functionalized cyclopentadienyl ligand C_5Me_4H-C_5H_4N to $Y(CH_2SiMe_3)_3(THF)_2$ generated the expected bis-Cp derivative $(C_5Me_4H\text{-}C_5H_4N)_2YCH_2SiMe_3$ together with the well-defined yttrium mono(alkyl) complex $(C_5Me_4H\text{-}C_5H_4N)[C_5HMe_3(\eta^3\text{-}CH_2)\text{-}C_5H_4N\text{-}\kappa]YCH_2SiMe_3$ ($\mathbf{86_Y}$) (Scheme 64; Table 7).[132]

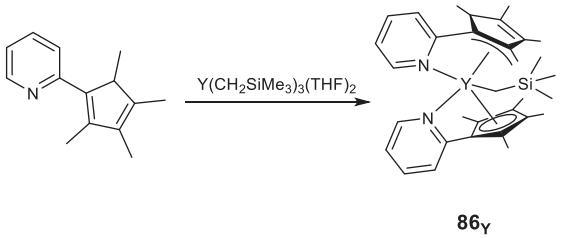

Scheme 64 Formation of complex $\mathbf{86_Y}$.

Table 7 Structural and analytical data of lanthanide complexes with unusual coordination mode (in brackets only the relevant complexes only, otherwise for all complexes).

Compound number	*Molecular formula*	*X-ray data Ln-C distances (Å)*	*NMR data*	*References*
82$_Y$, 82$_{Lu}$	$[C_5HMe_3(\eta^3\text{-}CH_2)\text{–}PPh_2{=}N\text{–}2,6\text{-}{}^iPr_2\text{-}C_6H_3]Ln(CH_2SiMe_3)_2(THF)$ (Ln = Y, Lu)	Y-C = 2.749(3), 2.669(3), 2.724(3)	^1H, ^{13}C, ^{31}P	131
83$_Y$	$(C_5Me_5)Y[(\eta^5\text{-}C_5Me_4CH_2\text{-}C_5Me_4CH_2\text{-}\eta^3)]$	Y-C = 2.6985(15), 2.9897 (16), 2.4502(16)	–	133
84$_{Sc}$, 84$_{Lu}$, 84′$_{Sc}$, 84″$_{Sc}$	[{MeC(NDipp)CHC(NDipp)Me}Ln(CHPPh$_3$)X] (**84$_{Sc}$**: R = Me; **84$_{Lu}$**: R = CH_2SiMe_3; **84′$_{Sc}$**: X = I; **84″$_{Sc}$**: X = OTf)	**84$_{Sc}$**: Sc-C = 2.105(2) **84′$_{Sc}$**: Sc-C = 2.044(5) **84″$_{Sc}$**: Sc-C = 2.060(3) **84$_{Lu}$**: Lu-C = 2.192(11)	^1H, ^{13}C, ^{31}P, ^{31}F (**84″$_{Sc}$**)	134
85$_{Lu}$	$[(NCN)LuH(THF)]_2(PhCHCHPh)$	Lu-C = 2.604(7), 2.785(6), 2.775(7)	^1H, ^{13}C	135
86$_Y$	$(\eta^5\text{-}C_5Me_4\text{–}C_5H_4N)[C_5HMe_3(\eta^3\text{-}CH_2)\text{–}C_5H_4N\text{-}\kappa]Y(CH_2SiMe_3)$	Y-C = 2.961(3), 2.792(3), 2.501(3)	^1H, ^{13}C	132
87$_{Ln}$	$(\eta^3\text{-}C_{13}H_8\text{-}C_5H_4N)Ln(CH_2SiMe_3)_2(THF)$ (Ln = Y, Sc, Lu)	Y-C = 2.689(2), 2.755(2), 2.916(2)	^1H, ^{13}C	78,136,137
87′$_Y$	$(\eta^3\text{-}C_{13}H_8\text{-}C_5H_4N)Y(CH_2C_6H_4\text{-}o\text{-}NMe_2)_2$	Y-C = 2.689(2), 2.755(2), 2.916(2	^1H, ^{13}C	78
88$_{Sc}$, 88$_{Lu}$, 88$_Y$	$(\eta^3{:}\eta^1\text{-}FluSiMe_2N{}^tBu)Ln(CH_2SiMe_3)(THF)_2$ (Ln = Sc, Lu, Y)	**88$_{Sc}$**: Sc-C = 2.065(3), 2.395(3), 2.730(3) **88$_{Lu}$**: Lu-C = 2.180(3), 2.504(4), 2.746(4) **88$_Y$**: Y-C = 2.213(3), 2.566 (3), 2.769(3)	^1H, ^{13}C	137

The X-ray diffraction analysis of complex [**86$_Y$**] exhibited a rare κ/η^3-allylic coordination mode, resulting from the unexpectedly C–H bond activation of one methyl group of the Cp ligand. The C–C bond distances of the $C_5HMe_3(\eta^3\text{-}CH_2)$ unit clearly showed that the electrons are delocalized over the three C atoms of the allyl group rather than in the Cp ring, with the Y-C(η^3-allyl) bonds being not symmetrical [Y-C(allyl) in the range of 2.50–2.96 Å] (Fig. 56).

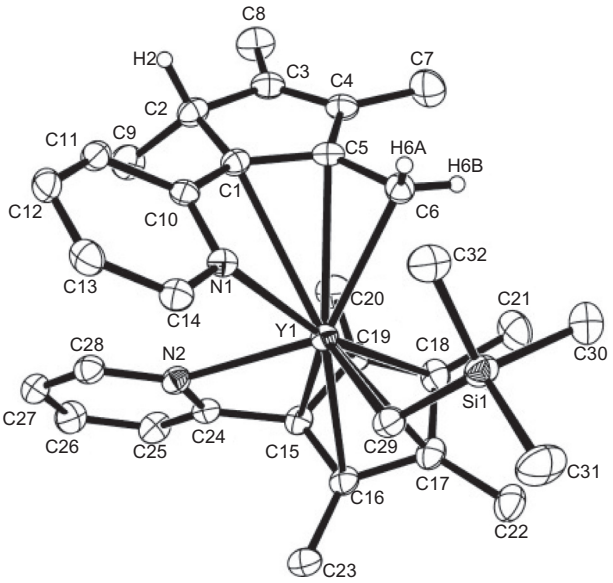

Fig. 56 ORTEP plot with thermal ellipsoids set at 40% probability level of **86$_Y$**. Hydrogen atoms are omitted for clarity. Reprinted from Jian, Z.; Cui, D. *Chem. Eur. J.* **2011**, *17*, 14578–14585, with the authorization of WILEY-VCH Verlag GmbH.

Deprotonation of the bulky pyridyl-Flu ligand ($C_{13}H_9\text{-}C_5H_4N$) in presence of Ln-$(CH_2SiMe_3)_3(THF)_2$ led to the rare earth-metal–dialkyl complexes of the type $(\eta^3\text{-}C_{13}H_8\text{-}C_5H_4N)Ln(CH_2SiMe_3)_2(THF)$ (**87$_{Ln}$**, Ln = Y, Sc, Lu) (Scheme 65).[78]

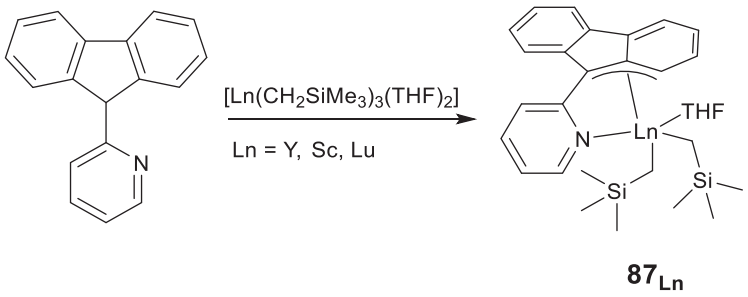

Scheme 65 Formation of complexes $\mathbf{87_{Ln}}$.

The crystal structure of the three complexes $\mathbf{87_{Ln}}$ has been successfully resolved and displays in each case an unusual asymmetric η^3-allyl bonding mode of the Flu moiety to the metal (Fig. 57, yttrium complex $\mathbf{87_Y}$). Computational studies of the scandium counterpart $\mathbf{87_{Sc}}$ also suggested that the ligand is coordinated to the metal in η^3-allyl/κ^1 fashion. On the other hand, it was found by calculation that upon alkyl abstraction, the ligand is preferably coordinated to the metal in η^5-cyclopentadienyl/κ^1 mode within the resulting cationic Sc complex.[136]

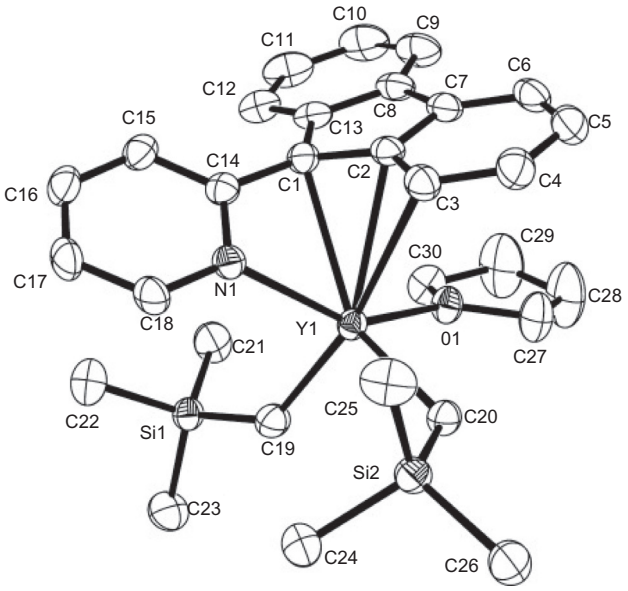

Fig. 57 Molecular structure of (η^3-$C_{13}H_8$-C_5H_4N)Y(CH_2SiMe_3)$_2$(THF) ($\mathbf{87_{Sc}}$). Displacement ellipsoids are drawn at the 40% probability level. Hydrogen atoms are omitted for clarity. Reprinted from Jian, Z.; Cui, D.; Hou, Z. *Chem. Eur. J.* **2012**, *18*, 2674–2684, with the permission of WILEY-VCH Verlag GmbH.

In addition, reaction of tris(aminobenzyl) yttrium with 1 equiv. of the same bulky pyridyl-Flu ligand produced the aminobenzyl unsolvated yttrium analog (η^3-$C_{13}H_8$-C_5H_4N)Y($CH_2C_6H_4$-*o*-NMe_2)$_2$ ($\mathbf{87'_Y}$) (Scheme 66), which exhibits similar coordination mode of the Flu moiety to the metal in an asymmetric η^3-allyl fashion (Fig. 58). Upon activation with $[Ph_3C][B(C_6F_5)_4]/Al^iBu_3$, this complex displayed poor activities toward the polymerization of styrene with moderate selectivity.

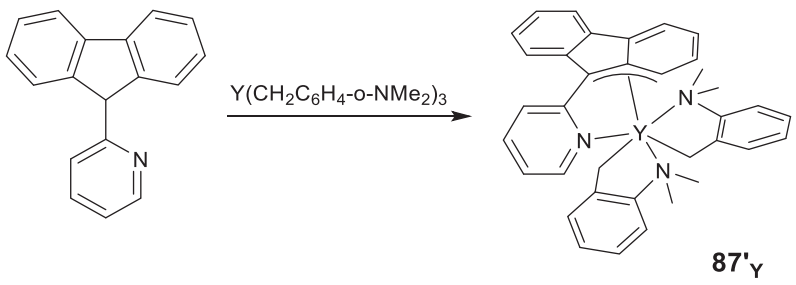

Scheme 66 Formation of complex $\mathbf{87'_Y}$ starting from tris(aminobenzyl) yttrium precursor.

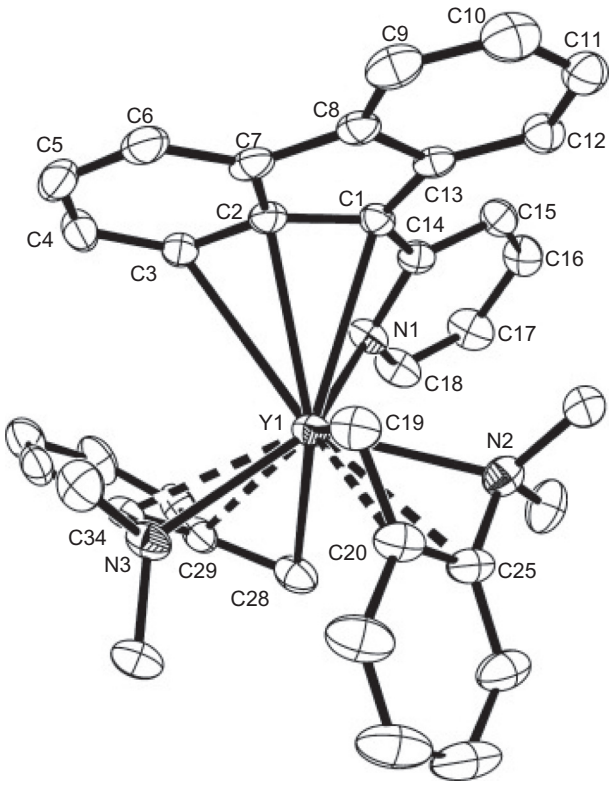

Fig. 58 Molecular structure of (η^3-$C_{13}H_8$-C_5H_4N)Y($CH_2C_6H_4$-*o*-NMe_2)$_2$ (**87′$_Y$**). Displacement ellipsoids are drawn at the 40% probability level. Hydrogen atoms are omitted for clarity. Reprinted from Jian, Z.; Cui, D.; Hou, Z. *Chem. Eur. J.* **2012**, *18*, 2674–2684, with the permission of WILEY-VCH Verlag GmbH.

With the aim to improve the activity and selectivity in the polymerization of olefins, Guo and coworkers reported the synthesis of a family of complexes (η^3:η^1-$FluSiMe_2N^tBu$)$Ln(CH_2SiMe_3)(THF)_2$ (**88$_{Ln}$**, Ln = Sc, Lu, Y) complexes by reacting the pro-ligand $FluSiMe_2NH^tBu$ with 1 equiv. of $Ln(CH_2SiMe_3)_3(THF)_n$ (Scheme 67).

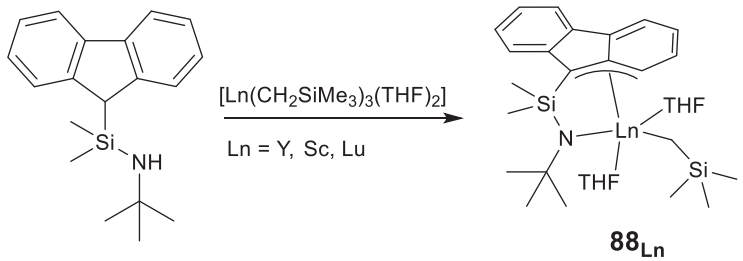

Scheme 67 Synthesis of complexes **88$_{Ln}$**.

X-ray diffraction studies of single crystals of the three complexes revealed a related asymmetric η^3-allyl mode of coordination of the Flu moiety to the metal (Fig. 59).[137]

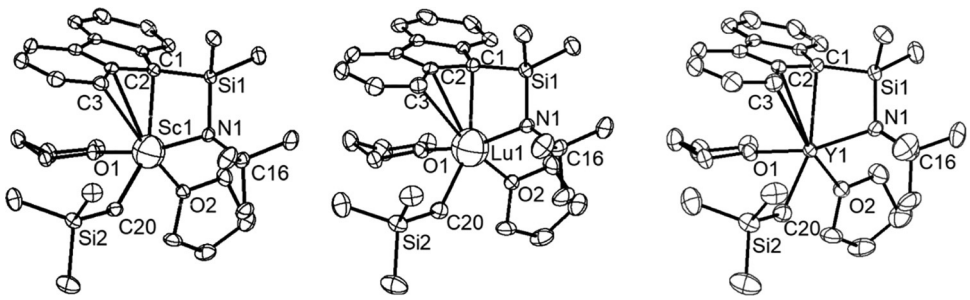

Fig. 59 ORTEP plots of complexes (η^3:η^1-$FluSiMe_2N^tBu$)$Ln(CH_2SiMe_3)(THF)_2$ (**88$_{Ln}$**, Ln = Sc, Lu, Y) with thermal ellipsoids set at the 30% probability level. Hydrogen atoms are omitted for clarity. Reprinted from Guo, G.; Wu, X.; Yan, X.; Yan, L.; Li, X.; Zhang, S.; Qiu, N. *Polymers* **2019**, *11*, 836, with the permission of MDPI.

When compared to $(\eta^3\text{-}C_{13}H_8\text{-}C_5H_4N)Y(CH_2C_6H_4\text{-}o\text{-}NMe_2)_2$ precatalyst, complexes $\mathbf{88_{Ln}}$ present enhanced catalytic activities and high regio-/seoselectivities in the 1,4-*cis* polymerization of isoprene and myrcene or in the syndiotactic polymerization of styrene, in presence of boron-based activator combined with aluminum alkyl.

3.6 Allyl complexes of the lanthanides as intermediates

Allyl lanthanide species have been postulated to be formed during some specific olefinic chemical processes that take place in the presence of lanthanides, like the lanthanum-mediated dehydrogenation of butenes[138] and C–H bond activation of propene,[139] based on spectroscopic analyses and theoretical calculations.

4 Conclusion

Allyl complexes of the lanthanides, as well as alkene(alkenyl) and alkyne(alkynyl) derivatives of these elements, have seen a considerable surge of interest in the last 15 years. A significant amount of new complexes with a wide variety of structures have been prepared, and among them new families of mono and bis-allyl complexes in particular have emerged, such as novel cationic complexes, which prefigure reactive species involved in some catalytic processes, or mixed allyl complexes sometimes including another type of reactive ligand. Otherwise, substituted allyl ligands or ligands incorporating a heteroatom have been the subject of several studies, allowing the synthesis of novel compounds.

Synthesis strategies are diversifying, using, for allyl derivatives and depending on the precursor used, traditional ionic metathesis or acid-base reactions with a pro-ligand, as an opportunity offered by the allyl ligand in a "soft" synthetic manner to subtly add a new ligand to the coordination sphere of a lanthanide. With regard to alkene(alkenyl) and alkyne(alkynyl) complexes, which generally result from C–H activation or non-common reduction processes, the variety of compounds reported is another illustration of the structural diversity observed with organometallic chemistry of the lanthanide elements. Quite often the families of complexes, from lanthanum to scandium, go hand in hand with the size of the lanthanides: we find typical structures with the largest, others with the smallest, where the choice of the lanthanide precursors and the reagents is of particular importance in that context.

As far as allyl complexes are concerned, the allyl ligand is rather versatile, often terminal, sometimes bridged, it can have a somewhat static or fluxional character, it is usually trihapto but can eventually slip into monohapto. This feature is apparent in crystalline structures, whereas in solution, NMR spectroscopy, even for paramagnetic compounds, is a very useful tool for studying the molecular arrangement of the allyl ligand on a metal.

In terms of reactivity, the chemistry of insertion into the lanthanide-allyl bond has continued to develop, or to generate hydrides or cationic species. Applications in catalysis have also largely been demonstrated, notably in hydrosilylation. Moreover, the use of allylic complexes has been particularly extended to polymerization reactions, following the initial work on the polymerization of dienes, and toward styrene and polar monomers as well. New allylic catalysts, including single-component systems—where the absence of cocatalyst may eventually be an advantage—with a strong stereoregulating and controlled character, have been specially designed and developed.

There is no doubt that this very special branch of the exciting organometallic lanthanide chemistry will continue to develop in the future.

References

1. Marks, T. J.; Ernst, R. D. In *Comprehensive Organometallic Chemistry*; Wilkinson, G., Stone, F. G. A., Abel, E. W., Eds.; Pergamon: Oxford, UK, 1982; pp 196–197. 205–206. Edelmann, F. T. In *Comprehensive Organometallic Chemistry II*; Abel, E. W.; Stone, F. G. A., Wilkinson, G., Eds.; Elsevier: Oxford, UK, 1995; pp 26–28; Edelmann, F. T. In *Comprehensive Organometallic Chemistry III*; Mingos, D. M. P.; Crabtree, R. H., Eds.; Elsevier: Oxford, UK, 2007; pp 17–21.
2. Carpentier, J.-F.; Guillaume, S. M.; Kirillov, E.; Sarazin, Y. *C. R. Chim.* **2010**, *13*, 608–625.
3. Taube, R.; Windisch, H.; Maiwald, S.; Hemling, H.; Schumann, H. *J. Organomet. Chem.* **1996**, *513*, 49–61.
4. Taube, R.; Maiwald, S.; Sieler, J. *J. Organomet. Chem.* **2001**, *621*, 327–336.
5. Sanchez-Barba, L. F.; Hughes, D. L.; Humphrey, S. M.; Bochmann, M. *Organometallics* **2005**, *24*, 3792–3799.
6. Robert, D.; Abinet, E.; Spaniol, T. P.; Okuda, J. *Chem. Eur. J.* **2009**, *15*, 11937–11947.
7. Abrams, M. B.; Yoder, J. C.; Loeber, C.; Day, M. W.; Bercaw, J. E. *Organometallics* **1999**, *18*, 1389–1401.
8. Porri, L.; Giarrusso, A. Conjugated Diene Polymerization. In *Comprehensive Polymer Science*; Eastmond, G., Ledwith, A., Russo, S., Sigwalt, P., Eds.; Pergamon: Oxford, UK, 1989; vol. 4; pp 53–108.
9. Evans, W. J.; Ulibarri, T. A.; Ziller, J. W. *J. Am. Chem. Soc.* **1990**, *112*, 2314–2324.
10. Taube, R.; Windisch, H.; Maiwald, S. *Macromol. Symp.* **1995**, *89*, 393–409.
11. Kuran, W. Coordination Polymerisation of Conjugated Dienes. In *Principles of Coordination Polymerisation*, J. Wiley and Sons: Chichester, 2001; pp 275–329. Chapter 5.
12. Fischbach, A.; Anwander, R. *Adv. Polym. Sci.* **2006**, *204*, 155–281.
13. Friebe, L.; Nuyken, O.; Obrecht, W. *Adv. Polym. Sci.* **2006**, *204*, 1–154.
14. Jothieswaran, J.; Fadlallah, S.; Bonnet, F.; Visseaux, M. *Catalysts* **2017**, *7*, 378.
15. Kirillov, E.; Saillard, J.-Y.; Carpentier, J.-F. *Coord. Chem. Rev.* **2005**, *249*, 1221–1248.
16. Gromada, J.; Carpentier, J.-F.; Mortreux, A. *Coord. Chem. Rev.* **2004**, *248*, 397–410.
17. Hou, Z.; Luo, Y.; Li, X. *J. Organomet. Chem.* **2006**, *691*, 3114–3121.

18. Porri, L.; Ricci, G.; Giarusso, A.; Shubin, N.; Lu, Z. Recent Developments in Lanthanide Catalysts for 1,3-Diene Polymerization. In *Olefin Polymerization: Emerging Frontiers*; Arjunan, P., McGrath, J. E., Hanlon, T. L., Eds.; ACS Symposium Series, American Chemical Society, 1999; vol. 749; pp 15–30.
19. Zhang, Z.; Cui, D.; Wang, B.; Liu, B.; Yang, Y. *Struct. Bond.* **2010**, *137*, 49–108.
20. Coperet, C. Hydrogenation With Early Transition Metal, Lanthanide and Actinide Complexes. In *Handbook of Homogeneous Hydrogenation*; De Vries, J. G., Elsevier, C. J., Eds.; Wiley-VCH Verlag GmbH & Co. KGaA: Weinheim, 2007; vol. 1; p 11.
21. Taube, R.; Windisch, H.; Görlitz, F. H.; Schumann, H. *J. Organomet. Chem.* **1993**, *445*, 85–91.
22. Hong, S.; Marks, T. J. *Acc. Chem. Res.* **2004**, *37*, 673–686.
23. Douglass, M. R.; Marks, T. J. *J. Am. Chem. Soc.* **2000**, *122*, 1824–1825.
24. Anwander, R. Rare Earth Metals in Homogeneous Catalysis. In *Applied Homogeneous Catalysis With Organometallic Compounds*; Cornils, B., Herrmann, W. A., Eds.; Wiley-VCH Verlag GmbH: Weinheim, 1996; vol. 2; p 866.
25. Nolan, S. P.; Marks, T. J. *J. Am. Chem. Soc.* **1989**, *111*, 8538–8542.
26. Casey, C. P.; Hallenback, S. L.; Pollock, D. W.; Landis, C. L. *J. Am. Chem. Soc.* **1995**, *117*, 9770–9771.
27. Casey, C. P.; Hallenback, S. L.; Wright, J. M.; Landis, C. L. *J. Am. Chem. Soc.* **1997**, *119*, 9680–9690.
28. Casey, C. P.; Fagan, M. A.; Hallenback, S. L. *Organometallics* **1998**, *17*, 287–289.
29. Casey, C. P.; Fisher, J. J. *Inorg. Chim. Acta* **1998**, *270*, 5–7.
30. Casey, C. P.; Fisher Klein, J.; Fagan, M. A. *J. Am. Chem. Soc.* **2000**, *122*, 4320–4330.
31. Casey, C. P.; Lee, T. Y.; Tunge, J. A.; Carpenetti, D. W., II *J. Am. Chem. Soc.* **2001**, *123*, 10762–10763.
32. Casey, C. P.; Tunge, J. A.; Lee, T. Y.; Carpenetti, D. W., II *Organometallics* **2002**, *21*, 389–396.
33. Casey, C. P.; Tunge, J. A.; Fagan, M. A. *J. Organomet. Chem.* **2002**, *663*, 91–97.
34. Casey, C. P.; Tunge, J. A.; Lee, T. Y.; Fagan, M. A. *J. Am. Chem. Soc.* **2003**, *125*, 641–2651.
35. Burns, C. J.; Andersen, R. A. *J. Am. Chem. Soc.* **1987**, *109*, 915–917.
36. Eaborn, C.; Hitchcock, P. B.; Izod, K.; Lu, Z. R.; Smith, J. D. *Organometallics* **1996**, *15*, 4783–4790.
37. Evans, W. J.; Perotti, J. M.; Brady, J. C.; Ziller, J. W. *J. Am. Chem. Soc.* **2003**, *125*, 5204–5212.
38. Schumann, H.; Schutte, S.; Kroth, H. J.; Lentz, D. *Angew. Chem. Int. Ed. Engl.* **2004**, *43*, 6208–6211.
39. Schumann, H.; Heim, A.; Schutte, S.; Lentz, D. *Z. Anorg. Allg. Chem.* **2006**, *632*, 1939–1942.
40. Berg, D. J.; Tosha, B.; Xuening, F. *J. Organomet. Chem.* **2010**, *695*, 2703–2712.
41. Selikhov, A. N.; Mahrova, T. V.; Cherkasov, A. V.; Fukin, G. K.; Larionova, J.; Long, J.; Trifonov, A. A. *Organometallics* **2015**, *34*, 1991–1999.
42. Zhang, G.; Deng, B.; Wang, S.; Wei, Y.; Zhou, S.; Zhu, X.; Huang, Z.; Mu, X. *Dalton Trans.* **2016**, *45*, 15445–15456.
43. Zhang, G.; Wei, Y.; Guo, L.; Zhu, X.; Wang, S.; Zhou, S.; Mu, X. *Chem. Eur. J.* **2015**, *21*, 2519–2526.
44. Selikhov, A. N.; Plankin, G. S.; Cherkasov, A. V.; Shavyrin, A. S.; Louyriac, E.; Maron, L.; Trifonov, A. A. *Inorg. Chem.* **2019**, *58*, 5325–5334.
45. Selikhov, A. N.; Shavyrin, A. S.; Cherkasov, A. V.; Fukin, G. K.; Trifonov, A. A. *Organometallics* **2019**, *38*, 4615–4624.
46. Selikhov, A. N.; Boronin, E. N.; Cherkasov, A. V.; Fukin, G. K.; Shavyrin, A. S.; Trifonov, A. A. *Adv. Synth. Catal.* **2020**, *362*, 5432–5443.
47. Khristolyubov, D. O.; Lyubov, D. M.; Shavyrin, A. S.; Cherkasov, A. V.; Fukin, G. K.; Trifonov, A. A. *Inorg. Chem. Front.* **2020**, *7*, 2459–2477.
48. Long, J.; Tolpygin, A. O.; Cherkasov, A. V.; Lyssenko, K. A.; Guari, Y.; Larionova, J.; Trifonov, A. A. *Organometallics* **2019**, *38* (4), 748–752.
49. Evans, W. J.; Giarikos, D. G.; Robledo, C. B.; Leong, V. S.; Ziller, J. W. *Organometallics* **2001**, *20*, 5648–5652.
50. Roitershtein, D. M.; Ziller, J. W.; Evans, W. J. *J. Am. Chem. Soc.* **1998**, *120*, 11342–11346.
51. Campazzi, E.; Solari, E.; Scopelliti, R.; Floriani, C. *Chem. Commun.* **1999**, 1617.
52. Coles, M. P.; Hitchcock, P. B.; Lappert, M. F.; Protchenko, A. V. *Organometallics* **2012**, *31*, 2682–2690.
53. Shapiro, P. J.; Cotter, W. D.; Schaefer, W. P.; Labinger, J. A.; Bercaw, J. E. *J. Am. Chem. Soc.* **1994**, *116*, 4623.
54. Huang, W.; Abukhalil, P. M.; Khan, S. I.; Diaconescu, P. L. *Chem. Commun.* **2014**, *50*, 5221–5223.
55. Selikhov, A. N.; Mahrova, T. V.; Cherkasov, A. V.; Fukin, G. K.; Kirillov, E.; Lamsfus, C. A.; Maron, L.; Trifonov, A. A. *Organometallics* **2016**, *35*, 2401–2409.
56. Guo, L.; Zhu, X.; Zhang, G.; Wei, Y.; Ning, L.; Zhou, S.; Feng, Z.; Wanf, S.; Mu, X.; Chen, J.; Jiang, Y. *Inorg. Chem.* **2015**, *54*, 5725–5731.
57. Zhu, X.; Li, Y.; Guo, D.; Wang, S.; Wei, Y.; Zhou, S. *Dalton Trans.* **2018**, *47*, 3947–3957.
58. Feng, Z.; Huang, Z.; Wang, S.; Wei, Y.; Zhou, S.; Zhu, X. *Dalton Trans.* **2019**, *48* (29), 11094–11102.
59. Zhang, F.; Zhang, J.; Zhang, Y.; Hong, J.; Zhou, X. *Organometallics* **2014**, *33* (21), 6186–6192.
60. White, R. E.; Carlson, C. N.; Veauthier, J. M.; Simpson, C. K.; Thompson, J. D.; Scott, B. L.; Hanusa, T. P.; John, K. D. *Inorg. Chem.* **2006**, *45*, 7004–7009.
61. Simpson, C. K.; White, R. E.; Carlson, C. N.; Wrobleski, D. A.; Kuehl, C. J.; Croce, T. A.; Steele, I. M.; Scott, B. L.; Hanusa, T. P.; Sattelberger, A. P.; John, K. D. *Organometallics* **2005**, *24*, 3685–3691.
62. Sanchez-Barba, L. F.; Hughes, D. L.; Humphrey, S. M.; Bochmann, M. *Organometallics* **2005**, *24*, 5329–5334.
63. Standfuss, S.; Abinet, E.; Spaniol, T. P.; Okuda, J. *Chem. Commun.* **2011**, *47*, 11441–11443.
64. Pu, M. P.; Li, Q.-S.; Xie, Y.; King, R. B.; Schaefer, H. F. *J. Phys. Chem. A* **2011**, *115*, 4491–4504.
65. Shannon, R. D. *Acta Crystallogr. Sect. A* **1976**, *32*, 751–767.
66. White, R. E.; Hanusa, T. P.; Kucera, B. E. *J. Am. Chem. Soc.* **2006**, *128*, 9622–9623.
67. White, R. E.; Hanusa, T. P.; Kucera, B. E. *J. Organomet. Chem.* **2007**, *692*, 3479–3485.
68. White, R. E.; Hanusa, T. P. *Organometallics* **2006**, *25*, 5621.
69. Kuehl, C. J.; Simpson, C. K.; John, K. D.; Sattelberger, A. P.; Carlson, C. N.; Hanusa, T. P. *J. Organomet. Chem.* **2003**, *683*, 149.
70. Rightmire, N. R.; Hanusa, T. P.; Rheingold, A. L. *Organometallics* **2014**, *33*, 5952–5955.
71. Taube, R. Catalytic Reaction Mechanisms and Structure-Reactivity Relationships in the Stereospecific Butadiene Polymerization. In *Metalorganic Catalysts for Synthesis and Polymerization*; Kaminsky, W., Ed.; Springer: Berlin, Germany, 1999; pp 531–546.
72. Porri, L.; Ricci, G.; Giarrusso, A.; Shubin, N.; Lu, Z. *ACS Symp. Ser.* **2000**, *749*, 15–30.
73. Ajellal, N.; Furlan, L.; Thomas, C. M.; Casagrande, O. L., Jr.; Carpentier, J.-F. *Macromol. Rapid Commun.* **2006**, *27*, 338–343.
74. Abinet, E.; Martin, D.; Standfuss, S.; Kulinna, H.; Spaniol, T. P.; Okuda, J. *Chem. Eur. J.* **2011**, *17*, 15014–15026.
75. Yu, N.; Nishiura, M.; Li, X.; Xi, Z.; Hou, Z. *Chem. Asian J.* **2008**, *3*, 1406–1414.
76. Cui, D.; Jian, Z.; Liu, X. *(Changchun Applied Chemistry), CN101704848A.*
77. Jian, Z.; Cui, D.; Hou, Z.; Li, X. *Chem. Commun.* **2010**, *46*, 3022–3024.
78. Jian, Z.; Cui, D.; Hou, Z. *Chem. Eur. J.* **2012**, *18*, 2674–2684.
79. Jian, Z.; Tang, S.; Cui, D. *Chem. Eur. J.* **2010**, *16*, 14007–14015.
80. Bonnet, F.; Violante, C.; Roussel, P.; Mortreux, A.; Visseaux, M. *Chem. Commun.* **2009**, *23*, 3380–3382.
81. Jian, Z.; Tang, S.; Cui, D. *Macromolecules* **2011**, *44*, 7675–7681.
82. Jende, L. N.; Hollfelder, C. O.; Maichle-Mössmer, C.; Anwander, R. *Organometallics* **2015**, *34*, 32–41.
83. Luo, Y.; Chi, S.; Chen, J. *New J. Chem.* **2013**, *37*, 2675–2682.
84. Fadlallah, S.; Terrier, M.; Jones, C.; Roussel, P.; Bonnet, F.; Visseaux, M. *Organometallics* **2016**, *35*, 456–461.
85. Maiwald, S.; Taube, R.; Hemling, H.; Schumann, H. *J. Organomet. Chem.* **1998**, *552*, 195–204.

86. Fadlallah, S.; Jothieswaran, J.; Capet, F.; Bonnet, F.; Visseaux, M. *Chem. Eur. J.* **2017**, *23*, 15644–15654.
87. Fadlallah, S.; Jothieswaran, J.; Del Rosal, I.; Maron, L.; Bonnet, F.; Visseaux, M. *Catalysts* **2020**, *10*, 820.
88. Cui, P.; Spaniol, T. P.; Okuda, J. *Organometallics* **2013**, *32*, 1176–1182.
89. Taube, R.; Windisch, H.; Weissenborn, H.; Hemling, H.; Schumann, H. J. *J. Organomet. Chem.* **1997**, *548*, 229–236.
90. Cui, P.; Spaniol, T. P.; Maron, L.; Okuda, J. *Chem. Commun.* **2014**, *50*, 424–426.
91. Martin, D.; Kleemann, J.; Abinet, E.; Spaniol, T. P.; Maron, L.; Okuda, J. *Eur. J. Inorg. Chem.* **2013**, 3987–3992.
92. Cui, D.; Nishiura, M.; Tardif, O.; Hou, Z. *Organometallics* **2008**, *27*, 2428–2435.
93. Tlpygin, A. O.; Linnikova, O. A.; Kovylina, T. A.; Cherkasov, A. V.; Fukin, G. K.; Trifonov, A. A. *Russ. Chem. Bull. Int. Ed.* **2020**, *69* (6), 1114–1121.
94. Barbier-Baudry, D.; Bonnet, F.; Dormond, A.; Finot, E.; Visseaux, M. *Macromol. Chem. Phys.* **2002**, *203*, 1194–1200.
95. Woodman, T. J.; Schormann, M.; Hughes, D. L.; Bochmann, M. *Organometallics* **2003**, *22*, 3028–3030.
96. Woodman, T. J.; Schormann, M.; Hughes, D. L.; Bochmann, M. *Organometallics* **2004**, *23*, 2972–2979.
97. Sánchez-Barba, L. F.; Hughes, D. L.; Humphrey, S. M.; Bochmann, M. *Organometallics* **2006**, *25*, 1012–1020.
98. Abinet, E.; Spaniol, T. P.; Okuda, J. *Chem. Asian J.* **2011**, *6*, 389–391.
99. Wu, C.; Liu, B.; Lin, F.; Wang, M.; Cui, D. *Angew. Chem. Int. Ed.* **2017**, *56*, 6975–6979.
100. Chen, R.; Yao, C.; Wang, M.; Xie, H.; Wu, C.; Cui, D. *Organometallics* **2015**, *34*, 455–461.
101. Chen, J.; Gao, Y.; Xiong, S.; Delferro, M.; Lohr, T. L.; Marks, T. J. *ACS Catal.* **2017**, *7*, 5214–5219.
102. Tsutsui, M.; Ely, N. *J. Am. Chem. Soc.* **1975**, *97*, 3551–3553.
103. Demir, S.; Lorenz, S. E.; Fang, M.; Furche, F.; Meyer, G.; Ziller, J. W.; Evans, W. J. *J. Am. Chem. Soc.* **2010**, *132*, 11151–11158.
104. Yoder, J. C.; Day, M. W.; Bercaw, J. E. *Organometallics* **1998**, *17*, 4946–4958.
105. Lorenz, S. E.; Schmiege, B. M.; Lee, D. S.; Ziller, J. W.; Evans, W. J. *Inorg. Chem.* **2010**, *49*, 6655–6663.
106. Evans, W. J.; Lee, D. S.; Johnston, M. A.; Ziller, J. W. *Organometallics* **2005**, *24*, 6393–6397.
107. Evans, W. J.; Seibel, C. A.; Ziller, J. W. *J. Am. Chem. Soc.* **1998**, *120*, 6745–6752.
108. Evans, W. J.; Kozimor, S. A.; Brady, J. C.; Davis, B. L.; Nyce, G. W.; Seibel, C. A.; Ziller, J. W.; Doedens, R. J. *Organometallics* **2005**, *24*, 2269–2278.
109. Peterson, J. K.; MacDonald, M. R.; Ziller, J. W.; Evans, W. J. *Organometallics* **2013**, *32*, 2625–2631.
110. Fieser, M. E.; Johnson, C. W.; Bates, J. E.; Ziller, J. W.; Furche, F.; Evans, W. J. *Organometallics* **2015**, *34*, 4387–4393.
111. Evans, W. J.; Montalvo, E.; Champagne, T. M.; Ziller, J. W.; DiPasquale, A. G.; Rheingold, A. L. *J. Am. Chem. Soc.* **2008**, *130*, 16–17.
112. Evans, W. J.; Montalvo, E.; Champagne, T. M.; Ziller, J. W.; DiPasquale, A. G.; Rheingold, A. L. *Organometallics* **2008**, *27*, 3582–3586.
113. Evans, W. J.; Montalvo, E.; Dixon, D. J.; Ziller, J. W.; DiPasquale, A. G.; Rheingold, A. L. *Inorg. Chem.* **2008**, *47*, 11376–11381.
114. Casely, I. J.; Suh, Y. S.; Ziller, J. W.; Evans, W. J. *Organometallics* **2010**, *29*, 5209–5214.
115. Demir, S.; Montalvo, E.; Ziller, J. W.; Meyer, G.; Evans, W. J. *Organometallics* **2010**, *29*, 6608–6611.
116. Demir, S.; Mueller, T. J.; Ziller, J. W.; Evans, W. J. *Organometallics* **2011**, *30*, 3083–3089.
117. Evans, W. J.; Lorenz, S. E.; Ziller, J. W. *Chem. Commun.* **2007**, 4662–4664.
118. Fieser, M. E.; Mueller, T. J.; Bates, J. E.; Ziller, J. W.; Furche, F.; Evans, W. J. *Organometallics* **2014**, *33*, 3882–3890.
119. Kirillov, E.; Lehmann, C. W.; Razavi, A.; Carpentier, J.-F. *J. Am. Chem. Soc.* **2004**, *126*, 12240–12241.
120. Rodrigues, A.-S.; Kirillov, E.; Lehmann, C. W.; Roisnel, T.; Vuillemin, B.; Razavi, A.; Carpentier, J.-F. *Chem. Eur. J.* **2007**, *13*, 5548–5565.
121. Rodrigues, A.; Kirillov, E.; Roisnel, T.; Razavi, A.; Vuillemin, B.; Carpentier, J. F. *Angew. Chem. Int. Ed.* **2007**, *46*, 7240–7243.
122. Rodrigues, A. S.; Kirillov, E.; Vuillemin, B.; Razavi, A.; Carpentier, J.-F. *J. Mol. Catal. A Chem.* **2007**, *273*, 87–91.
123. Perrin, L.; Sarazin, Y.; Kirillov, E.; Carpentier, J.-F.; Maron, L. *Chem. Eur. J.* **2009**, *15*, 3773–3783.
124. Fischbach, A.; Perdih, F.; Herdtweck, E.; Anwander, R. *Organometallics* **2006**, *25*, 1626–1642.
125. Perrin, L.; Kirillov, E.; Carpentier, J. F.; Maron, L. *Macromolecules* **2010**, *43*, 6330–6336.
126. Rodrigues, A. S.; Kirillov, E.; Vuillemin, B.; Razavi, A.; Carpentier, J.-F. *Polymer* **2008**, *49*, 2039–2045.
127. Sarazin, Y.; de Frémont, P.; Annunziata, L.; Duc, M.; Carpentier, J. F. *Adv. Synth. Catal.* **2011**, *353*, 1367–1374.
128. Annunziata, L.; Duc, M.; Carpentier, J. F. *Macromolecules* **2011**, *44*, 7158–7166.
129. Annunziata, L.; Rodrigues, A. S.; Kirillov, E.; Sarazin, Y.; Okuda, J.; Perrin, L.; Maron, L.; Carpentier, J. F. *Macromolecules* **2011**, *44*, 3312–3322.
130. Zhang, Z.; Bu, X.; Zhang, J.; Liu, R.; Zhou, X.; Weng, L. *Organometallics* **2010**, *29*, 2111–2117.
131. Jian, Z.; Petrov, A. R.; Hangaly, N. K.; Li, S.; Rong, W.; Mou, Z.; Rufanov, K. A.; Harms, K.; Sundermeyer, J.; Cui, D. *Organometallics* **2012**, *31*, 4267–4282.
132. Jian, Z.; Cui, D. *Chem. Eur. J.* **2011**, *17*, 14578–14585.
133. Evans, W. J.; Schmiege, B. M.; Lorenz, S. E.; Miller, K. A.; Champagne, T. M.; Ziller, J. W.; DiPasquale, A. G.; Rheingold, A. L. *J. Am. Chem. Soc.* **2008**, *130*, 8555–8563.
134. Mao, W.; Xiang, L.; Maron, L.; Leng, X.; Chen, Y. *J. Am. Chem. Soc.* **2017**, *139*, 17759–17762.
135. Cheng, J.; Wang, H.; Nishiura, M.; Hou, Z. *Chem. Sci.* **2012**, *3*, 2230–2233.
136. Wang, X.; Zhou, G.; Liu, B.; Luo, Y. *Organometallics* **2018**, *37*, 882–890.
137. Guo, G.; Wu, X.; Yan, X.; Yan, L.; Li, X.; Zhang, S.; Qiu, N. *Polymers* **2019**, *11*, 836.
138. Cao, W.; Hewage, D.; Yang, D.-S. *J. Chem. Phys.* **2018**, *148, 044312.*
139. Kumari, S.; Cao, W.; Hewage, D.; Silva, R.; Yang, D.-S. *J. Chem. Phys.* **2017**, *146, 074305.*

Appendix 2: ^{1}H NMR of I^{1} (a), I^{2} (b), I^{3} (c).

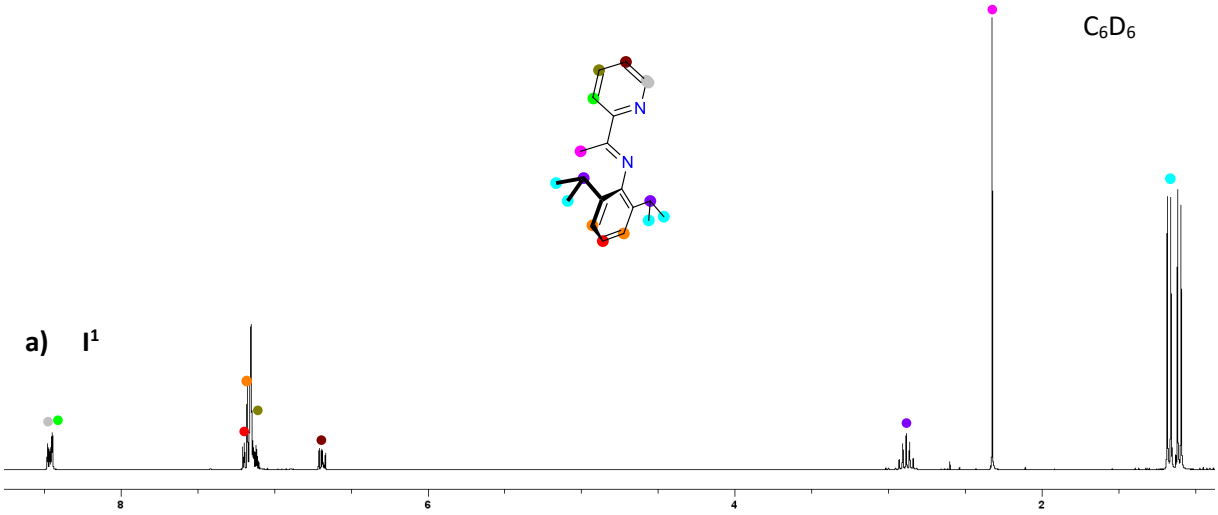

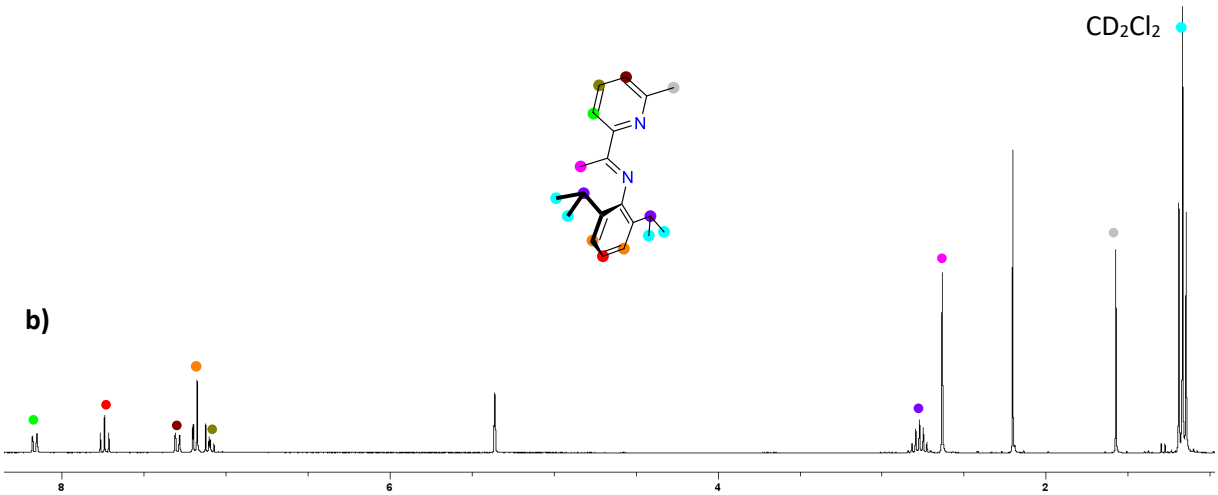

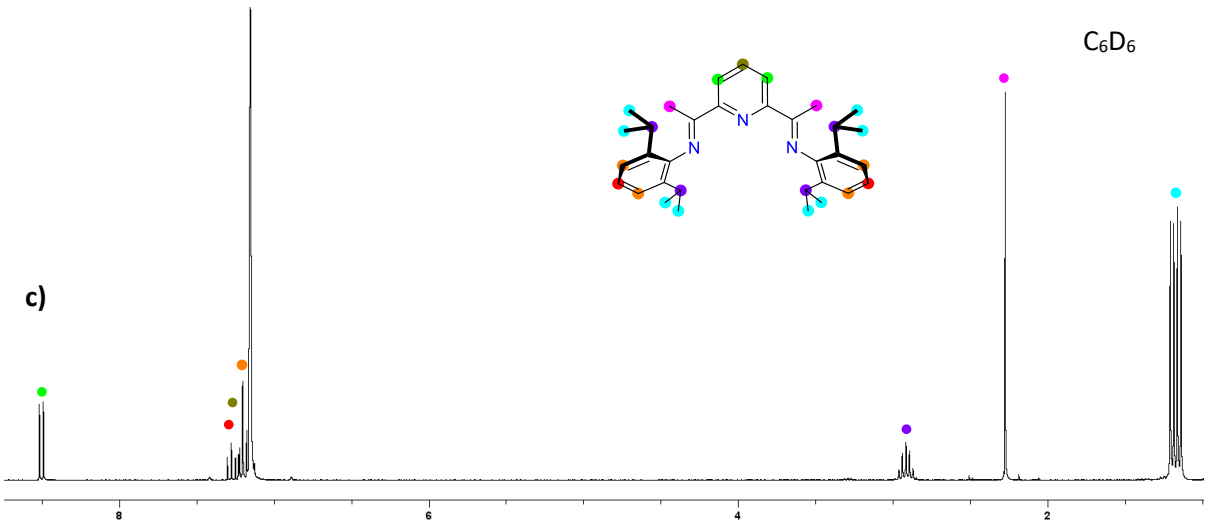

Appendix 3: ^{1}H NMR of $Z^{1}H$ (a), $Z^{2}H$ (b), $Z^{3}H$ (c).

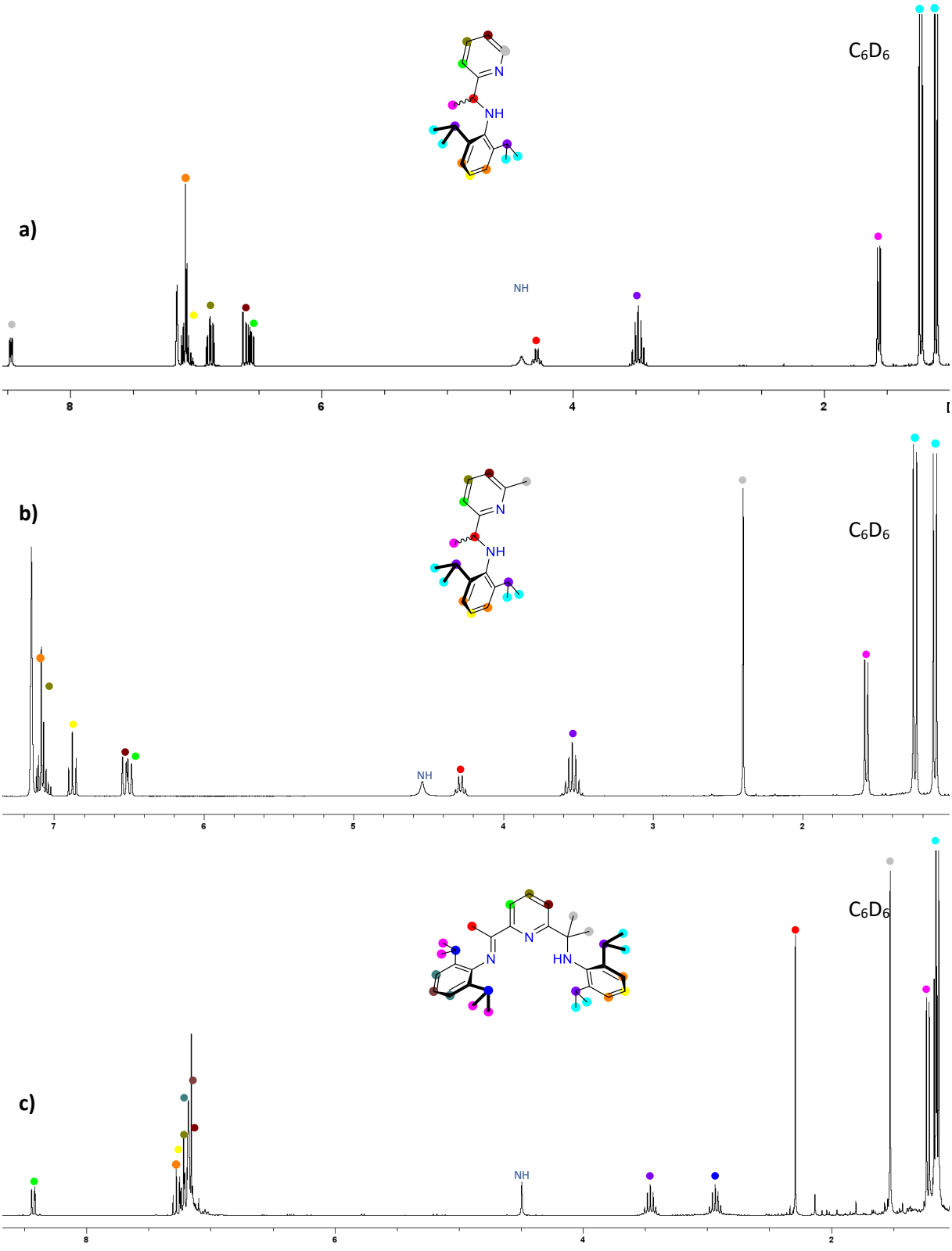

Appendix 4: Evolution of the ^{1}H NMR spectrum of $KN(TMS)_2.Z^{1}H$ (a) after three days at 50° C (b).

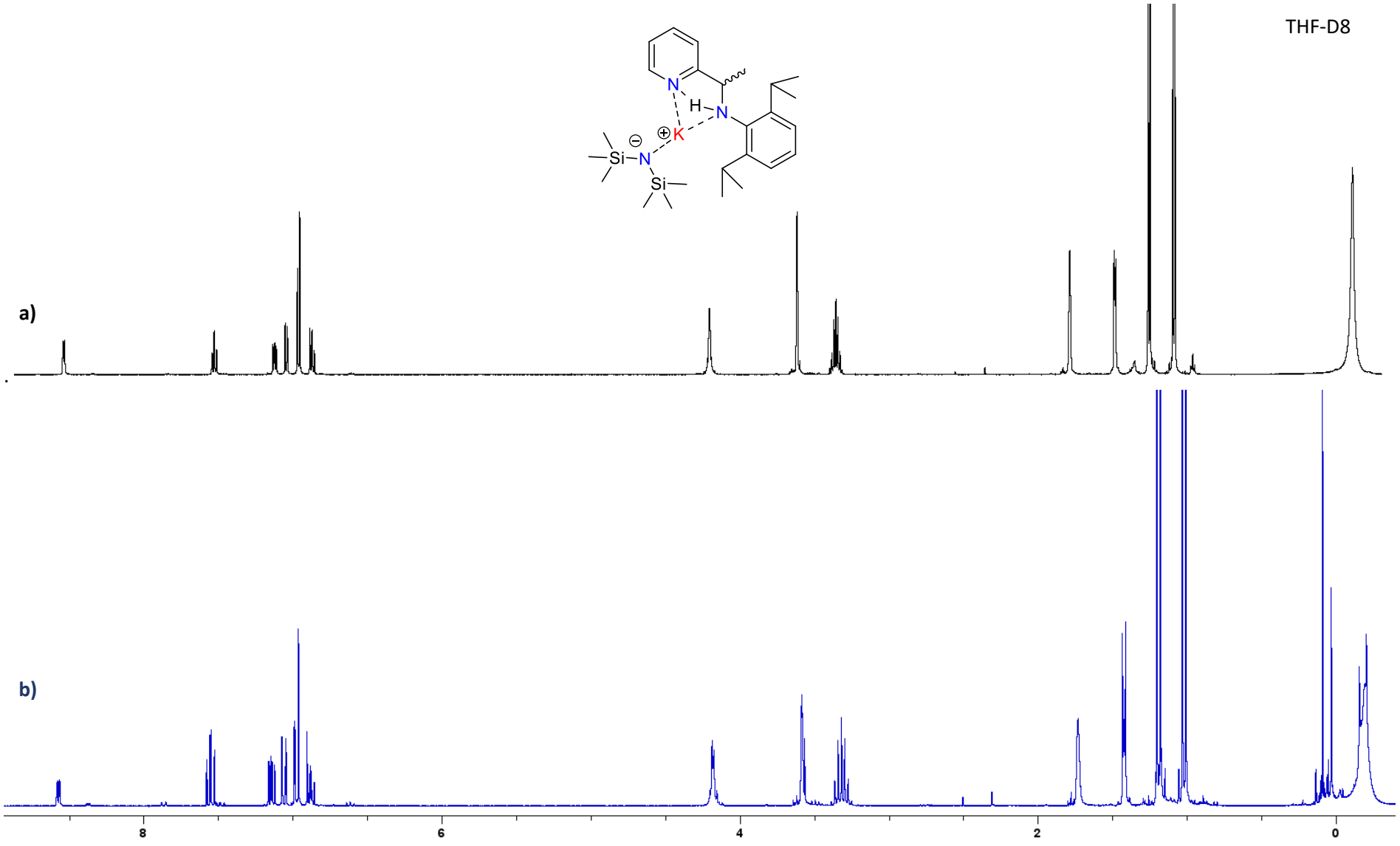

Appendix 5: Comparison between the in-situ obtain BEM complex (a) vs the crystallized complex 6 (b).

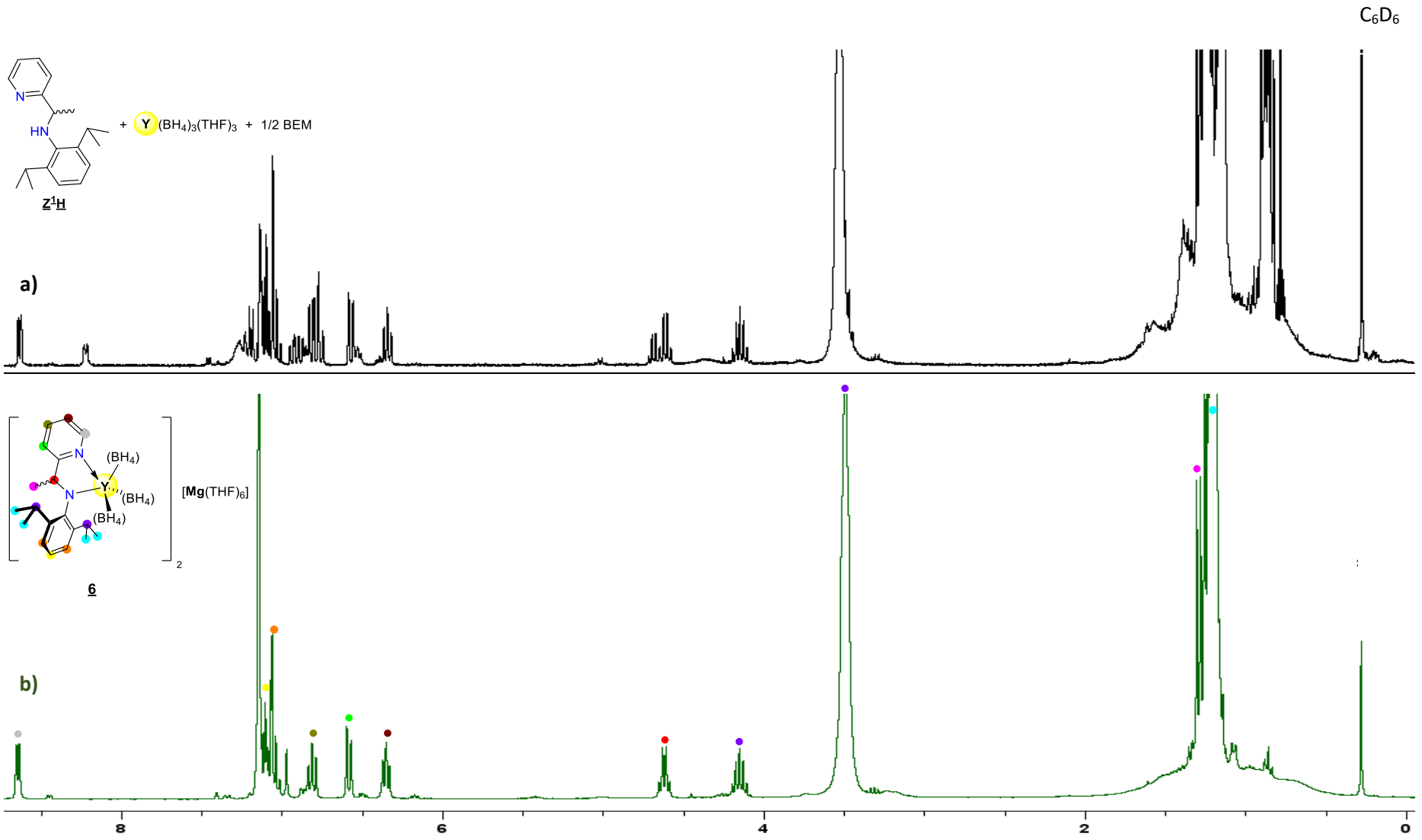

Appendix 6: ^{1}H NMR monitoring with BuLi as base to form the mon-substituted yttrium complex with Z^1 in C_6D_6.

C_6D_6

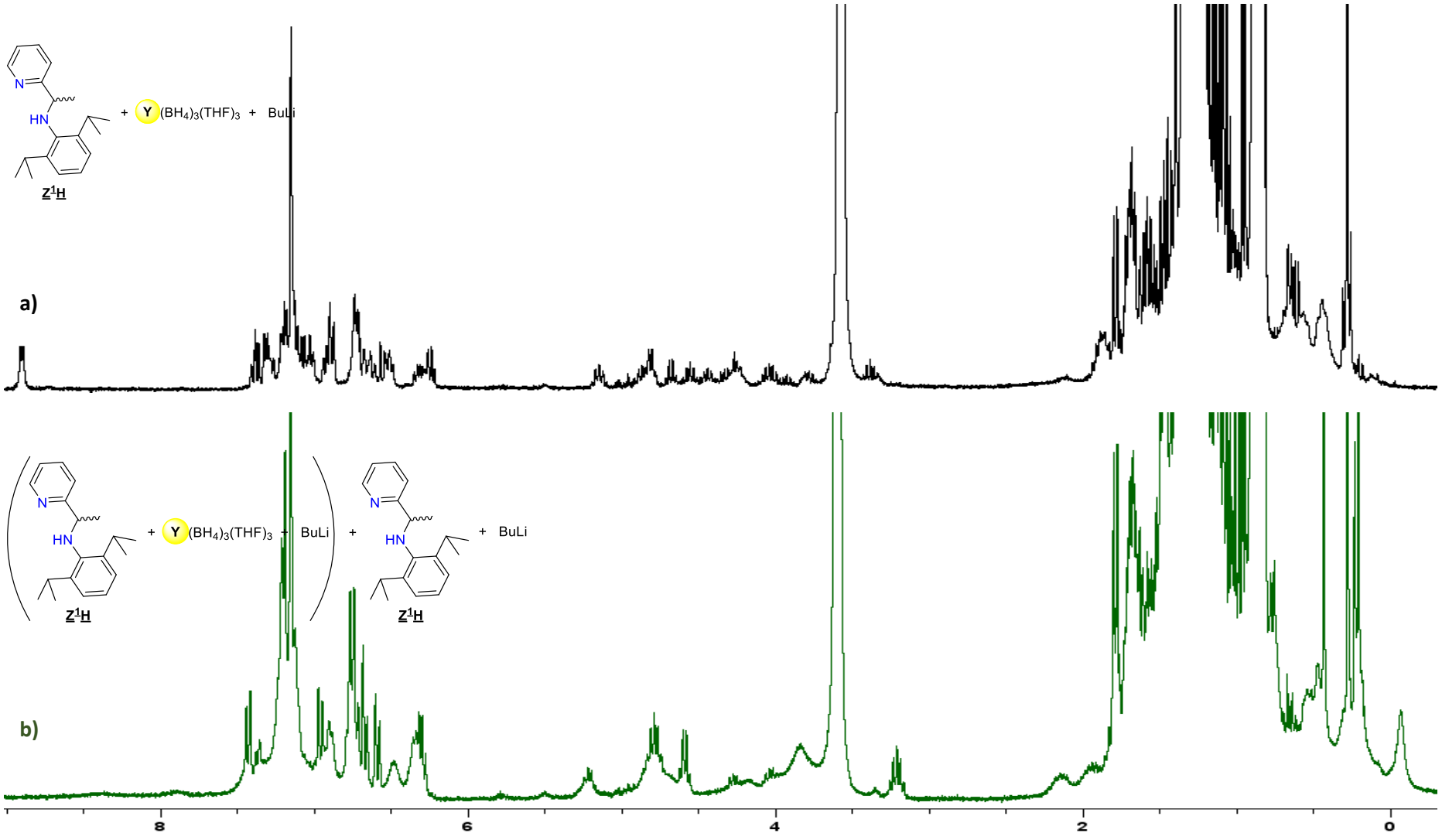

Appendix 7: Diferent attempt for the formation of mono-substituted yttrium complex supported by Z^3.

C_6D_6

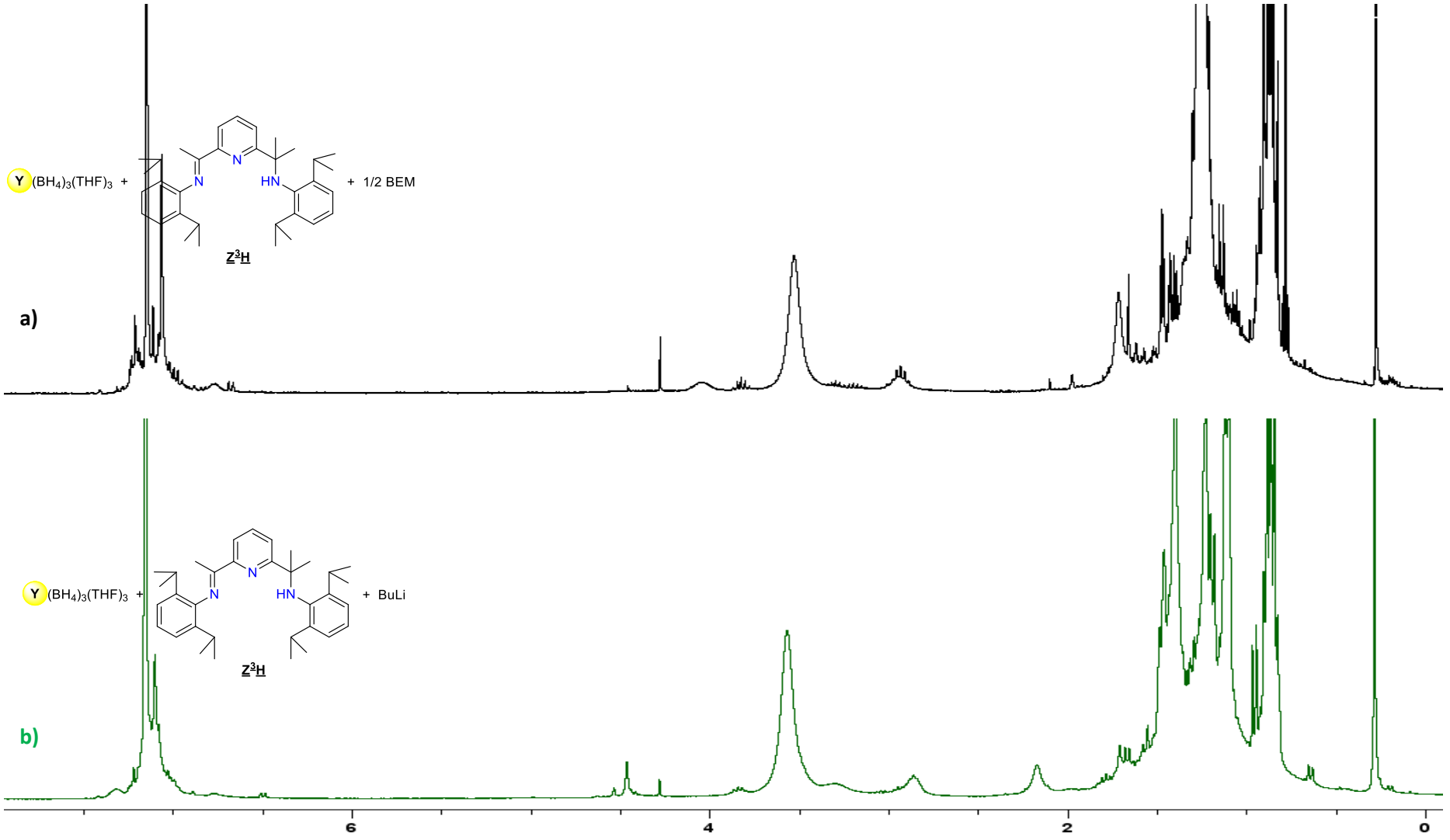

THF-D8

Appendix 8: ^{1}H NMR spectrum of $[Nd(C_3H_5)_2][B(C_6F_5)_4]$.

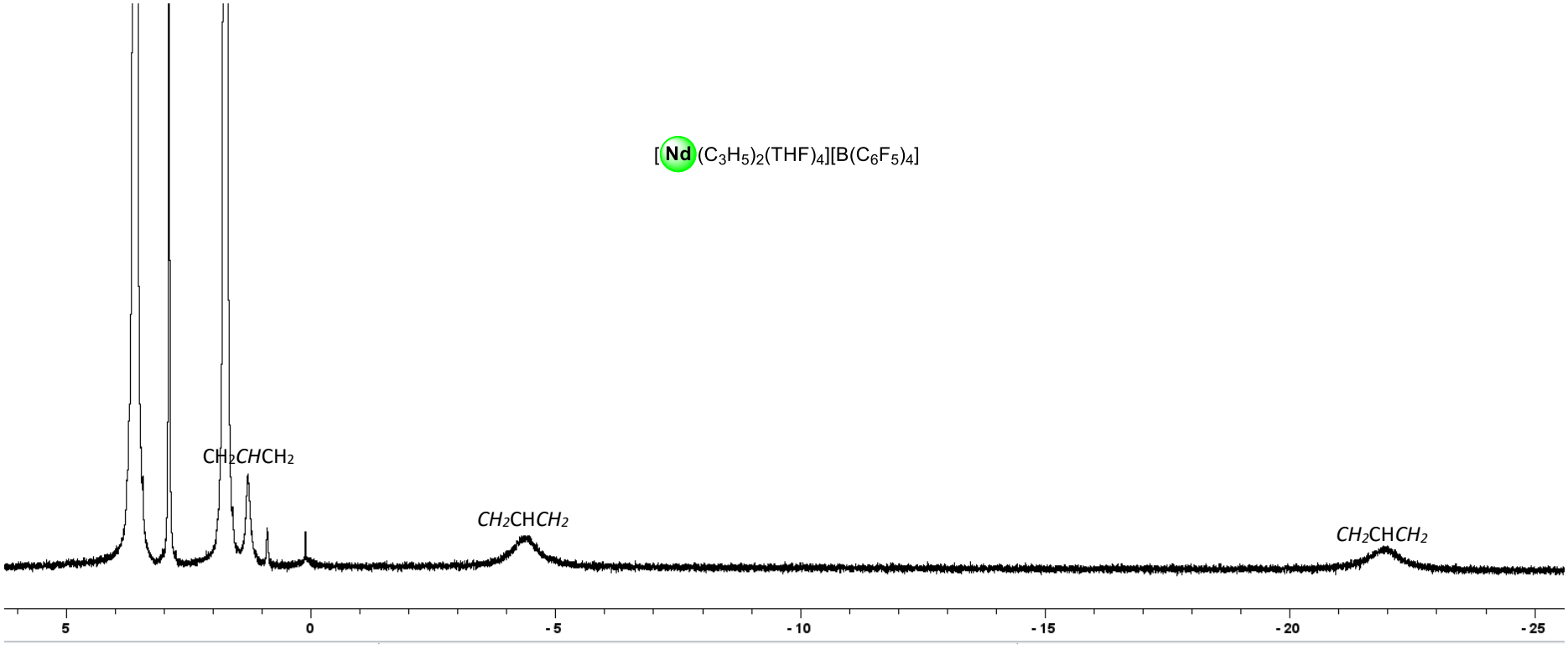

Appendix 9: ^{1}H NMR resulting from the reaction of $Nd(C_3H_5)_3(diox)$ with Z^2H in deuterate THF.

THF-D8

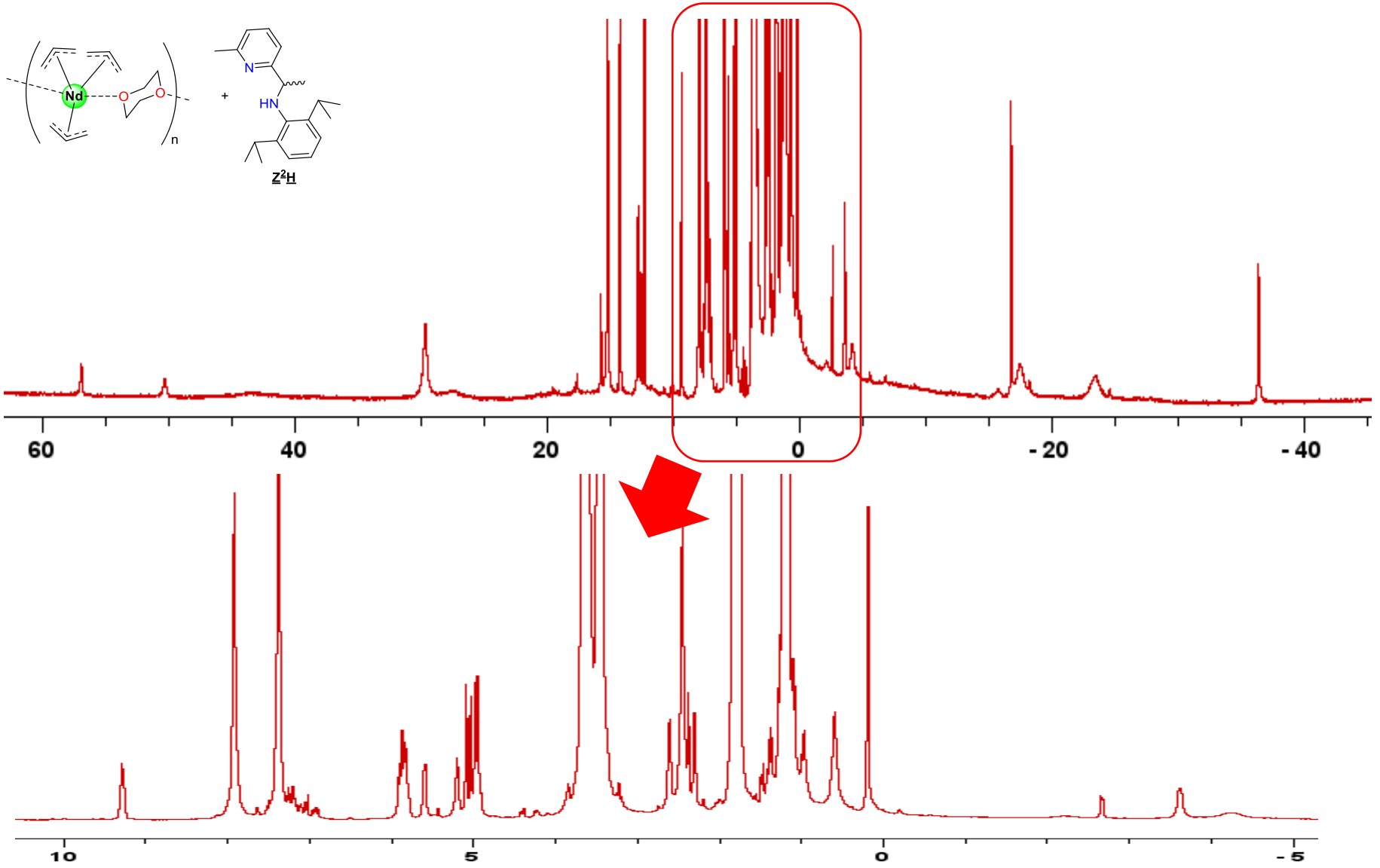

Appendix 10: ^{1}H NMR resulting from the reaction of $Nd(C_3H_5)_3(diox)$ with Z^3H in THF and deuterate benzene.